SEDIMENTOLOGY OF THE KAROO SUPERGROUP IN THE TULI BASIN (LIMPOPO RIVER AREA, SOUTH AFRICA)

A thesis submitted in fulfilment of the requirements for the degree of

DOCTOR OF PHILOSOPHY

of

RHODES UNIVERSITY

by

EMESE M. BORDY

2000

ABSTRACT

The sedimentary rocks of the Karoo Supergroup in the Tuli Basin (South Africa) consist of various terrigenous clastic and chemical deposits (parabreccias, conglo-breccias, conglomerates, sandstones, fine-grained sediments, calcretes and silcretes). Four stratigraphic units were identified: the Basal, Middle and Upper Units, and the Clarens Formation. The palaeo-environmental reconstructions of the four stratigraphic units are based on evidence provided by primary sedimentary structures, palaeo-flow measurements, clast size/shape analysis, petrographic studies, palaeontological findings, borehole data and stratigraphic relations.

The facies associations of the *Basal Unit* are interpreted as colluvial fan and low sinuosity, braided river channel with coal-bearing overbank and thaw-lake deposits. The interpreted depositional environment implies a cold climate, non-glacial subarctic fluvio-lacustrine system. The current indicators of the palaeo-river system suggest flow direction from ENE to WSW. The lithologies of the Basal Unit are very similar to the deposits of the fluvial interval in the Vryheid Formation (Ecca Group) of the main Karoo Basin. There is no indubitable evidence for glacial activity (e.g. striated pavements or clasts, varvites, etc.), therefore the presence of unequivocal Dwyka Group correlatives in the Tuli Basin remains uncertain.

The sedimentary structures and palaeo-current analysis indicate that the beds of the *Middle Unit* were deposited by an ancient river system flowing in a north-northwesterly direction. A lack of good quality exposures did not allow the reconstruction of the fluvial style, but the available data indicate a high-energy, perhaps braided fluvial system. The lack of bio- and chronostratigraphic control hampers precise correlation and enables only the lithocorrelation of the Middle Unit with other braided river systems either in the Beaufort Group or in the Molteno Formation of the main Karoo Basin.

The depositional environment of the *Upper Unit* is interpreted as a low-sinuosity, ephemeral stream system with calcretes and silcretes in the dinosaur-inhabited overbank area. During the deposition of the unit, the climate was semi-arid with sparse precipitation resulting in high-magnitude, low-frequency devastating flash floods. The sediments were built out from a distant northwesterly source to the southeast. The unambiguous correspondence between the Upper Unit and the Elliot Formation (main Karoo Basin) is provided by lithological similarities and prosauropod dinosaurs remains.

The palaeo-geographic picture of the *Clarens Formation* indicates a westerly winds-dominated erg environment with migrating transverse dune types. The ephemeral stream deposits, fossil wood and trace fossils are only present in the lower part of the Formation, indicating that the wet-desert conditions were progressively replaced by dry-desert conditions. Based on lithological and palaeontological evidence, the Formation correlates with the Clarens Formation in the main Karoo Basin.

At this stage, it remains difficult to establish the exact cause of the regional palaeo-slope changes during the deposition of the Karoo Supergroup in the Tuli Basin. It is probable that foreland system tectonics, which affected the lower part of the Supergroup (Basal Unit and Middle Unit?), were replaced by incipient continental extension and rift related tectonic movements in the Middle? and Upper Units, and Clarens Formation.

TABLE OF CONTENTS

LIST OF FIGURES

*The brackets contain the farm name where the figure was drawn.

LIST OF TABLES

1. Introduction

During 1998-2000 a comprehensive study was carried out on the Karoo Supergroup in the South African part of the Tuli Basin (Fig.1). This project was initiated in order to improve the understanding of palaeo-drainage patterns that developed in response to ice-movement during the Dwyka-age glaciation (± 300 Ma). Kimberlites, approximately 500 Ma old, occur along the southern margin of the Tuli Basin, and therefore proper understanding of the palaeo-geomorphology and reconstruction of palaeo-environments in the younger Karoo strata may yield economic implications for the exploration of heavy-mineral deposits such as diamonds.

This thesis presents the results of 32 months of research, comprising 8 months sedimentological field work followed by laboratory based analyses and interpretation of the collected data. The field work included mapping, logging and sampling, bed thickness measurements, bed morphology analysis, macrofabric analysis, palaeo-current and grain size/morphology measurements, and notes on weathering features. In addition, macroscopic sedimentary features and facies associations were analysed and recorded in detail. Laboratory studies consisted of statistical analysis and interpretation of the palaeo-currents, grain size and shape measurements, borehole records (thickness, sand:mud ratio, colouration features, etc.) and petrographic examinations (e.g. provenance, microfabric analyses).

The borehole records were obtained from the Coal Division of Anglo Operations Ltd. (50 detailed drill hole sections) and from De Beers Consolidated Mines Ltd. (9 less detailed core descriptions).

1.1. General geographic setting of the Tuli Basin

The transfrontier Tuli Basin (Fig. 2) is situated along the medial part of the Limpopo River and extends into E Botswana, SE Zimbabwe and into the Northern Province of South Africa. The basin lies between latitudes 28°10' E and 30°30' E, a total distance of approximately 230 km, and it covers an area of circa 9500 km^2. In the South African part of the Tuli Basin, the Karoo sedimentary rocks occupy an area of about 1000 km^2 (Fig. 3).

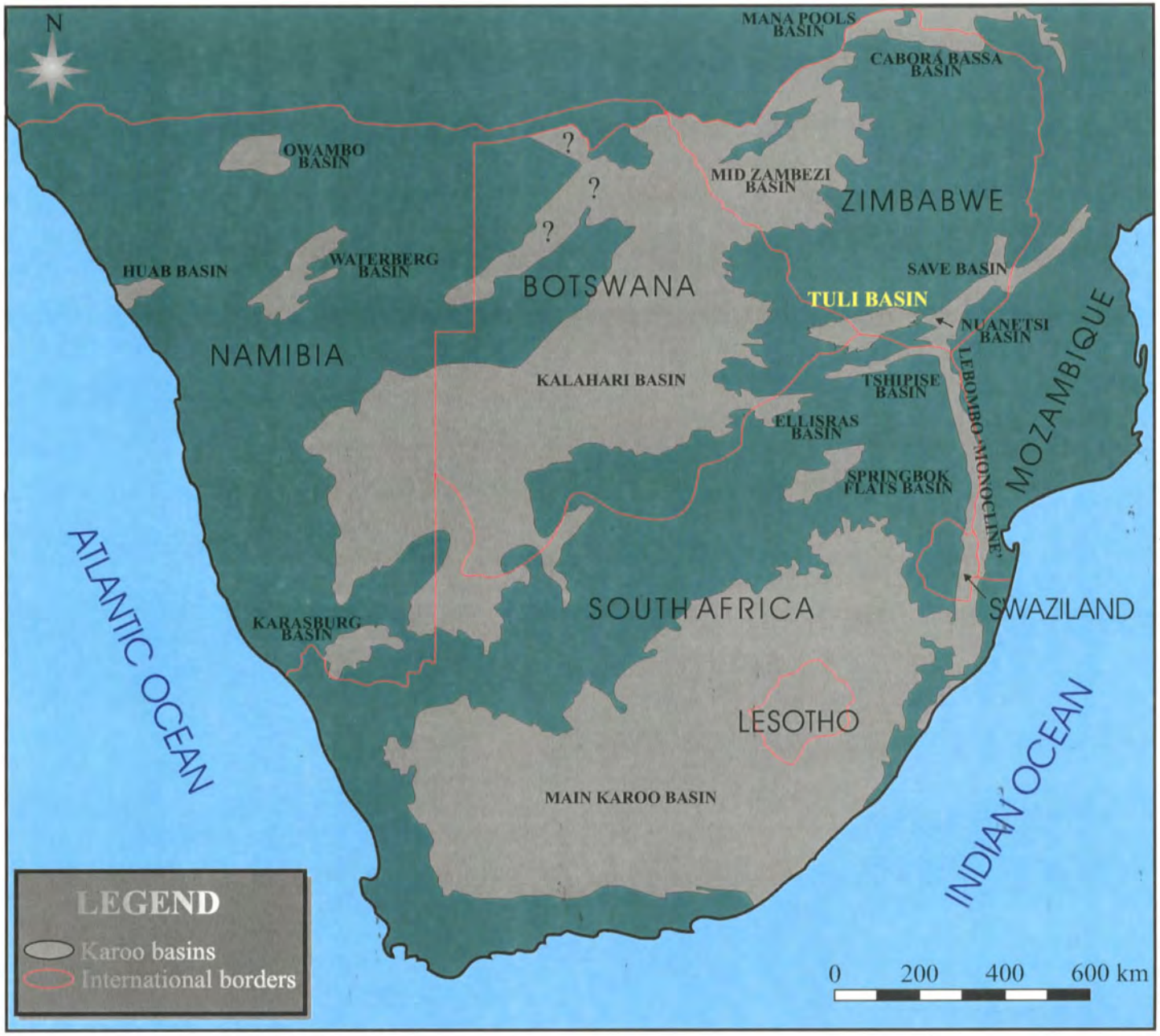

Fig. 1. The Karoo Supergroup in Southern Africa and the Tuli Basin (with yellow) (modified after Johnson et al., 1996).

Fig. 2. Geological Map of the Tuli Basin (modified after Brandl, 1992)

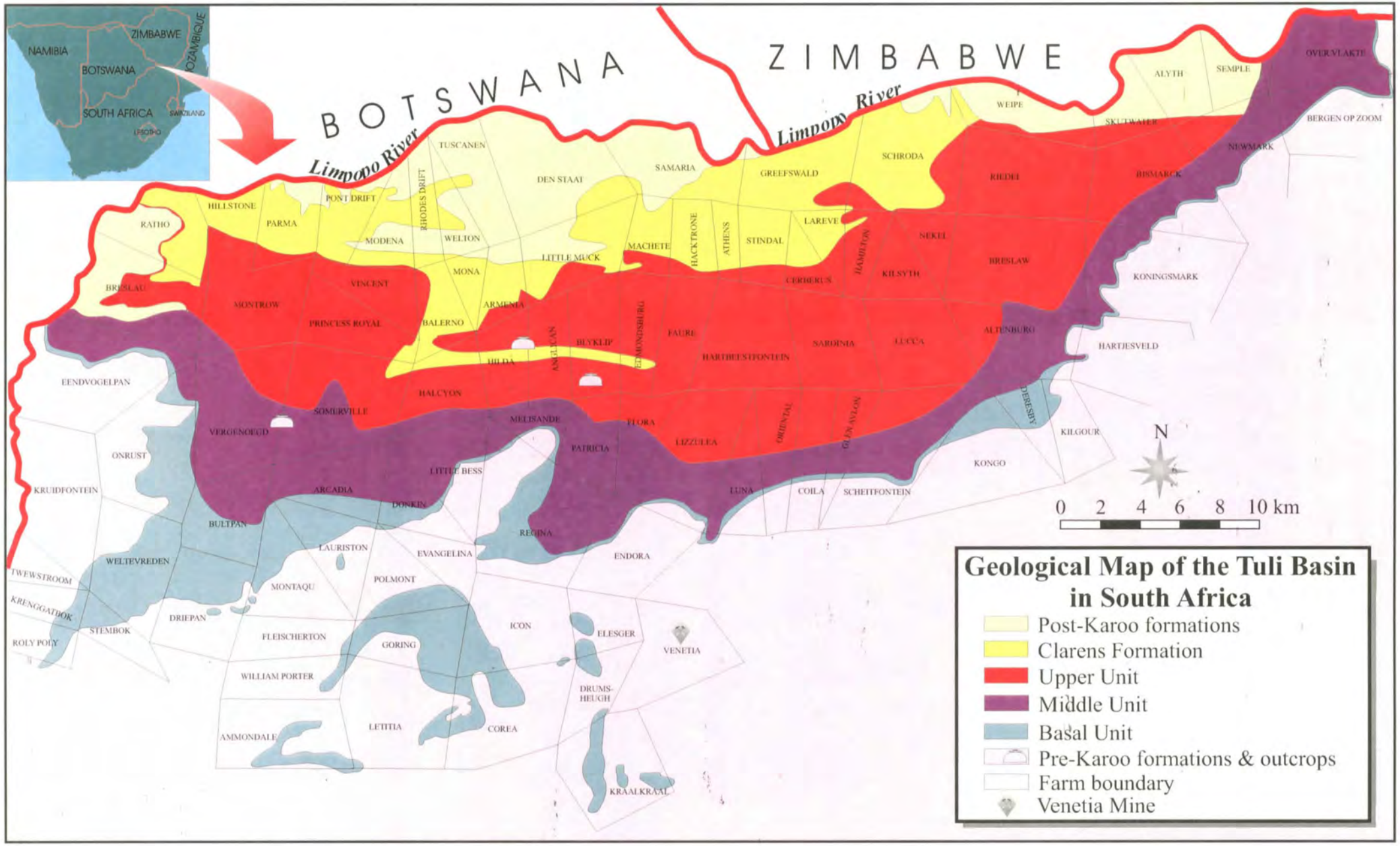

Fig. 3. Geological Map of the southern part of the Tuli Basin (modified after the Geological Map of Beit Bridge area, 1:250000, 1957).

The study area lies in the semiarid tropical climate region. The average annual rainfall is 339 to 400 mm. Most of the rain falls during summer (from October to March), when the average maximum temperature is above 31°C. The winter, with its little wind and clear skies, can also be quite hot (average maximum daily temperature of 27.3 °C) (SAWB, 1999).

Due to the semiarid tropical climate, the area has savanna vegetation dominated by a fairly dense mopani (*Colophospermum mopane*) scrub. Other characteristic tree species are the baobab (*Adansonia digitatai*), marula (*Sclerocarya birrea*) and wild fig (*Ficus sycomorus*) (Prof C. Strub, personal communication 1999).

The study area is subdivided into several sparsely inhabited farms, with no larger settlements. Most of the farms function either as game hunting areas or, to a much lesser extent, as game reserves. Some horticultural farms occur along the Limpopo River valley. All farm names used in the present study are those which appear on the 1:250000 Geological Map of the Beit Bridge area (1957). Though some of the farm names and a number of boundaries have been changed since 1957, the map delineates the outline of the Karoo Supergroup very well. Apart from the farming activity already mentioned, the Venetia Mine conducts the only industrial activity in the area (Fig. 3).

The study area is generally flat and covered by soils and loose sand and is part of the Limpopo lowveld. It does, however, contain two somewhat hilly zones, manifesting in small, 20-60 m high, plateau-like elevations, but rarely providing acceptable exposures for outcrop-based sedimentological field work. The lack of good quality exposures necessitated the visiting of every possible outcrop, which increased the length of time spent in the field searching for more or less continuous logging profiles and representative palaeo-current measuring points. Field work was also hampered by the large distances between the sites and the base camp, and poor quality farm tracks.

Along the southern margin of the basin, an elevated zone exposes very poor quality outcrops of the lower part of the Karoo Supergroup, consisting of highly eroded and weathered sandstone and mudstone, less commonly conglomerate/breccia units. The boulders and blocks of sandy units

were chiefly formed by insolation weathering. During this process the intergranular cement is loosened due to diurnal heating and cooling of the rocks (Blume, 1992). Apart from the insolation weathering, many exposures show salt weathering features represented by exfoliation of the beds. In this case, the weathering shells are formed by salt precipitation and concomitant pressures due to the growing crystals (Blume, 1992).

In the vicinity of the Limpopo River, the uppermost sandstone formation of the Karoo Supergroup produces the caprocks of the mainly flat-topped hills and long ridges. Where the bluff is eroded away, the underlying argillaceous deposits tend to form smooth graded slopes that are often strewn with giant sandstone boulders from the disintegrated caprocks *(Photo 1)*.

2. Geological background

The information presented in this sections is a compilation based on observations and results of the previous geological investigations carried out by several researchers. This summary does not contain research done by the author of this thesis.

2.1. Tectonic Setting

2.1.1. Tectonic Setting of the Karoo Supergroup in southern Africa

The Late Carboniferous-Middle Jurassic sedimentary and igneous rocks of the Karoo Supergroup occur in the main Karoo Basin, and in several other separated outcrop areas in southern and eastern Africa (Johnson et al., 1996) (Fig. 1).

Deposition of the Karoo Supergroup occurred in two broadly different tectonic settings (Rust, 1975). According to Catuneanu et al. (1998), the sedimentary rocks of the main Karoo Basin are retroarc foreland fills. North of the main Karoo Basin, the formations are preserved in separate, fault-bounded depositories which are interpreted either as rift basins or intracratonic thermal sag basins (Watkeys & Sweeney, 1988; Groenewald et al., 1991; Johnson et al., 1996). It is not known to what extent the basins were physically connected prior to post-Karoo erosion, thus the isolation of some of the present basins could be due to erosion that occurred in response to post-Karoo crustal movements (Visser, 1984; Johnson et al., 1996).

2.1.2. Tectonic Setting of the Lebombo-Save-Limpopo area

The Lebombo-Save-Limpopo area includes the Lebombo 'Monocline' (South Africa, Mozambique), the three basins of the Limpopo area: Tshipise (South Africa, partly Zimbawe), Nuanetsi (Zimbabwe), Tuli (South Africa, Zimbabwe, Botswana) and the Save Basin (Zimbabwe) (Fig. 1).

The dominant fault-pattern of these basins is interpreted as a modified southward extension of the East African Rift system (Vail, 1967 in Cox, 1970). It is believed that the Lebombo-Save-Limpopo area forms part of a failed rift triple-junction (Vail et al., 1969; Burke & Dewey, 1973). In this view, the Lebombo 'Monocline' is the southern, the Save Basin is the northern and the Limpopo area is the western arm of the triple junction. The location of the rift was perhaps influenced by the basement weaknesses which are present in the Archaean Limpopo Belt (Cox, 1970), and the genesis of the structure was associated with the Gondwana break-up (Burke & Dewey, 1973; Duguid, 1975).

The trends of the dominant extensional structures are N-S, ESE and ENE in the Lebombo 'Monocline'; ENE and WNW in the Limpopo area, and NNE in the Save Basin (Campbell et al., 1991; Bristow 1982).

The association of ENE-trending, right stepping, en echelon extensional faults with WNW-trending extensional faults, suggests some degree of ENE-directed, dextral strike-slip in addition to the dominant NNW-SSE extension (Campbell et al., 1991). The available data are insufficient for the accurate contouring of the basins in the Save-Limpopo area (Campbell et al., 1991).

2.1.3. Tectonic Setting of the Limpopo area

The Limpopo area, named after the river bordering Botswana, Zimbabwe and South Africa, consists of three basins: the Tshipise, the Nuanetsi and the Tuli. The fill of these basins covers unconformably the Archaean Limpopo Belt which separates the Zimbabwean Craton and the northern part of the Kaapvaal Craton (Pietersburg Block) (Watkeys, 1979; van Reenen et al., 1992) (Fig. 4). These cratons consist largely of Archaean granite-greenstones (van Reenen et al., 1992). Extending WSW-ENE for 700 km, the highly metamorphosed Limpopo Belt is subdivided into three discrete crustal domains: Northern Marginal Zone, Central Zone and Southern Marginal Zone (van Reenen et al., 1992).

The basins in the Limpopo area reflect the reactivation of structures within the Limpopo Belt (Cox, 1970; Campbell et al., 1991). The two prominent structural zones are the southerly-dipping Tuli-Sabi/Triangle Shear Zone in the north and the Palala Shear Zone in the south. These two zones separate the Central Zone from the Northern Marginal Zone and the Southern Marginal Zone, respectively (van Reenen et al., 1992).

Apart from the faults with the Limpopo trend (strike ENE), the major structural lines of the Limpopo area show ESE (Nuanetsi trend) and approximately N-S strikes (Cox et al., 1965).

There is a wide range in the age of the faults and many developed over long periods (Cox, 1970). The geology of the pre-Karoo rocks shows that the line of the Limpopo Belt was intensely reactivated in the post-Waterberg (<1.7 Ga), pre-Karoo period (Cox et al., 1965). After the faulting of the Waterberg rocks, a long period of tectonic quiescence and erosion ensued before the deposition of the Karoo strata (Cox et al., 1965). Accordingly, the pre-Karoo land surface was uneven, probably resembling the present day topography with small hills and ridges (Stagman, 1978). As a result of these erosional pre-Karoo irregularities, the thickness of the Karoo sedimentary rocks varies considerably from place to place (Cox et al., 1965).

Syn-Karoo faults are represented by those that cut the Karoo sedimentary rocks but which displace only the lower basalt flows (Lebombo Group, see p. 29) or fail to displace the basalts at all (Cox, 1970). The best examples is the Shurugwe Fault, marking the northern boundary of the Bubye Coalfield situated in the north-eastern extension of the Tshipise Basin in Zimbabwe

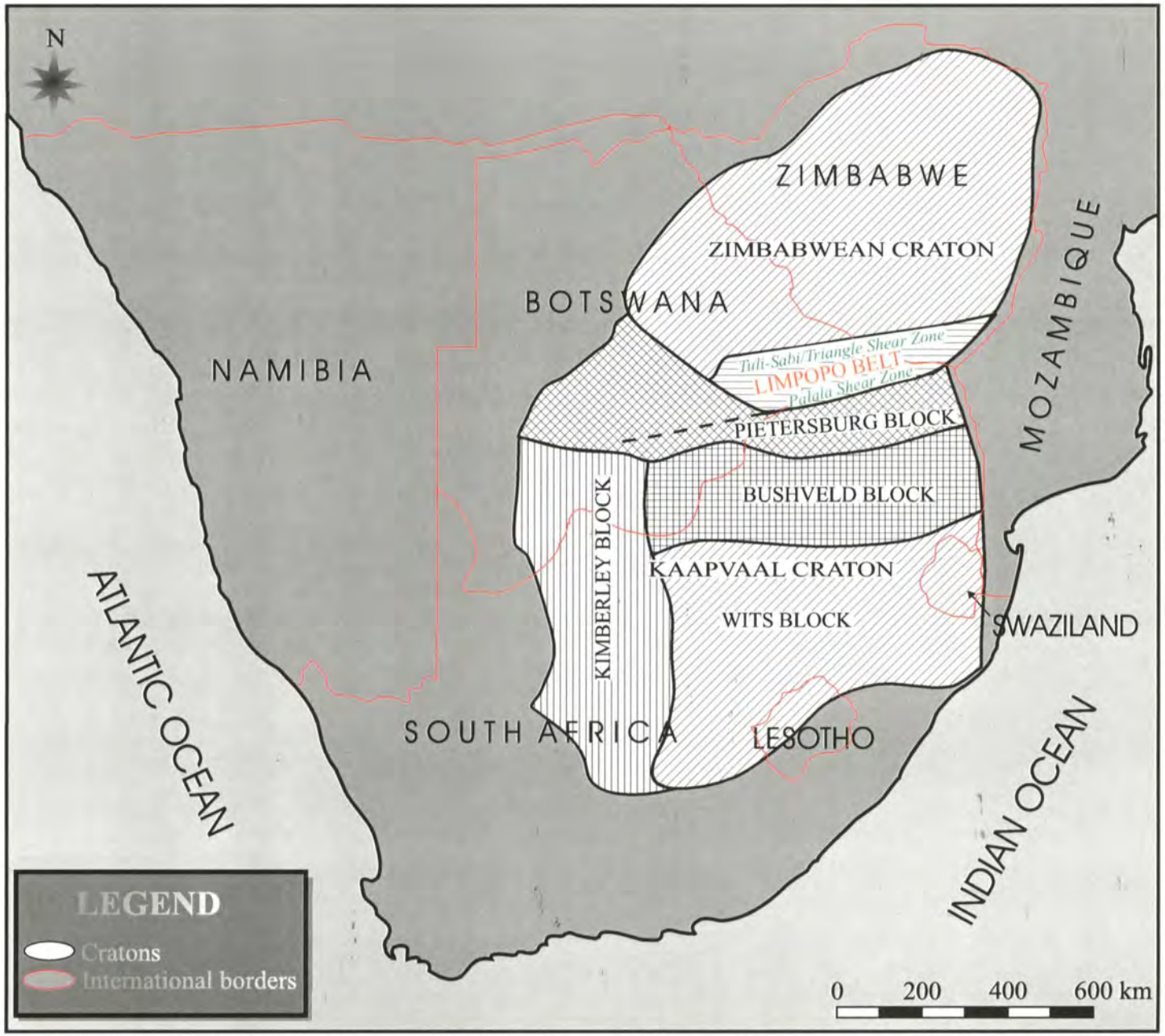

Fig. 4. Tectonic situation of the Limpopo Belt and the shear zones within it (modified after Skinner et al., 1992 and Brandl, 1992).

(Cox, 1970). This fault was active, possibly semi-continuously, during the Karoo sedimentation (Cox, 1970). There is evidence that there are some pre-Karoo faults (i.e. Tshipise Fault) which were reactivated during the deposition of the Karoo Supergroup (Cox, 1970). Generally, however, the literature contains virtually no evidence on the timing of syn-Karoo faulting.

The Karoo outcrops of the Tuli and Nuanetsi basins are separated from the Tshipise Basin by the highly deformed Messina Block (Fig. 5D), which may have acted as a consistently positive area during the accumulation of the Karoo strata (Cox, 1970). Therefore, the correlation of the Karoo outcrops of the northern (Tuli and Nuanetsi) basins and Tshipise Basin is difficult (Cox et al., 1965:123).

A number of major faults are post-Karoo in age (Cox, 1970). The great majority of the faults affecting the Karoo formations are of normal type, and no reverse faulting has been noted, thus there is no evidence for compressive tectonic phases in the Phanerozoic history of this area (Cox, 1970).

2.1.3.1. Tshipise Basin

The ENE-WSW orientated Tshipise Basin is situated south of the Limpopo River and north of the Soutpansberg in South Africa. The northeastern continuation of the Tshipise Basin is the Bubye Coalfield in Zimbabwe (Cox et al., 1965).

The northward-dipping Karoo rocks of the basin crop out in several long, narrow strips, striking approximately E-W and everywhere terminating against faults towards north (van Eeden et al., 1955; Cox et al., 1965). Intense post-Karoo and post-Waterberg faults with the same ENE trend occur, most of which are downthrown to the south (Cox et al., 1965). The normal faults which displace the Karoo rocks have a cumulative throw of a few hundred metres (Cox, 1970).

The palynological data show that complicated syndepositional tectonism occured during the accumulation of the Karoo Supergroup in this basin (MacRae, 1988). According to MacRae (1988), there were major periods of either non-deposition or sediment removal at different levels in the basin. Van Vuuren (1978 in MacRae, 1988) recorded that formation of narrow grabens or half-grabens occurred during the deposition of the Dwyka Group beds.

2.1.3.2. Nuanetsi Basin

The Nuanetsi Basin is situated NE of the Limpopo River in SE Zimbabwe. It is an approximately 100 km-long, E-W trending structure with pronounced eastward axial plunge (Cox, 1970). Tectonic data about the basin are limited, and the only available information is that the depository has been modified by numerous ESE and N-trending faults (Cox et al., 1965; Broderick, 1979).

2.1.3.3. Tuli Basin

As mentioned in the Introduction, the transfrontier Tuli Basin lies at the triple junction of the Zimbabwean, Botswanan and South African borders.

The northern boundary of the Karoo rocks is marked by a major, ENE trending fault which is continuous for about 100 km. The structure, which is parallel to the axis of the basin, can be traced through the Archaean basement (Cox et al., 1965; Vail et al., 1969). It is believed that this fault zone was active in post-Karoo times, because the Karoo rocks are virtually absent on the northern side of the fault (Smith, 1984). The only reported Karoo Supergroup outcrop north of this major fault seems to be a small outlier of basalts which mostly overlie basement rocks, but in some places they cover aeolian sandstones of the Tsheung Formation (Smith, 1984:186). This suggest that the fault was activated both prior to and after the deposition of the aeolian sandstones.

The fractures of the basin appear to cut the Karoo strata over considerable distances, thus giving the whole structure a graben character (Vail et al., 1969). The faults form part of the late- to post-Karoo fracture system, which broadly follows the axis of the Limpopo Belt (Vail et al., 1969; Thompson, 1975). This complex, bifurcating fracture system may have operated until quite recent times (Watkeys, 1979). Mapping and drilling has not disclosed any evidence of major faulting in the Karoo-age strata south of Limpopo River (Ortlepp, 1986).

According to Watkeys (1979:9), the Karoo rocks of the Tuli Basin "were flexurally downwarped along an ESE axis and subsequently downfaulted by a combination of NE- and ENE-trending fractures. This was accompanied by a minor faulting along a NW trend and later on along a N to NNE trend."

2.1.4. Tectonic model for the Limpopo area and Lebombo 'Monocline'

According to the tectonic model for the region suggested by Watkeys & Sweeney (1988), it may be considered in terms of two right-lateral strike slip systems (Fig. 5). The first one formed an ENE trending divergent wrench zone and was responsible for the generation of the Tuli Basin, the Nuanetsi Basin and Tshipise Basin (Watkeys & Sweeney, 1988). The tectonic displacement occurred along pre-existing ENE and NE trending faults during the sedimentation of the lower part of the Karoo Supergroup (Watkeys & Sweeney, 1988). In this interpretation, the Tuli Basin is a pull-apart rhombochasm due to a releasing overstep, while the Nuanetsi Basin is the result of a releasing fault junction (Fig. 5A). The extension in this divergent system was mainly accommodated by a major SSE dipping Archean thrust plane, with a central horst (i.e. Messina Block) above the flat portion of this fault (Watkeys & Sweeney, 1988) (Fig. 5D). The system involving half-grabens can be traced over the Tshipise Basin as well (Watkeys & Sweeney, 1988) (Fig. 5D). The rotative offlap of the "lower Karoo" strata took place during basin extension, while the rotative onlap of the "upper Karoo" strata occurred during a period of convergent right-lateral strike-slip movement (Watkeys & Sweeney, 1988) (Fig. 5D). This event was followed by asthenospheric upwelling and intracratonic rifting which initiated the Lebombo 'Monocline' (Watkeys & Sweeney, 1988) (Fig. 5B). The second right-lateral strike slip system was generated in the mid-Jurassic and is related to the southward migration of Madagascar (Watkeys & Sweeney, 1988). The fault system parallel to the Lebombo 'Monocline' resulted in a gentle WNW flexure across the Tuli Basin and the Nuanetsi Basin, and in the monoclinal folding of the southern part of the Lebombo 'Monocline' (Watkeys & Sweeney, 1988) (Fig. 5C).

Apart from the above model, a half-graben structure has also been suggested for the Tuli Basin, based on two arguments: the presence of the major fault in the north and the general gentle (<5°) northward dips of the Karoo Supergroup beds (Smith, 1984).

In the light of the observations and interpretations made during this study, a different tectonic development is proposed for the Tuli Basin (see discussion in Chapter 6.2.).

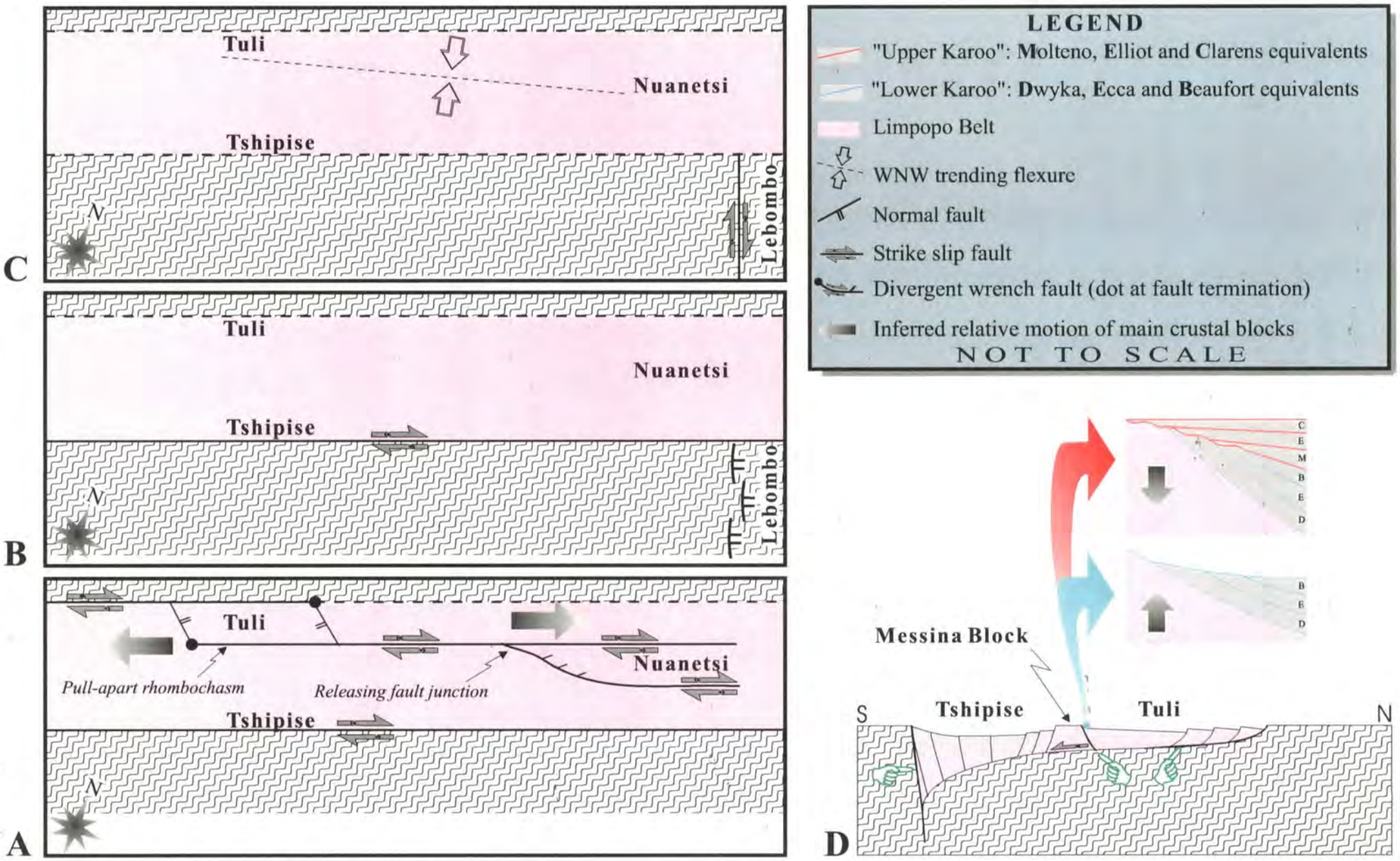

Fig. 5. Simplified model outlining the tectonic evolution of the Limpopo area and Lebombo 'Monocline' (modified after Watkeys & Sweeney, 1988). See text for explanation. The three tectonic lines marked in **D** are also recognised in the geophysical crustal profiles across the Limpopo Belt (Roering et al., 1992).

2.2. Stratigraphic setting

2.2.1. Stratigraphy of the Karoo Supergroup in southern Africa

Although the southern African basins containing Karoo Supergroup strata appear in different tectonic settings (Ch.2.1), the overall climatic overprinting resulted in similar vertical lithological profiles (Groenewald et al., 1991; Johnson et al., 1996).

Most commonly, the Karoo successions begin with diamictites and other glaciogenic rock types (Johnson et al., 1996). In the units following, the red colours are absent and coal seams are common, whereas in the higher strata both red and greenish mudrocks are present. According to Johnson et al. (1996), this reflects a change from generally reducing to generally oxidizing conditions as a result of increasingly subaerial deposition and a semi arid climate (Johnson et al., 1996). The aeolian sandstones in the uppermost part of the sedimentary succession reflect an arid climate. In most of the basins the sedimentation was terminated by intensive igneous activity (Johnson et al., 1996).

As the various basin fill sequences are comparable, the following brief presentation of the Karoo rocks is based on the stratigraphically most complete fill which occurs in the main Karoo Basin of South Africa. The principal stratigraphic dissimilarity between the main Karoo Basin and the other basins occurs in the lower part of the successions: the early formations of the Karoo Supergroup in the main Karoo Basin reflect marine/deltaic rather then lacustrine/fluvial conditions (Johnson et al., 1996). Other dissimilarities are due to the fact that some of these basins were subject to tectonism, leading to considerable thickness variation and intra-stratal unconformities (Johnson et al., 1996).

The Karoo Supergroup consists of five groups: Dwyka, Ecca, Beaufort, Stormberg and Drakensberg (Catuneanu et al., 1998). The Stormberg Group is a commonly used term for the uppermost strata of the Karoo Supergroup, but it is not approved by SACS (South African Committee of Stratigraphy) (Johnson, 1994).

The Dwyka Group comprises a basal unit of tillite, diamictite and associated sedimentary rocks (Johnson, 1994). The group reaches its maximum thickness of 750 m in the southwestern main

Karoo Basin (Groenewald et al., 1991; Catuneanu et al., 1998). Due to lithological differences, the name Elandsvlei Formation was suggested for the southern facies units consisting of glaciomarine sedimentary rocks, and the term Mbizane Formation for the northern facies units of glaciofluvial and lacustrine deposits (Johnson et al., 1997). The group was generated during Late Carboniferous to Early Permian times (Visser, 1987; Cole, 1992 in Catuneanu et al., 1998).

The Early Permian- Late Permian Ecca Group consists of two contrasting units. Alluvial strata are present only in the north-eastern part of the basin (part of Vryheid Formation) (Cadle et al., 1993); in the rest of the basin, the group was formed in a marine environment (Johnson, 1994). The lower part of the group was laid down in deep marine environment characterized by submarine fan depositories. These rocks consist of greywacke, siltstones and mudstones forming Bouma sequences (Visser & Lock, 1978 in Catuneanu et al., 1998) characteristic of turbidites. The upper part of the group is identified by the increasing dominance of arenaceous deposits formed in open shelf and then in shoreface and deltaic environments (Johnson, 1976; Kingsley, 1985).

The Beaufort Group of the Karoo Supergroup diachronously overlies the Ecca Group and was deposited on vast alluvial plain (Johnson, 1976; Groenewald et al., 1991; Catuneanu et al., 1998) from the Late Permian to early Mid Triassic times.

The Beaufort Group is overlain by the Late Triassic- early Middle Jurassic Stormberg Group. Starting with a coarse sediment wedge of a braided river system (Molteno Formation), this group also comprises laterally continuous floodplain mudstones and associated fluvial sandstones (Elliot Formation), as well as aeolian sandstones (Clarens Formation)(Johnson, 1976; Groenewald et al., 1991; Cairncross et al., 1995; Catuneanu et al., 1998).

The Drakensberg Group embodies mainly basaltic and some andesitic volcanic rocks (Johnson, 1994). The igneous rocks of the group are radiometrically dated at 183 ± 1 Ma, with a range between 184 to 179 Ma (Duncan et al., 1997). Outside of the main Karoo Basin, the Drakensberg Group is correlated with the Lebombo Group, which also consists chiefly of basic and acid volcanic rocks (Johnson et al., 1996).

2.2.2. Stratigraphy of the Karoo Supergroup in the Lebombo-Save-Limpopo area

The outcrop areas of the Lebombo-Save-Limpopo area embody various Karoo-aged successions. Fossils are scarce and correlation by palaeontological means is extremely tenuous (Stagman, 1978; Broderick, 1979). Similarly, there is no absolute certainty that lithologically-similar successions are synchronous (Stagman, 1978). Because of the diversities, local informal/formal nomenclature has been established for the different areas (Broderick, 1979). In general, the outcrop areas comprise more than 90% basalt, with thin rims of sedimentary rocks, commonly in fault contact with the gneisses and granulites of the Archaean basement. Attempts of stratigraphic correlations across the area have been made by the above authors without finality.

2.2.3. Lebombo 'Monocline'

The Lebombo 'Monocline' stretches between the Limpopo River and Empangeni (W of Richard's Bay, KwaZulu-Natal) for about 900 km in N-S direction (Bristow, 1982) (Fig.1). The rocks of the Karoo Supergroup overlie the eastern edge of the Pietersburg, Bushveld and Wits Blocks (Kaapvaal Craton).

The sedimentary groups of the Karoo Supergroup are well developed in the southern part of the Lebombo 'Monocline' (from Empangeni to S-Swaziland) (Haughton, 1969). This zone correlates well with the NE main Karoo Basin (Johnson, 1994). In the central part of the outcrop area, the sedimentary rocks are very thin (6-18 m) (Bristow, 1982). The *Dwyka Group* was only described from the southern part of the area and from S-Swaziland (Haughton, 1969). The glacial beds mainly occur as tillites and varved clays (Haughton, 1969). The *Ecca Group* is prominent in the south, but progressively wedges out towards the north (Haughton, 1969; Bristow, 1982). The coal-bearing strata are commonly missing from the northern-central part of the area (Bristow, 1982). The micaceous shales and sandy-shales of the *Beaufort Group* are represented only in the southern part of the outcrop area (south of Komatipoort, next to Mozambican border) (Bristow, 1982). The circa 570 m thick, fine-grained sedimentary rocks of the Emakwezini Formation are generally regarded as part of the lower Beaufort Group (Johnson, 1994).

The middle and upper part of the *Stormberg Group* is present along the whole western margin of the Lebombo 'Monocline' (Haughton, 1969; Bristow, 1982; Johnson, 1994). The red mudstones (Nyoka Formation) correlate with the Elliot Formation, and the off-white sandstones are assigned to the Clarens Formation of the main Karoo Basin (Johnson, 1994). In the southern part of the Lebombo 'Monocline', there are some coarse-grained sandstones interbedded with mudstones (Ntabene Formation) which may be equivalent to the Molteno Formation (Visser, 1984; Johnson, 1994). In NE Swaziland, the Molteno Formation consists of two, erosively-based upward-fining sequences comprising conglomerates, sandstones, siltstones and mudstones of a braided fluvial system. Palaeo-flow directions were from NW to SE (Turner & Minter, 1985). The diamond-bearing Elliot Formation also forms upward-fining cyclothems that developed in a low-sinuosity, ephemeral fluvial network, draining from WNW to ESE (Turner & Minter, 1985). The sedimentary beds of the Stormberg Group are 4000 m thick in the southern area (NE Kwazulu-Natal), but they show only ~170 m in thickness in NE Swaziland (Turner & Minter, 1985) and 60 m in the rest of the Lebombo 'Monocline'(Visser, 1984).

The Karoo volcanic rocks of the area belong to the Lebombo Group, which consists of the basic Letaba Basalt Formation (max. ~6500 m) and the acidic volcanic rocks of the Jozini Formation (max. ~5000 m) (Bristow, 1982; Johnson, 1994).

2.2.4. Save Basin

The north-trending Save Basin is situated NE of the Limpopo River in Zimbabwe. It lies on the south-eastern edge of the Zimbabwean Craton (Duguid, 1975) and contains the following groups of the Karoo Supergroup.

The Precambrian Umkondo Group is overlain by the glacial sedimentary rocks of the *Dwyka Group,* which comprise an alternating sequence of limno-glacial varved shale with dropstones, tillite and fluvioglacial outwash deposits (Duguid, 1975). The thickness of the group is between 40 and 70 m. Near the western end of the basin, there are several gently undulating, glacially striated pavements on the Umkondo Group. The glacial striations trend in a SSW direction (Duguid, 1975; Stagman, 1978).

The basin also contains deposits of the *Ecca Group* (Duguid, 1975). Coal seams dominate the southern part of the basin, whereas pebbly, arkosic, very coarse sandstones and mudstones occur in the northern part (Duguid, 1975). According to Duguid (1975), the south to north facies change can be explained by synsedimentary faulting.

There is limited and uncertain information regarding the deposition of strata during *Beaufort Group* times. According to Stagman (1978), the group is represented in a fairly condensed succession. In contrast, the *Stormberg Group* is more than 600 m thick (Stagman, 1978). It commences with the Molteno Formation-equivalent Escarpment Grit, which rests on a regional unconformity surface. The succeeding 530 m thick Red Beds (Elliot) are dominated by siltstone, followed by the Clarens Formation-equivalent aeolian Forest (Cave) Sandstones (Stagman, 1978).

The youngest formations of the Karoo Supergroup in this area are the igneous rocks of the *Lebombo Group*, comprising dolerite dykes, sills, basalts and acid ring complexes (Duguid, 1975).

2.2.5. Limpopo area

2.2.5.1. Tshipise Basin

The glacial beds of the *Dwyka Group* are represented by poorly sorted conglomerates (diamictites of the Tshidzi Formation) which attain a thickness of 20 m (van der Berg, 1980; Brandl, 1981; Johnson, 1994). The Formation consists of fragments of all shapes and sizes in an argillaceous to sandy matrix (McCourt & Brandl, 1980). In the type locality, the mostly subangular, poorly sorted fragments, up to 2 m in size, are set in a light-coloured, sandy or quartzitic, in some places argillaceous matrix (McCourt & Brandl, 1980). In other outcrops, the boulders, cobbles and pebbles are subrounded or rounded, and the matrix is more grey in colour. In places, with increasing sand content, the matrix may show cross-bedding (McCourt & Brandl, 1980). According to van der Berg (1980), the fluvioglacial sediments were transported in an E-ENE to W-WSW direction.

The *Ecca Group* is represented by three formations, the Madzaringwe Formation in the lower

part of the group, the Mikambeni Formation in the middle, and the Fripp Sandstone Formation in the upper part (McCourt & Brandl, 1980; Brandl, 1981; Johnson, 1994). However, according to van der Berg (1980), the Mikambeni Formation represents the Beaufort Group, and the Fripp Sandstone Formation correlates with the lower part of the Molteno Formation (lower Stormberg Group).

The Madzaringwe Formation consists of alternating sandstone, siltstone and shale, the latter containing coal seams. The feldspathic sandstone is usually micaceous and cross-bedded (McCourt & Brandl, 1980; Brandl, 1981). The maximum thickness of the Formation is 200 m, and the best developed coal seam is 3.9 m thick (McCourt & Brandl, 1980; Brandl, 1981). The shaly-coaly part of the Formation accumulated in a swamp environment, whereas the sandy part probably represents crevasse-splay deposits (Brandl, 1981). van Eeden (1955:53) reported that *Gangamopteris clyclopteroides, Glossopteris browniana,* and *Equisetales* were collected from the coal-zone.

The Mikambeni Formation consists of a series of massive, dark and pale mudstones and black shales; with a few thin, laminated sandstone layers toward the base (McCourt & Brandl, 1980; Brandl, 1981). There also are some scattered, very thin coal layers, and the total thickness of the Formation is about 120-150 m (McCourt & Brandl, 1980; Brandl, 1981). According to van Vuuren (1978 in MacRae, 1988), these beds were formed in a shallow-water lacustrine environment.

The Fripp Sandstone Formation consists of white feldspathic, trough-cross bedded, fine-grained and very coarse-grained sandstones with thin pebble horizons and occasional thin silty bands (Brandl, 1981). There are a few conglomerates containing pebbles of vein quartz, pegmatite, sandstone, quartzite and volcanic rocks (Brandl, 1981). Palaeo-current measurements (1325 readings) indicate transport directions from SE towards NW (van der Berg, 1980). The maximum thickness of the Formation is 110 m (Brandl, 1981). The sedimentary rocks are interpreted as point-bar sequences of meandering rivers and channel-bar deposits of braided rivers (van Vuuren, 1978 in MacRae, 1988; van der Berg, 1980).

The *Beaufort Group* is represented by the Solitude Formation (McCourt & Brandl, 1980; Brandl, 1981; Johnson, 1994). Consisting of alternating purple mudstones, grey shales and a few carbonaceous shales; the Formation is 170 m (max.) thick (Brandl, 1981). Cream and greenish grey, approximately 5 m thick siltstone intercalations are also present (McCourt & Brandl, 1980). The sedimentary rocks were formed as overbank deposits of a meandering system (van Vuuren, 1978 in MacRae, 1988). The lower part of these beds were named Joan Formation by van der Berg (1980) and correlated with the upper part of the Molteno Formation (Stormberg Group). In van der Berg's classification, the upper part of the original Solitude Formation of McCourt & Brandl (1980) has been correlated with the Elliot Formation of the main Karoo Basin. In van der Berg's (1980:97) table of correlation, the beds of the Beaufort Group are matched with the uppermost part of the Lilliput Formation and the erosional discordance that marks the base of the overlying Stormberg Group.

The *Stormberg Group* is reported to be present by several authors (McCourt & Brandl ,1980; van der Berg, 1980; de Jager 1983, in MacRae, 1988; Johnson, 1994), but the proposed correlation schemes of the local formations with the main Karoo Basin are rather complex and uncertain. According to van der Berg (1980) and de Jager (1983, in MacRae, 1988), the Klopperfontein (Sandstone) Formation corresponds to the Elliot Formation of the main Karoo Basin. McCourt & Brandl (1980) and Johnson (1994) do not mention correlatable stratigraphic units for the Formation. The Klopperfontein (Sandstone) Formation consists of medium-grained, white, feldspathic sandstones which are less quartzitic than those in the Fripp Sandstone Formation. Cross-bedding, pebble stringers and thin layers of green shale may occur. The maximum thickness of the Formation is 20 m in the Kruger National Park. It was probably deposited in a braided stream system (Brandl, 1981).

The middle part of the Stormberg Group is represented by the Bosbokpoort Formation. According to van Eeden (1955) and de Jager (1983, in MacRae, 1988), the Bosbokpoort Formation is correlated with the Elliot Formation (Red Beds) of the main Karoo Basin. The Bosbokpoort Formation is dominantly characterized by red mudstones and very fine sandstones, both with calcareous concentrations (McCourt & Brandl, 1980; Brandl, 1981). The maximum thickness of the Formation is about 100 m in the Tshipise area, but thins gradually towards the

east (McCourt & Brandl, 1980; Brandl, 1981). The fine-grained material represents a flood basin environment under hot and arid conditions (Brandl, 1981). According to van der Berg (1980: 114), the palaeo-current measurements (14 readings) indicate transport direction from SSE to NNW. Fossils of *Euskelosaurus, Melanorosaurus readi* and *Gryponyx* were collected on the Pelham Ranch (van Eeden, 1955: 53). *Melanorosaurus readi* is considered a synonym of *Euskelosaurus browni* (Cooper, 1980: 12; Kitching & Raath, 1984: 122), whereas *Gryponyx* is now thought to be synonym of *Massospondylus sp.*(Cooper, 1982: 92; Kitching & Raath, 1984: 122).

The upper part of the Stormberg Group is represented by the Clarens Formation. The Formation mainly comprises very fine- to fine-grained, white and cream-coloured sandstones (McCourt & Brandl, 1980; Brandl, 1981). The grains are well-sorted and only a small percentage of them are feldspar (Söhnge et al., 1948; van Eeden et al., 1955). Palaeo-current measurements (36 readings) on the locally developed large scale cross-bedding (van Eeden et al., 1955; Brandl, 1981) indicate a NNE transportation direction (van der Berg, 1980; van Eeden et al., 1955). The cumulative thickness of the Formation is about 300 m (McCourt & Brandl, 1980; Brandl, 1981). The sandstones accumulated as wind-blown dunes under arid climate conditions (Brandl, 1981).

The volcanic rocks of the Lebombo Group are represented by basalts (Letaba Formation) and rhyolites (Jozini Formation) (Brandl, 1981).

2.2.5.2. Nuanetsi Basin

The Nuanetsi Basin contains a thin sequence of clastic Karoo strata and an estimated 7000 m of volcanic rocks (Cox, 1970). Cut by innumerable small joints and faults, the thin Karoo sedimentary rocks are exposed only along the margins of the Nuanetsi Basin (Cox et al., 1965).

The presence of glacial beds (Dwyka Group) has not been confirmed from the western part of the Nuanetsi Basin (Broderick, 1979). The only suspected occurrence is a khaki-coloured, indurated rock, composed of 60-70% sericitic clay with randomly scattered, angular and fractured quartz grains, up to 5 mm across (Broderick, 1979).

The Bumburudza Formation (40 m max.) represents the *Ecca Group* (Broderick, 1979). The beds are largely argillaceous, and most of them are dark-grey or brown mudstones, flint clays, shales, thin sandstones and rare carbonaceous shales (Broderick, 1979). The Formation is well represented in the northern and western outcrops of the area, but it is extremely poorly exposed in the SW (Broderick, 1979). There are some fossiliferous shales with *Glossopteris browniana* and *Verterbraia indica* specimens (Broderick, 1979).

The *Beaufort Group* has not been reported from the area.

The lower part of the *Stormberg Group* is represented by the Bubye Grit Formation. The Formation is correlated with the Escarpment Grit (Broderick, 1979), which in turn correlates with the Molteno Formation of the main Karoo Basin (Watkeys, 1979). Coarse-grained, white, gritty (=very coarse) sandstones are common in the northern and western parts of the basin, where they attain 20-60 m in thickness (Broderick, 1979). Very coarse, ferruginous greywackes dominate the southern margin of the area (Broderick, 1979).

The middle part of the Stormberg Group is called Red Beds Formation and correlates with the Elliot Formation of the main Karoo Basin. The hard, massive, brick-red mudstone of the Formation is composed of a fine-grained, homogeneous mass of quartz and iron-stained clay. There are also some khaki-coloured siltstones with faint bedding and a few scattered angular quartz grains (Broderick, 1979). The Formation has only one significant outcrop in the southern part of the basin (Broderick, 1979).

The upper part of the Stormberg Group is the Forest Sandstone Formation, equivalent to the Clarens Formation of the main Karoo. The pale pink to off-white sandstones are mostly hard, fine-grained and massive (Broderick, 1979). Where metamorphosed, they contain numerous, sometimes perfectly spherical quartz-grain rich concretions up to 6 cm in diameter (Broderick, 1979). According to borehole data, the Formation is not thicker than 60 metres, but in outcrops it is the dominant member of the Karoo Supergroup (Broderick, 1979).

The volcanic rocks of the Lebombo Group attain an enormous thickness of circa 7 km (Broderick, 1979). In the eastern part of the basin, the upper part of the volcanic sequence

consists of several hundred metres of rhyolites with small amounts of interbedded basalt (Cox et al., 1965).

2.2.5.3. Tuli Basin

Due to the geographical position of the Tuli Basin (i.e. transfrontier), the following review of the Karoo Supergroup is based on descriptions given for the South African, Zimbabwean and Botswanan parts of the basin. Stratigraphic and palaeontological records are not sufficiently well known to allow an accurate correlation across the basin. Thus the correlation given in the following paragraphs should be considered as only tentative (Table 1).

South of the Limpopo River, the present-day preservation area of the Karoo rocks is limited by post-Karoo erosion events (Ortlepp, 1986). In this part of the basin, the pre-Karoo surface and the Karoo strata dip gently at a shallow angle of up to 2° to the north and north-west (Ortlepp, 1986). West of the Limpopo River, in Botswana, the dips are also less than 5° to N (Smith, 1984). Due to this shallow (<5°), northerly dip of the deposits, the facing direction of the Karoo Supergroup is from S to N.

In the *South African* part of the basin, the lowermost Karoo sedimentary rocks are described as infrequent, structureless, coarse diamictites (Chidley, 1985). These deposits are composed of angular blocks of basement rocks (up to 80 cm) floating in finer grained (mudstone and shale) material (Chidley, 1985). The maximum thickness of this rarely exposed formation is about 2 m (Chidley, 1985). Lithologically, this unit may correspond to the Tshidzi Formation described by McCourt & Brandl (1980) in the Tshipise Basin (Ch. 2.2.5.1.).

In *Zimbabwe*, the Karoo Supergroup commences with a similar, very rare sequence. The polymict conglo-breccias consist of unsorted, angular to subangular fragments of the basement rocks (up to 30 cm in diameter), which are randomly scattered in an argillaceous matrix (Thompson, 1975). The deposits, which are believed to be glacial in origin, attain approximately 9 m in thickness (Thomson, 1975:10: boreholes T3&T4). They have been incorporated into the Basal Beds together with other structureless, ill-sorted conglomerates, sandstones and a few mudstones (25 m) (Thompson, 1975).

Table 1. Summary of the lithostratigraphic nomenclature and correlation of the Karoo Supergroup strata of the transfrontier Tuli Basin and main Karoo Basin. Thick lines represent known unconformities.

<table>
<tr><th colspan="2">main Karoo Basin
(Johnson, 1994)</th><th colspan="2">Tuli Basin
(South African part)
(Chidley, 1985)</th><th>Tuli Basin
(Zimbabwean part)
(Thompson, 1975)</th><th colspan="2">Tuli Basin
(Botswanan part)
(Smith, 1984)</th></tr>
<tr><td rowspan="4">"Stormberg Group"</td><td>Clarens Formation</td><td rowspan="3">Clarens Formation</td><td>Tshipise Sandstone Member</td><td>"Forest Sandstone"</td><td rowspan="4">Lebung Group</td><td>Tsheung Sandstone Formation</td></tr>
<tr><td>Elliot Formation</td><td>Red Rock Member</td><td>Red Beds</td><td>Thune Formation</td></tr>
<tr><td rowspan="2">Molteno Formation</td><td colspan="2">Bosbokpoort Formation</td><td rowspan="2">"Escarpment Grit"</td><td rowspan="2">Korebo Formation</td></tr>
<tr><td colspan="2">Klopperfontein Formation</td></tr>
<tr><td colspan="2">Beaufort Group</td><td colspan="2">Solitude Formation</td><td></td><td colspan="2"></td></tr>
<tr><td colspan="2" rowspan="3">Ecca Group</td><td colspan="2">Fripp Formation</td><td></td><td colspan="2"></td></tr>
<tr><td rowspan="3">Basal Beds</td><td>Mikambeni Formation</td><td rowspan="2">Fulton's Drift Mudstones</td><td>Seswe Formation</td></tr>
<tr><td>Madzaringwe Formation</td><td>Mofdiahogolo Formation</td></tr>
<tr><td>Dwyka Group</td><td>diamictites</td><td>Basal Beds (undifferentiated)</td><td>??</td></tr>
</table>

In *Botswana*, no Karoo deposits are referred to the Dwyka Group, although there is a basal mudstone formation characterized by scattered boulders of quartzo-feldspathic gneisses (Smith, 1994).

The **Ecca Group** is represented all over the basin. In *South Africa*, at the base of the first formation of the Ecca Group (Madzaringwe Formation), a 5-6 m thick gritty-conglomeratic unit is described (Chidley, 1985). This unit is overlain by 12-15 m of grey, laminated and

homogeneous shale with plant debris which develops into a 20 m thick coal zone with 6 continuous seams (Chidley, 1985). According to Ortlepp (1986), the coal bearing series (10 m) are located at depths of less than 50 m along the southern margin, but attain a depth of over 300 m near the Limpopo River. The two major (1.6 m and 1.2 m thick) flat lying coal seams are overlain by mudstones and minor sandstones (Ortlepp, 1986). Even the economically important coal is interbedded with mudstones (Ortlepp, 1986). Relatively continuous coal seams are confined to the central and NE part of the study area; elsewhere, if present, they are thin and discontinuous (Ortlepp, 1986; Falcon, 1989). The upper Madzaringwe Formation is represented by cross-bedded, feldspathic quartz sandstones (10 m) (Chidley, 1985).

The following 15 m of grey, in places carbonaceous shales and siltstones are beds of the Mikambeni Formation containing *Glossopteris sp.* leaf impressions and occasional coal seamlets (Chidley, 1985). The overlying 5-10 m thick, well-sorted, medium- to coarse-grained, planar cross-bedded, arkosic, pinkish sandstones with abundant conglomerate intercalations are interpreted as fluvial channel deposits. According to Chidley (1985), this unit is the Fripp Formation, and it underlies the Beaufort Group's Solitude Formation. Söhnge et al. (1948) described some pale to reddish-brown sandstones, very coarse sandstones and conglomerates from the eastern part of the basin, which seem to form part of the Fripp Formation. The dip of these beds is of the order of 10 degrees to the W or SW (Söhnge et al., 1948).

In *Zimbabwe*, the Ecca Group is named Fulton's Drift Mudstones (Thompson, 1975). The 50 to over 120 m thick formation consists of grey to black argillaceous shales, mudstones, coal seams and a few discontinuous, lenticular white to light grey sandstones and pebble beds, especially near the base (Thompson, 1975; Watkeys, 1979; Cooper, 1980). The Formation appears to have been deposited in a shallow, stagnant basin under tundra conditions (Watkeys, 1979). The following fossils have been found: *Equisitites sp. (Clamites approximata?); Taeniopteris; Glossopteris indica; G. browniana; Phyllotheca sp.* (Watkeys, 1979).

In *Botswana*, the Ecca Group is represented by two formations (Smith, 1984). The 5.5 m thick basal mudstones of the Mofdiahogolo Formation are characterized by grey-brown mudstones with sandstone bands and scattered quartz grains. At the base of the unit, there is a fining-upward argillaceous sandstone unit. A "slump breccia" succession has also been described (Smith,

1984:188&191). The Formation is interpreted as deposits of post-glacial meltwater lakes which, from time to time, were entered by muddy debris flows ("slump breccia") (Smith, 1984).

The succeeding Seswe Formation comprises two members (Smith, 1984). The lower carbonaceous mudstone member with thin coals and sandstones is about 40 m thick. Some of the sandstone intercalations attain 1 to 2 m in thickness (Smith, 1984). The upper member is a 20 m thick succession of non-carbonaceous, variegated grey to khaki-coloured mudstones (Smith, 1984).

The clastic facies equivalents of the Formation occur only in the southern outcrops of the Botswanan part of the basin, where 12 m thick feldspathic sandstones with conglomerate lenses lie directly either on the basement or on the mudstones of the Mofidahogolo Formations (Smith, 1984). In places, these coarse beds are interbedded with mudstones containing indistinct plant fragments (Smith, 1984). Ironstones, nodular limestones, calcareous very coarse sandstones and mottled marls are also reported (Smith, 1984). The fine-grained facies is interpreted as lacustrine deposits, whereas the coarse-grained units were braided river sediments (Smith, 1984).

The **Beaufort Group** is only described from the *South African* part of the basin. It is represented by white, pink, green and khaki siltstones and very fine-grained sandstones, with grey mudstones of the Solitude Formation (Chidley, 1985). The maximum thickness of the planar and ripple-cross laminated formation is 25 m (Chidley, 1985). These beds were formed in the distal floodplain setting of a mature meandering system (Chidley, 1985).

The sedimentary rocks of the **Stormberg Group** are described from all three countries. In *South Africa*, the 10-12 m thick, trough cross-bedded, coarse sandstones and conglomerates of the Klopperfontein Formation are interpreted as proximal bedload-dominated, braided stream deposits (Chidley, 1985). The Formation is correlated with the Molteno Formation of the main Karoo Basin (Chidley, 1985).

In *Zimbabwe*, the 1-15 m thick, reddish Escarpment Grit consists of coarse- to very coarse-grained, white to pale grey or pink, upward-fining sandstones (Cooper, 1980). Commonly, layers

of small, angular to subangular pebbles of similar composition to those in the Dwyka Formation, lend an indistinct bedding to the otherwise unlaminated sandstone (Thompson, 1975). According to Watkeys (1979), the Formation has little or no unconformity with the underlying unit and probably a conformable contact with the overlying rocks. The Formation, also named the Gushu Formation (Cooper, 1980), is correlated with the Molteno equivalent Escarpment Grit of the Zambezi Karoo Basin (Thompson, 1975). Due to the lack of fossil remains, this correlation is based only on lithological grounds (Thompson, 1975).

In *Botswana*, the mudstones, siltstones and fine-grained sandstones of the Korebo Formation are 33 m thick in boreholes (Smith, 1984). These brown, finer-grained beds, described from boreholes, seem to be the facies equivalents of the coarser-grained, sometimes conglomeratic sandy units which are seen mostly in outcrops (Smith, 1984). The conglomerate pebbles consist of calcareous nodules, clay pellets and some quartz clasts (Smith, 19984). The depositional environment is thought to have been a playa-lake system with ephemeral floods under semi-arid climate conditions (Smith, 1984). The Formation is correlated with the Escarpment Grit and the Red Beds (lower part) from the Zimbabwean side of the basin (Smith, 1984).

The overlying succession is developed basinwide and it is dominated by *red* fine-grained strata. In *South Africa*, the 60 m thick brick-red, purplish mudstones and siltstones with calcareous nodules and concretions of the Bosbokpoort Formation are interpreted as floodplain deposits under semi-arid climate conditions (Chidley, 1985). Small bone fragments have been noted from beds containing poorly sorted calcareous conglomerates (Chidley, 1985).

The Red Rock Member of the Clarens Formation is about 60 m thick and consists of argillaceous, very fine- to fine-grained pinkish to red sandstones (Chidley, 1985). Irregular calcareous nodules and concretions are abundant and occasionally shell fragments have been found (Chidley, 1985). Reptilian remains have been described from the mudstones of the Formation (Chidley, 1985). The beds are believed to have formed under arid conditions in a distal overbank floodplain setting. The calcareous concretionary zone implies a period of non-deposition, while the conglomerates suggest the presence of wadi-type ephemeral stream systems (Chidley, 1985).

In *Zimbabwe*, there is a 300 m thick succession of red to purple mudstones, fine-grained sandstones and marls, frequently with scattered, very fine-grained red sandstone pebbles and calcareous nodules (Thompson, 1975; Cooper, 1980). There are occasional pebbly, very coarse sandstones and partly silicified limestones (Watkeys, 1979). Bedding is rare in the sandstones (Watkeys, 1979). Reptilian fossils have been found in this widespread formation, and the remains of an *Euskelosaurus* cf. *browni* allow a direct correlation with the lower part of the Elliot Formation in the main Karoo Basin (Cooper, 1980).

In *Botswana*, the Thune Formation is a transitional unit between the more argillaceous Korebo and the typical dune-bedded Tsheung Sandstone Formation (Smith, 1984). The Thune Formation (~65 m) contains fine-grained sandstones and siltstones with some cross-bedded sandstone intercalations (Smith, 1984). Due to its small fining-upward cyclothems, the Formation was interpreted to be fluvial in origin (Smith, 1984).

In *South Africa,* the 5-140 m thick Tshipise Sandstone Member of the Clarens Formation is very fine- to fine-grained, mostly cream-coloured, and displays large scale aeolian dune bedding with palaeo-currents from west to east (Chidley, 1985). The lithological characteristics of the Formation and the fossil remains of a *Massospondylus carinatus* (Cooper, 1980) allow direct correlation with the Clarens Formation of the main Karoo Basin.

In *Zimbabwe*, there is an 80-100 m thick formation consisting of pinkish-white to brownish, fine- to medium-grained, well-sorted sandstones, calcareous in their lower part and cross-bedded higher up (Thompson, 1975; Cooper, 1980). According to Thompson (1975), the lower part seems to contain sub-aqueous deposits. Because basalts were extruded on the undulating surface of the dunes, the sandstones are metamorphosed down to a depth of 2 metres (Watkeys, 1979). The cross-bedded sandstones are interpreted as aeolian dunes laid down under arid climate conditions (Watkeys, 1979).

In *Botswana*, the Tsheung Sandstone Formation is generally uniform, massive, fine- to medium-grained, well-sorted and occasionally trough cross-bedded (Smith, 1984). Thickness data are not available.

The Karoo basalts of the area are grouped in two formations of the **Lebombo Group**: the olivine-rich Letaba Basalt Formation and the Sabie River Basalt Formation, characterized by an augite-plagioclase phenocryst assemblage (Cox & Bristow, 1984). The latter name (Sabie River Basalt Formation) is not formally approved by the SACS (Johnson, 1994). According to Veevers et al. (1994), the alkaline complex of the Limpopo valley region is 186±3 Ma years old. The Letaba Basalt Formation crops out in the southern central part of the basin and it is overstepped by the Sabie River Basalt Formation, which in turn dominates the central and northern part of the basin (Cox & Bristow, 1984). In the central northern part of basin, in the Mazunga area (*Zimbabwe*), the total thickness of the extrusive rocks overlying the sedimentary beds is a few hundred metres (Cox, 1970; Cox & Bristow, 1984). In the lower part of the volcanic sequence, mainly along the southern contact, lenses of sandstone occur interbedded with the igneous rocks (Cox, 1970; Thompson, 1975; Smith, 1984; Chidley, 1985). This unit is called Mbaka Beds in *Zimbabwe* (Thompson, 1975) and Madikama Beds in *Botswana* (Smith, 1984). A 1.5 m thick, pollen and shell debris-bearing, fresh water limestone sequence was reported to interbed with the basalt (Aldis, 1982 in Smith, 1984; Aldis et al., 1984). In the *South African* part of the basin, the Clarens Formation is cut by numerous fractures frequently filled by dolerites and porphyritic andesites, which are usually 15 to 30 m thick, nearly vertical bodies (Vail et al., 1969; Chidley, 1985; Ortlepp, 1986). In the eastern part of the area, the sandstones alongside the dolerite dykes have locally developed an "amygdaloidal" texture due to the formation of concretions of brown calcite in the more argillaceous parts of the sandstone (Söhnge et al., 1948).

3. Methods of study

3.1. Lithofacies analysis

The sedimentary processes operating within depositional sedimentary environments generate particular structures/textures in the sediments. These observable characteristics preserved in the rock record define different sedimentary lithofacies. Therefore, a reasonable knowledge of the sedimentary processes and careful analysis of the preserved sedimentary features may provide a satisfactory explanation of the genesis of the sediments or sedimentary rocks.

3.1.1. The method

Facies analysis of sedimentary units means, first of all, very detailed observation and description of all physical and biological structures recorded in sedimentary rocks. For example, in the case of siliciclastic sedimentary rocks, it is essential to study the type, size, sorting, roundness, sphericity, orientation and grading of the grains; the quality, type and size of the matrix; the grain/matrix ratio; the fossil content of the beds (both body fossils and traces); the thickness and the lateral extent of the strata; the bedform types; the shape and length of the erosional surfaces; the synsedimentary deformation structures, and so on.

The next stage in the facies analysis is to interpret the depositional setting of the objectively described and classified facies.

Over the years, sedimentologists have worked out methods not only to define the sedimentary processes responsible for particular features, but also to determine the depositional environments of the facies association. During this phase of the analysis, the relationship between the different facies is examined.

This kind of palaeo-environmental reconstruction is based on facies models, which are "general summaries of particular depositional systems, involving many individual examples from recent sediments and ancient rocks" (Walker, 1992:2).

Facies models are idealizations, because they combine the features which may occur within a

sedimentary system. Facies models should not be rigidly followed in any sedimentological research, because this can lead to unnecessary confusion due to the high variability of sedimentary processes (Miall, 1996). Facies models only provide the framework to allow comparison between different case studies, and they are guidelines for future observation (Miall, 1996).

Among the existing sedimentary facies models, the more complete ones are those made for fluvial environments. A river consists of several depositional units, such as major and minor channels, sediment bars, sand flats, crevasse splay deposits, etc. (Miall, 1996). Their development is usually predictable and the sediments that comprise them have distinctive internal and external features (Miall, 1996). These features are termed "architectural elements". They are built up by various lithofacies assemblages and show some constant characteristics throughout rivers of all kinds (Miall, 1985, 1987). Although to some extent every river and every ancient fluvial unit is unique, the architectural elements are common to all rivers (Miall, 1987), and all alluvial formations are composed of varying proportions of these elements (Miall, 1992).

3.1.2. Fluvial lithofacies types

The simplest differentiation of fluvial deposits is based on their grain size (gravel, sand, silt and clay). Miall (1978) introduced a more sophisticated classification in order to simplify and codify the study of complex fluvial assemblages. His approach requires the bed-by-bed description of all sedimentary particulars, summarized in lithofacies codes. The capital letter of each code denotes the dominant grain size (G-gravel; S-sand; F - fines), while the lower case(s) identifies the internal sedimentary features and other particulars of the respective lithofacies. As Table 2 shows, there are seven major gravel lithofacies, seven sand lithofacies and six fine-grained lithofacies. The brief interpretation of each lithofacies is given in the fourth column of the table.

Facies code and symbol	Facies	Sedimentary structures	Interpretation
Gmm	Matrix-supported, massive gravel	Weak grading	Plastic debris flow (high-strength, viscous)
Gmg	Matrix-supported gravel	Inverse to normal grading	Pseudoplastic debris flow (low-strength, viscous)
Gci	Clast-supported gravel	Inverse grading	Clast-rich debris flow or pseudoplastic debris flow
Gcm	Clast-supported massive gravel	—	Pseudoplastic debris flow (inertial bedload, turbulent flow)
Gh	Clast-supported, crudely bedded gravel	Horizontal bedding, imbrication	Longitudinal bedforms, lag deposits, sieve deposits)
Gt	Gravel, stratified	Trough cross-beds	Minor channel fills
Gp	Gravel, stratified	Planar cross-beds	Transverse bedforms, deltaic growths from older bar remnants
St	Sand, fine to very coarse, may be pebbly	Solitary or grouped trough cross-beds	Sinuous-crested and linguoid (3-D dunes)
Sp	Sand, fine to very coarse, may be pebbly	Solitary or grouped planar cross-beds	Transverse and linguoid bedforms (2-D dunes)
Sr	Sand, very fine to coarse	Ripple cross-lamination	Ripples (lower flow regime)
Sh	Sand, very fine to coarse, may be pebbly	Horizontal lamination, parting or streaming lineation	Plane-bed flow (critical flow)
Sl	Sand, very fine to coarse, may be pebbly	Low-angle (<15°) cross-beds	Scour fills, humpback or washed-out dunes, antidunes
Ss	Sand, fine to very coarse, may be pebbly	Broad, shallow scours	Scour fill
Sm	Sand, fine to coarse	Massive or faint lamination	Sediment-gravity flow deposits
Fl	Sand, silt, mud	Fine lamination, very small ripples	Overbank, abandoned channel, or waning flood deposits
Fsm	Silt, mud	Massive	Backswamp or abandoned channel deposits
Fm	Mud, silt	Massive, desiccation cracks	Overbank, abandoned channel, or drape deposits
Fr	Mud, silt	Massive, roots, bioturbation	Root bed, incipient soil
C	Coal, carbonaceous mud	Plant, mud films	Vegetated swamp deposits
P	Paleosol, carbonate (calcite, siderite)	Pedogenic features: nodules, filaments	Soil with chemical precipitation

Table 2. Fluvial lithofacies (modified after Miall, 1996).

3.1.3. Architectural elements and bounding surfaces

As mentioned earlier, lithofacies assemblages with distinctive external geometries and orientation build up the architectural elements (Table 3). In a fluvial environment, the architectural elements are standard features that may combine and interbed with each other in an almost infinitely variable way (Miall, 1985). Architectural element analysis is a method of describing sedimentary structures which frees sedimentologists from rigid adherence to any "standard" fluvial model (Miall, 1985).

The architectural elements are laterally variable, three-dimensional depositional units bounded by various types and scales of surfaces (Fig. 6) (Miall, 1985). The bounding surfaces can rarely be used without an appropriate adaption in a particular case (Collinson, 1996). The terminology applicable to the bounding surfaces is presented in Table 4.

The first step in the sedimentological *modus operandi* is to define the small-scale lithofacies units, then to combine these closely related units into the larger scale facies associations which are the architectural elements. Once the three-dimensional building blocks have been identified, the local fluvial style can be reconstructed. Miall (1985,1996) proposed 16 fluvial styles based on this method. The differences among the end members of these 16 models are significant, but the similarities should also be noticed (Miall, 1996). For example, among the three major types of gravel-bed braided rivers there are only slight differences in terms of lithofacies and vertical profiles (Miall, 1996).

Although the well-known classification of alluvial channels by geometric characteristics (as braided, meandering, anastomosing and straight) is applicable to most of the fluvial styles described by Miall (1985,1996), there are some transitional styles as well. For instance, the 'gravel-bed wandering' or the 'low sinuosity river with alternate bars' are typical mixed-style fluvial systems.

Element code and symbol		Principal facies assemblage	Geometry and relationship
CH Channels	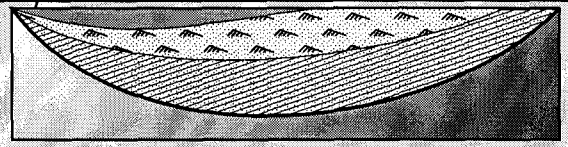	Any combination	Finger, lens or sheet: concave-up erosional base; scale and shape highly variable; internal concave-up 3rd-order erosion surfaces common
GB Gravel bars and bedforms	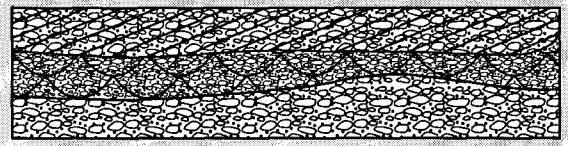	Gh, Gp, Gt	Lens, blanket; usually tabular bodies; commonly interbedded with SB
SB Sandy bedforms	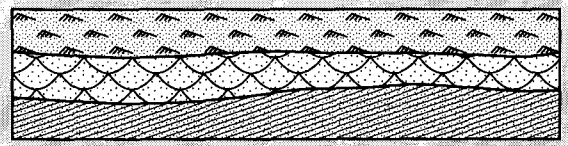	St, Sp, Sh, Sl, Sr, Ss	Lens, sheet, blanket, wedge, occurs as channel fills, crevasse splays, minor bars
DA Downstream-accretion macroform	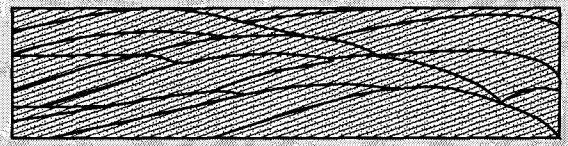	St, Sp, Sh, Sl, Sr, Ss	Lens resting on flat or channeled base, with convex-up 3rd-order internal erosion surfaces and upper 4th-order bounding surface
LA Lateral-accretion macroform	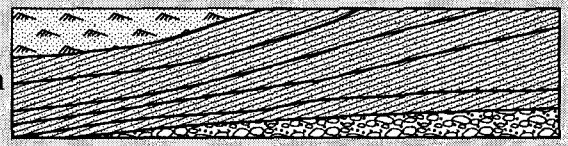	St, Sp, Sh, Sl, Sr, Ss, less commonly Gm, Gt, Gp	Wedge, sheet, lobe; characterized by internal lateral-accretion 3rd-order surfaces
HO Scour hollows	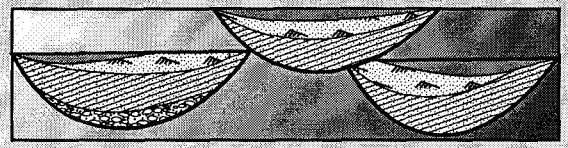	Gh, Gt, St, Sl	Scoop-shaped hollow with asymmetric fill
SG Sediment gravity flows	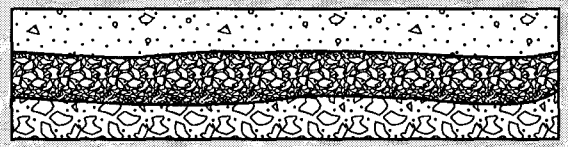	Gmm, Gmg, Gci, Gcm, Sm	Lobe, sheet; typically interbedded with GB
LS Laminated sand sheet	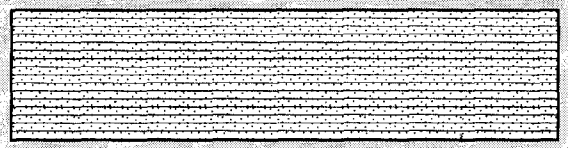	Sh, Sl; minor Sp, Sr	Sheet, blanket
FF Overbank fines	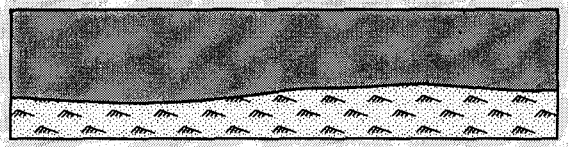	Fm, Fl	Thin to thick blankets; commonly interbedded with SB; may fill abandoned channels

Table 3. Architectural elements in fluvial deposits (modified after Miall, 1985; Miall, 1996). Not to scale.

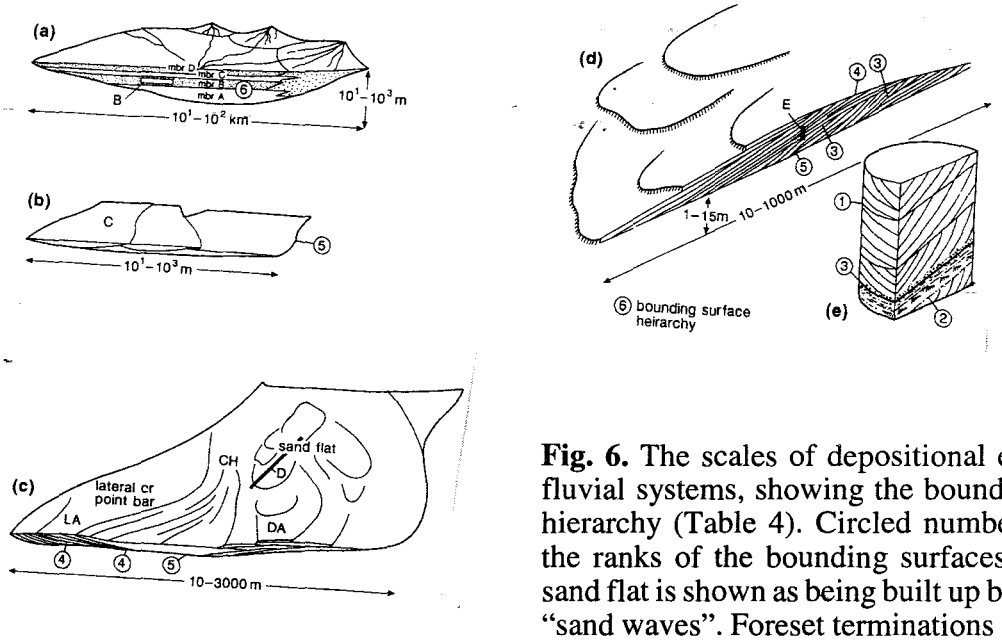

Fig. 6. The scales of depositional elements in fluvial systems, showing the bounding-surface hierarchy (Table 4). Circled numbers indicate the ranks of the bounding surfaces. In **C**, the sand flat is shown as being built up by migrating "sand waves". Foreset terminations of these are shown at the top of diagram, but the internal cross-bedding that results has been omitted for clarity (after Miall, 1988 in Miall, 1992).

Table 4. Bounding surfaces (after Miall,1988 in Collinson, 1996).

Order	Nature of the surface	Significance and process
1st	Separates individual cross-bedded sets	Migration of dune bedforms under steady flow conditions.
2nd	Separates cosets of contrasting set type	Change in hydrodynamic conditions through time, related to short-term unsteady flow or local non-uniformity.
3rd	Inclined erosion surfaces within coset or group of cosets	Medium-term change in hydrodynamic conditions related to stage fluctuation or major shifting of flow across/around a bar form.
4th	Separates units with discrete accretionary integrity	Shift of bar/subchannel pattern related to inherent channel-floor instability or to reorganization during a major flood.
5th	Surfaces with a marked shift in grain size, bedform scale, etc. Laterally extensive with relief	Shifting and erosion of a channel floor. Isolated channels with relief reflect channel switching. Extensive surfaces within larger sandbodies record channel migration.
6th	Separates major channel sandbodies from contrasting facies (fine-grained sediment or contrasting channel facies)	Major change in fluvial regime. May record shifts of base level or climatic or tectonic changes.

3.1.4. Applied lithofacies, architectural elements and bounding surfaces

A wide range of sedimentological features has been recognized from the Karoo Supergroup in the Tuli Basin (SA). Based on Miall's (1978 & 1996) lithofacies classification method, a total of 25 lithofacies types are described in this study (Table 5). In addition to Miall's lithofacies, the following lithofacies are newly introduced: Sd, Sc, Sb, Sf, Fp, Fs, Fb and S. Their more detailed description and interpretation is given in chapters: 4.2.4.1. & 5.4. (Sd); 4.2.3.2.3. & 5.3.2.3.(Sc); 4.2.1.3. & 5.1.3. (Sb, Sf, Fp, Fs, Fb) and 4.8. & 5.8. (S).

The lithofacies were grouped in 7 of the 9 architectural elements given in Table 3. The lateral-accretion macroform (LA) and the 'scour hollow' element (HO) were not observed in the field. The recognized architectural elements and bounding surfaces are marked on the outcrop drawing presented in Ch. 4.2. Due to their high frequency, the 1st order and most of the 2nd and 3rd order bounding surfaces were omitted from the figures. The other bounding surfaces are indicated by the number of their rank (i.e. 6th = 6th order bounding surface).

3.2. Palaeo-current analyses

Palaeo-current measurements are one of the most powerful tools in palaeo-drainage reconstructions, providing information on the direction of the local or regional palaeo-slope, depositional environment, direction of the sediment supply, geometry and trend of lithologic units (Miall, 1984).

A great number of palaeo-current features was noticed during the field work. The most valuable and abundant data resulted from the measurements carried out on the foresets of planar cross-bedded sandstones. In the Upper Unit, the trough cross-bedded strata yielded a significant palaeo-current record. Apart from these, information concerning palaeo-current flow patterns was obtained from current ripple and channel axes orientations, as well as from parting lineations. Only the large-scale cross-bedded strata were measured in the Clarens Formation.

The 704 measurements include readings obtained from medium- and large-scale planar cross-stratified beds. The ripples and small-scale cross-beddings were excluded from the

Facies code and symbol	Facies	Sedimentary structures	Interpretation
Gmm 	Matrix-supported, massive gravel	Weak grading	Plastic debris flow (high-strength, viscous)
Gcm 	Clast-supported massive gravel	—	Pseudoplastic debris flow (inertial bedload, turbulent flow)
Gh 	Clast-supported, crudely bedded gravel	Horizontal bedding, imbrication	Longitudinal bedforms, lag deposits, sieve deposits)
Gt 	Gravel, stratified	Trough cross-beds	Minor channel fills
Gp 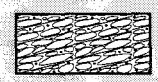	Gravel, stratified	Planar cross-beds	Transverse bedforms, deltaic growths from older bar remnants
Sd 	Sand, very fine to medium	Very large scale planar or trough cross-beds	Aeolian sand dunes
St 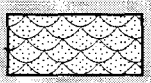	Sand, fine to very coarse, may be pebbly	Solitary or grouped trough cross-beds	Sinuous-crested and linguoid (3-D dunes)
Sp 	Sand, fine to very coarse, may be pebbly	Solitary or grouped planar cross-beds	Transverse and linguoid bedforms (2-D dunes)
Sr 	Sand, very fine to coarse	Ripple cross-lamination	Ripples (lower flow regime)
Sh 	Sand, very fine to coarse, may be pebbly	Horizontal lamination, parting or streaming lineation	Plane-bed flow (critical flow) or low velocity wind-blown depos.
Sl 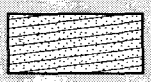	Sand, very fine to coarse, may be pebbly	Low-angle (<15°) cross-beds	Scour fills, humpback or washed-out dunes, antidunes
Ss 	Sand, fine to very coarse, may be pebbly	Broad, shallow scours	Scour fill
Sm 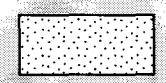	Sand, fine to coarse	Massive or faint lamination	Sediment-gravity flow deposits/ very high deposition rates
Sc 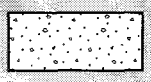	Sand, silt rich in intra-formational clasts	Massive	Sediment-gravity flow deposits
Sb 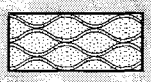	Sand, fine to very coarse, may be pebbly	Ball-and-pillow structure, may show internal lamination	Soft sediment deformation
Sf 	Sand, fine to coarse with mud	Massive, may be laminated	Sediment-gravity flow deposits
Fl 	Sand, silt, mud	Fine lamination, very small ripples	Overbank, abandoned channel, or waning flood deposits
Fsm 	Silt, mud	Massive	Backswamp or abandoned channel deposits
Fp 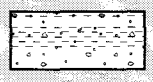	Mud with pebbles	Vague laminated mud with floating, isolated clasts	Lacustine deposits with dropstones
Fs 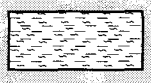	Mud with sand, fine to coarse	Massive, may be laminated	Sediment-gravity flow deposits
Fb 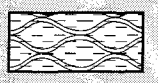	Mud, silt	Ball-and-pillow structure, may show internal lamination	Soft sediment deformation
Fm 	Mud, silt	Massive, desiccation cracks	Overbank, abandoned channel, or drape deposits
C 	Coal, carbonaceous mud	Plant, mud films	Vegetated swamp deposits
P 	Paleosol	Pedogenic features: nodules, filaments	Soil with chemical precipitation
S 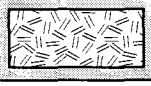	Silcrete	Pedogenic features: nodules, filaments	Chemical precipitation in soil

Table 5. The applied lithofacies (modified after Miall, 1996).

measurements, because these are believed not to be representative of regional trends, having been generated by less unimodal, local currents (Miall, 1984).

Most of the measurements were carried out in the western, south-western and northern central parts of the area where better quality outcrops were more available. Data was unobtainable from the badly or non-exposed southern central part of the area. The NE and NW parts of the study area also provided some good records, but to a lesser extent than the SW area.

3.3. Grain size/shape analysis

Grain size/shape studies can be applied either to differentiate between deposits of various origins or between deposits of similar origin but of different ages, in order to establish the lithostratigraphic relationship between them (Bridgland, 1986).

Limitations associated with grain size/shape studies, such as the necessity of a large number of readings and non-reproducible factors (e.g. inherited roundness) meant that such studies largely went out of favour during the 1980s (Miall, 1996). As Friedman & Sanders (1978:59) remark: "The factors responsible for ultimate shape of the particles are too many and too varied to allow us to draw definite conclusions from even the most elaborate studies based on elegant quantification of shape." Nevertheless, textural studies can be powerful when used as a complement to other sedimentological methods, such as palaeocurrent measurements, facies analysis, etc. (Bridgland, 1986).

In this study, the original purpose of clast counting was to analyze the particle size, roundness and sphericity changes across the area. A total of 28 separate clast counts of 100 particles were carried out. The conglomerate sampling localities are shown in Appendix 2: Fig.I. The raw parameters of each particle (short(C)- and long(A)-axes; roundness and sphericity) are presented in Appendix 2 (28x100x4 = 11200 readings). Bearing in mind the purpose of the clast counting and the fact that any change in the shape and size of the particles strongly depends upon the mineralogy of the clast itself, only the quartz and quartzite clasts were included in the statistical tests. The parameters of other clasts (e.g. gneiss) were only noted.

3.3.1. Sampling techniques for statistical tests

The application of statistical tests to sedimentary data has restrictions. One of the requirements is that each sedimentary particle must have an equal chance to form part of the sample; in other words, the sample must be drawn at random (Blatt et al., 1972). The fulfilment of this criterion might present difficulties, for example, in the case of a conglomerate bed. Therefore, in practice, it is assumed that a randomly chosen group of neighbouring specimens (i.e. clasts) will indeed show the properties of the whole population (i.e. bed). It is commonly accepted that in the field only visual justifications are carried out in order to ensure that the collected sample represents the entire tested sedimentary bed (Blatt et al., 1972).

In this study, the samples were selected on the basis of personal judgment in those exposures that provided easy access to sampling points. According to Bridgland (1986), this approach generates a close approximation to a random strategy, provided that opportunities for sampling occur on a random basis.

The clasts were first measured in millimetres, then the parameters were converted into phi (ϕ) scale units, which is a logarithmic grade scale (Table 6). The ϕ scale units represent the negative logarithm of the particle dimension in base 2 ($\phi = -\log_2 d$). The application of the logarithmic ϕ scale is for ease of presentation of the whole grain size range (a grain size change from 1 to 2 mm is a more significant one than a change from 101 to 102 mm).

In this study, the method of estimating roundness was by visual comparison of the particles with standard images of clasts prepared by Powers (1953 in Blatt et al., 1972). In the Powers chart each roundness class image corresponds to one of the six rho (ρ) scale units. In this way the 0.5 ρ value represents a very angular grain, while the 5.5 ρ value shows a well-rounded particle (Blatt et al., 1972). The sphericity of the clasts was also determined with the naked eye, and only low sphericity (1) and high sphericity (2) classes were observed. The adverse effects of subjectivity endemic to this method might be seen to be countered by the fact that all the measurements were taken by the same operator.

Table 6. Grain size scale and mm/ϕ conversion chart for the grain sizes applied in this study (modified after Prothero & Schwab, 1996).

	Clay	Silt	Very fine sand	Fine sand	Medium sand	Coarse sand	Very coarse sand	Granule	Very fine pebble	Fine pebble	Medium pebble	Coarse pebble	Cobble
mm	0.031	0.062	0.125	0.25	0.5	1	2	4	8	16	32	64	
ϕ	5	4	3	2	1	0	-1	-2	-3	-4	-5	-6	

mm	5	10	15	20	25	30	35	40	45	50	55	60	65
ϕ	-2.3	-3.3	-3.9	-4.3	-4.6	-4.9	-5.1	-5.3	-5.5	-5.6	-5.8	-5.9	-6.01

3.3.2. Factors determining the clast size/shape

Clast size and shape are functions of: the shape and size of the fragment prior to transportation; its chemical and mineralogical properties (resistance); the intensity (energy level of the transporting medium) and duration of abrasion; and the post-depositional effects (weathering) (Blatt et al., 1972; Fisher & Bridgland, 1986). In addition, the grain size distribution depends on the hydraulic sorting processes acting during transport and deposition (Blatt et al., 1972).

The initial sizes of the rock fragments are determined by the nature of the source materials and the block-making pattern of intersecting joints, faults, and bedding-surface partings (Blatt et al., 1972; Friedman et al., 1992).

Mechanical abrasion is a significant factor in changing the shape of the particles. As many experiments on particle abrasion have demonstrated, the effectiveness of the mechanical abrasion is chiefly controlled by the geological composition and size of the particle. Ergo, the mechanical abrasion is more pronounced for less durable rocks and for very coarse sand and pebble-size particles (Blatt et al., 1972). Simulating fluvial abrasion, it was concluded that a quartz cube 0.4

mm in diameter can be transformed into a sphere after several million kilometers of transport (Blatt et al., 1972:69). At the same time, weight loss values for fresh feldspar were about twice those for quartz sand. Apart from the composition and initial size of the grain, the rate of abrasion also depends on the grain roundness and the gradient of the streams.

In addition to these factors, the nature of the transportation floor also significantly determines the effects of the mechanical abrasion (Blatt et al., 1972). Although all these shape-modifying factors can be modeled in flumes, there are some others that appear only in natural systems, for example chemical solution during transport, inherited grain shape or partial fracturing of the source rock (Blatt et al., 1972).

In fluvial systems, roundness increases logarithmically with distance (Blatt et al., 1972). On the other hand, in mass movements, particle roundness reflects the source area because of dominant passive flow paths (Owen, 1994). Under such conditions, if the material has been derived from joint fragmented bedrock or rockfall deposits, the resultant deposit will consist of angular clasts (Owen, 1994).

Due to the fact that chemical weathering can easily destroy feldspars, any feldspar preserved in sediments may indicate that the rate of the mechanical detaching of pieces of the source rock exceeded the rate of chemical weathering. Therefore the survival of feldspars yields palaeo-topographic and/or palaeo-climatic information (Friedman et al., 1992). For example, high relief would ensure the exposure of unaltered bedrock and the rapid detachment of rock fragments. Under dry climate conditions chemical decomposition is insignificant, but mechanical disintegration of the fresh bedrock is prominent (Friedman et al., 1992). Similarly, during glacial erosion, significant amounts of feldspar-rich debris can be accumulated by the ripping up and crushing of the feldspar-bearing bedrock (Friedman et al., 1992).

4. Observations

4.1. Basement rocks

The Karoo Supergroup lies unconformably on the Central Zone of the Limpopo Belt containing 2.7 Ga metamorphic rocks assigned to Beit Bridge Complex and Alldays Gneiss (Brandl, 1992; van Reenen et al., 1992). The basement lithologies are light grey leucocratic gneisses and to a lesser extent, quartzites, leucogabbros, granites, migmatites. The predominant basement formation is a highly weathered quartzo-feldspathic gneiss which rarely tends to be mica (muscovite) rich, but which commonly contains thick, massive, *in situ*-fractured quartz veins.

The unconformity between the Archaean Complex and Karoo Supergroup is a gently undulating erosion surface. In outcrop the amplitude of the surface is never greater than circa 4-5 m on 100 m. Fig. 7 shows the morphology of the surface based on data from unevenly spaced coal prospecting boreholes in the basin. This three dimensional view shows that the depth of the basin increases towards the north and the basin floor seems to be rugged. Some of these Archaean irregularities rise through the entire Karoo sequence, forming small, isolated basement exposures or inselbergs (Fig. 3) (Vergenoeg, Somerville, Hilda, Blyklip). In the absence of evidence of any structural control at the site of outcrops, it is inferred that these conspicuously projecting domes and ridges of resistant Archaean lithologies are palaeo-hills. Even if these irregularities formed part of the pre-Karoo landscape, any further information about the morphology of the pre-Karoo surface can hardly be determined from these scanty erosional remnants.

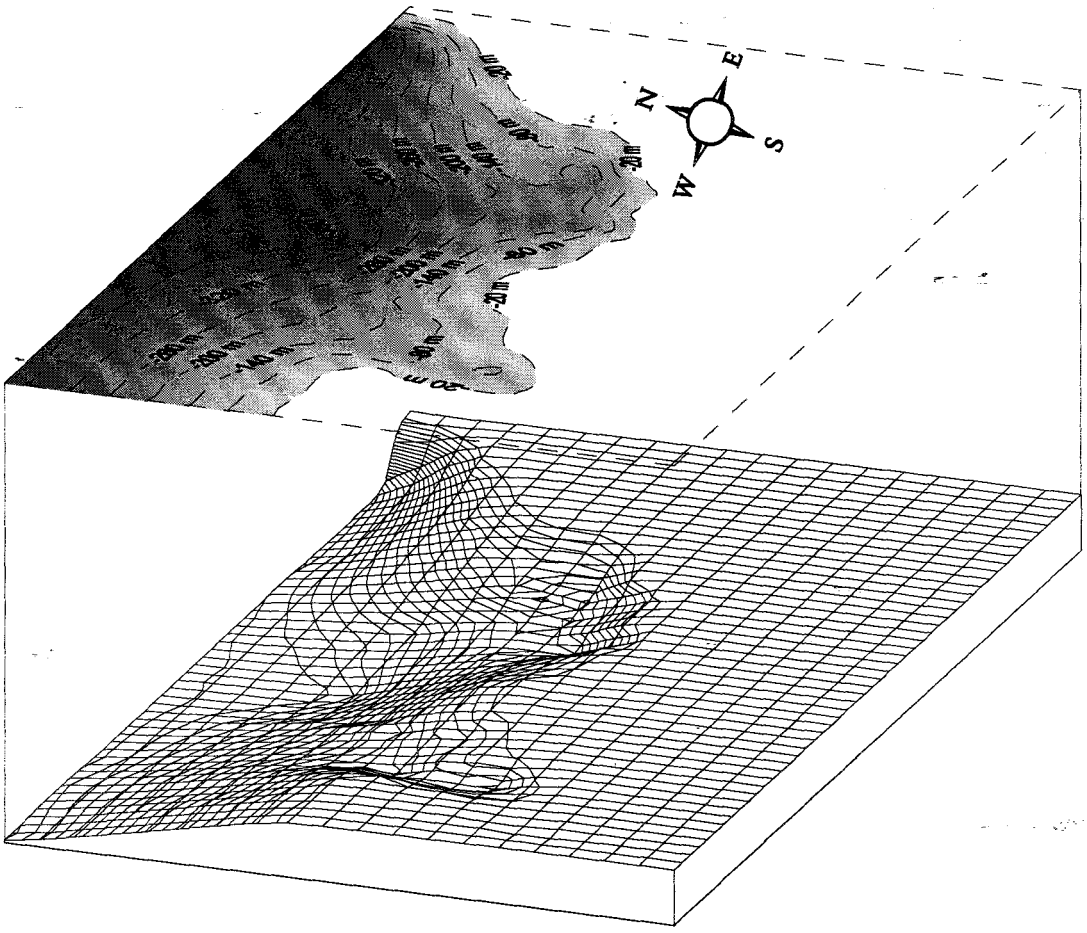

Fig. 7. Relief of the pre-Karoo surface in the southern part of the Tuli Basin.

4.2. Description of the sedimentary units

The available geological information and the lack of proper age indicators allows only a tentative application of the formal stratigraphic nomenclature used for the Karoo Supergroup in the Limpopo area (see Ch. 2.2.5. & 2.2.5.3.). Based on careful observations, the following four lithologically and genetically distinctive lithostratigraphic units are differentiated in the study area, namely the Basal, Middle and Upper Units, and Clarens Formation. These units are not recognised by the SACS, and therefore the use of their names here must be regarded as informal. The spatial distribution of the four units is indicated in Fig. 3. Detailed descriptions of the units are given in separate, subsequent chapters. The potential relation of the Tuli Basin units to the Karoo Supergroup strata in the main Karoo Basin is explained in Ch. 6.1. and Table 21.

Detailed sedimentological investigation of the four units resulted in more than 100 sedimentary logs. Appendix 1: Sections1-7; Fig. I. show the traverses of the sections for the Basal and Middle Units, whereas the vertical profiles logged in the Upper Unit and Clarens Formation are presented in Chapter 4.2.3. and 4.2.4., respectively. The scale is 1:80 for the majority of the vertical profiles, but there are some logs with different scales due to the extreme vertical thickness of the successions (Section 3: ST5, RE1, OV1). In the case of Roly Poly and Stembok, some of the logs reflect only the well-exposed parts of the outcrops. The favourable regional datum horizon should be at the base of the Middle Unit, as indicated in Section 1 and the north-eastern part of Section 3. Considering that the Middle Unit has no exposures in the SW part of the area, the datum horizon needs to be situated either at the base of the first major sandstone unit or at the base of the first fine-grained unit. This configuration applies to Section 2, and to the south-western parts of Section 3 and Section 4. In Section 5, the datum horizon is the base of the second major sandstone unit.

Because the Karoo Supergroup was affected by post-Karoo denudation events, the precise lateral thickness variation of the units could not be determined in the outcrops. Based on the borehole records provided by the Coal Division of Anglo Operations Ltd. (50) and De Beers Consolidated Mines Ltd. (9), thickness and basin floor morphology maps were produced for each stratigraphic unit with the aid of a map-plotting software package. Most of the boreholes were sunk in the southern, eroded edge of the basin. Because only one borehole was drilled (Den-1) in the northern part of the basin, the northward thickening of the stratigraphic units is therefore rather uncertain. All figures that are based on the borehole data should be treated with caution, bearing in mind that firstly, the boreholes were unevenly spaced within the basin; secondly, the boreholes were sunk in the erosional southern part of the basin and, thirdly, the map-plotting computer program performed extrapolation while producing the thickness figures.

4.2.1. Basal Unit

The lowermost unit of the Karoo Supergroup, the Basal Unit, consists of those strata which are situated between the Archaean metamorphic rocks and the Middle Unit (Ch. 4.2.2.). Bounded by two regional unconformities, the unit contains breccias, conglo-breccias, sandstones, mudstones and coal seams. The breccias and conglo-breccias are confined to the lowermost part of the unit. The sandstones containing minor conglomerates and the mudstones form two major fining-upward cyclothems. The main coal seam is developed in the lower cyclothem, and there are only thin coal bands in the upper cyclothem. According to this description, the lowermost part of the unit might correspond to the Tshidzi Formation of McCourt & Brandl (1980) in the Tshipise Basin (Ch. 2.2.5.1.). The lower fining-upward cyclothem seems to fit the lithological characteristics of the Madzaringwe Formation, while the upper one matches the Mikambeni Formation, both reported by Chidley (1985). These correlations are only speculative because the rock descriptions of these deposits in the above-mentioned study are preliminary. The maximum exposed thickness of the unit is 30 m (arenaceous deposits on Stembok, near Stinkwater River dam; argillaceous deposits on Regina, in the Kolompe River bend, next to the border of Patricia farm). The best outcrops can be seen on Roly Poly, Weltevreden, Stembok and Ammondale.

Based on coal prospecting and De Beers borehole data, the average thickness of the Basal Unit is ~56 m, the maximum thickness is ~111 m (Brombreek: Bro-1, isolated Karoo Supergroup outlier is situated between the main outcrops of the Tuli and Tsihipise Basins) (see Appendix 3: Table 1). Table 7 shows that the average thickness of the arenaceous deposits is 8.33 m, and the average thickness of the argillaceous strata is ~36 m. Fig. 8 shows the thickness map of the Basal Unit in the study area (data based on coal prospecting drill hole data only). Conforming to this, the thickness of the Basal Unit gradually increases northwards, as does the average depth of the pre-Karoo surface (Fig. 7). The average thickness of the so-called main coal zone is ~12 metres (Table 7). The actual coal is confined to 6-10 cm (max. ~2 m) thick bands that commonly alternate with other terrigenous rocks (mainly mudstone and siltstone). Fig. 9 shows the coal thickness map that has been compiled from the coal prospecting borehole data. Fig. 10 exhibits the sand:mud:coal ratio in the Basal Unit. According to this, only ~15% of the unit consists of arenaceous deposits, which seems to contradict field observations made, as the majority of the outcrops exhibit sandy deposits. This inconsistency could be explained by taking into

consideration the fact that the coal prospecting drill holes were sunk in order to determine the lateral distribution of the workable coal zone. Therefore, the boreholes are concentrated around the main coal reserves that are interbedded with argillaceous deposits. On the other hand, in outcrops, the fine-grained deposits that tend to weather easily are either vegetated or covered by surficial sandy deposits.

The Basal Unit is composed of three sedimentary facies assemblages:

1. Breccias and conglo-breccias (Gmm, Gcm) with subordinate sandstones (Sh, Sf) and siltstones (Fl);
2. Sandstones (Sp, St, Sh, Sr, Sm, Sb, Sf) with conglomerate and conglo-breccia intercalations (Gh, Gmm);
3. Fine-grained rocks (Fl, Fsm, Fp, Fs, Fb, Fm, C, P).

Table 7. Descriptive statistics of the Basal Unit. Data based on borehole records.

	Basal Unit	Arenaceous	Argillaceous	Coal
Mean	55.51	8.33	35.55	11.63
Standard Error	2.62	1.5	1.82	0.97
Median	51	4.88	33.98	10.03
Mode	NA	0.00	NA	9.24
Standard Deviation	20.15	1153	14.02	7.42
Variance	405.88	132.89	196.51	55.01
Kurtosis	0.46	5.5	-0.19	8.51
Skewness	0.75	2.30	0.13	2.55
Range	96.45	53.00	61.96	44.00
Minimum	14.55	0.00	6.00	0.00
Maximum	111.00	53.00	67.96	44.00
Sum	3275.06	491.53	2097.59	685.94
Count	59	59	59	59
Confidence Level (0.95)	5.14	2.94	3.58	1.89

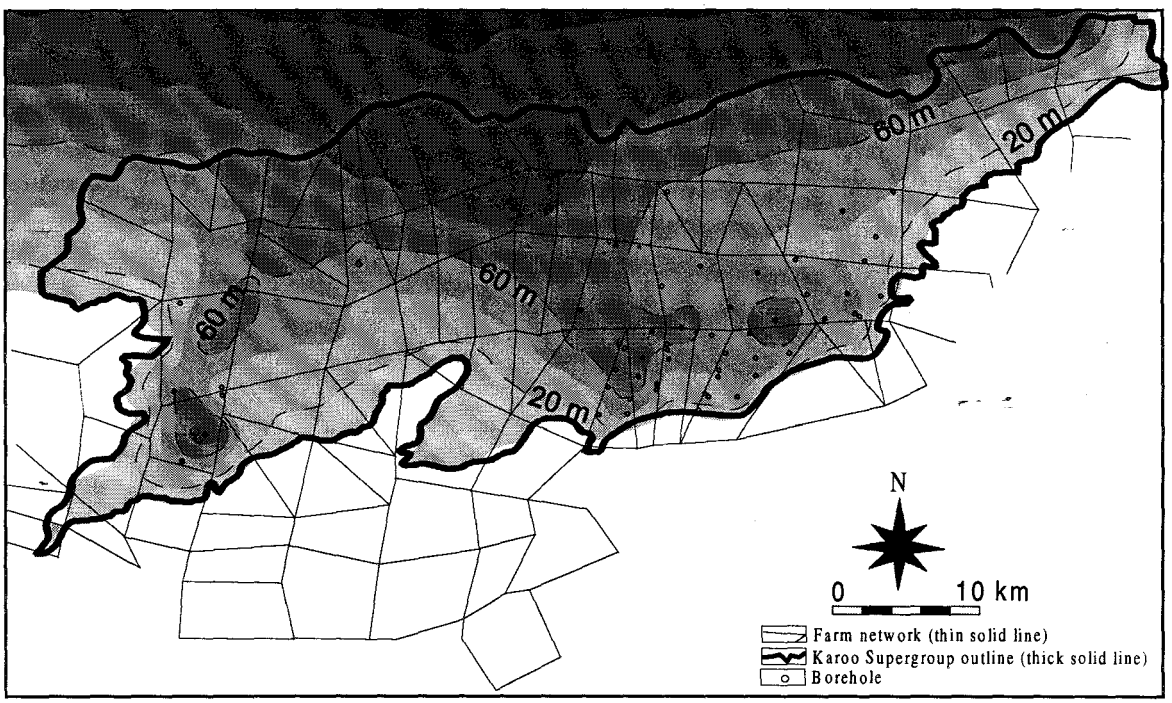

Fig. 8. Thickness map of the Basal Unit for the South African part of the Tuli Basin.

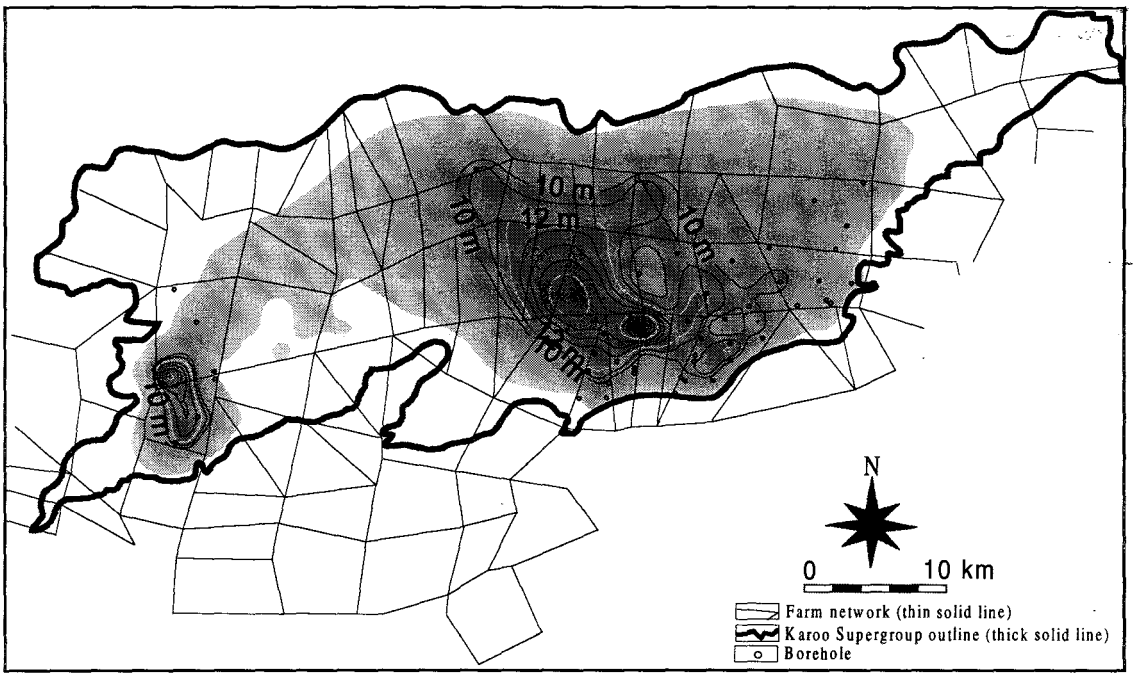

Fig. 9. Thickness map of the coal seam developed in the Basal Unit (data was available only for the South African part of the Tuli Basin).

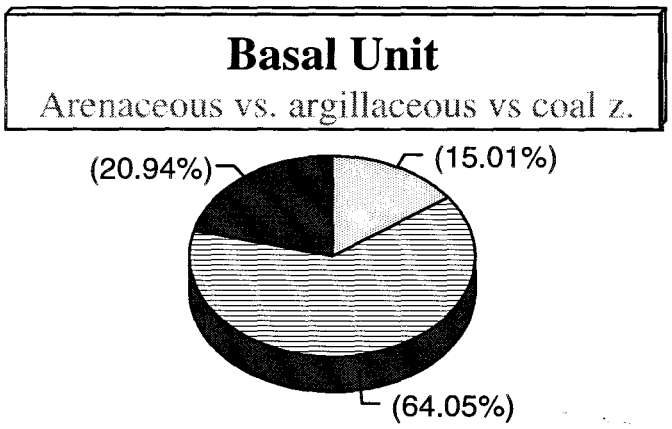

Basal Unit	Cumulative thickness in m	Percentage %
Arenaceous deposits	491.53	15.01
Argillaceous deposits	2097.59	64.05
Coal zone	685.94	20.94
Total	3275.06	100.00

Fig. 10. Sand:mud:coal ratio in the Basal Unit. Data based on borehole records.

4.2.1.1. Breccia and conglo-breccia facies assemblage

Based on textural and clast composition differences, two major lithofacies types are recognized: Gmm and Gcm. The massive Gmm lithofacies exhibits a wide range of grain sizes. The mainly structureless, occasionally slightly laminated, yellowish-brown or greyish, quartz-rich, feldspathic muddy-sandy matrix supports large clasts of angular and subangular vein quartz, quartzite (>90%), weathered gneisses (~8%) and micro-granites (~1%) *(Photo 2,3,4)*. Since more than 90% of the clasts are quartz-rich, this lithofacies type can be categorized as an oligomict parabreccia. The gneiss particles are very angular and form the coarsest grain size (up to 35 cm) *(Photo 5)*. Apart from these anomalously large clasts, the average particle size is about 2-2.5 cm. None of the clasts display striations on their surfaces. This poorly-sorted lithofacies lacks bedding and clast orientation *(Photo 6)*.

The whitish Gcm lithofacies consists predominantly of closely packed, angular to subangular, rarely subrounded vein quartz, quartzite (~95-100%) and rarely weathered gneiss (~0-5%) clasts *(Photo 7)*. The average size of the quartz clasts is 2 cm, but there are boulders of 20-30 cm in diameter as well *(Photo 8)*. The very angular gneiss particles are 8-30 cm in diameter *(Photo 9)*. Neither macroscopic clast surface striation nor clast orientation has been observed. This poorly-sorted lithofacies rarely displays a weak normal grading and a hardly visible bedding defined by the blade shaped clasts *(Photo 10)* (Lauriston, Kilgour). The medium sandstones and muddy siltstones associated with the above-described lithofacies appear either as rare lenses (20 cm x 1-1.5 m) or laterally inconsistent massive beds *(Photo 11)*.

Grain size/shape analysis was carried out on the quartz clasts of the facies assemblage, and the results are indicated in Ch. 4.4. (Figs. 84C, 85C & 86C and Appendix 2 (p.9,9a; 11,11a; 12,12a; 18,18a; 22,22a). The vertical profiles of these sedimentary rocks are shown in Appendix 1: Section 3 (RP1, RP2, AM2, LA2, LI1, KI1) and Section 4 (RP21).

Breccias and conglo-breccias with subordinate sandstones appear to be preserved either in small, isolated "pockets" of the overlying sandstone facies assemblage *(Photo 10 & 12)* or in small outcrops surrounded by basement rocks (Fig. 11). These outcrops are confined strictly to the southernmost margin of the area (Roly Poly, Ammondale, Lauriston, Lizzulea, Kilgour). The maximum outcrop thickness of this facies assemblage is ~2-3 m.

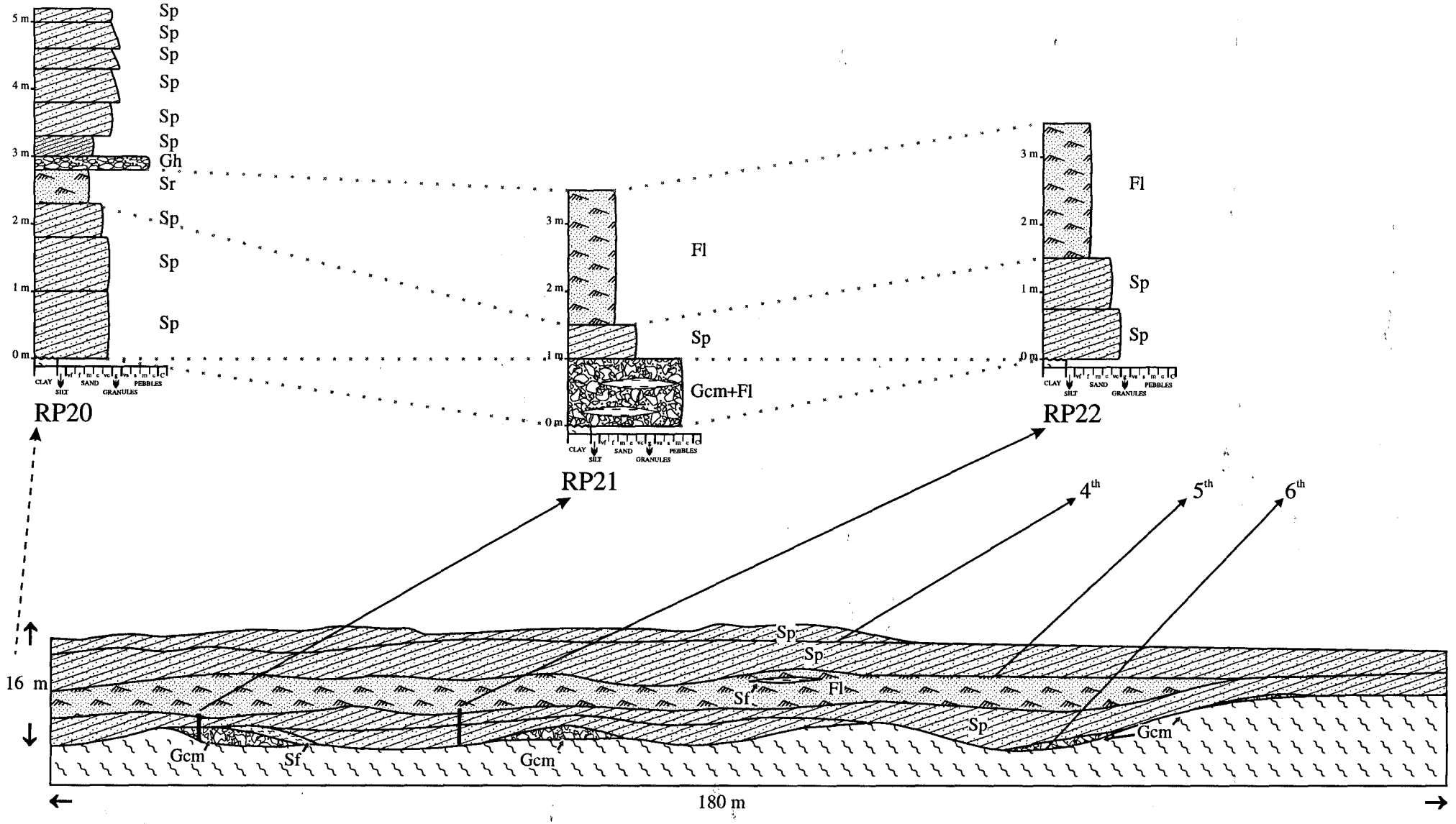

Fig. 11. Lithofacies Gcm is exposed in small pockets of the at the lower contact with the basement rocks. Note the two upward-fining cyclothems. The upper one is not complete (Roly Poly).

4.2.1.2. Sandstone facies assemblage

The coarse to very coarse-grained sandstones of this facies assemblage comprise angular to subangular, medium-sorted, quartz (~98%), weathered feldspar (~2%) and mica (<1%) particles. Macroscopically, there are no rock fragments in these beds. This yellowish-white coloured lithofacies assemblage is only rarely composed of medium- or fine-grained micaceous sandstones and is to date non-fossiliferous.

The most abundant lithofacies in the sandstone lithofacies assemblage is granular to coarse, planar cross-bedded sandstone (Sp) *(Photo 13)*. Planar cosets are mostly 0.3-0.8 m thick, but reach a maximum of 1 m. Other common facies are low-angle cross-stratified (Sl), horizontally stratified (Sh) *(Photo 14)*, massive (Sm) and ripple cross-laminated sandstones (Sr) *(Photos 15, 16)*. Trough cross-stratified sandstones (St) occur only in very few places (see Section 3, ST3).

Upward-fining cyclothems *(Photo 17)* and upward decrease in the scale of sedimentary structures are common (Fig. 12). Due to the frequent erosion and reactivation, the sandy facies has a multistorey appearance *(Photo 18)*. The erosion surfaces are straight *(Photo 18)*, convex-up (Fig.13) *(Photo 19)* or concave-up in shape. For ease of presentation, these extremely common erosion surfaces have been omitted from the vertical profiles.

Apart from the erosional surfaces, there are some other conspicuous convex-up surfaces as well. The dip directions of these surfaces are chiefly identical to the general dip directions of the underlying cross-bedded foresets (Fig.14). Since the surfaces are dipping in the direction of the sandbar movement, they have been interpreted as downstream accretion (**DA**) surfaces. Accordingly, the sandbodies bounded by these DA surfaces are DA macroforms.

These macroforms have internal lithofacies assemblages organized in a distinctive vertical sequence. The vertical sequence commences with *very thickly bedded* (0,8-2 m), planar and low-angle cross-stratified sandstones (Sp, Sl). These units are laterally continuous for at least a few tens of metres *(Photo 20)*. Apart from the cross-bedding, the tabular beds display laterally extensive, sharp, straight (Fig.15) and convex-up internal erosion surfaces.

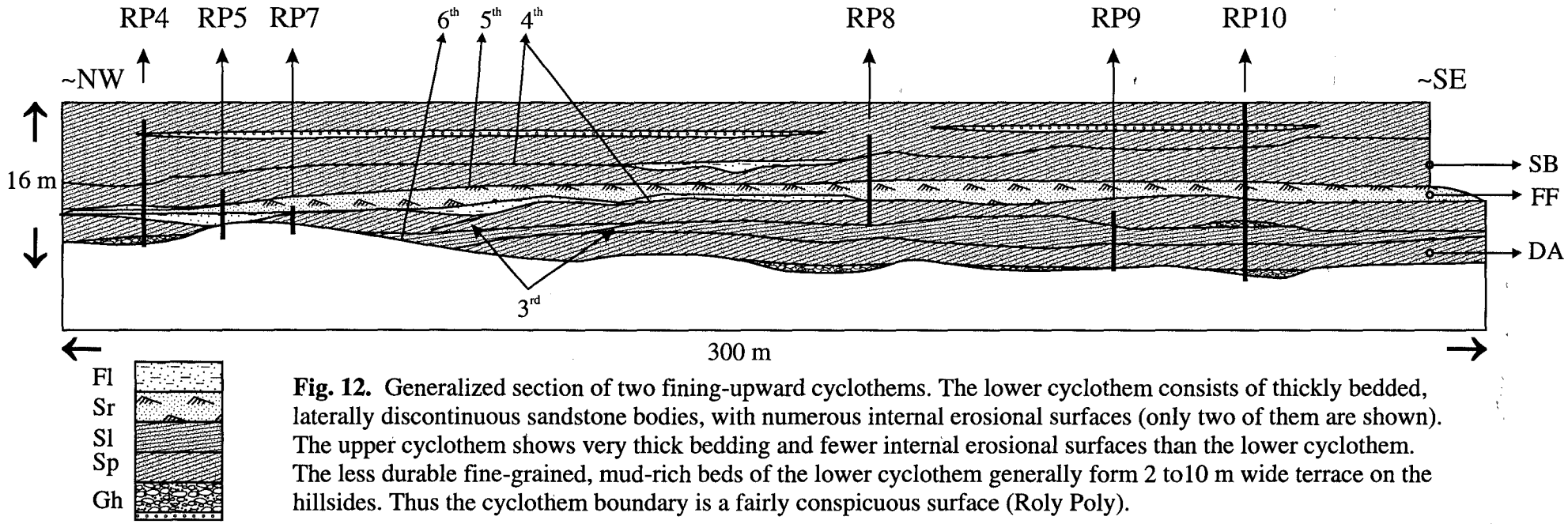

Fig. 12. Generalized section of two fining-upward cyclothems. The lower cyclothem consists of thickly bedded, laterally discontinuous sandstone bodies, with numerous internal erosional surfaces (only two of them are shown). The upper cyclothem shows very thick bedding and fewer internal erosional surfaces than the lower cyclothem. The less durable fine-grained, mud-rich beds of the lower cyclothem generally form 2 to10 m wide terrace on the hillsides. Thus the cyclothem boundary is a fairly conspicuous surface (Roly Poly).

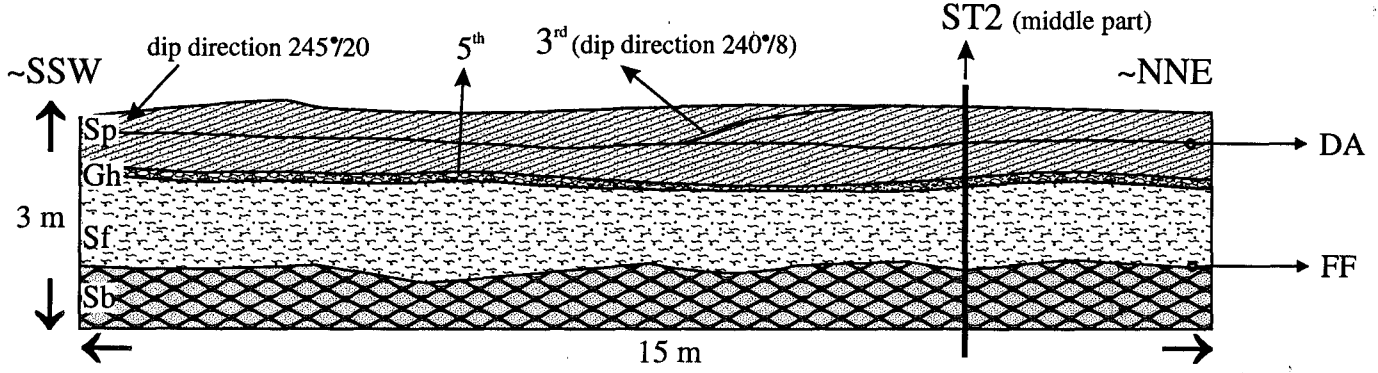

Fig. 13. Convex-up erosional surface (3rd) in thinly bedded, laterally discontinuous sandstone beds. The surface and the foresets show identical dip direction (~WSW) (Stembok).

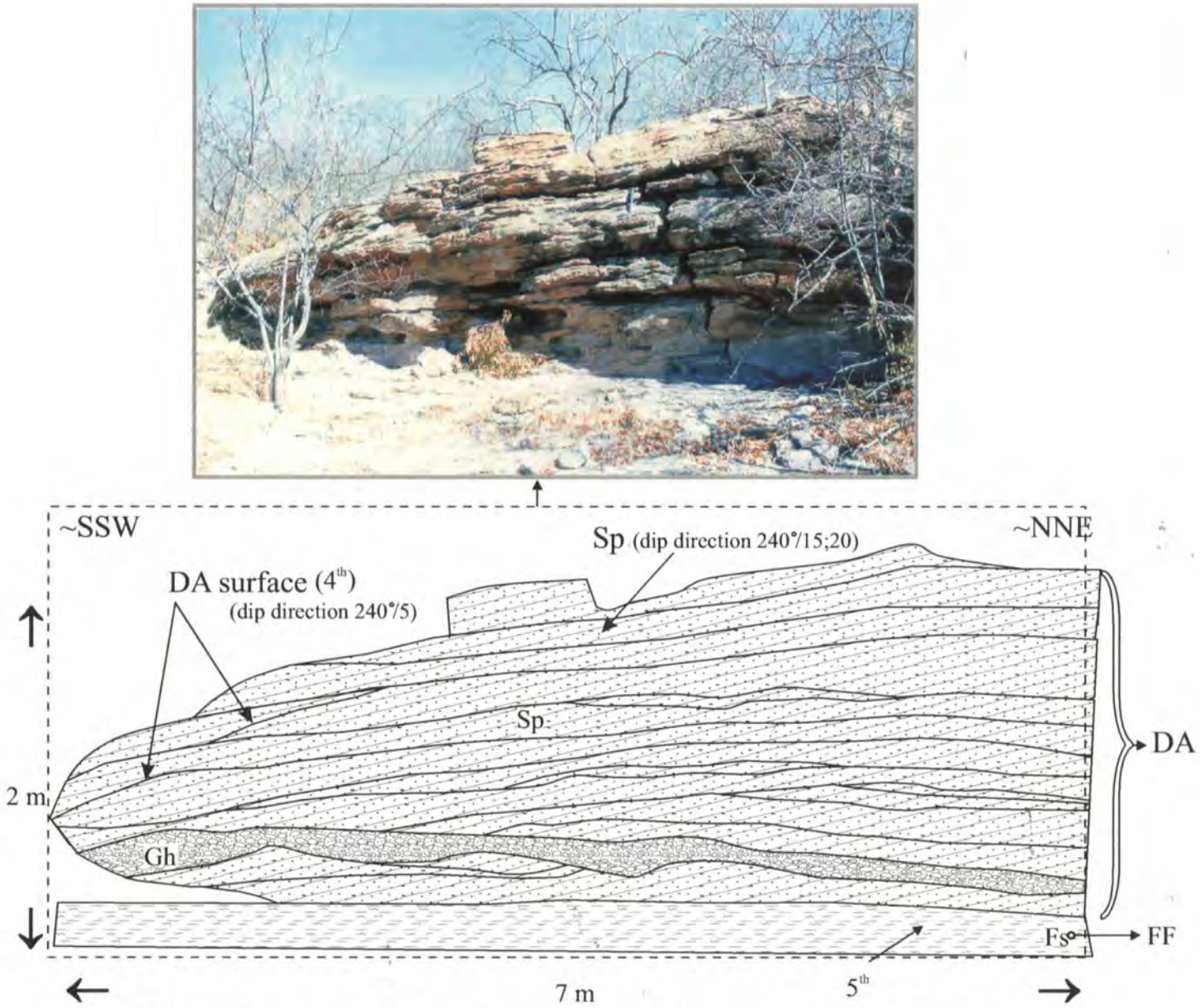

Fig. 14. Downstream Accretion surface (DA) bounding planar-cross stratified sandstones. The flat based sandstone lenses display convex-up internal erosion surfaces (Stembok).

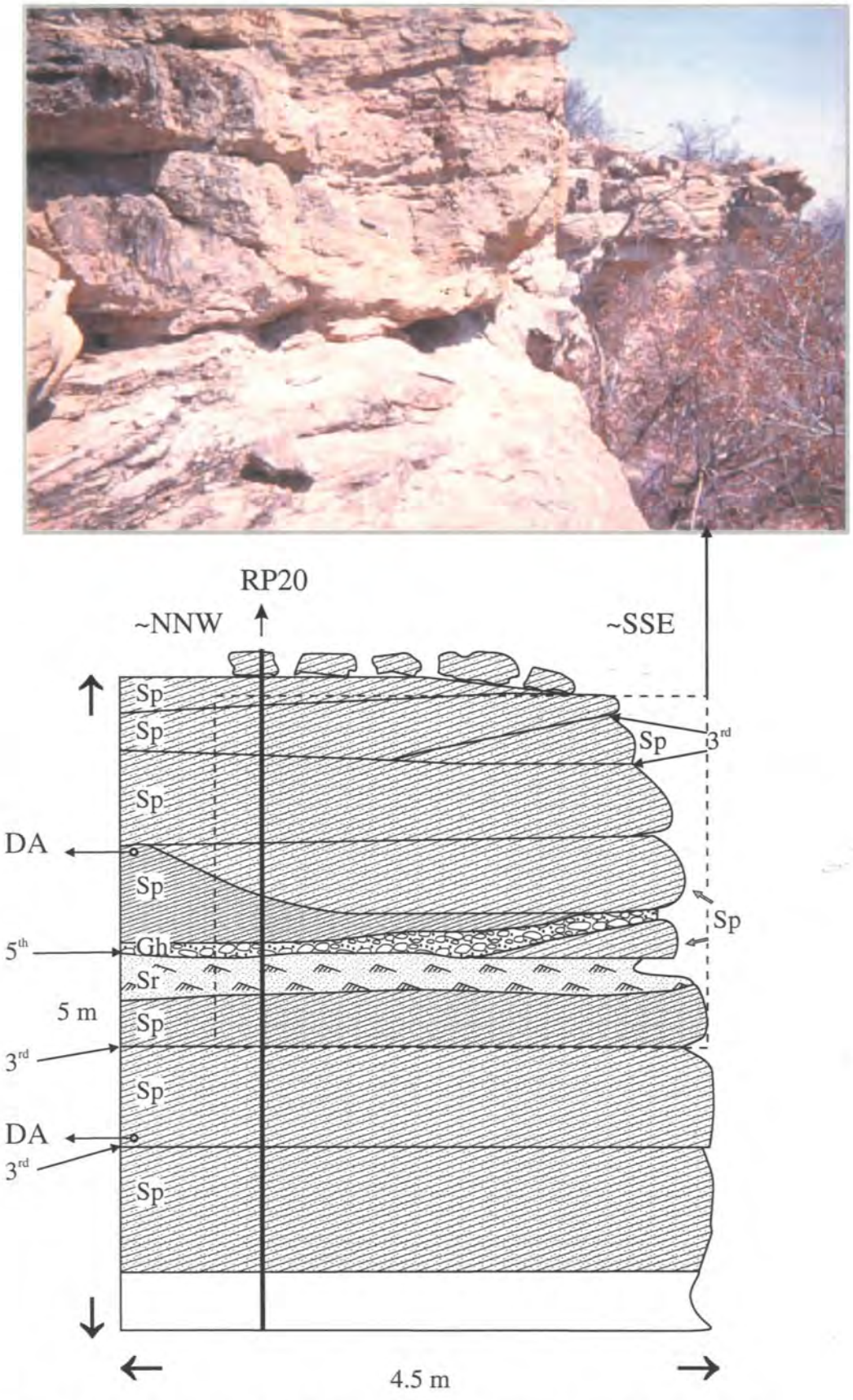

Fig. 15. Thickly bedded sandstones between straight internal erosion surfaces. The two fining-upward cyclothems are separated by a conspicuous erosion surface (Roly Poly).

The laterally discontinuous, *lens, wedge or sheet shaped units* (Fig.16) of superimposed sets of planar cross-bedded, coarse - medium sandstone (Sp) show an irregular upward decrease in set thickness (from 0.5 to 0.1 m). Basically, they display two different external geometries. Firstly, they may succeed the thick sandstone units *(Photo 21)*, in which case their upper boundary is convex-up (Fig.17) rather than straight or concave-up, thus representing Downstream Accretion (**DA**) macroforms. Secondly, they may be bounded by sharp, straight erosion surfaces (Fig.18) and divided by straight and concave-up internal erosional surfaces, giving the sandstones a small channel-shaped appearance (Fig.19). Within the sandstones, there are also small scour-and-fill structures (Ss) (Fig. 20), commonly consisting of small quartz-pebble conglomerates with a few intraformational mudclasts (Gh, Gcm) (Fig. 30).

The discontinuous lenses, wedges, channels and sheets *(Photo 22)* of sandstone are in places overlain by small sequences (max. 0.4-0.5 m) of Sh and Sr lithofacies, passing into very small ripples (Fl) (Fig. 21). These fine- and medium-grained, horizontally laminated sandstones (Sh), passing up to climbing ripples, followed by ripple-marks (Sr), are laterally non-persistent and lenticular in shape. The successions characterized by the geometry described above have been interpreted as Sandy Bedforms (**SB**). The lithofacies Sb also appears to be part of this architectural element, as indicated in Fig. 22. This lithofacies consists of ball-and-pillow structured sandstones which resemble closely packed ellipsoidal or kidney shaped bodies of various sizes (8-30 cm) *(Photo 23)*. There are some beds where these balls and pillows are linked to each other, but commonly they are isolated. Some of them show faint, deformed lamination.

Another association of lithofacies has also been classified as Sandy Bedform (**SB**), namely the horizontally laminated, low angle cross-laminated sandstones (Sh, Sl) and ripple-marks (Sr) where they occur as *sharp-based*, 0.1-1 m thick sandstone interbeds *(Photo 24)* in mudstones or siltstones. In these cases, the thin beds (0.1-0.2 m) of horizontally laminated sandstones (Sh) *(Photo 25)* show parting lineation, while the ripples are asymmetric, both undulatory and straight-crested. These ripples are made of poorly sorted, mainly fine and very fine sand grains. The sharp-based sandstones tend to have lenticular *(Photo 26)* or sheet-like geometry, sometimes displaying internal shallow truncation surfaces as well (Fig. 23). They attain 1-2 m in thickness and usually a few metres in width.

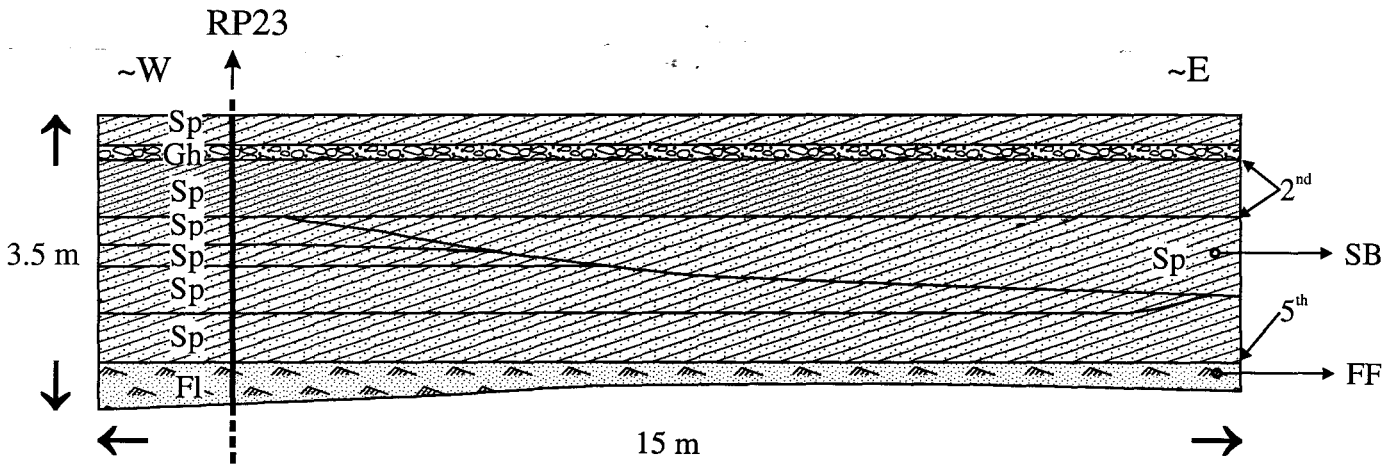

Fig. 16. Thinly bedded, wedge shaped sandstones (SB) overlying overbank fines consisting of grey, micaceous, horizontally and ripple laminated fine sandstone (FF) (Roly Poly).

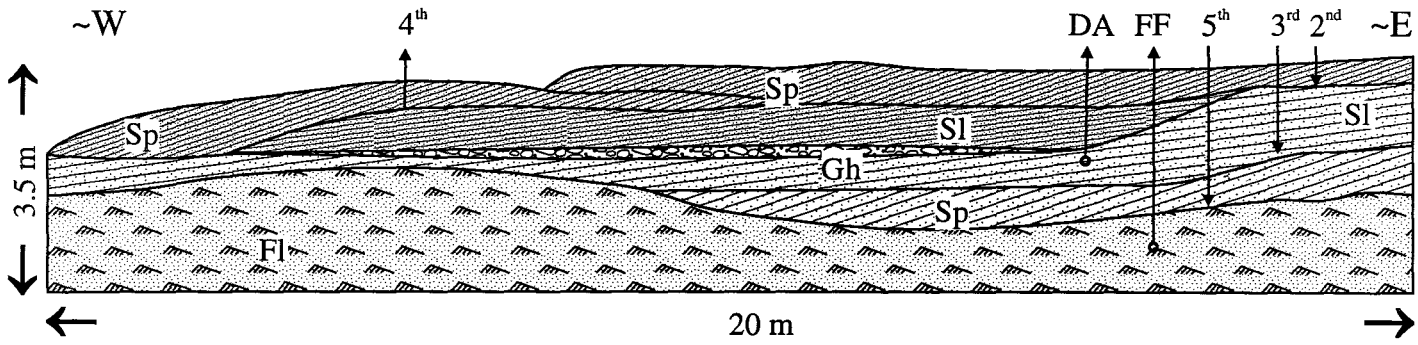

Fig. 17. A conspicuous downstream accretion (DA) surface within lenses of sandstone. The underlying overbank fines consist of grey, micaceous, horizontally and ripple laminated fine sandstone (FF) (Roly Poly).

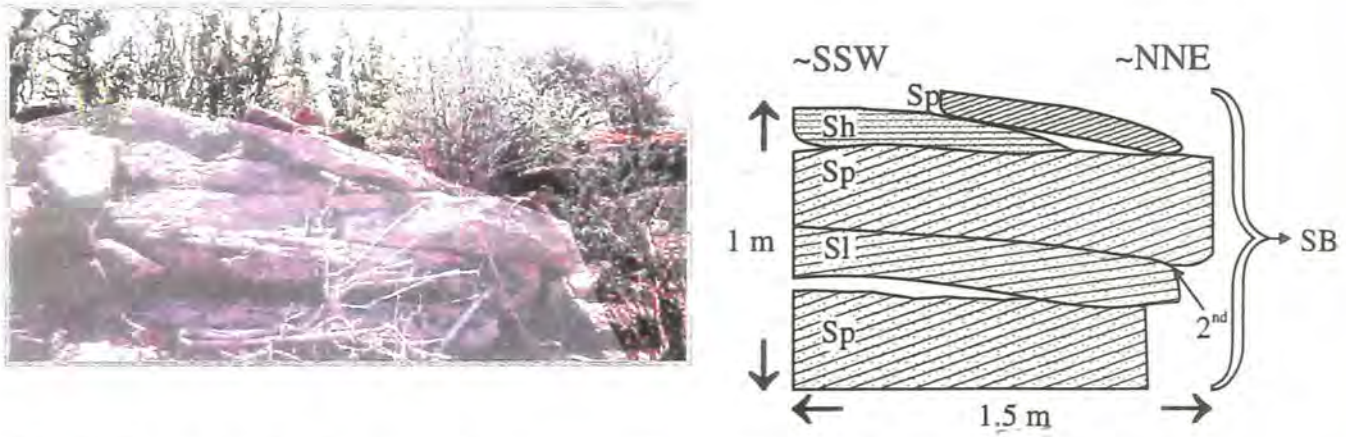

Fig. 18. Thinly bedded sandstones separated by straight erosional surfaces. The drawing shows the internal sedimentary structures (Lauriston).

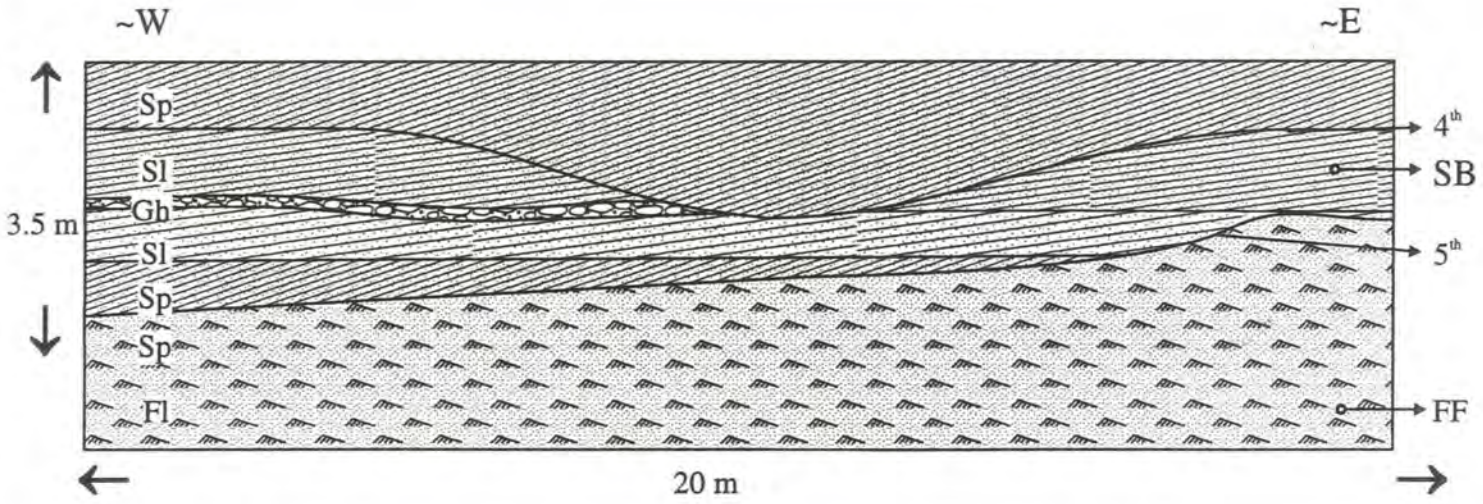

Fig. 19. A small channel sandstone incised in sandy bedforms (SB). The underlying overbank fines consist of grey, micaceous, horizontally and ripple laminated fine sandstone (FF) (Roly Poly) .

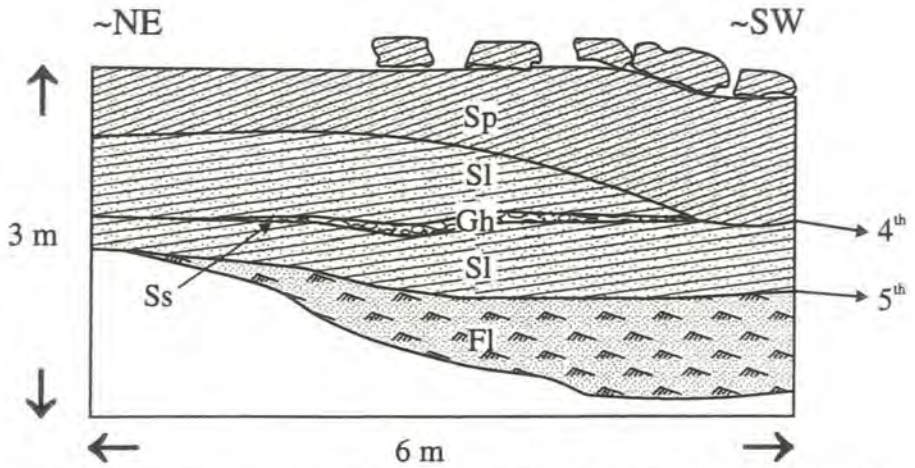

Fig. 20. Small scour-and-fill structure (Ss) filled by clast-supported conglomerate (Gh) (Roly Poly).

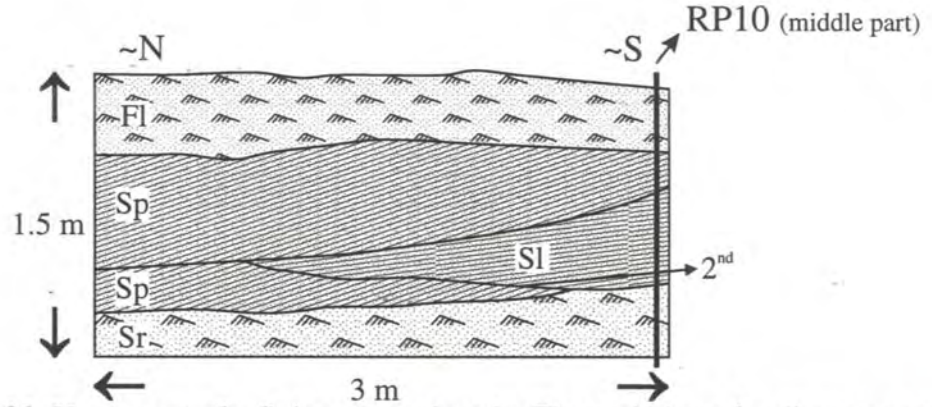

Fig. 21. Upper part of a fining-upward cycle. The variation of sedimentary structures (very fine sandstone and siltstone) indicates that flow strength fluctuated during deposition (Roly Poly).

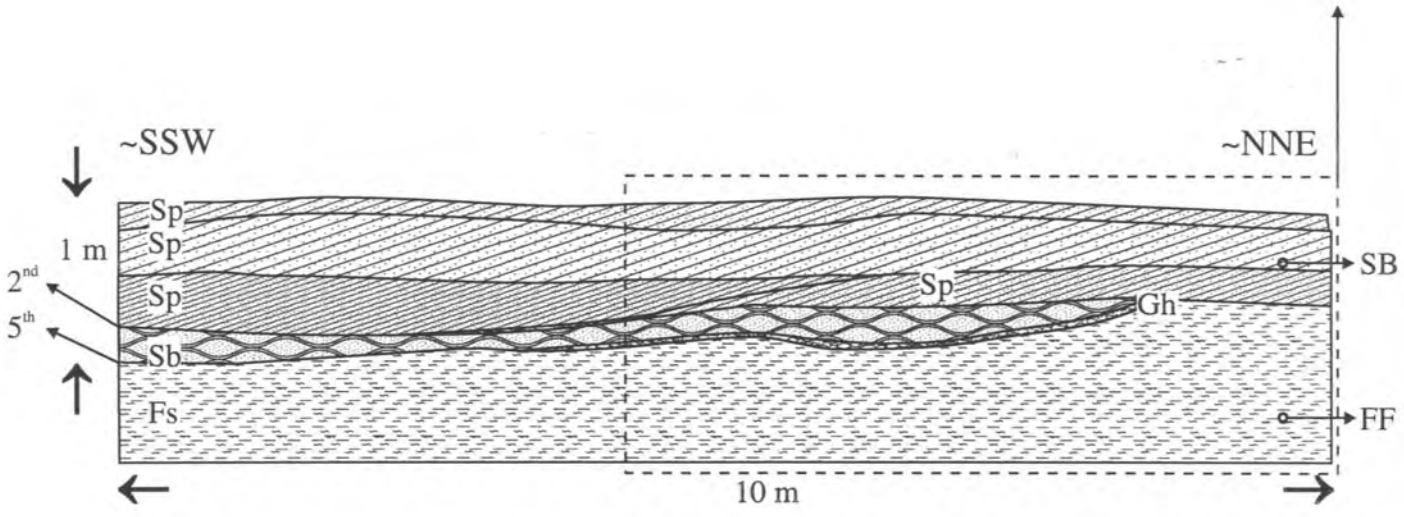

Fig. 22. Rarely, ball-and-pillow structures appear within the sandy bedforms (Stembok).

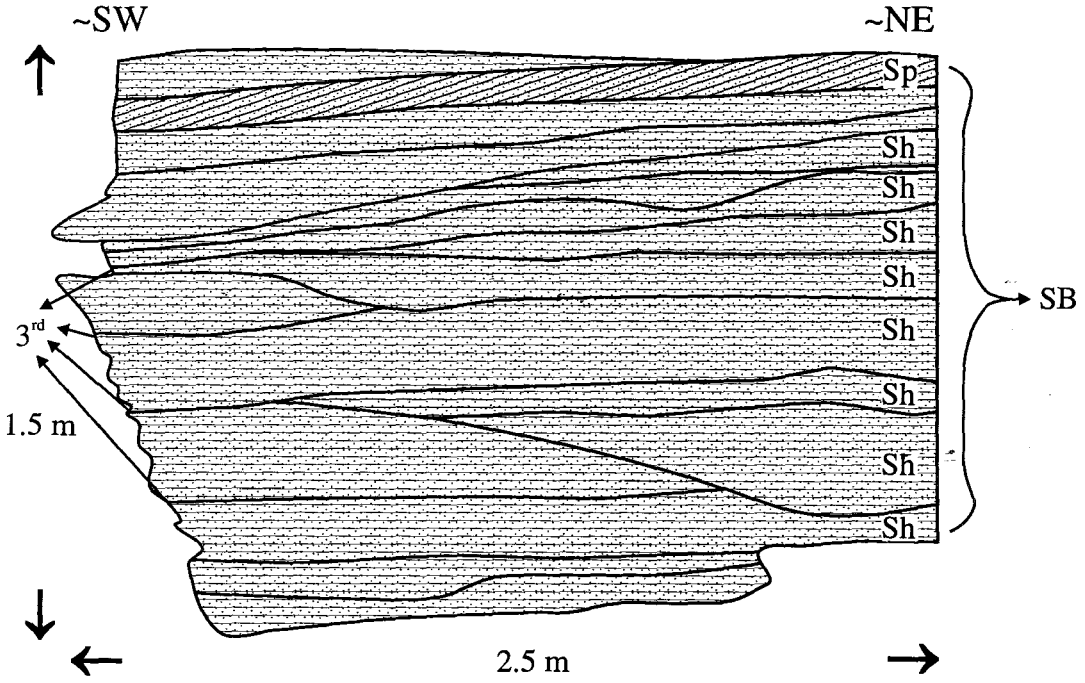

Fig. 23. Shallow reactivation surfaces in sandy bedforms (SB) consisting of horizontally laminated sandstones (Sh) (Weltevreden).

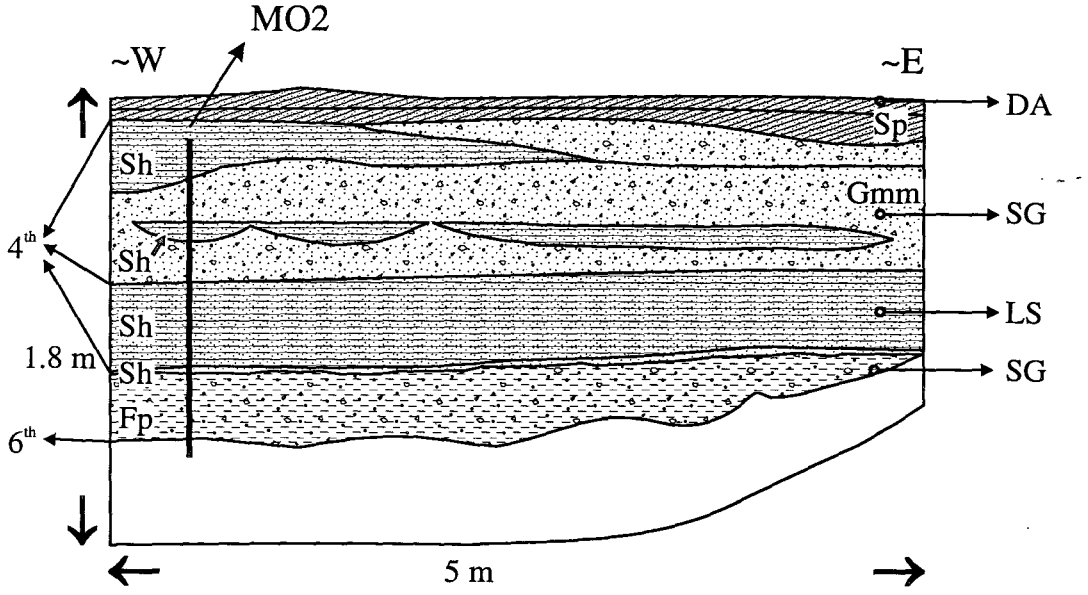

Fig. 24. Pebbly mudstone (Fp) fills the irregularities of the basement rocks. The succeeding coarser unit is composed of laminated sand sheets (LS) and sediment gravity flow deposits (SG). The upper part of the outcrop (+ 3-4 m) consists of lenses and wedges of medium-coarse sandstone (DA) (Montaqu).

The *sheet-like, tabular sandbodies* comprising horizontally laminated sandstones (Sh) *(Photo 27)* were classified as Laminated Sand sheets (**LS**) (Fig. 24). They may show primary current lineation and lateral continuity for ~10-25 m. A very few planar or low-angle cross-stratified sandstones might occur within these thin (0.1-0.3 m), continuous Sh strata.

The best example of the Channel architectural element is the exceptional outcrop on the farm Montaqu, where a well-defined concave-up erosional surface outlines a complete small channel sequence (**CH**) (Fig. 25). The stream cliff displays a 50 m long, 5 m thick channel, filled by low-angle cross-stratified (Sl, Sp), horizontally stratified (Sh) and ripple cross-laminated sandstones (Sr). The channel is incised into the massive and fine-laminated mudstones, siltstones (Fsm, Fl) and sandy mudstones (Fs) along an erosional, sharp basal scour. In the SE wing of the channel, below the basal erosion surface, a 10 cm thick nodular layer of silty mudstone crops out in a small patch. The grain size and the sedimentary structures are fining-upwards: large-scale planar cross-stratification (Sp) in coarse and very coarse sandstone becomes smaller in scale in the middle section of the channel. Here the tangential, planar-cross bedded sets are interbedded with low angle cross-stratified (Sl) and horizontally laminated (Sh) medium and coarse sandstones. The upper 3 m of the channel is dominated by highly micaceous, laminated, grey muddy medium-fine sandstone (Sh) overlain by sandy mudstones (Fs). The whole unit is overlain by thickly bedded, very coarse and coarse planar cross-stratified sandstones. The individual bedding units do not expose any lateral accretion surface. The calculation concerning the depth/width ratio of the channel is presented in Ch. 4.3.3.

Apart from the channel sequence described above, two other channel sequences were found in the study area: a major channel on the farm Stembok (Fig. 26) and a medium one on the farm Weltevreden (Fig. 30). Both channels are filled by upward-fining sequences. Figs. 26, 27, 28 & 29 show the details of the channels and the strong scour surfaces along which they were carved into the basement rocks.

Other channel-shaped, minor sandstone bodies are usually scoured into the upper part of Sandy Bedforms (SB) or (rarely) Downstream Accretion Macroforms (DA) (Figs. 31, 32, 33 & 34). There are a few units of *massive sandstone* (Sm) occurring within the cross-stratified sandstones.

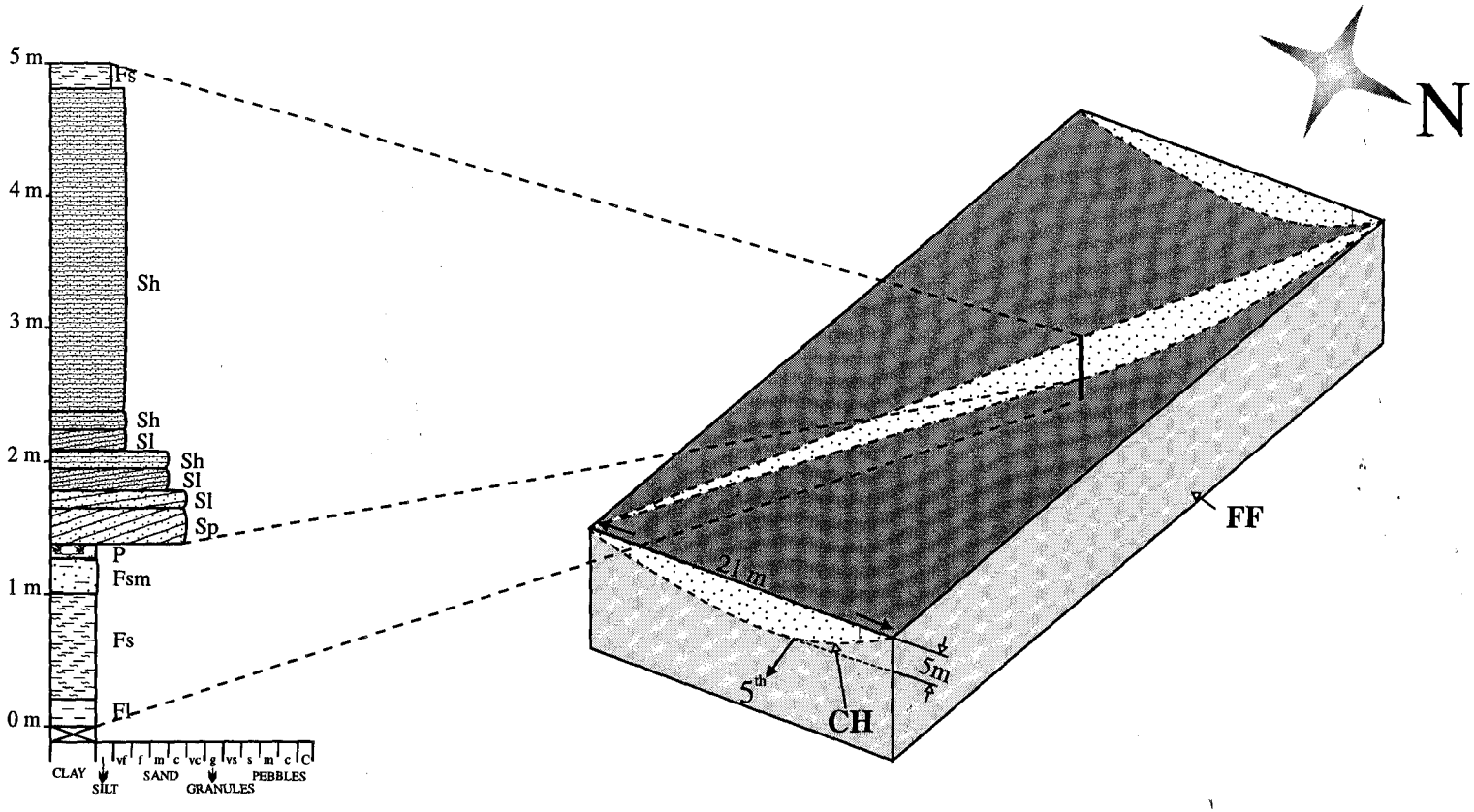

Fig. 25. A complete channel fill sequence of a medium sized channel (CH) (see explanation in text) (Montaqu).

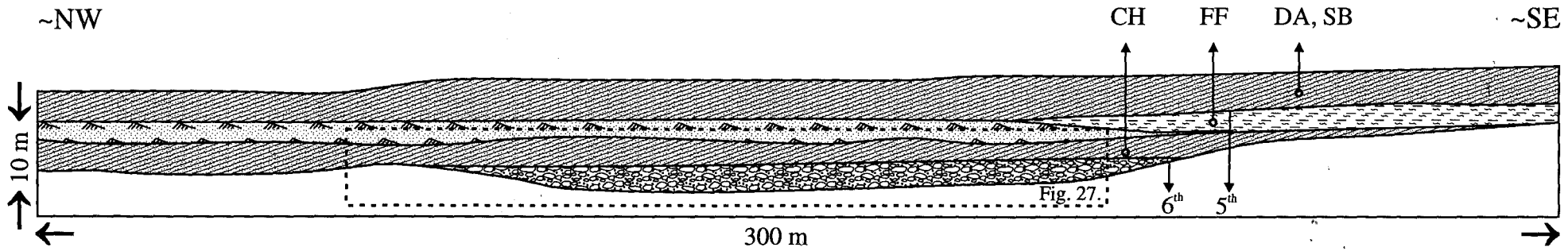

Fig. 26. Major channel (CH) filled by a fining-upward cyclothem of Gh, Sp, Sr. It is partly overlain by overbank fines (FF) and partly by downstream-accretion macroforms (DA) and sandy bedforms (SB) (Stembok).

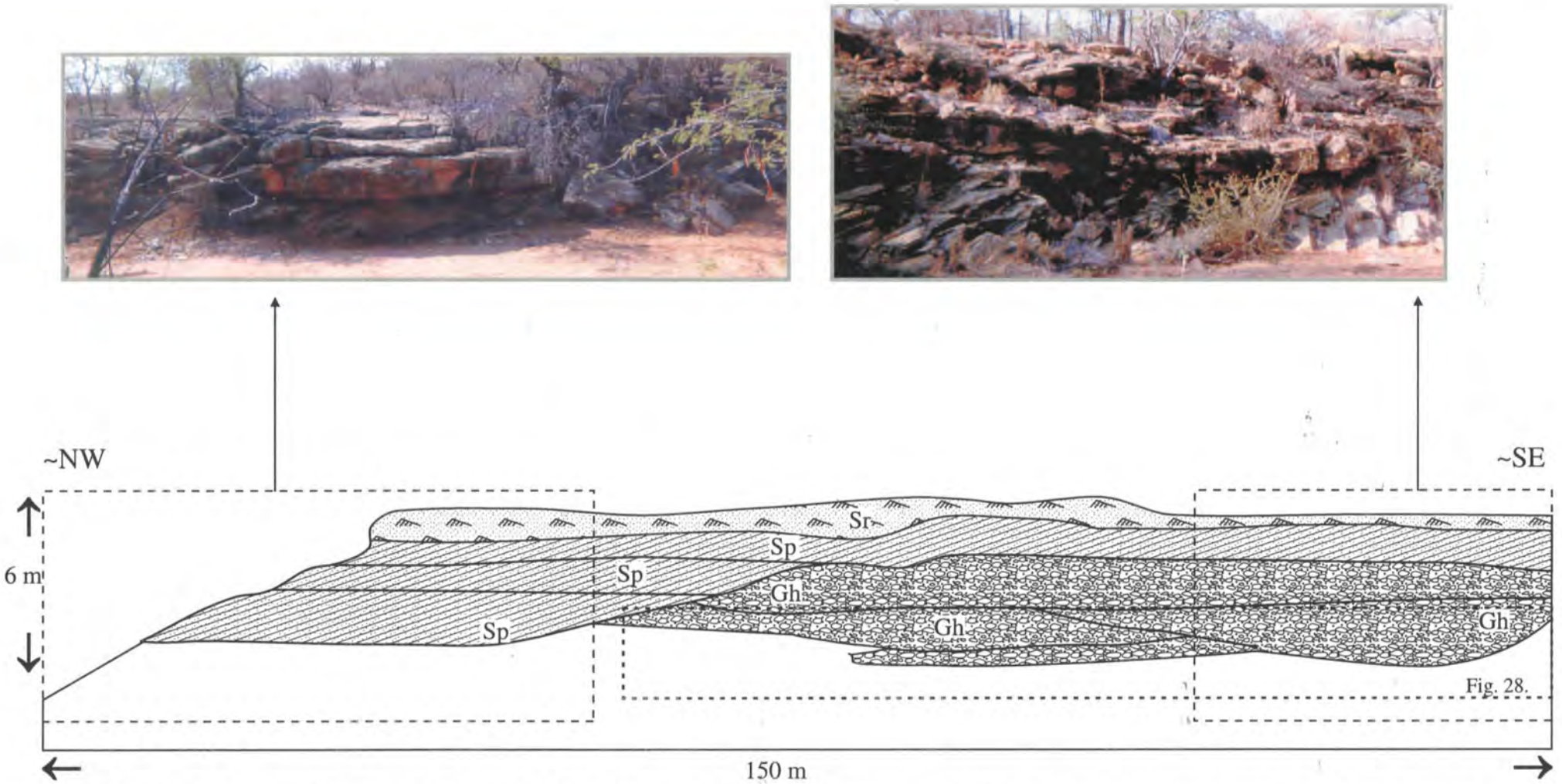

Fig. 27. Close-up pictures of a major channel fill. The difference in vertical and horizontal scales makes the basement irregularities more pronounced than is the case in the outcrop (Stembok).

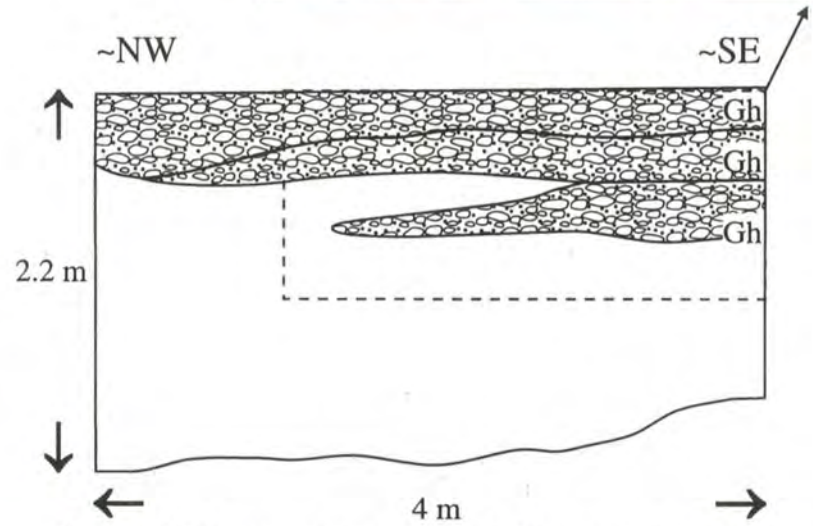

Fig. 29. Close-up pictures of the basement irregularities at the bottom of a major channel fill (Stembok).

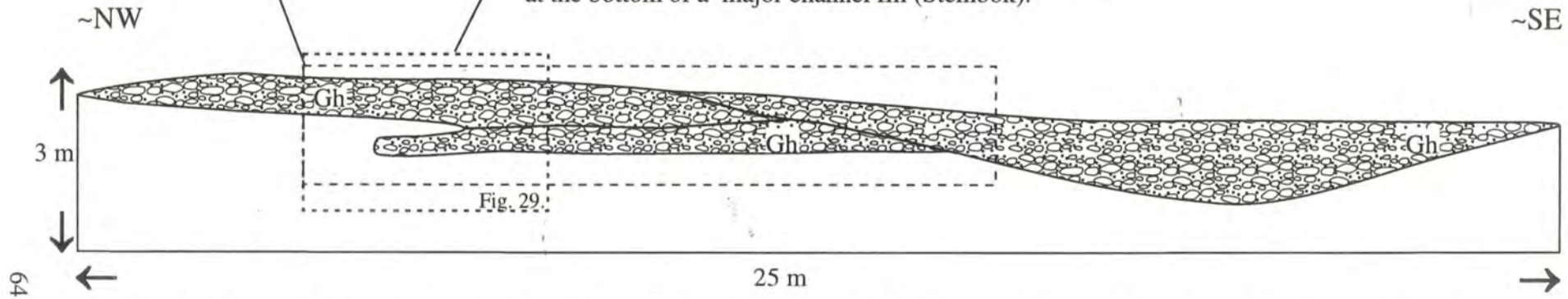

Fig. 28. Close-up pictures of a major channel fill. The width/depth ratio of the smaller channel shaped conglomerate body (on the right) has been calculated (see Fig. 82.). The difference in vertical and horizontal scales makes the basement irregularities more pronounced than is the case in the outcrop (Stembok).

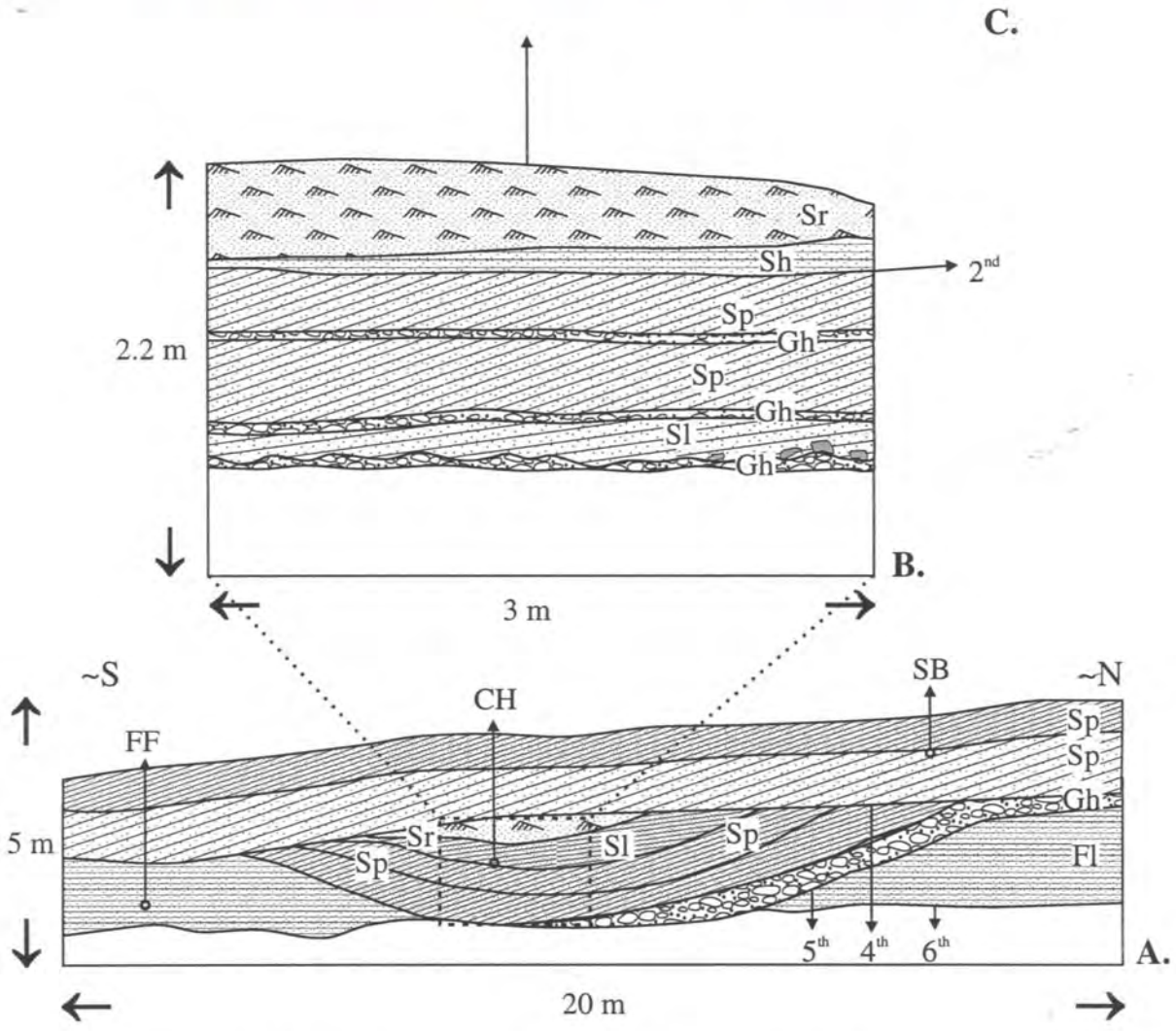

Fig. 30. **A.** Generalized picture of a small channel (CH) as well as of the under and overlying architectural elements (FF, SB). The channel is interpreted from very poor quality outcrops, thus its shape and width are only estimated. **B & C.** Detailed pictures of the internal sedimentary structures of the channel fill. The bases of the sandstones are frequently marked by 3-10 cm thick, stringers of subangular-subrounded pebbles. There also are a few rip-up mudstone-siltstone clasts (Weltevreden).

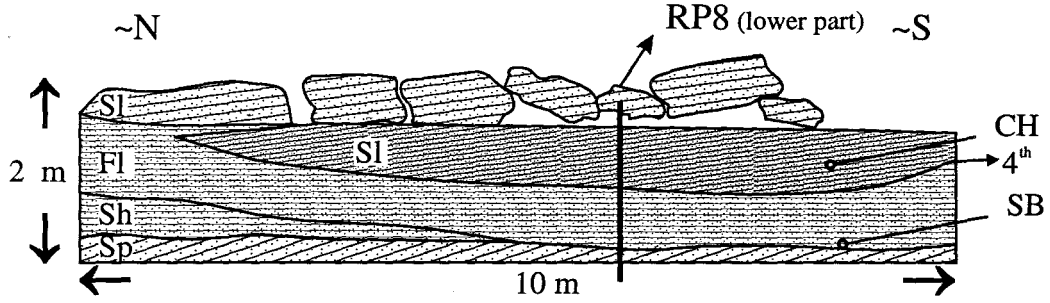

Fig. 31. Channel shaped medium-coarse sandstone (Sl) (CH) in micaceous, very fine-medium (Fl) sandstone (SB) (Roly Poly).

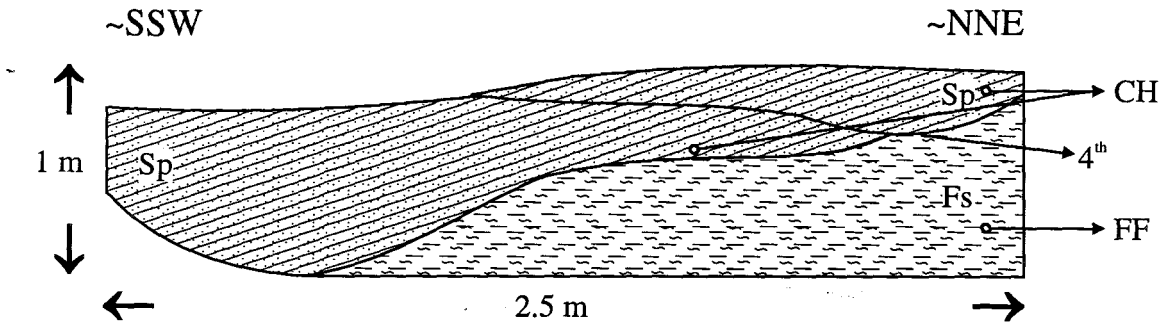

Fig. 32. Small channels (CH) scoured in fine-grained strata (FF) (Montaqu).

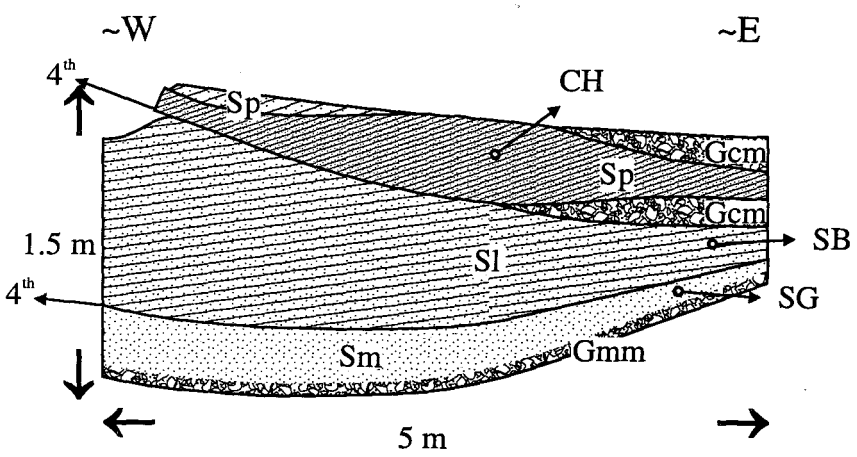

Fig. 33. Fining-upward cyclothems commencing with massive Gmm (Ammondale).

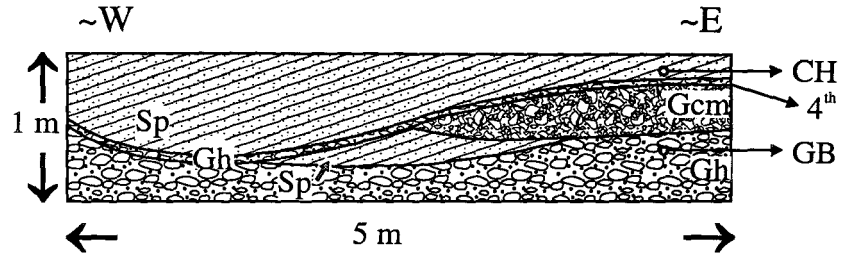

Fig. 34. Base of an upward-fining cyclothem. Small channel (CH) scoured in blanket like conglomerates and breccias (GB) (Ammondale).

Considering that the exposures of the area are highly weathered, some of the massive, tabular bedded sandstones may seem structureless.

Water-escape structures have been observed in a medium sandstone bed which shows slight faint lamination, but for most of its length the bed is massive (Weltevreden) *(Photo 28).*

In a few cases, where the massive sandstones are underlain by muddy-silty rock types, the underside of massive sandstone beds displays *load structures* (Weltevreden).

Gmm lithofacies of this facies assemblage is a rare, intermediate facies type between matrix-supported breccias and clast-rich massive sandstones. Gmm occurs at the base of the major fining-upward cyclothems (Section 3: ST4) and commonly passes into massive sandstones. Gmm and the massive sandstones (Sm) are therefore believed to form part of the Sediment Gravity Flows (**SG**) architectural element (Fig. 33). Occasionally, lithofacies Sm and Gmm are interbedded with minor lenses of lithofacies Sp *(Photo 29).* It was observed that those massive sandstones that are resting directly on basement rocks contain one or two boulder-sized, very angular vein-quartz fragments *(Photo 30).* Within a few metres, the basement gneisses were intruded by fractured 30-40 cm wide quartz veins *(Photo 31).*

Aside from the sandstones, the facies assemblage consists of some subordinate crudely bedded (Gh) *(Photo 32)* or massive, clast-supported conglomerates and conglo-breccias *(Photo 33A & B)* (Gcm). These lithofacies comprise subangular, subrounded 0.5-2 cm (-2.33 to -4.33 ϕ) clasts of vein quartz (97%), quartzite and chert. No clast orientation has been observed. Gcm lithofacies is massive, mainly clast-supported, but the matrix content may become higher in places *(Photo 34)*, and it appears as small isolated lenses. Gh lithofacies appears in the form of stringers, small lenses and as channel-shaped bodies above scour surfaces (Stembok) (Fig. 28) To a lesser extent, Gh also develops as 0.3-0.5 m thick, non-persistent beds at the base of the upward-fining sequences (Fig. 34) *(Photo 18)* (Section 3: RP14-20). The Gh and Gcm lithofacies have been identified as Gravel Bedforms (**GB**). The grain size/shape analysis results of the lithofacies are presented in Ch. 4.4. (Figs. 84C, 85C & 86C) and Appendix 2 (p.3,3a; 5,5a; 6,6a; 7,7a; 8,8a; 10,10a; 15,15a; 17,17a). The maximum outcrop thickness of the facies assemblage is ~20 m.

The clay-matrix rich, very poorly-sorted, coarse sandstones and sandy mudstones are intermediate between the sandy and the fine-grained facies. They are discussed in the next chapter as they appear more commonly in association with the fine-grained lithofacies.

4.2.1.3. Fine-grained facies assemblage

All lithofacies presented in the following paragraphs belong to the overbank fines (FF) architectural element. They not only overlie the sandstone facies assemblage but also alternate with them (Section 3, 4 and 5). When interbedded with the sandstones, they usually form the uppermost part of the fining-upward cyclothems.

The most abundant rock types of the fine-grained facies assemblage are the *laminated* and *massive mudstones* and *siltstones* (Fl, Fsm) *(Photo 35).* Depending on the organic matter content, their colour ranges from buff yellow and light grey to black, but generally they are grey. Some of the massive mudstone (Fm) displays desiccation cracks (Section 3: WE5).

Both mudstone types frequently contain abundant plant debris. The poorly preserved impressions of fossil leaves (mainly *Glossopteris sp.) (Photo 36)* and seed-bearing structures are confined to the laminated siltstones (Fl) (Weltevreden, Goring, Montaqu, Lauriston, Lizzulea). The 17 carbonaceous mudstone samples collected for pollen analysis were all non-fossiliferous. All fossil samples are catalogued and housed at the BPI (University of Witwatersrand, Johannesburg).

Although *coal* seams are not seen in any of the visited outcrops, their presence is indicated not only by borehole cores, but also by the black, carbonaceous mudstones (C).

Palaeosol horizons (P) are developed at the top of the laminated dark grey mudstones (Section 3: MO1 & Fig. 25). The palaeosol horizon shows homogenization by pedoturbation, desiccation cracks, slickensides and contains carbonate and clay-rich glaebules. According to the palaeosol classification by Mack et al. (1993), this horizon is a glaebular, calcic vertisol.

The *pebbly mudstones* (Fp) consist of a dark grey, rarely laminated mud or coarse sandy mud matrix, with scattered very angular to subangular coarse sand grains, granules, and fine to medium pebbles of quartz. The coarse, randomly sprinkled, poorly sorted clasts floating in the muddy matrix form a matrix-supported texture. The clasts lack orientation and the muddy matrix shows vague lamination. Due to their softness, the deposits form flat areas or appear in small patchy outcrops. Determination of the dimensions of this lithofacies was impossible.

The *massive sandy mudstones* (Fs) and the *massive muddy sandstones* (Sf) contain 10-20% to ~60% of fine to very coarse sand, respectively. Both lithofacies rarely show lamination and are commonly associated with massive mudstones (Fsm).

The *sandy siltstones* (Fl) are usually micaceous and display well-defined horizontal lamination (Fl/Sh) *(Photo 37)*. They commonly occur towards the top of the major, fining-upward sandstone units.

The ball-and-pillow structured siltstones and mudstones (Fb) *(Photo 38)* have the same characteristics as the ball-and-pillow structured sandstones (Sb) described in the previous chapter (see SB architectural element). The lithofacies Fb and Sb tend to develop together, underlying 2-5 m thick sandstone units (Figs. 35 & 22).

On Stembok farm there is a unique outcrop exposing Sf, Sb, Fp, Fs, Fsm, Fb and Fl lithofacies together. In this outcrop, the Fp, Sf and Fs lithofacies resemble plastic deformation features as they appear in the form of tongue-shaped lobes, and sausage- and roll-shaped bodies *(Photos 39, 40 & 41)*. These elongated structures do not display any favoured orientation, and their bottom is usually erosive *(Photo 42)*. The Fp, Sf and Fs lithofacies are characterized by chaotic mixtures of various grain sizes, where the muddy matrix supports the coarse sand grains and clasts up to 3 cm. The very poorly-sorted particles are weakly normal-graded at the bottom of the lobes and randomly scattered in the middle and upper part of the beds *(Photo 43)*. The 0.5-0.8 m thick lobes are laterally continuous for 3-4 m *(Photo 44)*. These chaotic beds are mainly overlain by Sb, Fb and Fl lithofacies, forming the upper part of the succession.

The maximum outcrop thickness of the facies assemblage is ~30 m.

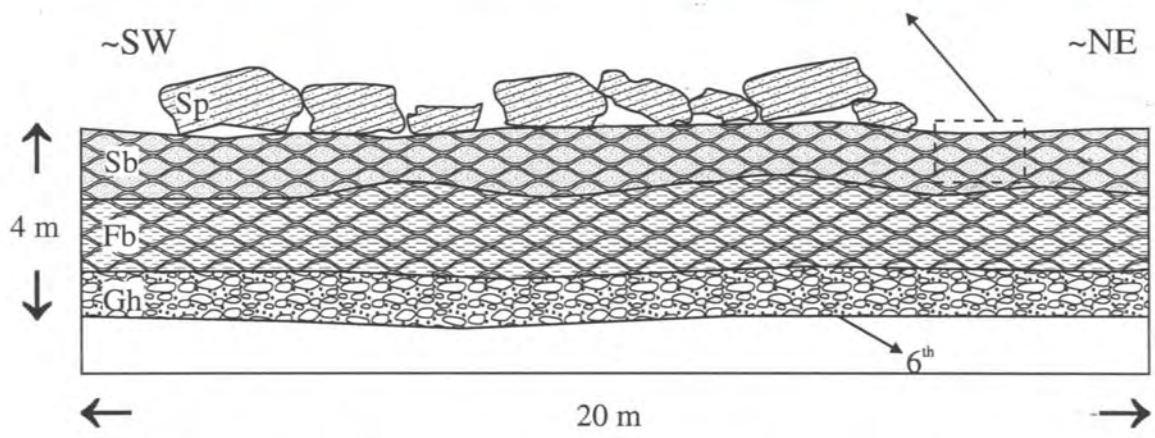

Fig. 35. Laterally continuous beds of ball-and-pillow structured mudstones and sandstones (Fb,Sb) (N - Drumsheugh).

4.2.2. Middle Unit

The Middle Unit has a ribbon-like outcrop belt running in a roughly E to W direction through the southern-central part of the study area (Fig. 3). The unit is defined by sharp lower and transitional, perhaps, conformable upper boundaries. The lower boundary of the unit is clearly detectable in several outcrops where the unit is separated from underlying carbonaceous mudstones and siltstones (Basal Unit) by a sharp, widespread surface (*Photo 45, 46*). There are a few outcrops along the eastern part of the Breslau/Eendvogelpan fence and along the southern-central part of the Vergenoeg/Sommerville fence, where the conglomerates of the lowermost Middle Unit directly rest on and/or lie against Archaean basement rocks that form inselbergs in the recent landscape. Although the hiatus is not directly measurable, it is documented that this lower boundary represents an unconformity which is traceable throughout the Limpopo valley basins (see Ch. 2.2.5.), Save Basin (Stagman, 1978) and the Lebombo 'Monocline' (NW Swaziland)(Turner & Minter, 1985). Hence, this erosional surface is a regional unconformity.

The upper boundary of the Middle Unit was not captured in any of the outcrops investigated, and this is mostly thought to be the consequence of the lithological similarities (i.e. softness) of the argillaceous upper part of the Middle Unit and succeeding mudstones of the Upper Unit. Therefore, this upper boundary had been arbitrarily established in the detailed core descriptions of boreheoles. The boundary was drawn at the first occurrence of the uniformly red-maroon mudstones and/or the reddish mudstones with carbonate glaebules. The drill core descriptions did not suggest any evident unconformity between the two units, the transition seems to be gradual, therefore the boundary is assumed to be conformable. The division of the Middle Unit into subunits was carried out in order to help clarify relations with the Tshipise Basin and other Karoo Supergroup satellite basins from the northern part of South Africa (e.g. Ellisras) (see Table 21 in Ch. 6.1.).

The Middle Unit comprises reddish-brown, white and mauve conglomerates, sandstones and siltstones (Fig. 36) *(Photo 47),* as well as varicoloured, red-green-purple-grey mudstones (the latter occur mostly in boreholes). The conglomerates, pebbly sandstones and sandstones of the lower part of the Middle Unit correspond to the Fripp Formation of Chidley (1985) (Ch. 2.2.5.3) (Table 1). The predominant siltstone and very fine-grained sandstones of the medial part of the

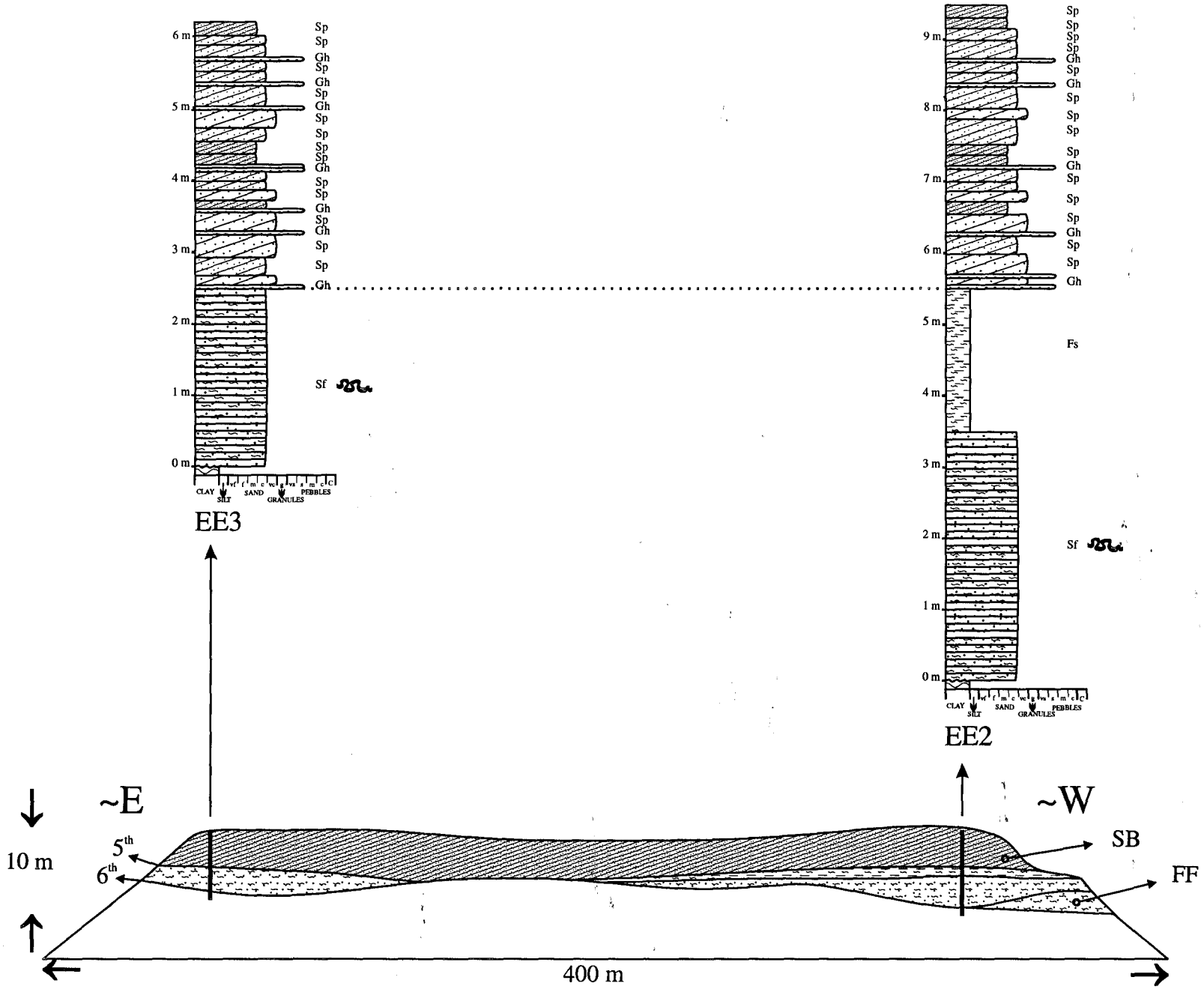

Fig. 36. The overbank fines (FF) fill the irregularities of the palaeo-topography. They are separated from the overlying sandy bedforms (SB) of the Middle Unit by a major erosional surface (Eendvogelpan).

Middle Unit are mentioned as Solitude Formation in Chidley's (1985) description. Rocks with similar lithological characteristics to these siltstones have been described as part of the Solitude Formation from the Tshipise Basin (McCourt & Brandl, 1980) (Ch. 2.2.5.1.). In the study area, the thirteen, *in situ* occurrences of the medial part of the Middle Unit - hardly larger than a few m^2 (thickness <1.5 m) - have been observed only in the northern vicinity and/or on top of the lower part of the Middle Unit deposits. These rocks are difficult to map in the field, and their outcrop belt outline is ambiguous (Fig. 37). Similarly, there are uncertainties regarding the distribution of the coarse sandstones and conglomerates (Klopperfontein Formation) reported by Chidley (1985) to stratigraphically succeed the siltstones of the medial part of the Middle Unit. This stratigraphic succession (i.e. siltstones overlain by conglomerates) has never been found, either in the field or in the borehole records. Based on Chidley's (1985) description, these rocks are lithologically indistinguishable from the sandstones and conglomerates of the lower part of the Middle Unit. The varicoloured mudstones of the upper part of the Middle Unit seem to fit the lower, variegated, non-calcareous part of Chidley's Bosbokpoort Formation.

The thinly bedded (0.2-0.5m) lower part of the Middle Unit appears to reach a maximum of 5-7 m in the exposures, the best of which are found in the extreme east (Over Vlakte) and extreme west (Breslau) of the study area. The pinkish, pale-red and white sandstones are medium- to coarse-grained, and consist of mainly subrounded, subangular and well-sorted grains. Based on macro- and microscopic determinations, the lower part of the Middle Unit contains very small amounts of feldspar, and therefore shows great compositional maturity. The sandstones are strongly planar cross-stratified (Sp), and there also are a few massive and horizontally stratified sandstones (Sm, Sh). Soft-sediment deformation resembling convolute bedding is exposed in one of the Sh beds *(Photo 48)*(Section 3: OV2). The conglomerates are usually horizontally bedded (Gh) and frequently form stringers at the base of the sandstone units *(Photo 49)*. The subrounded pebbles are 1-2 cm in diameter and consist of white, rose, green and black quartzite and vein quartz *(Photo 50)*. In places, rip-up siltstone and mudstone clasts were also observed (Halcyon). The lower part of the Middle Unit is shown in the vertical profiles of Sections 1 & 3 (from RG1 to OV2). The grain size/shape analysis results for this lithofacies are presented in Ch 4.4. (Figs. 84B, 85B & 86B) and Appendix 2 (p.1,1a; 2,2a; 4,4a; 13,13a; 14,14a; 16,16a; 19,19a; 21,21a; 23,23a to 27,27a). The detailed thin section descriptions are presented in Appendix 4.

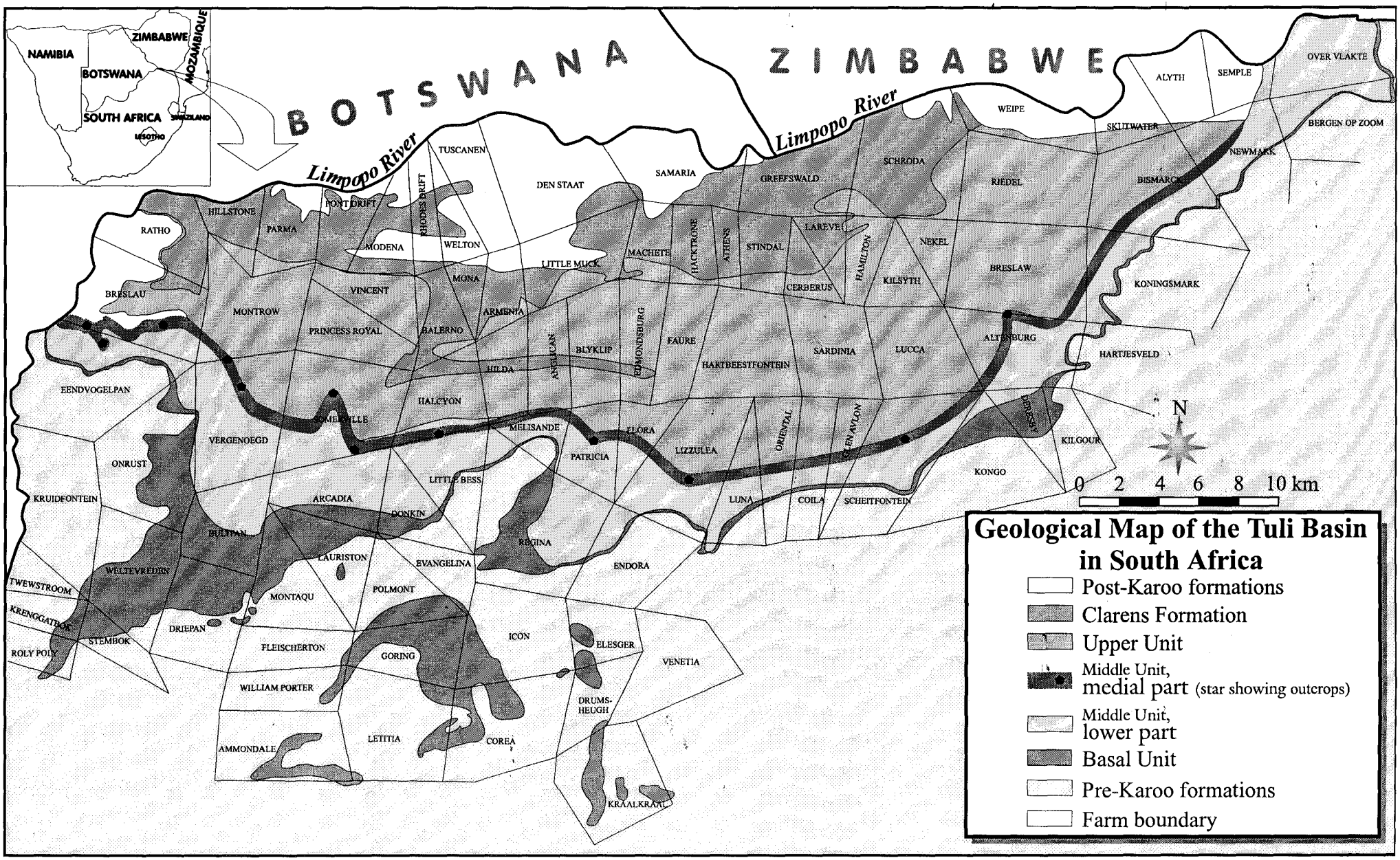

Fig. 37. Geological Map of the southern part of the Tuli Basin showing the outcrop belts of the lower and medial part of the Middle Unit.

The transition between the lower and medial part of the Middle Unit is difficult to detect in the outcrops, though it was observed that the *in situ* lower Middle Unit deposits are covered by numerous flaggy blocks of a mainly light pink, white or indurated greenish, friable, predominantly ripple-cross laminated siltstones *(Photo 51, 52)* or very fine-grained sandstones (Sr) *(Photo 53)* belonging to the medial part of the Middle Unit. The 10-20 cm thick, sharply bedded layers *(Photo 54)* show remarkable water escape structures *(Photo 55A)* and convolute bedding *(Photo 55B)*. The best outcrops of the medial part of the Middle Unit are on Eedvogelpan and Breslau (Fig. 37). The physical boundary between the conglomerates and the siltstones was captured in only one outcrop (Halcyon), where the conglomerates progressively grade into siltstones and muddy siltstones through a transitional zone of rip-up siltstone and silty mudstone clasts *(Photo 56, 57)* (also see HAL6 & 1,2,3 thin section description in Appendix 4 and Ch.4.5.3.). Because the material of these rip-up clasts is lithologically identical to the siltstones, silty mudstones and mudstones of the medial and upper part of the Middle Unit, it is assumed that these clasts are intraformational and that the three parts of the unit are, at least partially, synchronous facies equivalents.

The upper part of the Middle Unit is rarely exposed in the area (Halcyon/Little Bess boundary, W to the tar road), but data have been obtained from borehole records not only for this upper part but for the Middle Unit in general. According to these, the unit consists of an upward-fining sequence commencing with the conglomerates, pebbly sandstones and sandstones. These are overlain by either grey mudstones with reddish blotches of the upper part of the Middle Unit and/or the ripple-cross laminated siltstones (medial part of the Middle Unit) that grade up into the variegated, red-green-purple-grey mudstones of the upper part of the Middle Unit.

Based on borehole data, the average thickness of the Middle Unit is ~17 m (max. ~46 m in Vergenoeg: Ver-3) (see Appendix 3: Table 2). Table 8 also shows that the average thickness of the arenaceous deposits is ~7 m, whereas the argillaceous strata are ~10 m thick on average. Fig. 38 shows the sand:mud ratio of the Middle Unit, which is ~ 2:3. According to the thickness map of the Middle Unit (Fig. 39), there were two main depocentres (central western and central eastern part of the study area). The location of these depocentres chiefly correlates with the two areas of highest borehole density, which makes it likely that these depocentres are more apparent

than real. It seems more probable that the deposition took place on a northerly inclined palaeo-surface (Fig. 40), as this is confirmed by the palaeo-current data.

Table 8. Descriptive statistics based on the borehole data of the Middle Unit.

	Middle Unit	Arenaceous	Argillaceous
Mean	17.39	7.27	10.11
Standard Error	1.63	0.87	1.27
Median	13.38	5.88	8.50
Mode	NA	3.96	0.00
Standard Deviation	11.39	6.07	8.89
Variance	129.73	36.85	78.99
Kurtosis	-0.44	8.34	0.25
Skewness	0.80	2.58	0.94
Range	44.21	34.24	33.00
Minimum	2.01	0.40	0.00
Maximum	46.22	34.64	33.00
Sum	851.91	356.35	495.56
Count	49	49	49
Confidence Level (0.95)	3.19	1.70	2.49

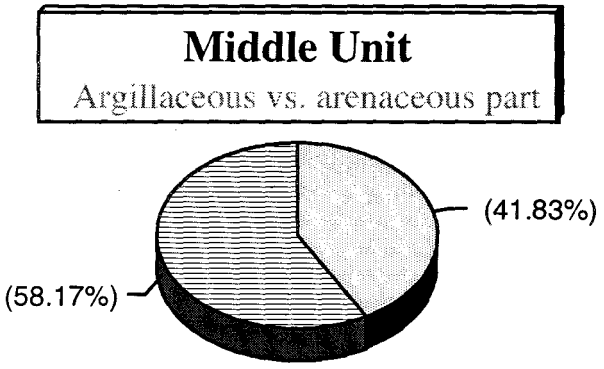

Middle Unit	Cumulative thickness in m	Percentage %
Argillaceous deposits	495.56	58.17
Arenaceous deposits	356.35	41.83
Total	851.91	100.00

Fig. 38. Sand:mud ratio of the Middle Unit.

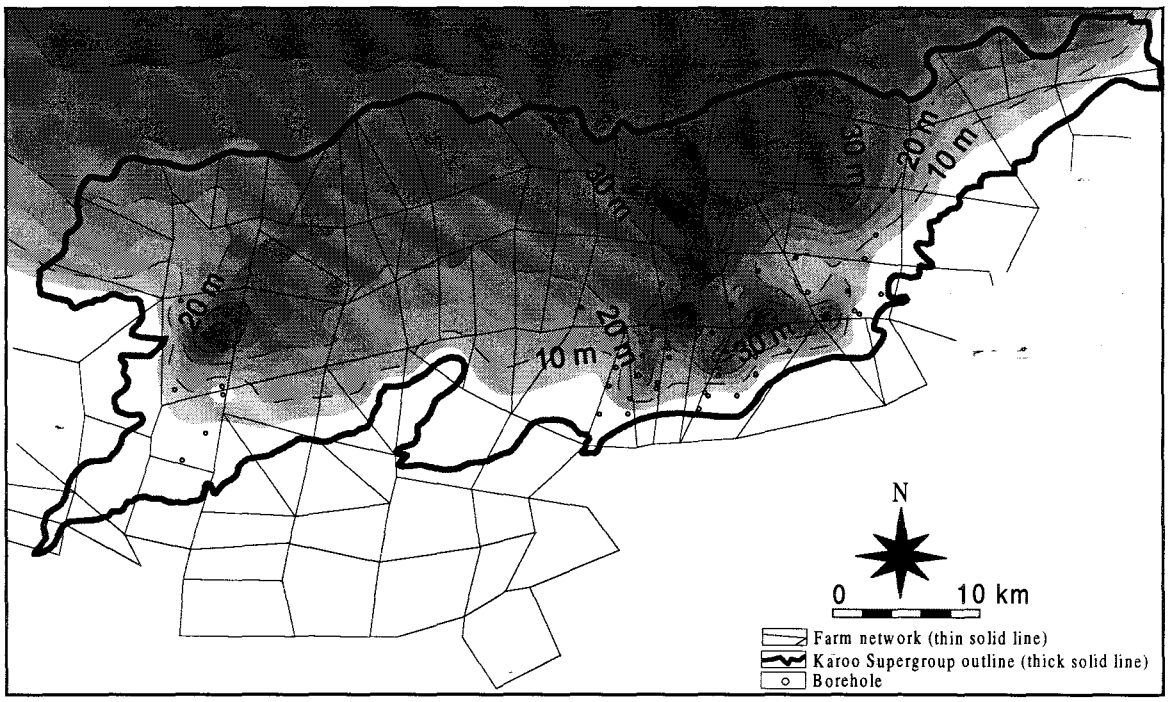

Fig. 39. Thickness map of the Middle Unit for the South African part of the Tuli Basin.

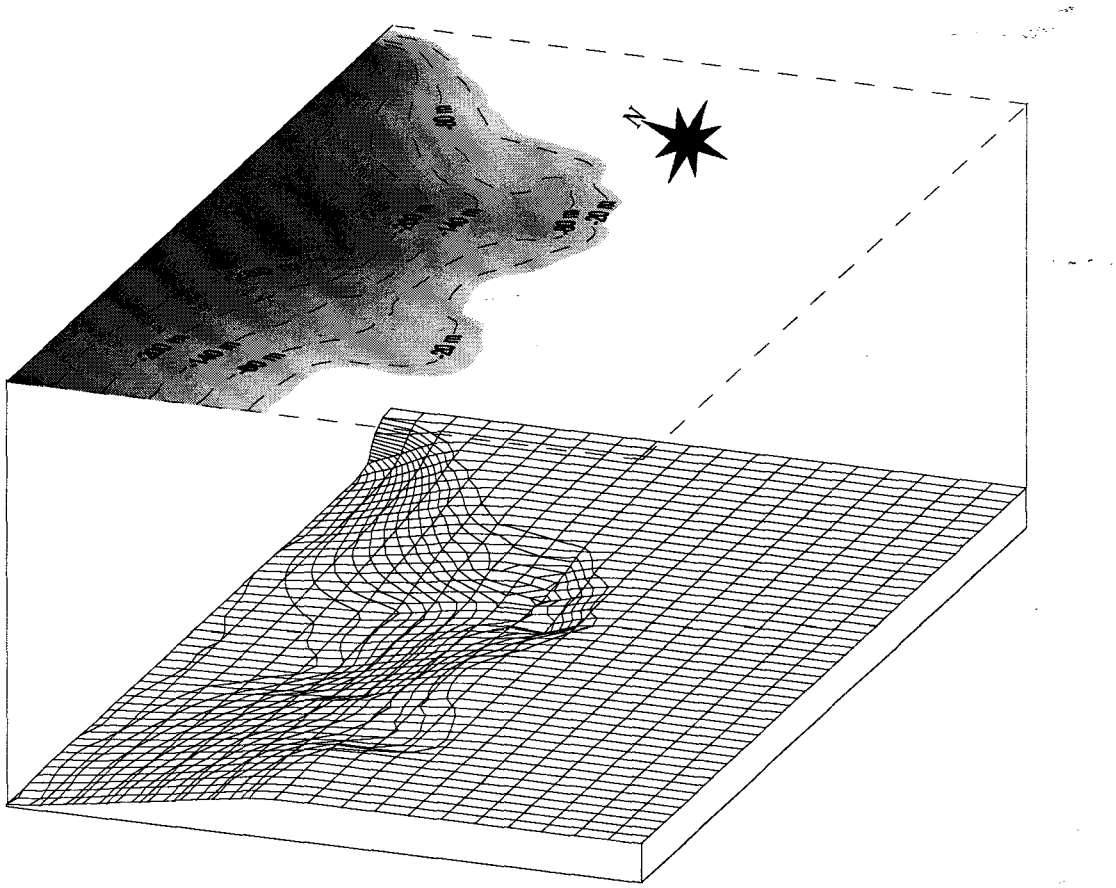

Fig. 40. Relief of the pre-Middle Unit surface.

4.2.3. Upper Unit

The outcrop belt of the Upper Unit runs in a roughly E to W direction through the northern-central part of the study area (Fig.3). The unit consists of arenaceous and argillaceous sedimentary rocks. The former are very well exposed in the northern part of Faure, Kilsyth, Nekel and Wiepe farms, while the finer-grained deposits have some excellent outcrops in the northern part of Breslau (Show of Rhodes koppie), the southwestern part of Balerno (Tsolwe koppie), and the southern parts of Armenia and Machete farms. In the geological cross-sections drawn from ~S to ~N, the estimated thickness of the Unit varies from ~200 m (Montrow, Hilda) to ~280 m (Lizzulea/Hartebeestfontein area). All calculations involved 2-5° northerly structural dip of the Upper Unit strata. Based on borehole data, the average thickness is ~60 m (max. ~207 m in Lareve: Rev-1) (Table 9 and Appendix 3: Table 3), while the maximum exposed thickness is 30 m (covered lower boundary). Fig. 41 shows that the thickness values increase towards north, as does the inclination of the pre-Upper Unit surface (Fig. 42). As mentioned in Ch. 4.2., the boreholes were mostly sunk in the erosional southern part of the basin, therefore the thickness figures and morphology of the pre-Upper Unit surface - which were derived from the boreholes - are very approximative.

The unit has conformable lower and upper boundaries. The exact delineation of the lower contact is difficult as the underlying red-green-purple mudstones of the Middle Unit are lithologically similar to the mudstones of the lower part of the Upper Unit. Therefore, the lower boundary had been established in boreholes at the first occurrence of the uniformly red, calcrete glaebule-bearing mudstones, even though this assumption can lead to chronostratigraphic misinterpretations. This arbitrary lower boundary is most likely to be diachronous, and for this reason it is shown with dashed line in the stratigraphic column (Fig. 100). The upper boundary of the unit was established at the top of that laterally continuous, white silcrete horizon which shows a gradual contact with the underlying more argillaceous (red or green-grey) Upper Unit and a sharp, clearly detectable - sometimes erosional - contact with the overlying yellow-creamy, large-scale cross-bedded sandstones of the Clarens Formation. This upper boundary is a diastem as little or no erosion could be detected between these two conformable successions of strata.

Table 9. Descriptive statistics based on the borehole data of the Upper Unit.

	Upper Unit	Arena-ceous	Arena-ceous [1] excl.Rev-1	Argilla-ceous	FUC[2]	FUC[3]	FUC[3]		Overbank mudstones[4]	Single sandbodies in overbank mudstones	Levee	
							coarse	fine			coarse	fine
Mean	59.66	11.88	9.96	19.65	15.7	19.61	12.28	7.33	28.07	5.21	2.86	3.07
Standard Error	7.72	2.07	0.79	1.86	1.07	1.39	1.09	1.22	2.07	0.5	0.33	0.41
Median	45	8.53	8.52	15.84	14.63	19.81	12.81	6.58	26.15	4.88	3.14	3.62
Mode	NA	3.62	3.62	3.62	10.97	19.81	14.02	NA	25.3	NA	3.62	3.62
Standard Deviation	46.97	17.95	6.83	15.25	7.28	5.38	4.23	4.71	13.45	2.18	1.00	1.24
Variance	2206.56	322.33	46.71	232.53	53.07	28.92	17.91	22.22	180.8	4.75	1.01	1.54
Kurtosis	3.15	54.32	0.22	-0.24	-1.10	0.04	0.10	-1.05	-0.48	-0.46	2.75	-0.55
Skewness	1.68	6.88	0.99	0.79	0.13	-0.03	0.19	0.54	0.51	0.42	-1.62	-0.01
Range	194.14	153.3	28.48	59.56	26.80	20.61	15.82	13.72	54.78	7.76	3.02	3.78
Minimum	12.79	0.6	0.6	1.4	2.74	8.93	4.88	2.13	6.18	2	0.60	1.40
Maximum	206.93	153.9	29.08	60.96	29.54	29.54	20.7	15.85	60.96	9.76	3.62	5.18
Sum	2207.44	890.78	736.88	1316.66	722.13	294.08	184.1	109.96	1079.03	98.94	25.77	27.67
Count	37	75	74	67	46	15	15	15	42	19	9	9
Confidence Level (0.95)	15.14	4.06	1.56	3.65	2.11	2.72	2.14	2.39	4.07	0.98	0.66	0.81

1 Based on the description of the Rev-1 borehole, the 153.9 m thick coarse unit could have been divided into cyclothems only in a speculative manner. To avoid this the data were omitted from this column and from any further calculation.

2 All fining-upward cyclothems: fully developed, half cyclothems as well as the coarse part of those cyclothems which were overlain by thick uniform mudstone units. The separation of the argillaceous units belonging to the fining-upward unit from the thickly bedded ("truly") overbank deposits was impossible in the latter case. For example, Har-1 commences with a 24.08 m thick coarse unit which is overlain by a 34.75 m thick argillaceous unit with a minor sandbody. The upper limit of the fining-upward cyclothem was placed at the base of the fine unit. Half cyclothems are those which lack of the argillaceous upper part. They are truncated either by the succeeding coarse unit or Quaternary deposits. For instance, the 2.74 m sandstone in the upper part of Bre-2 is probably a truncated half (or less?) cyclothem.

3 Only fully developed fining-upward cyclothems were analysed (half cyclothems or those overlain by thick fine-grained units were omitted).

4 Only those argillaceous rocks were included which were not part of the fining-upward cyclothems.

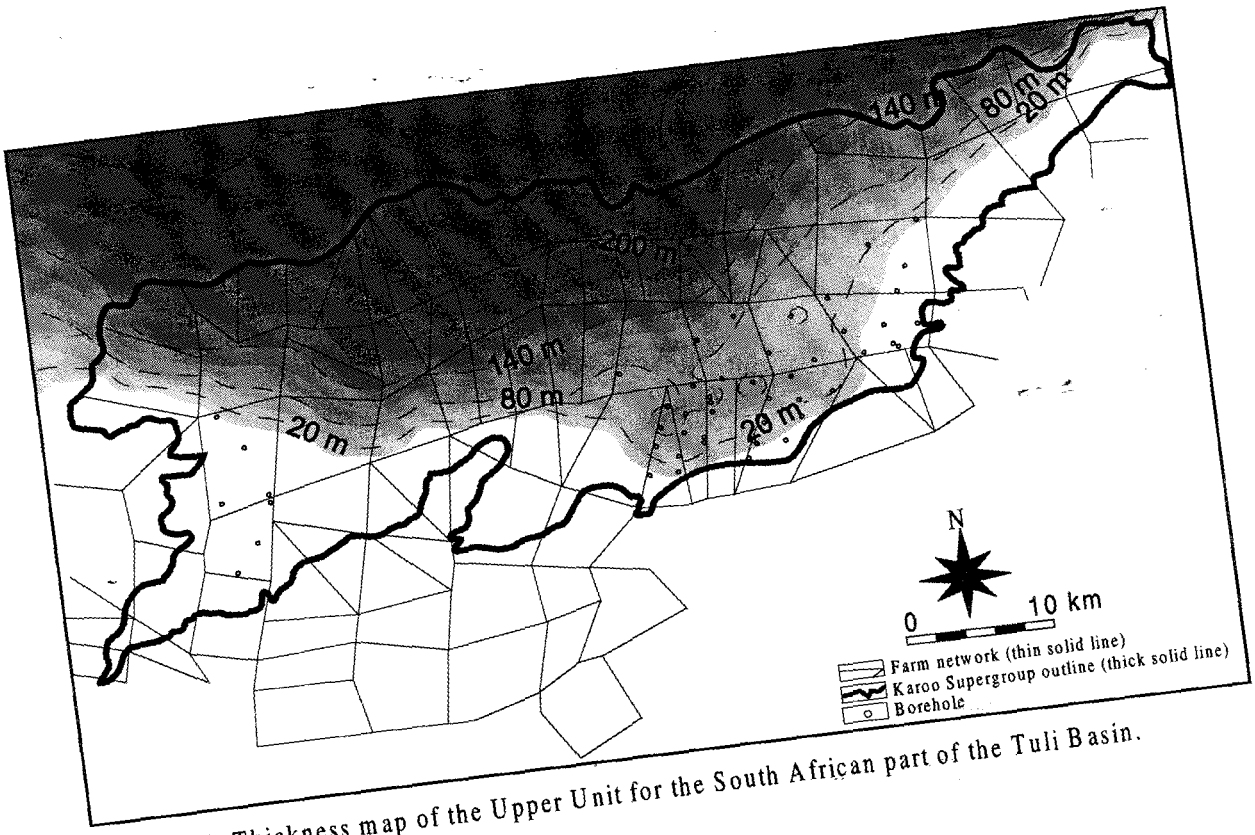

Fig. 41. Thickness map of the Upper Unit for the South African part of the Tuli Basin.

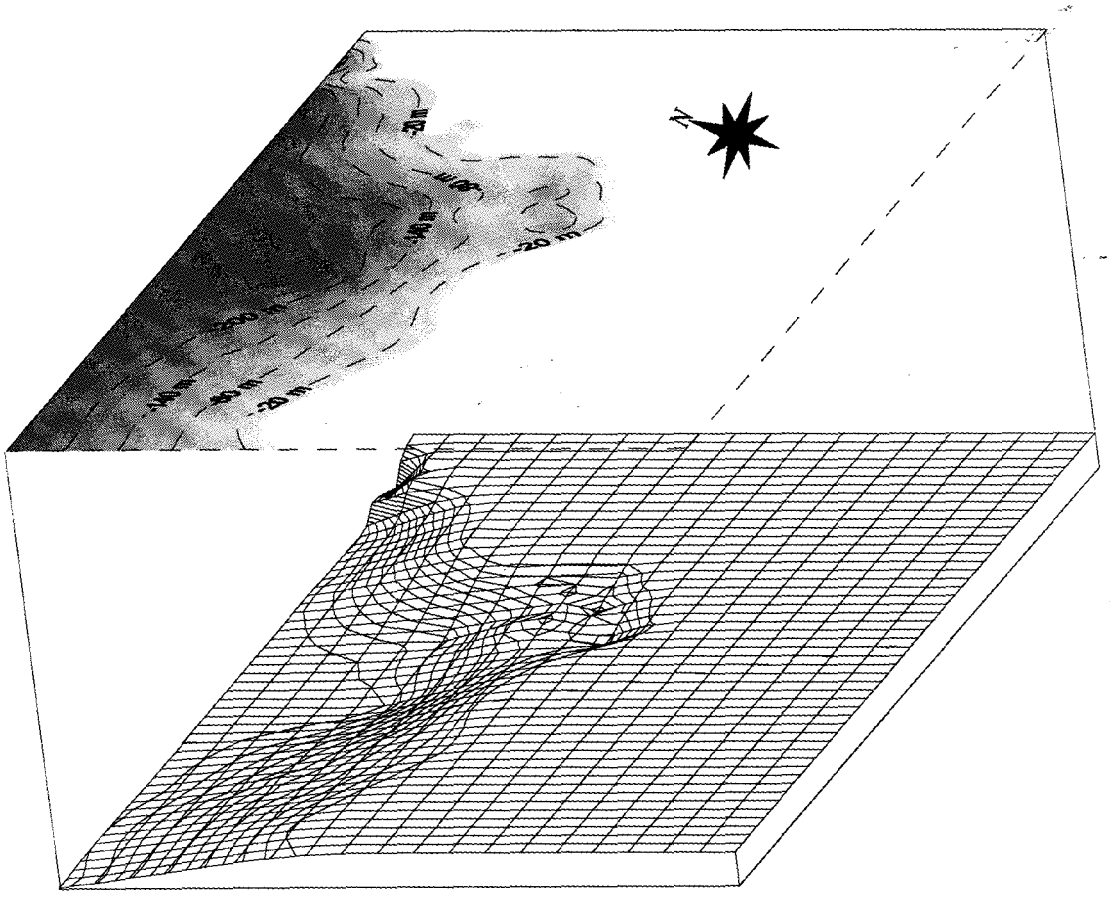

Fig. 42. Relief of the pre-Upper Unit surface.

The lowermost part of the above-defined Upper Unit may correlate with the upper, calcrete glaebule-bearing part of the Bosbokpoort Formation of Chidley (1985), whereas the rest of the unit corresponds to the Red Rock Member of Chidley's (1985) Clarens Formation.

The Upper Unit is composed of two sedimentary facies assemblages:

1. Sandstones (Sm, Sh, Sl, St, Sp, Sr) with subordinate (~1%) intraformational conglomerates (Gcm, Gh, Gp, Gt) and desiccated mud drapes (Fm);
2. Fine-grained strata (Fsm, Fs, Fl) containing glaebular calcretes; a silcrete horizon (S); subordinate sheet-like sandstones (Sm, Sh, Sp ~5%); intraformational breccias (Gmm <0.25%; Gcm <0.25%; Sc ~3%) and conglomerates (Gh <0.25%).

The outcrops of the two facies assemblages are confined to clearly distinguishable zones, but there are certain outcrops where the simple two-fold subdivision is inadequate to identify the complex of facies shown. For instance, some of the mudstones, either as mud drapes (Fm) or as <2 m thick beds (Fl, Fsm), sometimes do interbed with thicker sequences of sandstones. The statistical analysis of 37 boreholes intersecting the unit reveals that the sand vs. mud ratio is 1:1.5 (Fig. 43). This is in accordance with the outcropping frequency, as the two facies assemblages seem to be exposed in approximately equal proportion.

The generalized stratigraphic section of the unit is given in Fig. 104, and further details on the two previously mentioned facies assemblages are given in the following paragraphs.

Upper Unit	Cumulative thickness in m	Percentage %
Arenaceous deposits	890.78	40.35
Argillaceous deposits	1316.66	59.65
Total	2207.44	100

Fig. 43. Sand : mud ratio in the Upper Unit.

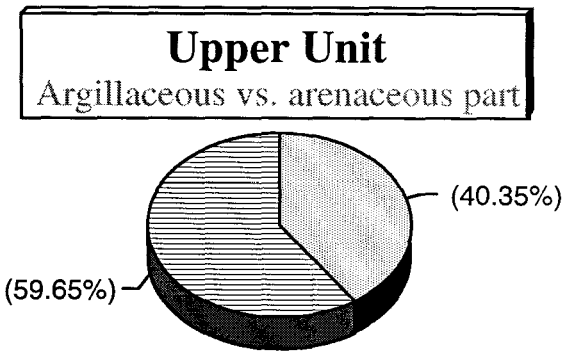

4.2.3.1. Sandstone facies assemblage

4.2.3.1.1. Sandstones

Sandstones of this facies assemblage comprise angular to subrounded, medium-well sorted, relatively clean, well-washed, predominantly very fine- to fine- or medium-grained, predominantly red-coloured quartz, feldspar and calcite particles. Detailed thin-section descriptions are presented in Appendix 4, while Ch. 4.5.4. & 5.5.3. contain the results of the modal analyses.

The sandstone beds exhibit the following internal bedding features:

- massive beds (Sm) (~70%) (*Photo 58*);
- horizontal lamination (Sh) (20%) (*Photo 59*);
- trough cross-bedding (Sh) (5%) (*Photo 60A & B, 61*);
- low-angle (Sl) and planar cross-bedding (Sp) (2.5%) (Fig. 44; Fig. 45; *Photo 62*);
- ripple cross-lamination (Sr) (type A and B) (2.5%) (*Photo 63, 64A, B & C*).

No preferential arrangement of these structures was clearly detectable in the coarse unit, although ripple cross-lamination (Sr) was more commonly found capping repetitions of Sh-St-Sp, Sh-St(Sp) and Sh-Sm (Fig. 46; Fig. 47).

Penecontemporaneous soft-sediment deformation was often observed in the form of convolute bedding (Fig. 48A, B & C; Fig. 49A & B).

The sandstones are often mud draped with mudfilms less than 0.5 cm thick, displaying desiccation features (Fm). *Photo 65A & B* present the delicate concave-up mud curls and the semi-orthogonal pattern of the mudcracks (on the bedding surface). Apart from the desiccation cracks, the bedding planes display abundant burrowing features (*Photo 66A, B, C, D & E*), rare vertebrate footprints (*Photo 67*) and other unidentified features (*Photo68A & B*). In the sandstones, broken bone fragments were observed only in two localities (*Photo 69*) (Greefswald SE & Schroda SW). Descriptions of these palaeontological findings are presented in Ch. 4.2.4.2.

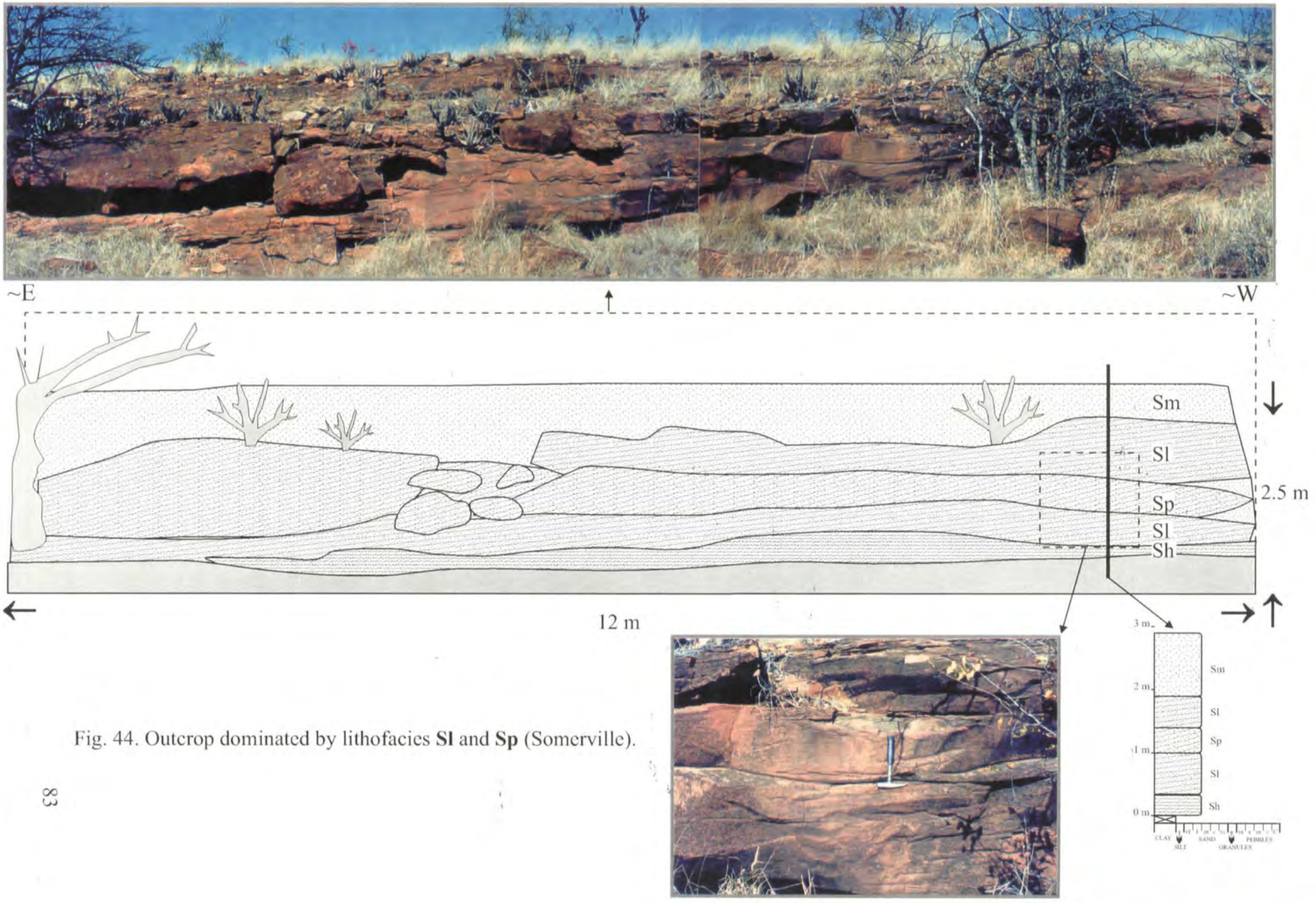

Fig. 44. Outcrop dominated by lithofacies **Sl** and **Sp** (Somerville).

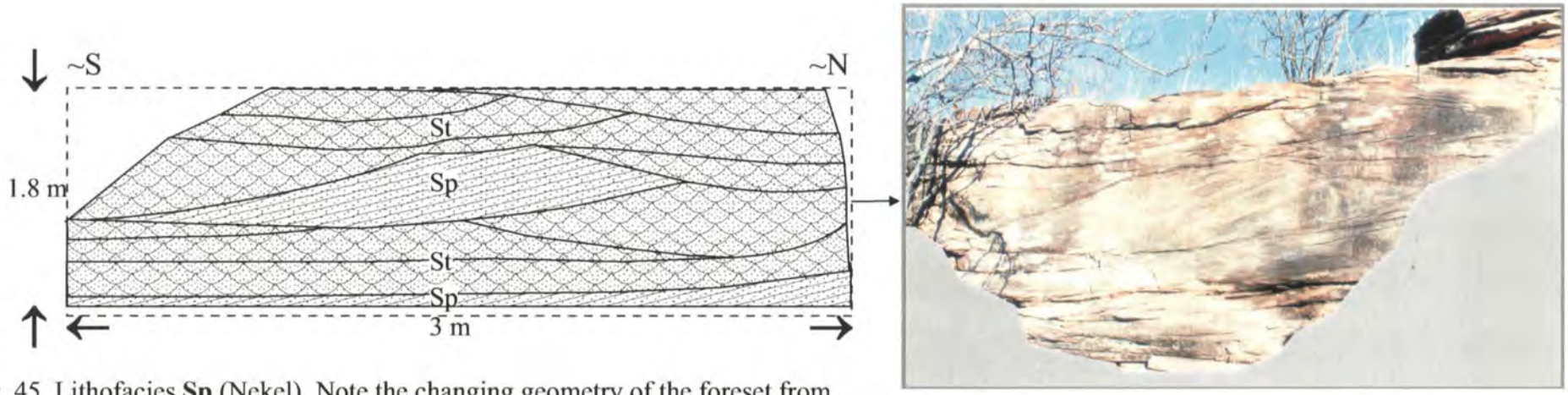

Fig. 45. Lithofacies **Sp** (Nekel). Note the changing geometry of the foreset from tangential to planar and the back to more tangential. Flow direction from right to left.

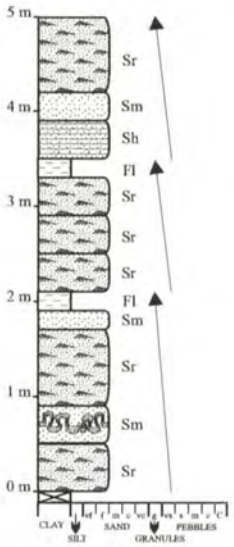

Fig. 46. Sedimentological log of three fining-upward cyclothems. The third cyclothem shows a common semi-sequence consisting of Sh-Sm-Sr (Lizzulea).

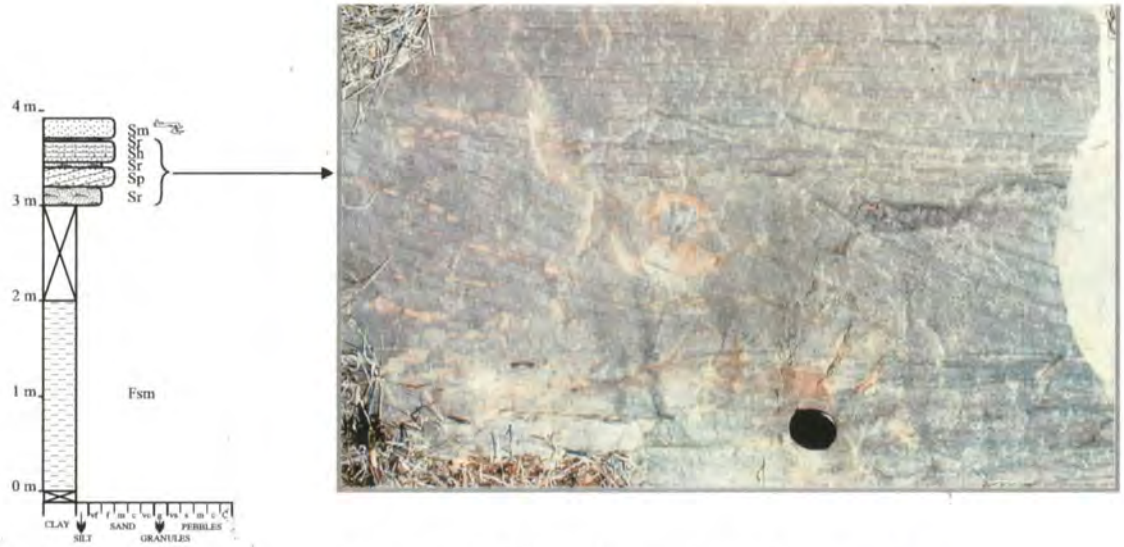

Fig. 47. Semi-sequence of Sp-Sr and Sh-Sr. The last Sr bed is covered by a mudfilm (Weipe).

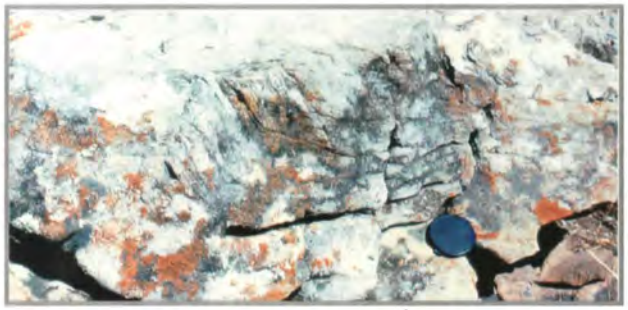

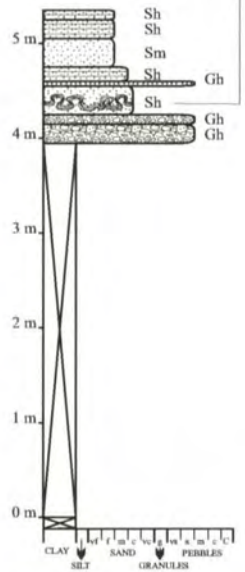

Fig. 48. Convolute bedding in coarse sandstone (Lucca).

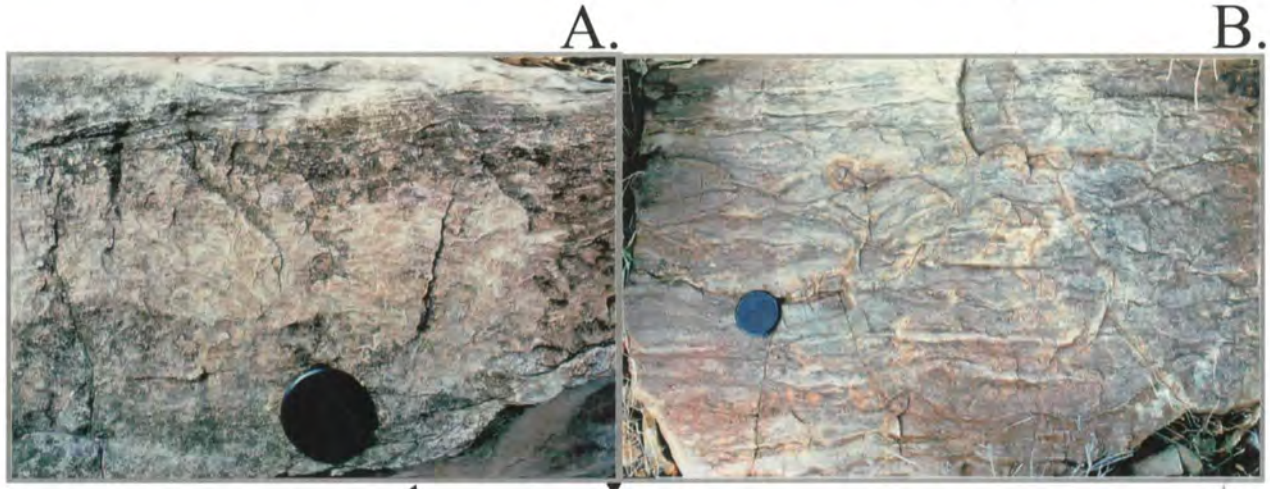

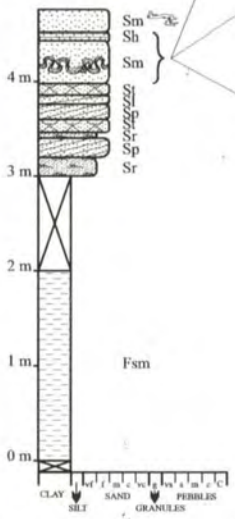

Fig. 49. Convolute (A, B) and slightly disturbed bedding (C) in fine sandstone (Weipe).

The outcrops of the sandstone facies assemblage have lateral extent in the order of less than a few tens (Fig. 50) to more than one hundred metres (*Photo 70*). The 10-30 cm, rarely more than 40 cm thick beds (Fig. 51A, B & C) have generally tabular geometry (Fig. 52; *Photo 71, 72)*, although lenticular bedforms were also noticed (Fig. 53; Fig. 54). The sandstones form multistoried *(Photo 73)*, stacked, slightly upward-fining cyclothems (Fig. 55A & B, *Photo 74*) capped by laminated or massive, 0.05 to about 1.5 m thick red siltstones and mudstones (Fm, Fl, Fsm) (Fig. 56). In outcrops, these cyclothems are rarely thicker than 10 metres (*Photo 75*). Fifteen cyclothems were statistically analysed from borehole records. The average fining-upward cyclothem consists of ~63% sand and ~37% mud (Fig. 57). The results also show that the coarse part of the cyclothems is generally 5 to 15 m thick (~73%), while the fine unit of the cyclothems is usually less than 5 m thick (40%) (Fig. 58A, B & C).

The cyclothems are characterized by sharp, non-channelized bases and truncated upper contacts (Fig. 59; *Photo 76A & B*). Very rarely, the individual, erosively based cyclothems commence with basal lag horizons of 0.5 m thick intraformational conglomerates or breccias of rip-up sandstone and mudstone clasts (*Photo 77*); however, in most cases basal lag deposits are absent. Within the cyclothems, shallow scour-and-fill structures were observed. In fact, most of the bedding surfaces within sandstones are erosive, and whereas, in the fine-grained beds, the surfaces are rather smooth, sharp and continuous (Fig. 60), the coarser-grained beds are often bounded by shallow scour surfaces (Fig. 61). Commonly, the cyclothems may not show grain size variation, but the bed thickness (Fig. 62) and the scale of the sedimentary structures decreases upwards. No evidence of lateral- or downstream-accretion nor channel-cutbanks have been found in any of the deposits.

4.2.3.1.2. Intraformational conglomerates

The reddish-greyish intraformational conglomerates form only about 1% of the sandstone facies assemblage and range in thickness from <0.1 m to 1 m. They consist of granule- to pebble-grade white, well-rounded carbonate concretions, septaria and nodules (~80%) (*Photo 78A & B*); white to reddish, subangular to subrounded mudstone clasts (~10%) (*Photo 79A & B*); red, subangular to

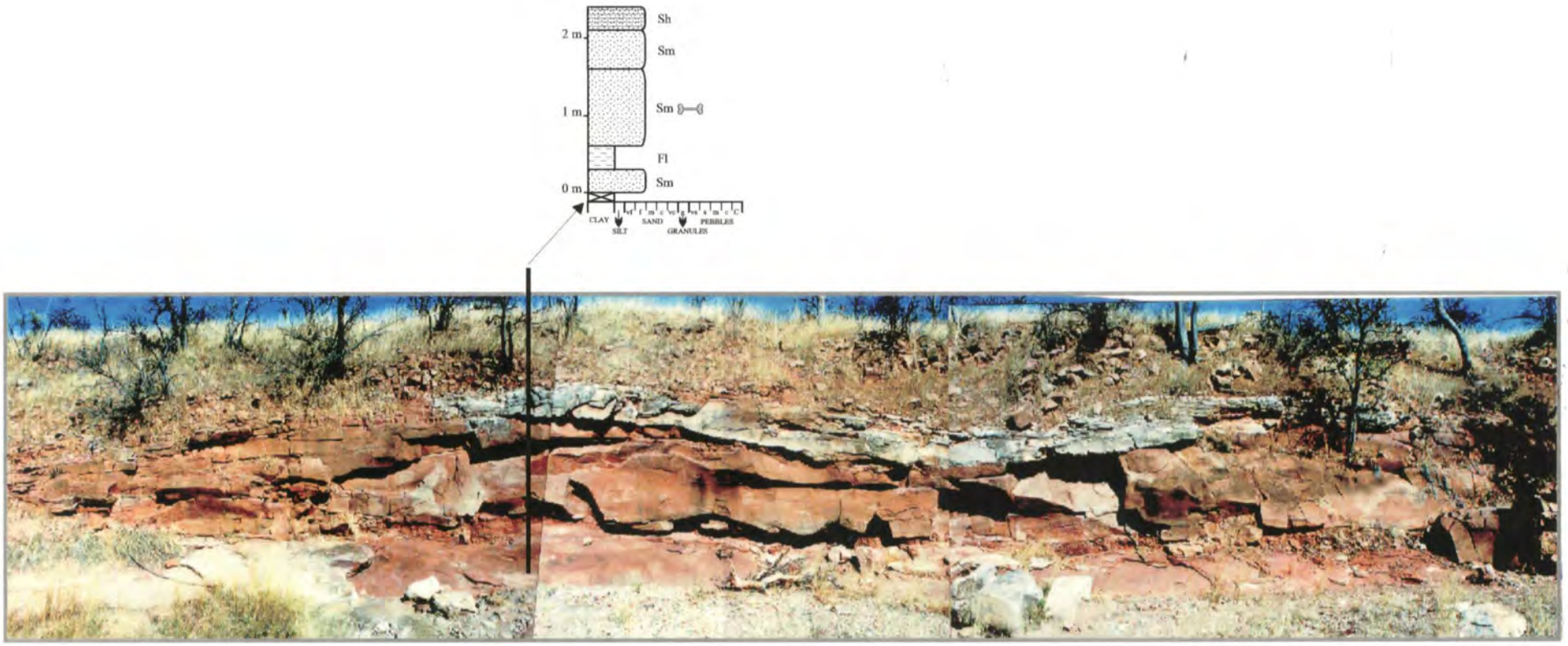

Fig. 50. Sandstone beds of limited lateral extent (Schroda). The top of the mudstone is terminated by a 5th order bounding surface.

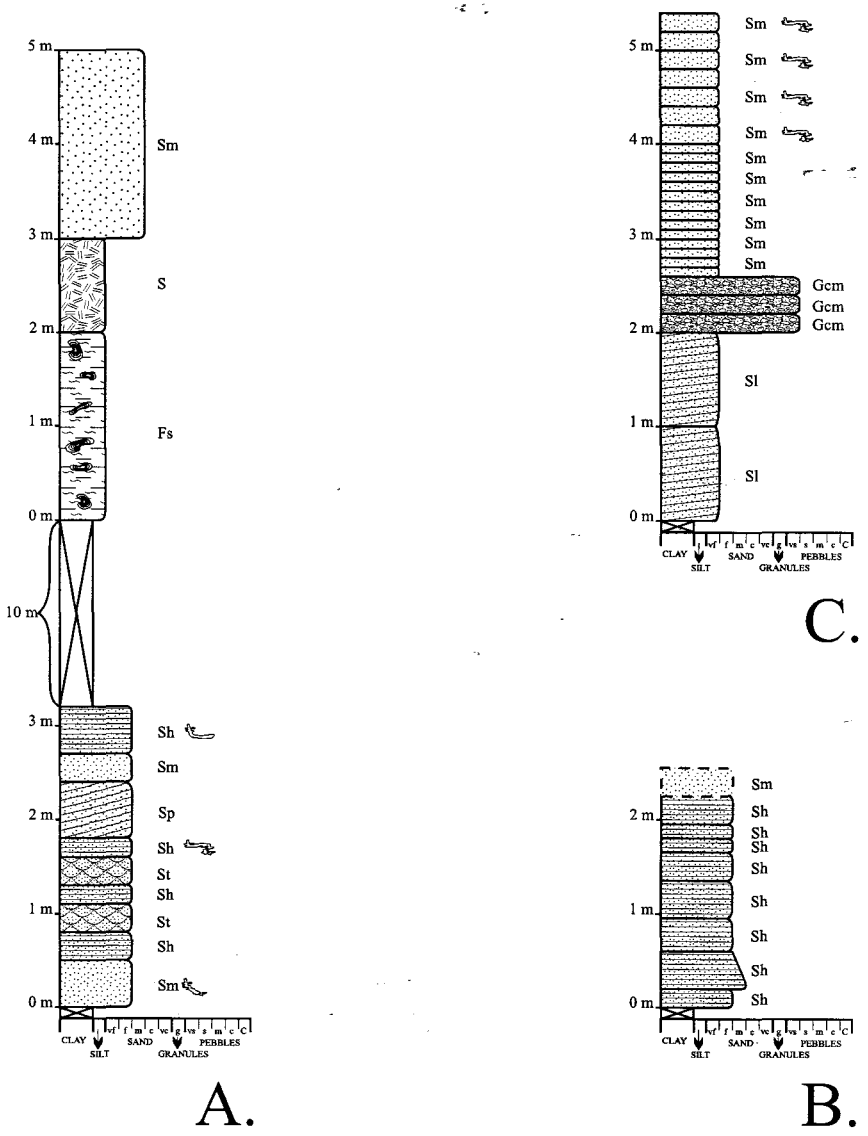

Fig. 51. Most of the sandstone beds are less than 0.5 m thick. Thicker beds are rare (lower part of log C) (A - Hamilton; B - Riedel; C - Edmonsburg).

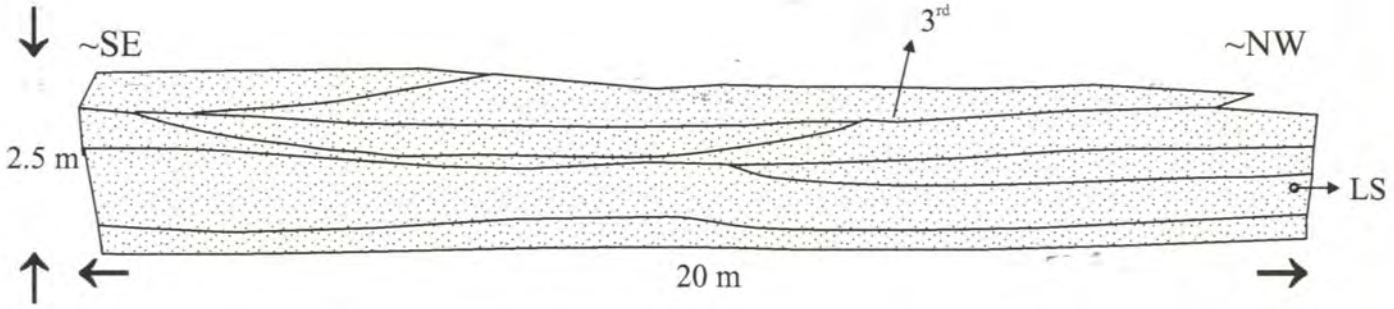

Fig. 52. Tabular sandbodies bounded by 3rd order surfaces in the middle part of the Laminated Sand Sheet (LS) architectural element (Edmondsburg).

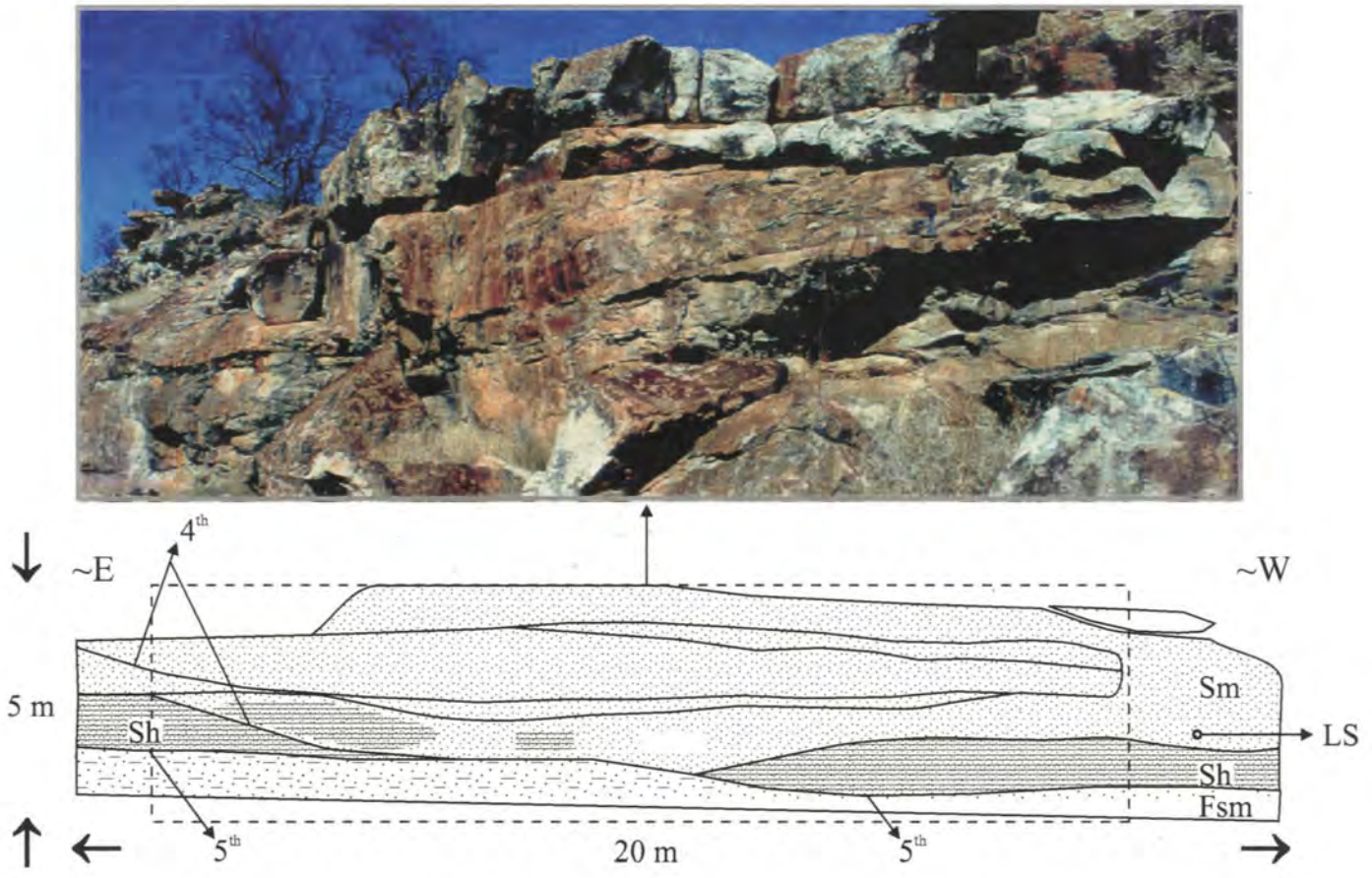

Fig. 53. Two slightly lenticular beds bounded by sharp, smooth 4th order surfaces. These two minor channels are found within a Laminated Sand Sheet (LS) architectural element bounded by 5th order surface (Parma).

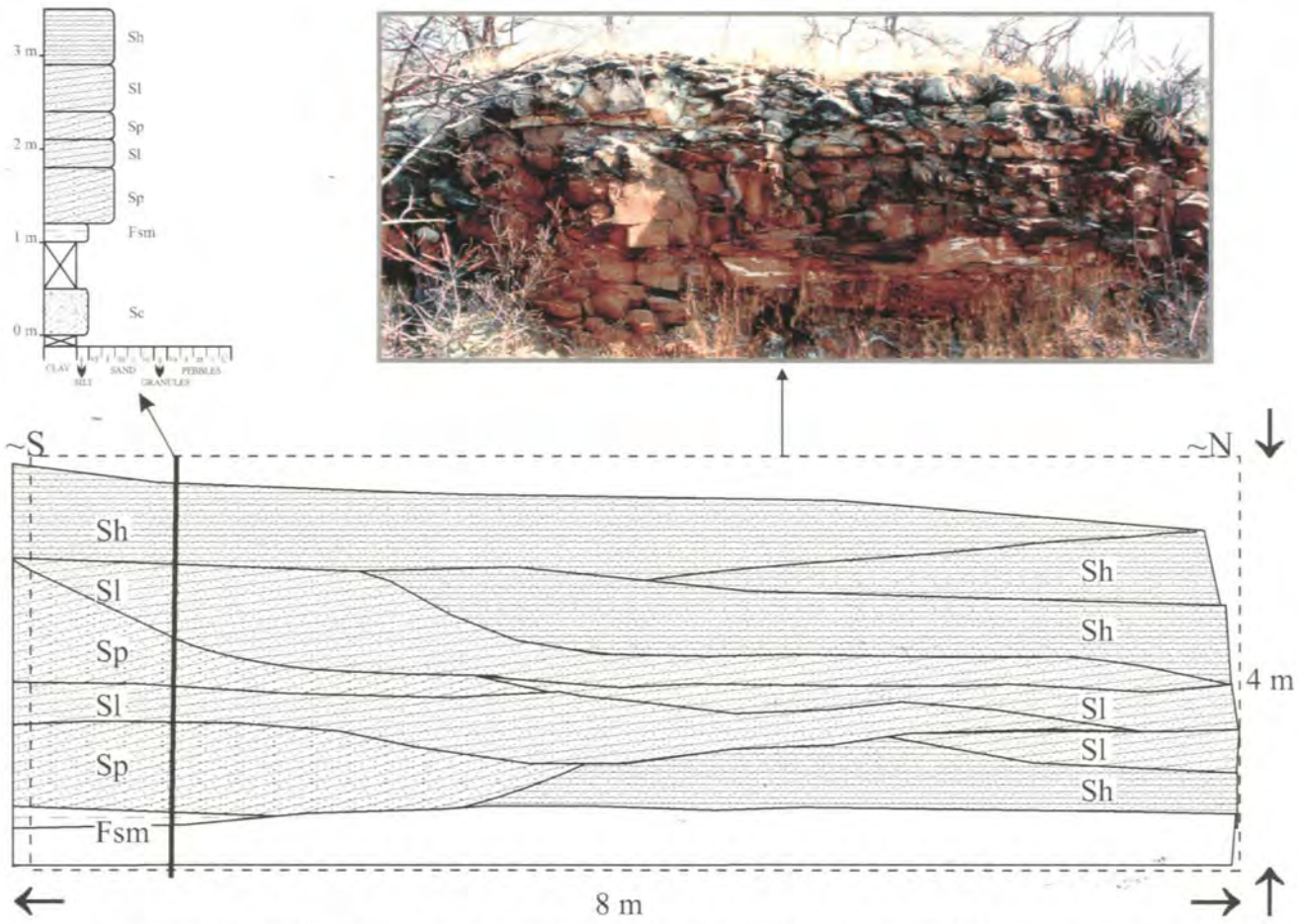

Fig. 54. Lenticular bedforms in the lower part of a Laminated Sand Sheet (LS) architectural element. Internal scour surfaces are of 3rd order (Hamilton).

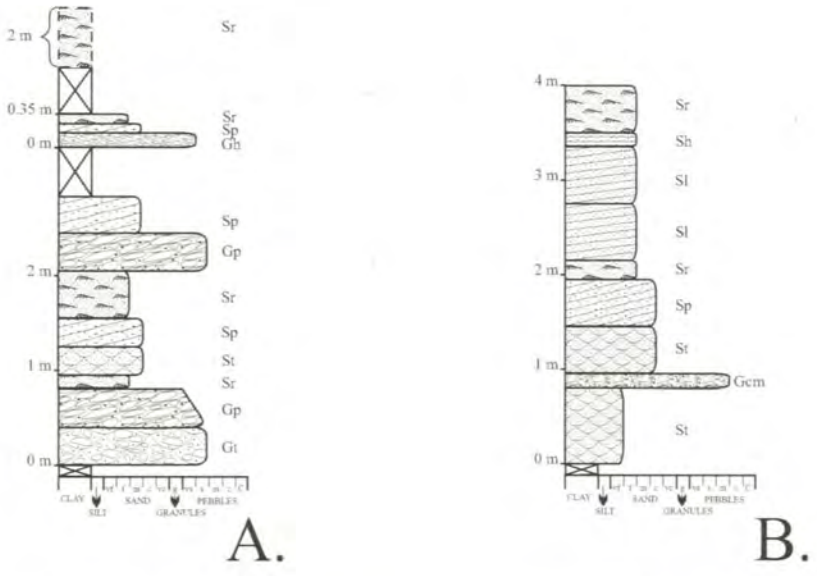

Fig. 55. Logs of slightly upward-fining cyclothems (A- Blyklip; B - Edmondsburg).

Fig. 56. The 1.5 m thick red, laminated mudstones (Fl) capping the top of a sandy facies association (guard stands on it) (Schroda).

FU Cyclothems	Cumulative thickness in m	Percentage %
Coarse part	184.13	62.62
Fine part	109.9	37.38
Total	294.08	100.00

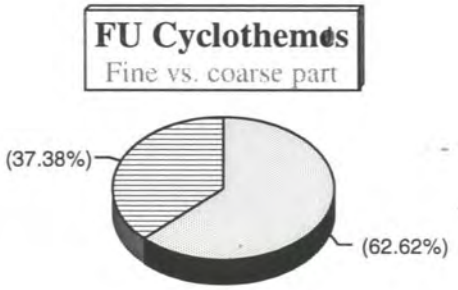

Fig. 57. Sand : mud ratio in the fining-upward units is roughly 1:3. Data based on 15 cyclothems identified in borehole record.

Bin	Frequency
0	1
5	4
10	7
15	2
20	1
25	0

A.

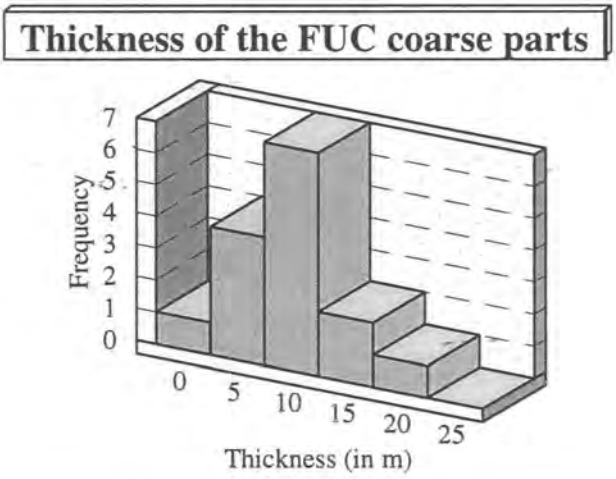

Bin	Frequency
0	6
5	4
10	4
15	1

B.

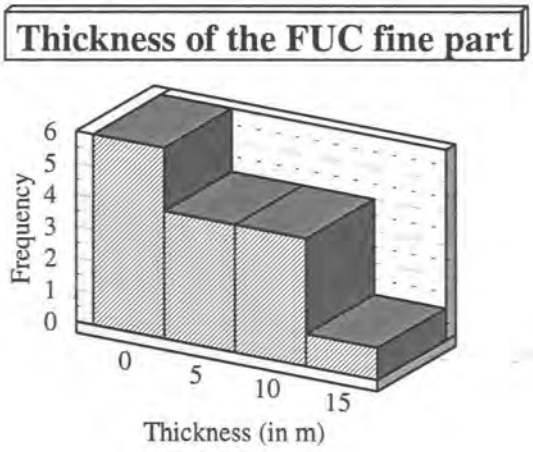

Bin	Frequency coarse part	Frequency fine part
0	1	6
5	4	4
10	7	4
15	2	1
20	1	0

C.

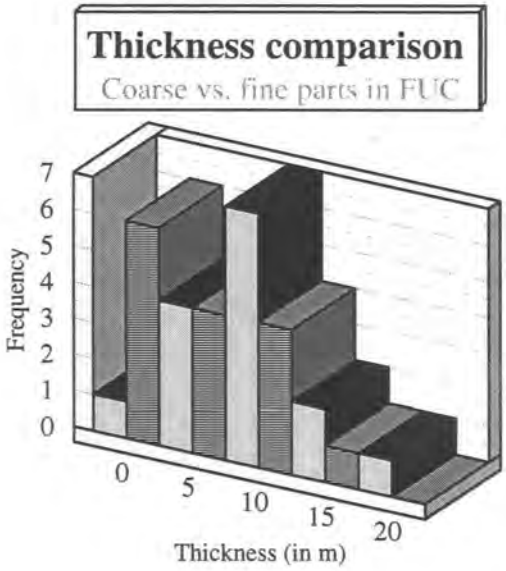

Fig. 58 A, B & C. Histograms showing the thickness of the coarse and fine part of the fining-upward cyclothems (FUC). Data based on 15 cyclothems identified in borehole record.

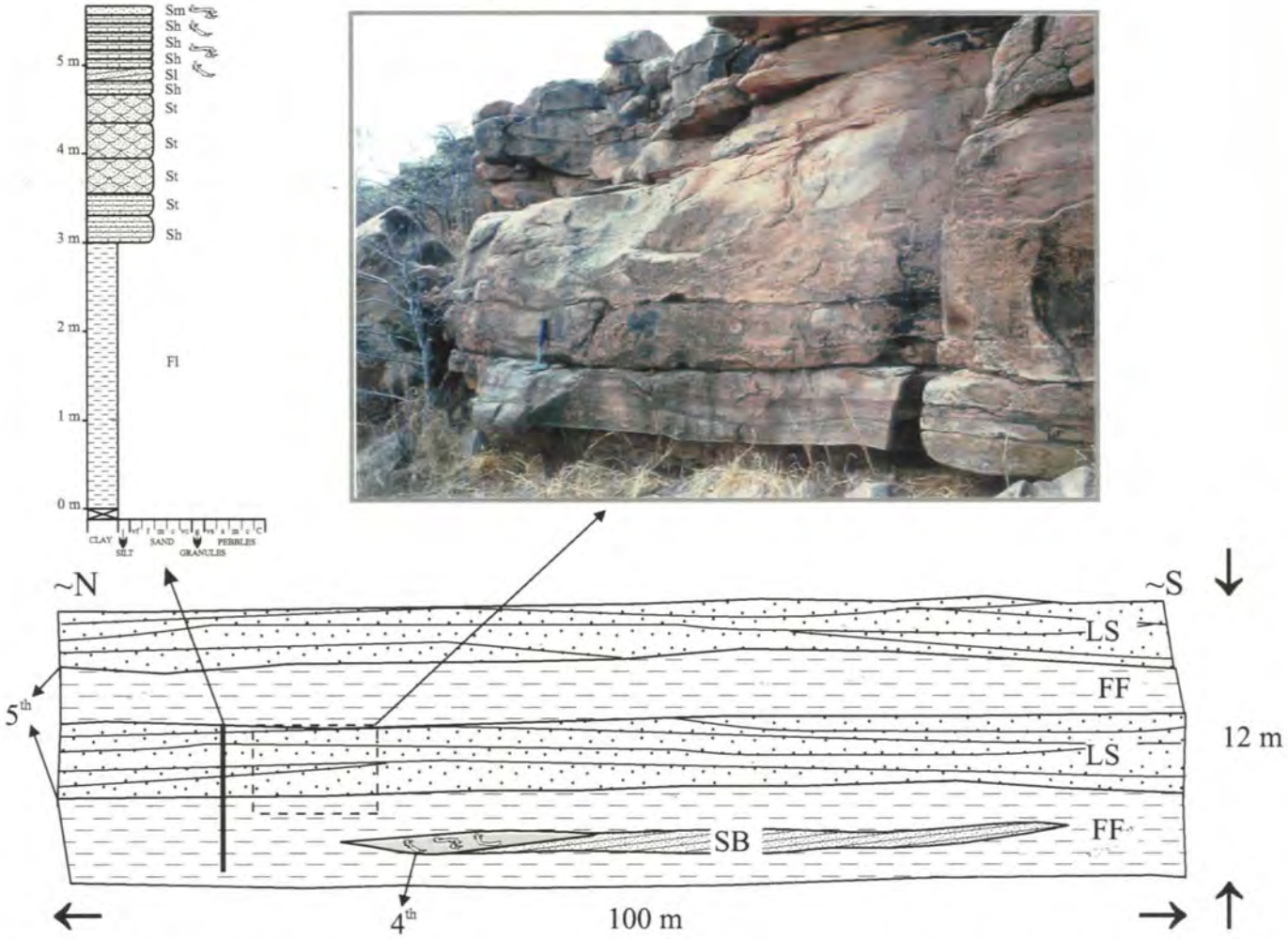

Fig. 59. The fully developed fining-upward cyclothem (in the middle of the outcrop outline) shows the sharp, non-channelized base and truncated upper contact of the architectural element LS. The truncating upper cyclothem is half way eroded. Other elements are overbank fines (FF) with a minor Sandy Bedform (SB) (lower part) (Weipe).

Fig. 60. Erosive, smooth, flat and continuous bedding surfaces (3rd order). Note the uniform bed thicknesses (Halcyon).

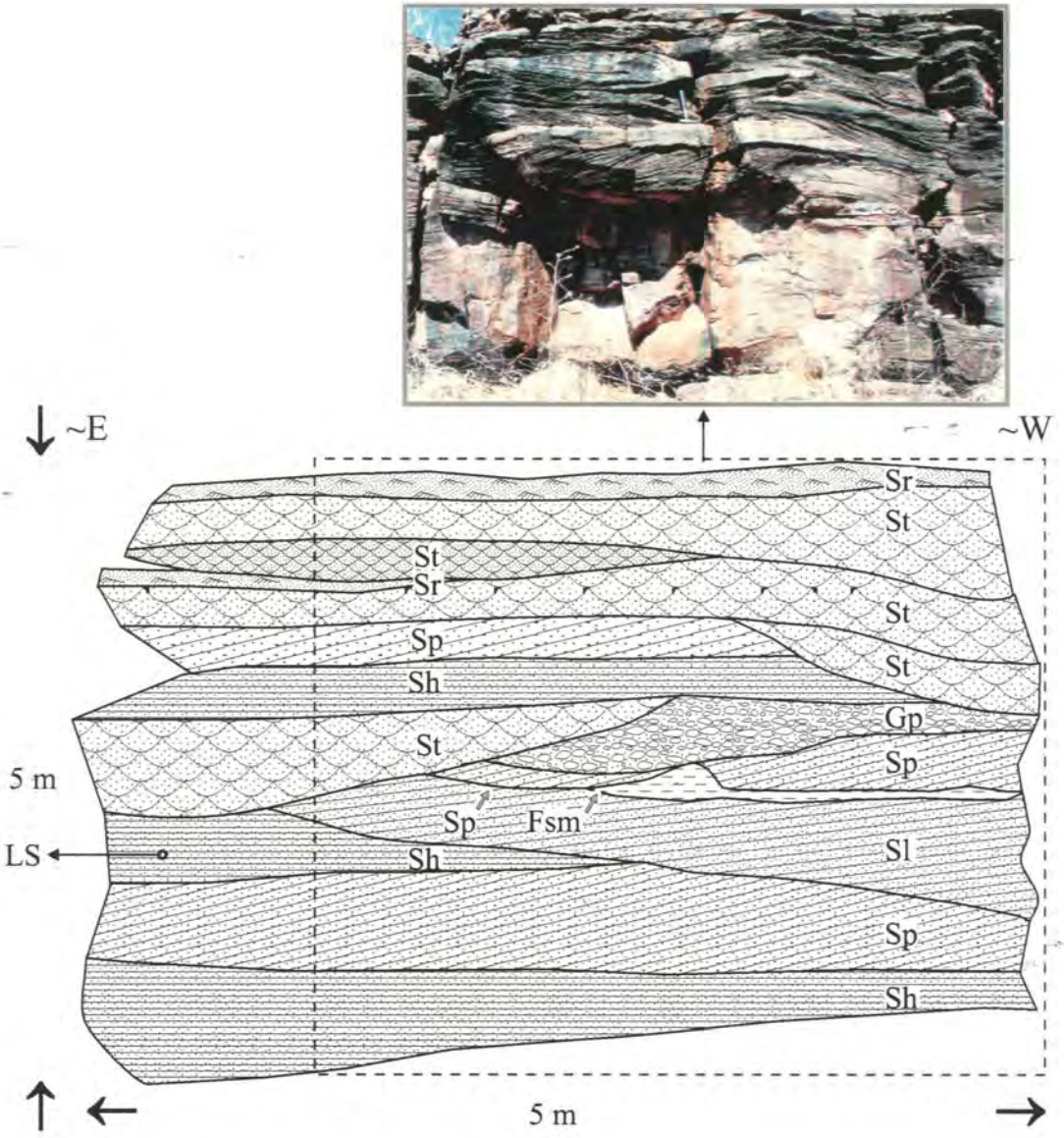

Fig. 61. Coarser grained beds bounded by shallow scour surfaces (3rd order). Note the slight fining-upward trend (Lizzulea).

Fig. 62. The beds in the upper part of the cyclothems are often thinner than those at the base. Bioturbation is also more abundant toward the top (Faure).

subrounded sandstone clasts (~10%) (*Photo 80*); reddish, subangular to subrounded isolated, broken and abraded bone fragments (<1%) (*Photo 81A & B*), and red to white, subrounded to rounded quartz pebbles (<1%). The average clast size in poorly-sorted and clast-supported conglomerates is ~2.5 cm, while the maximum diameter is 25 cm (*Photo 82*). The matrix is a red very fine sandstone, occasionally with coarse, rounded reddish quartz grains scattered throughout. The cement is uniformly carbonate, which indicates that the conglomerates are the most calcareous deposits in the unit. Most conglomerates lack stratification (Gcm) (*Photo 83*), though some display slight horizontal layering (Gh) (*Photo 84*) or cross-bedding (Gp, Gt) (*Photo 85*). The horizontal layering (*Photo 86*) as well as the foresets of the planar cross-stratified conglomerates are often defined by normal graded single pebble layers ranging in size from large pebble (6.4 cm) to granule (0.4 cm) (Fig. 63).

The intraformational conglomerates are often found at the base (Fig. 63) and/or at the middle section of the slightly fining-upward cyclothems (Fig. 64). The conglomerates are invariably topped by, or interbedded with, sandstone units. In places, the conglomerates are directly overlain by ripple cross-laminated (Sr) very fine sandstones (*Photo 87*).

In the field, the lowermost occurrence of intraformational conglomerates was observed 40 m above the lower boundary of the Upper Unit (Montrow). The thickness of the unit is estimated to be ±200 m in this area. The conglomerates were intersected by several boreholes (Lun-1, Lun-2, Gle-1,Ori-1, Ori-3, Den-1 see Appendix 3:**IX-XIV**). They seem not to be confined to one stratigraphic level, being present in various positions within the unit.

To summarise: the following features suggest that the slightly upward-fining cyclothems of the sandstone facies assemblage should be identified as Laminated Sand (**LS**) sheets:

- ❒ dominance of the lithofacies Sm, Sh with minor St, Sp, Sr, very rare (~1%) Gcm, Gh Gp, Gt;
- ❒ desiccated mud drapes on bedding planes;
- ❒ flat erosion surfaces;
- ❒ absence of channel-shape geometries.

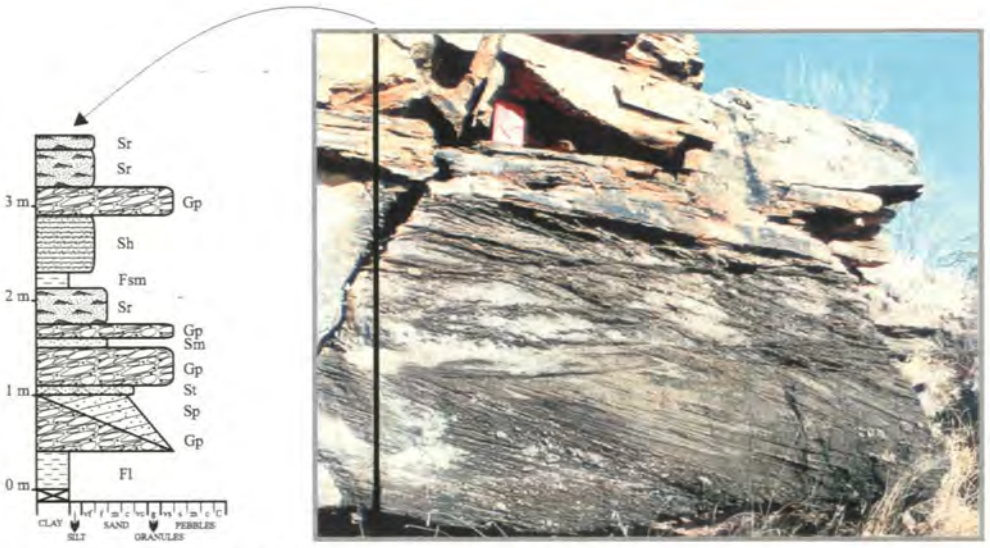

Fig. 63. A ~0.6 m **Gp** bed with foresets consisting of normal-graded, single-pebble layers ranging in size from granule (0.4 cm) to large pebble (6.4 cm). Note that within the same bed, from left to right the inclination of the foresets gradually changes from low-angle to high-angle and again low-angle (sandier) foresets. The photo captures a major fining-upward cyclothem with several internal truncation surfaces and conglomerate lenses (Lizzulea).

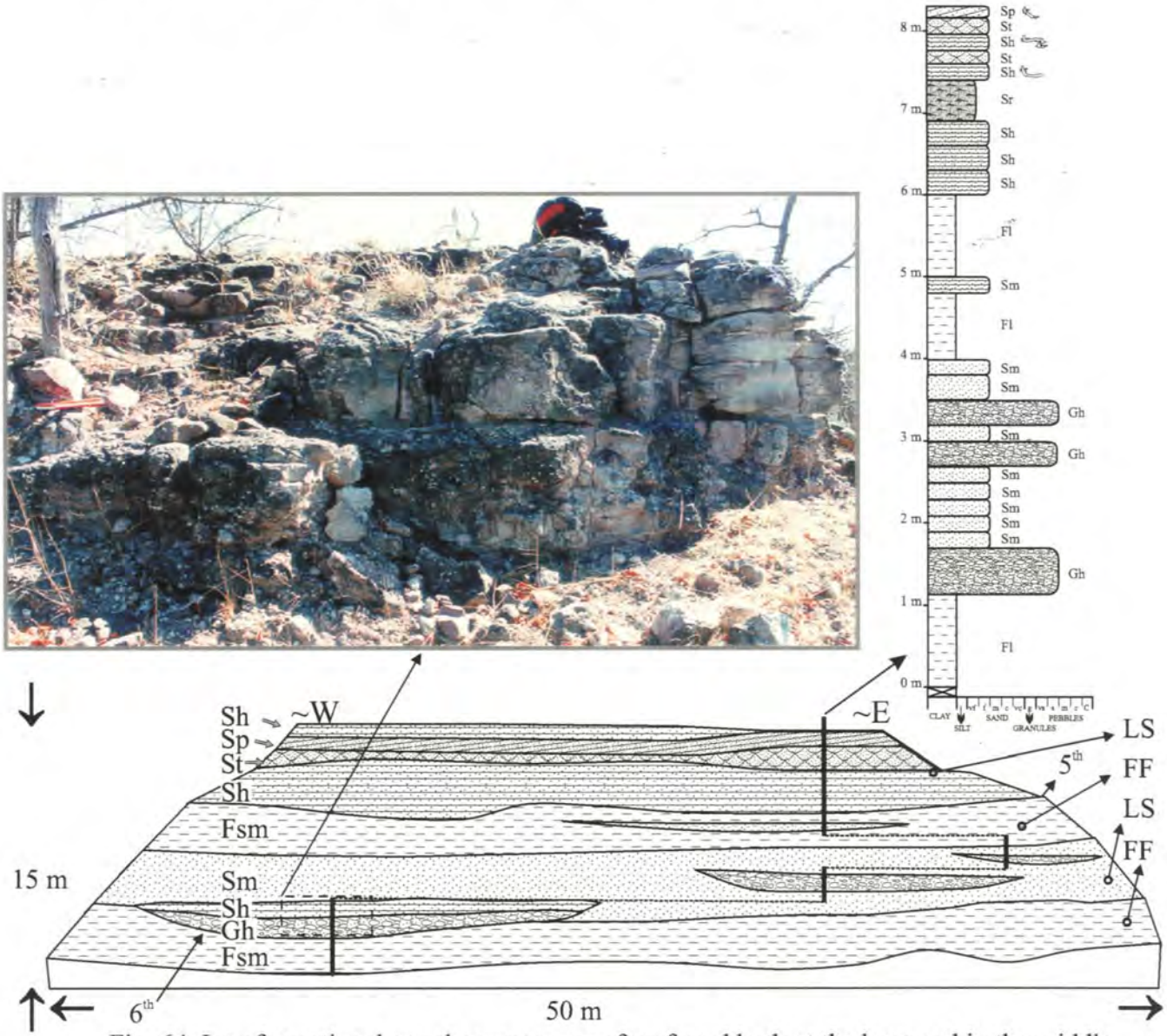

Fig. 64. Intraformational conglomerates are often found both at the base and in the middle section of the slightly fining-upward cyclothems (Nekel).

4.2.3.2. Fine-grained facies assemblage

4.2.3.2.1. Argillaceous strata

All argillaceous lithofacies types presented in the current section (4.2.3.2.) belong to the overbank fine (**FF**) architectural element. The fine-grained deposits that are found within the previously described (Ch. 4.2.3.1.) laminated sand sheet (**LS**) architectural element are relatively thinly bedded (<2 m) (Fig. 56), red, massive or laminated (Fm, Fsm, Fl) mudstones or siltstones. In contrast, argillaceous rocks that occur at certain lateral distances from the above-mentioned sandstones and thinly bedded, fine-grained strata, are thickly bedded (>2m) (*Photo 88*). Their colour varies from greenish to reddish (*Photo 89*). These rocks display intense colour and grain size mottling, sometimes showing a blotchy appearance (*Photo 90*). A detailed description of the colouration and its origin is given in Ch. 4.6. & 5.6. In composition, the argillaceous sediments range from pure mudstone to muddy fine sandstone or siltstones (greywacke). Most of the beds are massive (Fsm, Fs) with very rare relict lamination (Fl) (Fig. 65*; Photo 94, 110*). The mottled mudstones and siltstones often break up into equidimensional, centimetre-scale angular to subangular blocks (*Photo 91*). The carbonate cement has random patchy distribution within the fine-grained facies assemblage.

The best outcrops of the argillaceous sediments seem to be preserved only in those areas where a conspicuous 1-1.5 m thick silicrete (S) horizon underlies the succeeding Clarens Formation (*Photo 92*). The maximum outcrop thickness of the facies assemblage is 20-25 m (*Photo 88*). A detailed description of the silicrete (S) horizon and its origin is given in Ch. 4.8.

Based on differences in the frequency, thickness and grain size of the sediments as established in statistical analysis of the borehole data (Appendix 3: Table 3), the argillaceous deposits were arranged in the following three major groups:

1.) *Fine-grained strata interbedded with thicker coarse beds* of the sandstone facies assemblage. As already discussed in Ch. 4.2.3.1., these fine-grained deposits are relatively thinly (< 2 m) bedded, evenly grained mudstones or siltstones.

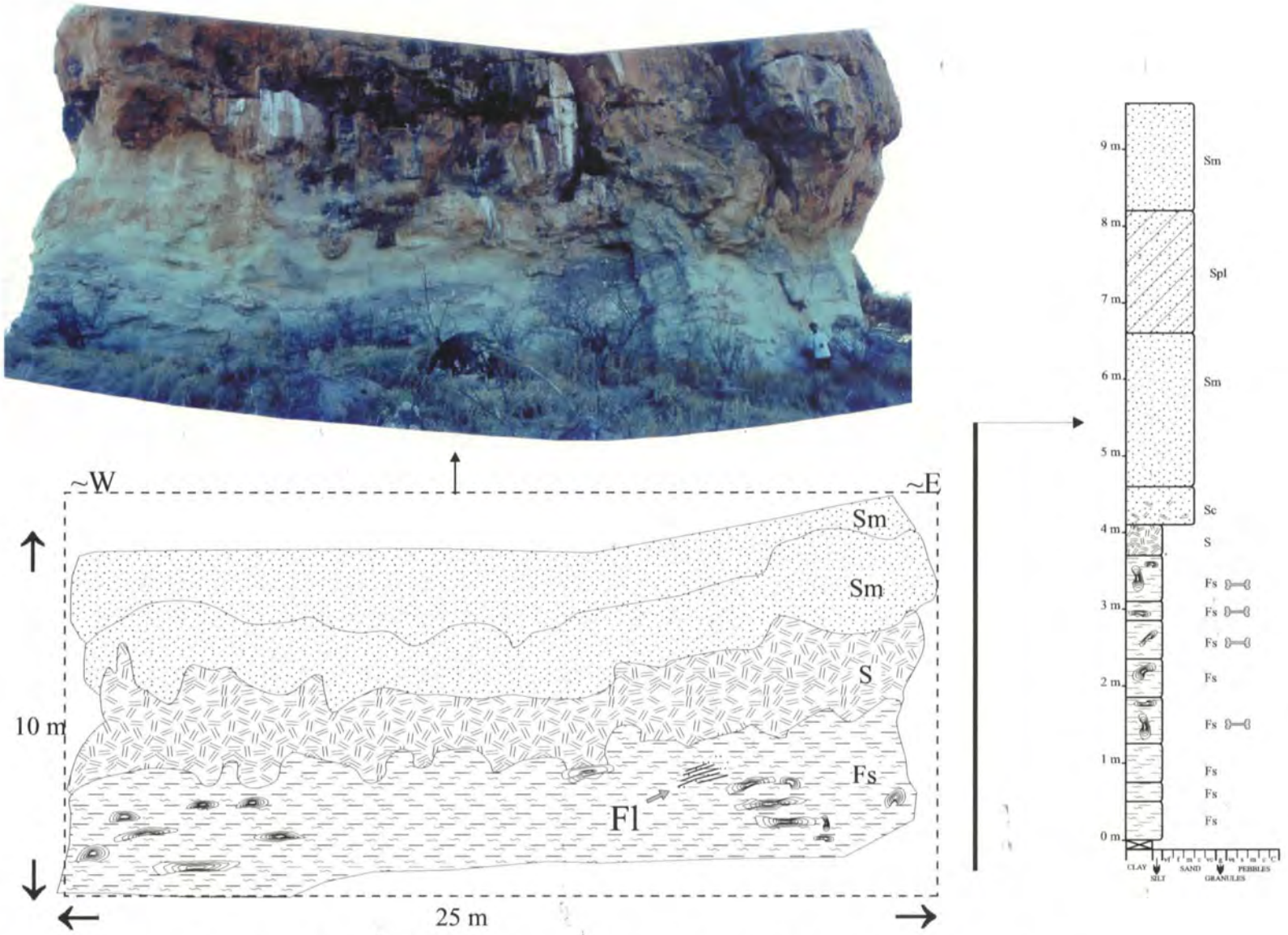

Fig. 65. Relict lamination (Fl) in otherwise massive, muddy-silty-sandy argillaceous rocks (Fs). The laminated blotch has purplish colour and lacks carbonaceous cement. The concentration of the carbonate glaebules is higher toward the top of the argillaceous beds (see log). Note the sharp upper and gradational lower boundary of the silcrete layer underlying the sandstones of the Clarens Formation (Breslau - Show of Rhodes).

2.) *Argillaceous strata without or with single, isolated sandbodies.* These argillaceous rocks are generally 10 to 30 m thick (Fig. 66)(they are referred as "overbank fines" in the figures). The average thickness is ~28 m (max. ~61 m; min. ~6 m) (Table 9). Fig. 67 is a comparative histogram of groups 1 and 2. The single, isolated sandbodies are generally 2 to 6 m thick (Fig. 68). The average thickness is ~5 m (max. ~10 m; min. ~2 m) (Table 9). The single sandbodies form ~7% of the overbank fines (Fig. 69).

3.) *Multiple sandbodies and mudstones.* These consist of alternating relatively thin sandstone and mudstone beds. The sandstone beds are generally 3 m thick (Fig.70). The average sandstone thickness is ~2.8 m (max. ~4 m; min. 0.60 m) (Table 9). The mudstone beds are generally 3 to 5 m thick (Fig. 70). The average mudstone thickness is ~3 m (max. ~5.1 m; min. ~1.4 m) (Table 9). The sand vs. mud ratio in the multiple sandbodies and mudstones is approximately 1:1 (Fig. 71).

In most places, the distinctive feature of the argillaceous sediments is the presence of isolated, hard carbonate glaebules in the form of nodules (*Photo 93, 94*), concretions (*Photo 95*) and septaria (*Photo 96 A & B*). These range in size from a few centimetres to decimetres, and are concentrated in the upper part of the individual argillaceous beds (see log in Fig. 65). The gradational lower and sharp upper contacts of the carbonate accumulations (*Photo 97*) are especially evident below the prominent silcrete already mentioned. Other occasionally observed, distinguishing features are the continuous horizons of carbonate glaebules (*Photo 98*), the meshwork of mainly horizontal and vertical white calcite veins and the pseudo-folded carbonate layers (*Photo 99*). The detailed description of the carbonate accumulations and their origin is given in Ch. 4.7. & 5.7.

The prominent silcrete horizon (*Photo 88, 91, 92)* is fully presented in Ch. 4.8. & 5.8.

In the outcrops, significant numbers of vertebrate fossils were found, besides the carbonate and silcrete accumulations, also towards the top of the beds. The lowermost *in situ* bone fossil (overlain by bone-bearing conglomerates) was found in an outcrop which is situated only 40 m above the lower boundary of the Upper Unit. This outcrop is located in the eastern part of the study area

Bin	Frequency
5	2
10	6
15	6
20	5
25	6
30	4
35	5
40	2
45	4
50	0
55	1
60	1

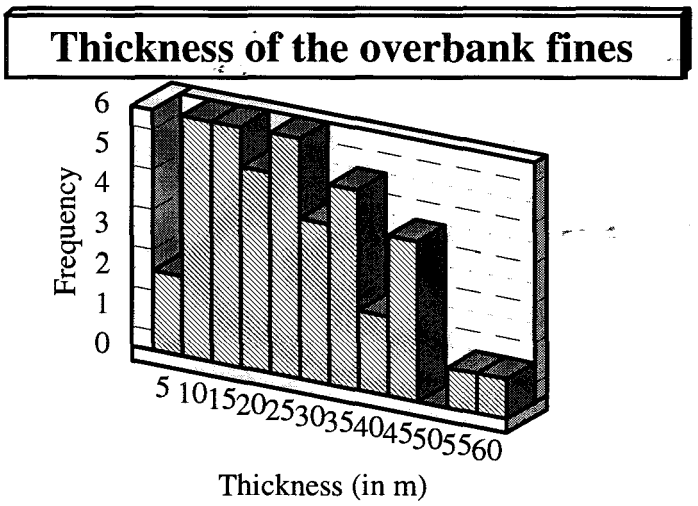

Fig. 66. Thickness of the argillaceous strata without or with single sandbodies (group 2). Thicknesses are calculated with the exclusion of the sandbodies.

Bin	Frequency overbank fines	Frequency FUC fines
0	0	6
5	2	4
10	5	4
15	6	1
20	4	0
25	5	0
30	2	0
35	5	0
40	2	0
45	3	0
50	0	0
55	1	0
60	2	0

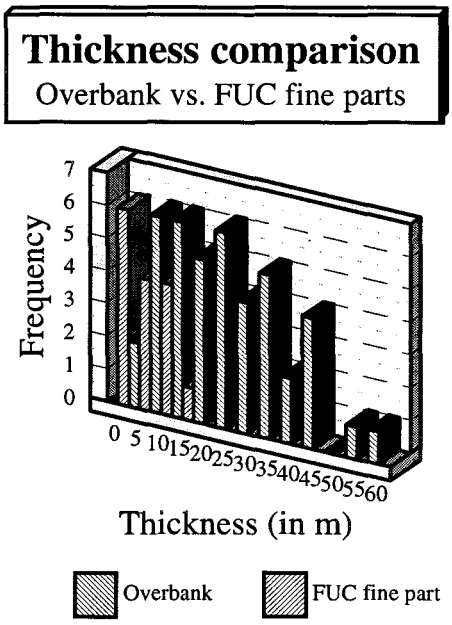

Fig. 67. Thickness comparison of the argillaceous strata without or with single sandbodies (group 2) and the fine part of the fining-upward cyclothems (FUC)(group 1).

Bin	Frequency
0	0
2	6
4	6
6	5
8	2

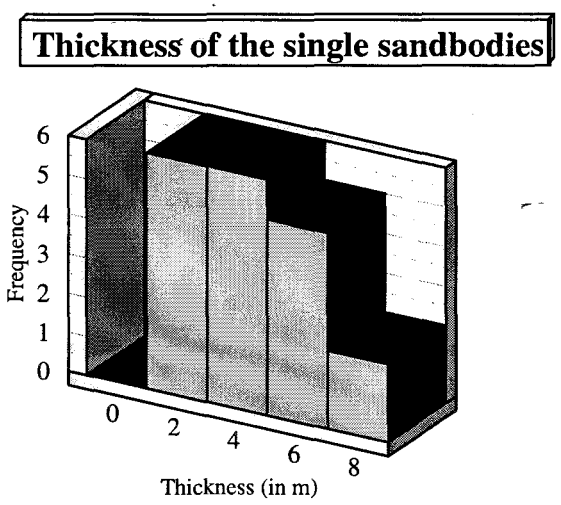

Fig. 68. Thickness of the single, isolated sandbodies.

Single sandbodies in overbank mudstones	Cumulative thickness in m	Percentage %
Coarse part (sand, silt)	98.94	6.99
Fine part (all overbank mudstones)	1316.66	93.01
Total	1415.60	100.00

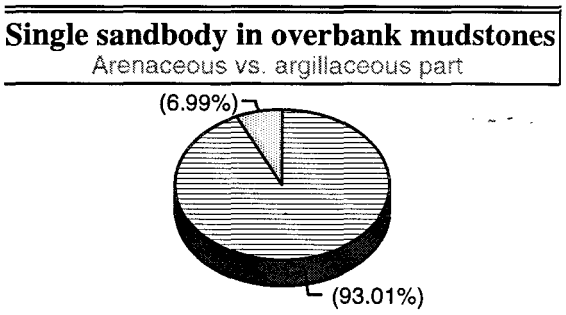

Fig. 69. Sand : mud ratio based on the thicknesses of the single sandbodies that are found isolated in thick mudstones.

Bin	Frequency sandstones	Frequency mudstones
0	1	0
1	0	3
2	3	0
3	5	5
4	0	0
5	0	1

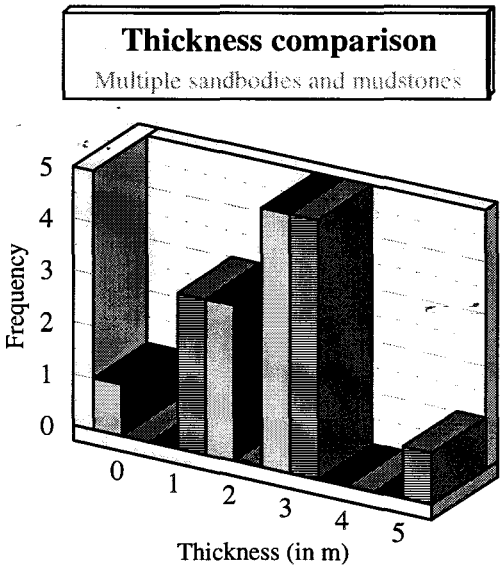

Fig. 70. Thickness comparison of the multiple sandbodies and mudstones.

Multiple sandbodies and mudstones	Cumulative thickness in m	Percentage %
Coarse part	25.77	48.22
Fine part	27.67	51.78
Total	53.44	100.00

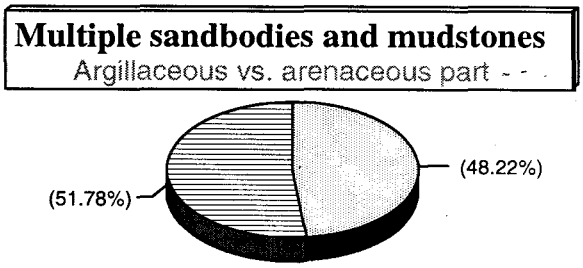

Fig. 71. Sand : mud ratio based on the thicknesses of the alternating sandbodies and mudstones.

(Montrow) where the thickness of the Upper Unit was estimated to be ~200 m (calculation based on field observations and geological cross-sections). Bone fossils were reported from two boreholes as well: Den-1 (62 m below the boundary between the Upper Unit and Clarens Formation, 140 m above the boundary between the Middle and Upper Units, in the lower upper part of the unit); and Rev-1 (145 m below the surface of the unit, 62 m above the boundary between the Middle and Upper Units, in the upper lower part of the unit). Most of the vertebrate remains are disarticulated; *Photo 100* portrays a relatively rare, exceptional case. In general, the fossils show little or no abrasion (*Photo 101 A, B, C, D, E & F*), but there are a few fragmented bones as well (*Photo 102 A, B, C & D*). The vertebrate fossils are presented in Chapter 4.2.3.3.

4.2.3.2.2. Sheet sandstones

In some of the outcrops, sheet like sandbodies were recognized within thick (>10 m) argillaceous deposits (lower part of Fig. 72) (see groups 2 & 3 in Ch. 4.2.3.2.1.). These beds form less than 5% of the fine-grained facies assemblage. The internally massive (Sm) and very rarely horizontal laminated (Sh) (*Photo 103*) or planar cross-laminated (Sp) (*Photo 104*), very fine- to fine-grained sandstone beds have sharp lower (*Photo 105*) and less definite, but planar upper surfaces, grading into laminated or bioturbated mudstone (*Photo 106*). Often, the sandstones are also bioturbated and may contain scattered angular mud pellets as well as very fine sandstone clasts (<5% e.g. Ratho, Schroda and Greefswald).

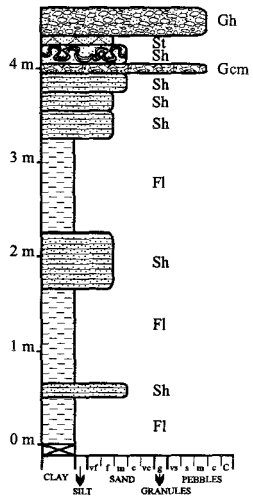

Fig. 72. Thick and thin sheet-like, single sandbodies within thick argillaceous deposits.

Two types of sandbodies were differentiated, according to their frequency of occurrence within the argillaceous deposits:

1.) *Single, tabular sandbodies (~1 m)* showing greater lateral continuity without any thinning for well over 50-80 m (*Photo 106*). Thinner (<0.5 m), narrower (<3 m) but also single, isolated sandstone beds with a lenticular or wedge shape *(Photo 107A & B)* were also observed in this category.

2.) *Multiple sandbodies and mudstones* are perhaps the outcrop equivalent of rocks presented in Group 3 (see section 1.2.1.). These superimposed sheets of sandstones and mudstones *(Photo 108A)* show great lateral continuity *(Photo 108B).* Their outcrop was found in the vicinity of major sand facies assemblage exposures.

These isolated, sheet-like sandstones were identified as sandy bedforms (**SB**) because of their internal structures, overall geometries and relations to the surrounding rock formations.

4.2.3.2.3. Intraformational breccias and conglomerates

The red intraformational breccias form <0.5% of the fine-grained facies assemblage. These lens or irregularly shaped, narrow (0.2-2 m), isolated bodies range in thickness from <0.1 m to 0.5 m and consist of red sandy siltstone and mudstone clasts, but lack carbonate glaebules. These granule- to large pebble-sized particles are angular, have a red clay-film coat and are set randomly in the mud-rich matrix forming either matrix- (*Photo 109*) or clast-supported fabric (Fig. 73). In addition, intraclast-bearing very fine sandstones and siltstones (Sc)(Fig. 73; *Photo 110)* were also observed with the same clast constitution. This lithofacies (and its code) was introduced because the very fine, randomly scattered, angular sandstone clasts (1-2 cm) usually represent about 5% of the rock type, so the matrix-supported breccia (Gmm) term would not be illustrative in this case. In addition, the relative dominance of the clast-rich sandstones (3% of the total fine-grained facies assemblage) as compared to the matrix-supported breccias makes clearer the necessity of this separation, even though there is a gradational boundary between one type and the other.

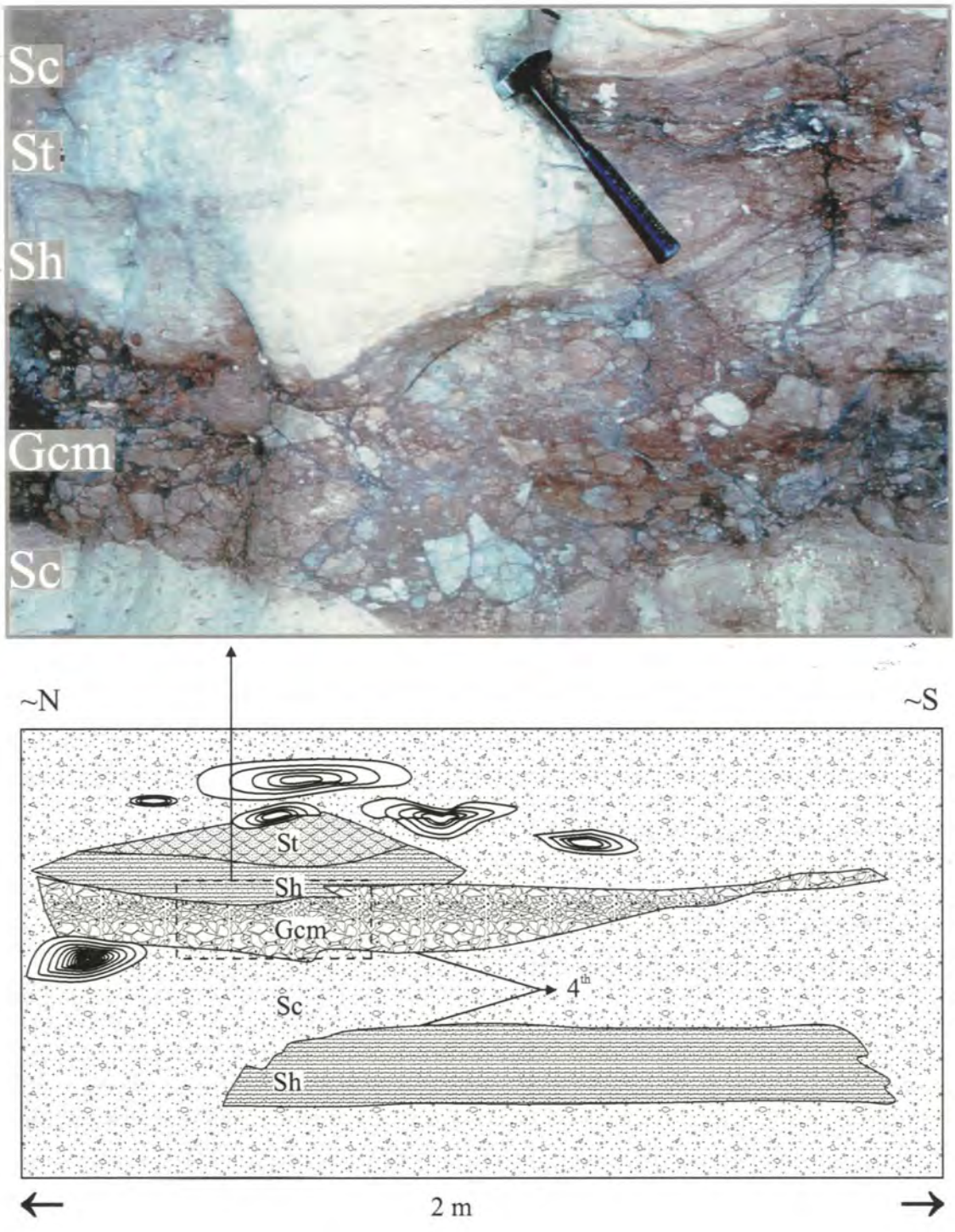

Fig. 73. Lithofacies **Gcm** is overlain by lithofacies **Sh** and **St**. Note the lenticular bedforms and the lack of erosive boundaries. The beds are surrounded by lithofacies **Sc** containing large carbonate concretions as well. Note the clay-coating on the breccia clasts (Balerno - Tsolwe).

The matrix-supported breccias (Gmm) (upper part of *Photo 110*) are commonly finer grained than the clast-supported ones (Gcm) (lower part of *Photo 110*). The sorting is generally poor, and grading was not observed. The clast-supported intraformational breccias occur in association with horizontally bedded, medium-grained sandstones, which grade into the surrounding muddy, silty deposits without a markedly erosive boundary. In one place, the laminated sandstone was overlain by trough cross-bedded sandstone (St) (Fig. 73). The absence of erosive relationship is valid for the base of the intraformational breccias as well as for the breccia/sandstone contact. The bed shapes are usually irregular, except for the clast-supported breccias and horizontally laminated sandstones which form isolated, laterally impersistent, 0.5-2 m long lenses. The intraformational breccias and the sandstones everywhere alternate with intraclast-bearing very fine sandstones and siltstones (Sc) (Fig. 73; *Photo 110).*

Because of the internal structures, bed geometries and stratigraphic position, the intraformational breccias and the clast-rich sandstones were identified as Sediment Gravity (**SG**) flow deposits.

At one locality (Montrow), two successive 0.3 m thick and 3 m wide, sheet-like layers of intraformational conglomerates were found in laminated, carbonate glaebular red mudstones (*Photo 111*). These clast-supported, poorly-sorted conglomerates consist of granule to pebble (3 cm) grade, mostly well-rounded carbonate glaebules with a minor amount of quartz granules (1%). The beds show ill-defined normal grading and display slight horizontal layering (Gh). The matrix is red muddy, very fine sandstone, the cement is uniformly carbonate. At the top of the first Gh layer, a well-preserved fossil bone was encountered (*Photo 112*). On the top of the second Gh layer, a small 8 cm thick, 1 m wide, planar (sigmoidal) cross-laminated very fine sandstone stratum was found. Such thin, cross-laminated sandstone sheets were also observed in other localities, and are described in Ch. 4.2.3.2.2.

These intraformational conglomerates were identified as gravel bedforms (**GB**).

4.2.3.3. Palaeontological findings

Vertebrate fossils

During this study, bone fossils were found in the rocks of the Upper Unit on the following farms: Ratho, Balerno, Armenia, Little Muck, Machete, Greefswald and Scroda. Most of these vertebrate remains are confined to argillaceous deposits *(Photo 100, 101 & 102)*.

Some easily removable samples were analysed by Dr M.A. Raath (Bernard Price Institute, University of Witwatersrand, Johannesburg). These bones which are not very well preserved include the metatarsal, femur, fibula, tibia, and odd isolated vertebrae of a medium sized prosauropod. These appear too small to be *Euskelosaurus* but are rather the size of *Massospondylus*. According to Dr M.A. Raath (written commun.), the postcranial skeletons of these two genera are very similar in many respects except for size, but a small (young) *Euskelosaurus* would be almost impossible to distinguish from a large (adult) *Massospondylus*, and *vice versa*. Because of this and other difficulties, the taxonomy and systematics of prosauropod dinosaurs is sorely in need of revision.

The following vertebrate fossils were reported from the beds equivalent to the middle and upper "Stormberg Group" deposits of the Tuli Basin:

Digit with claw of *Gryponyx africanus* (considered now synonym of *Massospondylus carinatus* (Cooper, 1981 in Kitching & Raath, 1984: 122)) - from the Zimbabwean part of the Tuli Basin (exact location unknown). This finding is mentioned by Bond (1973) and then repeated by Watkeys (1974) as well as by Thompson (1975). In the original reference given in Bond (*Broom, M.D. 1911. On the Dinosaurs of the Stormberg, South Africa. Ann. of S. Afr. Mus. 291-308.*), the Tuli Basin area is not mentioned at all.

Euskelosaurus cf. *browni* - in the red beds (Upper Unit equivalent) of Sentinel farm - from the Zimbabwean part of the basin (Cooper,1980). Prior to Cooper's (1980) revision, this specimen had been tentatively considered by Dr M.A. Raath as *Massospondylus carinatus*. He recognised this as a large individual, but did not consider it too large to be *Massospondylus*. Dr Raath (written commun.) considers that the Sentinel specimen is much smaller than many other well

preserved and provenanced specimens of *Euskelosaurus* in the BPI (Palaeontology - University of Witwatersrand, Johannesburg).

Massospondylus carinatus (i.e. it used to be termed as *Gryponyx transvaalensis*) - in the red beds (Upper Unit equivalent) of Weipe farm - South African part of the basin (Broom, 1912). Although Cooper (1980) mentioned it from the dune-bedded sandstones, the specimen seems to come from the red beds. The original description of Broom (1912) clearly states that these fossils were found in a red sandstone. The koppies of Weipe farm are made of red Upper Unit sandstones and argillaceous deposits, and there is only one koppie that has ~1-1.2 m of white, bioturbated Clarens Formation sandstone *(Photo 128)* (along the Schroda fence). The approximate distance between the last two fossil sites (Sentinel - Zim. and Weipe - S. Afr.) is about 10 km.

There appears to be some controversy over the identification of the *Euskelosaurus* specimen from Sentinel Ranch, and certainly all other remains from this area appear to be of *Massospondylus*.

Trace fossils

Trace fossils in the Upper Unit are developed on top of the massive, fine-grained sandstone beds, but very rarely may occur on top of the 0.1- 0.25 m thick horizontal or low-angle planar cross-stratified fine sandstones as well (see photographs in Ch. 4.2.3.1.1). The bioturbated beds are more common towards the upper parts of the 1-2.5 m thick fining-upward cyclothemes. Bioturbation seldom occurs in the lower part of these cyclothemes. Bioturbations are common in 1- 2.5 cm thick, mostly clay-rich silt- and mudstone beds (*Photo 66A*), and rare in sandstones (*Photo 66B*). Biogenic trace fossils have been observed on the following farms: Weipe, Schroda, Hamilton, Nekel, Lucca, Faure, Hartbeestfontein, Anglican, Halcyon and Ratho. Several boreholes (Gle-1, Ori-1, Ori-2, Ori-3, Den-1 and Sch-1) also record bioturbation features described as "patterns resembling worm-tracks". Based on outcrop observations, there are vertebrate trace fossils and at least two different forms of invertebrate trace fossils (type A and type B). Their characteristic features and possible interpretation are set out below.

Vertebrate trace fossil

Vertebrate tracks were found on a mudfilm-covered siltstone bedding plane of the Upper Unit in the southwestern part of Schroda farm *(Photo 67)*. The footprints (average 3.5 cm long) appear to have been made by a small four-toed animal. Most of the prints show only four or three digits. One of the footprints shows clearly that the digits ended in claws, but in the rest of the tracks the digits merely thin towards the toe tip. The minimum distance between two adjacent prints is 3 cm, while the maximum distance is about 6 cm. It seems that the tracks were made by a small quadrupedal animal with slightly larger pes than manus. It would be well worth trying to unroof more of the tracks in order to identify this small trackmaker, as the hostrock yields skeletal elements of only prosauropod dinosaurs.

Invertebrate trace fossil

Description

Type A (Weipe, Schroda, Hamilton, Nekel, Lucca, Faure, Hartbeestfontein, Anglican, Halcyon, Ratho)

The shape of the individual structures is cylindrical and their cross-section is circular. They are preserved as both casts and moulds (*Photo 66A*). The length of the unbranched segment varies from 1 centimetre to less than 10 centimetres. The diameters are uniform and range from 0.5 cm to 1 cm. Branching is extensively developed and orientation is mainly random (*Photo 66C*), forming complex interwoven networks (*Photo 66B*). The walls of the features are smooth, the fills are non-meniscate. *Photo 66D* shows structures that are organized in slightly polygonal patterns. Although it resembles desiccation cracks, the tube shape (eroded in the picture) of the structure indicates a probable biogenic origin.

Type B (Weipe)

One isolated specimen of a zig-zag mould *(Photo 66E)* was found on a mudfilm-covered sandstone bedding plane. The structure is 30 cm long with a uniform, circular cross-section of 1 cm. The walls of the feature are smooth, the fill is non-meniscate.

Interpretation

These bioturbations can hardly be explained as rhizoliths since the characteristics of rhizoliths such as downward bifurcation and orientated diameter changes (Klappa, 1980) are absent. The *Type A* occurrences are interpreted as feeding/habitation traces of organisms like aquatic (?annelid) vermiform animals *(Planolites?* of *Scoyenia* Ichnofacies).The *Type B* zig-zag mould is thought to record the burrows of crustaceans (i.e. aquatic crabs).

4.2.4. Clarens Formation

4.2.4.1. Lithofacies

The outcrop belt of the Clarens Formation runs in a roughly E to W direction through the northern part of the study area (Fig.3). The formation is exclusively composed of quartz sandstones and often forms the bluff of the hills. Some of the best exposures are found in the northern part of Hillstone, Pont Drift, Modena, Den Staat, Greefswald, Schroda, and the southwestern part of Balerno (Tsolwe koppie) farms. The formation is intersected in only one borehole (Den-1), where its thickness is 53.34 m. The maximum exposed thickness is circa 45-50 m (Balerno - Tsolwe koppie), while the average outcrop thickness is about 10-15 m.

The formation has a conformable, clearly detectable lower boundary, especially in those outcrops where it is underlain by the laterally persistent, white silcrete horizon developed in the uppermost beds of the Upper Unit. This lower boundary is traceable over several hundreds of metres (*Photo 89, 92*), and seems to be a rather smooth, sharp surface. This boundary is a diastem as there was little or no discernible erosion between the stratigraphic units. In the study area, the upper contact is only visible in a few outcrops where the sandstones are overlain by basalts (Ba) of the Letaba Basalt Formation (Balreno, Greefswald and Schroda/Weipe border) (Fig. 74A & B).

The strata described in this chapter correspond to the Tshipise Member of Chidley's (1985) Clarens Formation. Since there are outstanding lithological and generic analogies between these deposits and Clarens Formation of the main Karoo Basin, a revision of Chidley's Clarens Formation is required. It is suggested that in order to avoid confusion, the rank and name of the Tshipise Member in Chidley (1985) should be changed to Clarens Formation.

The cliff-forming sandstones of the Clarens Formation mainly display featureless, massive or large-scale cross-stratified beds of medium- to well-sorted, moderately rounded, fine- to very fine-grained quartz sandstones. Mudstones or coarse material are absent. The sandstones are off-white to orange, generally 2-6 m thick (Fig.75), but may attain a thickness of 12 m. The lateral continuity of the

Fig. 74. Clarens Formation sandstone (above the silcrete) overlain by basalt (Ba) of the Letaba Basalt Formation (A - Weipe; B - Greefswald).

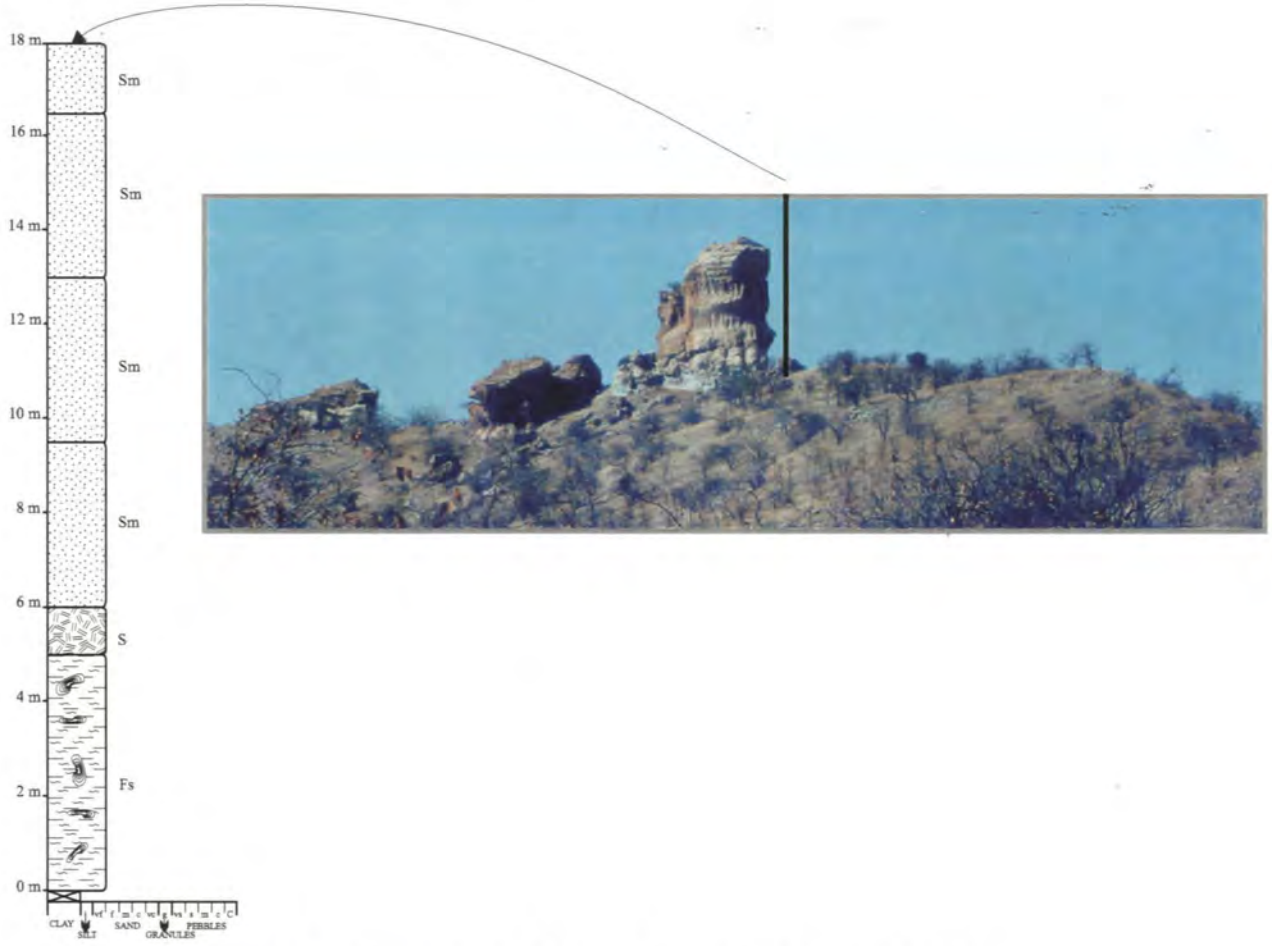

Fig. 75. Thickly bedded sandstones of the Clarens Formation (above the silcrete) (Breslau - Show of Rhodes koppie).

thicker beds is greater than that of the thinner ones. Generally, the thickly-bedded sandstones are traceable for distances ranging from a few tens of metres to more than a hundred metres, depending on the length of the outcrop.

Although the sandstones are commonly massive (Sm) (Fig. 76), the most abundant sedimentary structure is the large-scale cross-stratification (dune bedding) (Sd) (*Photo 113*). There also are some giant cross-beds (*Photo 114*) with finely laminated, highly inclined foresets (*Photo 115*).The individual foreset laminae are often structureless, rarely inversely graded (refer to Appendix 4 PON-2). The foreset dip direction in the successive beds is rather uniform (Fig. 80D), with slight variation in their orientation being observed only in a few places (Fig. 77). In places, the cross-stratified sandstones are aligned in connected crescent-shaped bedforms (*Photo 116, 117)* resembling rows of barchanoid ridges. Internally these beds show well-developed tangential bottomsets (*Photo 118).*

Three types of bounding surfaces were recognized. Third order internal bounding surfaces separate bundles of laminae within cosets (*Photo 119*). Second order bounding surfaces were observed only rarely, mainly towards the top of thick sets of cross-beds (*Photo 120, 121*). First order surfaces separate superimposed dune sets (*Photo 122A & B*). They are sharp, low-relief, cross-cutting and traceable for large distances.

There are a few sequences of horizontally bedded (Sh), low-angle cross-bedded (Sl), trough cross-bedded (St), and medium-scale planar cross-bedded (Sp) medium- to coarse-grained sandstones. These sequences occurred in thin (0.1-0.4 m) beds of flat-topped, channel-shaped bedforms (width 200 m, thickness 0 to 3 m) that were incised into neighboring large-scale cross-bedded or thickly bedded massive sandstones. They were observed only in the lowermost part of the formation, directly above the silcrete layer (Fig. 78).

Horizontal lamination (Sh) was infrequently recorded (Fig. 79) in 0.2-1 m thick, lens-shaped sandstones (*Photo 123*) that were also confined to the lower part of the formation. Lens-shaped, massive sandstones were observed to alternate with these horizontally laminated sandstones. Very

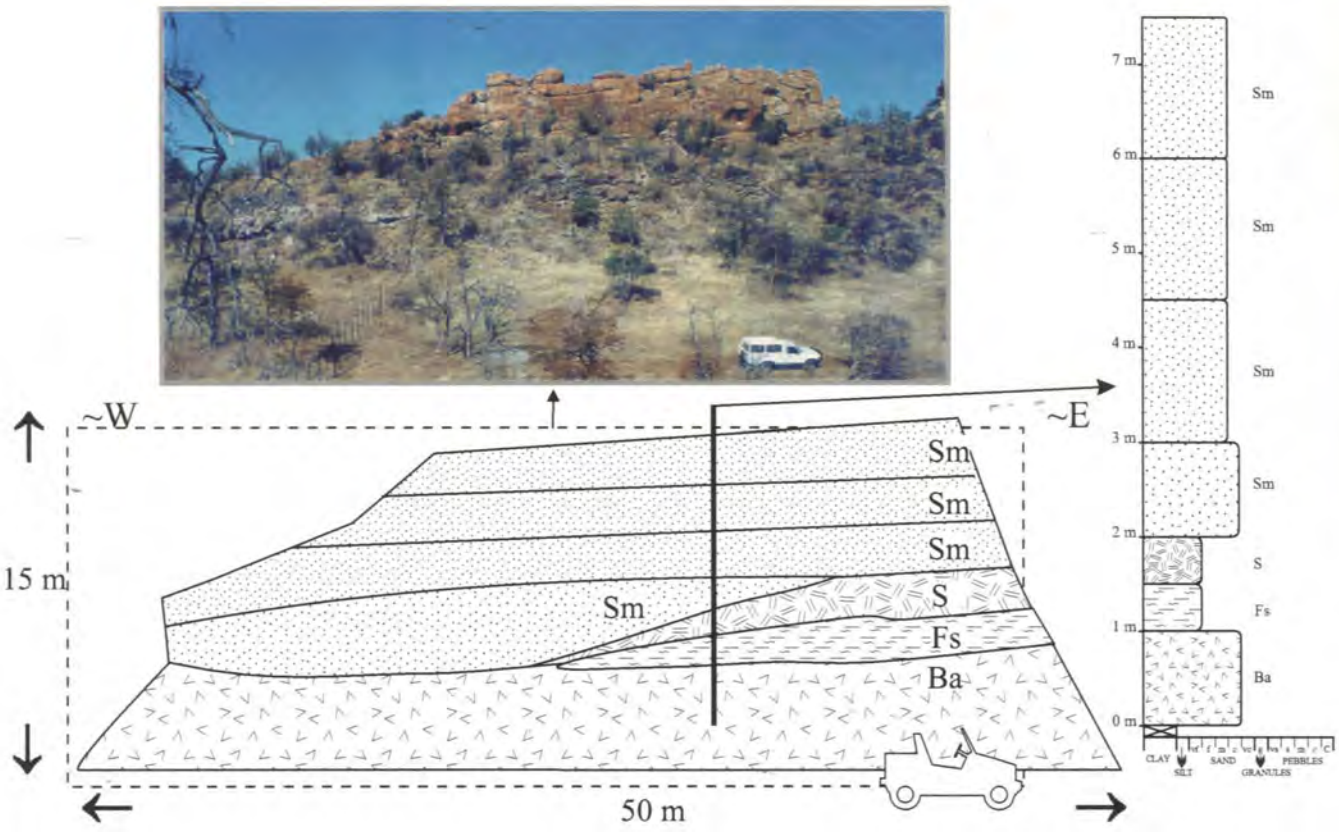

Fig. 76. Massive, featureless, thickly bedded sandstones of the Clarens Formation (above the silcrete) (Princes Royal).

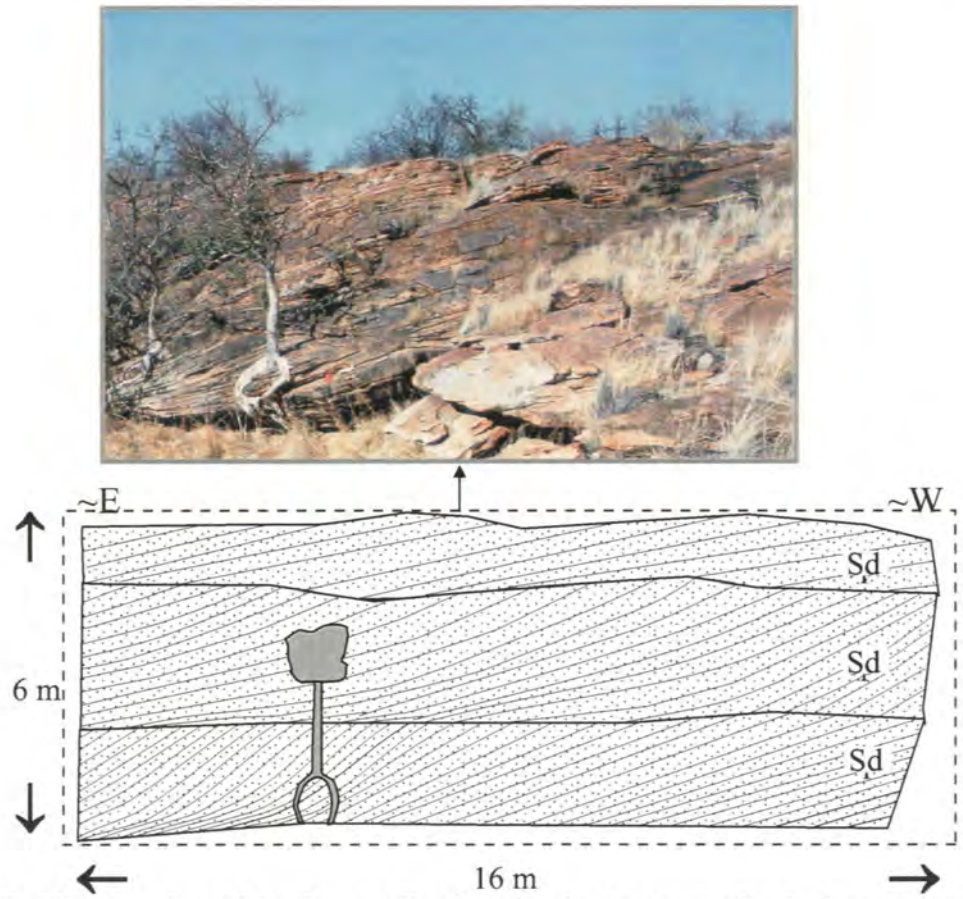

Fig. 77. The variation of the foreset dip direction in the successive beds range from 135°/30° to 150°/20° to 160°/20° (Den Staat).

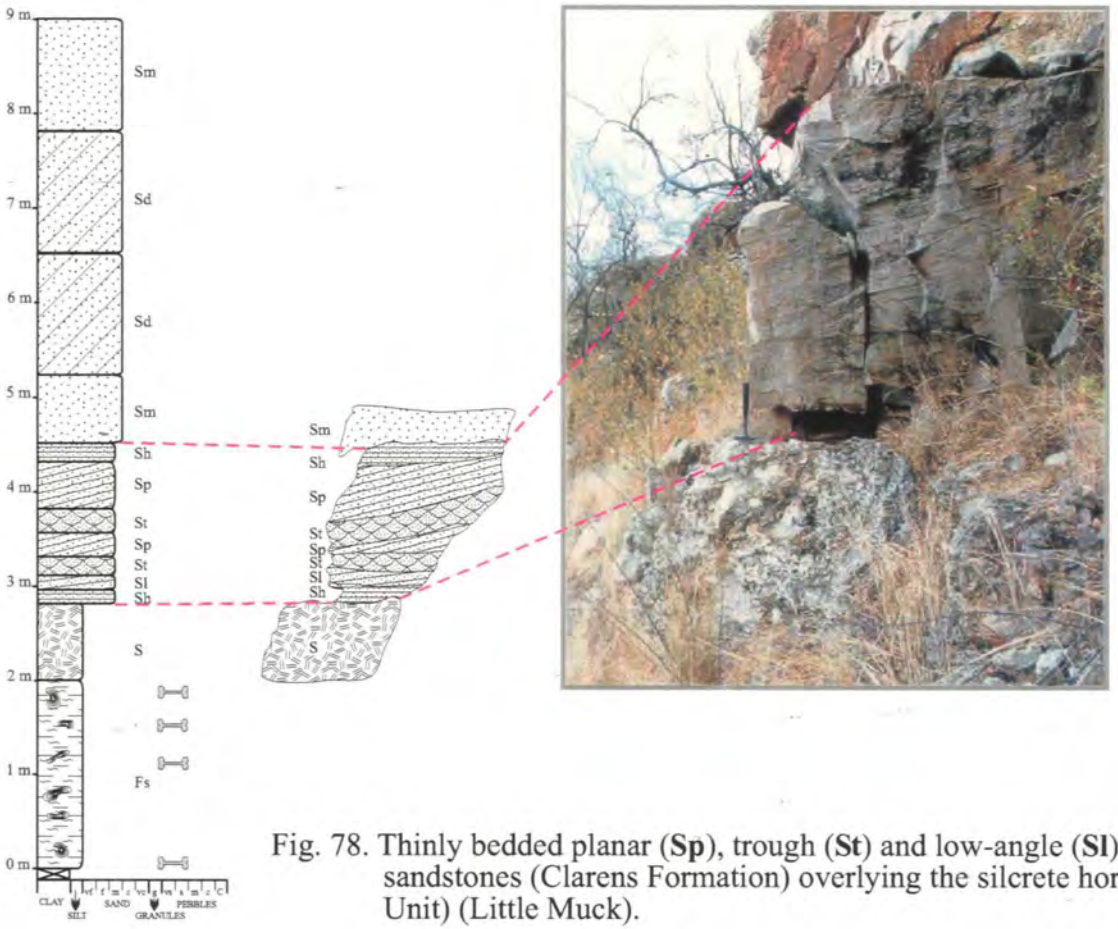

Fig. 78. Thinly bedded planar (**Sp**), trough (**St**) and low-angle (**Sl**) cross-bedded sandstones (Clarens Formation) overlying the silcrete horizon (Upper Unit) (Little Muck).

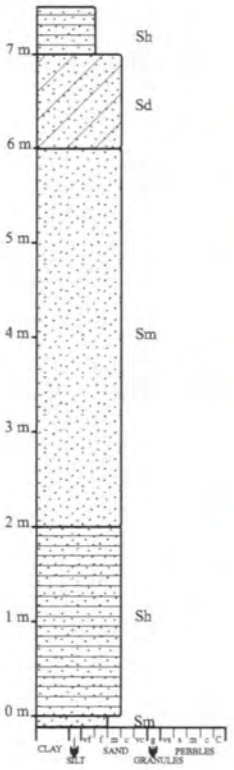

Fig. 79. Horizontal lamination (**Sh**) (lower right corner in the photo) is rare, confined mostly to the lower part of the formation (Breslau).

rarely, the massive beds contained scattered, angular silcrete fragments (Sc) (see log in Fig. 65). Some of the laminated and massive beds are slightly coarser grained (fine to medium sand) than the majority of the formation. These beds often display bioturbation features as described in Ch. 4.2.4.2. Wind ripples were not detected.

4.2.4.2. Palaeontological findings

Wood fossils

Poorly preserved, silicified fossil woods (*Photo 124)* were found on the surface of the Clarens Formation sandstones in the central part of Parma farm (22° 15' S; 29° 7' E, very approximate). Nine larger logs were measured (Table 10), whose average dimensions are the following: minimum diameter 27.56 cm, maximum diameter 36.22 cm and length 65.44 cm.

Table 10. Dimensions of silicified fossil logs.

Samples	A	B	C	D	E	F	G	H	I
Minimum diameter (in cm)	24	20	20	20	20	20	24	70	30
Maximum diameter (in cm)	40	32	30	24	32	20	48	30	30
Length (in cm)	85	80	38	24	48	24	80	120	90

These logs were lying about 1-2 m apart from one another but their similar diameters suggest they were part of one rather large tree. The petrified woods lack signs of abrasion and specimens are far too large to have been transported for a significant distance after silicification, and so it is assumed that the logs are virtually *in situ.*

The findings were identified as *Agathoxylon sp.* (= *Dadoxylon sp.*) by Dr M. Bamford (BPI, University of Witwatersrand, Johannesburg). *Agathoxylon sp.* type of wood is known from the Upper Triassic to the present and is found in several groups of plants. This type of wood often occurs in logs of more than 30 m long and more than 70 cm in diameter (Dr M. Bamford, written commun.). According to Dr Bamford's description, the collected specimen "is gymnospermous and has uniseriate, contiguous to slightly compressed pitting on the radial walls of the tracheids, of the

typical araucarian type and 10 microns in diameter. The cross-field pits are not preserved." The specimen shows growth-rings with very narrow latewood that indicates that "there was some seasonal variation in the climate, but the growth conditions were generally good, i.e. no dramatic water shortage"(Dr M. Bamford, written commun.). Interpretation of these fossil findings is included in Ch.5.4.

Similar petrified tree trunks are known from the Clarens Formation equivalents of southern Africa (Bamford, 1999). Beukes (1970:327) mentioned charred fossil wood log from the Clarens Formation in the main Karoo Basin. Truter (1945) reported silicified tree stems from the aeolian sandstones of the Tshipise Basin (Witfontein farm). Petrified trees also occur in the fluvial intercepts of the dominantly desert Forest Sandstone (~Clarens Formation) in the western Cabora Bassa Basin, Mid–Zambezi Valley, in the Dande west area (Oesterlen, 1991), but these have not yet been identified.

Trace fossils
Vertebrate trace fossils

Vertebrate tracks were reported by van Eeden and Keyser (1971). These Saurian fossil tracks were found in cross-bedded sandstone in the northeastern part of the study area (Pont Drift) and have been ascribed to the dinosaurs *Massospondylus* and *Syntarsus* (van Eeden & Keyser,1971).

Invertebrate trace fossils

Several biogenic trace fossils have been observed in the lower and medial part of the formation on the following farms: Hillstone, Schroda, Weipe, Machete and Greefswald. There are at least three different forms: types A, B and C. Their characteristic features and possible interpretation are set out below.

Description
Type A (Hillstone, Schroda)
The shape of the structures is cylindrical and their cross-section is circular. Their length varies from a few centimetres to less than a metre and the diameter ranges from 5 to 25 cm. Lateral bifurcations may occur (*Photo 125*), but downward bifurcation and higher order branching was not observed.

Whereas most of the structures are horizontal (*Photo 126*), there are several examples of vertical, cylindrical pipes with open apices as well (*Photo 127*). The latter project up to 15 cm above the surface. Diameters measured are about 10 cm at the top, but increase to 15 cm at the base.

Interpretation

These structures are not root casts of large trees because downward bifurcation and abundant branching with decreasing diameters of higher-order branches (Klappa, 1980) are absent. Similar cylindrical structures were also observed by de Villiers (1967) and van Eeden (1968) in the Clarens Formation (Schroda, Pont Drift). According to de Villiers (1967), the peculiar structures could be attributed "to the slow ascent of columns of ground-water through unconsolidated sand" or formed by steam which originated from volcanic activity. van Eeden (1968) supports the latter theory. However I consider that the morphology and large size of the structures suggest that they were perhaps produced by burrowing vertebrates (?reptiles or amphibians) for hibernation/resting/feeding purposes. According to Ahlbrandt et al. (1978), vertebrate burrows were recorded from ancient sediments with similar characteristics to the Clarens Formation.

Description

Type B (Weipe & Schroda, Machete)

Photo 128 shows an exceptional mould structure. The shape of the individual moulds is cylindrical and their cross-section is circular. Their length varies from 1 cm to 25 cm, but the structures frequently intersect the entire host bed which is in general 0.15-0.25 m thick (Fig.74A). Isolated occurrences were also observed (*Photo 129*). The diameter of the structures is about 0.5 cm and seems to be uniform along the length. Branching is absent and orientation is predominantly vertical, rarely slightly inclined. The host bed lithology is fine- or medium-grained sandstone. In places, around the upper cavities of these simple shafts, there is a 0.5 cm high, conical sand pile resembling in shape a mini sand volcano.

Interpretation

These moulds can hardly be explained as root moulds since characteristics of rhizoliths such as downward bifurcation, branching and tapering along their length (Klappa, 1980) are absent. The structures are believed to be produced by soft-sediment burrowing invertebrates (probably

arthropods, such as beetles, ants, crickets, spiders, wasps, etc.), therefore the shafts are fossil dwelling (?feeding) burrows. These trace fossils are very tentatively identified as *Skolithos sp.*, an ichnogenus which is a simple, unbranched tube oriented vertical to bedding planes (Ahlbrandt et al., 1978). *Skolithos sp.* has also been recorded from non-marine (Holocene aeolian) sediments by White & Curran (1988) and freshwater redbeds (Triassic) by Bromley & Asgaard (1979).

Description

Type C (Greefswald)

The shape of the structures is giant digit-like and their cross-section is circular (*Photo 130*). The height of the columns varies from 1.5 to 2.5 metres. Their diameter is not uniform, gradually decreasing from bottom to top, from 1 m into a convex peak. The average diameter is about 0.3-0.4 m. The surface of these medium sandstone columns is decorated by a web-like network of extensively branching, disorientated, cylindrical shaped, 0.5-1 cm thick structures which strongly resemble bioturbation (*Photo 131*). In cross section (*Photo 132*), the tubes are not meniscate and the giga-digits show a central empty shaft of 3-5 cm in diameter stretching through the sandstone pillar. Upward bifurcation of these exclusively vertical structures was observed only in two cases (*Photo 133).* There are a few twinned structures as well (*Photo 130*). The single giga-digits are widely spaced, usually 5-10 m from each other and they occupy an area about 300-400 m^2. Some of the giga-digits are situated on a conical dome-like elevation which rises about 0.2-0.3 m above the level of the surrounding plain (i.e. not a bedding plane). Such dome-like elevations are 0.3 m high (*Photo 134)* and consist of medium-grained, heavily bioturbated sandstone with identical characteristics to the bioturbation on the wall of the sandstone pillars.

In the Zimbabwean part of the Tuli Basin, similar columnar structures were also observed in the Clarens Formation by Thompson (1975) and Watkeys (1979:65). Thompson (1975:28) wrote: "East of the Umzingwane River and about 1,5 km south-east of the homestead on Cawood's Mazunga Ranch, numerous pipe-like structures stand for up to one metre above the ground, and extend for one or two metres below the surface, sometimes bifurcating like tree roots. Most are circular in cross-section and have an external diameter of about 40 to 50 cm and an internal diameter of 3 to 20 cm. Their walls consist of about 25 mm hard silicified sandstone."

Interpretation

These structures are not root casts since characteristics of rhizoliths such as downward bifurcation, tapering along the length and radiation from the central axis (Klappa, 1980) are absent. The heavily bioturbated, complex, columnar structures are thought to be a result of the coordinated activity of a large number of individuals. Cooperative habit is characteristic of organisms with social behavior (e.g. insects: ants, termites, etc.). The close morphological and structural resemblances of the columnar structures to some recent columnar termite nests that have been reported from southern Africa and Australia suggest that these structures may be interpreted as termite mounds (termitaria).

The group of termites constructing underground galleries and chambers that connect their food supply with the storage spaces are termed soil-dwelling/subterranean termites (Ratcliffe et al., 1952). The structure and morphology of the galleries and chambers (i.e. nest) are dependent on the colonizing termite species. There are numerous termite species that build mound-like nest extensions above the ground level. The structures built by *Macrotermes sp.* - a common genera in southern Africa - are not consistent, but this termite also shows tower-building habits (Howse, 1970) (*Photo 135*). *Macrotermes bellicosus* is reported to construct vertical pillars up to 4 m in Kenya (Harris, 1961). Other species that build chimney-like structures (ventilation shafts) projecting above the ground level, but having their nest underground are *Protermes sp.* and *Odontotermes sp.* (Howse, 1970), and have been reported from South Africa too (*O. transvaalensis*). In Australia, the following species have columnar nesting habit: *Nasutitermes triodiae, Tumulitermes (=Nasutitermes?) hastilis, Amitermes vitiosus, A. laurensis, A. meridionalis, Drepanotermes rubriceps* (Hill, 1942; Ratcliffe et al., 1952; Lee & Wood, 1971b).

The reason for mound-building behaviour is not well understood (Lee & Wood, 1971b); however, it is inferred that factors like climate, soil type and vegetation may influence such habits. For instance, in areas subject to frequent heavy rain, the mounds are usually domed, while in areas with severe winters, the nests are constructed deeper in the ground (Lee & Wood, 1971b). Lee & Wood (1971b) observed that *Amitermes meridionalis* retreat into their mounds during the rainy season and

consume the grass collected in the dry season. According to Luscher (1961), *Macrotermes bellicosus*, a fungus-growing termite, builds columnar features for air conditioning purposes. From these observations, it might be speculated that the columnar mound-building habit may be more dominant under hot climatic conditions that are subject to widespread seasonal flooding.

The relatively high preservation potential of the termite nests is due to a preferential cementation caused by early diagenetic consolidation of the nest-building saliva, excreta, wood and fungus-bound sand grains (Lee & Wood, 1971a; Brown, 1982). The type of substrate seems to play an important role in the distribution and type of termite mounds, with the availability of clay minerals being essential, especially in case of larger mounds (Lee & Wood, 1971a). The mound of one of the largest mound-building termites *(Nasutitermes triodate)* contains about 25% of clayey material (Lee & Wood, 1971a). Termite mounds are virtually absent in pure sands.

Termitaria elements were identified as follows. The central empty shaft could have functioned as part of an internal chamber system constructed for several purposes, such as a dwelling place for the royalty, storage of larvae, fungus gardens, ventilation shafts ("termite-aero"), etc. (Genise & Brown, 1994). The web-like network of the smaller burrows could be sand-filled passageways that were used to give access to storage chambers or to dumping sites where waste material was deposited (Retallack, 1991; Neke, 1994). The bioturbated dome-like elevations that surround the sandstone columns may be seen as the exposed subterranean part of the nest system.

Smith & Kitching (1997) reported a termitarium in the lower part of the Upper Elliot Formation from the main Karoo Basin, which makes the present sample the second oldest termitarium described from southern Africa.

4.3. Palaeo-current analyses

4.3.1. Palaeo-current measurements

The calculated statistical values and generated palaeo-current rose diagrams were based only on the orientation data derived from the foreset dip direction of the cross-bedded sandstones. In the Basal, Middle and Upper Units (Fig.80A, B & C), measurements were obtained from both medium and large-scale cross-beds, while in the Clarens Formation (Fig.80D) only the large-scale cross-bedded strata were measured. No structural correction was performed as the strata are undeformed (structural dip <5°). 43 palaeo-current rose diagrams were produced from a total of 704 measurements. The rose diagrams reveal unidirectional current patterns for all units.

The spatial distribution of the mean vectors are indicated in Fig. 81. The data were collected from the area surrounding the mean vector arrows. This map clearly displays that the regional mean current direction significantly changed during the Karoo Supergroup sedimentation. In the Basal Unit, this direction pointed from ENE to WSW (242°), in the Middle Unit from SE to NW (320°), in the Upper Unit towards SSE (156°), and from WNW to ESE (112°) during the Clarens Formation times. In the case of the Basal Unit, Middle Unit and Clarens Formation the current directional variation was insignificant, both vertically within the succession and laterally through the area. The Upper Unit shows the greatest dispersion of the palaeo-current data in the whole succession.

4.3.2. Calculations of the palaeo-channel sinuosity

The channel sinuosity (P) is a parameter reflecting the plan-view geometry of the river channel. Accordingly, high sinuosity values indicate tortuous, meandering channel patterns, and low sinuosity values imply straight, braided channel patterns.

Two different methods were applied to determine the sinuosity of the palaeo-channels. In order to obtain local channel sinuosity values, Le Roux's (1992) method was applied. This approach assumes that the river channel would swing through an arc represented by the arc of the rose diagram plotted from the data provided by the current indicators of the channel itself. The sinuosity value was given by:

$$\mathbf{P}\ (\text{sinuosity}) = \pi\ (\phi/360) \div \sin(\phi/2)$$

A.

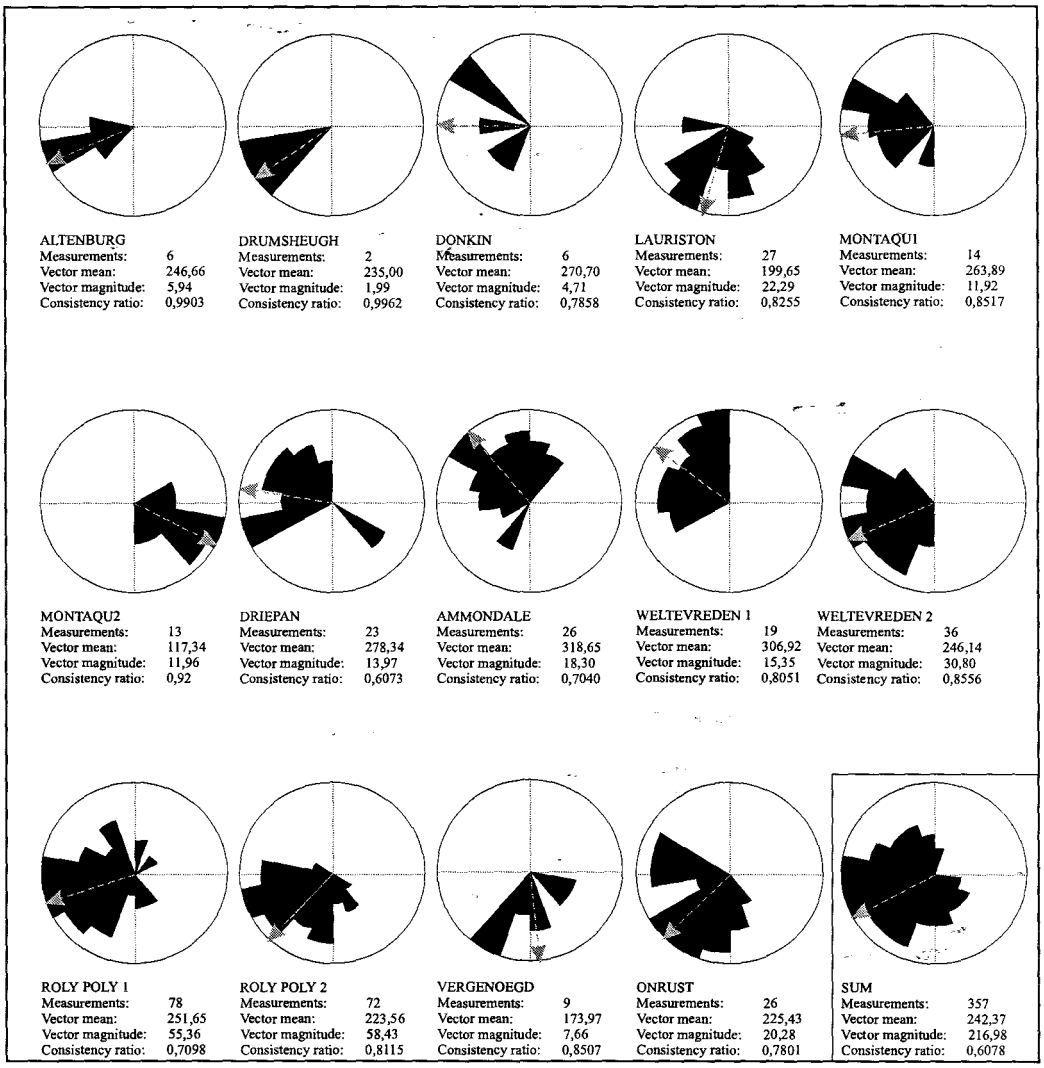

B.

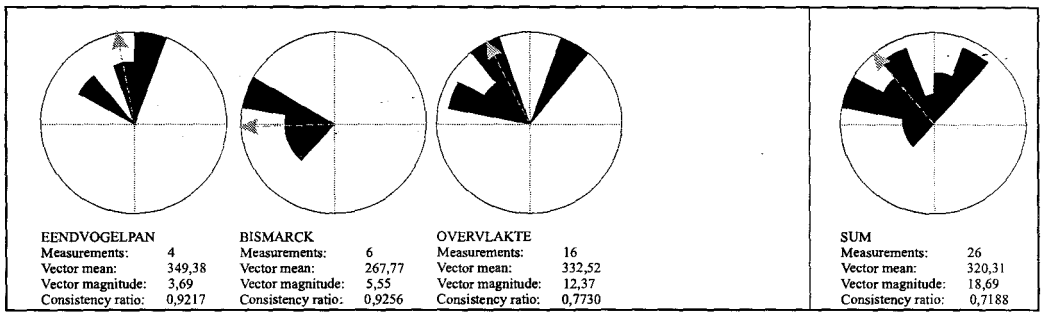

Fig. 80. Palaeo-current rose diagrams for planar cross-bedded sandstones. **A** - Basal Unit; **B** - Middle Unit; **C** - Upper Unit; **D** - Clarens Formation.

C.

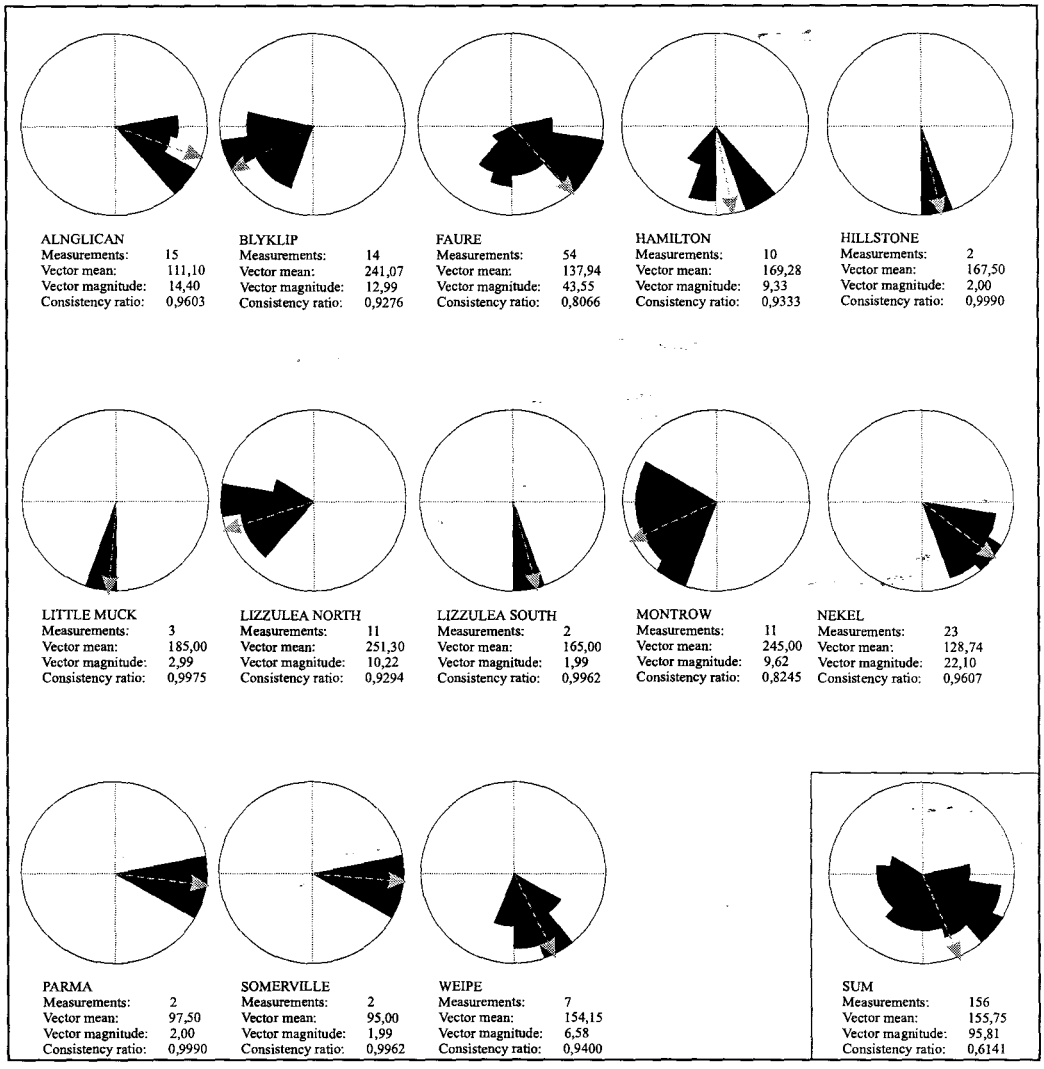

Fig. 80. Palaeo-current rose diagrams for planar cross-bedded sandstones. **A** - Basal Unit; **B** - Middle Unit; **C** - Upper Unit; **D** - Clarens Formation.

D.

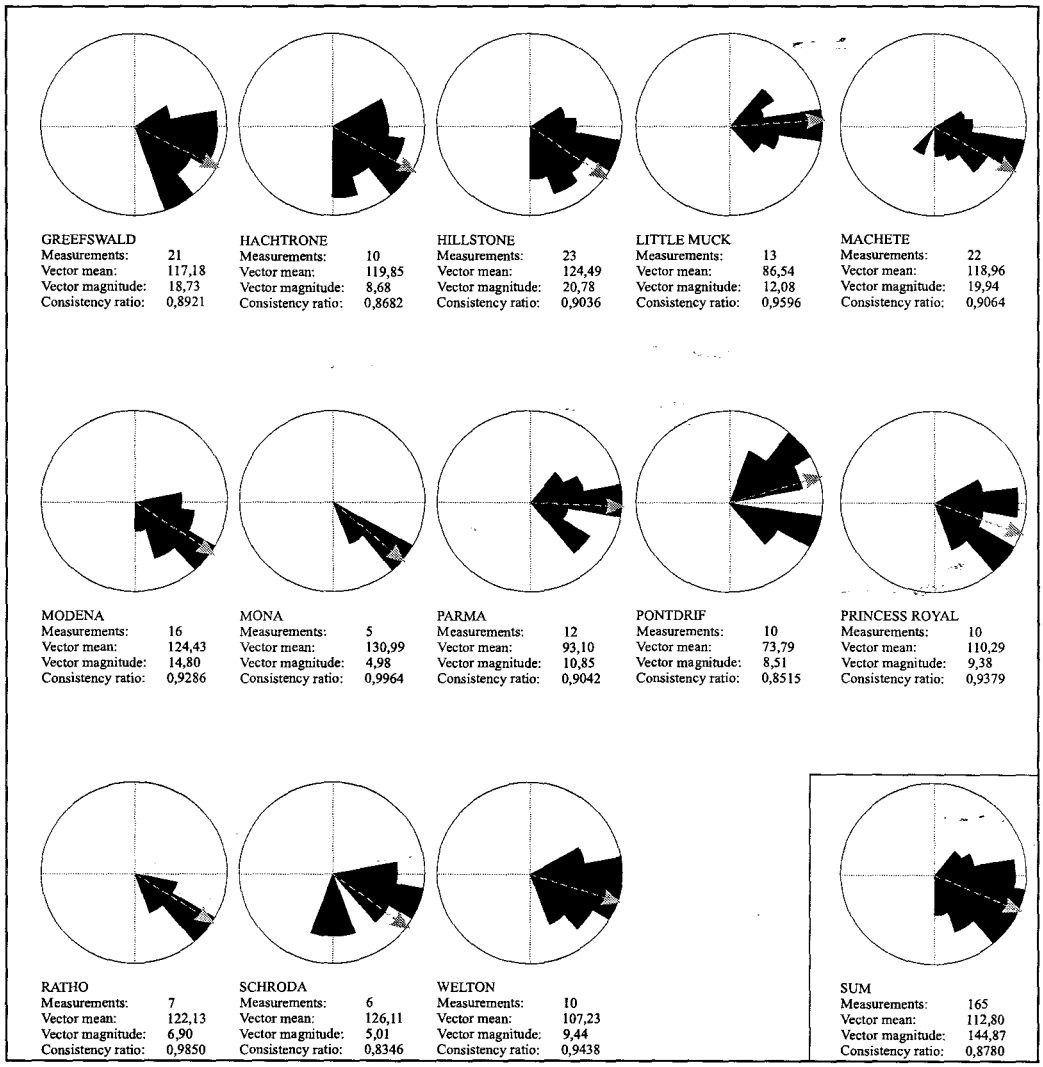

Fig. 80. Palaeo-current rose diagrams for planar cross-bedded sandstones. **A** - Basal Unit; **B** - Middle Unit; **C** - Upper Unit; **D** - Clarens Formation.

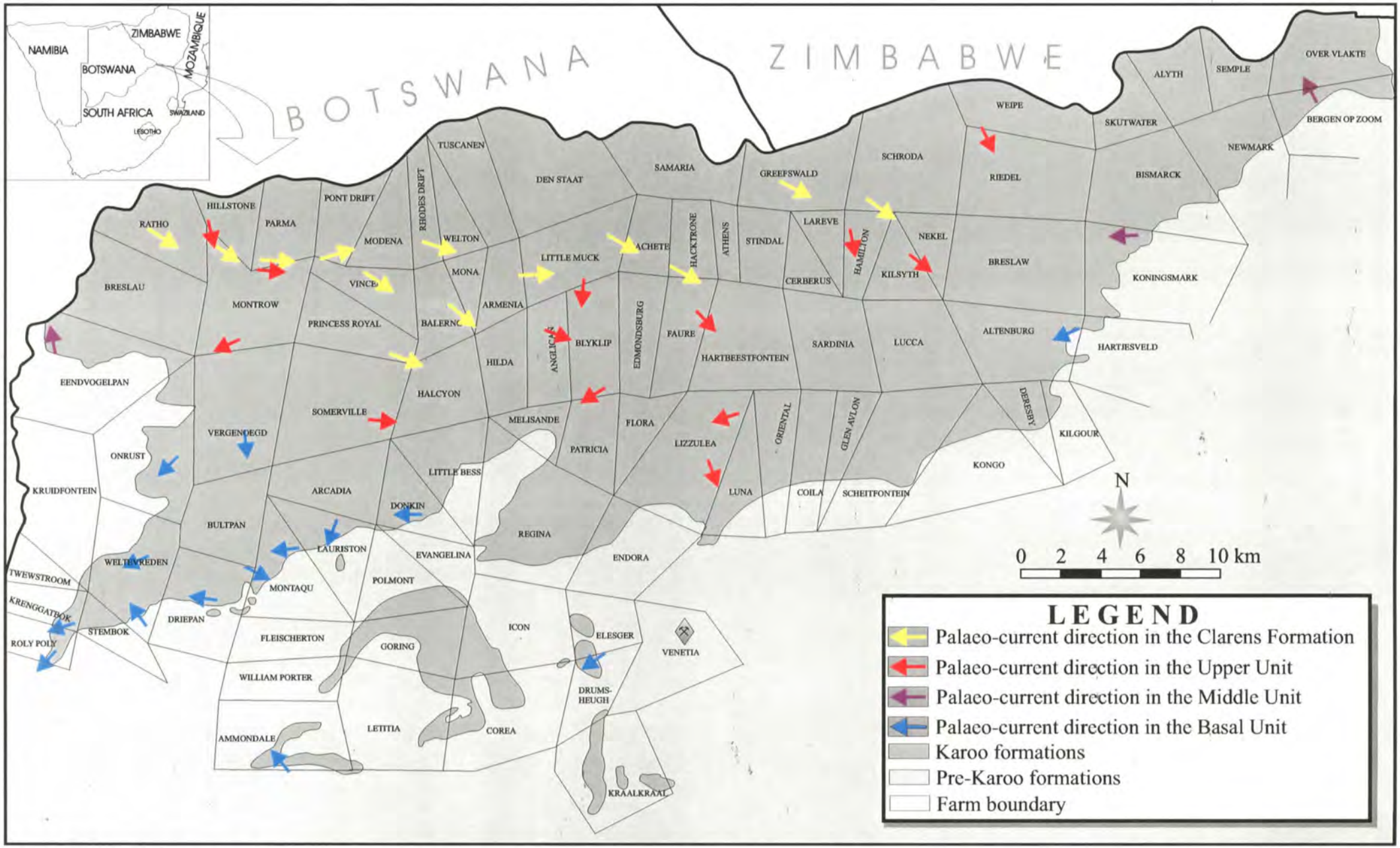

Fig. 81. Map showing the palaeo-current orientations inferred from planar-cross bedded sandstones. The arrows correspond to the mean vector of the measurements obtained from the adjacent outcrops to the arrow.

where ϕ is the angular range of the arc in degrees. This approach assumes that each rose diagram reflects a single meander belt (Le Roux, 1992). In the present study, this criterion was satisfied by the fact that the input data of each rose diagram shown in Fig. 80A was collected from areas less than 2 km in diameter, and this distance would correspond to the radius of any medium-sized meander belt. The theoretical sinuosity values of the method range from 0 to 5.24 ($0 \leq P \leq 5.24$), while ϕ has values between 0 and 300°. The ϕ reaches its maximum at 300° because neck cut-off would occur between the adjacent meander belts at any greater angular range (Le Roux, 1992).

Table 11. Calculated channel sinuosity values based on the Le Roux's method (1992).
A. Basal Unit **B.** Middle Unit. Note that the anomalous, infrequent data were omitted when calculating the arc range.

A.

Locality of measurements	ϕ	*P*	*Locality of measurements*	ϕ	*P*
Altenburg	*(235;250) **15***	**1.00**	Ammondale	*(20;270) **110***	**1.17**
Drumsgheugh	*(230;240) **10***	**1.00**	Weltevreden 1	*(240;350) **110***	**1.17**
Donkin	*(215;300) **85***	**1.04**	Weltevreden 2	*(190;300) **110***	**1.17**
Lauriston	*(135;230) **95***	**1.12**	Roly Poly 1	*(160;330) **170***	**1.48**
Montaqu 1	*(230;300) **70***	**1.06**	Roly Poly 2	*(140;275) **135***	**1.32**
Montaqu 2	*(108;160) **52***	**1.03**	Vergenoegd	*(160;200) **40***	**1.02**
Driepan	*(240;320) **80***	**1.08**	Onrust	*(180;280) **100***	**1.13**

B.

Locality of measurements	ϕ	*P*
Eendvogelpan	*(0;310) **50***	**1.03**
Bismarck	*(235;290) **55***	**1.03**
Overvlakte	*(30;280) **110***	**1.17**

The calculated local channel sinuosity values are low (<1.50) (Table 11): 9 samples out of the total 17 range between 1.00-1.10.

In order to obtain regional channel sinuosity values, another method was applied, which broadly follows the empirical equation described by Miall (1976):

$$\mathbf{P}\ (\text{sinuosity}) = \mathbf{1} \div \left[\ \mathbf{1} - (\theta \div 252)^2\ \right]$$

In the original work, θ was used to describe the maximum angular range of the mean azimuth of each sampling locality, while in the present study, θ represents the angular difference of the mean vector azimuths of the adjacent sampling areas. Owing to the scattered, discontinuous input data of the other units, this method was only applicable to the Basal Unit.

Table 12. Calculated channel sinuosity values based on Miall's method (1976) (Basal Unit).

Azimuth (locality)	*θ*	*P*
247 (Altenburg) - 235 (Drumsgheugh)	*12*	**1.00**
235 (Drumsgheugh) - 271 (Donkin)	*36*	**1.02**
271 (Donkin) - 200 (Lauriston)	*71*	**1.08**
200 (Lauriston) - 264 (Montaqu 1)	*64*	**1.06**
264 (Montaqu 1 - 278 (Driepan)	*14*	**1.00**
278 (Driepan) - 246 (Weltevreden 1)	*32*	**1.01**
246 (Weltevreden 1) - 252 (Roly Poly 1)	*6*	**1.00**
252 (Roly Poly 1) - 224 (Roly Poly 2)	*28*	**1.01**
174 (Vergenoegd) - 225 (Onrust)	*51*	**1.04**
307 (Weltevreden 2) - 318 (Ammondale)	*11*	**1.00**
264 (Montaqu 1) - 117 (Montaqu 2)	*147*	**1.51**
117 (Montaqu 2) - 278 (Driepan)	*161*	**1.68**

This method also produced low channel sinuosity values (Table 12), varying from 1.00 to 1.08. The only exception occurred in case of the Montaqu 2 (azimuth:117), where the sinuosity values were 1.51 compared to Montaqu 1 and 1.68 compared to Driepan (last two lines of Table 12).

In Miall's method, the theoretical P values range exponentially from 1.00 to 126.25 ($0 \leq \theta < 251°$). Table 13 compares some of the operational ranges and resulting P values of Miall's (1976) method with those calculated using the Le Roux (1992) method.

Table 13. Operational ranges and their corresponding sinuosity values calculated with Miall's (1976) and Le Roux's (1992) methods. Note the similar values at small operational ranges as well as the significant differences at greater ranges.

θ or ϕ	P (Miall, 1976)	P (Le Roux, 1992)
75°	1.09	1.07
150°	1.54	1.35
225°	4.93	2.12
251°	126.25	2.69

It can be concluded that the applied methods indicate low local and regional sinuosity values.

4.3.3. Estimation of the channel width/depth ratios

As mentioned earlier, there are two outcrops exposing major channel cross-cuts (Montaqu and Stembok). The description and illustration of the channel fills are presented in Ch. 4.2.3.2.: Fig.25 (Montaqu) and Figs.26-29 (Stembok).

In the case of Montaqu, the real trend (i.e. long axis) of this medium-sized channel is deduced from the palaeo-flow directions provided by the cross-bedded sandstones developed within the structure. In the case of Stembok, the real strike of the major channel is deduced from the strikes of the minor channel-shaped conglomerate bodies found within the major channel. The strikes of conglomerate bodies resulted from direct outcrop measurements.

Using the channel strike orientation data and the apparent widths, the true channel widths and the width-depth ratio is determined for the medium-sized channel of Montaqu (Fig.82A) and for the channel-shaped conglomerate body (Stembok) (Fig.82B).

As the western termination of the major channel (Stembok) is covered, the width of the channel is estimated to be a minimum of 300 m. Using the orientation data provided by the minor channel-shaped bodies, the true width of the channel is about (300 x $sin75° = 289.77\,m$). Fig.25 shows that the preserved channel fill is 10 m which indicates that the minimum depth of the channel was ~10 m. Accordingly, the width/depth ratio of the major channel is 29 ($290 \div 10$) (Table 14).

Table 14. The width/depth ratio of two larger channels in the study area.

Channel (locality)	*Width (m)*	*Depth (m)*	*Width/depth ratio*
Montaqu	21.13	5	4.22
Stembok	290	10	29

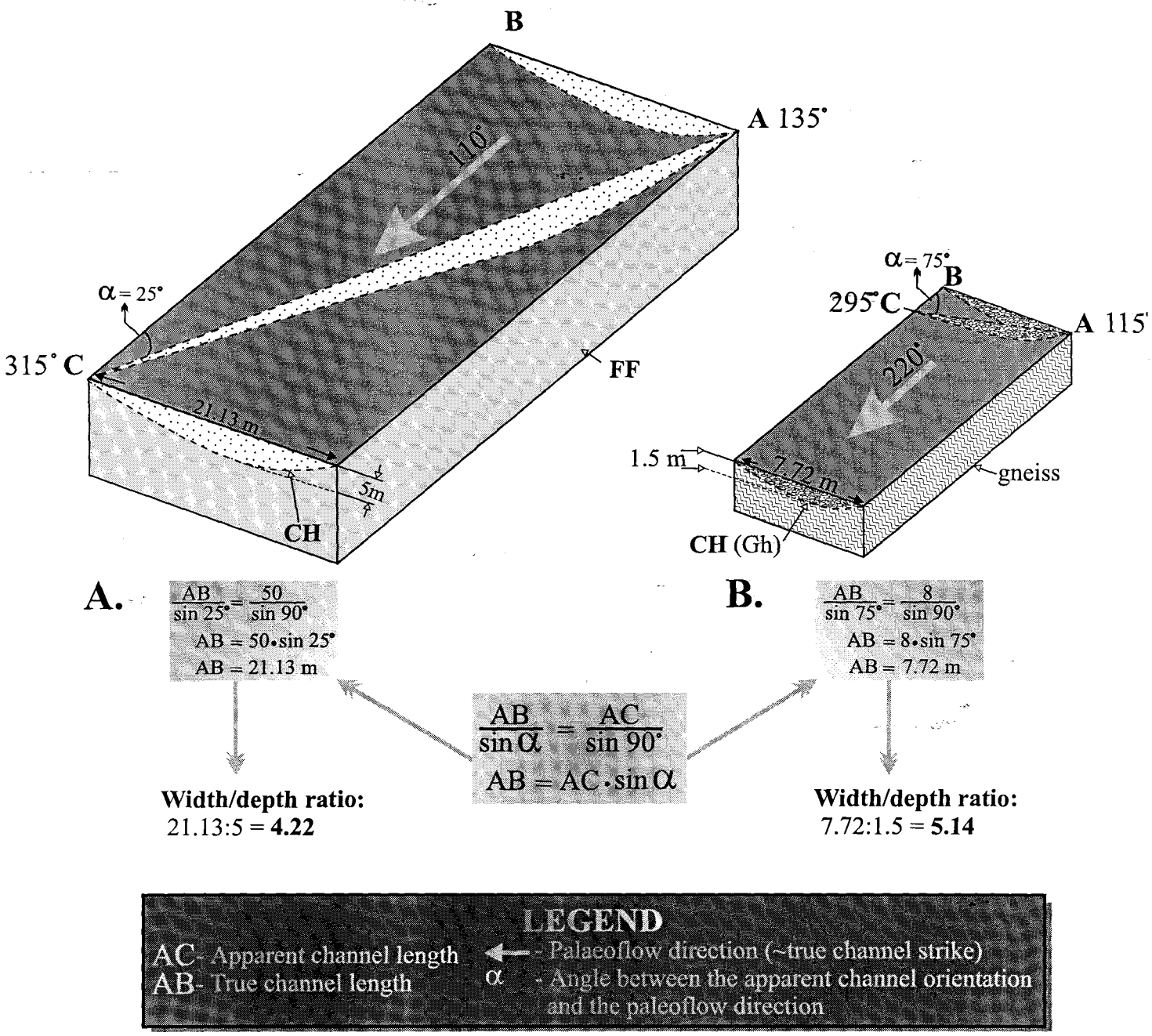

Fig. 82. Calculations of true channel-body orientation and width/depth ratio.
A. Channel sandstone (CH) scoured in fine grained sediments (FF) (Montaqu).
B. Minor channel-shaped conglomerate body (Gh) from a major channel (CH) (Stembok).

4.4. Grain size/shape analysis

The measured clast parameters (size/roundness/sphericity) are presented in the form of clast size distribution histograms, roundness histograms of the most frequent clast sizes (-3,91 & -3,33ϕ) and sphericity pie charts. The diagrams for each sampling point are attached after the table of raw measurements for the respective sampling locality (Appendix 2 p.1a - 27a). The calculated statistical parameters of each sampling point are given in Appendix 2 (p.28 - 41). The evaluation of the findings is discussed in Ch. 5 and 7.

The clast size distribution map (Fig.83) was based on the histograms of the longest (C)-axis of the clasts. Each circle represents the most frequent particle class of the respective sample. There is no observable change in the size of these circles: in other words, the clast size distribution is so random over the area that any kind of data grouping was unachievable. Hence a WSW transport direction (see Ch.4.3.1.), which might have been manifested as a slight WSW clast size decrease, was not detected. The lack of such patterns might be explained by the length of the study area relative to those distances over which remarkable textural changes would occur (Ch. 3.3.2.). Additionally, the fact that the E-W trending outcrop belt of the Middle Unit is perpendicular to the palaeo-current directions (Ch. 4.3.) would help account for the absence of progressive grain size change pattern.

The clast roundness variation maps (Fig. 84 & 85) were based on the roundness histograms of -3.9 and -3.3ϕ (150 & 100 mm) particle classes of each sample. There is an apparent difference between the samples of the Middle Unit and the those of the Basal Unit, the latter containing more angular clasts (Fig.84B & C; Fig.85B & C). This difference is more pronounced when the larger particle classes (-3.9ϕ) are compared (Fig.84). As in the case of the clast size distribution, there was no noticeable change parallel to the palaeo-transport directions. The roundness difference within the Basal Unit is caused by the fact that the lowermost conglo-breccia formation was incorporated into the conglomerate-sandstone-mudstone succession. As the roundness variation maps illustrate, the lowermost conglo-breccia formation is the most angular deposit of the whole analysed succession (Fig.84C & 85C: Roly Poly, Lauriston, Lizzulea and Kilgour sampling points).

The sphericity values are randomly distributed, and therefore data grouping was impracticable (Fig.86A,B & C.)

The standard deviations shown in the tables of calculated statistical parameters (Appendix 2, p.28-41) indicate that the Middle Unit samples are better sorted then those of the Basal Unit.

In conclusion, it can be stated that the clast size distributions and sphericity variations of the collected samples are patternless, while the clast roundness variations and standard deviations display a regional pattern indicating that the Basal Unit is texturally less mature than the overlying Middle Unit.

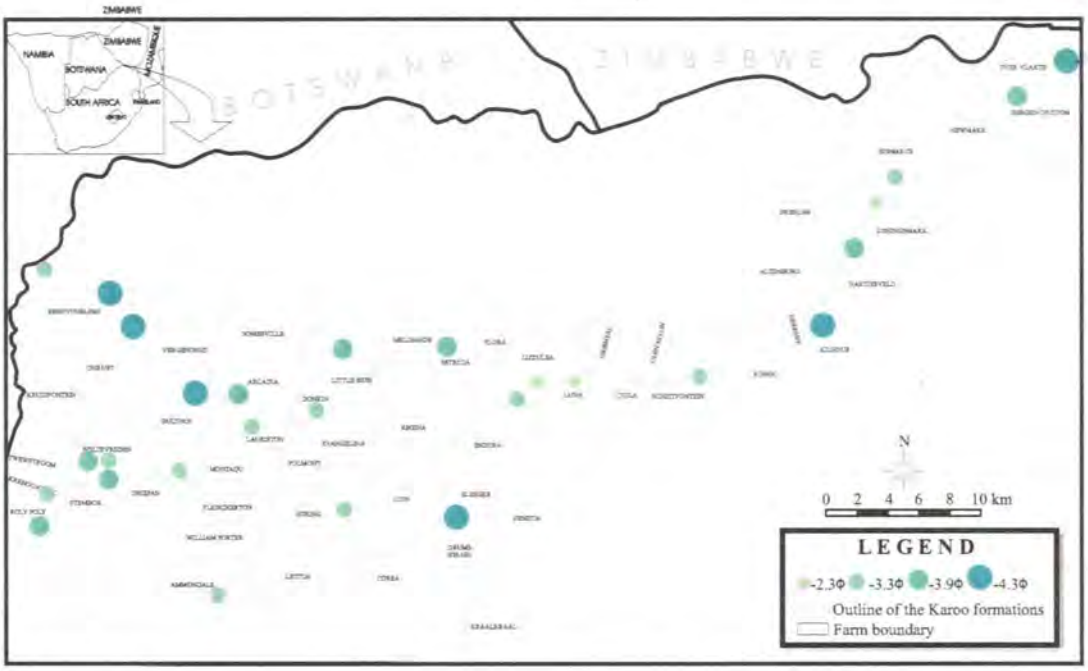

Fig. 83. Clast size distribution map. Circles represent the most frequent particle class.

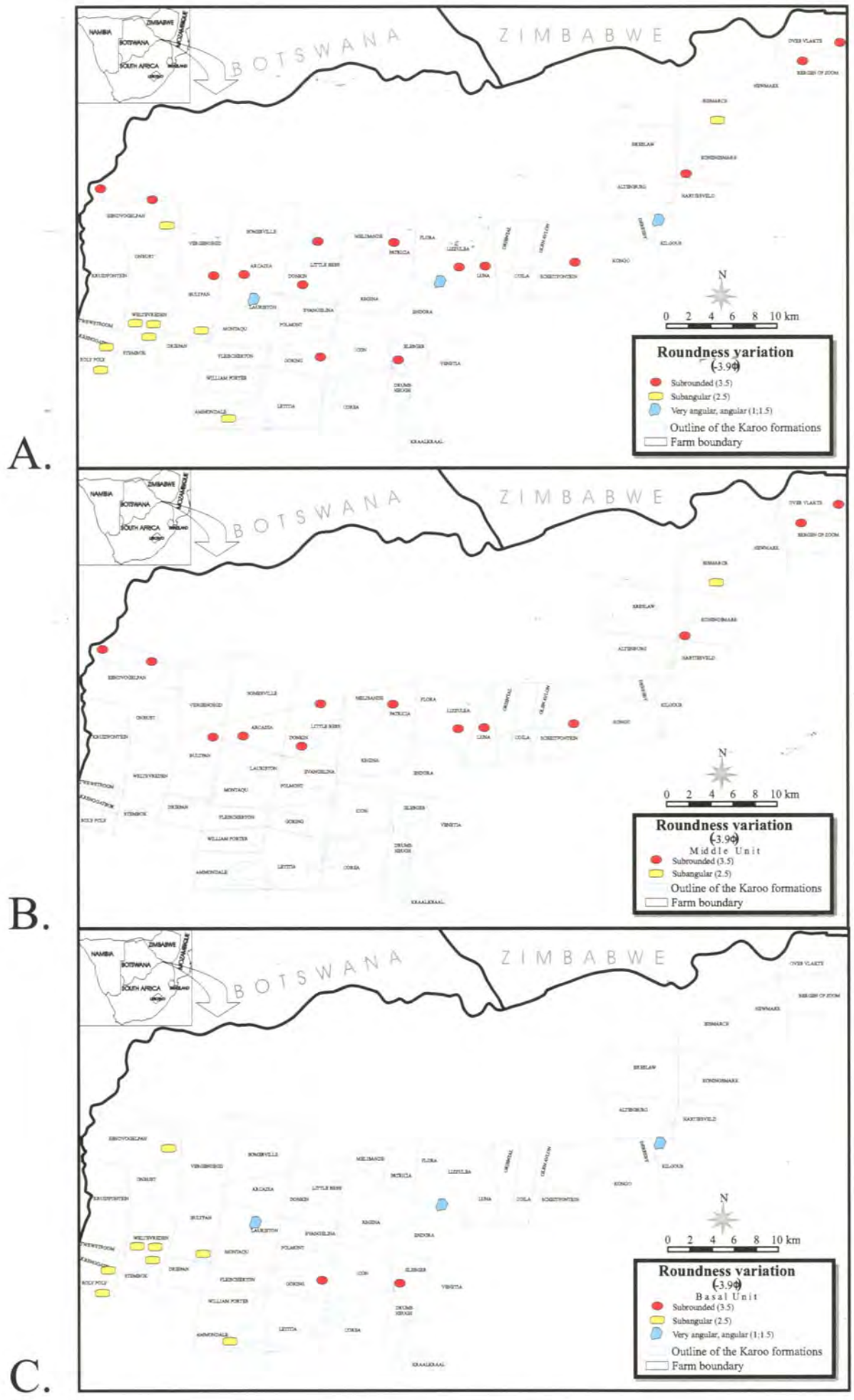

Fig. 84. Map of clast roundness variation (-3.9Φ) **A -** All sampling points. **B -** Middle Unit. **C -** Basal Unit (see text for explanation).

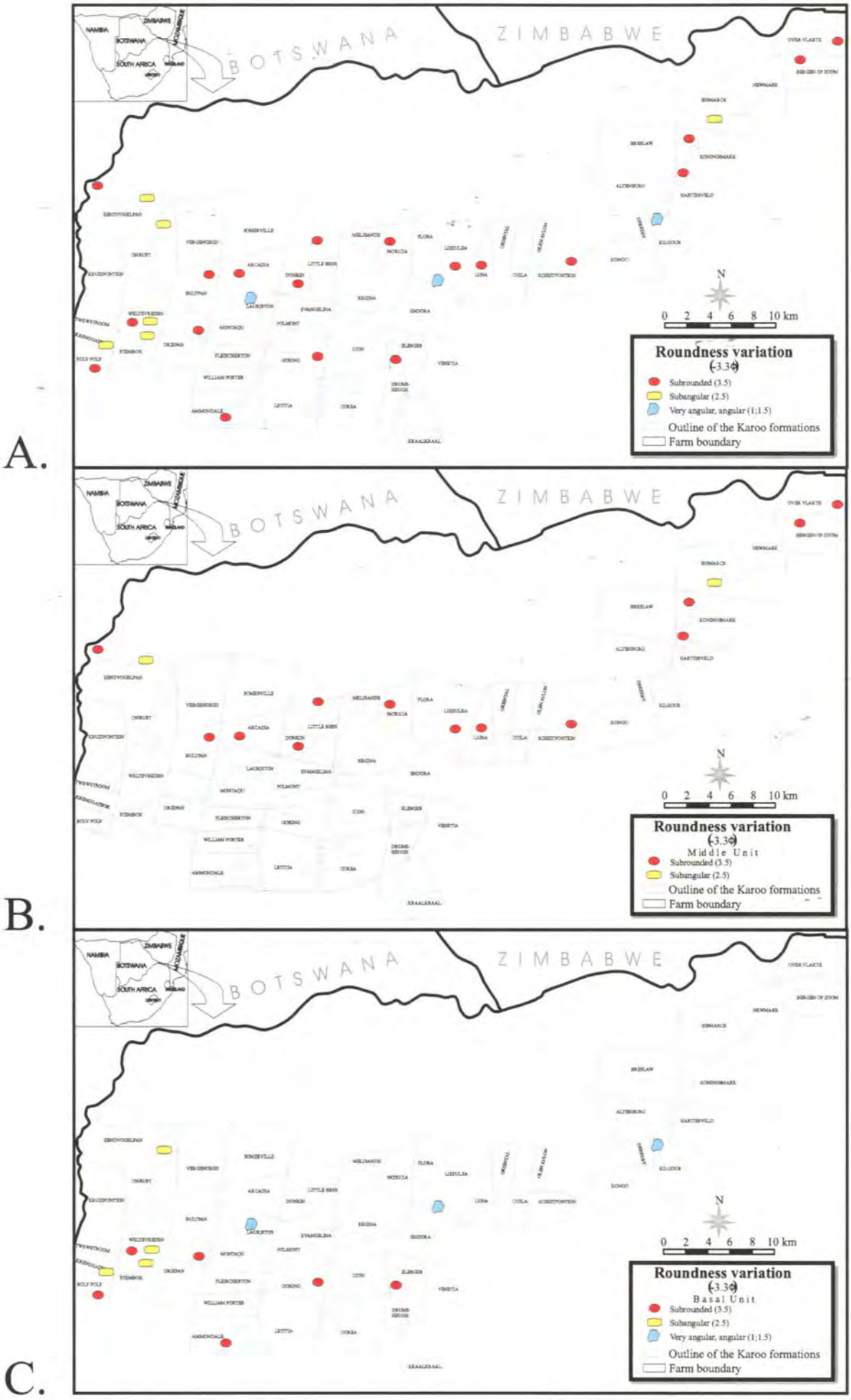

Fig. 85. Map of clast roundness variation (-3.3ϕ) **A -** All sampling points. **B -** Middle Unit. **C -** Basal Unit (see text for explanation).

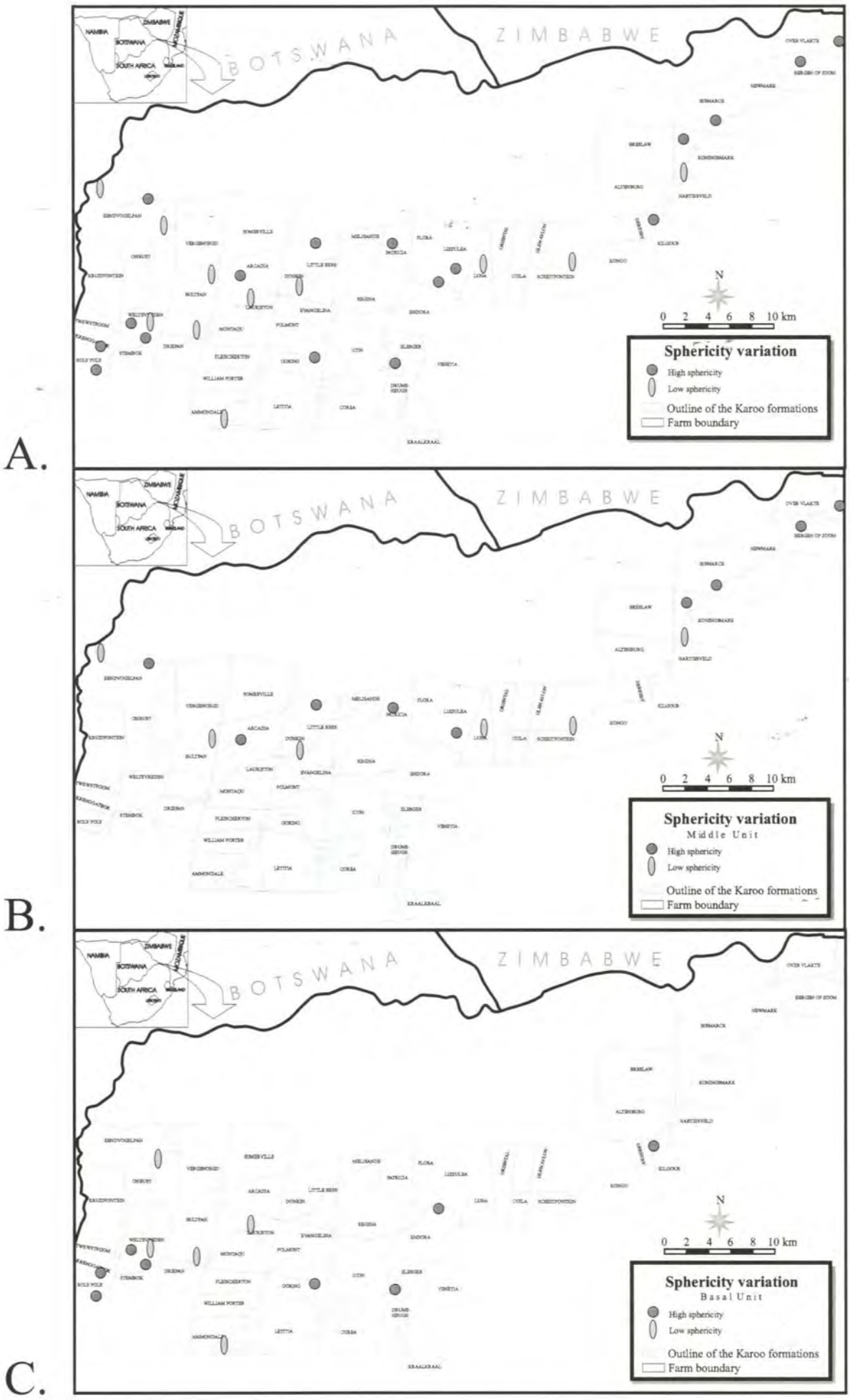

Fig. 86. Map of clast sphericity variation **A -** All sampling points.
B - Middle Unit. **C -** Basal Unit (see text for explanation).

4.5. Petrographic studies

The petrology of sedimentary rocks generally reflects the source of the detritus even though the original detrital composition may have been modified by extremely complex interactions among physical/chemical processes (e.g. weathering, rigour and duration of erosion/transportation, selective entrainment and transport, diagenesis), geological conditions (e.g. lithology, basin tectonics, base level changes, sediment supply) and climate (e.g. water discharge, sediment supply). Petrographic studies were carried out in order to gain a better understanding of the paleo-environment by supplying information about the dynamics of the sedimentation and the probable source rocks.

The petrographic studies comprise of detailed thin-section (72) descriptions, and graphical and statistical evaluations of the petrographic data by means of ternary diagrams and bar charts. The thin-section descriptions were based on qualitative observation and semi-quantitative visual estimates using composition charts for mineral percentage, grain size, sorting, roundness, sphericity, etc.

The collected samples macro/microscopically appeared to be rather pure quartz arenites/greywackes. Increasing the level of accuracy by intensive and time consuming point counting seemed to be unnecessary for the needs of the investigation. The original sampling strategy was designed to collect representative specimens of the different arenaceous lithofacies (arenites, greywackes and sandy mudstones), calcretes and silcretes. Hence the sampling points were not systematically distributed throughout the units.

The statistical investigation was selectively based on 53 quartz arenite and wacke samples. The reason for excluding the other 19 samples was because of the different durability characteristics of the grains other than quartz. Such differences in durability can obscure textural signals related to provenance. During the statistical analysis, the following parameters were evaluated and presented in bar charts: modal composition, sample grain size, polycrystalline and non-undulatory quartz grain frequency, quartz-grain sphericity, quartz-grain roundness and heavy mineral content.

Because the sample size of the medial part of the Middle Unit was too low (4) to bear statistically significant meaning, these four samples were studied together with the other Middle Unit samples. Ideally, all four stratigraphic units should be represented by the same number of samples, but as mentioned before, the original sampling strategy was not meant for detailed statistical comparisons. Therefore, the result of the statistical investigation should the treated with caution and used in conjunction with the results of the other methods applied. For instance, the results of the palaeo-current analysis were vital in the estimation of source regions.

4.5.1. General descriptions

The 72 detailed thin section descriptions of the four Karoo Supergroup units are presented in Appendix 4. The collected samples were grouped according to the Pettijohn et al. (1972 in Pettijohn et al., 1987) classification scheme. Table 15 shows the sample distribution among the five, microscopically identified rock categories (arenite, wacke, mudstone, calcrete glaebules and silcrete). The most commonly described arenaceous rock type of the collected sample population is quartz arenite (41 samples), followed by quartz wacke (12 samples). The ternary diagrams of Fig. 87A & B are based on the abundance of the main framework minerals in the arenites and wackes. Litharenites (5) were encountered only among the samples of the Upper Unit, while lithic greywackes belong to the Basal Unit (2) and Upper Unit (1). The two analysed sandy mudstone samples were described from the Basal Unit, and the four calcrete and four silcrete samples were described from the Upper Unit.

The statistical analysis of the mineral composition of the quartz arenites and wackes (Fig. 88) reveals that the samples have high (>97.5%) quartz and very low (<0.9%) lithic fragment content. The Upper Unit has the highest feldspar value (2.4%), and the Middle Unit the lowest (0.3%).

The grain size distribution (Fig. 89) indicates a progressive size decrease and sorting increase from the coarse and poorly sorted Basal Unit to the predominantly very fine- to fine-grained and better-sorted Clarens Formation.

Table 15. Microscopically identified sedimentary rock types in the Tuli Basin.

FORMATION (SAMPLE NUMBER)	ARENITE			WACKE		MUDSTONE	CALCRETE GLAEBULE	SILCRETE
	Quartz arenite	Sublitharenite	Litharenite	Quartzwacke	Lithic wacke			
Clarens Formation (8)	**9** (LIT2, GRE1, GRE2, HILL2, LIT3, PON2, PRI1, PRI2, WEI6)							
Upper Unit (25)	**7** (BRE1, FAU1, HAL8, PAR1A, PON1A, RAT4, TSO1)	**1** (MAC1)	**6** (BLY3, HIL2, LIZIIB, MON2, NEK1)	**3** (BAL5, LIT1, LIZIIA)	**1** (TSO2)		**4** (BAL2, NEK2, BRE2, RAT2)	**4** (BAL1A, BAL1B, HILL1, LIT4)
Medial part of the Middle Unit(4)	**3** (HAL1, HAL2, HAL3)			**1** (HAL6)				
Lower part of the Middle Unit (11)	**11** (ALT2, BIS1, DON2B, EEN1, EEN3, EEN8, HAL7, LIZ1, LIZ3, OVE2, REG7)							
Basal Unit (23)	**11** (ALT1, DON1, DON2A, DRU2, EEN5A, KIL1, LAU3, MOG10A, MOG10B, ROL3, WEL14)			**8** (AMM1, CIR1, LAU4, REG2, STE2, WEL2, WEL6, WEL18)	**2** (AMM3, REG5)	**2** (MOG8, STE3)		
Total 72	41	1	5	12	3	2	4	4

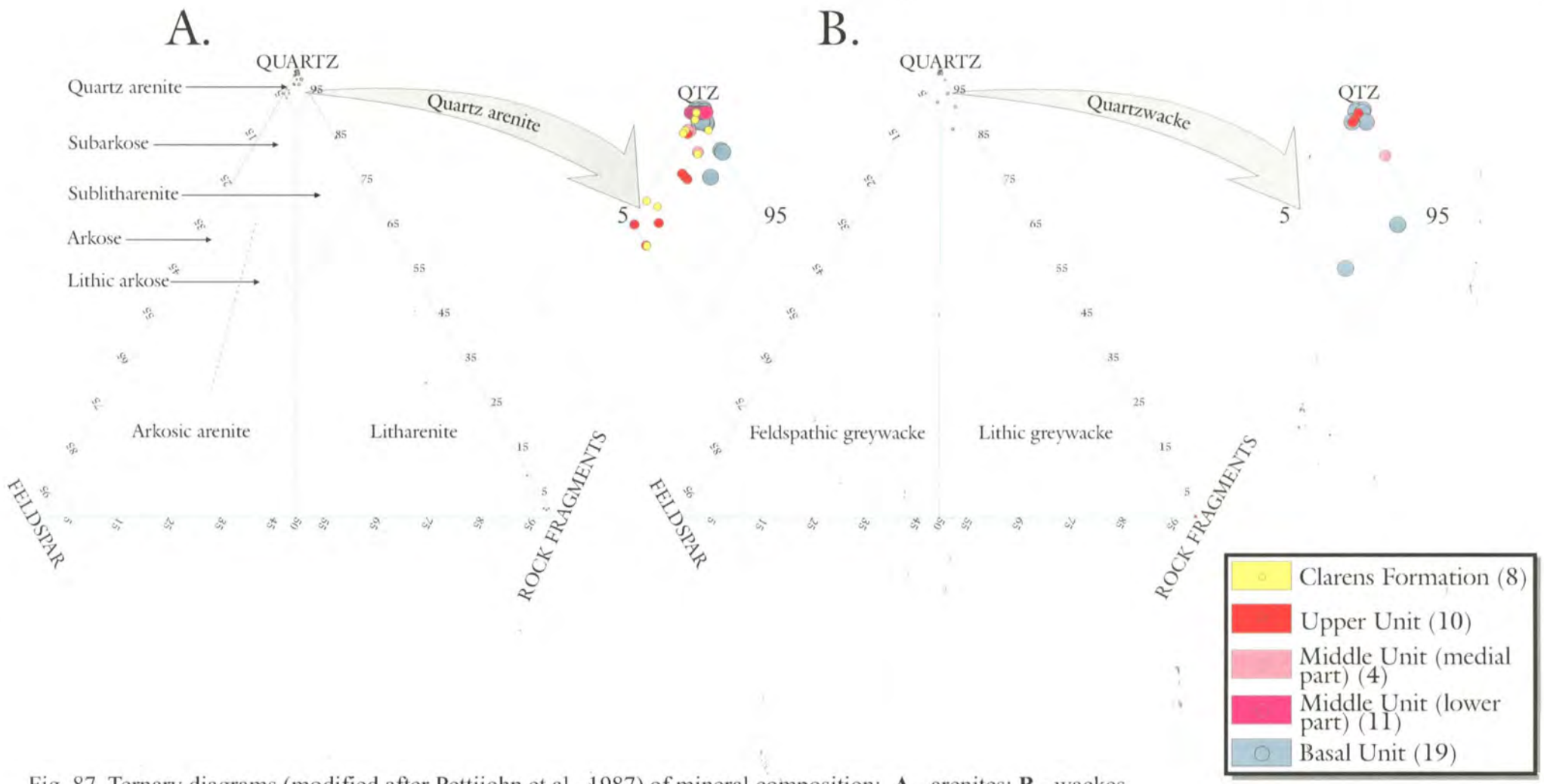

Fig. 87. Ternary diagrams (modified after Pettijohn et al., 1987) of mineral composition: **A** - arenites; **B** - wackes.

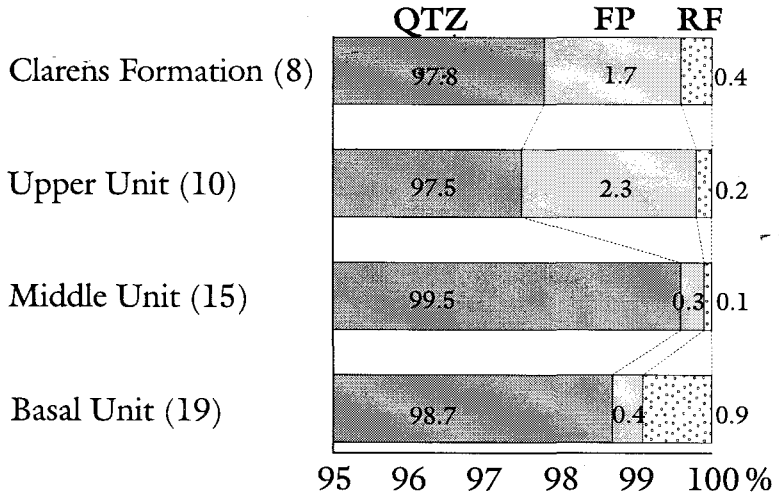

Fig. 88. Mineral composition of quartz arenites and wackes.

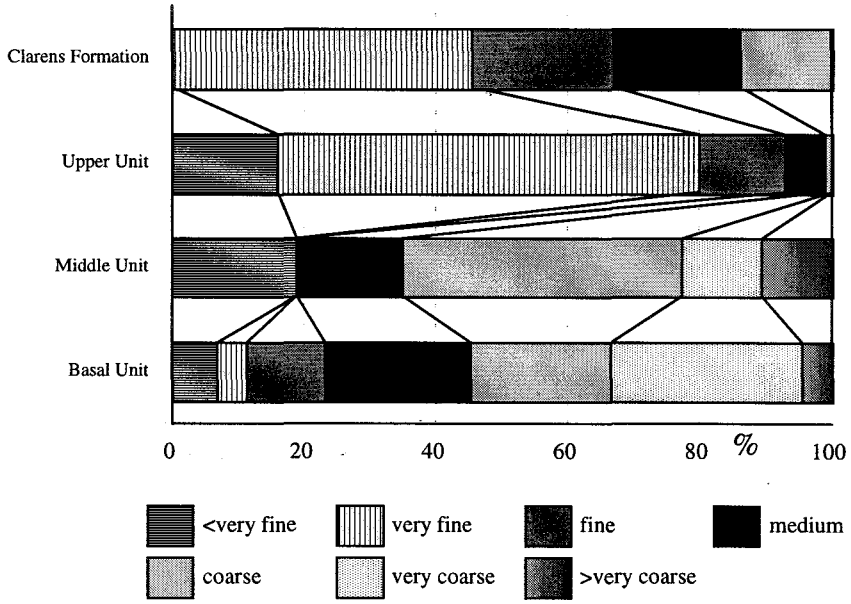

	<very fine	very fine	fine	medium	coarse	very coarse	>very coarse
Clarens Formation	0.00	45.48	21.48	19.26	13.67	0.00	0.11
Upper Unit	16.00	64.00	13.00	6.00	1.00	0.00	0.00
Middle Unit	18.87	0.00	0.00	16.07	42.53	12.00	10.53
Basal Unit	6.84	4.47	11.89	22.11	21.32	29.00	4.37

Fig. 89. Grain size distribution of arenites in the Tuli Basin.

The plots of the polycrystalline and undulatory quartz grains (Fig. 90) as well as the quartz grain sphericity (Fig. 91) demonstrate a progressive, consistent change from the Basal Unit to the Clarens Formation. Whereas the abundances of polycrystalline quartz grains and quartz grains with undulatory extinction decrease, the proportion of high-sphericity quartz grains increases from ~36% in the Basal Unit to ~60.55% in the Clarens Formation. On the other hand, the progressive change in the roundness (Fig. 92) and heavy mineral (Fig. 93) content are systematically interrupted by anomalies. For instance, the increase in the frequencies of the rounded and subrounded grains and heavy minerals from the Basal Unit (0%, ~32% & 0%) to the Clarens Formation (40%, ~51% & ~89%) are punctuated by the "out-of-trend" values ~26.5%, 55% & 100% of the Upper Unit. The frequency of the subangular (Fig. 92) grains decreases from ~45% (Basal Unit) to ~9% (Clarens Formation), but again it has a relative peak (~18.5%) in the Upper Unit. The validity of the anomalies is definite as they occur systematically in all analysed parameters, although the absolute values of the anomalies are related to the variable sample numbers (relatively small sample numbers being compared with larger sets).

Kimberlitic indicator minerals (e.g. garnet, ilmenite, spinel, chrome-diopside) have not been detected in any of the 72 examined samples.

	Polycrystalline qtz	Undulatory qtz
Clarens Formation	0.00	65.55
Upper Unit	1.00	67.50
Middle Unit	9.93	69.66
Basal Unit	18.42	79.47

Fig. 90. Polycrystalline and undulatory quartz distribution.

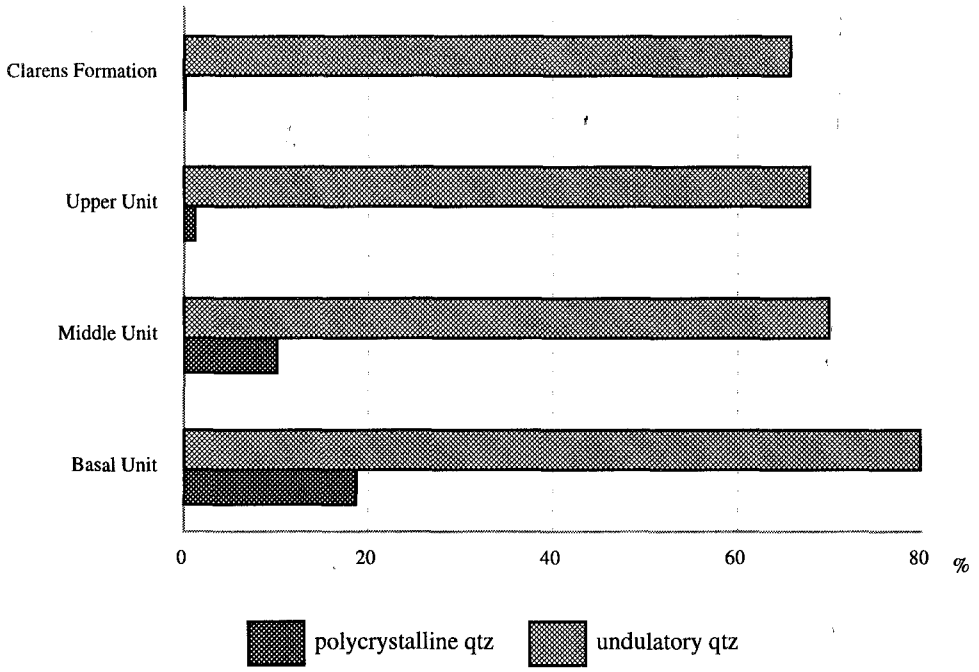

	High sphericity grains
Clarens Formation	60.55
Upper Unit	58.00
Middle Unit	48.33
Basal Unit	36.05

Fig. 91. Quartz grain sphericity

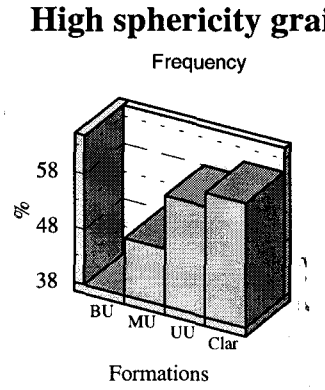

	subangular	subrounded	rounded
Clarens Formation	8.88	51.115	40
Upper Unit	18.50	55.00	26.50
Middle Unit	16.66	49.67	30.67
Basal Unit	45.26	32.37	0.00

Fig. 92. Roundness distribution of quartz grains.

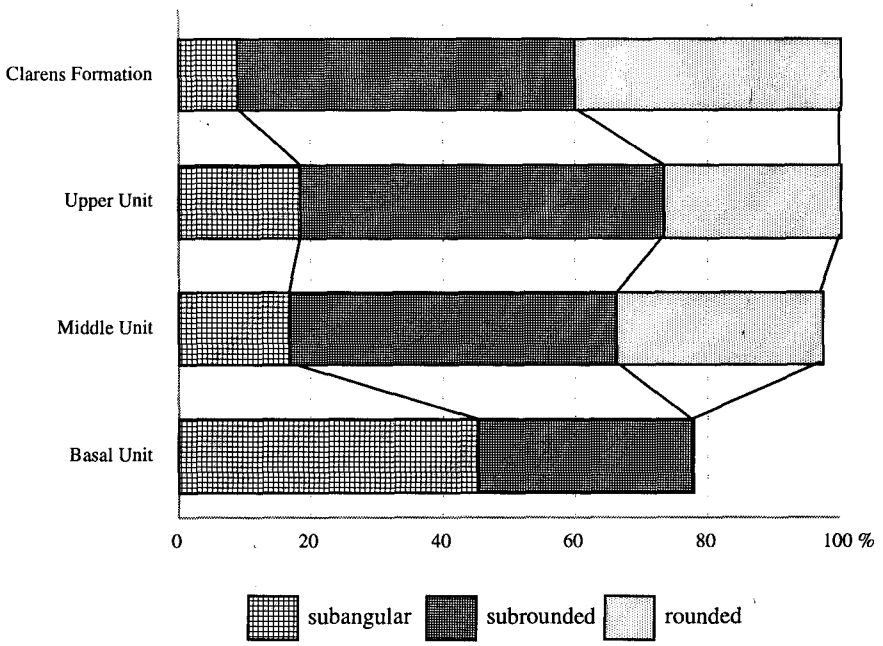

	Total sample number	Sample number containing heavy minerals	%
Clarens Formation	9	8	88.88
Upper Unit	10	10	100.00
Middle Unit	15	8	53.33
Basal Unit	19	9	47.30

Fig. 93. Heavy-mineral content.

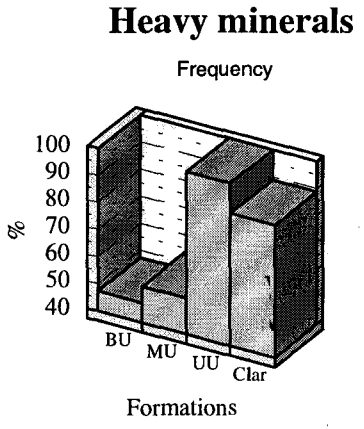

4.5.2. Basal Unit

The arenaceous rock samples from the Basal Unit (23) are quartz arenites (11), quartz wackes (8), lithic greywackes (2) and sandy mudstones (2).

Microtexture analysis of the samples showed that the framework grains are coarse-grained, poorly-sorted, mostly subangular-angular, elongated and randomly orientated. There were no downstream grain size changes across the sampling area. Most of the samples are immature or submature. When grain-supported, the particles show point contacts, but sutured grain contacts and authigenic overgrowths are rare. The porosity figures range from 0 to 35%.

Where present, the *matrix* consists of clay, mica, quartz and feldspar. The matrix, in most of the quartzwackes (CIR1, REG2, WEL2, WEL6, WEL18) and in both sandy mudstone samples (MOG8, STE3), displays slight lamination determined by the blade or lath-shaped clay and mica minerals. In these samples, the laminated matrix asymmetrically wraps around the coarser, angular detrital grains, so that usually the matrix below the grains is more bent/squashed then the matrix laminae overlying the grains. Microslumps (swirly structures) were also detected in laminated matrix of the quartzwackes (e.g. WEL2).

In the quartz arenites and wackes, the modal proportions of the framework quartz grains range from 93 to 100%, with an average value of 98.7%. Detrital feldspar grains constitute 0 to 4% of the samples (av.~ 0.4%), and lithic fragments range from 0 to 4% (av. ~0.9%). Heavy mineral concentrations are very low (<<0.01%, 1-2 grains per thin section) and more than half of the samples are heavy mineral free.

The quartz grains consist of ~82% monocrystalline, ~18.5 % polycrystalline grains. About 80% of the *monocrystalline quartz* grains show undulatory extinction. In addition, the poorly-sorted, very fine to granular monocrystalline quartz grains commonly exhibit fractured, shattered textures.

Polycrystalline quartz grains are predominantly coarse- or very coarse-grained, with plentiful fine- or medium-grained crystals. Coarse polycrystalline grains with low crystal number were very rarely

encountered. A few polycrystalline grains exhibit bimodal crystal sizes, and the crystals are rather well-sorted. The crystal shapes are mostly irregular, subequant and only very rarely slightly elongated. The crystal boundaries are mainly sutured, with non-sutured contacts being virtually absent.

The fine- to medium-grained detrital *feldspar* is plagioclase and microcline. Commonly the plagioclase is twinned on the albite law, while the microcline displays tartan (cross-hatched) twins. Generally the feldspars are altered, and sericitization seems to be advanced, especially in the quartzwacke samples where 'ghost' grains also occur (LAU4).

Rock fragments are muscovite-bearing metamorphic rock particles. The micas include both muscovite and biotite.

Heavy minerals contribute to the finer grain size group (~0.125-0.25 mm) and only the most resistant types are present (opaque minerals, zircon).

4.5.3. Middle Unit

Out of the15 Middle Unit samples, 11 quartz arenite and one quartz wacke (HAL6) were identified. Texturally, three samples are muddy siltstones, while the other 12 samples consist of sandstones and pebbly sandstones (EEN1, HAL7, LIZ3). Sample HAL6 was taken from the transition between the lower and medial part of the Middle Unit.

Microtexture analysis of the samples showed the framework grains to be usually coarse-grained, moderately-sorted, mostly subrounded-rounded and randomly orientated. There were no grain size changes across the sampling area. Cross-lamination was observed in the samples from the medial part of the Unit (HAL1, HAL2, HAL3), and sample HAL2 is flaser bedded. Most of the samples are supermature (lower part) or submature (medial part). When grain-supported, the particles are closely packed, showing point and concavo-convex contacts. Sutured grain contacts are rare, whereas authigenic overgrowths are common on the quartz grains. The porosity figures range from 0 to 40%.

The *matrix* consists of clay and quartz. It is present in all samples from the medial part of the Unit and in one sample (REG7) from the lower part. In the transitional sample (HAL6), the matrix is inhomogenous: among the closely packed grains, it is exclusively clean clay, whereas among the loosely packed grains, it consists of coarse silty mud and muddy coarse silt. Sample HAL6 also contains distinct lumps of slightly deformed siltstone clasts which seem to have a similar texture to the matrix between the loosely packed grains.

The modal proportions of the framework quartz grains range from 98 to 100%, with an average value of approximately 99.5%. Detrital feldspar grains constitute 0 to 1% of the samples (av.v.~ 0.3%). The proportion of lithic fragments ranges from 0 to 2% (av.v. ~0.1%). Although ~40% of the samples are heavy mineral free, the highest heavy mineral concentration per sample was recorded in the samples of the Middle Unit.

The quartz grains consist of ~91% monocrystalline and ~10 % polycrystalline grains. About 70% of the *monocrystalline quartz* grains show undulatory extinction. Occasionally, the larger monocrystalline quartz grains contain needle-like (rutile?) mineral inclusions and subparallel lines or randomly orientated very small fluid inclusions. There are a few quartz grains with zircon inclusions as well. The *polycrystalline quartz* grains are predominantly coarse- or very coarse-grained, with plentiful fine-grained, well-sorted crystals. The crystal shapes are mostly irregular, subequant and only very rarely slightly elongated. The crystal boundaries are mainly sutured, with non-sutured contacts being virtually absent.

The vast majority of the very fine sand or coarse silt-grained detrital *feldspar*s (plagioclase) are twinned on the albite law and slightly altered (sericitisation). *Rock fragments* are the previously mentioned lumps of slightly deformed muddy coarse siltstone. The micas consist of muscovite (only one sample EEN1). *Heavy minerals* usually contribute to the finer grain size group (~0.125-0.25 mm), but in the lower part of the Unit (e.g. EE1) the zircons and the brown tourmaline are relatively coarser (0.25-0.5 mm) grained and well rounded. In addition to the ultrastable types (zircon, tourmaline, opaque minerals), green hornblende was also observed (HAL7).

4.5.4. Upper Unit

The arenaceous rock samples from the Upper Unit (17) are quartz arenites (7), litharenites (6), quartz wackes (3) and lithic greywacke (1). A detailed description of the calcrete (4) and silcrete (4) samples is to be found in Appendix 4, while a summary and interpretation thereof are in Ch. 4.7. & 5.7. and Ch. 4.8. & 5.8., respectively.

Microtexture analysis of the arenaceous samples showed that the framework grains are generally very fine-grained, moderately-sorted, mostly subrounded-rounded, rather spherical and randomly orientated. The coarser grains (0.25 to 1 mm) are predominantly rounded or well rounded. There were no grain size changes across the sampling area. Most of the samples are mature. When grain-supported, the particles show point contacts, whereas sutured grain contacts and authigenic overgrowths are absent. The porosity figures range from 0 to 20%.

The *matrix* consists of microquartz, clay and calcite(sparite or micrite) in the wackes (BAL5, LIT1, LIZIIA, TSO1), and of microquartz and feldspar in the litharenites. In most litharenites, the upper grain size limit of the matrix was established at 0.125 mm and not 30 microns because of the strong bimodal grain size distribution (<0.125 mm and >0.5 mm).

In the quartz arenites and wackes, the modal proportions of the framework quartz grains range between 95 and 100%, with an average of ~97.5%. Detrital feldspar grains constitute 0 to 5% of the samples (av.~ 2.3%). In the litharenites and lithic wackes, the modal proportions of the framework quartz grains range from 0 to 85%, whereas the detrital feldspar grains constitute 0 to 10% of the samples. The proportion of lithic fragments ranges from 0 to <1% (av. ~0.2%) in the quartz arenites and wackes, and between 15 and 98% in the litharenites and lithic wackes. Heavy minerals are widespread in the Upper Unit, but their concentration is rather low as none of the samples contain more then 0.01% (2-3 grains per thin section) of heavy minerals. Only one litharenite sample (LIZIIB) is heavy mineral free.

The quartz grains consist of ~99% monocrystalline, ~1% polycrystalline grains. ~67.5% of the *monocrystalline quartz* grains show undulatory extinction. *Polycrystalline quartz* grains were detected only in two samples (BRE1, FAU1). These grains contribute to the coarsest grain fraction of these samples. The composite grains consist of more than 5 medium silt or medium sand grained crystals. The crystal shapes are mostly irregular, subequant and rarely slightly elongated. The crystal boundaries are mainly sutured, but non-sutured contacts are also present.

The fine- to medium-grained detrital *feldspar* is plagioclase and microcline. Commonly the plagioclase is twinned on the albite law, whereas the microcline displays tartan (cross-hatched) twins. A few feldspars are slightly altered (sericitisation, brown clouding). Alteration seems to be advanced in sample RAT4 where 'ghost' grains also occur.

Rock fragments in the samples of the Upper Unit are predominantly reworked carbonate glaebules. Chert, silty mudstone, siltstone, very fine sandstone and mica (muscovite) are minor components (<1%), and reworked silcrete chips are found only in one sample (MAC1). Reworked bone fragments were also noted in the litharenite samples (BLY3, HIL2, LIZIIB, MON2). The reworked carbonate glaebules and the terrigenous rock fragments have been matched with the *in situ* carbonate glaebules and other terrigenous rock types of the unit. Bioturbation features have been noticed in the reworked carbonate glaebules of the litharenites.

Heavy minerals (zircon, tourmaline, opaque minerals, hornblende) contribute to the finer grain size group (~0.1 mm) and are rounded or subrounded in their shape.

4.5.5. Clarens Formation

The rock samples from the Clarens Formation (9) are exclusively quartz arenties. All samples were collected from the lower part of the Formation.

Microtexture analysis of the samples showed that the framework grains are generally very fine-grained, moderately to well-sorted, mostly subrounded-rounded, rather spherical and randomly

orientated. Bimodal grain sizes and exceptionally well rounded, spherical, coarse (0.25-1mm) grains were also observed (e.g. GRE2). There is a total lack of silt- and clay-sized detrital grains (finer than 0.062 mm). Most of the samples were mature. Both evenly and inversely graded laminae occur (e.g. PON2). The individual laminae are well-sorted and show grain size differences. The adjacent laminae often show sharp grain size differences. Some of the laminae are inversely-graded. Bioturbation features were observed in GRE2, PRI1 and WEI6 samples, an interpretation of which is given in Ch.4.2.4.2. The particles show point contacts; sutured grain contacts are almost absent (the exception being PR2), though authigenic overgrowths are quite common (e.g. HILL2, LIT2, PON2, PRI1-2, GRE1). The porosity figures range from <5 to 20%.

Matrix, consisting of microquartz, limonite, mica (?) and clay mixture, was observed in only one sample (~5% of PRI2).

The modal proportions of the framework quartz grains range from 95.5 to 100%, with an average of ~97.8%. Detrital feldspar grains constitute <1 to 5% of the samples (av.~ 1.7%). Two samples (GRE1 & PRI2) are feldspar free. Lithic fragments range from 0 to <1% (av. ~0.4%). Heavy minerals are widespread, but their concentration is rather low as none of the samples contain more then 0.01% (2-3 grains per thin section) of heavy minerals. Only one sample (PRI2) is heavy mineral free.

The quartz particles consist of 100% monocrystalline grains and 65.5% show undulatory extinction.

The very fine-grained detrital *feldspar* consists of plagioclase and microcline. Commonly the plagioclase is twinned on the albite law, whereas the microcline displays tartan (cross-hatched) twins. A few feldspars are slightly altered (sericitisation, brown clouding).

Rock fragments are chert and reworked, subangular silcrete chips (the latter only in one sample, LIT2).

Heavy minerals (zircon, tourmaline, opaque minerals, hornblende) contribute to the finer grain size group (~0.1 mm) and are rounded or subrounded in their shape.

4.6. Colouration of the continental beds

The continental deposits of the Tuli Basin show a progressive colour change from the grey-whitish-yellowish Basal Unit through the purplish-pinkish Middle Unit, up to the predominantly red/reddish Upper Unit and yellowish-whitish Clarens Formation. The colour contrast between the lower and upper part of the Karoo Supergroup is thought to be the result of contrasting redox conditions in the depositional environments, red being indicative of oxidizing, and green of reducing conditions (Turner, 1980; Miall, 1996).

The huge and acrimonious literature on the origin of the colouration of the continental beds invariably agrees that the yellowish-brownish and reddish colours are caused by minerals containing ferric ions (e.g. goethite-limonite, hematite), and the green pigmentation by ferrous ion-bearing minerals (e.g. pyrite, clay minerals) (PiPujol & Buurman, 1994; Weibel, 1998). The origin of the iron oxides/hydroxides indeed causes debate: it is argued that these are formed either in syn-depositional and/or post-depositional settings.

Syn-depositional iron oxides/hydroxides may form by precipitation directly from the iron saturated transporting agent (i.e. river water in alluvial setting) (Blatt et al., 1972). In this case, the grain coatings would be expected to be of more-or-less uniform thickness (Turner, 1980). The redeposition of red formations, especially of the hematite grains either from pre-existing red beds or lateritic soils, can also lead to reddening of originally non-red deposits (Eriksson, 1987).

Post-depositional iron-oxide formation is caused by the weathering processes of rock-forming ferromagnesian silicates that were buried in the sedimentary pile. The alteration products of these detrital minerals are initially hydrated brownish iron oxides, which are later on dehydrated and recrystallized into iron oxides (Friedman & Sanders, 1978). The weathering mechanism can develop under both semi-arid/arid and moist tropical climatic conditions (Friedman & Sanders, 1978; Eriksson, 1987). It is believed that prolonged subaerial exposure in a hot, seasonally wet climate is required in a free-draining, above-watertable setting, in order progressively to dehydrate the detrital amorphous and semi-crystalline brown hydrated iron oxides (McPherson, 1979). Dehydration is also promoted by sediment compaction.

This *in situ* post-depositional reddening could take place during early and/or late diagenesis. Early diagenetic reddening develops when iron-bearing detrital clay minerals are washed into the alluvium through mechanical infiltration. In this way, the terrigenous grains obtain a clay coating which being bathed in oxygenated groundwater may lead to iron oxide formation (Turner, 1980). During late diagenetic processes, the terrigenous ferromagnesian silicate (hornblende, pyroxene, biotite) grains themselves are oxygenated by the circulating ground waters. On the other hand, according to Walker (1968 in Blatt et al., 1972), the distribution of such iron oxides is essentially independent of the rock permeability as they are transferred from the interior of the decomposing ferromagnezian silicates to their exterior.

When the circulating ground waters act as oxygenating agents, the alteration processes depend on the permeability of the formations, the pH-Eh condition and circulation pattern of the groundwater (Miall, 1996:443) in the particular depositional basin, and do not necessarily require a hot, arid climate (Turner, 1980).

Microscopic evidence for diagenetic reddening includes alteration and clay replacement of feldspars; pits and ooids in garnet; the euhedral shape and small size of the hematite as well as its presence in the interstitial matrix; pseudomorphs after biotite and chlorite; and martitization of the magnetite grains (Turner, 1980). Additional evidence for mechanically infiltrated clay is that apart from the framework grains the sample contains only clay-size matrix (i.e. any intermediate, silt sizes are missing due to the filtering effect of the framework fabric).

Green colouration in predominantly red continental beds in a semi-arid/arid climate is explained by the existence of locally-reducing conditions (Slate et al., 1996). Such conditions are generated in surface-water gleys where pluvial water is ponded above an impermeable layer in the form of stagnant, perched water bodies (PiPujol & Buurman, 1994). The presence of organic matter, as a local reductant, is particularly emphasized in the prevention of precipitation of the oxidized iron minerals (Weibel, 1998). The source of such organic matter could be floral and/or faunal. Examples of locally-reducing environments caused by vegetation decay are given in Turner (1985), whereas the effects of the post-burial decomposition of animal carcasses is mentioned in Smith (1995).

4.6.1. Macroscopic description

Basal Unit

In the outcrops, the arenaceous deposits of the Basal Unit are predominantly white or pale yellow. Red or pink colouration can only be observed in a very few sandstones and sandy mudstones, bordering post-Karoo faults and cracks. The argillaceous deposits are usually light to dark grey, bluish-green or dark brown. There are yellowish, pale orange mudstone varieties as well. The carbonaceous mudstones are often black. Based on borehole data, 0.19% of the arenaceous (Fig. 94A) and ~14% of the argillaceous (Fig. 94B) rocks show reddish or purplish colours, and these occur exclusively in the upper part of the succession. The majority of the deposits (99.81% sandstone, ~86% fine-grained) exhibit various hues of black, green and grey. Copper-sulphides (e.g. pyrite) have been reported from the boreholes.

Middle Unit

In outcrops, arenaceous deposits of the Middle Unit are grey, white, pink, light purple or red. The red colour increases in abundance in the upper part of the unit. The argillaceous deposits are mainly yellow, green and grey, and less frequently light pink; purple colours were also observed. Based on borehole data, ~15% of the arenaceous (Fig. 95A) and ~31% of the argillaceous (Fig. 95B) rocks show reddish or purplish colours, the remainder being grey, green or dark brown. The mudstones are often variegated, especially toward the top of the unit.

Upper Unit

In the outcrops, the argillaceous sedimentary rocks of the Upper Unit are red-pinkish with green-grey-white intercalations. The sandstones are mainly red or, rarely, faded reddish; no white or green sandstones were observed. The mudstones and siltstones interbedded with the red sandstones are outstandingly red. Contrarily, the thickly bedded mudstones and siltstones show mainly green-grey colours and less commonly red colouration.

	OXIDATIVE cum. thick in m	REDUCTIVE cum. thick in m
Arenaceous deposits	0.94	490.59
Argillaceous deposits	301.28	1796.31

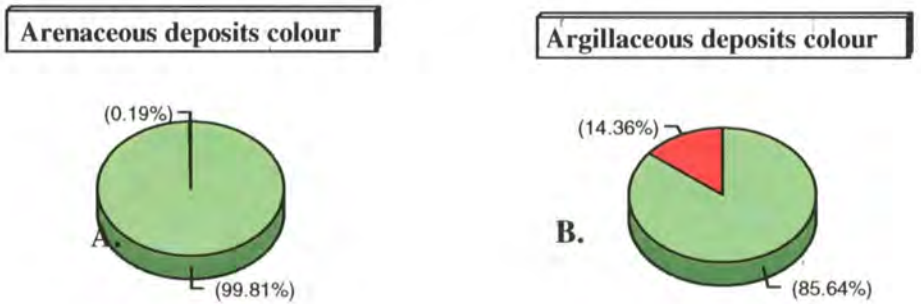

Fig. 94. Colour distribution in the Basal Unit. Diagrams
based on borehole data (Oxidative coloures in red, reductive coloures in green).

	OXIDATIVE cum. thick in m	REDUCTIVE cum. thick in m
Arenaceous deposits	54.19	302.16
Argillaceous deposits	154.62	340.94

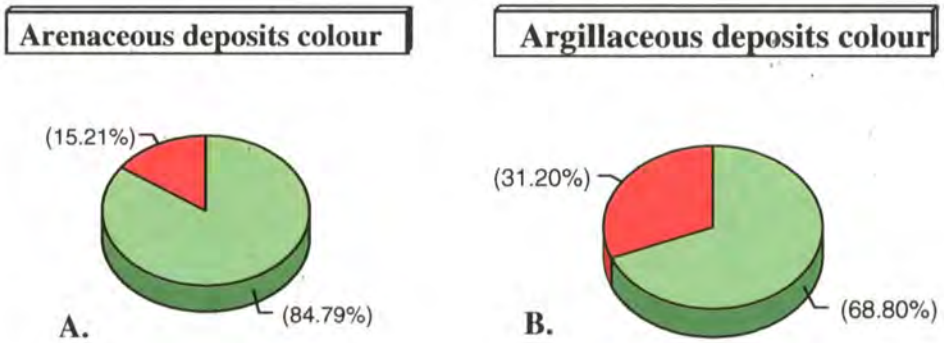

Fig. 95. Colour distribution in the Middle Unit. Diagrams based on borehole data (Oxidative coloures in red, reductive coloures in green).

Within the same unit, the contact between the red and green fine-grained strata is sharp. This demarcation line is unaccompanied by any other obvious change in physical properties such as grain size, porosity or permeability, and is never confined to single stratigraphic units nor to the sedimentary structures. Indeed, in some places the colour boundaries cut across bedding, which clearly indicates that at least one colour had developed post-depositionally.

The intraformational conglomerates are bimodal in colour as the matrix is usually red or pinkish-purple, while the sandstone and siltstone pebbles are either red or grey (*Photo 80*). The reworked carbonate glaebules are uniformly greenish-grey and white (*Photo 80, 82*).

The analysed borehole records show a slightly different colour distribution (Fig. 96A-D). According to the statistical analysis, up to ~10% of the total thickness of the sandstones exhibit green or white colour (Fig. 96A). This fgure was ~1% in the outcrops. Figure 96B shows that only ~12% of the total thickness of the fine-grained strata has a reductive colour, whereas in outcrops this colour seemed to be dominant. Again, the indicators of Fig. 96C are very dissimilar to the outcrop observations, showing that only ~13% of the overbank fine rocks have reductive colours, although in the field, this colour was more dominant in the thickly bedded argillaceous strata. The exclusive red colouration of the argillaceous sedimentary rocks interbedded with the sandstones is confirmed by the borehole record as well (Fig. 96D).

Clarens Formation

The Clarens Formation is generally pale yellow to cream coloured, whereas weathered surfaces are often deep yellow or light orange. The Clarens Formation has been intersected in only one borehole (Den-1) where it exhibits a cream to pale yellow colour.

	OXIDATIVE cum. thick in m	REDUCTIVE cum. thick in m
Arenaceous deposits	802.18	88.6
Argillaceous deposits	1166.25	150.41
Overbank fines	1029.24	149.78
FUC fines	109.34	0.62

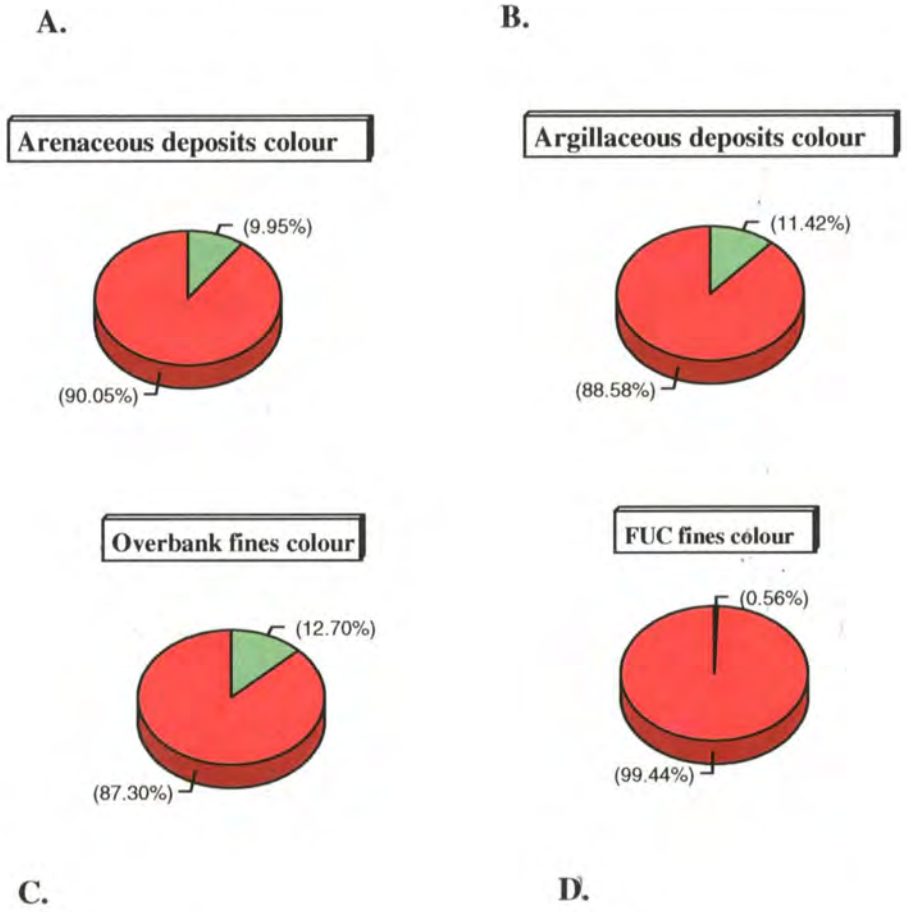

Fig. 96. Colour distribution in the Upper Unit.
Diagrams based on borehole data.
(Oxidative coloures in red, reductive coloures in green).

4.6.2. Microscopic description

During the petrographic investigation of the thin-sections (for detailed description see Appendix 4) of the Karoo Supergroup units, red colouration features were also studied. Statistically only the arenaceous rock types (63) were analysed (Fig. 97). In order to reduce the possibility of statistical errors owing to the variable sample numbers of the different units, 7 quartz arenite samples were randomly selected from each unit (Fig. 98).

The following three red pigmentation features were observed: diffuse microcrystalline stain, grain coating, and hematite blebs and crystals.

Microcrystalline staining is best developed in the argillaceous samples and macroscopically is hardly visible. This feature is also best developed in the Basal Unit, where 60% of the samples exhibit it (Fig. 97). Staining is absent in the Clarens Formation samples.

Grain coatings are most evident in the Middle Unit samples (80%), but are totally absent around the grains of the Basal Unit. They seem to be better developed in the quartz arenite samples of the Upper Unit, where more than two-thirds of the samples display red cuticles. The Fe-oxide coating is often absent at grain contacts, but there are samples where the adjacent grains are separated by thin iron-oxide rims (e.g. TSO2, DON2B). Samples LIZ3 and DON2B exhibit a "cement-supported" fabric, where most of the framework grains float in the hematite cement. In sample OVE2, the formation of the Fe-oxide rim predates the authigenic overgrowth of the quartz, as the overgrowths lack the red cuticles. In contrast, in sample BIS1, the authigenic overgrowths of the quartz grains pre- and post-date the Fe-oxide cementation and coating of the grains because most the overgrowths also have a thin rim of hematite/limonite.

Hematite blebs and crystals are extensively developed in all units (Fig. 98), especially in the quartz arenite samples of the Upper Unit (100%).

	diffuse stain	grain coating	blebs&crystals
Clarens Formation (9)	0.00	55.5	77.0
Upper Unit (17)	11.7	58.8	94.0
Middle Unit (15)	13.3	80.0	93.3
Basal Unit (23)	60.8	0.00	100

Fig. 97. Fe-oxide distribution in arenaceous samples. Note the different number of samples.

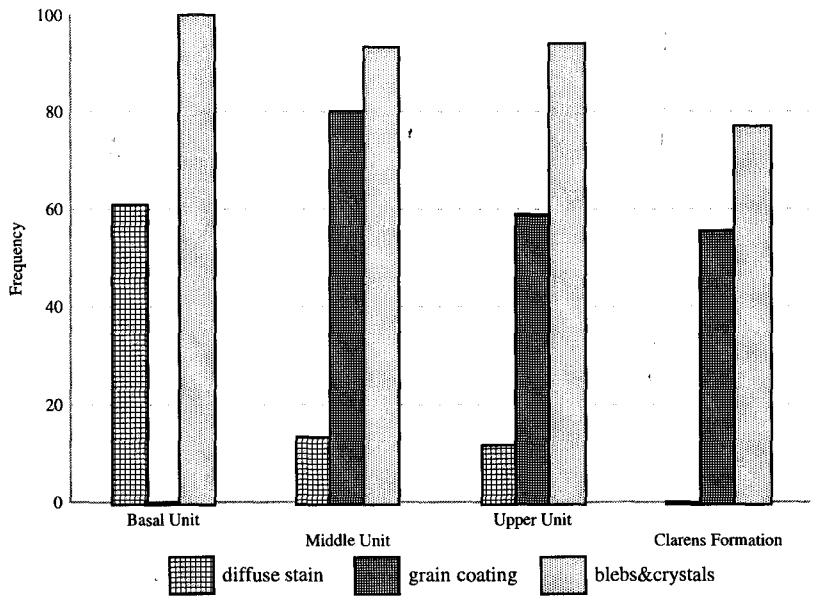

	diffuse stain	grain coating	blebs&crystals
Clarens Formation (7)	0.00	57.1	71.4
Upper Unit (7)	28.5	71.4	100
Middle Unit (7)	14.2	85.7	85.7
Basal Unit (7)	28.5	0.00	85.7

Fig. 98. Fe-oxide distribution in quartz arenite samples. Note the constant number of samples, 7 randomly selected samples were taken from each formation.

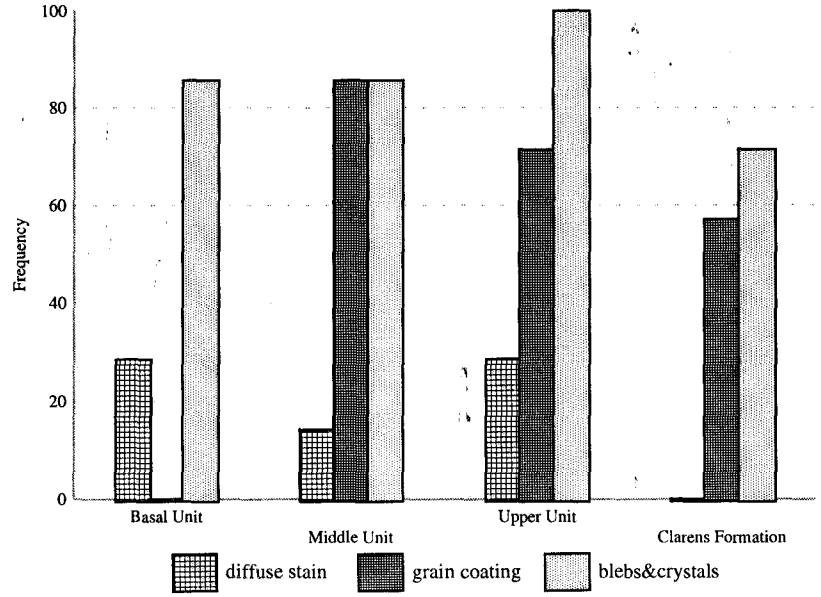

4.7. Calcrete

The carbonate glaebules of the Upper Unit necessitate a detailed description and interpretation as such carbonate accumulations are crucial in palaeo-environmental reconstructions.

4.7.1. Notes on classification and genesis

According to Wright (1990:1) "calcretes are secondary accumulations of calcium carbonate in near surface settings, which result from the cementation and/or replacement of host material by the precipitation of calcium carbonate from soil water or groundwater." There is no standard rate of calcrete generation as the formation of such accumulations strongly depends on the availability of calcium carbonate and other characteristics (e.g. microclimate) within the particular basin (Wright, 1990).

Microscopically, calcretes consist of a dense, finely crystalline groundmass of micrite and microsparite, with floating, micrite- or microsparite-enveloped detrital grains (Blodgett, 1988; Spotl & Wright, 1992). These detrital grains are displaced due to expansion related to the *in situ* carbonate precipitation (Arakel & McConchie, 1987).

4.7.1.1. Textural classification

Based on macrofeatures, calcretes may be classified into nine (non-genetic) types: calcareous soil; calcified soil; powder calcrete; pedotubule calcrete; glaebular calcrete; honeycomb calcrete; hardpan calcrete; laminar calcrete and boulder/cobble calcrete (Netterberg,1980; Wright & Tucker, 1991).

Glaebular calcrete consists of carbonate glaebules which are discrete, very hard, (semi)spherical, (semi)cylindrical or irregularly shaped, with high concentrations of carbonate minerals (Netterberg, 1980). In this study the following three carbonate glaebule-types were recognized: nodules (structureless fabric); concretions (concentric fabric); and septaria (glaebules with internal radial or circum-glaebular cracks) (classification according to Brewer & Sleeman,1964 in Netterberg, 1980). In addition to the glaebular calcrete, hardpan and laminar calcretes were also recognized.

4.7.1.2. Generic classification

Generically, there are groundwater and pedogenic calcretes. Macro- and microscopic differentiation between these two calcrete types is difficult as they share numerous identical features (Wright, 1990).

4.7.1.2.1. Groundwater calcretes

Groundwater or phreatic calcretes are formed around the water table by the precipitation of carbonate minerals from the laterally and vertically mobile groundwaters (Netterberg, 1980). The carbonate enrichment occurs during the migration of the water through different carbonate-bearing formations, while precipitation takes place where CO_2 degassing, or evaporation/evapotranspiration (H_2O loss) occurs, commonly in groundwater discharge zones within topographic depressions (Wright & Tucker, 1991). According to Arakel (1985), low annual rainfall, high evaporation potential, and the frequency and duration of the rainfall, are all important factors in supersaturation and subsequent carbonate precipitation from groundwaters. In alluvial settings, phreatic calcretes often occur in association with sediments of high primary permeability (i.e. channel sandbodies rather than the fine-grained overbank deposits) (Wright & Tucker, 1991; Spotl & Wright, 1992; Mozley & Davis, 1996).

Macroscopically, the groundwater calcretes could develop in the form of nodular to massive, porous, very thick (up to 20 m) carbonate bodies (Wright & Tucker, 1991; Spotl & Wright, 1992; Piementel et al., 1996). Features such as radial wedge-shaped and curvilinear circumgranular cracks filled with sparry calcite cement (in other words septaria) and concretions, are also common phreatic carbonate glaebule types (Boles et al., 1989). Morphologically, the phreatic carbonate glaebules are often elongated in the direction of palaeo-groundwater flow, which in turn is in direct relation to the primary permeability pattern of the formation (Boles et al., 1989; Johnson, 1989; Mozley & Davis, 1996).

Being formed in the zone of groundwater saturation, usually well below the main level of biological activity, phreatic calcretes lack evidence of vadose (meniscus/pendant cements), terrestrial (black

pebbles) and biological features (microbially coated grains) (Wright & Tucker, 1991; Spotl & Wright, 1992). However, sequences of mottled, nodular to massive or laminar calcrete developed in the deep vadose/phreatic zone interface may show the impact of rooting caused by phreatophytes (deep-rooted plants), which make use not only of vadose, but also phreatic waters, particularly in arid areas (Semeniuk & Meagher, 1981). All these imply that groundwater calcretes are not usually formed in near-surface settings (Wright & Tucker, 1991).

According to Piementel et al. (1996), saline and alkaline shallow groundwaters often have considerably variable redox behaviour, and therefore calcretes in grey to red, mottled, but otherwise red substratum may be explained by fluctuating, reducing groundwater levels in the zone of capillary-rise. Such fluctuating groundwaters can tremendously influence soil formation, resulting in hydromorphic soils, which are characterized by grey and red colour-mottles, and contain either a nodular or massive hydromorphic (capillary-fringe) carbonate horizon (Slate et al., 1996).

Microscopically, phreatic carbonate glaebules may show displacive and replacive growth features, microscopic glaebules, cracks and spheroidal to pod-like carbonate precipitations (Spotl & Wright, 1992). The dissolution features tend to be horizontally or subhorizontally orientated (Piementel et al., 1996). Locally, there may be authigenic silicification in the form of quartz and chalcedony (Spotl & Wright, 1992). Features such as desiccation cracks, pedoturbation or brecciation caused by plant roots are absent (Wright & Tucker, 1991). In conjunction with other evidence, the presence of sparry calcites with crystal size >40 microns might be indicative of groundwater calcretes (Wright & Tucker, 1991). Additionally, the unimodal euhedral fabric of the carbonate crystals may imply the relatively constant physicochemical conditions that are characteristic under the phreatic conditions (Colson & Cojan, 1996).

4.7.1.2.2. Pedogenic calcretes

Pedogenic or vadose calcretes are formed within soil profiles, between the surface and water table, typically under seasonally wet, semi-arid to arid climates (Spotl & Wright, 1992). Pedogenic calcretes are typically 1-2 m thick (Spotl & Wright, 1992).

According to the *per descensum* genetic model, during the wet season the downward percolating meteoric (rain) water leaches the carbonate from the upper soil horizon. Later, during dry periods, the carbonate is precipitated as $CaCO_3$ or Mg-rich $CaCO_3$ in the deeper parts of the soil profile (Leeder, 1975; Netterberg, 1980; Turner, 1980). Pedogenic calcretes are thought to be one of the most widely recognized climate indicators of seasonally wet, semi-arid to arid areas (Spotl & Wright, 1992).

Apart from the inorganic chemical conditions of the soil, pedogenic calcrete formation and morphology are directly influenced by biological processes in the soil (Pye&Tsoar, 1990). For instance, plant roots are believed to be responsible for the following features of pedogenic carbonates: the alveolar-septal fabrics; the predominantly vertical alignment of glaebules; horizontal sheet cracks, and *in situ* brecciation (Klappa, 1980; Wright & Tucker, 1991; Spotl & Wright, 1992). The organosedimentary structures of the pedogenic calcretes that originate from the preservation of plant roots are rhizoliths (Klappa, 1980).

The major external source of the Ca^{++} ions is believed to be calcareous aeolian dust which originates from desert areas adjacent to the semi-arid zones of calcrete formation (Leeder, 1975; Turner, 1980; Mayer et al., 1988). Goudie (1973) states that the calcretes found within overbank deposits of semi-arid/arid alluvial plains are precipitated from carbonate-saturated sheet-floods flowing across low relief geomorphic surfaces. In addition, Khadkikar et al. (1998) point out that the river water itself is thought to become carbonate-saturated through weathering in the upper catchment areas. Klappa (1983) lists an entire range of calcium carbonate sources, including breakdown of Ca-rich primary minerals of the host sediments; accumulation of carbonate within plant tissues; microbial synthesis of Ca-bearing minerals by biological (floral and fungal) processes, etc.

Glaebular pedogenic calcretes may develop in high relief areas; semi-continuous sheet-like massive and pisolitic calcrete horizons are present in lower relief areas; laminar calcretes develop at or near the rock-air interface (Arakel & McConchie, 1987; Pye&Tsoar, 1990). In addition, in fluvial settings, pedogenic calcrete often occurs in association with fine-grained deposits of the floodplains where most of the pedogenesis takes place (Blodgett, 1988; Spotl & Wright, 1992).

Microscopically, the inorganic pedogenic carbonate glaebules show similar features to the phreatic carbonate glaebules, although the former tend to have more complex forms, structure and composition than the latter (Wright,1990; Spotl & Wright, 1992).

According to Retallack (1991), one of the main differences seen microscopically is that groundwater calcretes have "simple cement that fills open spaces between larger grains", while pedogenic calcrete consists of micritic cements which often replace the host rock matrix and surround grains. In addition, the extremely loosely packed grains are irregular around the edges, showing dissolution embayment texture. According to Arakel (1985) the displacive and replacive growth features caused by *in situ* carbonate precipitation are more pronounced, whereas the sizes of the micrite/sparry mottled textures are smaller in pedogenic calcretes than in groundwater calcretes.

Curvilinear circumgranular and radial wedge-shaped cracks filled with sparry cement (i.e. septarias) and concretions also occur in the calcretes of soil profiles (Blodgett, 1988). Usually, pedogenic concretions consist of less than five indistinct, micritic laminae, and are less abundant and smaller in size than those formed in the phreatic zone (Tandon & Narayan, 1981).

Blodgett (1988:111) remarks that circumgranular crystallaria and septaria "result from differential drying and cementation between the interior and exterior" of the glaebules, and between the glaebules and the surrounding soil matrix. According to Spotl & Wright (1991), in well-drained soils, pedogenic septarias reflect fluctuation of oxygenation, while concretions indicate fluctuation of pedochemical conditions.

Authigenic silicification of calcretes developed by sub-aerial diagenesis was reported by Reevers (1970) and Steel (1974).

Although Leeder (1975) proposed a quantitative model for pedogenic calcrete development, Wright (1990) demonstrated that the rate of calcrete formation is highly variable and strongly depends on the Ca^{++} ion availability as well as other local factors (e.g. geomorphologic rainfall distribution, climate). In contrast, the qualitative model for pedogenic calcrete development (Gile et al., 1966; Machette, 1985 in Retallack, 1991) has been widely accepted. This concept is based on the progressive change of the pedogenic calcrete morphology and thickness with time, resulting in a sequence of 6 maturity stages. The timing of the individual stage development remains a difficult and sometimes impossible task. For instance, in the palaeosols of the Old Red Sandstone (South Wales) the isolated centimetre-scale carbonate glaebules are thought to be formed over periods of hundreds to thousands of years (Marriott&Wright, 1993). There are case studies documenting mature soil profiles with pedogenic calcrete development in only 3000 years (stage 4), yet there are others recording a minimum of 250 thousand years of development (stage 3) (Wright,1990). As Khadkikar et al. (1998) point out, assessment of paleosol maturity based on morphogenetic sequences could be misleading, especially in settings where the pedogenic calcrete formation is overprinted by groundwater calcrete formation (or *vice versa*). For instance, overprinted, originally pedogenic calcretes may reach anomalous sizes and shapes in a relatively shorter period of time, masking or reformatting the characteristics of the primary calcretes.

4.7.1.3. Calcrete and pedogenesis

Pedogenic calcrete or carbonate glaebule horizons may be indicative of well-drained alkaline soils (Miall, 1996). In present day settings, calcic soils are typical for dry subtropical climates with 500 mm annual rainfall, where evapotranspiration exceeds precipitation for most of the year. The depth of the calcrete horizon is related to mean annual rainfall, becoming deeper in wetter areas (Miall, 1996). Soil development rates in semi-arid climates depend on the subaerial exposure time, local variation in rainfall and Ca^{++} ion content (Wright, 1990).

In conjunction with the calcrete horizon, the following features also indicate calcareous pedogenesis: almost complete destruction of primary sedimentary structures mainly by floral bioturbation (Gustavson & Holliday, 1999), colour mottling associated with biological processes, soil horizonation with gradational lower contact into the unmodified parent material, slickensides, desiccation cracks, early diagenetic cementation, and poorly-sorted and floating-grain structures (Blodgett, 1988). Other calcareous soil features are sparry calcite veins and voids. The veins appear to be the result of desiccation cracks, while the voids are products of decayed roots (Blodgett, 1988). Among these, the most evident soil indicators are plant root trace fossils. Soil formation also requires a pause or reduction in the sediment supply.

4.7.2. Macroscopic description

The calcrete can be found predominantly in the outcrops of the thickly bedded fine-grained member of the Upper Unit. The host rocks are invariably massive, compact with a very little relict, mainly horizontal bedding (Fig. 65; *Photo 94, 110*), and consist of green and/or red, locally intensively mottled and carbonaceous, muddy, very fine sandstones (greywackes), muddy siltstones and mudstones. There is no evidence of any horizonation (i.e. illuvial accumulation of clays) other than that of the calcretes. The best outcrops of the carbonate glaebular fine-grained member seem to be preserved only in those areas where the overlying Clarens Formation commences above a conspicuous 0.5 to1.5 m thick silicrete horizon. According to the analysed borehole data, carbonate accumulation was mentioned in ~16.5% of the Upper Unit (Fig. 99A). About 11% of the sandstones (Fig. 99B) and ~20% of the muddy deposits (Fig. 99C) contained carbonate accumulation; in other words, ~26% of the total carbonate accumulation mentioned was found in sandy and ~74% in muddy strata (Fig. 99D). None of the figures (Fig. 99A-D) represents the true calcrete thickness as most of the carbonate glaebules are sparsely scattered throughout the host beds.

The most abundant form of the calcrete in the area are carbonate glaebules consisting of nodules, concretions and septaria. The size of the glaebules ranges from a few centimetres to decimetres,

	Total thickness	Calcrete host rock thickness	Percentage %
Upper Unit	2207.44	433.47	100
Coarse deposits	890.78	112.73	26.33
Fine deposits	1316.66	320.74	73.99

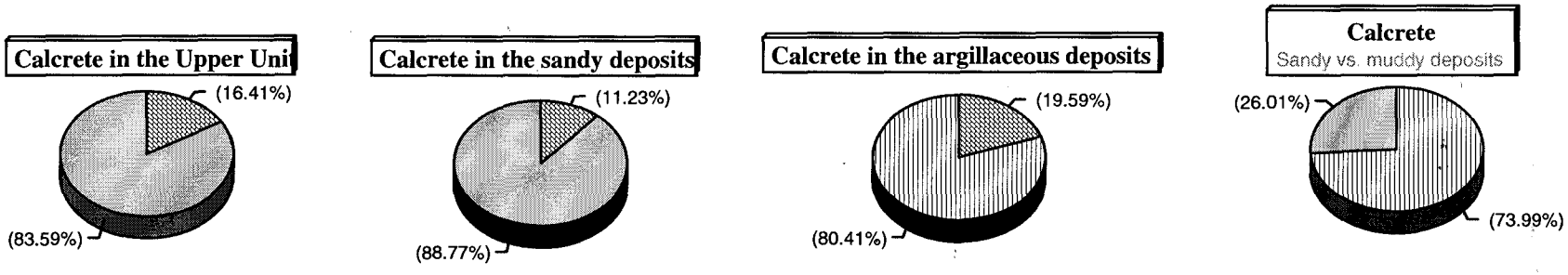

Fig. 99. Calcrete (brick pattern) distribution in the Upper Unit. Charts are based only on borehole data. See text for details.

and their shapes vary from diffuse, irregular to crudely cylindrical or spherical (Fig. 65; *Photo 93, 95*). The glaebules have sharply defined boundaries and smooth surfaces. Some concretions show truncated upper parts and accretionary growth rings on their lower surfaces (Ratho).

Although most of the glaebules are in horizontal and sub-horizontal positions *(Photo 93)*, smaller, individual glaebules may be vertically orientated (*Photo 94*). The particular glaebule shown in *Photo 94* has a rough surface, being formed by the amalgamation of numerous smaller glaebules resulting in a framboidal appearance. Apart from the sparsely scattered individual concretions, there are some large, twinned concretions (*Photo 95*).

Sometimes the carbonate glaebules are organized in semi-continuous, coalesced horizons (Fig. 65). *Photo 98* shows continuous layers of amalgamated, football-sized concretions and glaebules gradually passing downwards into isolated, irregularly spaced smaller glaebules. The upward continuation of the outcrop is captured in *Photo 97,* where the coalesced glaebular horizon passes into a solid carbonate layer which in turn is capped by a zone of horizontal lamellar carbonate veining.

The whole calcrete has gradational lower and sharp upper boundaries. It is overlain by a 0.3-0.5 m massive, continuous silcrete horizon with sharp lower and upper surfaces. The total thickness of the green, carbonaceous, massive, muddy-sandy host siltstone is 3 m, whereas the calcrete is about 2.5 m thick throughout the area.

In addition to the carbonate glaebules, meshworks of mainly horizontal and vertical white calcite veins and solid, pseudo-folded carbonate layers were also observed, especially within the red silty, fine sand host sediment (*Photo 99*). At this site, coalesced and isolated glaebules occur as well (not visible in the picture).

It is important to note that the glaebules are basically missing from the sandstone units. *Photo 136 A & B* shows one of those very rare situations when carbonate glaebules are developed in sandstones.

These concretions tend to be quite regularly spherical and 5-6 cm in diameter. As a rule, the host sandstone is always alongside the dolerite dykes (*Photo 137 A & B*). This phenomenon was described by Söhnge et al. (1948) as amygdaloidal texture. In addition, it has to be mentioned that these sandstones are invariably indurated and locally may also show small scale fold-like structures (*Photo 138*). All these features are likely to be related to dyke emplacements.

4.7.3. Microscopic description

The calcretes investigated in thin sections represent reworked calcrete glaebules (HIL2, BLY3, NEK1, LIZIIB, MON2), *in situ* concretions (BRE2, RAT2) and septaria (BAL2, NEK2). The detailed thin-section descriptions are presented in Appendix 4. The reworked calcrete glaebules are 85-98% nodules, 2-10% septarias and 5-10% concretions. To what extent the abundance of nodules of the intraformational conglomerates and glaebular granular sandstones represent allorthic nodules or reworked, rounded massive calcrete fragments, is unclear. The nodules largely consist of micrite, and <30% have microsparite matrix. The nodules incorporate <1% to >10% very fine silt size, corroded and sometimes calcite-replaced quartz grains floating in micrite matrix. The frequency of the dissolution features associated with the chemical corrosion of primary quartz grains is higher in those samples that show advanced grain displacements. About 3% of the miciritic nodules show crystal "mottling" in the form of elongated, tabular or spherical inhomogeneities filled by microsparite or sparite. The micritic septaria and concretions contain radial wedge-shaped and curvilinear circumgranular cracks filled with sparite and microsparite.

4.8. Silcrete

The silcrete horizon found at the top of the Upper Unit necessitates a detailed investigation as such silica accumulations are significant in palaeo-environmental reconstructions.

4.8.1. Notes on classification and genesis

Silcretes are thought to represent secondary near-surface silicification processes developing in and/or replacing the host material, which is progressively transformed into a resistant, silica-rich or completely silicified duricrust.

Compared to calcrete formation, the mechanism of the silcrete generation process is less well studied. Consequently, there is no standardized silcrete categorization available in the duricrust literature. The combination of different classifications is also a challenging task as the various authors select divergent features to distinguish between the different silcrete types. For instance, Summerfield (1982) based his silcrete classification on outcrop scale observations as well as geochemical and micromorphological differences. In this way, he distinguishes silcretes associated with a weathering profile from silcretes without a weathering profile. Whereas the former are generated through host rock weathering in a predominantly humid, low pH environment, the non-weathering profile silcretes are the result of surface or near-surface silicification in a significantly more arid and fluctuating but dominantly high pH environment.

Wopfner's (1983) silcrete division consists of three main groups which differ not only in microfeatures but also in macrofeatures, silica source, place and mode of origin, etc. Table 16 is a compilation of criteria given by both authors.

In a more recent work by Thiry (1999), silcrete duricrusts are divided into three main groups: pedogenic, groundwater and evaporite-like silicification. Characteristics of pedogenic silicification are the vertical arrangement of the sections into horizons and other pedogenic features (e.g. illuviation). Groundwater silcretes consist of lenses, nodules or pans, and do not destroy original host-rock structures (e.g. stratification, bioturbation). The characteristics of evaporite associated silicification are not well defined, and the legitimacy of indicator minerals such as quartzine (length-slow chalcedony) are not widely accepted.

Table 16. Classification of silcretes (based on Summerfield, 1983 and Wopfner, 1983).

Group	Matrix characteristics & type	Petrographic characteristics	Habit	Profile development	Geochemical characteristics	Forming conditions	Source of the silica	Origin	Climate
I	Crystalline quartz growth; F-(floating) or M-(matrix) fabric.	Optically continuous or chalcedonic overgrowths absent; Length-slow chalcedony void-fills absent; Authigenic glaebules & colloform features abundant.	Blocky; bulbous-pillowy	Yes	Enriched in TiO_2 and depleted in Fe, Al, Ca, K, Mg, and P	Very low pH (suitable for extensive bleaching)	Kaolinisation of feldspar and other silicates	Ground water/ diagenetic	Moist/ warm
II	Crypto-crystalline quartz aggregation; F-(floating) or M-(matrix) fabric.	Same as above.	Columnar, polygonal-prismatic; platy; botryoidal; pillowy	Yes	Same as above.	Same as above.	Same as above.	Pedogenic	Same as above.
III	A whole range of silica (from amorphous cristobalitic-tridimitic silica (opal CT) to megaquartz); F-(floating) abundant, GS-(grain supported), M-(matrix) & C-(conglomeratic) fabric common.	Optically continuous or chalcedonic overgrowths uncommon; Complex void-fills of length-slow and fast chalcedony, micro- and megaquartz common; Authigenic glaebules & colloform features absent.	Breccious; conglomeratic; replacements and infillings	No	Enriched in Al_2O_3 & Fe_2O_3	High pH; oxidising		Late-pedogenic	Arid / semi-arid

In more arid areas, one of the crucial chemical pathways of duricrust development is the gradual replacement of calcium carbonate by silica, although Summerfield (1982) has provided evidence of bidirectional replacement processes. The variable calcite/silica ratios are, in the first place, governed by pH changes due to the reciprocal solubility of the two minerals. In addition, the replacement processes result from the sophisticated interplay of other solubility controlling factors such as regional temperature, pressure, partial pressure of CO_2, presence of organic complexes, time, etc. (Reveers, 1970). Silica precipitation is also related to the presence of substances like Al_2O_3, Fe_2O_3, MgO, NaCl and Na_2SO_4 (Smale, 1972). According to Thiry (1999), increased salt concentration can decrease three to ten times the solubility of amorphous silica.

Retallack (1986) maintains that silicified calcrete horizons and chalcedony replacements of gypsum or barite roses are evidence of seasonally extremely dry climate. On the other hand, Summerfield (1983) states that the silicification of calcretes does take place in arid to semi-arid climate settings; however, it is not clear if silicification develops during significantly more humid interludes or relatively drier phases.

In fact, most dry climate silcretes are silicified calcretes and mud-rich playa deposits (Summerfield,1983). Three of the most significant characteristics of such silcretes are the presence of length-slow chalcedony, silicified glaebules as inherited features from calcretes, and the absence of weathering profiles (Summerfield, 1983). Silcretes associated with playa sediments tend to contain more cryptocrystalline silica, whereas those originated from calcretes show microquartz abundance (Summerfield, 1982). Commonly, these silcretes exhibit F-(floating) fabric (Table 17), which is believed to form either by displacement or partial replacement of skeletal grains or by matrix replacement in the originally matrix-supported host material (Summerfield, 1979). In contrast to calcretes, the displacive origin of the F-(floating) fabric is unlikely to be due to the difference in the crystallization kinetics of silica and calcite (Wright & Tucker,1991). For instance, silica does form adhesive ionic bonds with non-silica grains, whereas calcite is unable to do so with non-carbonate grains.

Table 17. Non-weathering profile silcrete fabric types and their host rocks (after Summerfield, 1982).

Fabric	**M-(matrix)**	**F-(floating)**	**GS-(grain supported)**	**C-(conglomeratic)**
Particle type	Skeletal quartz grains; less than 5%	Skeletal quartz grains; more than 5%	Self-supporting quartz grains	Pebbles
Matrix type	Microquartz, chalcedonic or cryptocrystalline/ opaline silica	Microquartz, chalcedonic or cryptocrystalline/ opaline silica	Void-filling chalcedony, microquartz or cryptocrystalline/ opaline silica	Microquartz, chalcedonic or cryptocrystalline/ opaline silica
Host material	Greywackes & sandy mudstones	Playa sediments & calcretes	Loose sediments	Conglomerates, breccias

The following main silica sources are recognized for the semi-arid and arid climate setting: fluvially transported silica originating from distant catchment bedrock weathering and entering the floodplains during inundations; (pene)contemporaneously released silica from the extensively replaced detrital grains in the calcrete forming processes; enhanced-solubility quartz dust from aeolian activity. Some arid climate (desert) grasses containing large amounts of silica are believed to be another significant silica source (Turner, 1980). According to Summerfield (1983), in the case of thick silcrete units, the capillary fringe silica source is unlikely because the initial thin silcrete crust would act as a seal preventing further evaporation of the silica-bearing solutions, thus blocking the development of thick silcrete.

4.8.2. Macroscopic description

The silcrete horizon is usually yellowish-whitish (*Photo 92*), but depending on the quantities and colour of the parent material still present, it could be pinkish, rosy-light red, reddish or greenish (*Photo 91*). Macroscopically, cryptocrystalline quartz is the most common silcrete-forming silica type, whereas crystalline quartz is absent.

Confined to the mainly sharp contact between the Upper Unit and Clarens Formation, the silcrete forms lenticular or laterally extensive, 0.4 to 2 m thick sheets with no evident relief (*Photo 88, 92*). Owing to the completely indurated texture, uniform thickness and laterally semi-continuous development, the silcrete seems to have formed a protecting mantle over the fine-grained, less permeable, muddy units of the Upper Unit, containing carbonaceous glaebules and other

pedogenic features. In other words, there is no silcrete developed above the red coloured, coarse-grained units of the Upper Unit.

Excellent exposures of this silcrete layer are presented across the study area, where none of the occurrences appears to be associated with weathering profiles. Two silcrete types were identified: non-gradational, massive and gradational forms. The contact between the silcrete and the over- and underlying formations seems to be generally abrupt (*Photo 88, 92)* (even in the case of gradational forms).

The *non-gradational, massive* silcrete forms are usually 1-1.5 m thick, extremely brittle, with glassy conchoidal fracture. They consist of well-cemented, randomly orientated, mainly spherical and/or elongated crypto crystalline glaebules, forming a botryoidal fabric (*Photo 139*). The randomly orientated tabular features have very rough, corrugated surfaces resembling candle-wax drippings. Both glaebules and tubules are internally structureless, though a few, mainly the tubules, may exhibit a central hollow *(Photo 140).* Voids, cavities and jointing are abundant. The voids and cavities have various shapes, from irregular to tunnel- or pipe-like hollows and pits *(Photo 141).* Most of the voids have millimetre-thin walls of microquartz and/or cryptocrystalline silica *(Photo 142).* Rarely, the voids display an agate texture due to the concentric colour banding caused by filling of the void by slightly differently coloured cryptocrystalline laminae. The diameter of circular voids varies from less than 0.5 cm to 3-4 cm. Owing to this cavernous development, the porosity of the silcrete is high. Macroscopically, there is no carbonate content and very little recognisable host rock material is present.

The *gradational* silcrete forms are 0.25 to 2 m thick and have sharp upper and transitional lower boundaries (Fig. 65). Grading upwards from the host rock, there is a transitional zone where laterally discontinuous silica laminations *(Photo 143)* and clay-coated silicified host rock lumps and lenses of 1 to 2 cm were often observed *(Photo 144, 145).* The upper parts are invariably well-cemented, showing the characteristics of massive silcrete forms with trace amounts of the host rock. Pipe-like, very thin walled features, >0.1 cm in diameter and >1.5 cm in length, are more readily recognisable in the transitional or lower parts which invariably contain minor amounts of carbonate.

4.8.3. Microscopic description

The matrix of the investigated silcrete specimens (BAL1A, BAL1B, HILL1, LIT4) consists of a mixture of a whole range of silica phases from cryptocrystalline silica to length-fast chalcedony and microquartz. The detailed thin-section descriptions are presented in Appendix 4. According to Summerfield's (1983) classification, most of the matrix types are F-(floating) fabrics, but GS-(grain supported) fabrics are also present.

The detrital grains in the silcretes are overwhelmingly primary quartz grains with embayment dissolution features and some feldspar grains (0.1%). The corrosion frequency of the grains is in linear relationship with the rate of grain displacement: detrital grains of the silcrete samples with F- (floating) fabric are more corroded than those with GS-(fabric). Other observed micromorphological features are the spherical voids (diameter: 0.04-0.8 mm), tubules (width: 0.04-0.2 mm; length: 1-2 mm) and veins (width: 0.04 to 10 mm) which are often completely filled by a systematic succession of Fe-oxide banded cryptocrystalline silica and/or fibrous, radial, multi-generation chalcedony, microquartz and equant quartz. Additionally, in some of the structures the cryptocrystalline silica may alternate with length-fast chalcedony, but the cavity centres are usually occupied by equant megaquartz. By far the most abundant void-filling silica phase is represented by radiating bundles of length-fast chalcedony fibres, whereas only a few voids are filled by lutecite ("zebraic chalcedony"). The crystal/bundle size increases toward the centre of the void/tubule/vein. There are also a few cavities with chalcedony or microquartz coated walls.

5. Interpretation of depositional environments

The results of the palaeo-current measurements and grain size/shape analysis are incorporated into the following sections, which are devoted to interpretation of the field observations.

5.1. Basal Unit

5.1.1. Breccia and conglo-breccia facies assemblage

The oligomict parabreccia Gmm lithofacies may be described as a diamictite, but in the absence of other supporting evidence (e.g. striated clasts/bedrocks, polimict clast fabric, varved clay sequences), only that part of the lithofacies which exhibits a laminated matrix is - tentatively - interpreted as a glacial diamictite. On the other hand, those Gmm lithofacies beds that show no matrix lamination of any kind are interpreted here as gravity flow deposits. Although "coarse-tail" inverse grading and tabular bedding have not been observed, the fact that the large clasts float in the mud-sand-rich matrix supports the interpretation of this lithofacies as high-viscosity debris flow deposits (Blikra & Nemec, 1998).

The Gcm lithofacies resembles the characteristics of rockfall deposits (Blikra & Nemec, 1998). These highly immature deposits, consisting of angular, disorderly "adjusted" larger clasts fining upward to sand size grains, are typical sediments resulting from colluvial processes.

The Gmm and Gcm lithofacies are fairly common deposits in postglacial colluvial fans/aprons dominated by avalanching (Blikra & Nemec, 1998). The plan-view radius of these fans is less than 0.5 km and they occur in mountainous areas. The immature debris, consisting of large blocks of rocks derived from the bedrock of the steep valley walls, is transported through avalanches (Blikra & Nemec, 1998). Not only the texture but also the relatively high bedrock content of the Gmm and Gcm lithofacies suggest rapid mechanical disintegration of the source rocks, which in turn might imply rapid detachment of the rock fragments in a high-relief palaeo-topography setting.

The distribution of these colluvial fan deposits exclusively along the southern margin of the area might suggest the existence of a preeminent, NE-SW extending palaeo-ridge, south to the present Tuli Basin.

The relative age of the facies assemblage can be deduced from its stratigraphic position (the lowermost deposit) and from the fact that it consists of the most angular clasts and contains angular gneiss particles. The conclusion to be drawn from these characteristics may be that the facies assemblage is the oldest formation. In this case, the reason for the complete absence of gneiss particles from the other assemblages may be explained by the changes of catchment-area position over time. Such changes are caused by the progressive denudation/burial of the source rocks, the reorganization of the drainage pattern within the catchment and, last but not least, the intrusion of external agencies (i.e. river capture) into the catchment area (Green & McGregor, 1986).

If it is accepted that the breccia and conglo-breccia facies assemblage is facies equivalent to the other lithofacies assemblages, it follows that gneiss particles are absent because of the dissimilarities of the dominant transportation processes acting in the different depositional environments: in colluvial fans, the gravity-driven sediment transport is short and sudden, thus little crushing or milling is taking place, while in fluvial environments the significant mechanical abrasion would break the soft, weathered basement gneiss fragments into sand-size quartz and feldspar grains.

5.1.2. Sandstone facies assemblage

The upward-fining cyclothems, the multistorey sand-bodies, the frequency of the erosion surfaces, and unidirectional palaeo-current directions are features consistent with fluvial environments. The upward-fining cyclothems indicate changes in water energy over flooding events: the initial high-competency phase is represented by coarser deposits, while the waning of the flow is indicated by finer grain sizes.

The multistorey and multilateral sand-bodies suggest frequent lateral shifting of the down-current migrating sand dunes (SB) or channel bars (DA). The lack of levee deposits also indicates that the channels were most probably unconfined.

The abundant erosion scours and reactivation surfaces may reflect abrupt changes in flow regimes. The convex-up macroform-bounding surfaces, the downstream dipping erosional

surfaces and the lack of lateral-accretional features, suggest a low sinuosity, multichannel fluvial system.

The *very thickly bedded* (0,8-2 m), laterally-persistent planar and low-angle cross-stratified sandstone (Sp, Sl) units may have originated from perennial flows, perhaps with bank attached and/or mid-channel bars, and sand islands (DA). The directional uniformity of the foreset dip directions suggests that the thick solitary sets were probably formed as downstream migrating linguoid or transverse bars (Collinson, 1996).

The *lens-, wedge- or sheet-shaped units* with their smaller-scale cross-bedded cosets may reflect the presence of periodic straight-crested sand dunes deposited during high discharge events (SB). The upward thinning of the sets probably records the decreasing flow velocities of single floods.

Since platy particles restrain ripple formation (Manz, 1978 in Collinson, 1996), the micaceous parallel laminated sandy siltstones and sandstones (Fl, Sh) may be interpreted as gentle flow products rather than upper flow regime deposits. As they always occur towards the top of the major channel type sandbodies, they may have developed during lower water levels (Collinson, 1996) (part of SB, DA).

The small sequences of thinly bedded, horizontally laminated sandstones, climbing ripples and ripple-marks could be formed during single flood events, under decreasing flow velocities (SB). The shape and orientation of the sand ripples and their grain size distribution indicate that they are subaqueous deposits, generated by relatively gentle, unidirectional currents.

The intraformational mudclasts along the scour surfaces were most probably locally derived. They may be related to the erosion of the overbank area during lateral channel migration.

The sharp-based sandstone bodies, with horizontal and low-angle cross-lamination (Sh, Sl) and less commonly ripple cross-lamination (Sr), are interpreted as proximal crevasse channel and distal splay (SB) (minidelta?) deposits because they always occur interbedded with mudstones and siltstones. The lensoid sandstone bodies were scoured into the floodplain deposits by

crevassing of the river banks during flooding (Collinson, 1996). In distal settings, they tend to have non-erosional, flat bases due to the loss of flow power away from the feeding channels (Miall, 1996). The internal erosional surfaces may indicate that the splays were originated by periodic or irregular sheet flooding (Miall, 1996:175).

The extensive sheet-like, parallel-sided sandbodies of horizontally laminated sandstones (Sh) reflect upper flow regime conditions and vertical accretion of the laminae (LS).

Within the channel-fill sequences (CH), the decreasing size of the grains and sedimentary structures imply a progressive decline in current competency from the lower to the upper part of the channels. The channel width/depth ratio (29) calculated for the major channel exposed on Stembok probably corresponds to the width of a single channel, considering that the channel width/depth ratio of a low sinuosity, multichannel system should be much greater (Collinson, 1996).

The low width/depth ratio (4.2) calculated from the channel sandbody (CH) on Montaqu is presumably due to the cohesive, clayey bank (Fs). Indicators of upper flow regime conditions (Sh, Sl) and the absence of lateral accretion surfaces probably indicate that this narrow channel, deposited within the floodplain succession, was associated with temporary flows which occurred on the surface of the floodplain. In this case the incision of the channel is a result of direct precipitation during short-lived storms with heavy rainfalls rather than overbank flooding (Collinson, 1996). In the light of this interpretation, the anomalous palaeo-current data set of this locality (Montaqu 2 Ch. 4.3.1. & 4.3.2.) may be explained as the result of a temporary, short-lived channel oblique to the main river flow. The sharp channel top suggests that channel evolution was abruptly terminated. Sandbodies with similar lenticular geometries and internal structures have been described as ribbon sandbodies, and also thought to be deposited by brief floods (Collinson, 1996).

The other channel-shaped, minor sandstone bodies are interpreted as minor channels crossing sandflats. These minor channels are formed during falling water after flooding (Figs. 31 & 33) (Miall, 1996). Those minor channels that are scoured in overbank fines may be seen as proximal crevasse channels that feed the distal splays on the floodplain (Fig. 32) (Miall, 1996).

The completely structureless *massive sandstones* (Sm) and matrix-supported breccias (Gmm) (SG) are often interpreted as gravity flow deposits triggered by collapsing riverbanks (Collinson, 1996). Massive sandstones (Sm) and matrix-supported breccias (Gmm) may also be rapidly deposited from short-lived currents with exceptionally high sediment yield. In cold climates, such devastating floods are likely to occur during spring time when non-glacial subarctic river discharge suddenly increases due to rapid snow melting.

The water escape structures and the load structures indicate that these strata were accumulated rapidly and heavily loaded shortly after their deposition.

The subordinate Gh lithofacies of the sandstone facies assemblage, with its horizontally bedded, lenticular or channel-shaped features, appear to represent gravel sheets of channel lags (Collinson, 1996). The other, also rare conglomeratic lithofacies, the poorly-sorted, mainly clast-supported Gcm may correspond to "ice jam" deposits described by Martini et al. (1993). These deposits develop in cold-climate, non-glacial subarctic rivers. The deposition occurs during spring floods, when the jammed ice floes melt and their rafted sediments settle out. According to Martini et al. (1993), the anchor ice can obtain the coarse-sediment load by picking up particles from the river floor.

5.1.3. Fine-grained facies assemblage

The abundance of the fine-grained facies contrasts with the fluvial style recorded in the sandy units (i.e. multichannel, low sinuosity river), making it unlikely that the origin of the overbank fines was exclusively fluvial. A more appropriate explanation may be that the fine-grained facies were initially deposited in lakes of glacial origin. These lakes may have developed upon the irregular topography left after the retreat of a major ice sheet. Many of these lakes were strongly affected by the major multichannel river flowing through the area. The lakes proximal to the river would sustain more frequent and drastic flooding effects (i.e. coarser sediment supply) than those of distal setting. The calcareous mudstone horizon reported by Chidley (1985) may also support the partly lacustrine origin of the fine-grained facies, considering that lime-rich sediments commonly occur at the base of lake-infill sequences (Collinson,1996).

From evidence of coal-quality investigation, Falcon (1989) also deduces a limnic origin for the coal seams of the area. The frequency and geometry coal seams described in the coal prospecting drill hole sections and also by Falcon (1989) (see Ch. 2.2.5.3.) further indicate that they were formed in lakes near the active river channels. In such settings coals tend to be thin and of limited lateral extent (Collinson, 1996).

The shallow, low relief of the overbank area is documented by the palaeosol and coal horizons, as well as by the rare desiccation cracks. The organic-rich, dominantly grey fine-grained rocks are also indicative of lowland topography, as these characteristics record a high palaeo-water-table and reductive pore water (Collinson, 1996). This high water table was probably sustained by glacial meltwater input.

The subaerial exposure indicated by the palaeosol horizon of Montaqu is not a regional event and the length of the time period represented by this structure is unknown.

The sedimentary structures of the fine-grained strata also reflect a variety of different depositional settings within the overbank area. Within the larger lakes, the environments are subdivided into proximal (marginal) and distal (basinal) sub-environments (Miller, 1996).

The randomly laminated (Fl) and non-laminated (Fsm) mudstones, siltstones and pebbly mudstones (Fp) are probably *distal* lake deposits. The laminated lithofacies were deposited from suspension, while the massive ones could have developed as the result of mass-flows. The paucity of lithofacies Fp implies the possible presence of rare and small-sized, floating icebergs that rafted some debris on their backs (Miller, 1996). As the iceberg melted, the debris landed on the soft mudstones and disrupted the lamination (see Ch. 4.5.2., MOG8 & STE3 thin-section descriptions in Appendix 4). The homogeneous, laminated carbonaceous mudstones, grey siltstones (Fl) and continuous coal seams (C) probably represent transition between the distal and proximal lake zones.

Representing relatively stable periods, the laminated muddy-silty facies are frequently interrupted by sharp-based, lenticular or sheet/blanket-like sandstone bodies (Sh, Sl, Sr) as well as by massive, muddy-silty-sandy deposits (Fsm, Fs, Sm, Sf, Gmm). These deposits are the likely

products of episodic, short-lived events, such as major flooding and sudden storms in *proximal* lakes. The sharp-based sandstone bodies are interpreted as small-scale delta (crevasse splay?) sands (SB), while the massive facies are associated with gravity flow deposits (Blikra & Nemec, 1998). The tongue-shaped lobes, the sausage-shaped bodies, and the erosive furrows filled by Sf, Fs lithofacies are typical features of low-viscosity debris flows (Blikra & Nemec, 1998).

Debris flows can occur on any slightly rolling landscape where a mass of water-saturated mud and unconsolidated debris is available. Such conditions are believed to be favoured in glacial or post-glacial lakes where the glacially carved, irregular topography is draped by silts and clays which become water-saturated due to glacial meltwaters (Potter & Pettijohn, 1977). The debris flow deposits may have been triggered by slope failure along lake margins (Miller, 1996). This mechanism could have been set in motion by rapid spring melting of the snow or short-lived storms. During these extreme weather conditions, the massive mudrock lithofacies were rapidly dumped from hyperconcentrated flows in the shallow lakes of the overbank area (Collinson, 1996).

Ellipsoidal or kidney-shaped, ball-and-pillow structured sandstones, siltstones and mudstones are formed by vertical sediment transfer in response to inverse density stratification (Dżułyński, 1966; Anketell et al., 1970). When water saturated, non-mobile sediment is overlain by a denser member, unstable density stratification occurs, leading to the development of regular convective patterns within the members (Anketell et al., 1970). This may result in soft-sedimentary deformation such as ball-and-pillow structures or convolute bedding. According to Dżułyński (1966), such unstable stratification is characteristic of cold, subarctic regions where the heavier clastics are deposited upon frozen silty sediments which subsequently melt.

All soft sedimentary deformation found in the area (load casts, ball-and-pillow structures, water-escape structures) and debris flow deposits are diagnostic of environments with high sedimentation rates, where the rapidly deposited, unconsolidated sediments are loaded or mobilized by denser, suddenly deposited materials.

The fine-grained facies assemblage and the overlying and underlying coarse, planar cross-bedded sandstones ought to be pene-contemporaneous in order to display any of the above structures. Therefore it is concluded that the fine-grained and sandstone facies assemblages are facies equivalents having been deposited in different parts of the same sedimentation system.

5.1.4. Discussion

Fig. 100 shows the general vertical profile of the Basal Unit in the study area, illustrating the major lithology types. The thicknesses shown in this figure are compiled from the estimated outcrop and the calculated (average) subsurface thickness records.

The lower part profile indicates that the sandstone with subordinate conglomerate intercalations and the fine-grained facies assemblage are the most abundant deposits in the lower part of the Karoo Supergroup strata. Thick units of coarse-grained strata appear in the lower part of the sequence, implying that maximum depositional rates occurred in earlier periods. These features may be explained by the fact that this succession was deposited in a deglaciated area immediately after glacial retreat (Le Blanc Smith & Eriksson, 1979).

The breccia and conglo-breccia facies assemblage of the Basal Unit seems to be the oldest Karoo Supergroup rocks in the southern part of the Tuli Basin. A portion of these basal strata (i.e. the parabreccias with laminated matrix) may have been deposited under glacial conditions, but as most of the beds represent colluvial fan deposits, the facies assemblage is interpreted as cold climate, non-glacial deposits. The facies assemblage is exposed exclusively along the southern margin of the area, which could hint at the former existence of a NE-SW Archaean basement palaeo-ridge south of the present basin. The abundant, fragmented quartz veins and the weathered gneisses of the Archaean basement must have been one of the significant local source materials for these deposits.

The succeeding coarse-grained rocks include upward-fining units of planar cross-bedded (Sp), coarse-grained to granule-grade sandstones and subordinate, thin, laterally intermittent lenses of subangular, subrounded conglomerates (Gh, Gcm). The sandstones display frequent erosion surfaces as well as downstream-dipping accretion surfaces. Neither lateral-accretion surfaces nor large-scale convex-up surfaces have been observed. Levee and point-bar deposits are also absent. Palaeo-current data analysis of the cross-bedded (Sp, Sl) sandstones indicates a low sinuosity river system with consistent current directions pointing toward WSW. All these features imply a multichannel, low sinuosity braided river, transporting large amounts of very coarse to coarse sand and subordinate gravel. The thickness of the fining-upward cyclothems could not be used

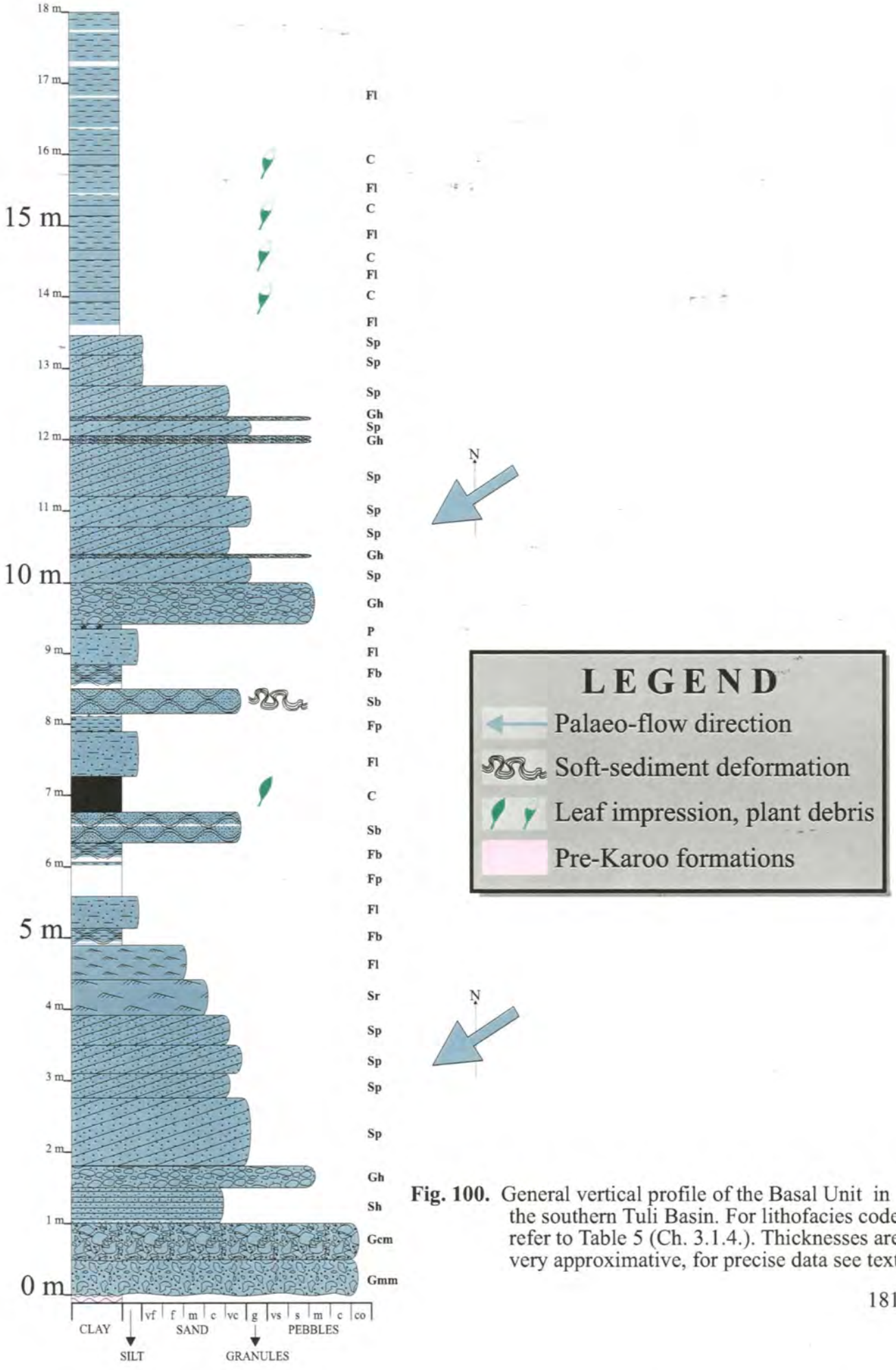

Fig. 100. General vertical profile of the Basal Unit in the southern Tuli Basin. For lithofacies codes refer to Table 5 (Ch. 3.1.4.). Thicknesses are very approximative, for precise data see text.

for stream depth estimation as the cyclothems consist of multistory sand bodies. The facies assemblages described as well as the data base provided by measurements and calculations point to a fluvial style which shows similarities with the "shallow, perennial braided" river facies model of Miall (1996). This fluvial style, also called "Platte-type", is characterized by large, flat-topped 3-D dunes constructed of planar cross-bed sets (Miall, 1996).

The palaeo-current data not only support the existence of this low sinuosity, multichannel fluvial system, but also indicate that at least one trunk river (stream system?) was draining obliquely to the main WSW flowing river system (see anomalous data set of Ammondale-Weltevreden Ch. 4.3.1. & 4.3.2.).Within the sandstones, the vertical variability of the current directions was insignificant; thus the flow patterns may be assumed to have remained consistent during deposition.

The fine-grained strata vary in grain size from fine sandstones to siltstones and mudstones, and in structure from massive to laminated. These units are interpreted as floodplain, mainly lacustrine deposits inter-bedded with minidelta (crevasse splay?) sandstones and fine- to coarse-grained gravity-flow deposits. The depositional settings were in shallow lakes and swamps proximal and distal to the main braided fluvial system. The lakes may initially have been carved during the previous glaciation. The flourishing vegetation of this overbank area is revealed by the presence of rooted palaeosol horizons, the abundant plant debris, fossil leaves, seeds and coal seams. The formation of swamps in the area was enhanced by the shallow ground-water level in the lowland areas and other direct climatic factors.

5.1.5. The model and a recent analogue

It may be concluded that the strata of the Basal Unit were deposited in a cold climate, non-glacial subarctic fluvio-lacustrine system. The palaeogeographic reconstruction of the area is illustrated in Fig. 101 (the lowermost colluvial fan deposits are omitted from this sketch). According to this figure the coarse- and fine-grained strata are facies equivalents and the lateral facies change is explained by the existence of the different depositional environments side by side.

There is a close affinity between the reconstructed depositional environment of the Basal Unit of the Tuli Basin (SA) and some regions of Alaska (USA) (Fig. 102). The marshy area of the Yukon Flats Ecoregion is patterned by numerous thaw- and a few oxbow-lakes. The braided segment of the Yukon River annually replenishes the shallow lakes during spring breakup of the river ice (Gallant et al., 1995). The region has a cold, subarctic climate, with temperatures above freezing only from June to August (Gallant et al., 1995). The area is covered by dense vegetation consisting of thick forests as well as tall scrub thickets and swamps (Gallant et al., 1995).

In other regions of Alaska, the finer-grained medial and distal areas of the glacial outwash fans also support an extensive vegetation between the active braids (Boothroyd & Ashley, 1975).The overbank area is characterized by muddy-silty facies interbedded with sandier crevasse splay deposits (Boothroyd & Ashley, 1975), where the meltwater-hollows and other depressions of glacial origin are excellent environments for coal-forming peat accumulation (Stach et al., 1975).

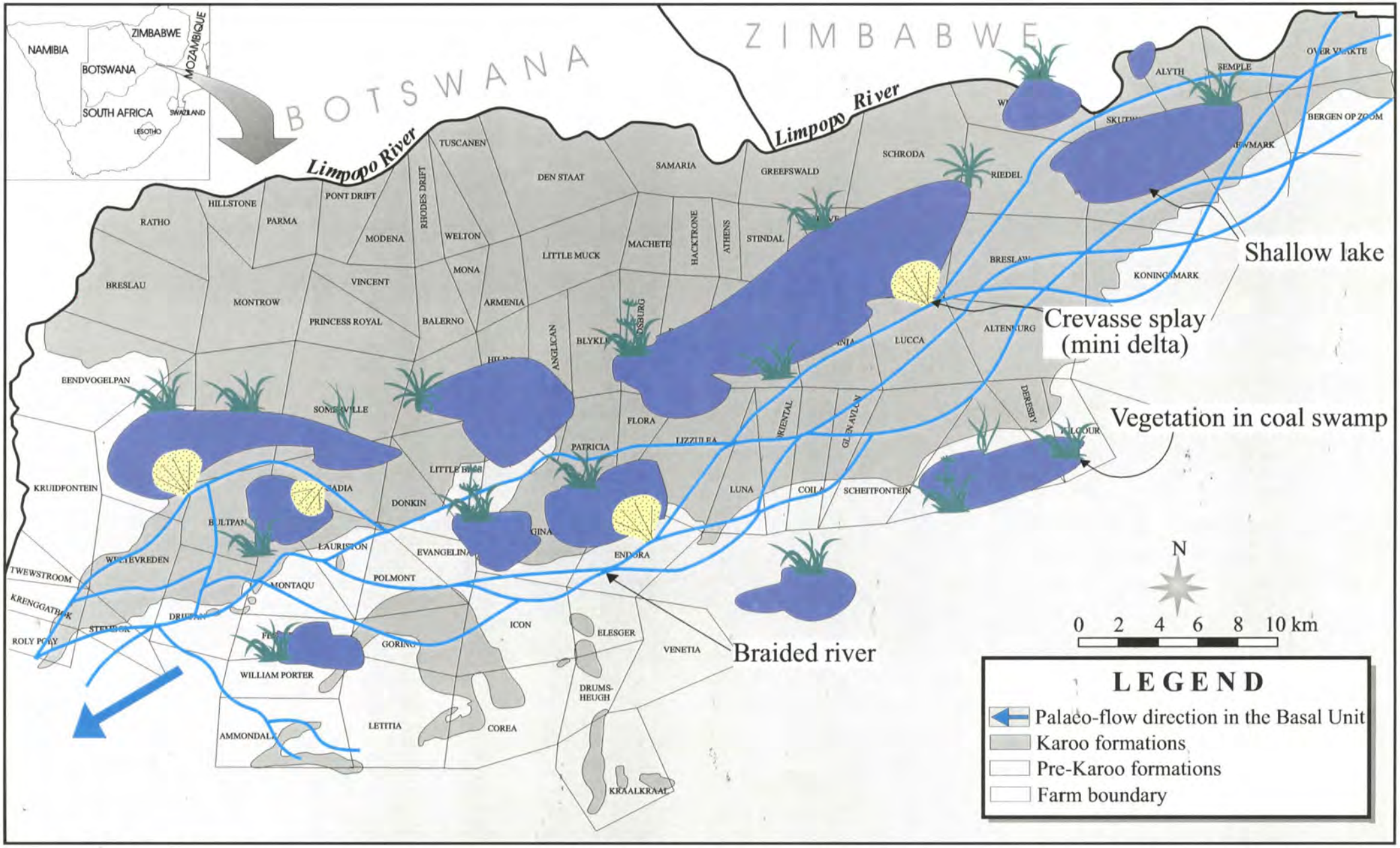

Fig. 101. Map showing the palaeo-environmental reconstruction of the Basal Unit. The fine-grained strata were deposited mostly in quiet overbank environments dominated by lakes, while contemporaneously the coarse-grained deposits were formed in the channels of a braided river system.

Fig. 102. The recent analog of the palaeo-environmenal setting (Yukon River, Alaska, USA) proposed for the Basal Unit..

5.2. Middle Unit

The very poor quality outcrops only allowed tentative recognition of the following architectural elements: gravel bars (GB) and sandy bedforms (SB) in the arenaceous rocks, and overbank fines (FF) in the argillaceous deposits. The conglomerates are believed to have formed as channel lag deposits. The planar cross-bedded sandstones and ripple cross-laminated very fine sandstones are interpreted here as intrachannel migrating, straight crested sand dunes and ripples. The abrupt passage from arenaceous into argillaceous deposits (mostly mudstones, less commonly siltstones) (Fig. 103) could represent rapid channel shifting and abandonment. The intraformational, rip-up, siltstone and silty mudstone clasts indicate the coexistence of high- and low-energy processes and intensive fluctuation in the energy levels (see also Ch. 5.5.2.). These characteristics, the regular distribution of both arenaceous and argillaceous deposits, lack of point-bar successions, crevasse-splay or levee deposits and desiccation cracks, indicate a braided perennial river system rather than an anastomosing or meandering fluvial regime.

The unidirectional palaeo-current directions and low palaeo-channel sinuosity are also consistent with the braided fluvial-system interpretation. The drainage direction of the channels was from SE to NW, a diversion from the palaeo-flow directions recorded in the Basal Unit (ENE to WSW). This difference implies that the general dip direction of the regional palaeo-slope was changing through time.

The overall fining-upward trend of the unit may reflect weakening intensity of the initial tectonic uplift and denudation processes in the source area. This decline resulted in decreasing of the regional slope gradients and coarse sediment input.

The roundness difference between the Basal Unit and Middle Unit (Fig. 84 & 85) yields provenance information: the more rounded quartz particles of the Middle Unit may have been partly derived from the underlying Basal Unit. The better sorted texture of the Middle Unit may also indicate that reworking of the Basal Unit occurred (for details on provenance, see Ch.5.5.2.).

The maps of the quartz pebble roundness variation (Fig. 84 & 85) show that the clast roundness increases towards north. This trend is clearly parallel to the facing direction of the Karoo Supergroup in the basin. That the Middle Unit is younger then the underlying Basal Unit is thus not only indicated by stratigraphic evidence, but might be considered proven by the clast statistical tests.

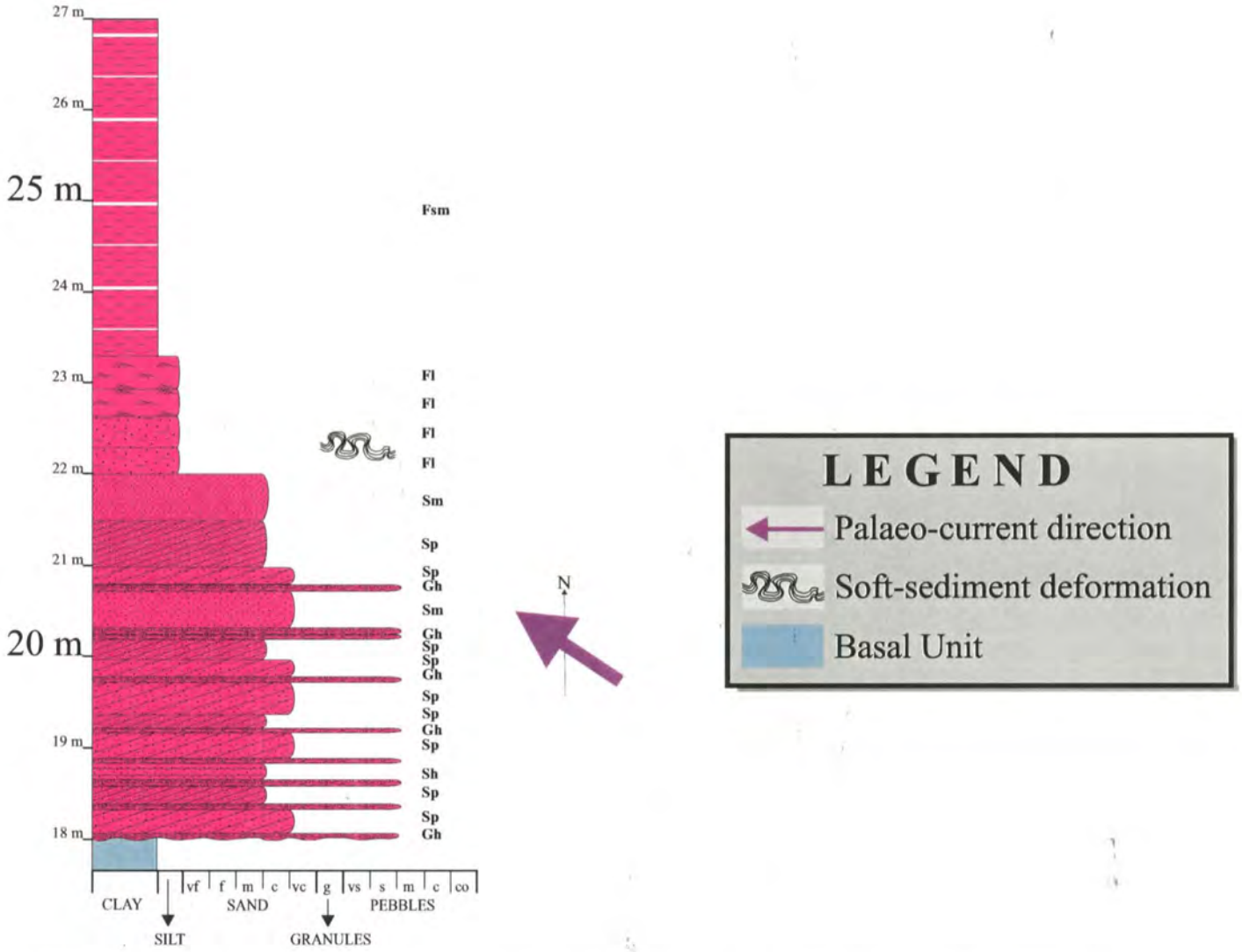

Fig. 103. General vertical profile of the Middle Unit in the southern Tuli Basin. For lithofacies codes refer to Table 5 (Ch. 3.1.4.). Thicknesses are very approximative, for precise data see text.

5.3. Upper Unit

5.3.1. Sandstone facies assemblage

The suite of the lithofacies found in the laterally continuous, thinly-bedded sandstone facies assemblage not only resembles unidirectional upper flow-regime sedimentary structures, but also records wide energy fluctuations of the transporting agent, as indicated by the presence of intraformational conglomerates sometimes overlain by ripple cross-laminated sandstones (*Photo 87).* On the other hand, the desiccated mud drapes that often separate the predominantly tabular bedforms are indicative of erratic sedimentation. This evidence paints a picture of a high-energy but ephemeral depositional milieu. In continental settings, such episodically vigorous environments exist in the flash-flood dominated ephemeral stream/river systems of semi-arid/arid climates. Therefore the relatively thinly bedded, upward-fining, multistoried cyclothems of the sandstone facies assemblage are thought to have formed in wide, shallow, channels of an ephemeral stream/river environment draining from NW to SE.

5.3.1.1. Sandstones

Hot, arid areas are characterized by influent stream systems with downstream decreasing discharge due to water losses caused mainly by seepage into the alluvium and by evaporation (Báldi, 1992). Seepage into the alluvium largely depends on the permeability and thickness of the channel substratum (Knighton & Nanson, 1997). The short-lived nature of the floods as well as the transmission losses caused by evaporation and infiltration into the sandy channel substrate could be responsible for the formation and predominance of the massive sandstones (Sm). These common, structureless beds originate from rapid sedimentation from short-lived currents with exceptionally high sediment yield. Due to sudden drop in discharge, the transported particles were rapidly dumped on the channel floor as structureless mounds of sediments. As bioturbation is common in the unit, a significant proportion of the Sm sandstones may have resulted from the burrowing activity of living organisms disrupting internal sedimentary structures.

Experimental studies show that in 0.25-0.4 m-deep water courses (Ashley, 1990), the very fine- or fine-grained sands tend to develop horizontal lamination (Sh) only at flow velocities higher than 0.8-1 m/sec. On the other hand, it is well known that while ephemeral stream depths are low, their flow velocities are high (Langford & Bracken, 1983). Thus, the common horizontal lamination of the very fine- and fine-grained sandstones are interpreted here as testimony of upper flow-regime conditions.

According to Allen (1963), trough cross-bedding (St) is attributed to the migration of sinuous-crested dunes in the deepest part of the channels, while the tabular sets (Sp) are formed during migration of straight-crested transverse bars. For a given grain size, lithofacies St is formed in 3-D dunes at higher velocities, while lithofacies Sp is generated as 2-D dunes in weaker currents (Ashley, 1990). Apart from the fact that flashy, ephemeral systems are dominated by short-lived, high-energy flows that mainly generate horizontal lamination and/or massive beds, the paucity of cross-bedding may also be explained by the predominant very fine and fine grain size of the sandstones. In shallow water courses (depth 0.25-0.4 m) the development of cross-bedded strata in very fine- or fine-grained sands is limited: when the flow velocity decreases, the upper flow regime horizontal lamination is abruptly followed by ripple cross-lamination (Ashley, 1990).

Low-angle cross-bedded (Sl) sandstones that are often found in association with horizontal-laminated sandstones are thought to represent flow velocities transitional to the upper flow-regime current conditions (Miall, 1996).

Ripple cross-laminated sandstones (Sr) are interpreted as deposits of migrating small scale ripples. Depending on the flow conditions, different ripple forms are generated. Type A is generated at low net sediment deposition, while type B is formed at higher deposition rates (lower flow velocities) (Blatt et al., 1972). The latter type is also called climbing ripple cross-lamination, and it is commonly deposited from very low-velocity currents overloaded by very fine sand and silt (Miall, 1996). In the present case, the ripple cross-laminated sandstone is thought to have been formed during the waning phase of floods.

The repeated semi-sequences of Sh-St-Sp-Sr and Sh-Sm-Sr are attributed to velocity fluctuations, perhaps even within a single flood event. In addition, the frequent scour surfaces and intraformational conglomerates, not only as basal lags, but also within the sandstone beds, confirm the pulsating hydrodynamic conditions. The boulder-sized intraclasts within the basal-lag deposits (*Photo 77*) may indicate the intensity of the intrachannel flows which caused the underscouring and collapse of the river banks into the channel. The unsteady flow pattern is a distinctive characteristic of ephemeral streams with multiple-peak discharges. During a vigorous storm the overland flow is generated within minutes, with the water reaching the channels from several entry points. As a result, the intrachannel discharge has unpredictable, forceful wave-like pulses (at least two), which are thought to be generated mainly by widely separated storm cells with fluctuating intensities (Lucchitta & Suneson, 1981; Reid & Frostick, 1997). Frostick et al. (1983) showed that the intensity and frequency of such discharge pulses depend also on the drainage network-density, for instance, the size and extent of interconnection of the tributaries. The discharge pulses (i.e. water level and energy fluctuations) are crucial in the formation of various sedimentary structures during a single flood.

Along with the common bedding surface features (desiccated and bioturbated mud drapes, etc.), the soft sediment deformation structures provide a record of the processes that occurred shortly after the flood water receded. Therefore, the convolute beds may be attributed to quicksand conditions which commonly develop in water-saturated and disturbed sands through water expulsion in late flood stages. According to Blatt et al. (1972:169), these contorted beds "suggest rapid deposition from suspension and plastic deformation of partially liquefied sediments produced by shear stress on the bed".

The mud drapes with desiccation cracks, bioturbation and vertebrate footprints argue for repeated periods of non-deposition and subaerial exposure of the intrachannel deposits. Additionally, the mud drapes may be used as measures of the palaeo-channel bathymetry, assuming that each set of sandstone-mud drape units is the result of a single dynamic flood event. In this way, the thinly bedded (<0.5 m), mud draped, laterally continuous sandstones suggest rather shallow and wide courses. The internal structures (massive, horizontal- and (rarely) planar-cross bedding, ripple cross-

lamination) of the sandstones and their organization in sequences imply high-stage flows succeeded by minor low-stage conditions. Wide, shallow channels and poorly connected drainage networks are characteristic of the ephemeral river/stream systems in semi-arid/arid zones (Knighton & Nanson, 1997). Additionally, the wide channels have high sediment-transport capacities in small- to medium-sized semi-arid/arid basins (Knighton & Nanson, 1997).

Accepting that the multistoried, mud-draped sandstone beds are the result of several flood events, it can be concluded that the slightly upward-fining arenaceous units without channel cutbank surfaces may comprise many palaeo-channel fills superimposed one upon the other. The thinner beds towards the top of the cyclothems may indicate progressive filling of channels resulting in shallower channels (Friend, 1978). The absence of waning flood-phase sedimentary rocks (lithofacies Sr) within the multistoried sandstone beds and their rare presence in the upper part of these stacked sandstone bed are explained by the fact that the waning flood-phase deposits (lithofacies Sr) of earlier floods were eroded in subsequent rainstorms. Possibly the absence of the Sr lithofacies within fining-upward cyclothems is not caused only by subsequent erosion, but by non-deposition because the water level dropped too rapidly. The possibility of such sudden water level falls may be indicated by the presence of the previously mentioned massive beds (Sm). All these features show that deposition took place in short time intervals.

The fine-grained mudstone and siltstone (Fm, Fsm, Fl) interbeds in arenaceous deposits are interpreted as thick mud drapes which settled from suspension in intrachannel stagnant pools that dried out in time. During the rainy days of the 1998 field-work season, I had the opportunity to witness some present-day ephemeral stream processes in the semi-arid study area. One of the observations was that after the flood receded, the murky water in such thalweg scour pools often survived for some time, and attracted thirsty animals not only for drinking, but for wallowing purposes as well. Being trampled by these animals, the soft and delicately laminated mud dried out as a massive, bioturbated mud unit. These intrachannel mud deposits are excellent sources of intraformational mud clasts, as subsequent floods often remove the fine-grained deposits from the channels.

5.3.1.2. Intraformational conglomerates

The carbonate glaebules, mud- and sandstone clasts and bone fragments of intraformational conglomerates (Gcm, Gh, Gp, Gt) originate from a nearby source as they display low abrasion effects and poor sorting.

These gravel beds, together with the other sedimentary structures of the sandstone facies assemblage, indicate the high strength of the floods. Sundborg (1956 in Allen & Williams, 1979) showed that calcrete pebbles are transported in currents running with speeds of at least 1-2 m/s. However, as the classical article of McKee et al. (1967) demonstrates, the maximum preserved rock grain-size does not always reflect the maximum stream power. In their example, the largest rock particles deposited after a major flood in the semi-arid Bijou Creek (Colorado) were granules and pebbles, but the very same flood picked up and transported large iron bars and other concrete masses from a washed-away highway bridge for a minimum of 335 metres. Therefore, the maximum preserved particle size represents the lower limit of the strongest stream power (and preserved maximum available grain size) rather than the maximum transporting ability of the current in the catchment area.

The gravel lithofacies (Gcm, Gh, Gp, Gt) are thought to be formed in traction currents with constantly changing strength and sediment-yields. They most probably represent channel-bottom lag deposits in the form of gravel sheets, straight (2-D) and sinuously (3-D) crested gravel dunes. The normal graded foresets resulted from the segregation of gravel-sand mixtures on the avalanche slope of the forward-accreting foreset aprons in those large gravel dunes (Allen, 1983c in Miall; 1996).

The presence of the locally-derived intraformational conglomerates and the lack of distinct paleosol horizons might be taken as an indication of a depositional system where the streams/rivers often abandoned their channels, eroding the paleosols down to their carbonate-bearing horizons and occasionally even eroding into older channel deposits (*Photo 80*). The absence of LA macroforms indicates that the rivers/streams did not migrate laterally across their floodplains. It is believed that periodic but significant overbank erosion was generated by powerful overland flows during exceptional cloud bursts. These overland sheet flows were competent to wash away the relatively thin topsoil of the calcisols (*sensu* Mack et al., 1993), remove the resistant calcrete glaebules from the calcic horizon and transport them to the larger channels.

5.3.2. Fine-grained facies assemblage

In arid climates where intermittent heavy rainfalls deliver high water volumes exceeding the rate of infiltration into the floodplain deposits, overland flows and pluvial water ponding are important factors in both landscape formation and sedimentary processes (Baird, 1997). Therefore, the sediment transportation in the overbank area is dominated by forceful overland (Hortonian) flows rather than by overspilling flows from major channels.

Frostick et al. (1983) observed that in flash-flood environments, the sediment-transport capacities of the overland flows are influenced by the rainfall intensity, exposed lithology-types, vegetation and geomorphology. The extremely flashy regimes, generated by high intensity storms, easily mobilize the otherwise dry, loose surface sediments, especially after prolonged dry periods. The development of current structures is often prevented because of the short-lived nature of the storms and by the rapid dissipation/evaporation of the floodwater (Tunbridge, 1984; Tirsgaard & Øxnevad, 1998).

5.3.2.1. Argillaceous strata

The highly argillaceous strata of the overbank area imply low surface-infiltration capacities, and therefore intense overland flows with mixed sediment load (Frostick et. al., 1983). In turn, these rapid Hortonian flows probably speeded up the beginning of the intrachannel processes in arid climate. On the other hand, the muddy deposits with reduced permeability may also have enhanced the subsequent deposition from ponded pluvial waters. Thus the argillaceous strata dominated by homogenous mudstones and siltstone (Fsm, Fs) possibly settled out from mixed Hortonian flows of the interchannel area. The laminated argillaceous deposits reflect subsequent deposition from ponded pluvial waters (ephemeral lakes). Just as in the channel subenvironment, the overbank area was also subject to episodic flooding and drying out, but because of the different geomorphological gradients and available loose-sediment particle sizes, the intensity of the sedimentation processes turned out to be significantly different.

The common clay-rich sandstones (greywacke) (Fs) within the fine-grained facies assemblage may originally have been deposited from mixed load Hortonian flows, but due to the mechanical infiltration of clays through influent seepage of muddy pluvial water ponds, the initial low mud:sand ratio has been increased.

The rounded, silt-sized quartz grains of the argillaceous rocks may be indicative of aeolian dust or loess derived within the unit or from the neighbouring desert environments via dust storms. Aeolian material is thought to be a significant contributor to the sediment supply in semi-arid floodplain settings (Smith & Kitching, 1997).

The calcretes and silcretes are evidence of duricrust formation in arid climate soil. The calcretes indicate calcisols *(sensu* Mack et al., 1993), whereas the blocky structures seen in *Photo 91* and the clay coated clasts (*Photo 110*) are interpreted as peds and argillans, being early stages of vertisol formation (Talbot et al., 1994). The abundance of massive, structureless, colour-mottled argillaceous rocks may also be indicative of plant root horizons within paleosol profiles. Palaeosol features (calcrete; silcrete; silicified rootlets; soil peds; clay coated argillans; massive, colour-mottled deposits) indicate that the landscape was stable over relatively extended periods (i.e. no clastic deposition). The palaeosols, palnt traces and vertebrate bone fossils indicate that the fine-grained facies assemblage accumulated on surfaces that supported a complex ecosystem.

The distribution and abundance of disarticulated vertebrate bone fossils and the absence of whole articulated skeletons may be suggestive of rare but powerful floods that punctuated extended periods of non-deposition when the drying out of the ligaments and bone weathering could take place. Probably, the skeletal elements of the disarticulated carcasses were transported and scattered by torrential overland flows before being buried in the overbank strata (Smith, 1995). The rare articulated bone fossils may imply that in some cases the animals died not long before a major flood and the bones were rapidly buried prior to complete decomposition of ligaments. On the other hand, the preservation of some articulated and unbroken fossil bones supports the interpretation that the fine-grained rocks accumulated in an area dominated by less vigorous sedimentation processes than those of the channel subenvironment.

5.3.2.2. Sheet sandstones

The tabular bedforms and the internal structures of the single, sheet-like sandstones enclosed by fine overbank rocks indicate non-channelized, high-energy currents away from the main, ephemeral channels. Thus the isolated, sheet-like thickly and thinly bedded sandbodies (**SB**) are interpreted as deposits of short-lived, unconfined, major and minor sheet floods, respectively. Such ephemeral, sediment-laden, sheet-like flows are common features of the very slightly elevated interfluvial areas of flash flood stream/channel systems. Blanket-like sheet sand within sequences of muddy flood plain deposits are well-documented in the literature of semi-arid sedimentary processes (e.g. van Dijk et al., 1978; Allen & Williams, 1979; Tunbridge, 1984; Demicco & Kordesch, 1986, etc.).

The superimposed sheets of sandstone and mudstone that show great lateral continuity are explained here as rare, preserved examples of well-developed 'rhythmites' formed by cyclic sedimentation in natural levees (Farrell, 1987). The sequences of rapidly alternating sandstones and mudstones are extremely rare and are exclusively found adjacent or proximal to major exposures of the channel sandstones (**LS**).

5.3.2.3. Intraformational breccias and conglomerates

The locally derived sandstone and siltstone clasts, the poor sorting, the very angular fabric, the infrequency of the bedding in the intraformational breccias (Gmm, Gcm) and clast-rich sandstones (Sc), all suggest that the strata were deposited after short transportation distances. The red clay coated, angular and relatively soft intraclasts resemble blocky structures (peds) with clay coatings (argillans) of aridisols (Talbot et al., 1994). Thus the breccias might be seen as local accumulations of redeposited soil peds. The initial brecciation probably took place within the soil profile, where during pedogenesis the original sandstone and siltstone were fissured, and later coated by illuviated clays. This process is relatively common in modern semi-arid mud playa/pan environments (Demicco & Kordesch, 1986).

The poor sorting, the lack of bedding structures and the general absence of erosional surfaces indicates that the intraformational breccias (Gmm, Gcm), clast-rich sandstones (Sc) and accompanying laminated sandstones were formed in a higher viscosity medium than the normal stream traction currents (Steel, 1974). While matrix-supported breccias (Gmm) and clast-rich sandstones (Sc) are interpreted as debris flow deposits, perhaps the clast-supported massive breccias (Gcm) are high-density flow deposits which represent transition between normal stream and debris flow conditions (Hartley, 1993). Accordingly, the horizontal laminated and trough cross-bedded sandstone sequence that consistently overlies the clast-supported breccia (Fig. 73) may point to the coexistence of normal stream currents and debris flows.

Debris flows, and the more channelled, stream-flow sedimentation were triggered by high-magnitude floods resulting in intensive overland wash processes of varying strength and sediment/water ratio. These processes interrupted the quiet aggradation of the floodplain sequence, and after short transportation distances, deposited their locally derived sediment load in small-scale, shallow hollows and rainstorm-eroded gullies of the otherwise flat, muddy floodplain surface (Allen & Wiliams, 1979).

The glaebular calcrete conglomerates that were found as narrow, sheet-like layers (**GB**) within the fine-grained, argillaceous rocks were also formed during high intensity, devastating rainstorms in short-lived, rapid runoff processes (Allen & Wiliams, 1979). The carbonate glaebules were denuded from the adjacent soil (calcisol *sensu* Mack et al., 1993) profiles of the flood plain. After short transportation distances, these carbonate glaebules were redeposited in local, shallow depressions in the form of isolated, sheet-like intraformational conglomerates.

5.3.3. Discussion

The subtle upward-fining pattern of the semi-sequences of Sh-St-Sp-(Sr) or Sh-Sm-(Sr) punctuated by desiccated mud drapes; the abundance of the Sr towards the upper portion of the cyclothems; the relative dominance of the Sm, Sh lithofacies; the intraformational conglomerates; the bedforms and lateral continuity of bedforms; together show strong similarities to deposits of ephemeral stream/river channel sequences (Parkash et al., 1983; Rust & Legun, 1983; Langford & Bracken, 1983). These observations combined with the recognized lithofacies assemblages of the overbank area (Fig. 104) and their organization into architectural elements (LS, SB, GB, SG & FF) reinforce the interpretation of an ephemeral stream/river system controlled by flash floods in an increasingly arid environment.

Supported by outcrop and subsurface observations, the spatial relationships of the lithofacies assemblages suggest that the stacked palaeo-channel deposits form laterally and vertically isolated zones within the fine, overbank sedimentary rocks. These indicate periodically confined, multichannel alluvial systems with well-developed channel and overbank subenvironments. The abrupt termination of the multistoried, tabular palaeo-channel sandbodies against the surrounding fine-grained strata invoke the picture of former wide arroyos (Dreyer, 1993) cut into the cohesive muddy deposits which inhibited the lateral migration of the channels.

In the absence of syn-sedimentary faults and other evidence of syn-depositional tectonics, the initial incision of the valley together with the generation of the intraformational conglomerates perhaps took place during severe torrential floods, following extended dry periods when the regional base-level (i.e. groundwater level) dropped below the equilibrium profiles of the ephemeral stream system (Smith & Kitching, 1997). Such base-level lowering could be generated by prolonged droughts when the generally low groundwater table falls even further.

The upper flow-regime sedimentary structures suggest the dominance of high-flow velocities and high sediment concentrations, which in turn reflect relatively elevated upland and/or higher regional-slope gradients than in the present day Channel Country of semi-arid to arid central Australia (Gibling et al., 1998). Palaeo-current data indicate a regional slope inclined to the SSE. These data, which show high overall variability (consistency ratio: 0.6), but low dispersal for the individual measuring points (average consistency ratio: 0.9), imply low-sinuosity wandering channels.

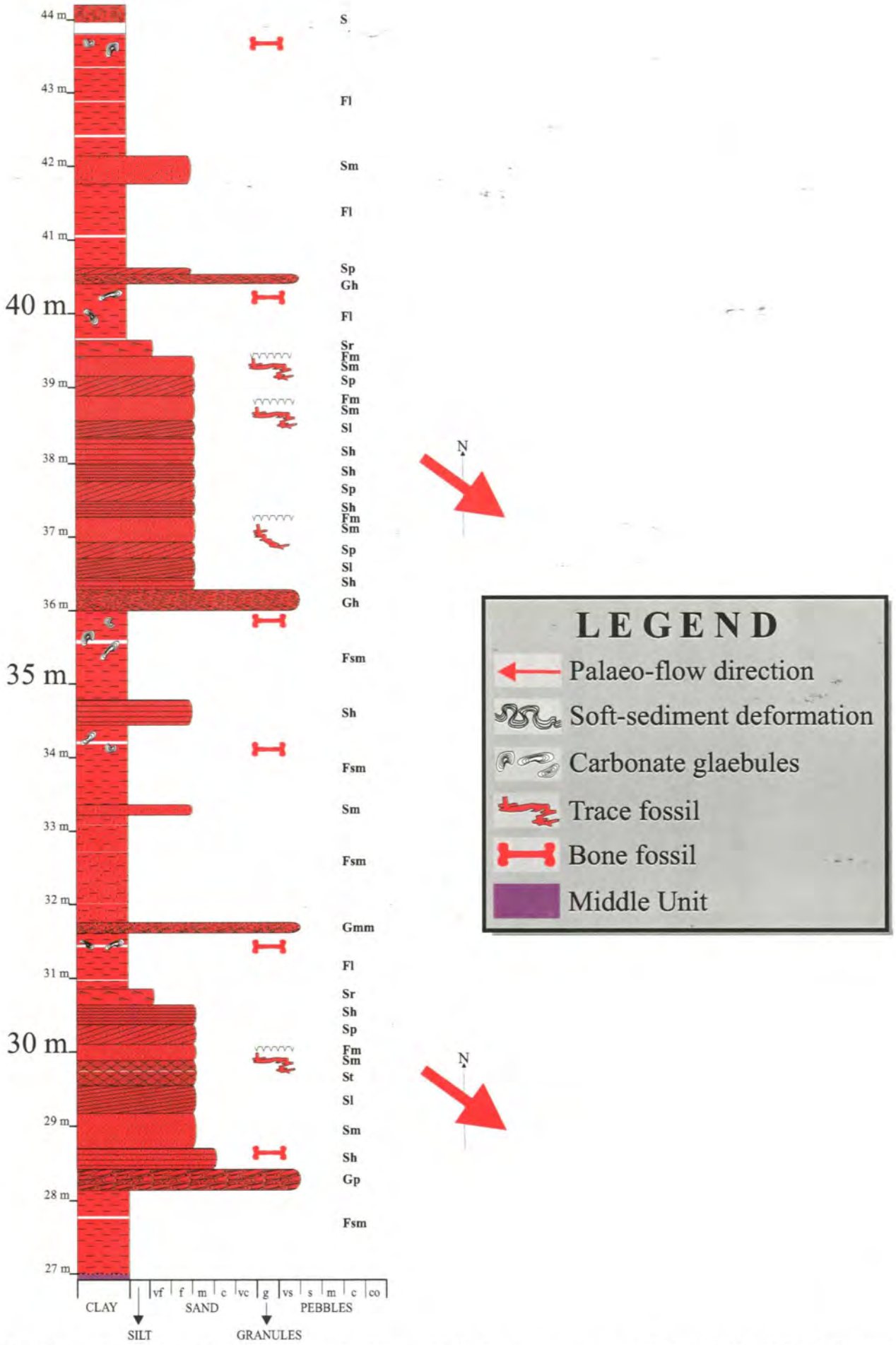

Fig. 104. General vertical profile of the Upper Unit in the southern Tuli Basin. For lithofacies codes refer to Table 5 (Ch. 3.1.4.). Thicknesses are very approximative, for precise data see text.

Based on subsurface data, levee deposits constitute less than 3% of the formation (Fig. 105). This low percentage, which is also confirmed by outcrop observations, reinforces the postulated concept of fixed ephemeral channels that rarely ovetopped their banks. The periodically fixed channels imply the relative stability of regional slope gradient which was high enough to prevent the dominance of unconfined flows, but low enough to allow ephemeral, muddy pools of ponded rain water in the overbank area.

	Cumulative thickness in m	Percentage %
Channel	865.01	39.19
Levees	53.44	2.42
Overbank deposits (all mudstones and single sandbodies)	1288.99	58.39

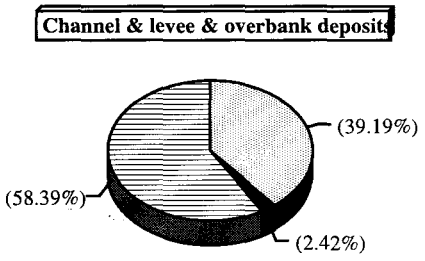

Fig. 105. Relative frequencies of channel, levee and overbank deposits in the Upper Unit. Data based on borehole records.

The various sedimentological parameters (e.g. palaeo-current indicators, abundance of muddy overbank deposits (~58%), absence of downward- and lateral-accretion macroforms, absence of point-bar sequences and channel-shaped lithosomes) imply that the wide, shallow water courses were neither braided nor meandering. Deposition might have occurred in an alluvial system with an interconnected and periodically-fixed ephemeral-channel network. Sedimentation took place via vertical aggradation in both the channel and overbank subenvironments (see Parkash et al., 1983; Wells, 1983; Gibling et al., 1998). In both of these subenvironments, the sediments were supplied by competent overland (Hortonian) flows which reworked both older deposits and the contemporaneous aeolian silts and sands. The aeolian influence was significant, as it is important in present day semi-arid settings (Tirsgaard & Øxnevad, 1998). Additionally, in the ephemeral intrachannel subenvironment, one of the most important sediment sources for aeolian transport is the loose sand cover of the river bed itself (Knighton & Nanson, 1997).

5.3.4. The model and analogues

The fluvial system under investigation is equally dominated by stacked sequences of Laminated Sand Sheets (LS) and Floodplain Fines (FF). While the former represents the channel subenvironment, the latter is testimony of interchannel areas where, during major flooding, minor amounts of Sandy Bedforms (SB), Gravel Bars (GB) and Sediment-Gravity-Flow (SG) deposits were also laid down. It may be concluded that the strata were deposited under semi-arid climate conditions, in an ephemeral fluvial and clay-pan system. The palaeogeographic reconstruction of the area is illustrated in Fig. 106. According to this figure, the sandy and fine-grained facies assemblages were deposited simultaneously in different parts of the depositional system. None of the available semi-arid/arid climate fluvial facies models (Miall, 1996) can be applied without minor modifications. This is partly because each fluvial system is somehow unique, and partly because the processes dominating in semi-arid/arid areas are still insufficiently known. Because of the hazardous, infrequent and unpredictable character of the floods (Reid & Frostick, 1997), it is difficult to form facies models, thuis the rigid application of existening models is inappropriate.

5.3.4.1. Ancient analogues

Most of the architectural characteristics listed for flashy, ephemeral sheetflood ("Bijou Creek type") river style are displayed by the strata of the Upper Unit, though the "criteria" of sand predominance and lack of well-developed floodplain areas are not met here (Miall, 1996). On the other hand, the characteristics described in the terminal fan (middle part) model of Kelly & Olsen (1993) seem to be partially applicable to the present study as well, although there is insufficient palaeo-current data to support the fan-shaped geomorphology and the radially divergent nature of the distributary system. The other major difference in the case of the Upper Unit is that there are no consistent downstream trends in the various sedimentary parameters (downward decrease in grain size and increase in the proportion of fine-grained sediment). In other words, the sandstone and fine-grained facies assemblages cannot be separated into only two discrete zones because they are laterally interspersed.

The facies associations of the Upper Unit correspond in some respects with the ephemeral stream system and clay-playa model of Tunbridge (1984). Although there are some major differences, the

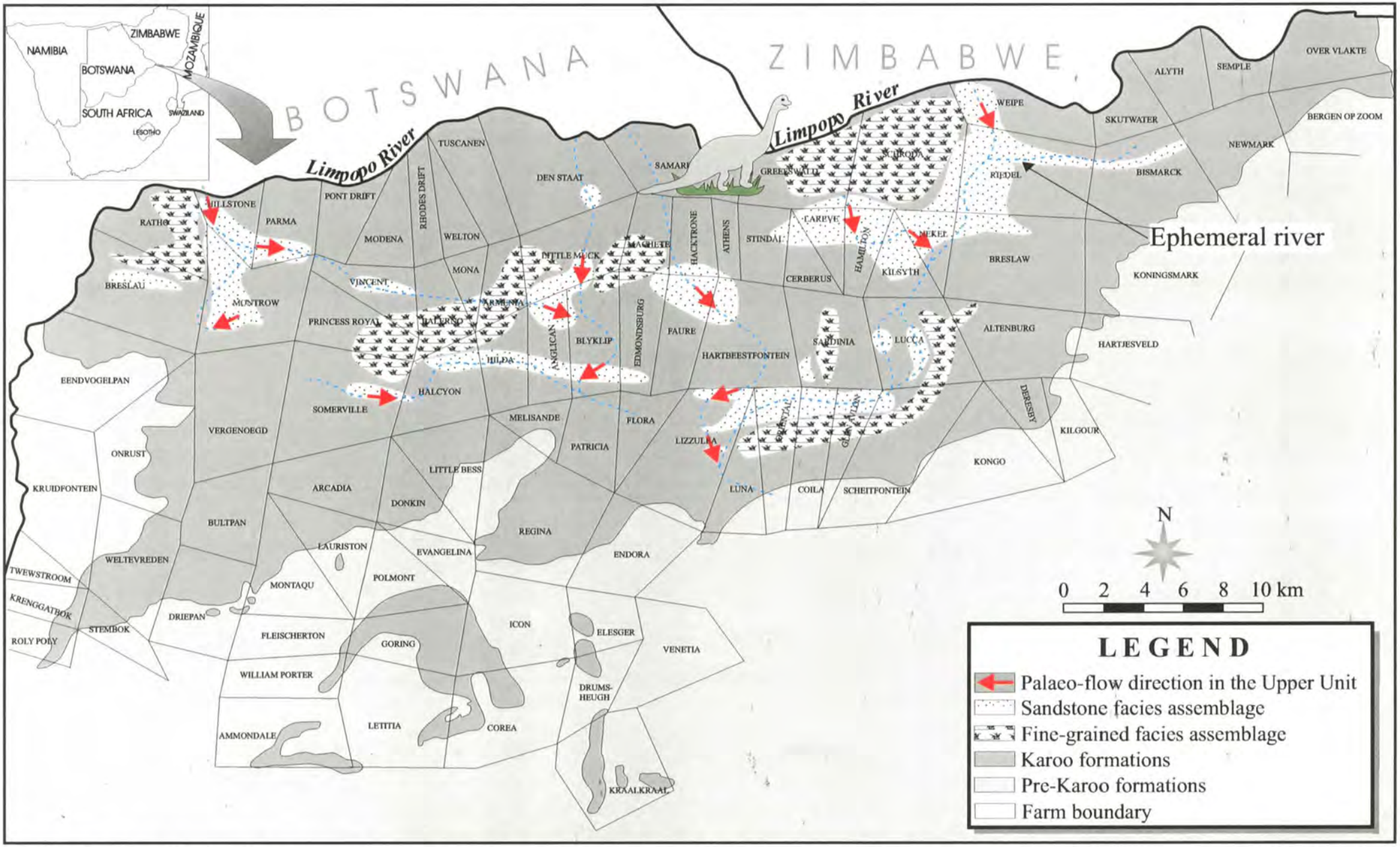

Fig. 106. Map showing the palaeo-environmental reconstruction of the Upper Unit. Distribution of the facies assemblages is based on outcrop and borehole data. The arrows correspond to the mean vector of the palaeo-current measurements obtained from the outcrops adjacent to the arrow.

medial to distal transitional sequences (distributary-channel, sheet-flood and clay-playa deposits) may be comparable to the overall succession of the Upper Unit.

In addition, the fine-grained facies assemblage shows similarities with the confined and the terminal floodplain sequences described by Sneh (1986) from Wadi El Arish, northern Sinai. The confined floodplain deposits occur as mud draped sandstones forming upward-fining units of horizontal and cross-bedded strata capped by climbing ripples. Scour-and-fill structures are common and pebble-sized particles may be present. Terminal floodplain deposits are characterized by laminated and massive mudstones alternating with minor cross-laminated sandstones.

Regarding the overbank area sedimentation processes, the clay-floored pan/playa depositional model of Rosen (1994) seems to be applicable. Such pans usually develop in flat-lying areas, over sandy clay and/or clay surfaces, and are relatively well vegetated (Shaw & Thomas, 1997). In addition, the clay-floored pans (*sensu* Rosen, 1994) are characterized by low salt and high carbonate inputs and a low-lying groundwater table (Rosen, 1994). Pans of this type and adjacent areas are the sites of pedogenic duricrust accumulations (calcrete and silcrete). The sediments of the overbank area, including the clay-floored pans, are supplied by episodic inundations and aeolian inputs (Shaw & Thomas, 1997).

The ephemeral stream-playa lake palaeoenvironment reconstructed from the rock record of the Permian lower Beaufort Group, Main Karoo Basin (Stear, 1983), is broadly similar to the one which existed at the Triassic-Jurassic transition in the Tuli Basin. The internal sedimentary structures and the lithofacies associations are similar, and the main differences arise from the very different morphology and internal geometry of the sandstone bodies. As already mentioned, channel cutbank and lateral accretion surfaces are absent, and none of the overbank sandstone sheets could be identified as crevasse splays or ribbon sandstones.

5.3.4.2. Recent analogues

The present day climate, landscape and sedimentary processes of the study area seem to be reasonable contemporary analogues of the sedimentary dynamics that prevailed during the deposition

of the Upper Unit in the Tuli Basin. Generally speaking, the semi-arid climatic conditions (average annual rainfall 339-400 mm) are characterized by prolonged dryness punctuated by rare, but intense rainstorms. The relatively flat, barren terrain is dominated by an ephemeral stream system, draining into the Limpopo River, which itself flows only during major thunderstorms.

The 5 to 25 m wide, shallow, mostly straight sandy riverbeds have relatively low banks and flat-bottomed floors, and are virtually dry through the year. Following thunderstorms in their catchments, water courses along them for only a few hours, maybe a few days, depending on the rainfall intensities. Water starts flowing in the riverbeds after runoff from the overbank area reaches the channels. Because the discharge in the channels is not steady, but depends on factors like storm intensity, storm cell density, tributary network, catchment area size and vegetation, wave-like pulses of discharge may be observed. Such standing waves have great and unpredictable energy, being capable of overturning a normal pick-up truck (bakkie) even in a 0.5 m deep by 15 m wide channel. During medium intensity storms, the flowing water partially occupies the wide river bed, so bank-full channel stages are only seen in the low gradient reaches where the water spreads over a wide area, forming either numerous smaller braids or wide, shallow sheetflows (*Photo 146*). The flood waters infiltrate very rapidly into the thick sandy channel substratum, resulting in a downward decrease in the river discharge. Flash flood events with high sediment-transport capacities are normally followed by long, hot desiccation periods of decreased, mainly aeolian sedimentation. During the dry season, sunbaked, cracked mud drapes or layers are formed, not only in thalweg scour pools of rivers, but also in the marginal parts of man-made dams (*Photo 147).*

The fairly well-developed floodplain area is relatively flat and covered by loose alluvial sands/silts, thin topsoils of sandy and/or calcareous soils and other regolith with isolated inselbergs rising above it. Depending on the storm magnitude and frequency, the flash floods may generate shallow, ephemeral ponds and lakes as well as blanket-like sandy-silty sheets over this flat interchannel area. The sandy/calcareous soils sustain a sparse vegetation and a relatively rich fauna (both being strongly influenced by game/cattle farming). The soils of the overbank area are fragile: at some places the soil erosion rate is high, and gully and rill formation processes are present (*Photo 148, 149*). Aeolian processes are present mainly in form of dust storms which occur primarily during the dry period. Wind-blown sand and silt are often trapped by the bushes. Contemporaneous calcrete formations (*Photo 150*) are relatively common in the near surface deposits, and evaporites (NaCl and $CaSO_4.2H_2O$) were occasionally observed (Weltevreden, Regina).

5.4. Clarens Formation

The general vertical profile of the Clarens Formation is presented in Fig. 107. The lithofacies associations of the Formation indicate an arid climate, desert and ephemeral fluvial depositional environment (Fig. 108).

The massive, thickly-bedded sandstones (Sm) interbedded with large-scale planar cross-bedded sandstones are interpreted as secondary massive dune sandstones. The original dune cross bedding is interpreted to have been destroyed by precipitation onto the dune surfaces or by rising ground/dune water (Chakraborty & Chaudhuri, 1993). According to Eriksson (1986), even in modern aeolian deposits, sedimentary structures are not always readily visible. It is therefore possible that part of the thickly-bedded massive sandstones is just apparently structureless. This is indeed an interpretation which has been given for the thickly-bedded, massive sandstones of the Clarens Formation in the main Karoo Basin (Beukes, 1970; Eriksson, 1981 and 1986).

Large-scale cross-bedded sandstones (Sd) separated by planar, first-order bounding surfaces indicate simple migrating wind dunes such as barchan dunes, barchanoid and transverse ridges (Brookfield, 1992). The aligned and connected crescent-shaped bedforms are interpreted here as barchanoid ridges, while the low dispersion values of the foreset dip directions are believed to indicate fairly straight crested transverse ridges. The high-angle foresets and their internal structures (i.e. inversely graded and indistinct laminae) suggest accretion by grainflow (avalanche) and grainfall processes in dry sand dunes (Glennie, 1987). The paucity of second-order bounding surfaces indicates simple dune systems (Pye & Tsoar, 1990; Nickling, 1994). Palaeo-current data show minor variation in average foreset dip directions and indicate constant, unidirectional westerly winds (Fig. 108). Although it is negative evidence, the lack of ripples on avalanche slopes also indicates unimodal winds (i.e. lack of cross-winds). The presence of both barchanoid ridges and transverse dunes implies, firstly, limited sediment supply (Glennie, 1987); secondly, slight fluctuations in sand supply (Nickling, 1994) and, thirdly, winds with little directional variability (Glennie, 1987). According to Pye & Tsoar (1990), the migrating transverse dune types form in vegetation-free areas, and Cooke & Warren (1973) state that such aeolian bedforms tend to develop upon hard surfaces. In the present

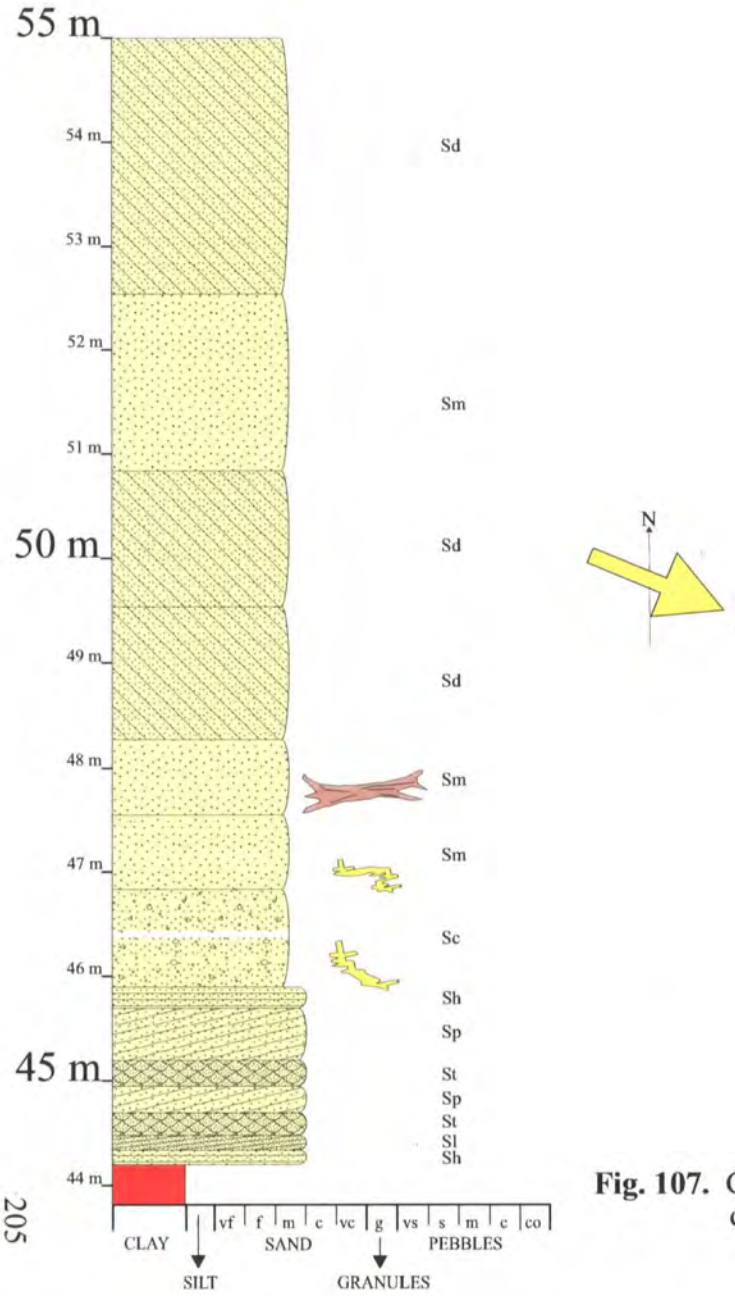

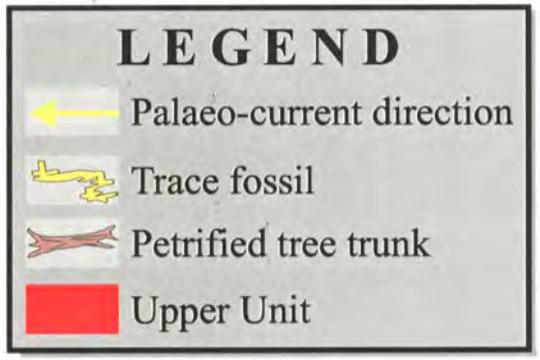

Fig. 107. General vertical profile of the Clarens Formation in the southern Tuli Basin. For lithofacies codes refer to Table 5 (Ch. 3.1.4.). Thicknesses are very approximative, for precise data see text.

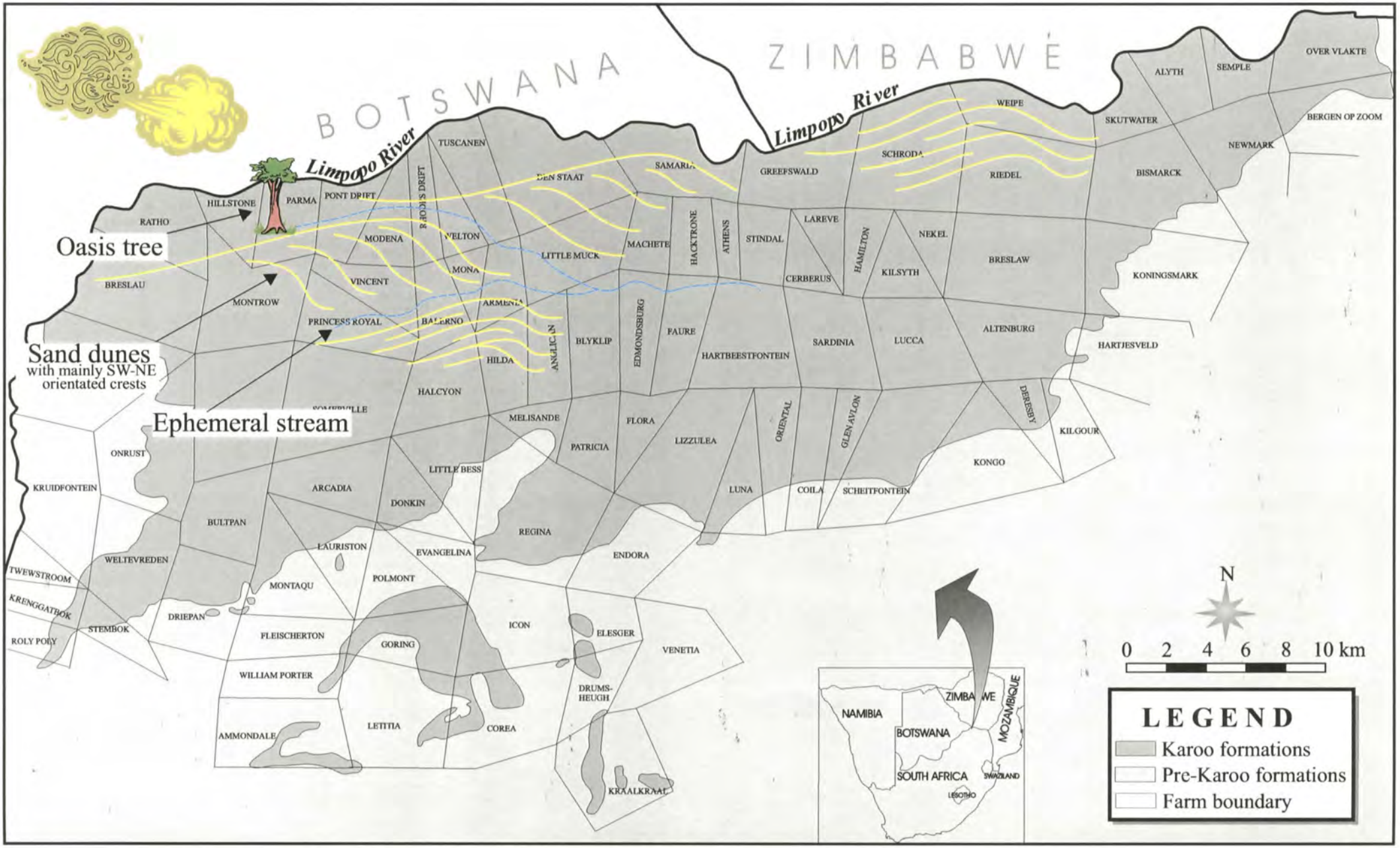

Fig. 108. Map showing the palaeo-environmental reconstruction of the Clarens Formation.

case, the hard silcretized upper surface of the Upper Unit provided an ideal even pavement over which the migrating dune types could rapidly develop.

The sedimentary features (horizontal-bedded (Sh), low-angle cross-bedded (Sl), trough cross-bedded (St) and medium-scale planar cross-bedded (Sp) sandstones) that occurred in the lower part of the Formation are thought to represent the channel deposits of ephemeral streams. Assuming that the sequence in Fig. 78 was formed in a single flood event, the Sh-Sl-St-Sp-St-Sp-Sh bedforms indicate decreasing water velocities from upper-flow regime (Sh-Sl) to lower-flow regime (Sp-Sh) and finally flow cessation. The repeated St-Sp structures may suggest changes in the flow conditions (energy fluctuation?). The short, shallow and wide channel-shaped bedforms suggest that the temporal water courses were transient, and that the channel water dissipated very quickly before it could reach a semi-permanent body of water (Olsen, 1987). The magnitude of the rainfalls must have been significant, because in semi-arid/arid areas surface runoff from aeolian dunes is minimal because rainwater quickly soaks into the permeable sand. According to Warren (1983), only 5% of the infiltrated water reaches the dune water table, the rest evaporates. The scarcity of palaeo-current indicators and exposures does not allow the proper reconstruction of channel morphology, but the channel-fill pattern points to a rather low-sinuosity, perhaps single- or braided-stream system.

The horizontally laminated sandstones that are found in the lower part of the Clarens Formation are interpreted as wet/damp interdune deposits that were formed by aqueous reworking of aeolian sand. According to Langford & Chan (1989) such sediments are likely to be deposited under quiet-water (i.e. lower-flow regime) conditions between the dunes. Such water bodies are formed by ponding of rain or ground water after severe floods (Langford, 1989). In the present case, it is unclear what controlled the water ponding processes (rain water ponding versus temporary water table rise). Furthermore, these deposits may be interpreted as products of rapid but short-lived sheet flush (i.e. upper-flow regime) processes that washed away the loose sand dunes. According to Brookfield (1992), laminated, tabular bedforms may also form through exclusively aeolian processes when the wind velocities are too high for ripple/dune formation. The coarse grain sizes of these deposits also indicate stronger currents than the average prevailing wind speed (Pye & Tsoar, 1990). However,

the lens-shaped, horizontally laminated and massive sandstones are confined to the lower part of the Formation where most of the fluvial deposits occurred, and are therefore interpreted here as the fluvially derived strata of non-channelized, intermittent, rapid shallow flows.

The presence of fluvial strata implies that the interdune areas were seasonally inundated. Such wet interdune bottoms commonly support flourishing flora and fauna, and have a relatively high potential for preserving trace fossils (Langford & Chan, 1989). Therefore the bioturbation features described in Ch. 4.2.4.2. are interpreted here as additional, although indirect, evidence of a wet aeolian system. Moreover, the original structures of the thinly bedded, massive sandstones might have been destroyed by bioturbation because inhabited sand dunes often lack internal structures.

The growth-rings of the *Agathoxylon sp.* wood type also imply some seasonal variation in the climate. These petrified wood specimens are interpreted here as part of a large oasis tree, that possibly flourished in a rare, fertile spot in the desert (Fig. 108). The internal structure of the specimen shows that there was no dramatic water shortage, suggesting a continuous water supply in the oasis through the year. Thermal springs may have played a role. Evidence for this is common in the Limpopo Belt (Jackson, 1975; Chidley, 1985) and there are some active springs in the study area (e.g. Evangelina, Icon farm). It has been observed that around such springs/wells the vegetation is lush and includes giant mopani trees.

The micro- and macroscopic evidence supports the conclusion that the Clarens strata were formed as migrating sand dunes, generated by westerly winds of an erg milieu. The progressive aridification of the climate is indicated by the absence of the ephemeral stream deposits and trace fossils in the upper part of the Formation. The wet dune field environment was thus replaced by a dry sand sea milieu.

Recent analogues of the environments described above are the semi-arid areas of western central Australia, or the northern part of the Sahara Desert, where the depositional environments are dominated by westerly winds.

5.5. Petrographic studies

The evidence from microscale observations supports the conclusion reached from the study of outcrop-scale sedimentary structures, namely that the sedimentation of the Basal, Middle and Upper Units occurred in high energy, mechanically destructive environments.

The highly quartzose composition of the units indicates derivation from craton interiors (Pettijohn et al., 1987), whereas the virtual lack of unstable rock components, and the trends of increasing sorting, roundness, sphericity and maturity, demonstrate that the deposits were progressively recycled.

These trends originate in the fact that the Karoo Supergroup forms an evolutionary, quasi-continuous basin fill. In other words, the reworking of the older Karoo Supergroup sedimentary rocks became more pronounced with time. Even though igneous and metamorphic rock sources were always present, the geographic situation of the multiple source areas changed during the formation of the Karoo Supergroup. This is attested by the regional palaeo-current patterns as well.

Although the limited sample set is probably not representative, the absence of kimberlitic indicator minerals might imply that none of the adjoining kimberlite intrusions (Venetia - South Africa, River Ranch - Zimbabwe) were unroofed during the deposition of the sedimentary units of the Karoo Supergroup. This assumption need to be confirmed by a more extensive sampling survey.

5.5.1. Basal Unit

The following microscopic observations suggest that the sediments of the Basal Unit are first cycle deposits: coarse grain sizes, poor sorting, high angularity, low sphericity, high proportions of polycrystalline and undulatory quartz grains, low maturity and low concentration of heavy minerals.

The lack of downstream grain size changes among the collected samples may be explained by the masking effect of the local-sediment input and the relatively small sampling. Downstream

changes are in the first instance attributed to abrasion, but as Hoey & Bluck (1999) have pointed out, there are potentially several other contributing and/or controlling factors. The downstream fining could be influenced by interactions among physical processes (e.g. selective entrainment and transport), geological conditions (e.g. lithology, basin tectonics, base level changes, sediment supply, tributary input) and climate (e.g. water discharge, sediment supply).

Detrital micas and laminated clay-rich matrix may easily wrap around the larger detrital grains because of differential compaction of the sediments, leading to symmetrical deformation of the laminated matrix around the grains (Pettijohn et al., 1987). On the other hand, the deformation of the laminated matrix is confined only to the lower part of the larger detrital grains, suggesting that the contortion is due to a gravitational wrapping effect that developed under the load of the quartz grains settled on top of the laminated, but still plastic, muddy deposits. This laminated and plastically deformed matrix together with the predominance of the rather angular detrital grains suggest that the particles settled from suspension. The coarser grains may have been transported and embedded via processes like drop-stones. The microslumps (swirly structures) in the matrix are commonly generated by movements in debris flow sediments (Owen, 1994:24).

The finely crystalline composite quartz grains, with their irregular crystal shapes and high crystal number, indicate a metamorphic source area. Besides, the composite grains with poorly sorted crystals also suggest derivation from metamorphic terrains. As the polycrystalline quartz grains and the strained (undulatory) quartz grains are mechanically unstable, their presence in the Basal Unit suggest that, to some extent at least, metamorphic source components were proximal to the site of deposition. Additionally, the high proportion of angular, shattered quartz grains implies that the fragments were not far-travelled, so the idea of partially local provenance is reinforced. Macroscopic observations reconfirm the existence of local sediment input as quartz vein boulders were seen incorporated in the lower part of the Basal Unit (*Photo 30, 31*). The low proportions of composite quartz grains with coarse crystals and monocrystalline grains with mineral inclusions suggest that igneous plutonic rocks had a less significant function in the proximal sediment supply, while the relative high percentage of coarser (0.25 to 1 mm), monocrystalline, undulatory grains implies that igneous plutonic rocks were probably present in the catchment area.

Low proportions of feldspar and metamorphic rock fragments and the angularity and shattered textures of quartz grains indicate transportation in a high-energy environment where the less-durable materials were mostly destroyed. This accords with the sedimentological observation of a high-energy, braided fluvial system. Furthermore, the virtual lack of feldspar apart from the selective loss could also be explained by derivation from a source area blanketed with a deep residual regolith that was already depleted in feldspar. The alteration of feldspar to mica and clay minerals suggests that the original modal compositions were slightly modified in the diagenetic processes, perhaps by dissolution and replacement caused by migrating, chemically charged ground water (Salem et al., 1998).

Controlling processes for the concentration of heavy minerals are governed chiefly by the density contrasts between the sediment grains (Reid & Frostick, 1994). Conditions for heavy mineral concentration are best developed in alluvial systems due to the frequent energy fluctuations that crucially enhance the hydraulic sorting processes. For instance, it is widely known that concentrating processes are greatly amplified by stream flow separation that occurs, for instance, at channel confluences, channel-width alterations, around channel-floor irregularities (potholes or gravel lag, sand bars, dunes and ripples) (Reid & Frostick, 1994). In the light of this, the above-mentioned high-energy, braided river system must have been characterized by high erosion/sedimentation rates, rapid denudation and most importantly, insignificant sorting, thereby inhibiting the operation of mineral concentration processes (Sutherland, 1985). Furthermore, according to Pettijohn et al. (1987), diagenetic processes may also account for the minor amount of heavy minerals, as interstratal solution can destroy the unstable components and increase the relative concentration of the most resistant minerals (e.g. zircon).

The Basal Unit had a significant metamorphic source component. This is indicated by the metamorphic-rock and quartz-vein fragments, undulatory and finely crystalline composite quartz grains, a lack of reworked sedimentary rock fragments and insignificant concentrations of heavy minerals. Palaeo-current indicators suggest that this highly weathered, quartz-vein rich metamorphic rock source was situated northeast of the study area.

5.5.2. Middle Unit

The following microscopic observations suggest that the sedimentary rocks of the Middle Unit are multicycle deposits: dominance of quartz grains, moderate to well-sorted, high roundness and sphericity, high proportions of monocrystalline undulatory quartz grains, well-rounded heavy mineral grains.

Because the outcrop belt of the unit is perpendicular to the fluvial transportation directions, there are minimal changes in grain size among the collected samples. The relatively small sampling area and the high durability (quartz) of the analysed grains may also have been factors.

The matrix inhomogeneity feature is interpreted as the result of heterogeneity in the grain packing and pene-contemporaneous matrix filtering processes; where the grains were closely packed, only the very-fine matrix fraction (clay) could filter through the narrow pore throats between framework grains. Soft-sedimentary deformation in the muddy, coarse-siltstone clasts indicates that the clasts were ripped up from a proximal unlithified bed. Additionally, the silty-muddy matrix, the rip-up clasts and the flaser-bedding indicate significant energy fluctuation on the part of the transporting agent.

Due to the fact that monocrystalline grains with mineral inclusions (rutile?, zircon) and fluid inclusions tend to be eliminated through recycling and weathering, their presence in the unit indicates proximal derivation, presumably from quartz veins and/or plutonic igneous rocks (granite, pegmatite). Likewise, the large (>1 mm) monocrystalline quartz grains are likely to have originated from quartz veins, massive plutonic rocks or pre-existing sedimentary rocks. Because this unit contains quartz grains with the most pronounced roundness in the whole sequence, it is likely that most of the quartz grains were recycled, although the high proportions of undulatory grains may indicate the presence of igneous plutonic rocks in the catchment area.

The finely-crystalline composite quartz grains, with their irregular crystal shapes and high crystal number, indicate a metamorphic provenance, but the low proportion of feldspars, micas and the

absence of metamorphic rock fragments reveal the dominance of a (composite?) quartz-rich source area (e.g. the underlying Basal Unit).

Despite the fact that the well-rounded zircon grains may imply long transportation distances, their coarse (0.25-0.5 mm) grain sizes, relatively high concentrations and accompaniment by coarser (0.5-2 mm), highly rounded monocrystalline quartz grains, indicate that the zircons were reworked from a proximal, alluvial source via highly abrasive processes. In addition to this sedimentary source, subangular polycrystalline quartz and less-stable hornblende grains point to a multiple source area containing metamorphic and igneous rocks as well. Brown tourmaline in the rocks also indicates a metamorphic source (Pettijohn et al., 1987), but its coarse (0.25-0.5 mm) grain size, and highly spherical and rounded shapes, again indicate rather abrasive transportation processes.

5.5.3. Upper Unit

The following microscopic observations suggest that the sedimentary rocks of the Upper Unit are multicycle deposits: dominance of quartz grains, fine grain sizes, good sorting, high roundness and sphericity (especially of the coarser grains), mature texture, high proportions of monocrystalline and undulatory quartz grains, and the virtual absence of polycrystalline quartz.

The lack of grain size changes among the collected samples may be explained as the result of the outcrop belt of the Upper Unit lying perpendicular to the fluvial transportation directions, but the relatively small sampling area and the high durability (quartz) of the analysed grains may also be factors. High proportions of undulatory, monocrystalline, finer-grained quartz are interpreted as derived from disintegrated, finely-crystalline composite quartz, perhaps reworked from the underlying Karoo Supergroup units. The virtual lack of polycrystalline quartz grains supports the idea of secondary provenance.

The relatively high feldspar content of the Upper Unit compared to the other Karoo Supergroup units may suggest not only different source rock areas (see palaeo-currents), but also a more arid climate in which chemical weathering was probably more restricted.

The presence of carbonate glaebules and fragments of silty mudstone, siltstone and very fine sandstone in the litharenites may suggest less vigorous abrasion which has inhibited clast destruction. However large (>4 mm), rounded, elongated quartz particles in the same litharenites imply strong currents. The relatively local provenance of these litharenites is indicated, firstly, by the intraformational carbonate glaebules and terrigenous rock particles, and secondly, by those quartz particles that resemble the fabric of the underlying Middle Unit. Therefore the apparent contradiction described above may be explained by strong but short-lived transportation processes within the depositional environment. The fragmented bone fossils and the silcrete chips also suggest local, relatively high-energy reworking processes. As the silcrete fragment-bearing sample (MAC1) was taken below the prominent silcrete horizon that basinwide marks the cessation of the Upper Unit deposition, this sample may imply that minor(?) silcretization occurred prior to the formation of the prominent silcrete bed.

The presence of heavy minerals in practically all Upper Unit samples is primarily a consequence of the unroofing and denudation of a different, northwesterly situated source area which did not contribute to the underlying units. Secondly, the fluvial regime responsible for the accumulation of the Upper Unit could also explain the high frequency and low concentrations of heavy minerals. According to Sutherland (1985), as a result of the short-lived nature and high sediment load of ephemeral semi-arid rivers, heavy mineral concentrations are low in these types of fluvial systems, which tend to liberate, transport and spread heavy minerals rather then concentrate them in placers. The rounded shape of the heavy minerals and the predominance of the ultrastable types (zircon, tourmaline, opaque minerals) indicate their reworked origin from pre-existing sedimentary deposits. However, the presence of hornblende grains implies acid igneous or metamorphic source rocks as well.

5.5.4. Clarens Formation

The following microscopic observations suggest that the sedimentary rocks of the Clarens Formation are multicycle deposits: dominance of quartz grains, fine grain sizes, good sorting, high roundness

and sphericity (especially of the coarser grains), mature texture, high proportions of monocrystalline and undulatory grains, and a lack of polycrystalline quartz. The absence of silt- and clay-sized particles is explained by wind winnowing in an arid area environment, which effectively separates clay-size dust/mica from the coarser grains and also selectively removes the fine-sand fraction (0.125-0.25 mm), leaving behind a bimodal grain size population consisting of very fine (0.062-0.125 mm) and coarse (>0.25 mm) grains (Pettijohn et al., 1987). An aeolian origin is also supported by the following: the larger grains are well rounded whereas the finer are subrounded-rounded, the individual laminae are well sorted, there are sharp grain size differences between the adjacent laminae, some of laminae are inversely graded, and there is no mica (Glennie, 1987).

The high proportions of the undulatory, monocrystalline, finer-grained quartz are interpreted as evidence of disintegrated finely crystalline composite quartz reworked from the underlying Karoo Supergroup units. The lack of polycrystalline quartz grains supports the idea of secondary provenance.

The general occurrence of feldspar compared to the other pre-Upper Unit Karoo Supergroup formations may suggest both different source rock areas (see palaeo-currents) and a more arid climate in which chemical weathering was probably more restricted.

The silcrete chips and the presence of subangular-subrounded grains also suggest local, high-energy transportation processes. In fact, it is possible that the sample population includes some ephemeral fluvial deposits, even though at the sampling sites there were no particular sedimentary features indicating fluvial activity.

According to Pettijohn et al. (1987), desert sandstones usually exhibit the most restricted heavy mineral suite of any sands due to the fact that aeolian currents are not competent enough to concentrate heavy minerals (Sutherland,1985). Rare aeolian placers would therefore suggest nearby primary or secondary sources. The presence of rounded, ultrastable (zircon, tourmaline, opaque minerals) heavy minerals implies that they were probably reworked from older sedimentary rocks. There are a few hornblende grains indicating metamorphic and/or acid igneous source rock as well.

5.6. Origin of the colouration of the continental beds

The progressive shift in the colouration of the Karoo Supergroup units from grey, white and green to red and purple and then to light orange and yellow presumably reflects the gradual climatic change from high-latitude glacial through cool, humid to warm, semi-arid and, finally low-latitude, hot conditions.

The predominance of grey, white and green colours in the Basal Unit is believed to represent the highly reducing conditions that prevailed during and perhaps after the deposition of the succession. These conditions are demonstrated by the abundance of coal seams and the occurrence of copper-sulphides. The scarce red colouration features in the Basal Unit sandstones that are associated with faults and cracks are perhaps related to thermal spring activity that is common in the Limpopo Belt (Chidley, 1985). These waters not only affected the Basal Unit, but also the underlying Archaean gneisses.

The colour differences between the mainly red sandstones and the partially red, mainly green-grey, fine-grained strata of the Upper Unit can be explained in the following manner. In the overall oxidizing conditions of the semi-arid environment, the ground waters were probably oxidizing too. The reddening was caused by precipitation of the iron-oxides/hydroxides from ground waters during diagenesis. The more permeable, organic-poor sandstones and conglomerates were easily infiltrated by these iron oxide-rich groundwaters, whereas the less-permeable, organic-rich parts of the overbank deposits were less affected by these diagenetic changes. Therefore, green mottles are more likely to represent locally reducing circumstances. In the same way, the ~10% of reduced (whitish-greenish) sandstones reported from the borehole cores could represent locally reductive spots caused, for instance, by the decaying organic matter from riparian vegetation. On the other hand, assuming that the overbank fines were not impermeable to groundwater migration, these fine sedimentary rocks not only must have resisted the oxidation, but must even have played a crucial role in the reduction of colloidal ferric iron brought by the ground waters because of their carbonaceous content. The existence of reducing ground waters is not favoured, mostly because of the hot, arid climate and the fact that meteoric ground waters are usually unable to reduce ferric iron oxides (Salem et al., 1998).

In the Upper Unit, the various oxidizing conditions must have prevailed shortly after deposition because there are some intraformational conglomerates consisting of both white and greenish-grey carbonate glaebules and bioturbated, red sandstone pebbles (*Photo 80*). These clasts were surely lithified and coloured prior to deposition of the conglomerates, because clast colours are thought not to be modified subsequently (Miall, 1996). In the Middle Unit, the hematitic "cement-supported" fabrics as well as the rare Fe-oxide coatings, which are present at the points of contact of adjacent quartz grains and which pre-date authigenic overgrowth, indicate that the oxidizing conditions occurred prior to any significant compaction. As the hematite coating of the authigenic overgrowths implies, the chemical precipitation of the hematite films may have continued (returned?) for a long period after burial. In those Clarens Formation samples that were collected from near to Karoo dolerite dykes, the Fe-oxide coating pre-dates the authigenic overgrowth of the quartz grains. Therefore, the reddening occurred prior to the emplacement of these volcanic intrusions. Perhaps some of the red sand grains of the Clarens Formation inherited their colour from reworking of the underlying red Upper Unit.

Although negative evidence is generally not, by itself, compelling, the lack of rock-forming ferromagnesian silicate minerals and their weathering products (e.g. clay minerals) within the arenite samples supports the interpretation of reddening as the result of processes other than the *in situ* alteration of iron-bearing minerals.

5.7. Origin of the calcrete

5.7.1. Macroscopic evidence

The spacial distribution pattern of *in situ* carbonate glaebules is an indication of their pedogenic origin because the coarser-grained (channel fill) sequences are essentially glaebule free, whereas the finer-grained deposits (of the flood plain area) are dominated by carbonate glaebules. Their stratigraphic distribution pattern, e.g. occurrence toward the top of the thickly bedded unit, but not along or across the bedding planes, and the gradational lower and sharp upper boundaries of the calcretes profiles,
argue against a phreatic (groundwater) origin for the carbonate glaebules (Khadkikar et al., 1998). Additional evidence of pedogenic origin are the thickness of the calcrete horizons (never more than 2-2.5 m) and the accretionary growth rings on the lower surface of some of the concretions, indicating downward percolating vadose waters (Spotl & Wright, 1992).

Despite the fact that carbonate glaebules also may develop during deep burial or recent exposure (Spotl & Wright,1992), in this case those possibilities are ruled out by the presence of glaebule bearing intraformational conglomerates within the Upper Unit. These conglomerates, consisting mainly of nodules, concretions and septaria, indicate that the *in situ* carbonate glaebules of the fine-grained (overbank) deposits were formed in near-surface settings shortly after the deposition of the host sediments.

Although discrete palaeosol profiles have not been positively identified in the study area, the following features might indicate the former presence of advanced palaeosol development (stages 2&4 *sensu* Retallack, 1991). The evidence of former moderately-developed calcic soils in stage 2 development (*in sensu* Retallack,1991) is seen in those horizons which consist of discrete, isolated septaria and concretions (*Photo 96 A & B*) identical to carbonate glaebules described from well-drained aridosols. Fissuring of the original muddy substratum into recognizable peds, the presence of argillans and the paucity of relict bedding structures (because of the destruction of original structures by pedoturbation) provide additional evidence for soils in stage 2 development.

Advanced paleosol development (in stage 4 *sensu* Retallack, 1991) is indicated by the following features: football-sized, coalesced carbonate glaebules; solid, pseudo-folded carbonate layers; meshwork of mainly horizontal and vertical lamellar carbonate veining.

Other pedogenic features, such as desiccation cracks, slickenslided slip surfaces, calcretized rectilinear shrinkage cracks, meniscate burrows, clay-filled voids, anastomosing and branching clay films, etc. were not observed in the outcrops. This may only be an apparent absence, due to the restricted number of outcrops or simply because the features have not been recognized. A third - and most likely - explanation for the lack of these features is that these upper, vulnerable soil horizons were eroded during major flood events. In fact, intraformational conglomerates with reworked nodules, concretions, septaria and bioturbated sandstone clasts indicate that erosion was able to remove even the A and part or all of the calcic B horizon of the calcareous paleosols, together with some already lithified sandstones.

Although neither hydromorphic (capillary-fringe) nor groundwater processes can be confidently excluded as potential calcrete producers, both mechanisms would imply a rather fluctuating, near-surface groundwater table, which is in conflict with widely accepted southern African Triassic/Jurassic palaeo-climatological reconstructions, which traditionally picture a hot, arid climate. Despite the fact that fluctuating, reducing groundwaters might have promoted the grey-red colour mottling of the host rock, a more logical explanation of the phenomenon could be achieved by postulating the sometime existence of surface water gleys where pluvial water was ponded above impermeable inhomogeneities within more permeable host rock (i.e. perched water bodies)(Pimentel et al., 1996). Thus, due to locally reducing conditions, the green mottles and the green fine-grained sediments may indicate burial processes in presence of organic matter (Slate et al., 1996). In contrast with the general view (e.g. Summerfield, 1983) that an abundant production of humic acids is associated with the decomposition of buried organic matter, Klappa (1983) states that during organic matter decay, pH-increasing substances might be released too, which in turn would enhance the precipitation of calcium carbonates in the form of calcretes. Therefore, in the present case, the origin of the green colouration is believed to be triggered by the discharge of alkaline substances in a locally reducing environment.

In conclusion, it is proposed that the calcretes found in the Upper Unit formed through pedogenic processes predominantly in the overbank area of a semi-arid ephemeral stream system. In this case, the carbonate entered the system mostly via laterally migrating surface sheet floods supersaturated with respect to Ca^{++}. These surface waters provided Ca^{++} for calcrete formation both by infiltration into the substratum (e.g. accretionary growth rings of some glaebules) and surface evaporation (e.g. laminar structures). Another probable carbonate source is calcareous aeolian dust that might have originated from the neighboring desert areas, most probably (palaeo-) north of the study area. The summary of the macroscopic evidence is presented in Table 18.

5.7.2. Microscopic evidence

The crystal "mottling" of the micritic nodules is interpreted as rhizoliths resulting from calcification of root hairs. The radial and circumgranular sparite and microsparite cracks of the septaria and concretions are thought to represent alternating shrinkage and expansion processes in soils and are typical of calcretes with alpha-fabric (Theriault & Desrochers, 1993; Wright & Tucker, 1991). In addition to these features, the nodules with floating sediment grains and "clean" micritic textures indicate that the reworked glaebules originate from calcretes with predominantly alpha-fabric (Wright & Tucker, 1991). Thus the observed micromorphological features imply that the calcretes are pedogenic, and that they developed under an arid climate with relatively low biological activity.

Table 18. Comparative list of macroscopic features observed in the calcretes.

OBSERVED MACROSCOPIC FEATURES	PHREATIC CRITERIA	PEDOGENIC CRITERIA
Subhorizontal, horizontal orientation of the elongated glaebules (predominant)	✔✔	✔
Vertically elongated glaebules (rare)		✔
Septaria	✔	✔✔
Abundance of the concretions	✔✔	✔
Presence of the glaebules in the intraformational conglomerates as intraclasts (predominant)	✔	✔✔
Association of glaebules with more stable surfaces of the overbank area (predominant)	✔	✔✔
Presence of the glaebules in the channel deposits (very rare)	✔	
Pendant rings on lower glaebule surfaces (rare)		✔
Discontinuous nature of the glaebules	✔✔	✔
Continuous nature of the glaebules	✔	✔✔
Anomalously large glaebule sizes	✔✔	✔
Small size of the concretions		✔
Meshwork of mainly horizontal and vertical white calcite veins (rare)		✔
Solid, pseudo-folded carbonate layers (rare)		✔
Authigenic silicification	✔✔	✔✔
Thickness not more than 2 m		✔
Gradational basal & sharp upper contacts within the substratum		✔
Colour mottling of the substratum, reducing colours	✔	✔
Traces of relict bedding in the substratum		✔
Crumbling, cracked original muddy substratum (soil peds?)		✔
Total number of ✔	15	22

5.8. Origin of the silcrete

5.8.1. Macroscopic evidence

The stratigraphic position of the silcrete at the transition between semi-arid fluvial deposits and arid desert sandstones, demonstrates beyond doubt that the process leading to silcrete formation occurred in a rather hot environment. This conclusion may be contradicted only by introducing the idea of a considerable time gap between the silcretization and the deposition of the overlying sediments, when a relatively short-term climate change could have taken place from predominantly arid climate to a humid one and back to arid.

On the other hand, the rip-up silcrete chips found randomly scattered throughout the lowermost part of the Clarens Formation, indicate that the silcrete had formed and there was a considerable erosive agent that was able to break up fragments from the hard silcrete horizon. The occurrence of water-lain deposits at the base of the Clarens Formation points to fluvial activity. Obviously, during such fluvial erosion any less resistant formation overlying the silcrete would have been eroded away. The former existence of such strata cannot be excluded with total confidence, though there are no records confirming their existence. Ergo, the final conclusion is that at the time of the Upper Unit/Clarens Formation transition, the climate had become increasingly arid without any major climatic shifts towards a wetter climate.

In addition, the presence of the silcrete horizon exclusively at the top of the Upper Unit indicates that in the final stage of the deposition of the Upper Unit, the land surface reached relative stability and the erosional and depositional rates decreased, thus creating an ideal environment for silcretization. In this way, the silcrete horizon represents a palaeo-landscape surface. These reduced erosion/deposition rates are related to the increasing aridity of the area.

Despite the fact that the silcrete occurs in a more or less continuous horizon, the capillary fringe origin of the silica may have some local importance, being significant only in groundwater discharge areas because the general ground water table could neither be in a near-surface position nor could it fluctuate under increasingly arid climate conditions. Therefore, the more likely explanation of the sheet-like, laterally extensive silcrete, especially in the light of the fact that the silcrete horizon invariably overlies the fine-grained (floodplain) deposits without any noticeable

relief amplitude, is that it was formed in the flat-lying floodplain area, in close proximity to the mature land surface. The lack of deeply weathered strata and the other semi-arid climate indicators point to the fact that the investigated silcrete was formed under similar conditions to those near-surface non-weathering profile silcretes that are found in the Kalahari Basin in southern Africa (Summerfield, 1983).

The fact that the silcrete occurs exclusively in areas subject to fluvial inundation indicates that the silica might have been transported by sheet floods supersaturated with respect to quartz. The precipitation of the silica from these chemically charged surface waters occurred as a "result of either infiltration into underlying material or evaporation at the surface" (Goudie, 1973:122). It may be assumed that after dry periods, the salt concentration in the ephemeral ponds of the overbank area would increase, which could act as a significant catalyst in the precipitation of the contained silica (Thiry, 1999). As indicated by the significant amount of quartz grain dissolution features seen in the calcretes, considerable volumes of silica might have been released during the calcrete formation. Additional, less significant silica sources include aeolian input and siliceous plant material.

The apparent contradiction that arises between the enhanced silica solubility triggered by temperature increase and the abundance of silcrete at the boundary between the semi-arid Upper Unit/ arid Clarens Formation might be explained in a far too simplistic manner by a pH drop that could offset the effects of temperature rise. However, as mentioned previously, the very complex relationship among the controls of silica/calcite solubility does not allow for oversimplified explanations of the silcrete forming conditions.

The pipes and other open tubules may represent some type of bioturbation, perhaps of plant origin. Whereas the small tubes appear to resemble silicified grass (?) hair rootlets, the larger might be taken as the fossilized roots of larger plants (Gustavson & Holliday, 1999). All these features suggest near surface, perhaps pedogenic conditions. This is in accordance with the other observed pedogenic features (soil peds, clay coated argillans, abundance of massive, colour mottled rocks), all indicating near-surface, soil-forming processes.

Macroscopic evidence for the silicification of former calcretes is scarce; the only essential proof seems to be the botryoidal fabric of the silcretes, where the glaebules are likely to be pseudomorphs after calcareous glaebules (Wopfner, 1978). Additionally, the fact that gradational silcretes develop mainly from calcretes may indicate that the silcretization post-dates the calcrete formation, the silcrete being the last depositional unit of the Upper Unit. Therefore, the minimum age of the silicification is pre-Clarens (see detrital silcrete chips), while the maximum age is late-Upper Unit.

5.8.2. Microscopic evidence

Despite the fact that geopetal or other illuviation structures are absent, the following micromorphological features indicate that the silcretes were formed as non-weathering profile silcretes (Group III of Wopfner, 1983) in a near-surface setting:

- ❒relative dominance of length-fast chalcedony in most of the vug-fills;
- ❒presence of complex void-fills of chalcedony, microquartz and megaquartz;
- ❒matrix being a mixture of a whole range of silica (from cryptocrystalline silica to length-fast chalcedony, microquartz);
- ❒lack of authigenic glaebules and colloform features;
- ❒abundance of F-(floating) fabric and limited occurrence of GS-(grain supported) fabric (Summerfield, 1983);
- ❒presence of length-slow chalcedony void-fills which are believed to occur as replacements after either evaporites (Folk & Pittman, 1971; Thirty & Milnes, 1991) or calcretes (Summerfield, 1983);
- ❒Fe-oxide banded crytocrystalline silica and chalcedony (Watts, 1978);
- ❒vertically and subhorizontally oriented tubules;
- ❒partially filled voids resembling hair-rootlets.

According to Thirty & Milnes (1991), a host material that contains abundant clay and/or other high levels of impurities in the intergranular area promotes the precipitation of less crystallized silica phases. Therefore the lack of optically continuous quartz overgrowths and, on the other hand, the dominance of cryptocrystalline silica, length-fast chalcedony and microquartz, imply that precipitation took place from highly concentrated silica solutions around numerous nuclei with low growth rate in the investigated samples. The exclusive association of the silcrete with

the finer-grained, clay-rich overbank deposits of the Upper Unit, explains the predominance of poorly crystallized silica phases of the matrix of the investigated silcretes. In addition, the overwhelming presence of length-fast chalcedony in the matrix in contrast with length-slow chalcedony (which occurs only as void-filling) reflects the high carbonate and low sulfate concentration in the host rock (Thirty & Milnes, 1991).

The comparison between the silcrete and calcrete samples shows that the rate of detrital-grain corrosion is similar. This and the relative dominance of the length-fast chalcedony which is indicative of calcrete replacement (Thirty & Milnes, 1991) may suggest that the silcrete was formed through silicification of calcrete. This idea is supported by the specimens showing a gradational matrix-composition change from calcite to a mixture of a whole range of poorly crystallized silica phases. Therefore the corroded primary quartz grains of the silcretes are interpreted here as inherited features from the pre-existent calcretes.

The systematic succession from poorly crystallized silica phases to well-developed quartz is interpreted as indicative of silica solutions that - with time - became progressively depleted with respect to dissolved silica (Thirty & Milnes, 1991). This could indicate decreased evaporation and/or increased dilution of the silica-bearing solutions and/or elimination of the silica source from the system. Decreased evaporation and intensified silica dilution by fresh surface waters are rather unlikely as the silcrete is uniformly overlain by aeolian dune deposits, indicating progressive aridification. At the same time, the increased aridity and the subsequent change in depositional environment from fluvial to aeolian may readily explain the cessation of silica supplied from sheet flooding.

6. The Tuli Basin as part of Southern Gondwana

The palaeo-environmental reconstruction of the Karoo Supergroup in the Tuli Basin shows that the entire deposition took place in a continental setting. There is a clear transition from non-glacial, cold climate to semi-arid then to arid environments, and this is in accordance with the palaeo-climatological investigations in other Karoo Supergroup depositories across the southern African region (Smith at al., 1993; Johnson et al., 1996). The climatic change is attributed to Africa's latitudinal drift from cold/glacial to desert climatic belts during Late Carboniferous - Middle Jurassic (Raath, 1972; Catuneanu et al., 1998). Moreover, according to Scotese et al. (1999), the dry subtropical climate belt was expanded poleward during the 'Hot House' conditions of Late Permian-Jurassic times. This implies that the climate change from cool temperate/polar to warm temperate/dry-subtropical occurred not only as a result of the latitudinal continent drift, but also due to global warming at that time.

6.1. Stratigraphic correlations to the main Karoo Basin

The Tuli Basin contains a thinner (estimated max. ~450-500 m) and less continuous sequence than that in the main Karoo Basin. These differences present difficulties when attempting to correlate the Karoo Supergroup beds of the these two basins. In this work, correlations are based mainly on lithological grounds due to lack of bio- and chronostratigraphical controls.

6.1.1. Basal Unit

The coal-bearing fluvio-lacustrine deposits of the Basal Unit are very similar to the deposits of the fluvial interval in the Vryheid Formation of the main Karoo Basin. High energy, braided channel deposits characterized by cross-bedded, coarse sandstones, and peat-swamp, overbank deposits are typical for both stratigraphic units (Johnson et al., 1997).

Kocsács-Endrődy (1983, in Chidley, 1985) identified the leaf impressions of the Basal Unit (Lizzulea) with the *Glossopteris* flora of the Vryheid Formation from the main Karoo Basin. According to Ortlepp (1986), the coal zone in the Basal Unit correlates with the base of the Vryheid Formation (Late Early Permian).

The matrix-supported breccias in the lowermost part of the Basal Unit lack indubitable evidence for glacial activity (e.g. striated pavements or clasts, varvites, etc.), therefore the presence of unequivocal Dwyka Group correlatives in the Tuli Basin remains uncertain.

6.1.2. Middle Unit

A period of considerable uplift and erosion is marked by the regional unconformity at the conglomeratic base of the Middle Unit and its lithological equivalents in the north-eastern part of the southern African region (i.e. at the base of the Escarpment Grit and Angwa Sandstone Formation in Zimbabwe: Raath, 1972; Stagman, 1978; Oesterlen, 1991). The intensity of this erosional period in the study area is demonstrated by the fact that the succeeding Middle Unit beds rest directly upon the pre-Karoo Archaean basement, suggesting that the older Karoo beds were removed (see Ch. 4.2.2.). Similar situations have been reported from other northeastern Karoo Supergroup depositories (e.g. Zimbabwe - Visser, 1984).

The Middle Unit contains one upward-fining cyclothem commencing with medium- to well-sorted, subrounded-subangular, exclusively quartz-pebble conglomerate. The succeeding white to pink medium sandstones fine up into mudstones and siltstones which are grey to brownish grey, yellow with reddish blotches scattered throughout. Purplish-grey colours become more dominant towards the top. These non-fossiliferous lithologies were formed in a braided river system with inter-channel floodplains.

The lack of bio- and chronostratigraphic control hampers precise correlation and enables only the lithocorrelation of the Middle Unit with the formations of the main Karoo Basin. There are several upward-fining cyclothems of former braided river systems both in the Beaufort Group and in the Molteno Formation of the main Karoo Basin, so precise correlations are uncertain.

Tables 19 and 20 present the lithological comparisons of the Middle Unit to the braided river deposits of the lower (e.g. Koonap Formation) and upper (e.g. Katberg Formation) beds of the Beaufort Group. The palaeontological differences between the lower and upper beds of the Beaufort Group (i.e. *Glossopteris sp., Schizoneura sp., Equisetum sp.* plant, fish and therapsid reptile remains of the lower Beaufort, and *Dicroidium sp., Schizoneura sp., Dadoxylon sp.* plant,

fish, amphibia and therapsid reptile remains of the upper Beaufort) were non-beneficial for the correlation to the non-fossiliferous Middle Unit. In the other northeastern Karoo depositories, strata equivalent to the Beaufort Group are either not present (Tshipise, Nuatetsi Basins and northern Lebombo 'Monocline')(Visser, 1984; MacRae, 1988) or are found in the form of condensed, non-fossiliferous successions (Save, Springbok Flats and Ellisras Basins)(Stagman, 1978; MacRae, 1988; Faure et al., 1996).

Table 19 Lithological comparison between the Middle Unit (Tuli Basin) and lower Beaufort strata (main Karoo Basin). Data were derived from Johnson et al., 1997 and Rubidge et al., 2000.

Lithological comparison between the Middle Unit (Tuli Basin) and lower Beaufort (main Karoo Basin):
1. Erosively-based channel lags of upward-fining cyclothems consist of pebble- to cobble sized clasts of intraformational clay pebbles, carbonate nodules and fossilized bone fragments in the lower Beaufort. The upward-fining cyclothem in the Middle Unit commences with medium to well-sorted, subrounded-subangular, predominantly quartz pebble conglomerate. Intraformational mud clasts were observed in only one sample.
2. Point-bar sequences characterized by lateral accretion surfaces common in the lower Beaufort, absent in the Middle Unit
3. The massive argillaceous mudstones are dark grey, green and no maroon rocks are present in the lower Beaufort. The mudstones and siltstones of the Middle Unit are grey to brownish grey, yellow with reddish blotches scattered throughout. Purplish-grey coloured become more dominant towards the top.
4. Evidence of subaerial exposure (e.g. raindrop impressions, wrinkle marks, mudcracks) is present in the lower Beaufort, absent in the Middle Unit.
5. Calcareous nodules are present in the lower Beaufort, absent in the Middle Unit.

Table 20 Lithological comparisons between the Middle Unit (Tuli Basin) and upper Beaufort strata (main Karoo Basin). Data were derived from Johnson, 1976; Stavrakis, 1980 and Johnson et al., 1997.

Lithological comparison between the Middle Unit (Tuli Basin) and upper Beaufort (main Karoo Basin):
1. In some places, the erosively-based, upward-fining cyclothems commence with intraformational conglomerates of mudball and shale flake clasts in the upper Beaufort. The upward-fining cyclothem in the Middle Unit commences with medium to well-sorted, subrounded-subangular, predominantly quartz pebble conglomerate. Intraformational mud clasts were observed in only one sample.
2. The greenish grey sandstones are characterized by upper flow regime structures (horizontal bedding, streaming lineation) in the upper Beaufort. The arenaceous deposits of the Middle Unit are grey, white, pink, light purple or red. The sandstones are mainly planar cross-stratified, massive and horizontally stratified sandstones are less common.
3. Ripple cross-lamination is scanty in the upper Beaufort (e.g. Katberg F.), abundant in the Middle Unit.
4. The massive argillaceous mudstones are greyish red or greenish grey in the upper Beaufort. The mudstones and siltstones of the Middle Unit are grey to brownish grey, yellow with reddish blotches scattered throughout. Purplish-grey coloured become more dominant towards the top.
5. Sand-wedge polygons, calcareous duricrusts, mud draped surfaces and mudcracked surface are present in the upper Beaufort, absent in the Middle Unit.

There is a somewhat stronger lithological resemblance between upward-fining cyclothem of the Middle Unit (Tuli Basin) and the braided river deposits of the Indwe Member in the Molteno Formation of the main Karoo Basin. According to description of the lexicon of South African stratigraphy (Johnson, 1994:18), the Indwe Member commences with the Kolo Pebble Bed which is a "coarse pebbly unit" (Christie, 1986:2068). The lithology of this basal succession of the Indwe Member is pictured as a conglomerate or pebbly sandstone layer by the following authors: Johnson (1976:276 "relatively thin coarse-grained layer containing numerous clasts eroded from underlying material, as well as scattered quartzite pebbles and boulders"), Turner (1983:79, Fig. 3), Eriksson (1984:239 "lenses and beds of apparently massive conglomeratic sandstone"), Cairncross et al. (1995:455 "basal conglomeratic lag"), Johnson et al. (1997:301 "erosively-based pebble and cobble horizon"). According to Catuneanu (written commun.), the basal section of the Indwe Member seems to be much finer than the fine (1.5 cm) pebble-grade conglomerates of the Middle Unit in the Tuli Basin. Based on Turner's (1983:79) and Cairncross et al.'s (1995:455) descriptions, the clasts comprise mainly quarzite, vein quartz, chert and rare rock fragments and are well-rounded and spheroidal. The basal conglomerate unit fines upward to coarse- and medium-grained, cross-bedded sandstones, and then into fine sandstones, siltstones, shales and rare coal seams. The Indwe Member is reported to be basin-wide (i.e. found throughout in the present outcrop area of Molteno Formation) by Turner (1977:242; 1983:79), and this distribution pattern is accepted by Eriksson (1984:240), Cairncross et al. (1995:453) and Johnson et al. (1997:301).

In addition, there are noticeable similarities between the lithofacies associations of the Middle Unit and the Molteno Formation described from NE Swaziland (see Ch 2.2.3.). According to Turner & Minter (1985), the Molteno Formation in the Hlane area rests on an erosion surface and consists of two fining-upward cyclothems. The conglomerates contain subangular and subrounded pebbles, predominantly of quartzite and vein quartz. The middle part of these fining-upward cyclothems (Hlane), consisting of sandstones and ripple-cross laminated siltstones, clearly resembles the medial part of the Middle Unit. However, it should be pointed out that the argillaceous deposits in the Middle Unit are not carbonaceous and lack coal seams.

Although it seems to be non-fossiliferous, the Middle Unit shows a strong lithological and stratigraphical similarity to the *Dicroidium*-bearing strata both in the Tshipise Basin (Fripp and

Joan Formation - van den Berg,1980:55) and Zimbabwe (Escarpment Grit, Angwa Sandstone Formation, Ripple Marked Flagstones - Bond, 1973; Oesterlen, 1991). These *Dicroidium*-bearing Zimbabwean strata have been correlated with the Molteno Formation (Wilson, 1970; Cooper, 1982). All these stratigraphic units are underlain by an unconformity surface which is assumed to be regional in extent.

6.1.3. Upper Unit

The red, maroon and green ephemeral stream and floodplain deposits of the Upper Unit are very similar to the alternating sequences of fine- to medium-grained sandstones and argillaceous beds of the Elliot Formation in the main Karoo Basin. The following features - which are common in both stratigraphic units - highlight strong lithological similarities: predominance of upper-flow regime sedimentary structures (horizontal lamination, massive beds); trough cross-bedding; slumping; intraformational breccias/conglomerates; desiccation cracks; mud drapes; carbonate concretions; bioturbation; vertebrate foot prints; multistoried sandbodies (Botha, 1968; Visser & Botha, 1980; Kitching & Raath, 1984; Eriksson, 1985).

Numerous medium sized prosauropod dinosaurs remains have been collected throughout the Upper Unit, but these could not be identified on generic level. The other reported dinosaur fossils from the Tuli Basin appear to be of *Massospondylus*, and there is one controversial *Euskelosaurus* specimen (Ch.4.2.3.3.). Kitching & Raath (1984) proposed two biozones in the Elliot Formation in the main Karoo Basin: a lower *Euskelosaurus* Range Zone, and an upper *Massospondylus* Range Zone. Because of the uncertainties mentioned above, and in Ch.4.2.3.3., it is debatable whether the fossil fauna of the Upper Unit represents only the upper biozone or whether it belongs to both of them. Nevertheless, the presence of the prosauropod dinosaurs remains, in conjunction with the lithological similarities presented above, provide an unambiguous correspondence between the Upper Unit and the Elliot Formation.

6.1.4. Clarens Formation

The Clarens Formation, with fine- to medium-grained, very large-scale cross-bedded and massive sandstones, is doubtless correlative of the aeolian Clarens Formation in the main Karoo Basin. Both of the depositories received aeolian material from a westerly direction. Wet desert (e.g. ephemeral stream) deposits are confined to the lower Clarens Formation in the Tuli Basin. In the main Karoo Basin, similar subaqueous units are not reported from the northern outcrop area (Clarens, Harrismith) of the Formation, but are common in the southern zone (Drakensberg Gardens, Giants Castle, Bulwer) where they seem to be more abundant in the lower part of the Formation (Eriksson, 1981; 1986).

The silicified fossil wood (Ch. 4.2.4.2.) found in the Clarens Formation in the Tuli Basin seems to hold no significance for correlation, firstly, because it belongs to the stratigraphically widespread *Agathoxylon sp.* genus, and secondly, because the silicified tree trunks found in the Clarens Formation (main Karoo Basin) have not yet been identified. Although saurian bone fossils have not yet been described from the Clarens Formation in the Tuli Basin, the reported *Massospondylus* and *Syntarsus* footprints suggest a strong biostratigraphic relation between the hostrock and the Clarens Formation in the main Karoo Basin.

The proposed correlation of the units in the Tuli Basin with those in the main Karoo Basin is shown in Table 21.

Table 21 Summary of the lithostratigraphic nomenclature and tentative correlation of the Karoo Supergroup strata of the transfrontier Tuli Basin and main Karoo Basin (* See text for the two possible correlations of the Middle Unit). Thick lines represent known unconformities.

main Karoo Basin (Johnson, 1994)		Tuli Basin (South African part) (Bordy, this study)		Tuli Basin (South African part) (Chidley, 1985)		Tuli Basin (Zimbabwean part) (Thompson, 1975)	Tuli Basin (Botswanan part) (Smith, 1984)	
"Stormberg Group"	Clarens Formation	Clarens Formation		Clarens Formation	Tshipise Sandstone Member	"Forest Sandstone"	Lebung Group	Tsheung Sandstone Formation
								Thune Formation
	Elliot Formation	Upper Unit			Red Rock Member	Red Beds		Korebo Formation
				Bosbokpoort Formation				
	Molteno Formation		Middle Unit*	Klopperfontein Formation		"Escarpment Grit"		
Beaufort Group		Middle Unit*		Solitude Formation				
Ecca Group		Basal Unit (undifferentiated)		Fripp Formation				
				Basal Beds	Mikambeni Formation	Fulton's Drift Mudstones		Seswe Formation
					MadzarIndwe Formation			Mofdiahogolo Formation
Dwyka Group					diamictites	Basal Beds (undifferentiated)		??

6.2. Tectonic development of the Tuli Basin

This section outlines the various tectonic models proposed for the evolution of the Karoo basins in the southern African region, and explores their relevance to the Tuli Basin.

The formation of the Karoo Supergroup in southern Africa occurred in two contrasting tectonic regimes: an initial compressive system which was replaced by an extensive regime related to the break-up of Gondwana. With regard to this change in the tectonic regime, two main questions arise: "When did the transition occur?" and "How is the transition preserved in the sedimentary rock record of the Tuli Basin?"

According to Catuneanu et al. (1998), the compressive foreland system, which existed north of the Cape Fold Belt, developed in response to the Late Palaeozoic-Early Mesozoic subduction of the palaeo-Pacific plate below the Gondwana plate. Due to the flexural warping of the lithosphere, three distinct areas developed across the warped profile of the system: a foredeep, forebulge and back-bulge zone. The main Karoo Basin preserves sediments that accumulated in both foredeep and forebulge flexural provinces (Catuneanu et al., 1998). In the Karoo foreland system, the relatively thinner sediment pile of the back-bulge basin could be expected to be preserved in a roughly E-W trending zone, approximately 1500-1800 km north of the subduction zone/orogenic belt (Catuneanu et al., 1998: Fig. 13). The Tuli Basin may be identified with this back-bulge basin setting on the basis of its distance (~1500 km) from the northern margin of the Cape Fold Belt and its relatively thin sedimentary sequence.

The orientation of this postulated ENE-WSW striking back-bulge basin is consistent with measured and reported palaeo-current directions in the Basal Unit: palaeo-drainage was from E and NE to WSW (Fig. 109). Similar depositional environments and drainage patterns (Fig. 110) have been determined for the Dwyka and Ecca Group equivalents of the Tshipise (Van Der Berg, 1980) and Ellisras Basins (Faure et al., 1996). Within the northeastern part of the main Karoo Basin, the paraglacial outwash fans and fluvio-deltaic deposits of the lower Ecca Group were built out from a northeasterly source (Johnson et al., 1997). Therefore these strata may be identified as deposits of the southerly inclined foredeep slope which were derived form the northerly situated mountainous regions of the forebulge (Fig. 109-5A).

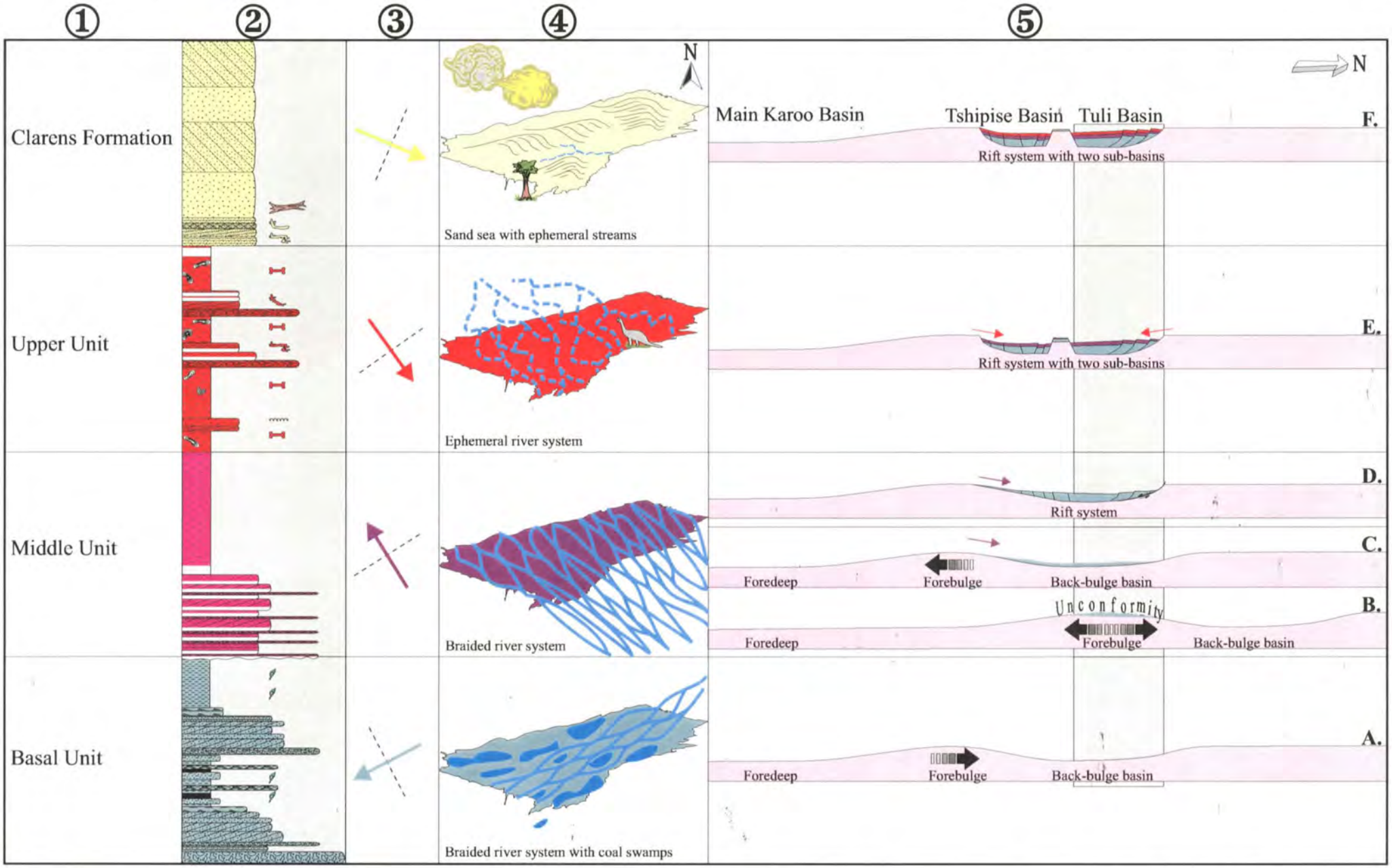

Fig. 109. Summary of the stratigraphic column (1, 2), palaeo-currents (3), environments of sedimentation (4) and tectonic setting (5) during each stage of deposition in the Tuli Basin. Dashed arrow (in 5) indicates the forebulge migration along the flexural profile of the foreland system. Not to scale.

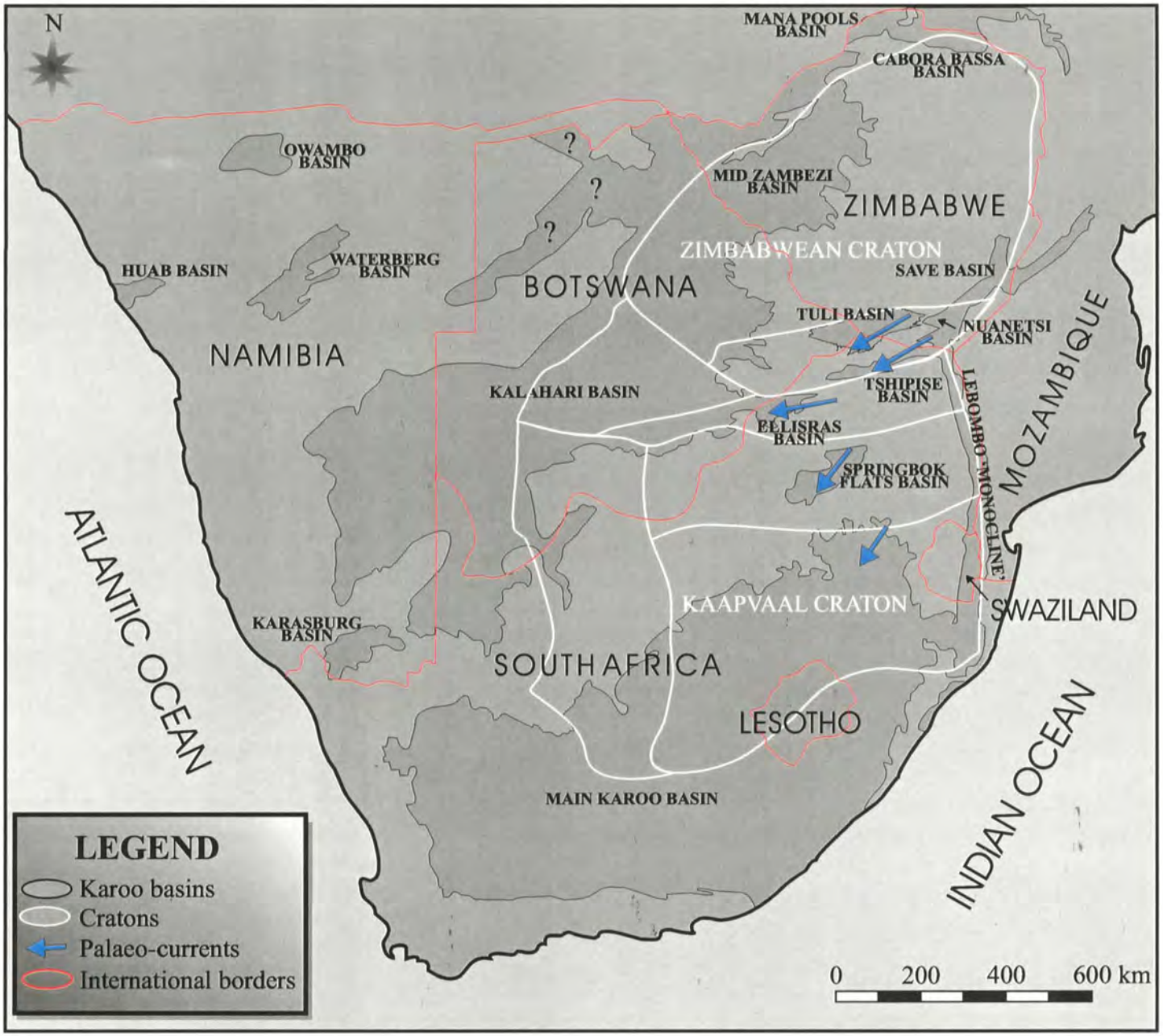

Fig. 110. Palaeo-current directions of the upper Early Permian Karoo Supergroup deposits. Data from Faure et al. (1996), Johonson et at. (1997), van der Berg (1980). Tuli Basin personal measurements.

However, despite the fact that palaeo-drainage patterns and the position of the Tuli Basin relative to the main Karoo Basin can be identified within the overall foreland basin model, it remains a challenge to correlate the sequences of the two basins as discussed in the previous section. These difficulties arise from paucity of bio- and chronostratigraphic control in the Tuli Basin, but scarcity of unconformity surfaces creates a more complicated situation. In other words, the several unconformity bounded sequences of the main Karoo Basin, which are related to tectonic deformation in the Cape Fold Belt, are extremely difficult to recognize in the Tuli Basin where only one well-documented unconformity-bounded sequence (i.e. Basal Unit) exists. Therefore, the origin of the unconformity surface between the Basal and Middle Units is an important factor in resolving the differences between the predictions of the foreland system model and the actual rock record in the Tuli Basin.

The long-wavelength subsidence, which affected the foreland system during the Late Carboniferous-Early Triassic (Pysklywec & Mitrovica , 1999), would predict the accumulation and preservation of the Dwyka-Ecca-Beaufort Group equivalents across the entire foreland system. As highlighted in Ch. 6.1., in the Tuli Basin, the unconformity bounded Basal Unit is correlated with the Dwyka?-Ecca Group (main Karoo Basin), but the relationship of the non-fossiliferous Middle Unit to the Karoo Supergoup in the main Karoo Basin has not been established. At least two possibilities exist: correlation of the Middle Unit with some formations of the Beaufort Group (main Karoo Basin) or correlation with the Molteno Formation (main Karoo Basin). Each of these potential correlations have different consequences for the tectonic evolution of the Tuli Basin.

The assumption that the Middle Unit corresponds to the Beaufort Group would imply that the Middle Unit was also formed in the back-bulge setting of the Karoo foreland system prior to the last major orogenic unloading and cessation of the subduction (see Catuneanu et al., 1998; Pysklywec & Mitrovica, 1999). The early Late Permian foreland system configuration (see Catuneanu et al., 1998: Fig. 13B) shows that the foresag region (i.e. main Karoo Basin) underwent subsidence, whereas the foreslope region and back-bulge setting experienced uplift, hence explaining the unconformity surface between the Basal and Middle Units in the back-bulge Tuli Basin (Fig. 109-5B). According to Catuneanu et al. (1998: Fig. 13C) the consequence of the

renewed orogenic loading in the Cape Fold Beld was the cratonward migration of forebulge along the flexural profile of the foreland system during the late Late Permian. This may explain the northerly dip direction of the surface profile during the deposition of the Middle Unit (Fig. 109-5C).

If the correlations between the Middle Unit and Beaufort Group (main Karoo Basin) as well as the Upper Unit and Elliot Formation (main Karoo Basin) are correct, there should be a time gap between the Middle and Upper Units of the Tuli Basin. Currently, there are no available field observations about the nature of this contact, and as described in Ch. 4.2.2 & 4.2.3., the boundary between the two units is assumed to be conformable from the borehole descriptions.

The assumption that the Middle Unit is a correlative of the Molteno Formation (main Karoo Basin) opens up the long-debated controversy on the possible causes and effects with regard to uplift in extensional tectonic regimes. Currently, there are two main explanations of the origin of uplift in such settings: the active and passive rifting models (Allen & Allen, 1990). According to the active rift model a mantle plume is emplaced under the lithosphere, and the thermal expansion above the plume generates a regional domal uplift which subsequently results in crustal extension, and associated magmatism. The amount of uplift is estimated to be about 1000 m above the plume centre and it affects an area of 1500-2000 km in diameter (White & McKenzie,1989; Cox, 1989; Hill, 1991). In the passive rifting model the regional/local tensional stress formulate the stretching and thinning of the lithosphere, and passively enable the upwelling of hot mantle material, which produces magmatic activity by decompression melting. An important consequence of the stretching is the uplift of the rift shoulders. The causes of this uplift are explained later in this chapter. The original model of sudden thinning and stretching of the crust and mantle lithosphere (McKenzie, 1978) has been subsequently modified by several authors, but the presentation of their models is beyond the scope of this thesis as these can be found in textbooks of basin analysis (e.g. Allen & Allen, 1990; Miall, 1990).

In the section that follows the implications of these models for the basin evolution of the study area are investigated. First an active model and its implications will be discussed, and later, the section will focus on the consequences of the passive model for the deposition of the Middle and Upper Units.

The assumption that the Middle Unit is Molteno Formation equivalent is based on lithological similarities and on the fact that both stratigraphic units rest on a well-defined regional unconformity surface (for Molteno Formation see Hancox, 1998; Turner, 1999). Although it is agreed that this Late Triassic erosion surface is the result of regional downcutting in response to uplift, the origin of the uplift itself is controversial (Turner & Thomson, 1998). The foreland system model (Catuneanu et al., 1998; Hancox, 1998) suggests that after the Late Ladinian orogenic loading (i.e. tectonic activities) in the Cape Fold Belt, Late Triassic orogenic unloading took place. This resulted in the erosion and reworking of older foredeep deposits and the accumulation of reworked sediment in the foresag setting (Catuneanu et al., 1998: Fig. 14H). Pysklywec & Mitrovica (1999) states that a regional uplift occurred in the Early Triassic and it was induced by the cessation of the subduction of the palaeo-Pacific plate below the Gondwana plate. Their geodynamic modelling shows that the entire Karoo foreland system was regionally uplifted shortly (~0-20 Ma) after the subduction was terminated.

The explanation of the Late Triassic uplift by exclusively late orogenic unloading processes has been challenged by Turner & Thomson (1998) and Turner (1999). In addition to foreland basin tectonics, Turner (1999) proposes that the regional uplift may be explain in term of the active rifting model related to a thermal anomaly. Additional effects of this thermal anomaly were crustal extension and minor volcanic activity prior to the outpouring of the Karoo lavas. It is proposed that minor mafic volcanic activity is documented by volcanic detritus in the Molteno, Elliot, and Clarens Formations of the main Karoo Basin - see Turner, 1999:230 & Fig. 14.

The origin of the thermal anomaly and uplift is ascribed to the emplacement of a mantle plume such as the so-called Karoo Plume (Burke & Dewey, 1973; White & McKenzie, 1989; Cox, 1989). Originally, Burke & Dewey (1973) located this Karoo Plume under the Nuanetsi Basin, whereas White & McKenzie (1989) and Cox (1989) placed it ~450 km ENE of Maputo (Mozambique). According to Turner (1999:234), the uplift by the plume is supported by "the presence of northeast-southwest trending block faults and small-scale folding in the Clarens and Elliot Formations, eroded and truncated by lavas"; and "radial drainage patterns outlining a domal topography imposed by pre-basalt eruptive updoming of the crust (Cox, 1989)". Turner (1999: Fig. 15), who places the Karoo Plume in the present Maputo area, indicates that the zone

of crustal uplift and extension stretched in a northeastern-southwestern direction, parallel to the present southeast coast of South Africa. Based on petrographic evidence and palaeo-current analysis in the main Karoo Basin, it seems that the following five fluvial transport directions were responsible for the denudation during Molteno-times: southerly, south-southeasterly, southeasterly, east-southeasterly and east-northeasterly (Eriksson, 1984; Turner 1977, 1983, 1984, 1999; Cairncross et al., 1995). Turner (1999) suggests that the dominant directions were from SE and ESE (Turner, 1999: Fig. 15). He explains this palaeo-current trend by the thermally-elevated 'Eastern Highland Provenance' which was situated in the SE. In this regard it is noteworthy that the mean vector in Turner (1977:247) and Turner (1983: Fig. 3) indicates that the main transport direction was from south-southeast to north-northwest and not the SE and ESE directions preferred by Turner (1999). In addition Cairncross et al. (1995:468-9) reported denudation only from the south.

Accepting that the Karoo plume (i.e. thermal anomaly) existed, a number of problems remain in connection with the model proposed by Turner (1999). Firstly, the geochemical similarities between the volcanic detritus in the Upper Karoo deposits and the overlying 183±1 Ma old Karoo basalts, which suggested to Turner (1999:235) a genetic link between the early volcanism and Gondwana rifting, are debatable. For instance, the mafic chemistry of the volcanic detritus is clearly contradicted in the reference given by Turner himself (1999: Fig. 14) because the mineralogical composition of the tonsteins from the Molteno Formation revealed a "rhyolitic composition of the pyroclastic material" from which the tonsteins were derived (Heinemann & Buhmann, 1987:296). Similarly, the bentonite layer and the "violent gaseous explosions" mentioned by Botha & Theron (1967:473) in the Elliot Formation indeed suggest silicic volcanic activity, as bentonite and explosively ejected widespread pyroclastic rocks are not typical of mafic volcanism (Lajoie & Stix, 1992). In the same way, laumontite often occurs in association with silicic igneous rocks, therefore it is not an exclusive indicator of mafic volcanism (Kubovics, 1993). In addition, the agglomerates mentioned from the Clarens Formation (Botha & Theron, 1967) firstly do not contain any volcanic rock fragments, and secondly, their stratigraphic relation to the Clarens Formation is unclear: there is no field evidence to indicate that these agglomerates were formed contemporaneously or after the deposition of the Clarens Formation. To summarize the chemistry of the volcanic detritus in the Upper Karoo deposits is

rather indicative of silicic volcanism than mafic. On the other hand, the evidence of Upper Karoo silicic volcanism evokes the question: "Where did this silicic volcanism take place?" As previously mentioned, Pysklywec & Mitrovica (1999) propose that subduction ceased in pre-Upper Karoo times, therefore, if assuming that volcanism ceases with cessation of subduction then it is very difficult to imagine that the source of these silicic volcanic materials is the same magmatic arc to south (Johnson et al., 1997: Fig. 32; Pysklywec & Mitrovica, 1999: Fig. 2a, b & c) that supplied silicic volcanic detritus into the Dwyka, Ecca and Beaufort Groups in the main Karoo Basin. However, there is clear evidence of magmatic arc activity in the rock record of the Antarctic Peninsula and southern South America during Late Triassic and Early Jurassic (Storey et al., 1992; Storey et al., 1996), thus it is possible that the source of the Upper Karoo silicic volcanism was palaeo-southeast and palaeo-southwest of the main Karoo Basin.

The second major problem with Turner's (1999) model emerges from the controversies about the importance of the Karoo and other plumes in the continental break-up of Gondwana, and timing of the plume-related uplift, crustal extension and outpouring of large volumes of basaltic lavas.

Although the presence of a mantle plume beneath the Karoo province and its contribution to the break-up are, in general, accepted (White & McKenzie, 1989; Hill, 1991; Cox, 1992; Storey et al. 1992; Smith, 1999), other researchers, for example Hawkesworth et al. (1999:257) doubt the significant role of mantle plumes in the initiation of the widespread, ~180 Ma continental flood basalts, and favour a model explaining the volcanic activity by "partial melting within the lithosphere in response to thermal incubation over 300 Ma".

Turner's (1999:235) model suggests that the plume-generated uplift predates the magmatic activity by some 40 Ma. The validity of his model therefore depends on whether this relationship is a feature of plume activity. This is examined below.

White & McKenzie (1989:7718) suggest that the sudden onset of the Karoo magmatic events indicates that the "plume had only then impinged on the base of the lithosphere" implying that magmatism is contemporaneous with the uplift. They also suspect that there was a long phase of rifting prior to the plume emplacement and the coeval, lava extrusion. This early rifting was not

accompanied by significant volcanism (White & McKenzie, 1989:7721). The fact that the plume-generated uplift is contemporaneous or postdates the volcanic activity is suggested by the conglomerates overlying the Karoo volcanic rocks (Martin & Hartnady, 1986 in White & McKenzie, 1989:7721).

The general plume model of Hill (1991) suggests that significant uplift above the plume head may begin significantly before the initiation of volcanism. His estimation (p. 400) of the time interval between the uplift and magmatism is 10-20 Ma, whereas Campbell & Griffiths (1990 in Hill, 1991:400) suggest that the interval is 20-40 Ma. It appears that the interval between the uplift and magmatism seems to be strongly dependent on ascending velocities of the plume, and the latter is influenced by the initial temperatures within the penetrated material.

To summarize, in the case of the proposed Karoo plume, there is considerable uncertainty in the timing of uplift versus magmatism but most estimates seem to be significantly shorter than the 40 Ma years required by Turner's model (1999:235).

If the speculations that the plume-induced regional uplift occurred shortly before Molteno-times is correct, these would have the following implications for the Tuli Basin. Considering Cox's (1989) remark that such updomed areas supply large volumes of clastic sediment in a radial drainage pattern, it might be speculated that during Middle Unit-times, the Tuli Basin was situated on the northwestern flank of the regional domal topography that was caused by the thermal anomaly discussed in Turner (1999). This could explain the northwesterly dip of the regional palaeo-slope in the Middle Unit (Fig. 109). The palaeo-flow indicators in the Fripp Formation of the Tshipise Basin also suggest denudation from a south-easterly source, therefore this area is also identified as a depository on the north-westerly dipping slope of the regional domal topography (Fig. 111).

In contrast to the predicted radial drainage pattern, the Molteno-strata of the southern Lebombo 'Monocline' (Fig. 111) were deposited on the south-southeasterly dipping slope, as determined by SE foreset inclination of the cross-bedded Molteno Formation (Turner & Minter, 1985). One way this could be reconciled with Turner's (1999) plume model is to suggest that the Molteno Formation in this region developed in small-scale rift basins which trended NNE-SSW parallel to the rifted 'crest' of the thermally-uplifted area. An additional explanation may be given by the

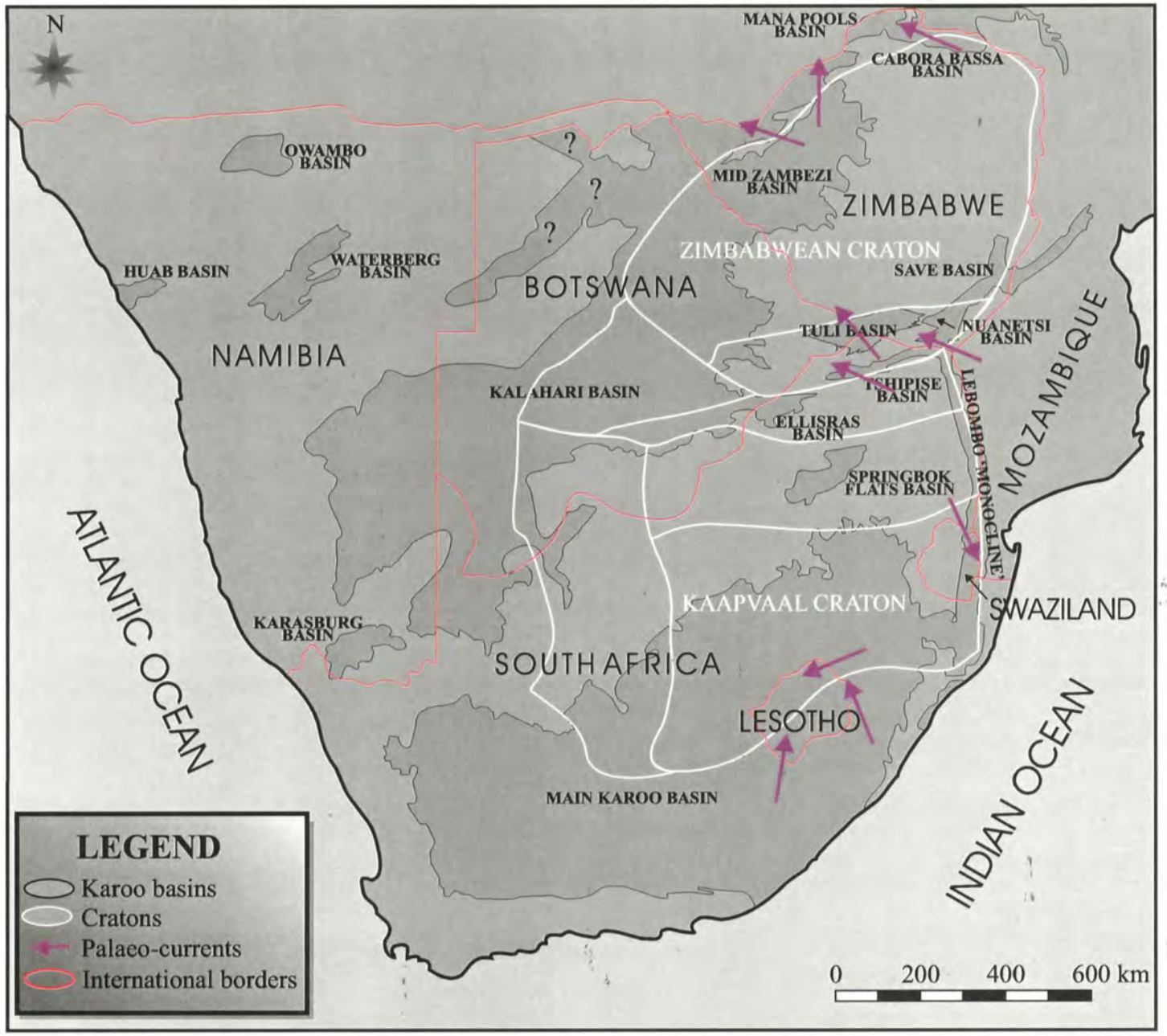

Fig. 111. Palaeo-current directions in the Middle Unit (Tuli Basin), Molteno Formation (main Karoo Basin) and other Molteno Formation equivalents. The data of the Tuli Basin are recent measurements; whereas the other data are from Fick (1970), Grant (1972), Jackson (1975), Oesterlen (1991), van der Berg (1980), Turner & Minter, (1985); Eriksson (1984) and Botha (1968).

fact that within the uplifted area above the plume, there are surface irregularities originating from the interaction between the rising plume and lithosphere (Hill, 1991:406). However deposits of such small-scale basins would be expected to show distinct sedimentary lithofacies, but as mentioned in Ch. 6.1., the Upper Karoo formations in this region are surprisingly similar to those in the Tuli and main Karoo Basins.

Apart from the plume model pictured above, the unconformity surface at the base of the supposedly Molteno-equivalent Middle Unit may be explained in terms of the passive rifting. The legitimacy of the passive rifting model for the Tuli Basin is seen in the fact that Gondwana break up-related extensional tectonics are documented to have existed in the region (see Ch. 2.), having been responsible for the intracontinental rift system in the zone of the Archaean Limpopo Belt and also for the half-graben geometry of the Tuli Basin (Cox, 1970; Burke & Dewey, 1973; Duguid, 1975; Smith, 1984; Watkeys & Sweeney, 1988; Cox, 1992). However, it needs to emphasized that during the course of this study, neither syn-sedimentary nor reverse faults have been observed. Because the study area lies within the eroded margin of the original basin, there are only scanty data on lateral thickness variations of the units, and the presence of faults may have gone undetected. As previously mentioned (Ch. 4.2.), the lateral thickness variations cannot be adequately evaluated from the available borehole record, mostly because the of the lack of information from the northern part of the study area.

Accepting that passive rifting occurred in the study area, the uplift inferred from the unconformable base of the Middle Unit may be related to uplift of the rift shoulder. In passive rifting models, such uplift is explained by a number of processes all taking place in the syn-rift phase of the rift evolution. Firstly, Cochran (1983:291) states that rift shoulder uplift of several hundred metres results from the lateral heat conduction from the upwelled asthenosphere to the cooler surrounding lithosphere. Secondly, small-scale, secondary mantle convection beneath rifts causes the progressive heating of the lower corner of the rift flank, resulting in uplift of the rift shoulder (e.g. Gulf of Suez) (Steckler, 1985 in Allen & Allen, 1990). Thirdly, Rowley & Sahagian (1986:34) propose that the uplift may be caused by "the replacement of relatively cooler, more dense lithosphere with warmer, less dense asthenosphere below a region of unstretched crust". However, it should be emphasized that these mechanisms were described with

regard to well developed intracontinental rifts characterized by large amounts of extension, and therefore it is uncertain if the same processes would be applicable to a small-scale rifting scenario such as the Tuli Basin.

Based on examples of extended syn-rift tectonics in other intracratonic rift basins (e.g. Paris Basin, France at ~ 60 Ma and Sirte Basin, Libya at ~120 Ma as discussed in Cochran, 1983:291), it is possible that syn-rifting started in post-Basal Unit times and lasted throughout the deposition of the Middle and Upper Units, and the Clarens Formation (i.e. for ~40-50 Ma). The duration of the syn-rift phase is thought to be influenced by several factors like rate of stretching (finite or instantaneous) and regional distribution of deviatoric stresses.

In this framework, it may be proposed that the sedimentary rocks of the Middle and Upper Units, and the Clarens Formation represent syn-rift deposits which were accumulated in the E-W trending rift system comprising the Tuli and Tshipise basins (Fig. 109-5D, E, & F). The major problem of this proposal is that it may explain the unconformity at the base of the Middle Unit as being the result of a pronounced rift shoulder uplift, but cannot explain the absence of the similar, distinct boundary between the Middle and Upper Units. Regarding the contrasting palaeo-current directions of the two units (i.e. from ~SE to ~NW in the Middle Unit and from ~NW to ~SE in the Upper Unit), it is possible that the dip direction of the regional palaeo-slopes varied with time due to the evolution of the major faults within the rift system. In other words, it can be imagined that the master fault of the rift system (i.e. the northern boundary of the Tuli Basin) was the major active fault during the accumulation of the Middle Unit and its equivalents. This set up would have generated a northerly inclined palaeo-slope stretching from the southern rift shoulder to the northern master border fault. The similar palaeo-current directions of the Middle Unit in the Tuli Basin and its equivalent (Fripp and Joan Formation - van den Berg,1980) in the Tshipise Basin may imply that both areas formed part of the same ~E-W trending depository (Fig. 109-5D). By the time of the accumulation of the Upper Unit, the rift system reached the stage when due to intrabasin fault activity individual, ~E-W trending sub-basins were created (Fig. 109-5E). This set up would explain why the palaeo-drainage pattern in the Tuli Basin is opposite to that of the north-easterly inclined depositional ramp of the neighbouring Tshipise Basin (Fig. 112). If during the deposition of the Upper Unit, the Tuli and Tshipise

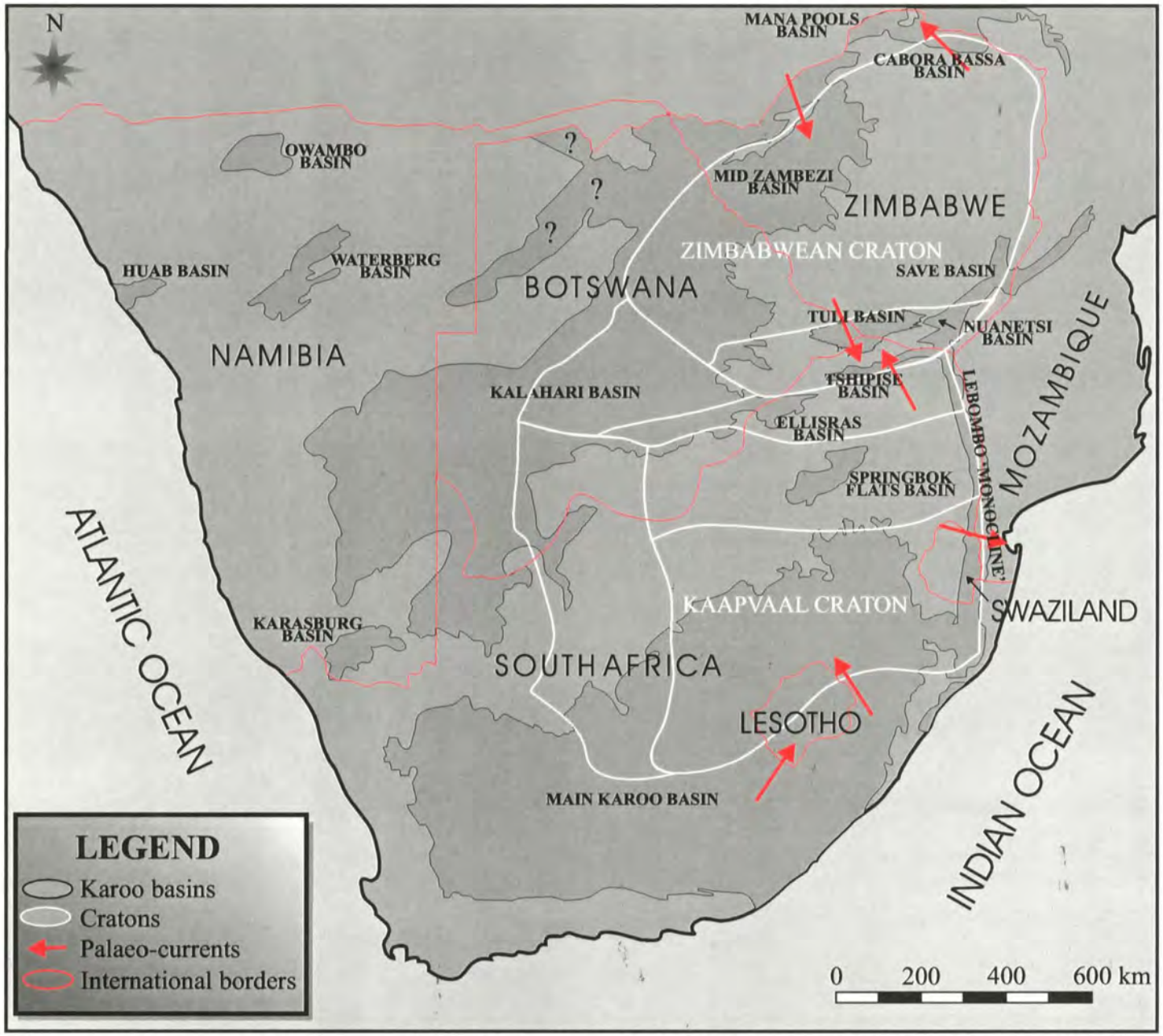

Fig. 112. Palaeo-current directions in the Upper Unit (Tuli Basin), Elliot Formation (main Karoo Basin) and other Elliot Formation equivalents. The data of the Tuli Basin are recent measurements; whereas the other data are from Visser (1984), Oesterlen (1991), van der Berg (1980), Turner & Minter (1985) Eriksson (1985) and Botha (1968).

basins were two individual sub-basins parallel to each other and within the E-W trending rift system (see also Fig. 5D in Ch. 2.1.4.), these two depocentres may have been supplied with sediments from different sources: the Tuli Basin mainly from north, and the Tshipise Basin mostly from south.

In conclusion, the reason for the various regional palaeo-slope directions that prevailed during the deposition of the Karoo Supergroup (Tuli Basin) remains uncertain for the time being. It is tentatively suggested that foreland system tectonics, which definitely affected the deposition of the Basal Unit, were replaced by incipient continental extension either shortly before the deposition of the Middle Unit, or at a later stage (i.e. during the accumulation of the Upper Unit). However, it must be emphasized that because of the scanty data on lateral thickness variations of the individual units, as well as lack of unambiguous bio- and chronostratigraphic evidence, the tectonic evolution of the Tuli Basin cannot be adequately explained at this stage. On the other hand, the results of this study show that the model of Watkeys & Sweeney (1988) (Ch. 2.1.4.) is subject to modification as extensional rift tectonics did not occur during the deposition of the Basal Unit, which was formed in the back-bulge basin setting of the Karoo foreland system.

7. Conclusions

The palaeo-environmental reconstruction of the Karoo Supergroup in the southern part of the Tuli Basin produced the following results:

1. The Tuli Basin contains a sedimentary sequence composed of four stratigraphic units, namely the Basal, Middle and Upper Units, and Clarens Formation. The units were deposited in continental settings from approximately Late Carboniferous to Middle Jurassic. These units yield subarctic, non-glacial fluvio-lacustrine to low-latitude desert deposits that formed during long-term climatic change from cold climate towards a more arid, hot environment.

2. The palaeo-geographic picture of the Basal Unit is a high-energy, braided fluvial regime draining to WSW on a relatively low relief, deeply weathered crystalline basement, composed mainly of high grade metamorphic and granitoid rocks. The marshy overbank area dotted by several lakes supported a flourishing vegetation characterized by various *Glossopteris* species. The unit contains a relatively well-developed coal seam, thus this lacustrine environment had suitable conditions for coal-forming peat accumulations.

3. Based on scanty field evidence, the Middle Unit was generated in a bed-load dominated, braided river system. This unit is non-fossiliferous and overlies a regional unconformity. The conglomerates, sandstones, siltstones and mudstone were derived mainly from weathered, quartz-rich metamorphic and - to a lesser extent - felsic plutonic and sedimentary source rocks situated SSE of the study area.

4. The Upper Unit was deposited by ephemeral fluvial systems characterized by sheet-flood processes. These transported mainly fine-grained arenaceous and argillaceous sediment from a weathered, quartz-rich craton interior and other sedimentary source rocks located NNW of the semi-arid study area. The fining-upward channel-fill sequences were built up by numerous flooding events as indicated by the desiccated mud drapes and internal erosion surfaces. The overbank area supported both flora and fauna as evidenced by indicators of soil-forming processes (e.g. pedogenic calcrete and silcrete) and palaeontological findings (e.g. ichnofossils and prosauropod? dinosaur remains).

5. The sandstones of the Clarens Formation were generated as transverse and barchanoidaeolian dunes blown by westerly winds in a somehow wet erg milieu. Direct evidence of aquatic subenvironments comes from the small ephemeral stream deposits, whereas indirect evidence is in the abundance of massive sandstones interpreted to result from slow rain-water seepage through the dunes, and palaeontological findings. Fossils of the Formation include petrified logs of *Agathoxylon sp.* wood type and several trace fossils which were produced by insects and vertebrates. The upper part of the Formation lacks both direct and indirect evidence of aquatic conditions, and this suggests aridification that lead to the dominance of dry sand sea conditions.

6. The Tuli Basin developed in the back-bulge basin setting of the south-Gondwana foreland system during the accumulation of the Basal Unit. The tectonic history of the basin during the deposition of the Middle and Upper Units, and Clarens Formation, however is still debatable. During the sedimentation of the non-fossiliferous Middle Unit, it appears that there are two equally possible explanations of the tectonic setting: in terms of a foreland system mechanism the Middle Unit seems to be a back-bulge basin fill, whereas in terms of rift-basin processes the Middle Unit may represent early syn-rift sediments. A third, rather unlikely possibility is that during the deposition of the Middle Unit, the Tuli Basin occupied a distal dome-flank position within the area which was regionally elevated by the Karoo plume. During the accumulation of the Upper Unit and Clarens Formation, the Tuli Basin seems to have undergone extensive tectonic movements, which finally led to the present half-graben geometry of the area.

8. Acknowledgments

I would like to thank De Beers Consolidated Mines Ltd. for providing the opportunity to undertake this PhD study by sponsoring me during the three years of study. Dr. E.M.W. Skinner is particularly thanked for proposing the research to the main sponsor. I also gratefully acknowledge funding received from NRF as well as from György Soros. South African National Parks are also acknowledged for permission to undertake research within their reserves.

I express my sincere gratitude to all who assisted me during the course of this study. First, I would like to thank my supervisor Prof. O. Catuneanu, as well as my co-supervisors Prof. R.E. Jacob and Prof. B.S. Rubidge for their assistance, guidance and patience. The foreland tectonic model was debated for long hours with Prof. O. Catuneanu. Prof. R.E. Jacob critically read and improved the English of the whole thesis, whereas Prof B.S. Rubidge gave his comments on the chapters dealing with the palaeontological findings. Prof J.S. Marsh was of great assistance being always keen to discuss the various aspects of this study, and also for his advises and critical evaluations of the final chapters.

I am grateful to all the members of the Geology Department: to Dr. Frank Holzförster and Dr. M. Roberts for being consistently encouraging, and to Miss J. Wright and Mrs. A. Goddard (secretaries) and Mr. J.R. Hepple (technical officer) and his team for their assistance during the course of the study.

I thank the following palaeontologists for professional assistance: Dr. M. Bamford, Dr. A. Cadman, Dr. M.A. Raath (BPI, University of Witwatersrand, Johannesburg) and Dr. W.J. de Klerk (Albany Museum, Grahamstown).

I would also like to thank my two office and soul mates, Kimberley Machin and Laura Quinton, not only for professional company, but also for their invaluable support in the last two years of this study. The second and third year undergraduate students, whom as a graduate assistant I taught some sedimentology, also contributed to the progress of my PhD studies by often putting me under sedimentological "cross-fire", endlessly challenging me with questions and demanding correct answers. Cheers guys, I learned a lot from you!

I am also indebted to Adriaan Stander. Without his assistance and encouragement (especially during the field work), it would have been difficult for me to cope alone with all those barricading thorny bushes, mopani-fly invasions, tricky sandy farm tracks, oversized sandstone samples, etc. I am also grateful to his family for providing for me a home thousands of kilometres away from my own. Baie dankie!

I wish to acknowledge with gratitude all the farmers, landowners and their employees in the study-area. Apart from their hospitality and interest, they provided me with useful information relevant to the field work, mostly during lekker braais. Special thanks go to Prof. C. Strub and Mrs. M. Stub as well as Mrs. and Mr. S. Lemmer for their sincere interest, the lovely conversations and last, but not least, for reading the first year progress report. I think they all contributed to the fact that after all, I left the "hell hot" lowveld not only with full field notebooks, but also with nice memories and friendships that I will never forget.

Finally, my sincere thanks go to the all De Beers Co. Mines Ltd. employees at the Geology Division, especially to the people at the Icon Camp (Far North) for their co-operation and interest during the field work.

9. References

Ahlbrandt, T.S.; Andrews, S. & Gwynne, D.T. (1978) Bioturbation in eolian sediments. *J. Sedim. Petrol.*, **48**, 839-848.

Aldis, D.T.; Benson; J.M. & Rundle, C.C. (1984) Early Jurassic pillow lavas and palynomorphs in the Karoo of eastern Botswana. *Nature*, **310**, 302-304.

Allen, J.R.L. (1963) The classification of the cross-stratified units with notes on their origin. *Sedimentology*, **2**, 93-114.

Allen, J.R.L. & Williams, B.P.J. (1979) Interfluvial drainage on Siluro-Devonian alluvial plains in Wales and the Welsh Borders. *J. Geol. Soc. London*, **136**, 361-366.

Allen, P.A. & Allen, J.R. (1990) Basin analysis: principles and applications. Oxford: Blackwell Scientific Publications.

Anketell, J.M; Cegła, J. & Dżułyński, S. (1970) On the deformational structures in systems with reversed density gradients. *Rocz. Pol. Tow. Geol. (Ann. Soc. Geol. Pol.), Kraków*, **XL (1)**, 3-29.

Arakel, A.V. (1985) Evolution of calcrete in palæodrainages of the Lake Napperby area, Central Australia. *Palæogeogr., Palæoclimatol., Palæoecol.*, **54**, 283-303.

Arakel, A.V. & McConchie, D. (1987) Classification and genesis of calcrete and gypsite lithofacies in paleodrainage system of inland Australia and their relationship to carnotite mineralization. *J. Sedim. Petrol.*, **52**, 1149-1170.

Ashley, G.M. (1990) Classification of large-scale subaqueous bedforms: a new look at an old problem. *J. Sedim. Petrol.*, **60**, 160-172.

Baird, A.J. (1997) Overland flow generation and sediment mobilisation by water. In: D.S.G. Thomas (ed.): Arid Zone Geomorphology: Process, Form and Change in Drylands. Chichester: John Wiley & Sons Ltd., 2nd edition, 166-184.

Báldi, T. (1992) Physical Geology. Budapest: Eötvös Loránd University, *Manuscript*, 489-504.

Bamford, M. (1999) Permo-Triassic fossil woods from the South African Karoo Basin. *Palaeont. Afr.*, **35**, 25-40.

Beukes, N.J. (1970) Stratigraphy and sedimentology of the Cave Sandstone Stage, Karoo System. In: S.H. Haughton (ed.): Proc. 2nd IUGS Symposium on Gondwana Stratigraphy and Palaeontology. Pretoria: CSIR, 321-341.

Blatt, H.; Middleton, G. & Murray, R. (1972) Origin of the Sedimentary Rocks. New Jersey: Prentice-Hall, Inc.

Blikra, L.H. & Nemec, W. (1998) Postglacial colluvium in Norway. *Sedimentology*, **45**, 909-959.

Blodgett, R. H. (1988) Calcareous paleosols in the Triassic Dolores Formation, southwestern Colorado. In: J. Reinhardt (ed.): Paleosols and Weathering Though Geologic Time: Principles and Application. *Geol. Soc. Amer. Spec. Paper,* **216**, 103-122.

Blume, H. (1992) *Colour Atlas of the Surface of the Earth.* London: Belhaven Press

Boles, J.R.; Landis, C.A. & Dale, P. (1989) The Moeraki boulders - anatomy of some septarian concretions. *J. Sedim. Pertol.,* **55**, 398-406.

Botha, B.J.V. (1968) The stratigraphy of the Red Beds Stage, Karoo System, at Elliot, C.P. *Trans. Geol. S. Afr.*, **71**, 101-113.

Botha, B.J.V. & Theron, J.C. (1967) New evidence for the early commencement of Stormberg volcanism. *Tydskrif Natuurwet*, **6**, 469-473.

Boothroyd, J.V. & Ashley, G.M. (1975) Process, bar morphology, and sedimentary structures on braided outwash fans, northeastern Gulf of Alaska. In: A.V. Jopling & B.C. McDonald (eds.): Glaciofluvial and Glaciolacustrine Sedimentation. *Soc. Econ. Paleont. Mineral. Spec. Publ.*, **23**, 192-222.

Brandl, G. (1981) The geology of the Messina area. Explanation of the Sheet 2230. Geol. Surv. S. Afr., 1-35.

Brandl, G. (1992) Geological Map of the Limpopo Belt and its Environs. Contribution to "A field workshop on granulites and deep crustal tectonics, 1990". Scale 1:500000. Geol. Surv. S. Afr.

Brandl, G. (1996) The geology of the Ellisras area. Explanation of the Sheet 2326. Geol. Surv. S. Afr., 1-49.

Bridgland, D.R. (1986). Discussion of procedures and recommendations. In: D.R. Bridgland (ed.): Clast lithological analysis. Cambridge: Quaternary Research Association.

Bristow, J.W. (1982) Geology and structure of Karoo volcanic and sedimentary rocks of the northern and central Lebombo. *Trans. geol. Soc. S. Afr.,* **85**, 167-178.

Broderick, T.J. (1979) Explanation of the Geological Map of the Country South of Nuanetsi, Nuanetsi and Bietbride Districts Salisbury. *Short Report No.* **46**, *Rhodesia Geol. Surv.*

Bromley, R. & Asgaard, U. (1979) Triassic freshwater inchnocoenoses from Carlsberg Fjord, East Greenland. *Palæogeogr., Palæoclimatol., Palæoecol.,* **28**, 39-80.

Brookfield, M.E. (1992) Eolian systems. In: R.G. Walker & N.P. James (eds.): Facies Models: Response to Sea Level Change. Geol Assoc of Canada, 142-156.

Brown, T.M. (1982) Ichnofossils and rhizoliths of the nearshore fluvial Jebel Qatrani Formation (Oligocene), Fayum Province, Egypt. *Palæogeogr., Palæoclimatol., Palæoecol.,* **40**, 255-309.

Burke, K.C.A. & Dewey, J.F. (1973) Plume-generated triple junctions: key indicators in applying plate tectonics to old rocks. *J. Geol.*, **86**, 406-433.

Cadle, A.D.; Cairncross, B.; Christie, A.D.M. & Roberts, D.L. (1993) The Karoo basin of South Africa: type basin for the coal-bearing deposits of southern Africa. *Int. J. Coal Geol.*, **23**, 117-157.

Cairncross, B.; Anderson, J.M. & Anderson, H.M. (1995) Palaeoecology of the Triassic Molteno Formation, Karoo Basin, South Africa - sedimentological and palaeontological evidence. *S. Afr. J. Geol.*, **98**, 452-478.

Campbell, S.D.G.; Oesterlen, P.M.; Blenkinsop, T.G.; Pitfield, P.E.J. & Munyanyiwa, H. (1991) A provisional 1 : 2 500 000 scale tectonic map and the tectonic evolution of Zimbabwe. *Ann. Zimb. Geol. Surv.* **XVI,** 31-52 (p.44).

Catuneanu, O.; Beumont, C. & Waschbusch, P. (1997) Interplay of static loads and subduction dynamics in foreland basin: Reciprocal stratigraphies and the "missing" peripheral bulge. *Geology*, **25**, 1087-1090.

Catuneanu, O.; Hancox, P.J. & Rubidge, B.S. (1998) Reciprocal flexural behaviour and contrasting stratigraphies: a new basin development model for the Karoo retroarc foreland system, South Africa. *Basin Research*, **10**, 417-439.

Chakraborty, T. & Chaudhuri, A.K. (1993) Fluvial-aeolian interactions in a Proterozoic alluvial plain: example from the Mancheral Quartzite, Sullava Group, Pranhita-Godavari Valley, India. In: K. Pyes (ed.): The Dynamics and Environmental Context of Aeolian Sedimentary Systems. *London: Geol. Soc. Spec. Publ.*,**72**, 127-144.

Chidley, C.M. (1985) The geology of the country around Evangelina and Pontdrift (1:50000 Sheets 2228BD&2229A). Unpublished S. Afr. Geol. Surv. Report. Pietersburg, South Africa.

Christie, A.D.M. (1986) Molteno coalfield. In: C.R. Anhaeusser & S. Maske (eds.): *Mineral Deposits of Southern Africa. Geol. Soc. S. Afr.*,Vol. **II**, 2063-2069.

Cochran, J.R. (1983) Effects of finite rifting on the development of sedimentary basins. *Earth & Plan. Sci. Lett.*, **66**, 289-302.

Collinson, J.D. (1996) Alluvial sediments. In: H.G. Reading (ed.): Sedimentary environments: Processes, Facies and Stratigraphy. Oxford: Blackwell Scientific Publications, 37-82.

Colson, J. & Cojan, I. (1996) Groundwater dolocretes in a lake-marginal environment: an alternative model for dolocrete formation in continental setting (Danian of the Provence Basin, France). *Sedimentolgy,* **43**, 175-188.

Cooke, R.U. & Warren, A. (1973) Geomorphology in Deserts. London: BT Batsford Ltd.

Cooper, M.R. (1980) The first record of the Prosauropod dinosaur *(Euskelosaurus)* from Zimbabwe *Arnoldia*, **9**, No.3, 1-17.

Cooper, M.R. (1982) A mid-Permian to earliest Jurassic Tetrapod biostratigraphy and its significance. *Arnoldia*, **9**, No.7, 77-103.

Cox, K.G. (1970) Tectonics and vulcanism of the Karoo period. In: T.N. Clifford & I.G. Gass (eds.): African magmatism and tectonics. Edinburgh: Oliver&Boyd, 211-236.

Cox, K.G. (1989) The role of mantle plums in the development of continental drainage patterns. *Nature*, **342**, 873-876.

Cox, K.G. (1992) Karoo igneous activity, and the early stages of the break-up of Gondwanaland. In: B.C. Storey; T. Alabaster & R.J. Pankhurst (eds.): Magmatism and the Causes of Continental Break-up. *London: Geol. Soc. Spec. Publ.*, **68**, 137-148.

Cox, K.G. & Bristow, J.W. (1984) The Sabie River Basalt Formation of the Lebombo Monocline and South-East Zimbabwe. *Spec. Publ. geol. Soc. S. Afr.*, **13**, 125-147.

Cox, K.G.; Johnson, R.L.; Monkman, L.J.; Stillman, C.J.; Vail, J.R.& Wood, D.N. (1965) The geology of Nuanetsi Igneous Province *Phil. Trans. Royal Soc. Ser. A.*, **257**, 71-218.

Demicco, R.V. & Kordesch, E.G. (1986) Facies sequences of a semi-arid closed basin: the Lower-Jurassic East Berlin Formation of the Hartford Basin, New England, U.S.A. *Sedimentology,* **33**, 107-118.

de Villiers, S.B. (1967) Sundervormige Structure in Holkranssandsteen van die Serie Stromberg, Distrik Messina. *Ann. Geol Surv. S. Afr.*, **6**, 69-71.

Dreyer, T. (1993) Quantified fluvial architecture in ephemeral stream deposits of the Esplugafreda Formation (Palaeocene), Tremp-Graus Basin, northern Spain. *Publs Int. Assoc. Sedim.*, **17**, 337-362.

Duguid, K. (1975) Dwyka and Ecca sedimentation in the Karoo basin of the Sabi Valley, and its tectonic control. *Detritus Mennell Society Journal*, University of Rhodesia, **X**, 22-37.

Duncan, R.A; Hooper, P.R.; Rehacek, J.; Marsh, J.S. & Duncan, A.R. (1997) The timing and duration of the Karoo igneous event, southern Gondwana. *J. Geophys. Res.*, **102**, No. B8, 18127-18138.

Dżułyński, S. (1966) Sedimentary strictures resulting from convection-like pattern of motion. *Rocz. Pol. Tow. Geol. (Ann. Soc. Geol. Pol.), Kraków,* **XXXVI (1),** 3-21.

Eriksson, P.G. (1981) A palaeoenvironmental analysis of the Clarens Formation in the Natal Drakensberg. *Trans. Geol. S. Afr.*, **84**, 7-17.

Eriksson, P.G. (1984) A palaeoenvironmental analysis of the Molteno Foramtion in the Natal Drakensberg. *Trans. Geol. S. Afr.*, **87**, 237-244.

Eriksson, P.G. (1985) The depositional environment of the Elliot Formation in the Natal

Drakensberg and north-east Orange Free State. *Trans. Geol. S. Afr.*, **88**, 19-26.

Eriksson, P.G. (1986) Aeolian dune and alluvial fan deposits in the Clarens Formation of the Natal Drakensberg. *Trans. Geol. S. Afr.*, **89**, 389-393.

Eriksson, P.G. (1987) A note on the red colouration in sedimentary rocks of the Molteno, Elliot and Clarens Formations. *Ann. Geol. Surv. S. Afr.*, **21**, 89-94.

Esteban, M.C. (1976) Vadose Pisolite and Caliche. *Amer. Assoc. of Petr. Geol. Bulletin*, **60**, 2049-2057.

Falcon, R.M.S. (1989) Macro- and micro-factors affecting coal-seam quality and distribution in southern Africa with particular reference to the No. 2 seam, Witbank coalfield, South Africa. *Int. J. Coal Geol.*, **12**, 681-731.

Farrell, K.M. (1987) Sedimentology and facies architecture of overbank deposits, of the Mississippi River, False River Region, Louisiana. In: F.G. Ethridge & R.M. Flores (eds.): Recent developments in fluvial sedimentology. *Soc. Econ. Paleontol. Mineral Spec. Publ.*, **39**, 111-120.

Faure, K; Armstrong, R.A., Harris, C. & Willis, J.P. (1996) Provenance of mudstones in the Karoo Supergroup of the Ellisras Basin, South Africa: geochemical evidences. *J. Afr. Earth Sci.*, **23** (2), 189-204.

Fick, V. (1970) Note on Investigations on Current Directions in the Karoo Molteno Outcrop Around Sinamwenda, Lake Kariba. *Detritus*, **6**, 36-38.

Fisher, P.F. & Brindgland, D.R. (1986). Analysis of pebble morphology. In: D.R. Bridgland (ed.): *Clast lithological analysis*. Cambridge: Quaternary Research Association

Folk, R.L. & Pittman, J.S. (1971) Length-slow chalcedony: a new testament for vanished evaporites. *J. Sedim. Petrol.*, **41**, 1045-1058.

Friedman, G.M.; Sanders, J.H. & Kopaska-Merkel, D.C (1992) Principles of Sedimentary Deposits. New York: Macmillian Publishing Company

Friedman, G.M. & Sanders, J.H. (1978) Principles of Sedimentology. New York: Wiley.

Friend, P.F. (1978) Distinctive features of some ancient river systems. In: A.D. Miall (ed.): Fluvial Sedimentology. Calgary: Can. Soc. Petrol. Geol., Memoir **5**, 531-542.

Frostick, L.E.; Reid, I. & Layman, J.T. (1983) Changing size distribution of suspended sediment in arid-zone flash floods. In: J.D. Collinson & J. Lewin (eds.): Modern and ancient fluvial systems. *Spec. Publs Int. Assoc. Sedim.*, **6**, 97-106.

Gallant, A.L.; Binnian, F.E; Omernik, J.M. & Shasby, MB. (1995) Ecoregions of Alaska. *US Geol. Surv. Professional Paper*, Washington, **1567**

Geological Map, Beit Bridge (1957) Scale 1:250000, Sheet 2228. Geol.Surv., Department of Mines, Union of South Africa.

Genise, J.F. & Brown, T.M. (1994) New trace fossils of termites (Insecta: Isoptera) from the late Eocene - early Miocene of Egypt, and the reconstruction of ancient isopteran social behavior. *Icnos*, **3**, 155-183.

Gibling, M.R.; Nanson, G.C. & Maroulis, J.C. (1998) Anastomosing river sedimentation in the Channel Country of central Australia. *Sedimentology*, **45**, 595-619.

Glennie, K.W. (1987) Desert sedimentary environments, present and past - a summary. *Sedim. Geol.*, **50**, 135-165.

Goudie, A. (1973) Duricrusts in tropical and subtropical landscapes. London: Oxford University Press.

Grant, D. (1972) The Karoo Sediments of the Country South of the Nebiri Coalfield, Gokwe District. *Detritus*, **7**, 24-27.

Green, C.P. & McGregor, D.F.M. (1986). The utility of intercomponent ratios in the interpretation of stone count data. In: D.R. Bridgland (ed.): Clast lithological analysis. Cambridge: Quaternary Research Association

Groenewald, P.B.; Grantham, G.H. & Watkeys, M.K. (1991) Geological evidence for a Proterozoic to Mesozoic link between southeastern Africa and Dronning Maud Land, Antarctica. *J. Geol. Soc.*, London, **148**, 1115-1123.

Gustavson, T.C & Holliday, V.T. (1999) Eolian sedimentation and soil development on a semiarid to subhumid grassland, Tertiary Ogallala and Quaternary Blackwater Draw Formations, Texas and New Mexico High Plains. *J. Sedim. Research,* **69**, 622-634.

Hancox, P.J. (1998) The Beaufort-Molteno contact revised: ramifications for the development of the Karoo retro-foreland basin during the Triassic. *J. Afr. Earth Sci.*, **27** (1A), 103-104.

Harris, V. (1961) Termites: their recognition and control. London: Longmans.

Hartley, A.J. (1993) Sedimentological response of an alluvial system to source area tectonism: the Seilao Member of the Late Cretaceous to Eocene Purilactis Formation of northern Chile. *Publs Int. Assoc. Sedim.*, **17**, 489-500.

Haughton, S.H. (1924) The fauna and stratigraphy of the Stormberg Series. *Ann. S. Afr. Mus.*, **12**, 323-495.

Haughton, S.H. (1969) Geological History of Southern Africa. Cape Town: Geol. Soc. S. Afr.

Hawkesworth, C.; Kelly, S.; Turner, S.; leRoex, A. & Storey, B. (1999) Mantle processes during Gondwana break-up and dispersal. *J. Afr. Earth Sci.*, **28**, 239-261.

Heinemann, M. & Buhmann, D. (1987) Coal-tonsteins from the Molteno Formation of the Maluti

District, Tanskei. *S. Afr. J. Geol.*, **90** (3), 296-304.

Hill, G.F. (1942) Termites (Isoptera) from the Australian Region. Melbourne: C.S.I.R.

Hill, R. I. (1991) Starting plumes and continental break-up. *Earth & Plan. Sci. Lett.*, **104**, 398-416.

Hoey, T.B. & Bluck, B.J. (1999) Identifying the controls over downstream fining in river gravels. *J. Sedim. Research,* **69/1**, 40-50.

Howse, P.E. (1970) Termites: a study in social behaviour. London: Hutchinson University Library

Jackson, A. (1975) The Geology of the Area between Chipise Hot Springs and Mazondo, near Beit Bridge. *Detritus*, **10**, 64-70.

Johnson, M.R. (1976) Stratigraphy and sedimentology of the Cape and Karoo sequences in the eastern Cape Province. Unpubl. PhD Thesis, Rhodes University, South Africa.

Johnson, M.R. (1989) Paleogeographic significance of orientated calcareous concretions in the Triassic Katberg Formation, South Africa. *J. Sedim. Petrol.*, **59**, 1008-1010.

Johnson, M.R. (ed.) (1994) Lexicon of South African Stratigraphy. Part1: Phanerozoic Units. Pretoria: SACS, Council for Geoscience

Johnson, M.R.; Van Vauuren, C.J.; Hegenberger, W.F.; Key, R. & Shoko, U. (1996) Stratigraphy of the Karoo Supergroup in southern Africa: an overview. *J. Afr. Earth Sci.*, **23**(1), 3-15.

Johnson, M.R.; Van Vuuren, C.J.; Visser, J.N.J.; Cole, D.I.; Wickens H. de V.; Christie, A.D.M.; Roberts, D.L. (1997) The Foreland Karoo Basin, South Africa. In: R.C. Selly (ed.): African Basins. Sedimentary Basins of the World, **3**. Amsterdam: Elsevier Science B.V, 269-317.

Kelly, S.B. & Olsen, H. (1993) Terminal fans - a review with references to Devonian examples. *Sedim. Geol.*, **85**, 339-374.

Khadkikar, A.S.; Merh, S.S.; Malik, J.N. & Chamyal, L.S. (1998) Calcretes in semi-arid alluvial systems: formative pathways and sinks. *Sedim. Geol.*, **116**, 251-260.

Kingsley, C.S. (1985) Stratigraphy and sedimentology of the Ecca Group in the eastern Cape Province. Unpubl. PhD Thesis, University of Port Elisabeth, South Africa.

Kitching, J.W. & Raath, M.A. (1984) Fossils from the Elliot and Clarens Formations (Karoo Sequence) of the northeastern Cape, Orange Free State and Lesotho, and a suggested biozonation based on tetrapods. *Palæont. Afr.*, **25**, 111-125.

Klappa, C.F. (1980) Rhizoliths in terrestrial carbonates. *Sedimentology*, **27**, 613-629.

Klappa, C.F. (1983) A process-response model for the formation of pedogenic calcretes. In: R.L.C. Wilson (ed.): Residual deposits: surface related weathering processes and materials. Geol.

Soc. Spec. Publ. Oxford: Blackwell Scientific Publication, 211-220.

Knighton, D. & Nanson, G. (1997) Distinctiveness, diversity and uniqueness in arid zone river systems. In: D.S.G. Thomas (ed.): Arid Zone Geomorphology: Process, Form and Change in Drylands. Chichester: John Wiley & Sons Ltd., 2nd edition, 185-203.

Kubovics, I. (1993) Petrological microscopy. Budapest: Tankonykiado.

Lajoie, J. & Stix, J. (1992) Volcaniclasic rocks. In: R.G. Walker & N.P. James (eds.): Facies Models: Response to Sea Level Change. Geol. Assoc. Can., 119-142.

Langford, R.P. (1989) Fluvial-aeolian interactions: Part I, modern systems. *Sedimentology*, **36**, 1023-1035.

Langford, R.P.& Bracken, B. (1983) Medano Creek, Colorado, a model for upper-low-regime fluvial depostion. *J. Sedim. Petrol.*, **57**, 863-870.

Langford, R.P. & Chan, M.A. (1989) Fluvial-aeolian interactions: Part II, ancient systems. *Sedimentology*, **36**, 1037-1051.

Lee, K.E. & Wood, T.G. (1971a) Physical and chemical effects on soils of some Australian termites, and their pedological significance. *Pedobiologia*, **11**, 376-409.

Lee, K.E. & Wood, T.G. (1971b) Termites and soil. London: Academic Press

Leeder, M.R. (1975) Pedogenic carbonates and flood sediment accretion rates: a quantitative model for alluvial arid-zone lithofacies. *Geol. Mag.*, **112**, 257-270.

Le Roux, J.P. (1992) Determining the channel sinuosity of ancient fluvial systems from paleocurrent data. *J. Sedim. Petrol.*, **67** (2), 283-291.

Le Blanc Smith, G. & Eriksson, K.A. (1979) A fluvioglacial and glaciolacustrine deltaic depositional model for Permo-Carboniferous coals of the north-eastern Karoo basin, South Africa. *Palæogeogr., Palæoclimatol., Palæoecol.*, **27**, 67-84.

Lucchitta, I. & Suneson, N. (1981) Flush flood in Arizona - observations and their application to the identification of flash-flood deposits in the geologic record. *Geology*, **9**, 414-418.

Luscher, M. (1961) Air-conditioned Termite Nests. *Scientific American, Inc.*

Mack, G.H.; James W.C. & Monger, C.H. (1993) Classification of paleosols. *Geol. Soc. Amer. Bulletin*, **105**, 129-136.

MacRae, C.S. (1988) Palynostratigrafhic correlation between the lower Karoo sequence of the Waterberg and Pafuri Coal-bearing Basins and the Hammanskraal plant macrofossil locality, Republic of South Africa. Geol. Surv. S. Afr., Memoir **75**, 1-217.

Marriott, S.B. & Wright, P.V. (1993) Paleosols as indicators of geomorphic stability in two Old

Red Sandstone alluvial suites, South Wales. *J. Geol. Soc. London,* **150**, 1109-1120.

Martini, I.P.; Kwong, J.K. & Sandura, S. (1993) Sediment ice rafting and cold climate fluvial deposits: Albany River, Ontario, Canada. *Spec. Publs Int. Assoc. Sedim.*, **17**, 63-76.

Mayer, L.; McFadden, L.D. & Harden, J.W. (1988) Distribution of calcium carbonate in desert soils: A model. *Geology,* **16**, 303-306.

McCourt, S. & Brandl, G. (1980) A lithostratigraphic subdivision of the Karoo sequence in the north-eastern. *Transvaal Annals Geol. Surv. S. Afr.*, **14** (1), 51-56.

McKee, E.D.; Crosby, E.J. & Berryhill, H.L., JR. (1967) Flood deposits, Bijou Creek, Colorado, June 1965. *J. Sedim. Petrol.*, **37**, 829-851.

McKenzie, D. (1978) Some remarks on the development of sedimentary basins. *Earth & Plan. Sci. Lett.*, **40**, 25-32.

McPherson, J.G. (1979) Calcrete (caliche) Paleosols in fluvial redbeds of the Aztec Siltstone (Upper Devonian), Southern Victoria Land, Antarctica. *Sedim. Geol.*, **22**, 267-285.

Miall, A.D. (1976) Palæocurrent and palæohydrologic analysis of some vertical profiles through a Cretaceous braided stream deposit, Banks Island, Arctic Canada. *Sedimentology*, **23**, 459-483.

Miall, A.D. (1978) Lithofacies types and vertical profile models in braided river deposits: a summary. In: A.D. Miall (ed.): Fluvial Sedimentology. Calgary: Can. Soc. Petrol. Geol. Memoir **5**, 597-604.

Miall, A.D. (1984) Principles of sedimentary basin analysis. New York: Springer-Verlag.

Miall, A.D. (1985) Architectural-element analysis: a new method of facies analysis applied to fluvial deposits. *Earth Sci. Rev.*, **22**, 261-308.

Miall, A.D. (1987) Recent developments in the study of facies model. In: F.G. Ethridge & R.M. Flores (eds.): Recent developments in fluvial sedimentology. *Soc. Econ. Paleontol. Mineral Spec. Publ.*, **39**, 1-9.

Miall, A.D. (1990) Principles of sedimentary basin analysis. New York: Springer-Verlag. 2nd ed.

Miall, A.D. (1992) Alluvial deposits. In: R.G. Walker & N.P. James (eds.): Facies Models: Response to Sea Level Change. Geol. Assoc. Can., 119-142.

Miall, A.D. (1996) The Geology of Fluvial Deposits. Oxford: Blackwell Scientific Publications.

Miller, J.M.G. (1996) Glacial sediments. In: H.G. Reading (ed.): Sedimentary environments: Processes, Facies and Stratigraphy. Oxford: Blackwell Scientific Publications, 454-484.

Mozley, P.S & Davis, J.M. (1996) Relationship between orientated calcite concretions and permeability correlation structure in an alluvial aquifer, Sierra Ladrones Formation, New Mexico. *J. Sedim. Research*, **66**, 11-16.

Neke, K.S. (1994) "Heuweltjies" in the Fort Beaufort Region, eastern Cape - identity and origins. Unpublished Honours Thesis. Grahamstwon: Rhodes University, Zoology and Entomology Department.

Netterberg, F. (1980) Geology of Southern African Calcretes: 1. Terminology, Description, Macrofeatures and Classification. *Trans. geol. Soc. S. Afr.*, **83**, 255-283.

Nickling, W.G. (1994) Aeolian sediment transport. In: K. Pye (ed.): *Sediment Transport and Depositional Processes*. Oxford: Blackwell Scientific Publications, 293-345.

Oesterlen, P.M. (1991) A further report on the geology of the Dande west area (western Cabora Bassa Basin, Mid–Zambezi Valley). *Ann. Zimb. Geol. Surv. Bulletin,* **15**, 1-5.

Olsen, H. (1987) Ancient ephemeral stream deposits: a local terminal fan model from Bunter Sandstone Formation (L. Triassic) in the Tonder-3, -4 and -5 wells, Denmark. In: L.E. Frostick & I. Reid (eds.): Desert Sediments: Ancient and modern. *Geol. Soc. Spec. Publs.*, **35**, 69-87.

Ortlepp, G.J. (1986) Limpopo Coalfield. In: C.R. Anhaeusser & S. Maske (eds.): *Mineral Deposits of Southern Africa*. *Geol. Soc. S. Afr.*,Vol. **II**, 2057-2061.

Owen, L.A. (1994) Glacial and non-glacial diamictions in the Karakoram Mountains and Western Himalayas. In: W.P. Warren & D.G. Croot (eds.): Formation and Deformation of Glacial Deposits. Rotterdam: Balkema, 9-37.

Parkash, B.; Awasthi, A.K. & Gohain, K. (1983) Lithofacies of the Markanda terminal fan, Kurukshetra district, Haryana, India. In: J.D. Collinson & J. Lewin (eds.): Modern and ancient fluvial systems. *Spec. Publs Int. Assoc. Sedim.*, **6**, 337-344.

Parnell, J. (1983) Ancient duricrust and related rocks in perspective: a contribution from the Old Red Sandstone. In: R.L.C. Wilson (ed.): Residual deposits: surface related weathering processes and materials. Geol. Soc. Spec. Publ. Oxford: Blackwell Scientific Publication, 197-209.

Pettijohn, F.J., Potter, P.E. & Siever, R. (1987) Sand and Sandstone. 2nd Edition. New York: Springer Verlag.

Pimentel, N.L.; Wright, V.P. & Azevedo, T.M. (1996) Distinguishing early groundwater alteration effects from pedogenesis in ancient alluvial basins: examples from the Palæogene of southern Portugal. *Sedim. Geol.*, **105**, 1-10.

PiPujol, M.D. & Buurman, P. (1994) The distinction between ground-water gley and surface-water gley phenomena in Tertiary paleosols of the Ebro basin, NE Spain. *Palæogeogr., Palæoclimatol., Palæoecol.,* **110**, 103-113.

Potter, P.E. & Pettijohn, F.J. (1977) Paleocurrents and basin analysis. 2nd Edition. New York: Springer Verlag

Prothero, D.R. & Schwab, F. (1996) Sedimentary Geology. New York: W.H.Freeman and Company

Pye, K. & Tsoar, H. (1990) Aeolian sand and sand dunes. London: Unwin Hyman.

Pysklywec, R.N. & Mitrovica, J.X. (1999) The role of subduction-induced subsidence in the evolution of the Karoo Basin. *J. Geol.*, **107**, 155-164.

Raath, M.A. (1972) The Succession of Life in the Rhodesian Gondwana Period. *Detritus*, **7**, 11-19.

Ratcliffe, F.N.; Gay, F.J. & Greaves, T. (1952) Australian termites. Melbourne: Morris& Walker Pty. Ltd. (C.S.I.R.O.)

Reevers, C.C. (1970) Origin, classification, and geologic history of caliche on southern High Plain, Texas and eastern New Mexico. *J. Geol.*, **78**, 352-362.

Reid, I. & Frostick, L.E. (1994) Fluvial sediment transport and deposition. In: K. Pye (ed.): Sediment Transport and Depositional Processes. Oxford: Blackwell Scientific Publications, 89-155.

Reid, I. & Frostick, L.E. (1997) Channel form, flows and sediments in desert. In: D.S.G. Thomas (ed.): Arid Zone Geomorphology: Process, Form and Change in Drylands. Chichester: John Wiley & Sons Ltd., 2nd edition, 205-229.

Retallack, G.J. (1986) Fossil soils as grounds for interpreting long-term controls on ancient rivers. *J. Sedim. Petrol.*, **56**, 1-18.

Retallack, G.J. (1991) Soil of the past: an introduction to paleopedology. Hammersmith: HarperCollins Academic.

Roering, C.; van Reenen, C.A.; Barton Jr, J.M.; de Beer, J.H.; de Wit, M.J.; Stettler, E.H.; van Schalkwyk, J.F.; Stevens, G. & Pretorius, S. (1992) Tectonic model for the evolution of the Limpopo Belt. *Precambrian research,* **55**, 539-552.

Rosen, M.R. (1994) The importance of groundwater in playas: A review of playa classification and the sedimentology, hydrology of playas. In: M.R. Rosen (ed.): Paleoclimate and Basin Evolution of Playa Systems. Boulder, Colorado: Geological Society of America, Special Parer 289, 1-18.

Rowley, D.B. & Sahagian, D. (1986) Depth-dependent streching: a different approach. *Geology*, **14**, 32-35.

Rubidge, B.S.; Hancox, P.J. & Catuneanu, O. (2000) Sequence analysis of the Ecca-Beaufort contact in the southern Karoo of South Africa. *S.Afr.J.Geol.*, **103**, 81-96.

Rust, B.R. & Legun, A.S (1983) Modern anastomosing-fluvial deposits in arid central Australia,

and a Carboniferous analogue in New Brunswick, Canada. In: J.D. Collinson & J. Lewin (eds.): Modern and ancient fluvial systems. *Spec. Publs Int. Assoc. Sedim.*, **6**, 385-392.

Rust, I.C. (1975) Tectonic and sedimentary framework of Gondwana basins in southern Africa. In: K.S.W. Campbell (ed.): Gondwana Geology. Canberra: Australian National University Press, 537-564.

SAWB South African Weather Bureau (1999) Climate of South Africa, WB42. Climate statistics-1961-1990 (22°41`S & 31°1`E). Pretoria.

Scotese, C.R.; Boucot, A.J. & McKerrow, W.S. (1999) Gondwanan paleogeography and paleoclimatology. *J. Afr. Earth Sci.*, **28** (1), 99-114.

Semeniuk, V. & Meagher, T.D. (1981) Calcrete in quaternary costal dunes in southwestern Australia: a capillary-rise phenomenon associated with plants. *J. Sedim. Petrol.*, **51**, 47-68.

Shaw, P.A. & Thomas, D.S.G. (1997) Pans, playas and salt lakes. In: D.S.G. Thomas (ed.): Arid Zone Geomorphology: Process, Form and Change in Drylands. Chichester: John Wiley & Sons Ltd., 2nd edition, 293-317.

Skinner, E.M.W.; Clement, C.R.; Gurney, D.B.; Apter, D.B. & Hatton, C.J. (1992) The distribution and tectonic setting of South-African Kimberlites. *Russian Geology and Geophysics,* **33** (10), 26-31.

Slate, J.L.; Smith, G.A.; Wang, Y. & Cerling, T.E. (1996) Carbonate-paleosol genesis in the Plio-Pleistocene St. Davis Formation, Southeastern Arizona. *J. Sedim. Research*, **66**, 85-94.

Smale, D. (1972) Silcretes and associated silica diagenesis in southern Africa and Australia. *J. Sedim. Petrol.*, **43**, 1077-1089.

Smith, A.G. (1999) Gondwana: its shape, size and position from Cambrian to Triassic times. *J. Afr. Earth Sci.*, **28**, 239-261.

Smith, R.A. (1984) The lithostratigraphy of the Karoo Supergroup in Botswana. *Botsw. Geol. Surv. Dept., Bulletin,* **26**, 184-205.

Smith, R.M.H. (1995) Changing fluvial environments across the Permian-Triassic boundary in the Karoo Basin, South Africa and possible causes of tetrapod extinctions. *Palæogeogr., Palæoclimatol., Palæoecol.,* **117**, 81-104.

Smith, R.H.M.; Eriksson, P.G. & Botha, W.J. (1993) A review o the stratigraphy and sedimentary environments of the Karoo-aged basins of Southern Africa. *J.Afr. Earth Sci.*, **16**, 143-169.

Smith, R.M.H & Kitching, J. (1997) Sedimentology and vertebrate taphonomy of the *Tritylodon* Acme Zone: a reworked palæosol in the Lower Jurassic Elliot Formation, Karoo Supergroup, South Africa. *Palæogeogr., Palæoclimatol., Palæoecol.,* **131**, 29-50.

Sneh, A. (1984) Desert stream sequences in the Sinai Peninsula. *J. Sedim. Petrol.*, **53**, 1271-1279.

Söhnge P.G.; le Roex H.D. & H.J. Nel (1948) The geology of the country around Messina. An Explanation of Sheet No. 46, Department of Mines, Geol. Surv., p. 81.

Spotl, C. & Wright, V.P. (1992) Groundwater dolocretes from the Upper Triassic of the Paris Basin, France: a case study of an arid, continental diagenetic facies. *Sedimentology,* **39**, 1119-1136.

Stach, E.; Mackowsky, M.-Th.; Teichmuller, M.; Taylor, G.H., Chandra, D. & Teichmuller, R. (1975) Coal petrology. Berlin: Gebruder Borntraeger

Stagman, J.G. (1978) An Outline of the Geology of Rhodesia. *Rhodesia Geol. Surv. Bulletin,* **80**, p. 126.

Stavrakis, N. (1980) Sedimentation of the Katberg Sandstone and adjacent formtions in the south-eastern Karoo Basin. *Trans. Geol. S. Afr.*, **83**, 361-374.

Stear, W.M. (1983) Morphological characteristics of ephemeral stream channel and overbank splay sandstone bodies in the Permian Lower Beaufort Group, Karoo Basin, South Africa. *Spec.,* In: J.D. Collinson & J. Lewin (eds.): Modern and ancient fluvial systems. *Spec. Publs Int. Assoc. Sedim.,* **6**, 405-420.

Steel, R.J. (1974) New Red Sandstone floodplain and piedmont sedimentation in the Hebridean Province, Scotland. *J. Sedim. Pertol.,* **44**, 336-357.

Storey, B.C.; Alabaster, T.; Hole, M.J.; Pankhurst, R.J. & Wever, H.E. (1992) Role of subduction-plate boundary forces during the initial stages of Gondwana break-up: evidence form the proto-Pacific margin of Antarctica. In: B.C. Storey; T. Alabaster & R.J. Pankhurst (eds.): Magmatism and the Causes of Continental Break-up. *London: Geol. Soc. Spec. Publ.,* **68**, 149-163.

Storey, B.C.; Vaughan, A.M.J.; & Millar, I.L. (1996) Geodynamic evolution of the Antarctic Peninsula during Mesozoic times and its bearing on Wendell Sea history. In: B.C. Storey; E.C. King & L.A. Livermore (eds.): Wendell Sea Tectonics and Gondwana Break-up. *London: Geol. Soc. Spec. Publ.*, **108**, 87-103.

Summerfield, M.A. (1979) Origin and palæoenvironmental interpretation of sarsens. *Nature.,* **281**, 137-139.

Summerfield, M.A. (1982) Distribution, nature and probable genesis of silcrete in arid and semi-arid southern Africa. In: Yaalon, D.H. (ed.): Aridic soils and geomorphic processes. *Catena Suppl.,* **1**, 37-65.

Summerfield, M.A. (1983) Silcrete as a palaeoclimatic indicator: evidence from southern Africa. *Palæogeogr., Palæoclimatol., Palæoecol.,* **41**, 65-79.

Sutherland, D.G (1985) Geomorphological controls on the distribution of placer deposits. *J. Geol. Soc. London*, **142**, 727-737.

Swift, W.H. (1961) An Outline of the Geology of Southern Rhodesia. *Southern Rhodesia Geol.*

Surv. Bulletin, **50.**

Talbot, M. R.; Holm, K. & Williams, M.A.J. (1994) Sedimentation in low-gradient desert margin systems: A comparison of the Late Triassic of northwest Somerset (England) and the Late Quaternary of east-central Australia. *Geol. Soc. Amer., Spec. Paper*, **289**, 97-117.

Tandon, S.K. & Narayan, D.(1981) Calcrete conglomerate, case-hardened conglomerate and cornstone - a comparative account of pedogenic and non-pedogenic carbonates from the continental Siwalik Group, Punjab, India. *Sedimentology,* **28**, 353-367.

Theriault, P. & Desrochers, A. (1993) carboniferous calcretes in the Canadian Arctic. *Sedimentology*, **40**, 449-465.

Thirty, M. & Milnes, A.R. (1991) Pedogenic and groundwater silcretes at Stuart Creek Opal Field, South Australia. *J. Sedim. Petrol.*, **61**, 111-127.

Thirty, M. (1999) Diversity of continental silicification features: examples from the Cenozoic deposits in the Paris Basin and neighboring basement. *Spec. Publs Int. Assoc. Sedim.*, **27**, 87-127.

Thompson, A.O. (1975) The Karoo Rocks in the Mazunga Area, Beitbridge District. *Short Report No.* **40**, *Rhodesia Geol. Surv.*

Tirsgaard, H. & Øxnevad, I.E.I. (1998) Preservation of pre-vegetational mixed fluvio-aeolian deposits in a humid climatic setting: an example from the Middle Proterozoic Eriksfjord Formation, Southwest Greenland. *Sedim. Geol.,* **120**, 295-317.

Truter, F.C. (1945) The geology of a post-Karoo fault trough in the Zoutpansberg District, Transvaal. *Geol. Soc. S. Arf.*, **48**, 143-159.

Tucker, M.E. (1981) Sedimentary petrology An Introduction. Oxford: Blackwell Scientific Publication, p. 252.

Tunbridge, I.P. (1984) Facies model for a sandy ephemeral stream and clay playa complex; the Middle Devonian Trentishoe Formation of North Devon, U.K. *Sedimentology*, **31**, 697-715.

Turner, P. (1980) Continental red beds. Developments in Sedimentology **29**. Amsterdam: Elsevier Scientific Publishing Company

Turner, B.R. (1977) Fluviatile cross-bedding patterns in the Upper Triassic Molteno Formation of the Karoo (Gondwana) Supergroup in South Africa and Lesotho. *Trans. Geol. S. Afr.*, **80**, 241-252.

Turner, B.R. (1981) The occurrence and stratigraphic significance of bone-bearing mudstone pellet conglomerates from the Beaufort Group in the Jansenville District, Cape Province, South Africa. *Palæont. Arf.*, **24**, 63-73.

Turner, B.R. (1983) Braidplain deposition of the Upper Triassic Moteno Formation in the main

Karoo (Gondwana) Basin, South Africa. *Sedimentology,* **30**, 77-89.

Turner, B.R. (1984) Palaeogeographic implications of braid bar deposition in the Triassic Molteno Formation of the eastern Karoo Bsain, South Africa. *Palæont. Afr.,* **25**, 29-38.

Turner, B.R. (1999) Tectonostratigraphical development of the Upper Karoo foreland basin: orogenic unloading versus thermally-induced Gondwana rifting. *J. Afr. Earth Sci.*, **28**, 215-238.

Turner, B.R. & Minter, W.E.L. (1985) Diamond-bearing upper Karoo fluvial sediments in NE Swaziland. *J. Geol. Soc. London,* **142**, 765-776.

Turner, B.R. & Thomson, K. (1998) Tectonostratigraphical development of the Upper Karoo foreland basin: orogenic unloading versus Gondwana rifting. Implication for the Mesozoic evolution of the Falkland Plateau and West Gondwana. *J. Afr. Earth Sci.*, **27** (1A), 201-202.

Vail, J.R.; Hornung, G. & Cox, K.G. (1969) Karoo basalts of the Tuli Syncline, *Rhodesia Bull. Volcan.*, **33**, 398-418.

van der Berg, H.J. (1980) Die sedimentologie van die Soutpansberg-steenkoolveld met spesiale verwysing na steenkoolvorming .Unpublished M.Sc. Thesis, Bloemfontein: University of Orange Free State.

van Dijk, D.E.; Hobday, D.K. & Tankard, A.J. (1978) Permo-Triassic lacustrine deposits in the Eastern Karoo Basin, Natal, South Africa. *Spec. Publs Int. Assoc. Sedim.*, **2**, 225-239.

van Eeden, O.R. (1968) Die Ontstaan van Silindervormige Structure in die Holkranssandsteen. *Ann. Geol Surv. S. Afr.*, **7**, 81.

van Eeden, O.R.; Visser, H.N. & van Zyl, J.S. (1955) The geology of the eastern Soutpansberg and the Lowveld to the north. An Explanation of Sheet No. 42 Department of Mines, Geol. Surv. S. Afr.

van Eeden, O.R. & Keyser, A.W. (1971) Fossielspore in die Holkranssandsteen op Pont Drift, Distrik Southpansberg, Transvaal. *Ann. Geol Surv. S. Afr.,* **9**, 135-137.

van Reenen, D.D.; Roering, C.; Ashwal, L.D. & de Wit, M.J. (1992) Regional geological setting of the Limpopo Belt. *Precambrian Research*, **55**, 1-5.

Veevers, J.J.; Cole, D.I. & Cowan, E.J. (1994) Southern Africa: Karoo Basin and Cape Fold Belt. In: J.J. Veervers & McA. Powell: Permian-Triassic Pangean Basins and Foldbelts Along the Panthalassan Margin of Gondwanaland. *Geol. Soc. of America*, Memoir **184**, 223-280.

Visser, J.N.J (1984) A review of the Stromberg Group and Drakensberg Volcanics in Southern Africa. *Palæont. Afr.,* **25**, 5-27.

Visser, J.N.J. & Botha, B.J.V. (1980) Meander belt, point bar, crevasse splay and aeolian deposits from the Elliot Formation in Barkly Pass, northeastern Cape. *Trans. Geol. S. Afr.*, **83**, 55-62.

Walker, R.G. (1992) Facies, facies models and modern stratigraphic concepts. In: R.G. Walker & N.P. James (eds.): Facies Models: Response to Sea Level Change. Geol Assoc of Canada,1-15.

Warren, J.K. (1983) Pedogenic calcrete as it occurs in quaternary calcareous dunes in costal South Australia. *J. Sedim. Petrol.*, **53**, 787-796.

Warren, A. & Damiani, R. (1999) Stereospondyl amphibians from the Elliot Fromation of South Africa. *Palaeont. Afr.*, **35**, 45-54.

Watkeys, M.K. (1979) Explanation of the Geological Map of the Country west of Bietbride - Salisbury, *Short Report,* **45**, *Rhodesia Geol. Surv.*

Watkeys, M.K. & Sweeney, R.J. (1988) Tuli-Lebombo volcanism and Gondwana rifting Extended abstracts - Geocongress '88, Durban: University of Natal, **38**, 725-728.

Watts, S.H. (1978) A petrographic study of silcrete from inland Australia. *J. Sedim. Petrol.*, **48**, 987-994.

Weibel, R. (1998) Diagenesis in oxidising and locally reducing conditions - an example from the Triassic Skagerrak Formation, Denmark. *Sedim. Geol.*, **121**, 259-276.

Wells, N.A. (1983) Transient streams in sand-poor redbeds: early-Middle Eocene Kuldana Formation of northern Pakistan. In: J.D. Collinson & J. Lewin (eds.): Modern and ancient fluvial systems. *Spec. Publs Int. Assoc. Sedim.*, **6**, 393-403.

Wilson, A.H. (1970) Fossil plant sites in the Karoo Molteno Series, the Border Road, Binga District. *Detritus.*, **6**, 31-32.

White, B. & Curran, H.A. (1988) Mesoscale physical sedimentary structures and trace fossils in Holocene carbonate eolianites from San Salvador Island, Bahamas. *Sedim. Geol.*, **55**, 163-184.

White, R.S. & McKenzie, D.P. (1989) Magmatism at rift zones: the generation of volcanic continental margins and flood basalts. *J. Geophys. Res.*, **94**, 7685-7729.

Wopfner, H. (1978) Silcretes of northern South Australia and adjacent regions. In: T. Langford-Smith (ed.): Silcrete in Australia. Armidale: Department of Geography, University of New England, 93-141.

Wopfner, H. (1983) Environment of silcrete formation: a comparison of examples from Australia and the Cologne Embayment, West Germany. In: R.L.C. Wilson (ed.): Residual deposits: surface related weathering processes and materials. Geol. Soc. Spec. Publ. Oxford: Blackwell Scientific Publication, 151-158.

Wright, P.V. (1990) Estimating rates of calcrete formation and sediment accretion in ancient alluvial deposits. *Geol. Mag.*, **127**, 273-276.

Wright, V.P. & Tucker, M.E. (1991) Calcretes: an introduction. In: V.P. Wright & M.E. Tucker (eds.): Calcretes. *Int. Assoc. Sedim. Reprint Series.*, **2**, 1-22.

COLOURED PLATES

LIST OF PHOTOS

*The brackets contain the farm name where the figure was drawn.

Photo	Plate
Photo 24. Laterally continuous, laminated (**Sh**) sandstone bed (20 cm) in finely laminated, grey mudstone (**Fl**) (Weltevreden).	5
Photo 25. Thinly bedded, horizontally laminated (**Sh**) sandstones (Weltevreden).	5
Photo 26. Sharp-based sandstones tend to have lenticular shape as well (upper middle part of the photo) (Montaqu).	5
Photo 27. Laterally continuous, horizontally laminated (**Sh**) sandstones are rarely interbedded with planar-cross stratified (**Sp**) sandstones (Roly Poly)	5
Photo 28. Water-escape structure in otherwise massive sandstone (Weltevreden).	5
Photo 29. Matrix supported breccias (**Gmm**) occur at the base of the fining upward cycles. They pass into massive sandstones (**Sm**). Also note the cross-bedded sandstone (**Sp**) lense below the camera cap (Weltevreden).	6
Photo 30. Lithofacies **Sm** with outsized vein quartz boulder (Roly Poly).	6
Photo 31. Quartz vein crossing basement gneisses (Roly Poly).	6
Photo 32. Lithofacies **Gh**. Crudely bedded conglo-breccias passing into Sh sandstones. For scale see camera cap in the centre (Ammondale).	6
Photo 33A & B. Lithofacies **Gcm**. Clast-supported, massive conglomerates (**A** - Ammondale) and conglo-breccias (**B** - Montaqu).	7
Photo 34. Lithofacies **Gcm**. Occasionally the matrix content may become higher in places (Roly Poly).	7
Photo 35. Lithofacies **Fl** and **Fsm**. The laminated and massive mudstones and siltstones are rarely well exposed (Regina). The rectangle is 2 m high at the bottom of the outcrop.	8
Photo 36. Poorly preserved impressions of *Glossopteris sp.* (Lizzulea).	8
Photo 37. Well-defined horizontal lamination in micaceous, muddy and sandy siltstones (**Fl**). Height of the cliff is ~0.7 m (Eendvogelpan).	8
Photo 38. Lithofacies **Fb**: ball-and-pillow structured siltstones and mudstones (lower part of the picture) (Roly Poly).	8
Photo 39. Tongue-shaped pebbly mudstones (**Fp**), muddy sandstones (**Sf**) and sandy mudstones (**Fs**) in massive mudstones (**Fsm**). Height of the scrub is ~1.2 m (Stembok).	9
Photo 40. Sausage-shaped pebbly mudstones (**Fp**), muddy sandstones (**Sf**) in laminated silty-mudstones (**Fl**)(Weltevreden).	9
Photo 41. Roll-shaped pebbly mudstones (**Fp**), muddy sandstones (Sf) and sandy mudstones (**Fs**) in massive mudstones (**Fsm**) (Stembok). The hammer lies in the continuation of a "roll".	9
Photo 42. Erosive furrow filled by muddy sandstone (**Sf**) (Stembok).	9
Photo 43. Weak normal grading at the bottom of a lobe (Stembok).	9
Photo 44. The lobes of the **Fp**, **Sf** and **Fs** lithofacies are continuous for 3-4 m (Stembok).	9
Photo 45. Erosional surface (dashed and arrowed line) separating the carbonaceous mudstones of the Basal Unit from the overlying Middle Unit (20 cm conglomerate and 30 cm massive, medium grained sandstone (Somerville).	10

Photo	Plate
Photo 46. Erosional surface separating the laminated, carbonaceous mudstones of the Basal Unit from the overlying Middle Unit (20 cm conglomerate and 25 cm massive, medium grained sandstone) (Lizzulea).	10
Photo 47. Reddish-brown sandstones and conglomerates of the Middle Unit (Eendvogelpan).	10
Photo 48. Soft sediment deformation (convolute bedding) in otherwise laminated (**Sh**) sandstone. Pencil for scale (Middle Unit, lower part, Over Vlakte).	10
Photo 49. Horizontally bedded conglomerates (**Gh**). Height of the cliff ~ 2 m (Eendvogelpan).	10
Photo 50. Subrounded pebbles of quartzite and vein quartz (Bismarck).	10
Photo 51. Laminated (**Fl**) and ripple-cross laminated (**Sr**) silty, very fine grained sandstone (Breslau).	11
Photo 52. Ripple-cross laminated (**Sr**) siltstone (Breslau).	11
Photo 53. Ripple-cross laminated (**Sr**) very fine grained sandstone (Halcyon).	11
Photo 54. Well-bedded, thin (12-20 cm) layer of silty, very fine grained sandstone (Breslau).	11
Photo 55A & B. Convolute lamination (**A**) and water escape structures (**B**) in silty, very fine grained sandstone (Eendvogelpan).	12
Photo 56. Lower bedding plane of a siltstone bed showing the remains of the underlying conglomerate bed with rip-up clasts (Halcyon).	12
Photo 57. Transitional zone containing small pebble, granule sized rip-up clasts. The lower part of the overlying siltstone bed is ripple-cross laminated, the upper part is massive (Halcyon).	12
Photo 58. Lithofacies **Sm**. Except for the bed in the front (Sh), all the beds in the picture are lacking internal bedding structures (Edmonsburg).	13
Photo 59. Lithofacies **Sh** (Nekel).	13
Photo 60 A & B. Well preserved cosets of lithofacies **St** (Faure). Flow direction from left to right. Note the numerous 1st and 2nd order bounding surfaces.	13
Photo 61. Lithofacies **St** (Hamilton).	13
Photo 62. Lithofacies **Sp** in coarse sand (Montrow). Flow direction from right to left. Note that the beds are slightly tilted in the paleoflow direction.	13
Photo 63. Lithofacies **Sr**. The ripple cross-lamination in the bed under the notebook is characterized by many small scale scour surfaces resulting in the poor preservation of the ripple form (type A) (Lizzulea).	14
Photo 64A, B & C. Lithofacies **Sr**. The ripples in these beds are characterized by the preserved lee sides and truncated stoss sides of the ripples (type B). Flow direction in the first two pictures toward the right, in the **C** toward the left (Edmonsburg, Lizzulea).	14
Photo 65A & B. Delicate concave-up mud curls (**A**) and semi-orthogonal pattern of the mudcracks (**B** - on the bedding surface) (Weipe).	14
Photo 66A, B, C, D & E. Burrowing features (for explanation see Ch. 4.2.4.2.) (Weipe, Halcyon, Ratho, Blyklip, Weipe).	15

Photo	Plate
Photo 67. Vertebrate tracks (Schroda). The footprints are average 3.5 cm long, and appear to have been made by a small four-toed animal(s), although most of the prints show only four or three digits. One of the footprints shows that the digits clearly ended in claws, but in the rest of the tracks the digits just thin towards the toe tip. The minimum distance between two adjacent print is 3 cm, while the maximum distance is about 6 cm.	15
Photo 68A & B. Unidentified features on bed surfaces (Kilsyth, Weipe).	16
Photo 69. Broken bone fragment in sandstone (Schroda SW).	16
Photo 70. Laterally continuous sandstone beds. Note the tabular, non-channelized geometries. The three Laminated Sand Sheet (**LS**) architectural elements bounded by 5th order surfaces are best visible in the middle of the picture. Height of the cliff is ~20 m (Blyklip).	17
Photo 71. Tabular, thin sandbodies (Lareve).	17
Photo 72. Tabular, thick sandbodies (Weipe). Scale the ~2 m thick bush on the top of the ridge.	17
Photo 73. Superimposed sheets of sandstone. Lower part of a fining upward cycle (architectural element **LS**). Note that although most of the beds are tabular, there are wedge shaped sandstones as well (Hartebestfontein).	17
Photo 74. Slightly upward fining cycles (architectural element **LS**). The picture on the left shows at least 2.5 cycles. The first two cycles are fully developed with strongly vegetated upper parts (Parma). The cycles in the right photo have no fine grained upper part (Hillstone).	18
Photo 75. Three succeeding, laterally continuous cycles (architectural element **LS**), each about 6 m thick. The dashed lines are 5th order bounding surfaces. Notebook for scale (Reidel- NW).	18
Photo 76A & B. Superimposed sheets of sandstone with non-channelized bases (architectural element **LS**). In **B**, the total height of the cliff is ~8 m (Weipe, Riedel).	18
Photo 77. Base of a fining-upward cyclotheme commencing with a shallow scour and very fine, rip-up sandstone and mudstone clasts. The size, roundness as well as the identical lithologies of the clast and the underlying laminated bed indicates that the clasts were torn up and transported from the immediate vicinity. Note lithofacies differences below and above the surface (5th order) (Edmondsburg).	19
Photo 78A & B. Poorly sorted, clast supported (**Gcm**) intraformational conglomerates mainly consist of granule to pebble grade white, well rounded carbonate concretions, septaria and nodules (Nekel).	19
Photo 79A & B. White to reddish, subangular to subrounded mudstone particles in poorly sorted, massive, clast supported (**Gcm**) intraformational conglomerates (Vergenoegd).	19
Photo 80. Red, subangular to subrounded sandstone clasts. The 8 cm long pebble in the middle is bioturbated. The other red clasts in the upper right are bone fragments (Blyklip).	19
Photo 81A & B. Reddish, isolated, broken and abraded bone fragments contribute to the subangular, subrounded clast fraction of the conglomertes (Montrow).	20
Photo 82. Some 10 cm large pebbles in poorly sorted conglomerates. At this location a 25 cm pebble was also found (Nekel).	20
Photo 83. Lithofacies **Gcm**: massive, clast supported intraformational conglomerates (Blyklip)	20
Photo 84. Lithofacies **Gh**: slight horizontal layering in the intraformational conglomerates (Montrow).	21
Photo 85. Lithofacies **Gp, Gt**: cross-bedding. Lower part of the picture shows layer of **Gp** being overlain by a faddishly, through cross-bedded (**Gt**) conglomerate (Lareve).	21

Photo	Plate
Photo 86. Lithofacies **Gh**: in slight horizontal stratification defined by normal grading (Lizzulea).	21
Photo 87. Lithofacies **Gcm** being directly overlain by ripple cross-laminated (**Sr**) very fine sandstones (Blyklip).	21
Photo 88. Thickly bedded argillaceous rocks. The upper part of the picture shows the thickly bedded sandstones of the Clarens Formation. The hard silcrete horizon is between the last white, thick argillaceous bed and the first yellow-brown, very thick, sharp based sandstone bed (Ratho - Boscamp).	22
Photo 89. Greyish-greenish and reddish thickly bedded argillaceous rocks. The upper part of the picture shows the thickly bedded sandstones of the Clarens Formation. The height of the cliff is ~20 m (Greefswald - near Mapungubwe).	22
Photo 90. Blotchy colour mottling in massive, thickly bedded argillaceous rocks. Hammer for scale (Hilda).	22
Photo 91. Equidimensional, centimeter-scale angular to subangular blocks of greenish mudstone. Hammer rest on 0.4 m thick, greenish silcrete layer underlying the sandstones of the Clarens Formation (Machete).	22
Photo 92. Well preserved, circa 20 m high outcrop of the argillaceous sediments. Note the contrasting red and greyish-greenish colouration of the beds and also the prominent, white silcrete horizon sharply separating the mudstones and yellow-brown sandstones of the Clarens Formation (Parma - Tsolwe).	22
Photo 93. Irregular and crudely cylindrical and spherical carbonate glaebules in horizontal and sub-horizontal position. The hammer is 28 cm long (the millipede - lower left is very large). The host rock is red, carbonaceous, massive muddy siltstone (**Fs**) with very fine sand grains. (Parma - Tsolwe).	23
Photo 94. Vertically orientated carbonate glaebules with framboidal texture. The notebook (19 cm) rests on a coalesced carbonate glaebule horizon. The surrounding host rock is green, carbonaceous, massive (**Fs**) muddy siltstone with very fine sand grains. Note the spot of relict lamination (**Fl**) (Breslau - Show of Rhodes). Compare this picture with *Photo 150* showing contemporaneous carbonate glaebules with framboidal texture.	23
Photo 95. Large, twined carbonate concretion (notebook length 19 cm) in red, locally carbonaceous, massive silty-sandy host rock (**Fsm**). (Breslau - Pyramid Koppie).	23
Photo 96A & B. Septaria in massive, green mudstone (Machete).	23
Photo 97. Carbonate accumulations with gradational lower and sharp upper contacts within thickly bedded silty mudstones (Parma - Tsolwe).	24
Photo 98. Continuous, coalesced glaebule horizons within thickly bedded silty mudstones (Parma - Tsolwe).	24
Photo 99. Meshwork of mainly horizontal white calcite veins and pseudo-folded carbonate layers (Modena).	24
Photo 100. In situ fossilised and articulated vertebrate limb bones in siltstones of Upper Unit (Armenia).	24
Photo 101A, B, C, D, E & F. In situ vertebrate remains showing little or no abrasion. Note the perimineralization with haematite (*A, E, F* - Armenia; *B* - Little Muck; *C, D* - Balerno).	25

Photo	Plate
Photo 102A, B, C & D. Single disarticulated, abraded bone fossils (*A, B* - Balerno; *C* - Machete) and bone bed within equidimensional, centimeter-scale angular to subangular blocks of greenish mudstone (*D* - Armenia).	26
Photo 103. Lithofacies **Sh** in sheet like sandbodies (Lizzulea).	27
Photo 104. Lithofacies **Sp** in sheet like sandbodies (Montrow).	27
Photo 105. Sheet-like sandbodies within sharp lower surfaces (Lizzulea).	27
Photo 106. Laterally continuous, thick, tabular sandbodies with planar upper surfaces grading into laminated or bioturbated mudstone (Lizzulea).	27
Photo 107A & B. Thin and narrow sandstones with wedge (**A** - Montrow) and lens (white parts in **B** - Ratho) shapes are isolated as single beds in thick, massive or laminated, red mudstones.	28
Photo 108A & B. Multiple sandstone and mudstones forming laterally continuous superimposed sheets (Hilda SW).	28
Photo 109. Lithofacies **Gmm** (Schroda).	29
Photo 110. Lithofacies **Sc** surrounding irregularly shaped Gcm and Gmm beds. Note the rare relict lamination (**Fl**) in the otherwise massive silty mudstones (**Fsm**) (upper left), as well as the clay coating of the breccia clasts (Balerno - Tolwe).	29
Photo 111. Two sheet-like layers of intraformational conglomerates (**Gh**) in red, laminated and massive mudstones (**Fl, Fsm**) (Montrow).	29
Photo 112. Well preserved fossil bone at the top of a **Gh** layer (Montrow).	29
Photo 113. Large-scale cross-stratification. Height of the cliff is ~15 m (Pont Drift).	30
Photo 114. Giant cross-beds. Notebook length is 19 cm (Parma).	30
Photo 115. Finely laminated foresets of giant cross-beds (Parma).	30
Photo 116. Alined, connected, crescent-shaped cross-stratified sandstones resembling rows of barchanoid ridges. Foreset dip direction to left. Note the vegetated shallow hollows between the bedforms (Hillstone).	30
Photo 117. Alined, connected, crescent-shaped cross-stratified sandstones resembling rows of barchanoid ridges. Foreset dip direction from the viewer to the scale. The dark zone in the background is a lava flow (Greefswald).	30
Photo 118. Well-developed tangential bottom sets in cross-stratified, crescent-shaped sandstones. Hammer for scale (Hillstone).	31
Photo 119. Third order surfaces between cosets of cross laminae (see arrow). The picture shows two separate dunes with forsets dipping form the viewer's right to the left corner of the pictures (Balerno - Tsolwe koppie).	31
Photo 120. Rare second order bounding surfaces separating the lower, thick set of crossbeds from smaller bedforms. Height of the cliff is ~25 m (Balerno, Tsolwe koppie).	31
Photo 121. Reactivation (2nd order) surface separating cosets of slightly different dip directions. See arrow pointing at the notebook (19 cm) (Parma).	31
Photo 122A & B. Sharp, low-relief first order bounding surfaces (dashed line). See arrow at the third order surfaces. Person for scale (Balerno).	32

Photo	Plate
Photo 123. Lenticular beds of horizontal laminated (Sh), 0.2-1 m thick sandstones. Person for scale (Greefswald).	32
Photo 124A & B. Silicified fossil woods found on the surface of the Clarens Formation sandstones. It was identified as *Agathoxylon sp.* (= *Dadoxylon sp.*) (Parma).	33
Photo 125. Large scale trace fossils (*Type A*) showing lateral bifurcations (Schroda).	33
Photo 126. Large scale horizontal trace fossils (*Type A*) (Hillstone).	33
Photo 127. Vertical, cylindrical pipes with open apex (*Type A* trace fossils)(Hillstone).	33
Photo 128. Simple, mostly vertical shafts-like trace fossils frequently intersect the entire, 0.15-0.25 m thick host bed (*Type B*)(Weipe & Schroda).	33
Photo 129. Simple, isolated, unbranched trace fossils (*Type B*)(Machete).	33
Photo 130. Digit-like (giant finger-like), vertical trace fossils (*Type C*). Note the twinned structures and person sitting in the 0.5 m wide saddle between the two digits (Greefswald).	34
Photo 131. Close up of the wall of the digit-like structure showing extensive branching with random orientation (*Type C*). Person for scale (Greefswald).	34
Photo 132. Polished slab showing non-meniscate tubes and the central shapt of the digit-like structures (Greefswald).	34
Photo 133. Rare upward bifurcation (in the center of the photo) (*Type C*). Person for scale (Greefswald).	34
Photo 134. Dome-like elevations at the base of the digit-like structures is heavily bioturbated (*Type C*) (Greefswald).	34
Photo 135. Recent columnar termite nests are rather common in the study area (Ammondale).	34
Photo 136A & B. Carbonate glaebules in indurated sandstones found in immediate vicinity of dolerite dykes (**A** - Parma; **B** - Lareve).	35
Photo 137A & B. Dolerite dyke intrusions in sandstones. **A** - Indurated and bleached sandstones on the sides of a large dyke (Parma); **B** - The young boy stands on the bleached, white boundary between the dyke (right) and the muddy red sandstones (left) (Lareve).	35
Photo 138. Small scale fold-like structure in indurated sandstone. The structure is above the geological hammer (circled). The outcrop is the inner, near vertical wall of a parallel, double crested sandstone ridge flanking a dolerite dyke which being less resistant, had been eroded away.	35
Photo 139. Botryoidal fabric of coalesced silcrete glaebules forming brittle, massive horizon (Breslau - Show of Rhodes).	35
Photo 140. Massive silcerete with internally massive, rough surfaced tubules (see arrow). The tubule in the centre of the picture has a very small white walled central hollow.	35
Photo 141. Massive silcerete with irregular to tunnel or pipe like hollows and pits.	36
Photo 142. Massive silcerete with voids that show millimeter thin walls of microquartz and/or cryprocrystalline silica. Well developed in the upper part of the picture.	36
Photo 143. Gradational silcrete with laterally discontinuous silica laminations in the red silty-mud host rock.	36

Photo	Plate
Photo 144. Gradational silcrete with clay coated silicified host rock lumps and lenses in the transitional lower part.	36
Photo 145. Gradational silcrete with clay coated silicified host rock lumps grading into massive, cavernous silcrete.	36
Photo 146. Rapid sheet flow during an early summer storm (Montrow/Breslau border).	37
Photo 147. Large dessication cracks developed in thick mud (Halcyon dam).	37
Photo 148. Contemporaneous example of shallow hollows and rainstorm eroded gullies of an otherwise flat, muddy floodplain surface. Picture shows the interchannel area of ephemeral stream system of the study area. Note the sparse vegetation and the patches of coarse, loose sediments in the foreground (Montrow).	37
Photo 149. Contemporaneous rainstorm erosion feature developed in laminated mudstone. Also note the angular sandstone slabs lying on the dry gully floor (This picture was taken at Brosterlea, near Molteno, South Africa. Similar features are common in the study area too). Scale 20 cm.	37
Photo 150. Contemporaneous carbonate glaebules with framboidal texture. Compare this picture with *Photo 94.*	37

INTRODUCTION

Photo 1. The gentle slopes of the argillaceous Upper Unit are strewn with large blocks of sandstone that commonly form the bluff of the hills. The more resistant sandstone typically forms scarp slopes.

BASAL UNIT

Photo 2. Lithofacies **Gmm**. Large clasts of angular, subangular vein quartz, quartzite, weathered gneisses and micro-granites set in mainly structureless, greyish muddy matrix (Ammondale)*

*The brackets contain the farm name where the figure was drawn.

Photo 3. Lithofacies **Gmm**. Occasionally the yellowish-brown and greyish muddy matrix may be slightly laminated (upper half of the picture). Note the almost vertical orientation of the angular blade shaped clast (upper center). The clast is surrounded by slickenslide surfaces (Ammondale).

Photo 4. Lithofacies **Gmm**. Slightly lamination in yellowish-brown sandy (Ammondale).

Photo 5. Lithofacies **Gmm**. Very large angular gneiss particle in muddy, massive matrix (bottom left corner)(Roly Poly).

Photo 6. Lithofacies **Gmm**. Poorly-sorted breccia with randomly orientated clasts (Ammondale).

1.

2.

3.

4.

5.

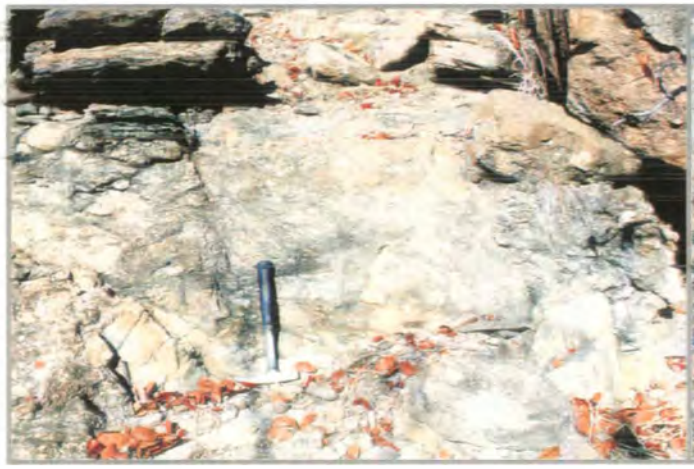

6.

Plate 1

Photo 7. Lithofacies **Gcm**. Closely packed, angular to subangular, rarely subrounded vein quartz, quartzite (~95-100%) and rarely weathered gneisses (~0-5%) clasts (Ammondale).
Photo 8. Lithofacies **Gcm** with outsized quartz clasts (Kilgour).
Photo 9. Lithofacies **Gcm** with outsized gneisses clasts (left center). Note the black quartzite clast too (right center) (Drumsheugh).
Photo 10. A 30 cm layer of lithofacies **Gcm** with hardly visible bedding, defined by flat clasts. It is underlain by gneisses and overlain by a pebbly mudstone (Fp) strata which is succeeded by sandstones (Drumsheugh).
Photo 11. Lithofacies **Gmm** is rarely associated with sandstones (Kilgour).
Photo 12. Breccias, conglo-breccias in a small, isolated "pocket". The **Gmm** matrix supported is overlain by the sandstone facies assemblage forming a fining upward cycle (Ammondale).

7.

8.

9.

10

11.

12

Plate 2

Photo 13. Lithofacies **Sp.** The large scale foresets of the most abundant lithofacies in the sandstone facies assemblage indicate flow direction from left to right (Roly Poly).
Photo 14. Sequence of lithofacies **Sh-Sp-Sl**. Scale: the lower (Sh) bed is 20 cm thick (Montaqu).
Photo 15. Lithofacies **Sr.** Asymmetric, sinuous-crested ripples in fine sandstone (Weltevreden).
Photo 16. Lithofacies **Sr.** Asymmetric, straight-crested ripples in fine sandstone (Weltevreden).

13.

14.

15.

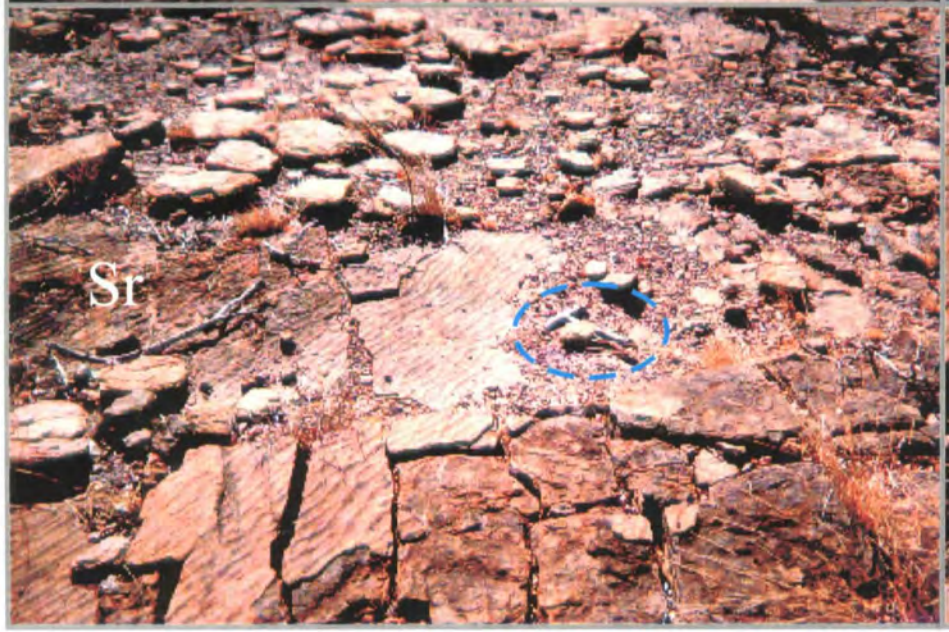

16.

Plate 3

Photo 17. Fining upward cycle (Ammondale).
Photo 18. Upward decrease in the bed thickness (and in grain size and sedimentary structures as well). Note the frequent erosion surfaces (both straight and inclined) (Roly Poly).
Photo 19. Convex-up erosion surface in thickly bedded sandstone (Weltevreden).
Photo 20. Laterally continuous, thickly bedded sandstones (Weltevreden).
Photo 21. Thickly bedded sandstones succeeded by lenses and wedges of thinly bedded sandstones (Onrust).
Photo 22. Tabular, thinly bedded sandstones (Weltevreden).

17.

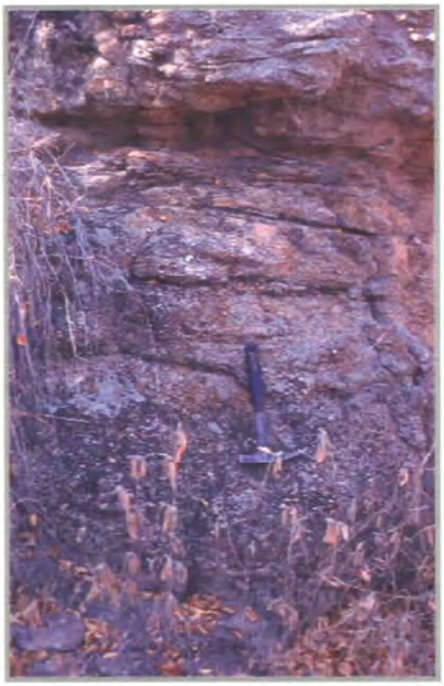

18.

20.

19.

21.

22.

Photo 23. Lithofacies **Sb.** Kidney shaped sandstone bodies form ball-and-pillow structures (Montaqu).
Photo 24. Laterally continuous, laminated (**Sh**) sandstone bed (20 cm) in finely laminated, grey mudstone (**Fl**) (Weltevreden).
Photo 25. Thinly bedded, horizontally laminated (**Sh**) sandstones (Weltevreden).
Photo 26. Sharp-based sandstones tend to have lenticular shape as well (upper middle part of the photo) (Montaqu).
Photo 27. Laterally continuous, horizontally laminated (**Sh**) sandstones are rarely interbedded with planar-cross stratified (**Sp**) sandstones (Roly Poly)
Photo 28. Water-escape structure in otherwise massive sandstone (Weltevreden).

23.

24.

25.

26.

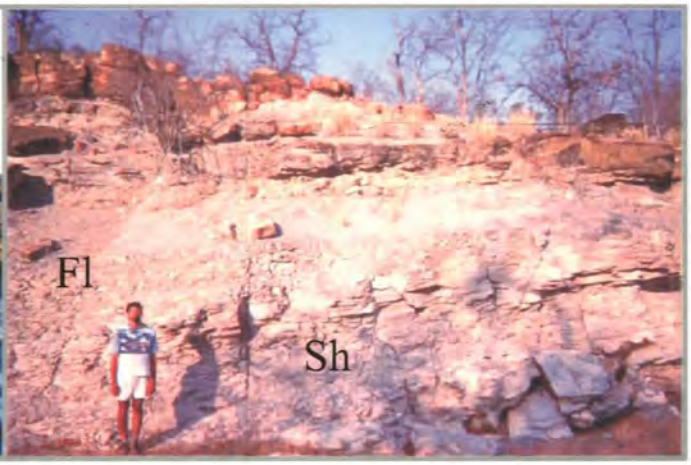

27.

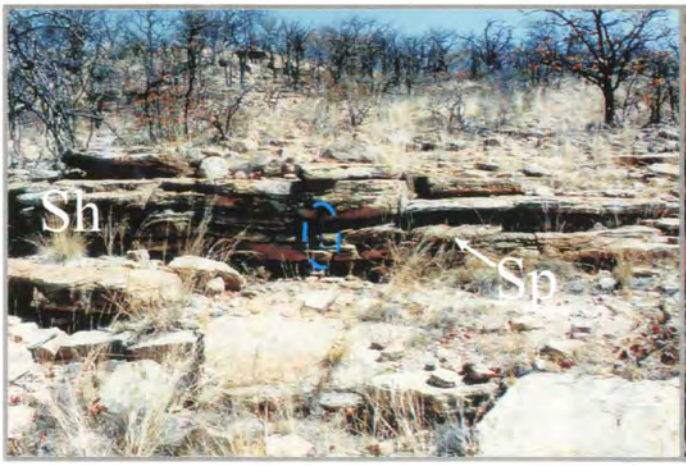

28.

Photo 29. Matrix supported breccias (**Gmm**) occur at the base of the fining upward cycles. They pass into massive sandstones (**Sm**). Also note the cross-bedded sandstone (**Sp**) lense below the camera cap (Weltevreden).
Photo 30. Lithofacies **Sm** with outsized vein quartz boulder (Roly Poly).
Photo 31. Quartz vein crossing basement gneisses (Roly Poly).
Photo 32. Lithofacies **Gh**. Crudely bedded conglo-breccias passing into Sh sandstones. For scale see camera cap in the centre (Ammondale).

29.

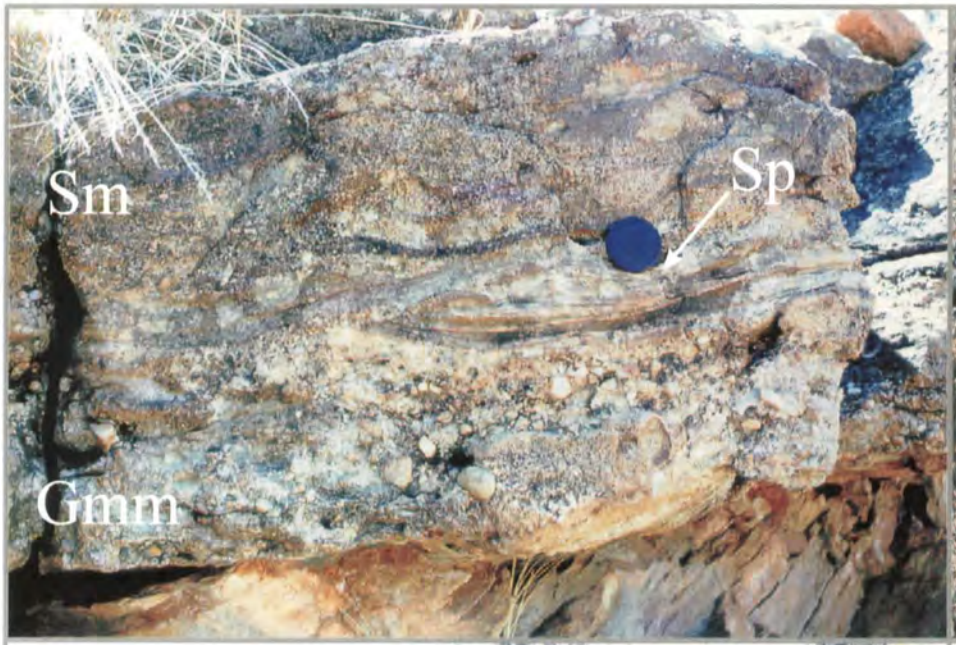

30.

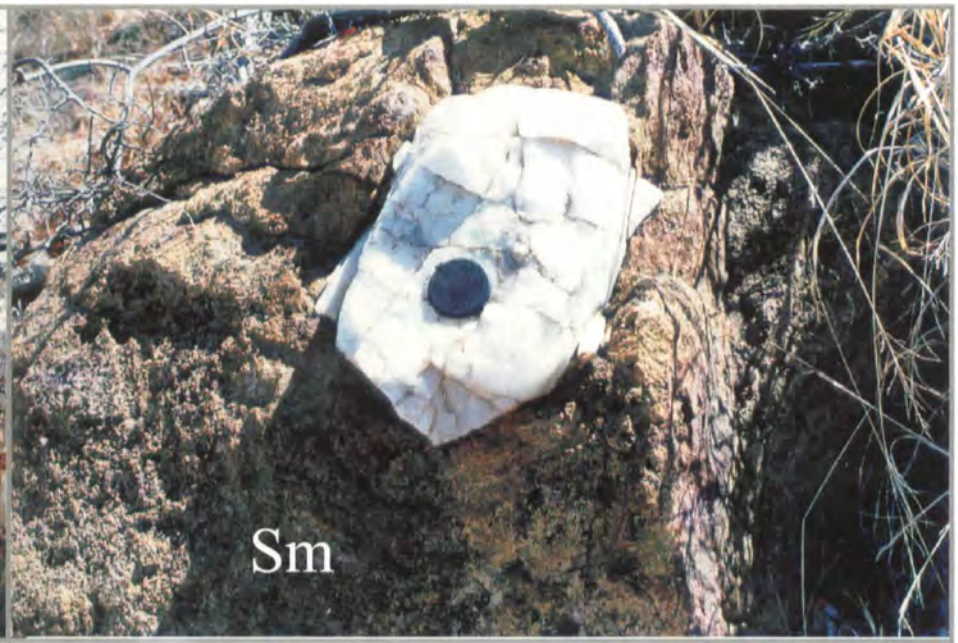

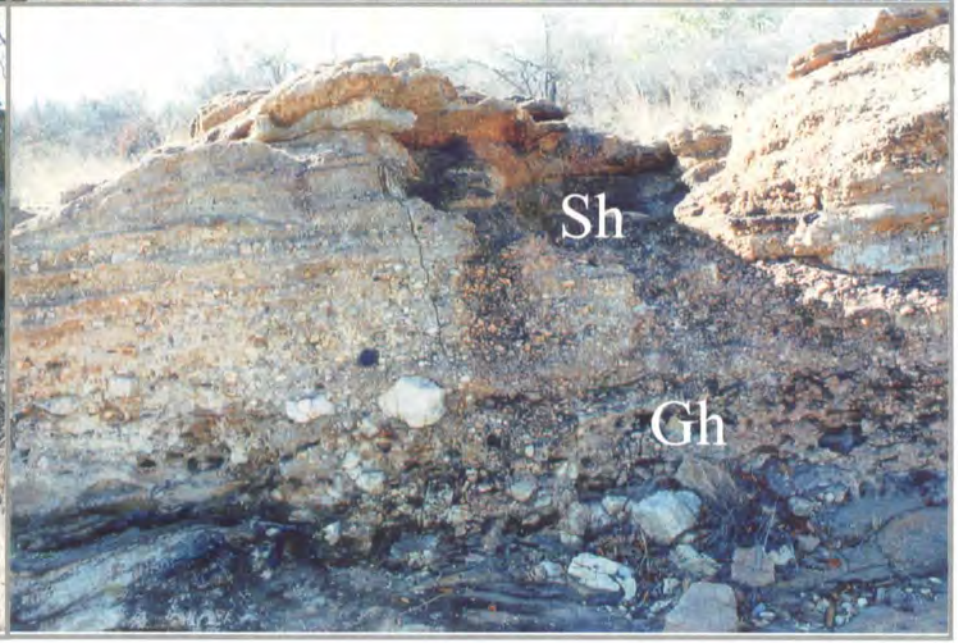

31.

32.

Plate 6

Photo 33A & B. Lithofacies **Gcm**. Clast-supported, massive conglomerates (**A** - Ammondale) and conglo-breccias (**B** - Montaqu).
Photo 34. Lithofacies **Gcm**. Occasionally the matrix content may become higher in places (Roly Poly).

33A.

33B.

34.

Plate 7

Photo 35. Lithofacies **Fl** and **Fsm**. The laminated and massive mudstones and siltstones are rarely well exposed (Regina). The rectangle is 2 m high at the bottom of the outcrop.
Photo 36. Poorly preserved impressions of *Glossopteris sp.* (Lizzulea).
Photo 37. Well-defined horizontal lamination in micaceous, muddy and sandy siltstones (**Fl**). Height of the cliff is ~0.7 m (Eendvogelpan).
Photo 38. Lithofacies **Fb**: ball-and-pillow structured siltstones and mudstones (lower part of the picture) (Roly Poly).

35.

36.

37.

38.

Plate 8

Photo 39. Tongue-shaped pebbly mudstones (**Fp**), muddy sandstones (**Sf**) and sandy mudstones (**Fs**) in massive mudstones (**Fsm**). Height of the scrub is ~1.2 m (Stembok).
Photo 40. Sausage-shaped pebbly mudstones (**Fp**), muddy sandstones (**Sf**) in laminated silty-mudstones (**Fl**)(Weltevreden).
Photo 41. Roll-shaped pebbly mudstones (**Fp**), muddy sandstones (Sf) and sandy mudstones (**Fs**) in massive mudstones (**Fsm**) (Stembok). The hammer lies in the continuation of a "roll".
Photo 42. Erosive furrow filled by muddy sandstone (**Sf**) (Stembok).
Photo 43. Weak normal grading at the bottom of a lobe (Stembok).
Photo 44. The lobes of the **Fp**, **Sf** and **Fs** lithofacies are continuous for 3-4 m (Stembok).

39.

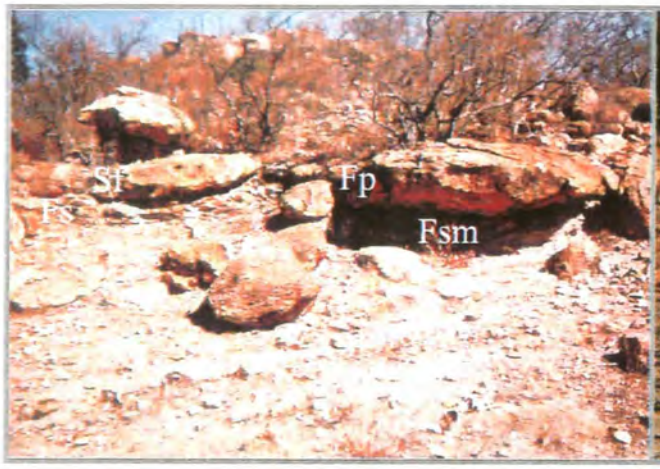

40.

41.

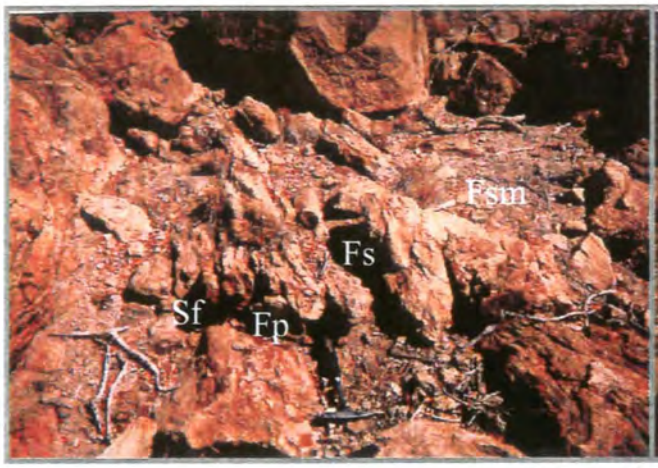

42.

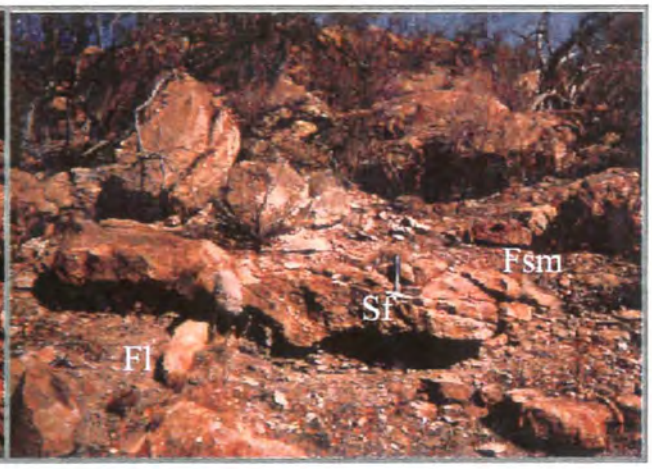

43.

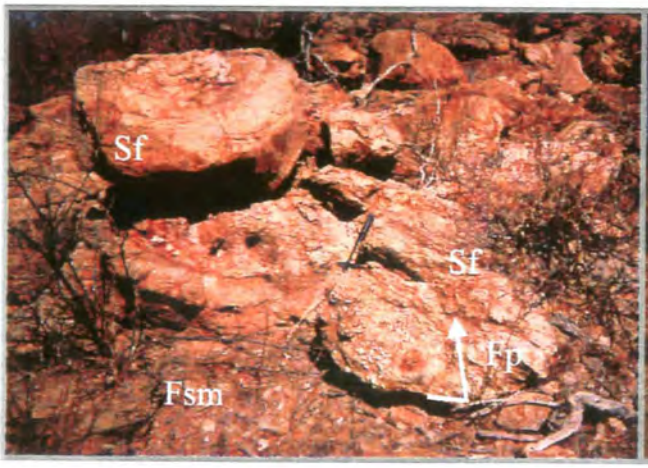

44.

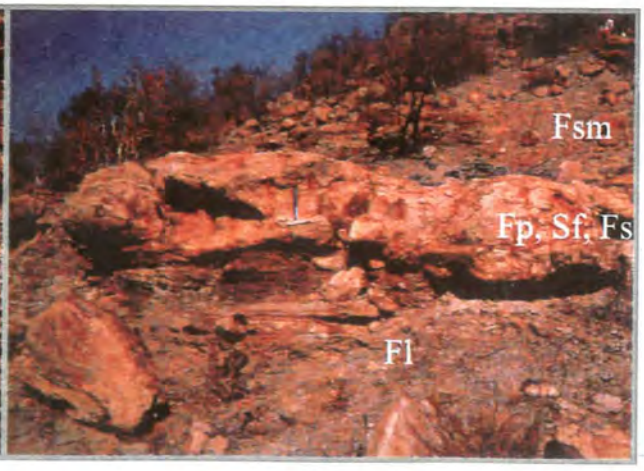

Plate 9

MIDDLE UNIT

Photo 45. Erosional surface (dashed and arrowed line) separating the carbonaceous mudstones of the Basal Unit from the overlying Middle Unit (20 cm conglomerate and 30 cm massive, medium grained sandstone (Somerville).

Photo 46. Erosional surface separating the laminated, carbonaceous mudstones of the Basal Unit from the overlying Middle Unit (20 cm conglomerate and 25 cm massive, medium grained sandstone) (Lizzulea).

Photo 47. Reddish-brown sandstones and conglomerates of the Middle Unit (Eendvogelpan).

Photo 48. Soft sediment deformation (convolute bedding) in otherwise laminated (**Sh**) sandstone. Pencil for scale (Middle Unit, lower part, Over Vlakte).

Photo 49. Horizontally bedded conglomerates (**Gh**). Height of the cliff ~ 2 m (Eendvogelpan).

Photo 50. Subrounded pebbles of quartzite and vein quartz (Bismarck).

45.

46.

47.

48.

49.

50.

Plate 10

Photo 51. Laminated (**Fl**) and ripple-cross laminated (**Sr**) silty, very fine grained sandstone (Breslau).
Photo 52. Ripple-cross laminated (**Sr**) siltstone (Breslau).
Photo 53. Ripple-cross laminated (**Sr**) very fine grained sandstone (Halcyon).
Photo 54. Well-bedded, thin (12-20 cm) layer of silty, very fine grained sandstone (Breslau).

51.

52.

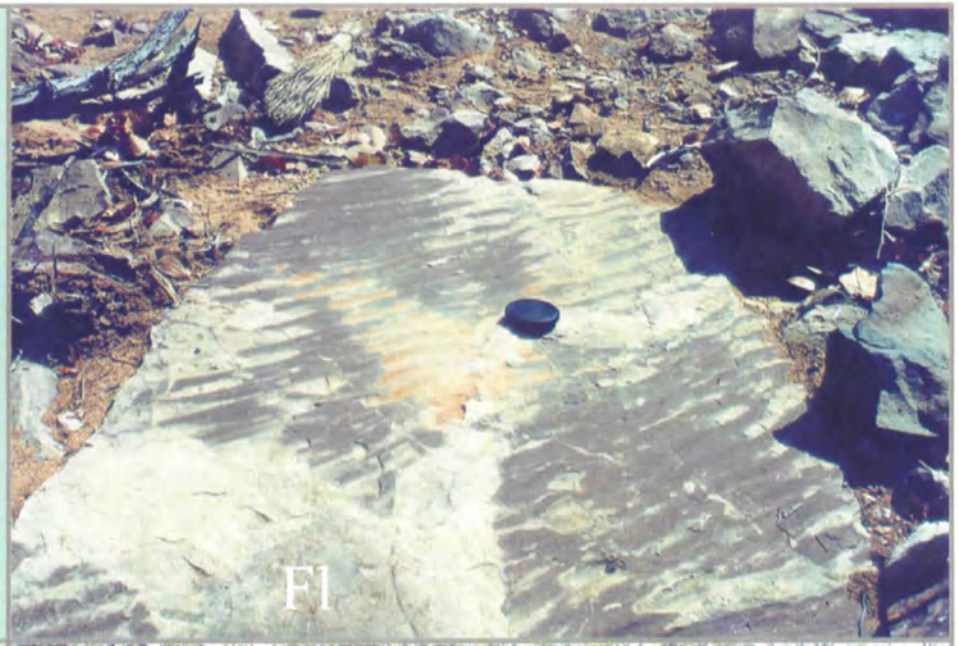

53.

54.

Plate 11

Photo 55A & B. Convolute lamination (**A**) and water escape structures (**B**) in silty, very fine grained sandstone (Eendvogelpan).
Photo 56. Lower bedding plane of a siltstone bed showing the remains of the underlying conglomerate bed with rip-up clasts (Halcyon).
Photo 57. Transitional zone containing small pebble, granule sized rip-up clasts. The lower part of the overlying siltstone bed is ripple-cross laminated, the upper part is massive (Halcyon).

55A.

55B

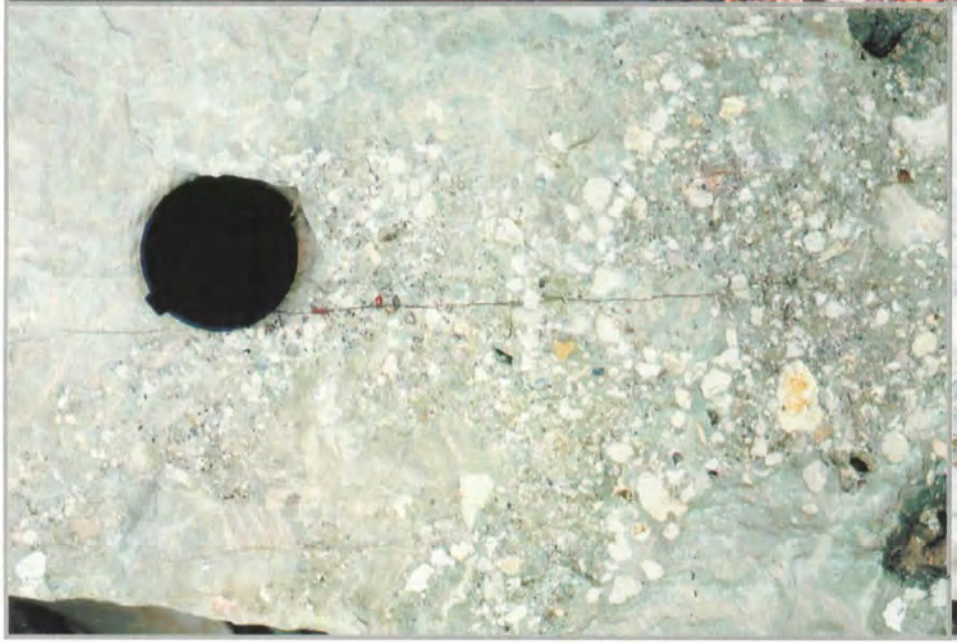

56.

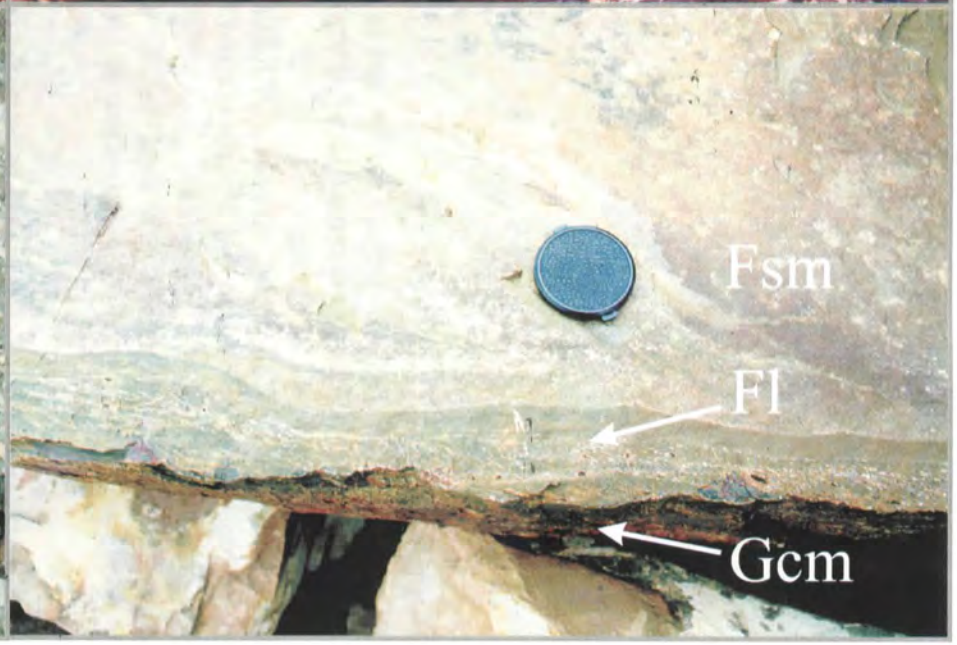

57.

Plate 12

UPPER UNIT

Photo 58. Lithofacies **Sm**. Except for the bed in the front (Sh), all the beds in the picture are lacking internal bedding structures (Edmonsburg).

Photo 59. Lithofacies **Sh** (Nekel).

*Photo 60 **A** & **B***. Well preserved cosets of lithofacies **St** (Faure). Flow direction from left to right. Note the numerous 1st and 2nd order bounding surfaces.

Photo 61. Lithofacies **St** (Hamilton).

Photo 62. Lithofacies **Sp** in coarse sand (Montrow). Flow direction from right to left. Note that the beds are slightly tilted in the paleoflow direction.

58.

59.

60A.

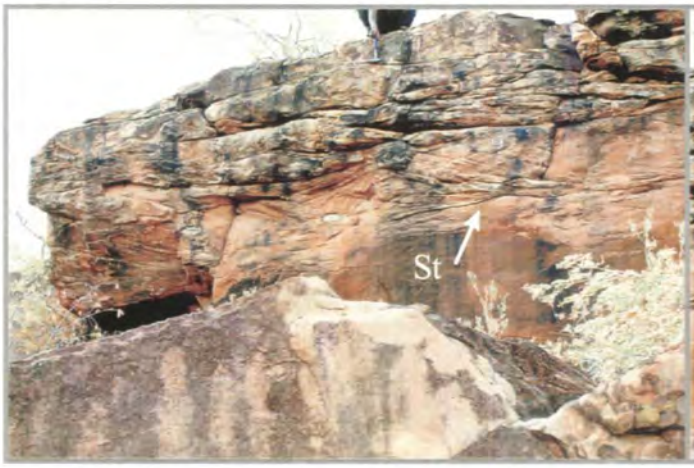

60B.

61.

62.

Photo 63. Lithofacies **Sr**. The ripple cross-lamination in the bed under the notebook is characterized by many small scale scour surfaces resulting in the poor preservation of the ripple form (type A) (Lizzulea).

*Photo 64A, **B** & **C***. Lithofacies **Sr**. The ripples in these beds are characterized by the preserved lee sides and truncated stoss sides of the ripples (type B). Flow direction in the first two pictures toward the right, in the **C** toward the left (Edmonsburg, Lizzulea).

*Photo 65A & **B***. Delicate concave-up mud curls (**A**) and semi-orthogonal pattern of the mudcracks (**B** - on the bedding surface) (Weipe).

63.

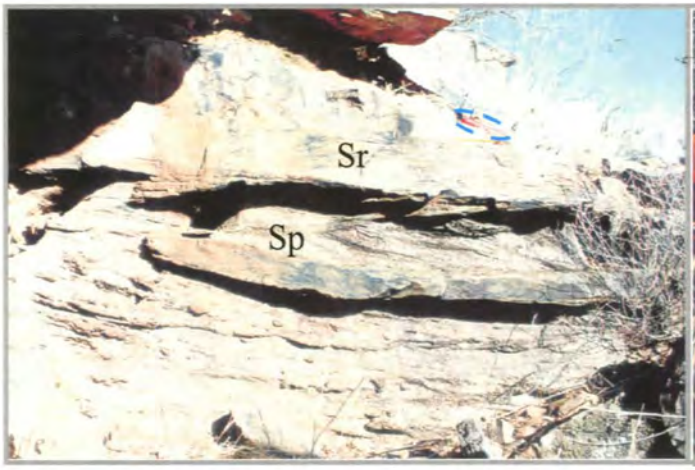

64A.

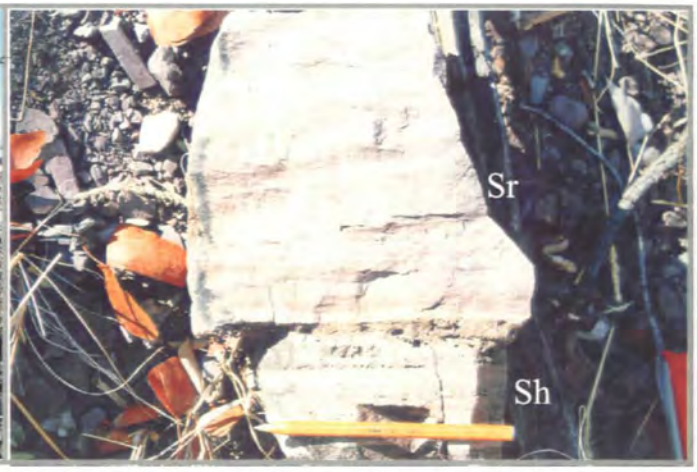

64B.

64C.

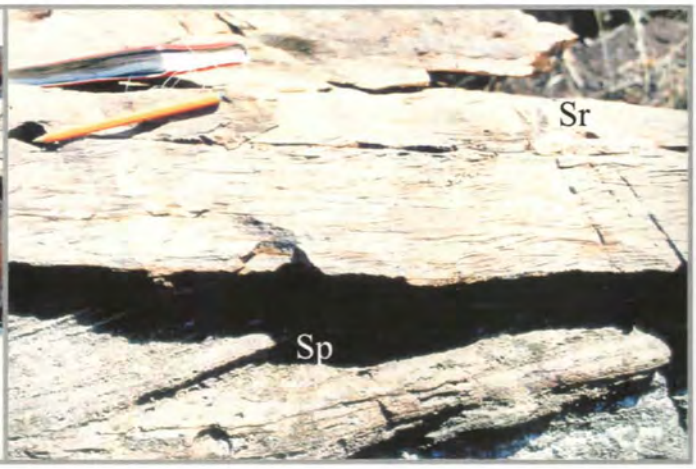

65A.

65B.

Photo 66A, B, C, D & E. Burrowing features (for explanation see Ch. 4.2.4.2.) (Weipe, Halcyon, Ratho, Blyklip, Weipe).

Photo 67. Vertebrate tracks (Schroda). The footprints are average 3.5 cm long, and appear to have been made by a small four-toed animal(s), although most of the prints show only four or three digits. One of the footprints shows that the digits clearly ended in claws, but in the rest of the tracks the digits just thin towards the toe tip. The minimum distance between two adjacent print is 3 cm, while the maximum distance is about 6 cm.

66A.

66B.

66C.

66D.

66E.

67.

Plate 15

*Photo 68**A** & **B***. Unidentified features on bed surfaces (Kilsyth, Weipe).
Photo 69. Broken bone fragment in sandstone (Schroda SW).

68A.

68B.

69.

Photo 70. Laterally continuous sandstone beds. Note the tabular, non-channelized geometries. The three Laminated Sand Sheet (**LS**) architectural elements bounded by 5^{th} order surfaces are best visible in the middle of the picture. Height of the cliff is ~20 m (Blyklip).
Photo 71. Tabular, thin sandbodies (Lareve).
Photo 72. Tabular, thick sandbodies (Weipe). Scale the ~2 m thick bush on the top of the ridge.
Photo 73. Superimposed sheets of sandstone. Lower part of a fining upward cycle (architectural element **LS**). Note that although most of the beds are tabular, there are wedge shaped sandstones as well (Hartebestfontein).

70.

71.

72.

73.

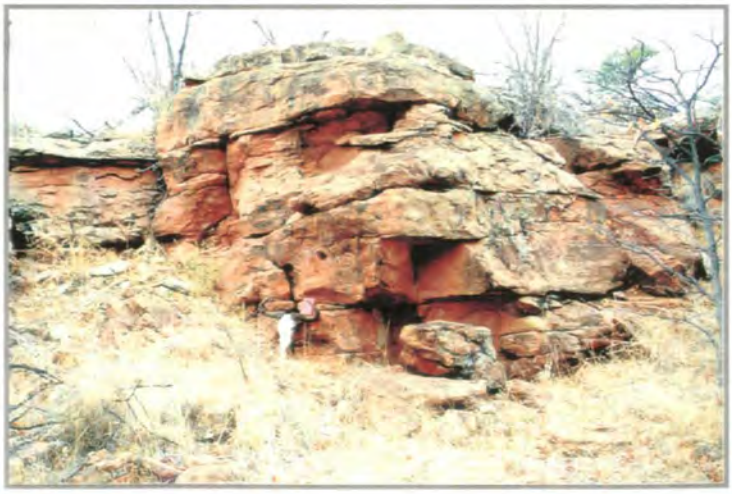

Plate 17

Photo 74A & B. Slightly upward fining cycles (architectural element **LS**). The picture on the left shows at least 2.5 cycles. The first two cycles are fully developed with strongly vegetated upper parts (Parma). The cycles in the right photo have no fine grained upper part (Hillstone).
Photo 75. Three succeeding, laterally continuous cycles (architectural element **LS**), each about 6 m thick. The dashed lines are 5^{th} order bounding surfaces. Notebook for scale (Reidel- NW).
Photo 76A & B. Superimposed sheets of sandstone with non-channelized bases (architectural element **LS**). In **B**, the total height of the cliff is ~8 m (Weipe, Riedel).

74.

75.

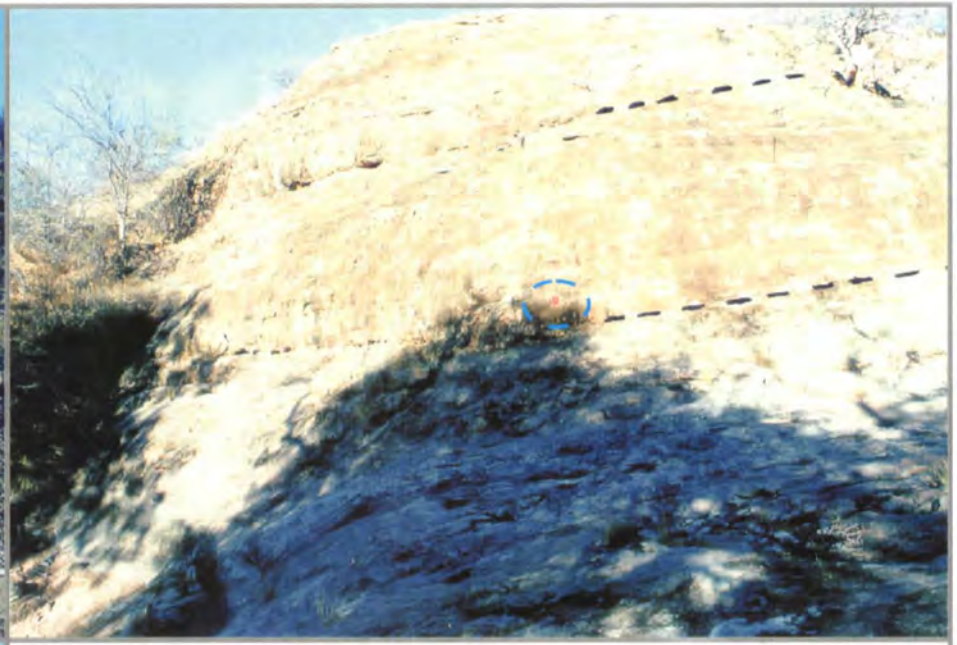

76A.

76B.

Photo 77. Base of a fining-upward cyclotheme commencing with a shallow scour and very fine, rip-up sandstone and mudstone clasts. The size, roundness as well as the identical lithologies of the clast and the underlying laminated bed indicates that the clasts were torn up and transported from the immediate vicinity. Note lithofacies differences below and above the surface (5^{th} order) (Edmondsburg).

*Photo 78A & **B**.* Poorly sorted, clast supported (**Gcm**) intraformational conglomerates mainly consist of granule to pebble grade white, well rounded carbonate concretions, septaria and nodules (Nekel).

*Photo 79A & **B**.* White to reddish, subangular to subrounded mudstone particles in poorly sorted, massive, clast supported (**Gcm**) intraformational conglomerates (Vergenoegd).

Photo 80. Red, subangular to subrounded sandstone clasts. The 8 cm long pebble in the middle is bioturbated. The other red clasts in the upper right are bone fragments (Blyklip).

77.

79A.

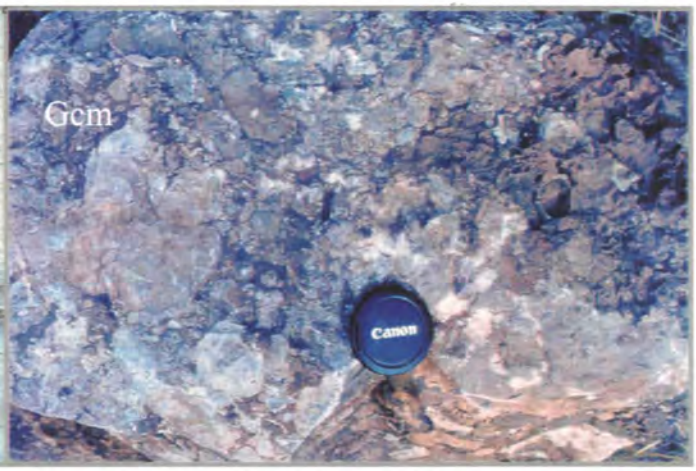

78A.

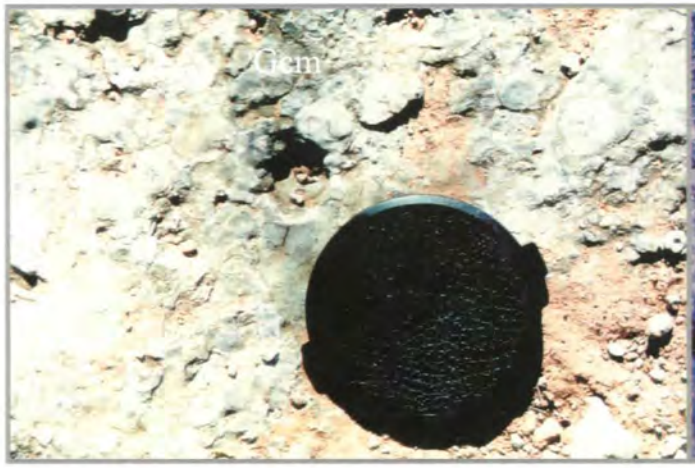

79B.

78B.

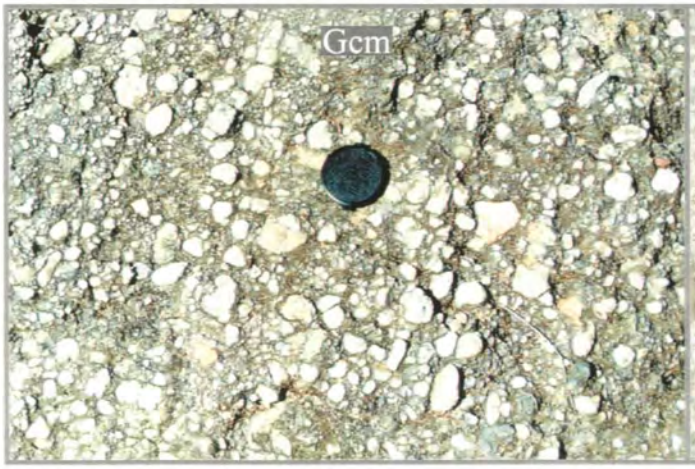

80.

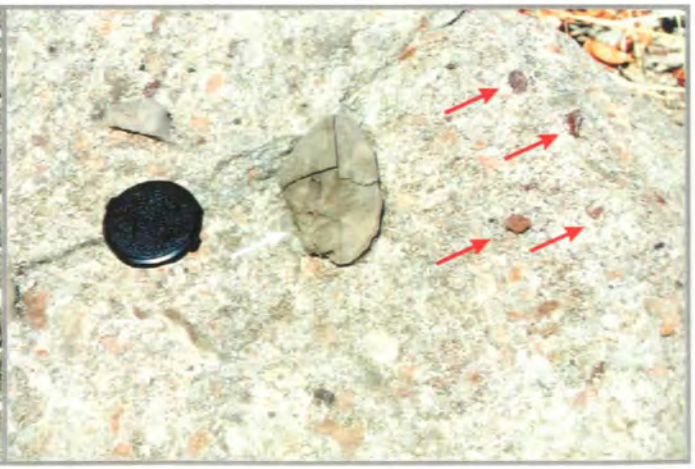

Photo 81A & B. Reddish, isolated, broken and abraded bone fragments contribute to the subangular, subrounded clast fraction of the conglomertes (Montrow).
Photo 82. Some 10 cm large pebbles in poorly sorted conglomerates. At this location a 25 cm pebble was also found (Nekel).
Photo 83. Lithofacies **Gcm**: massive, clast supported intraformational conglomerates (Blyklip)

81A.

81B.

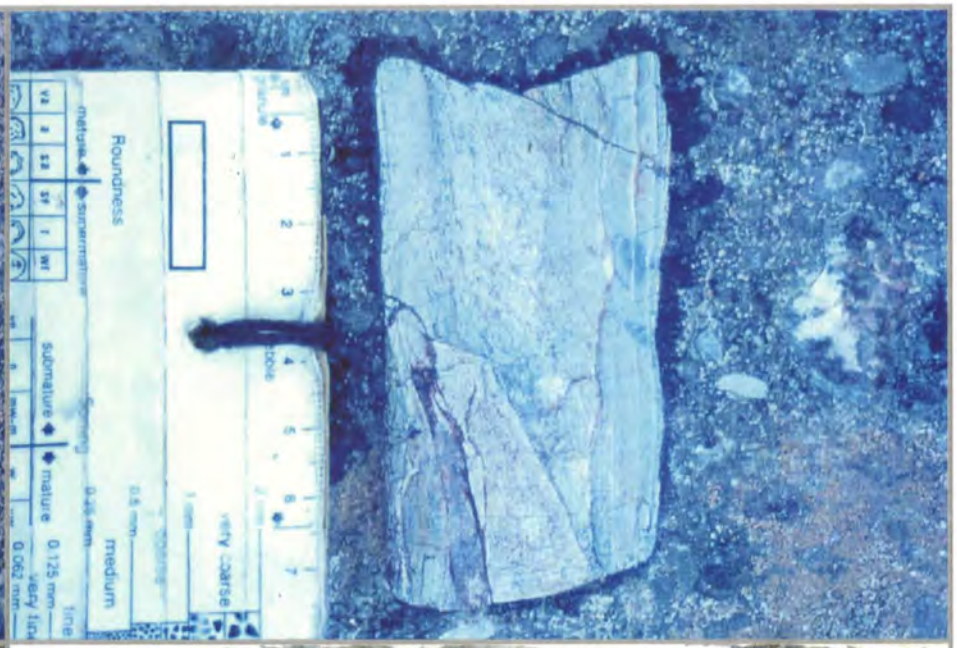

82.

83.

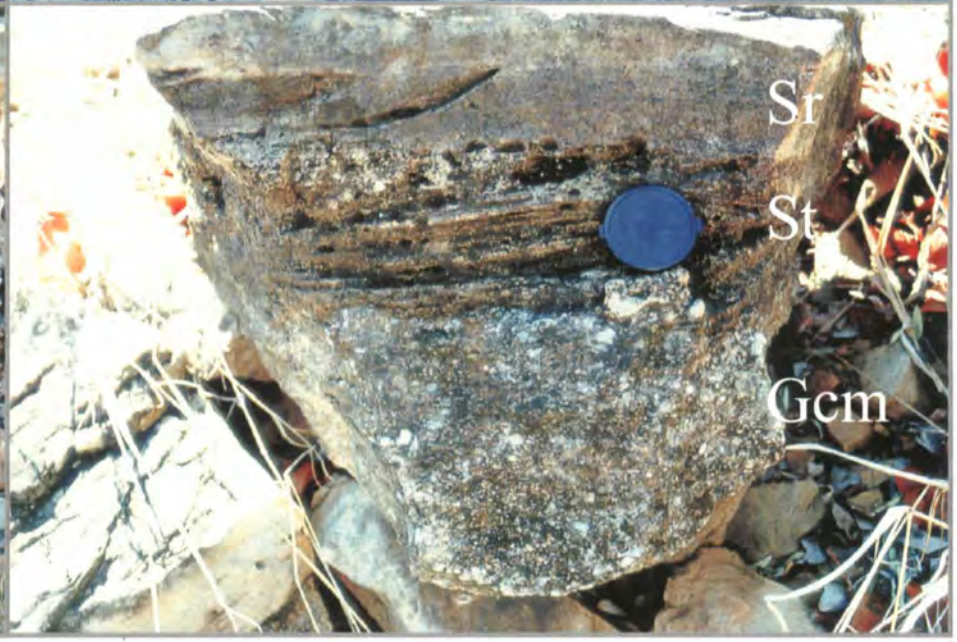

Plate 20

Photo 84. Lithofacies **Gh**: slight horizontal layering in the intraformational conglomerates (Montrow).
Photo 85. Lithofacies **Gp, Gt**: cross-bedding. Lower part of the picture shows layer of **Gp** being overlain by a faddishly, through cross-bedded (**Gt**) conglomerate (Lareve).
Photo 86. Lithofacies **Gh**: in slight horizontal stratification defined by normal grading (Lizzulea). *Photo 87*. Lithofacies **Gcm** being directly overlain by ripple cross-laminated (**Sr**) very fine sandstones (Blyklip).

84.

85.

86.

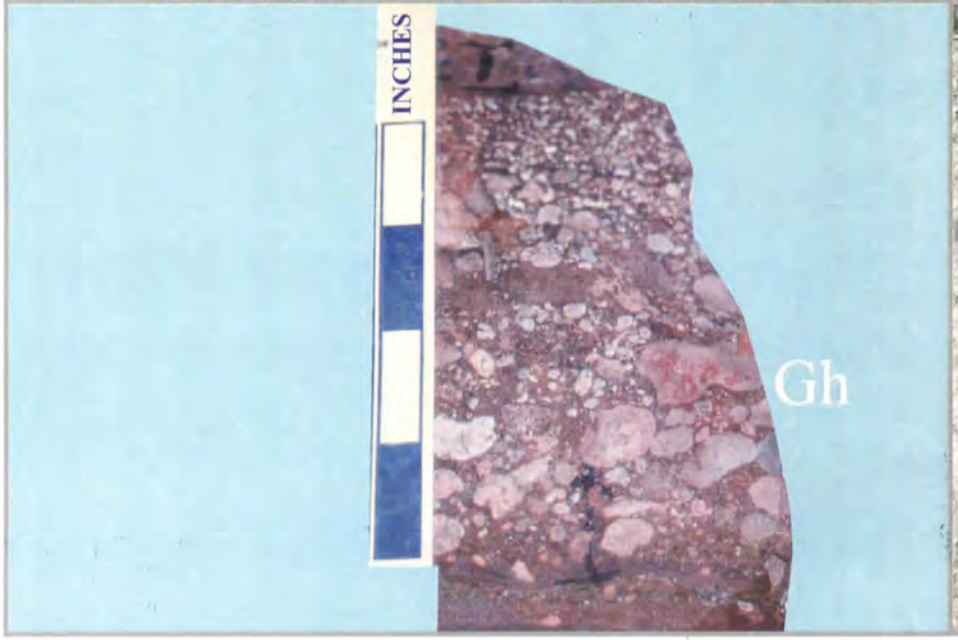

87.

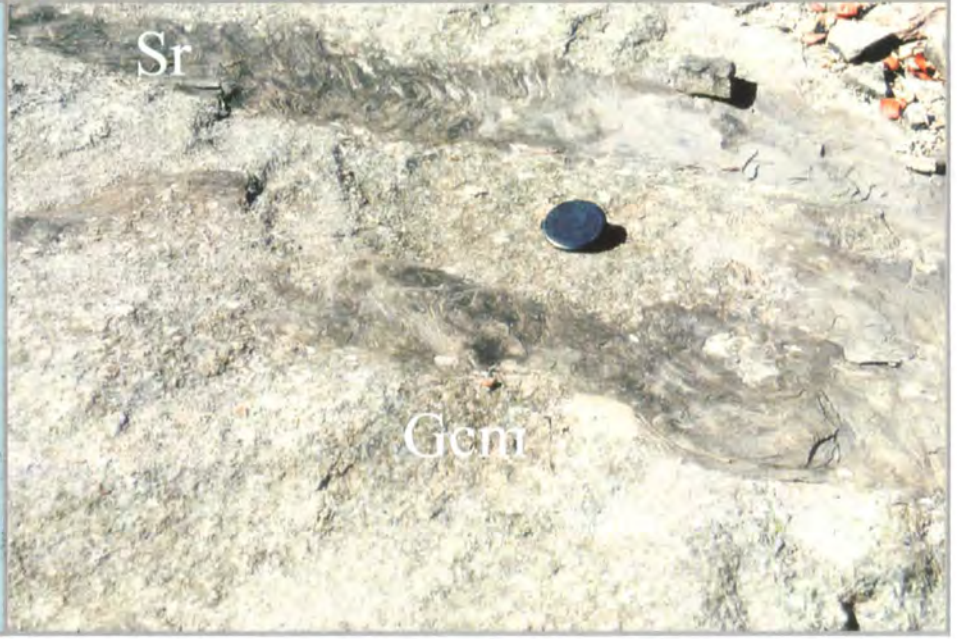

Plate 21

Photo 88. Thickly bedded argillaceous rocks. The upper part of the picture shows the thickly bedded sandstones of the Clarens Formation. The hard silcrete horizon is between the last white, thick argillaceous bed and the first yellow-brown, very thick, sharp based sandstone bed (Ratho - Boscamp).

Photo 89. Greyish-greenish and reddish thickly bedded argillaceous rocks. The upper part of the picture shows the thickly bedded sandstones of the Clarens Formation. The height of the cliff is ~20 m (Greefswald - near Mapungubwe).

Photo 90. Blotchy colour mottling in massive, thickly bedded argillaceous rocks. Hammer for scale (Hilda).

Photo 91. Equidimensional, centimeter-scale angular to subangular blocks of greenish mudstone. Hammer rest on 0.4 m thick, greenish silcrete layer underlying the sandstones of the Clarens Formation (Machete).

Photo 92. Well preserved, circa 20 m high outcrop of the argillaceous sediments. Note the contrasting red and greyish-greenish colouration of the beds and also the prominent, white silcrete horizon sharply separating the mudstones and yellow-brown sandstones of the Clarens Formation (Parma - Tsolwe).

88.

89.

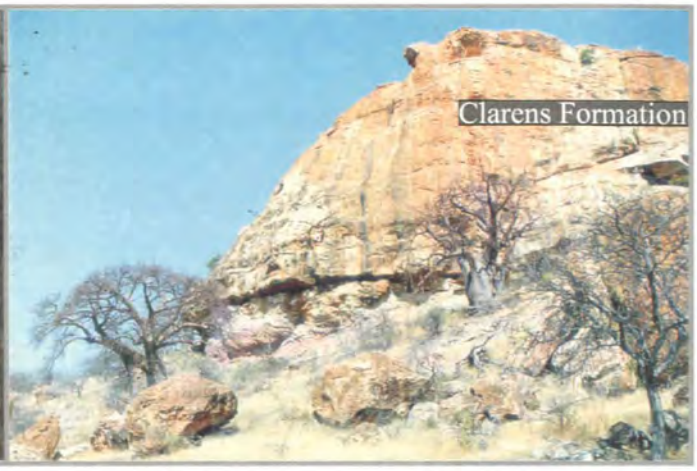

90.

91.

92.

Plate 22

Photo 93. Irregular and crudely cylindrical and spherical carbonate glaebules in horizontal and sub-horizontal position. The hammer is 28 cm long (the millipede - lower left is very large). The host rock is red, carbonaceous, massive muddy siltstone (**Fs**) with very fine sand grains. (Parma - Tsolwe).

Photo 94. Vertically orientated carbonate glaebules with framboidal texture. The notebook (19 cm) rests on a coalesced carbonate glaebule horizon. The surrounding host rock is green, carbonaceous, massive (**Fs**) muddy siltstone with very fine sand grains. Note the spot of relict lamination (**Fl**) (Breslau - Show of Rhodes). Compare this picture with *Photo 150* showing contemporaneous carbonate glaebules with framboidal texture.

Photo 95. Large, twined carbonate concretion (notebook length 19 cm) in red, locally carbonaceous, massive silty-sandy host rock (**Fsm**). (Breslau - Pyramid Koppie).

Photo 96A & B. Septaria in massive, green mudstone (Machete).

93.

94.

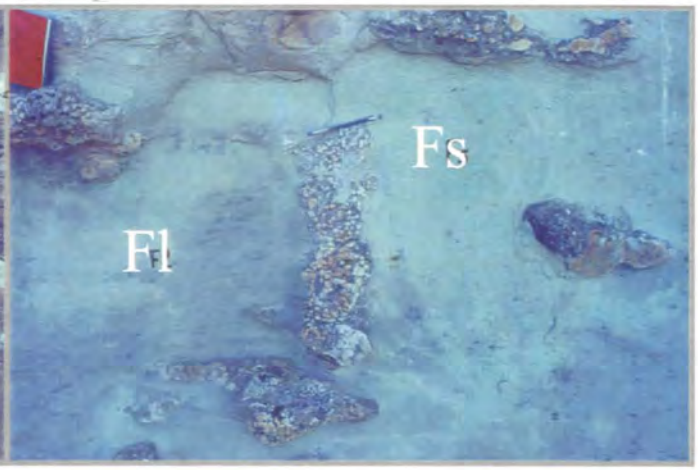

95.

96A.

96B.

Plate 23

Photo 97. Carbonate accumulations with gradational lower and sharp upper contacts within thickly bedded silty mudstones (Parma - Tsolwe).
Photo 98. Continuous, coalesced glaebule horizons within thickly bedded silty mudstones (Parma - Tsolwe).
Photo 99. Meshwork of mainly horizontal white calcite veins and pseudo-folded carbonate layers (Modena).
Photo 100. In situ fossilised and articulated vertebrate limb bones in siltstones of Upper Unit (Armenia).

Plate 24

Photo 101A, B, C, D, E & F. In situ vertebrate remains showing little or no abrasion. Note the perimineralization with haematite (*A, E, F* - Armenia; *B* - Little Muck; *C, D* - Balerno).

101A. 101B.

101C. 101D.

101E. 101E.

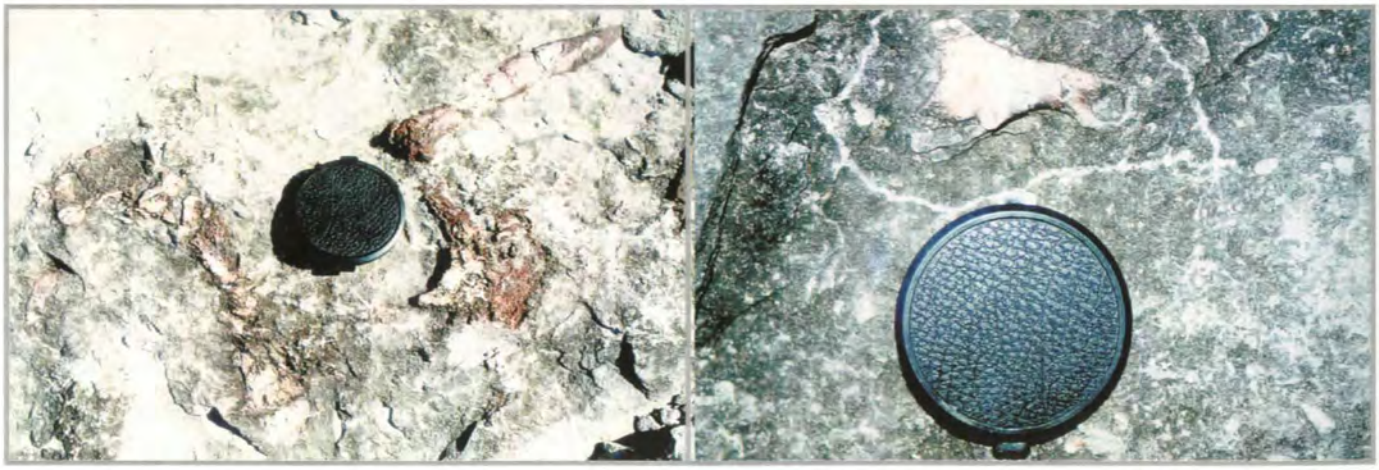

*Photo 102**A, B, C** & **D**. 69, 70, 94, 124/a* Single disarticulated, abraded bone fossils (*A, B* - Balerno; *C* - Machete*)* and bone bed within equidimensional, centimeter-scale angular to subangular blocks of greenish mudstone (*D* - Armenia*)*.

102A.

102B.

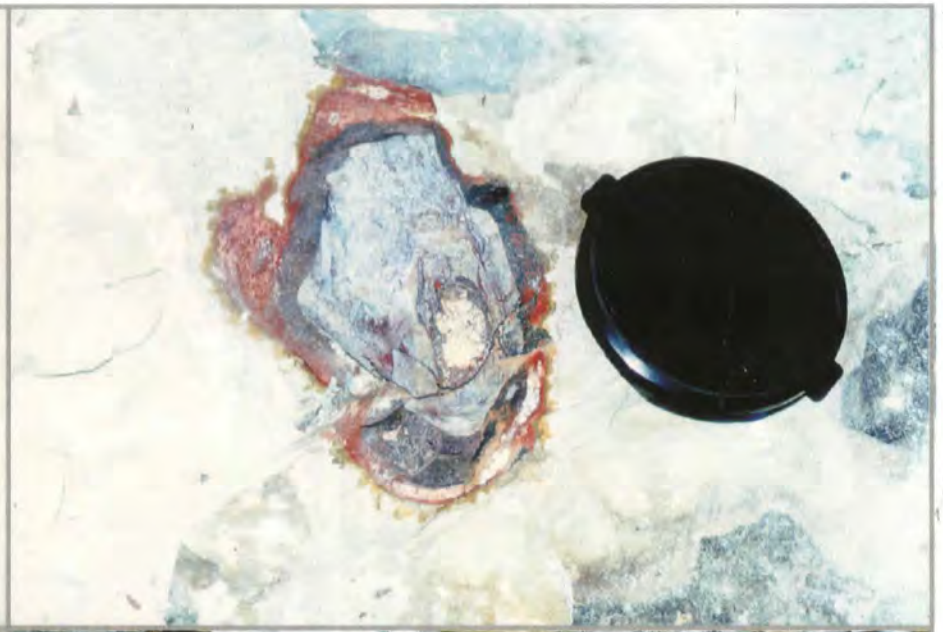

102C.

102D.

Plate 26

Photo 103. Lithofacies **Sh** in sheet like sandbodies (Lizzulea).
Photo 104. Lithofacies **Sp** in sheet like sandbodies (Montrow).
Photo 105. Sheet-like sandbodies within sharp lower surfaces (Lizzulea).
Photo 106. Laterally continuous, thick, tabular sandbodies with planar upper surfaces grading into laminated or bioturbated mudstone (Lizzulea).

103.

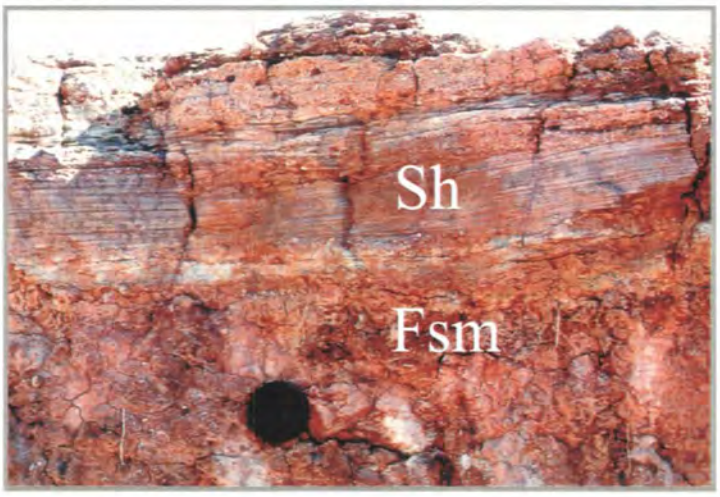

104.

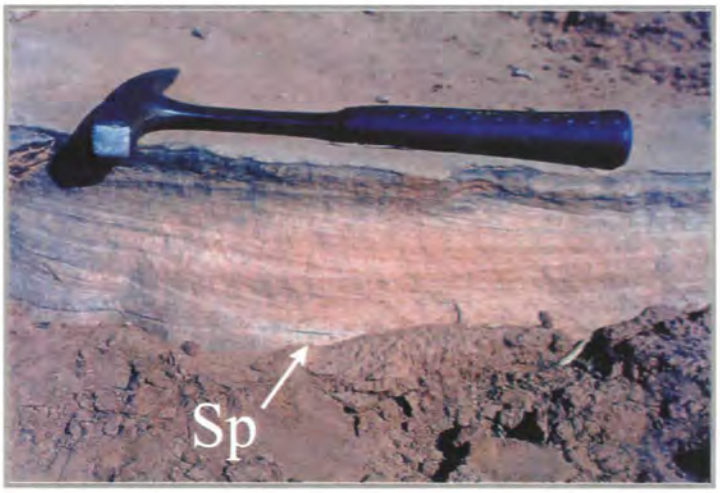

105.

106.

Plate 27

Photo 107A & B. Thin and narrow sandstones with wedge (**A** - Montrow) and lens (white parts in **B** - Ratho) shapes are isolated as single beds in thick, massive or laminated, red mudstones.
Photo 108A & B. Multiple sandstone and mudstones forming laterally continuous superimposed sheets (Hilda SW).

107A.

107B.

108A.

108B.

Plate 28

Photo 109. Lithofacies **Gmm** (Schroda).
Photo 110. Lithofacies **Sc** surrounding irregularly shaped Gcm and Gmm beds. Note the rare relict lamination (**Fl**) in the otherwise massive silty mudstones (**Fsm**) (upper left), as well as the clay coating of the breccia clasts (Balerno - Tolwe).
Photo 111. Two sheet-like layers of intraformational conglomerates (**Gh**) in red, laminated and massive mudstones (**Fl, Fsm**) (Montrow).
Photo 112. Well preserved fossil bone at the top of a **Gh** layer (Montrow).

109.

110.

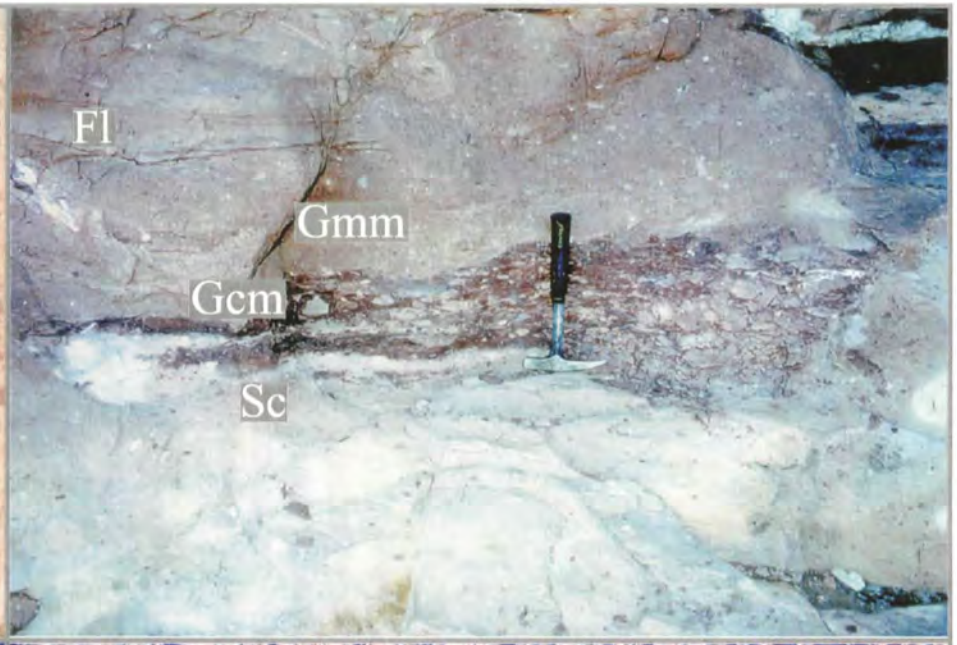

111.

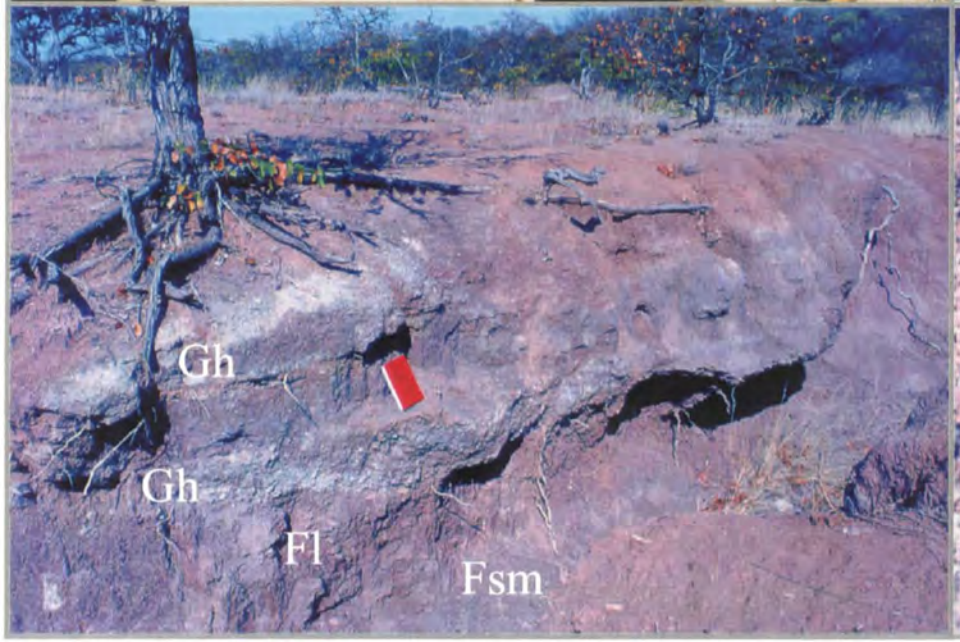

112.

Plate 29

CLARENS FORMATION

Photo 113. Large-scale cross-stratification. Height of the cliff is ~15 m (Pont Drift).

Photo 114. Giant cross-beds. Notebook length is 19 cm (Parma).

Photo 115. Finely laminated foresets of giant cross-beds (Parma).

Photo 116. Alined, connected, crescent-shaped cross-stratified sandstones resembling rows of barchanoid ridges. Foreset dip direction to left. Note the vegetated shallow hollows between the bedforms (Hillstone).

Photo 117. Alined, connected, crescent-shaped cross-stratified sandstones resembling rows of barchanoid ridges. Foreset dip direction from the viewer to the scale. The dark zone in the background is a lava flow (Greefswald).

113.

114.

115.

116.

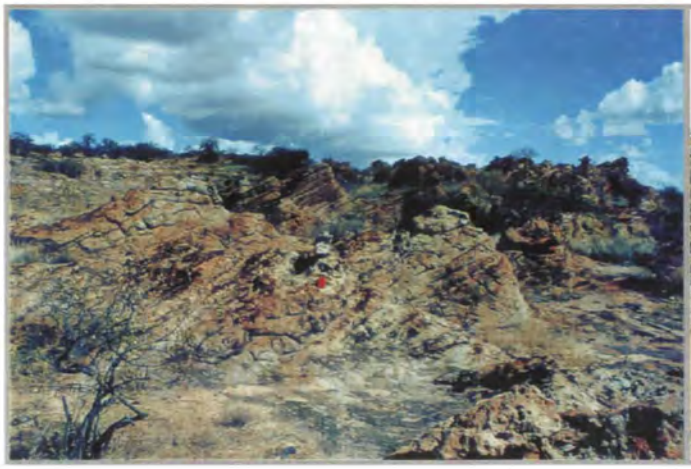

117.

Photo 118. Well-developed tangential bottom sets in cross-stratified, crescent-shaped sandstones. Hammer for scale (Hillstone).
Photo 119. Third order surfaces between cosets of cross laminae (see arrow). The picture shows two separate dunes with forsets dipping form the viewer's right to the left corner of the pictures (Balerno - Tsolwe koppie).
Photo 120. Rare second order bounding surfaces separating the lower, thick set of crossbeds from smaller bedforms. Height of the cliff is ~25 m (Balerno, Tsolwe koppie).
Photo 121. Reactivation (2^{nd} order) surface separating cosets of slightly different dip directions. See arrow pointing at the notebook (19 cm) (Parma).

118.

119.

120

121.

Plate 31

*Photo 122**A** & **B***. Sharp, low-relief first order bounding surfaces (dashed line). See arrow at the third order surfaces. Person for scale (Balerno).

Photo 123. Lenticular beds of horizontal laminated (Sh), 0.2-1 m thick sandstones. Person for scale (Greefswald).

122A.

122B.

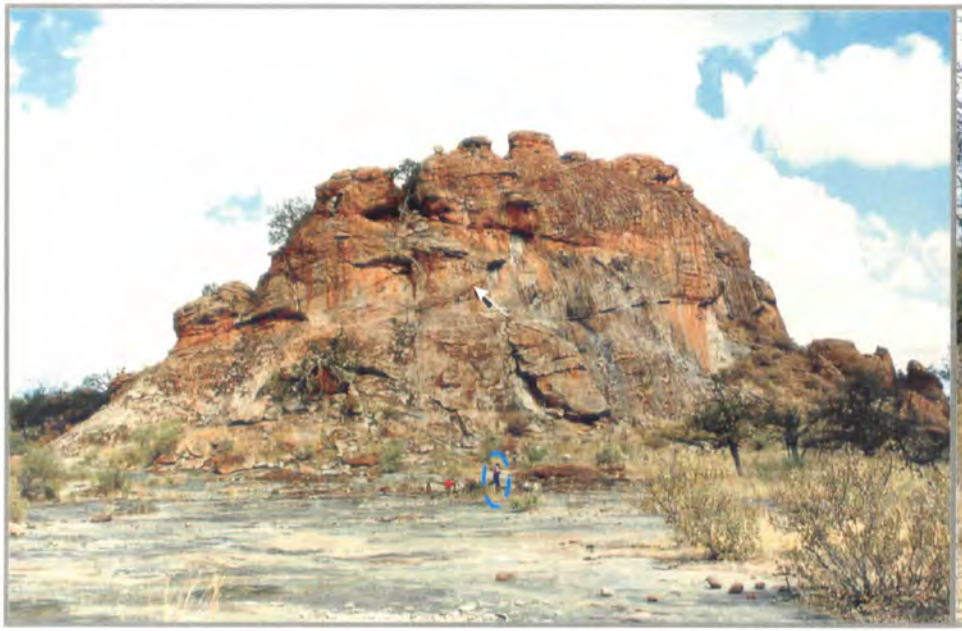

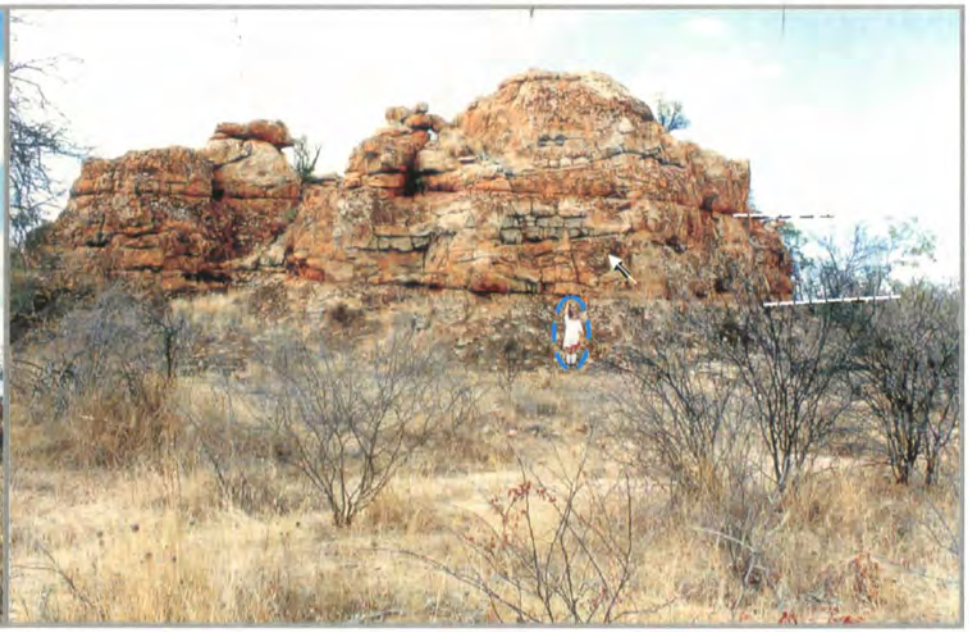

123.

*Photo 124A & **B***. Silicified fossil woods found on the surface of the Clarens Formation sandstones. It was identified as *Agathoxylon sp.* (= *Dadoxylon sp.*) (Parma).
Photo 125. Large scale trace fossils (*Type A*) showing lateral bifurcations (Schroda).
Photo 126. Large scale horizontal trace fossils (*Type A*) (Hillstone).
Photo 127. Vertical, cylindrical pipes with open apex (*Type A* trace fossils)(Hillstone).
Photo 128. Simple, mostly vertical shafts-like trace fossils frequently intersect the entire, 0.15-0.25 m thick host bed (*Type B*)(Weipe & Schroda).
Photo 129. Simple, isolated, unbranched trace fossils (*Type B*)(Machete).

124.

125.

126.

127.

128.

129.

Plate 33

Photo 130. Digit-like (giant finger-like), vertical trace fossils (*Type C*). Note the twinned structures and person sitting in the 0.5 m wide saddle between the two digits (Greefswald).
Photo 131. Close up of the wall of the digit-like structure showing extensive branching with random orientation (*Type C*). Person for scale (Greefswald).
Photo 132. Polished slab showing non-meniscate tubes and the central shapt of the digit-like structures (Greefswald).
Photo 133. Rare upward bifurcation (in the center of the photo) (*Type C*). Person for scale (Greefswald).
Photo 134. Dome-like elevations at the base of the digit-like structures is heavily bioturbated (*Type C*) (Greefswald).
Photo 135. Recent columnar termite nests are rather common in the study area (Ammondale).

130.

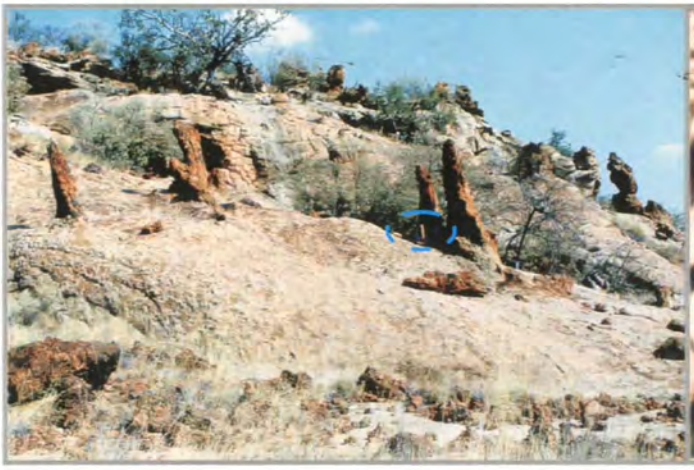

131.

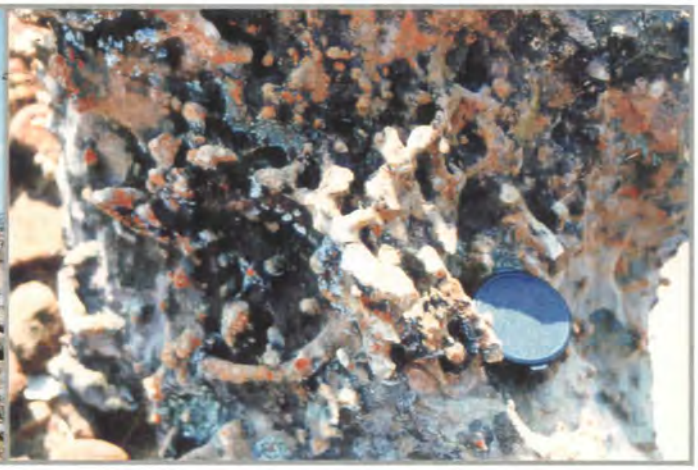

132.

133.

134.

135.

CALCRETE & SILCRETE

Photo 136A & B. Carbonate glaebules in indurated sandstones found in immediate vicinity of dolerite dykes (**A** - Parma; **B** - Lareve).

Photo 137A & B. Dolerite dyke intrusions in sandstones. **A** - Indurated and bleached sandstones on the sides of a large dyke (Parma); **B** - The young boy stands on the bleached, white boundary between the dyke (right) and the muddy red sandstones (left) (Lareve).

Photo 138. Small scale fold-like structure in indurated sandstone. The structure is above the geological hammer (circled). The outcrop is the inner, near vertical wall of a parallel, double crested sandstone ridge flanking a dolerite dyke which being less resistant, had been eroded away.

Photo 139. Botryoidal fabric of coalesced silcrete glaebules forming brittle, massive horizon (Breslau - Show of Rhodes).

136A.

136B.

137A.

137B.

138.

139.

Photo 140. Massive silcerete with internally massive, rough surfaced tubules (see arrow). The tubule in the centre of the picture has a very small white walled central hollow.
Photo 141. Massive silcerete with irregular to tunnel or pipe like hollows and pits.
Photo 142. Massive silcerete with voids that show millimeter thin walls of microquartz and/or cryprocrystalline silica. Well developed in the upper part of the picture.
Photo 143. Gradational silcrete with laterally discontinuous silica laminations in the red silty-mud host rock.
Photo 144. Gradational silcrete with clay coated silicified host rock lumps and lenses in the transitional lower part.
Photo 145. Gradational silcrete with clay coated silicified host rock lumps grading into massive, cavernous silcrete.

140.

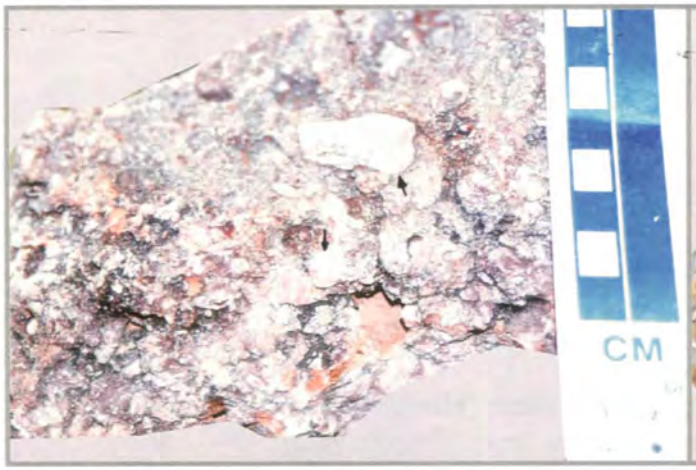

141.

142.

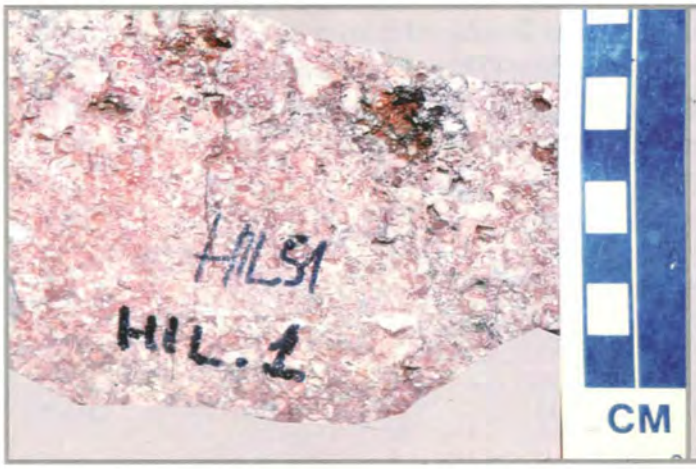

143.

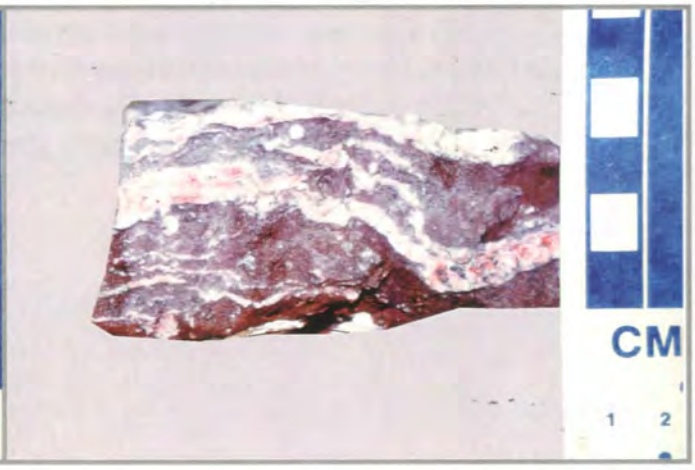

144.

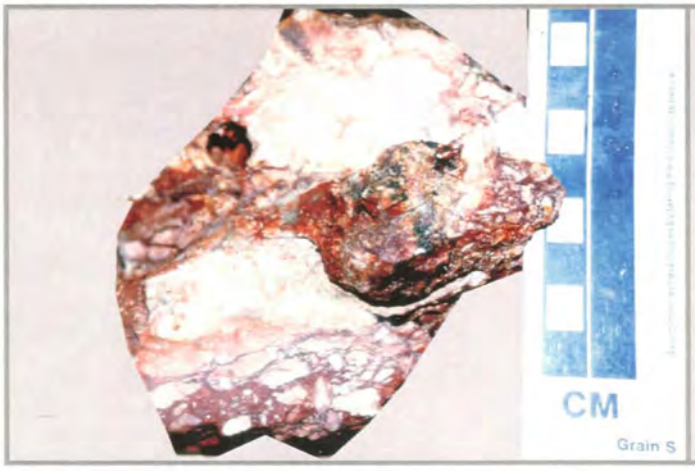

145.

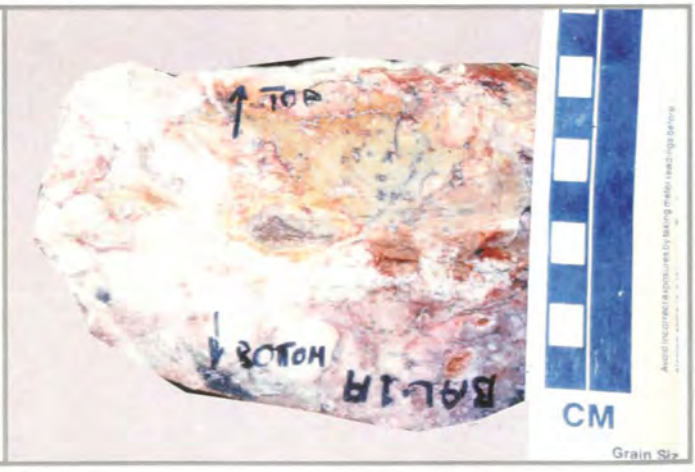

INTERPRETATION

Photo 146. Rapid sheet flow during an early summer storm (Montrow/Breslau border).

Photo 147. Large dessication cracks developed in thick mud (Halcyon dam).

Photo 148. Contemporaneous example of shallow hollows and rainstorm eroded gullies of an otherwise flat, muddy floodplain surface. Picture shows the interchannel area of ephemeral stream system of the study area. Note the sparse vegetation and the patches of coarse, loose sediments in the foreground (Montrow).

Photo 149. Contemporaneous rainstorm erosion feature developed in laminated mudstone. Also note the angular sandstone slabs lying on the dry gully floor (This picture was taken at Brosterlea, near Molteno, South Africa. Similar features are common in the study area too). Scale 20 cm.

Photo 150. Contemporaneous carbonate glaebules with framboidal texture. Compare this picture with *Photo 94.*

146.

147.

148.

149.

150.

Plate 37

APPENDIX 1

Sedimentological vertical profiles

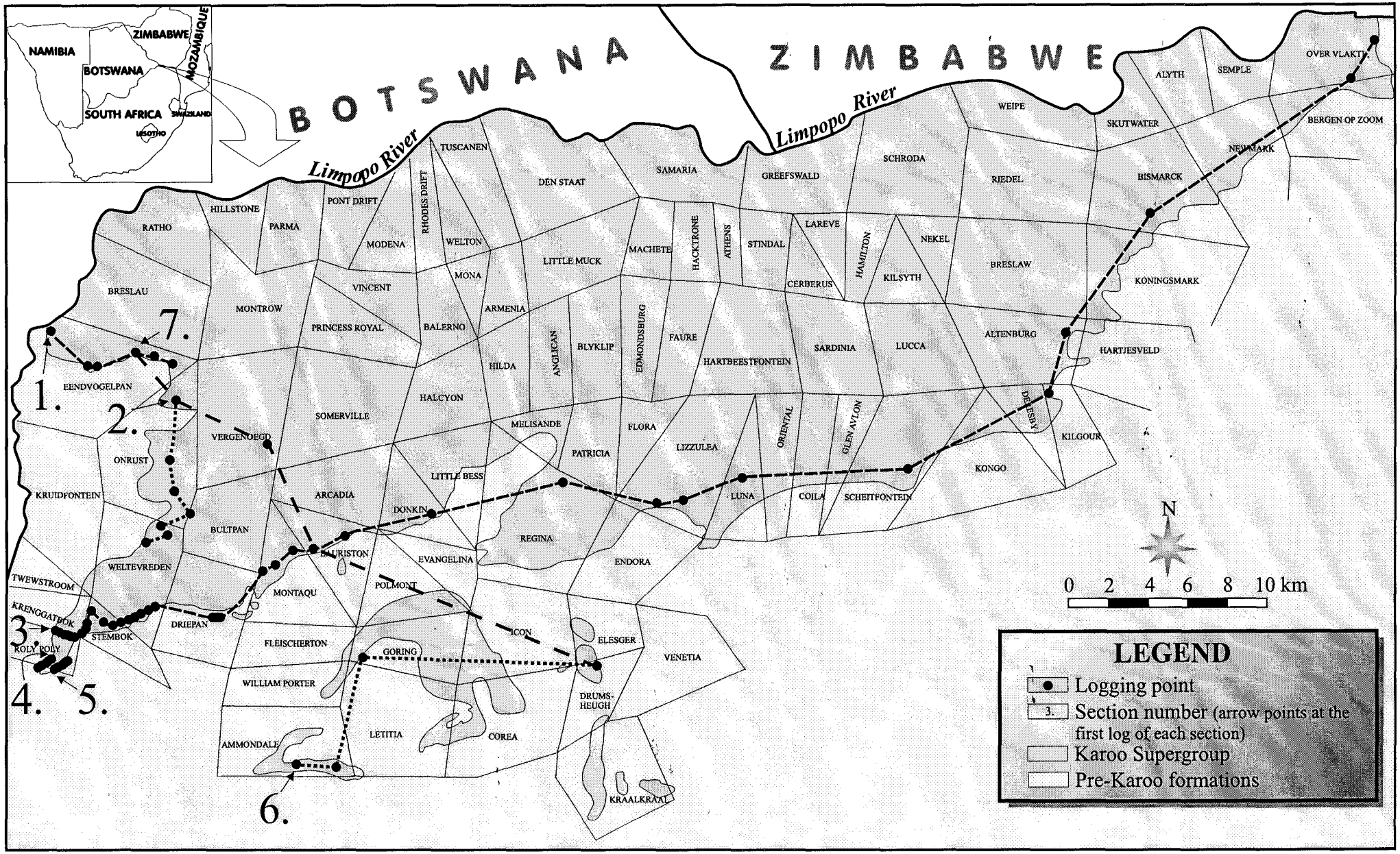

Fig.I. Map showing the traverses of Section 1-7.

FARM NAME	Section number	Vertical profile symbol
Altenburg	3	AL1
Ammondale	6	AM1
		AM2
Bismarck	3	BI1
Bultpan	2	BU1
Donkin	3	DO1
Driepan	3	DP1
		DP2
		DP3
		DP4
Drumsheugh	6, 7	DR1
Eendvogelpan	1	EE1
		EE2
		EE3
	1, 7	EE4
		EE5
		EE6
Goring	6	GO1
Kilgour	3	KI1
Lauriston	3	LA1
	3, 7	LA2
Lizzulea	3	LI1
		LI2
Luna	3	LU1
Montaqu	3	MO1
		MO2
		MO3
Onrust	3, 7	ON1
	3	ON2
		ON3

FARM NAME	Section number	Vertical profile symbol
Overvlakte	3	OV1
		OV2
Regina	3	RE1
Roly Poly	3	RP1
		RP2
		RP3
		RP4
		RP5
		RP6
		RP7
		RP8
		RP9
		RP10
		RP11
		RP12
		RP13
	4	RP14
		RP15
		RP16
		RP17
		RP18
		RP19
		RP20
		RP21
		RP22

FARM NAME	Section number	Vertical profile symbol
Roly Poly	4	RP23
		RP24
		RP25
	5	RP14
		RP26
		RP27
		RP28
		RP29
		RP30
		RP31
Schietfontein	3	SC1
Stembok	3	ST1
		ST2
		ST3
		ST4
		ST5
		ST6
Vergenoegd	7	VE1
Weltevreden	3	WE1
		WE2
		WE3
		WE4
		WE5
		WE6
	2	WE7
		WE8
		WE9

~W

~E

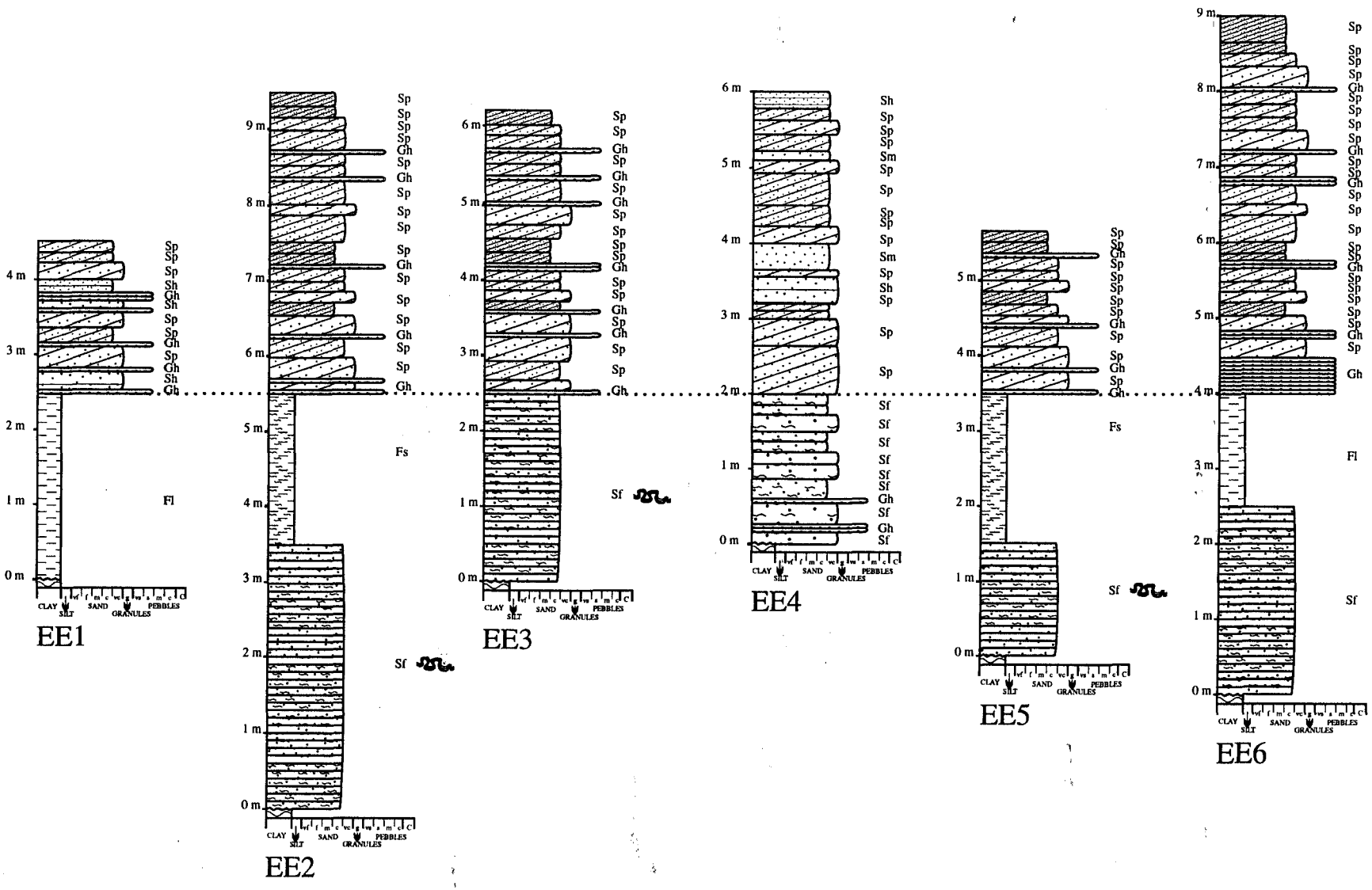

1.

~N

~S

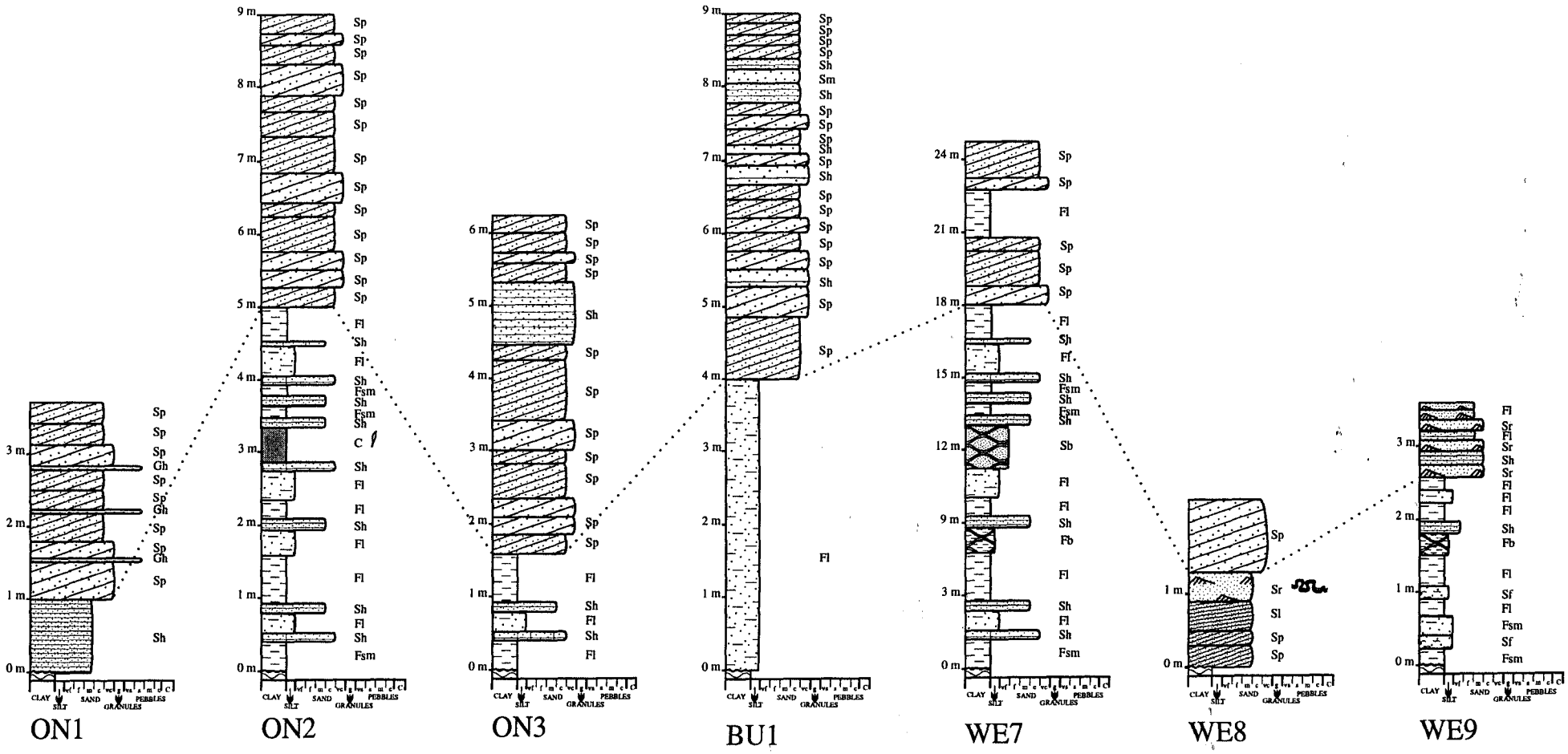

2.

~SW

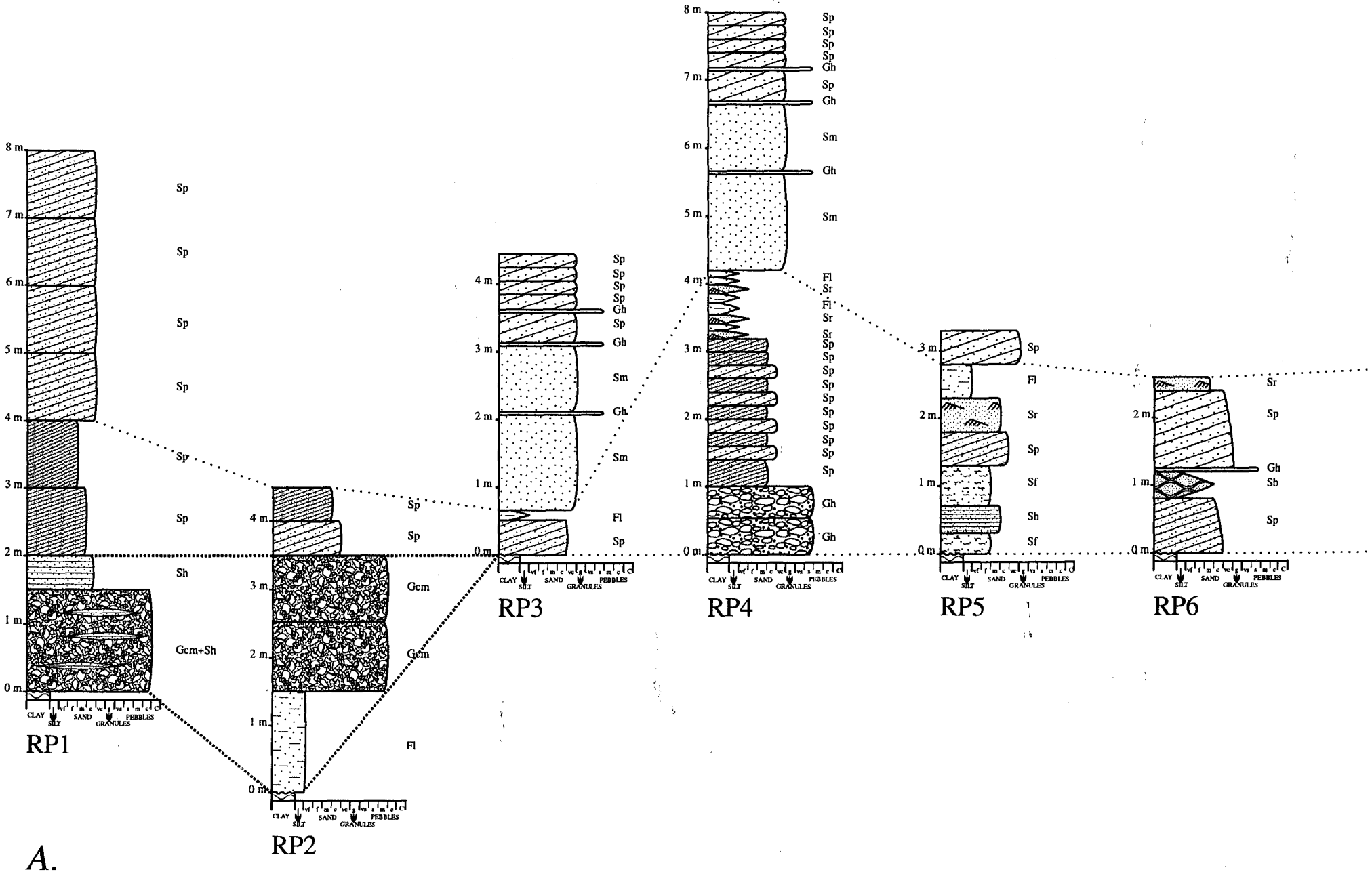
8 m
7 m
6 m
5 m
4 m
3 m
2 m
1 m
0 m
Sp
Sh
Gcm+Sh
Gcm
Fl
Sm
Gh
Sr
Sf
Sb
CLAY
SILT
SAND
GRANULES
PEBBLES
RP1
RP2
RP3
RP4
RP5
RP6

A.

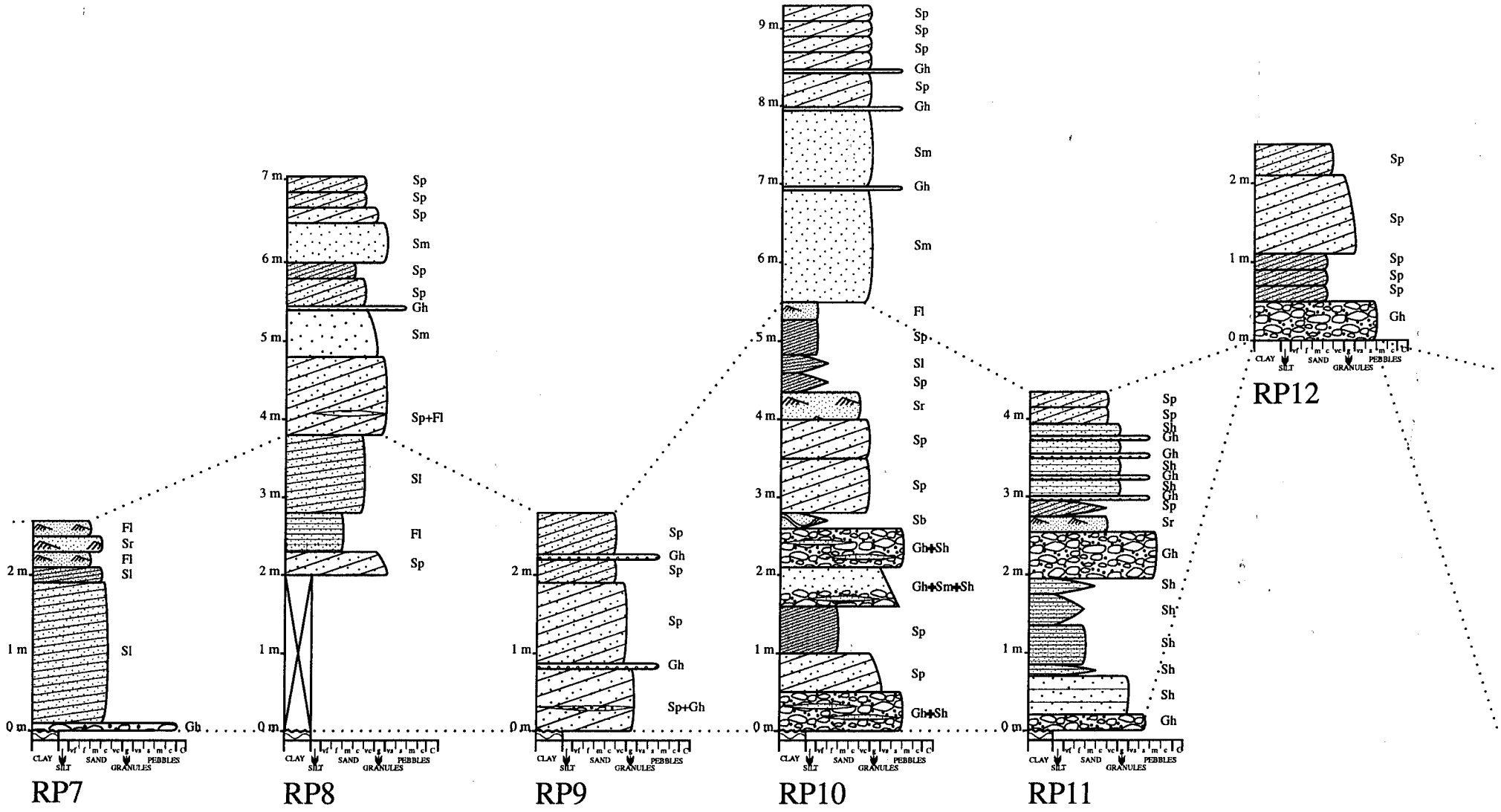

B.

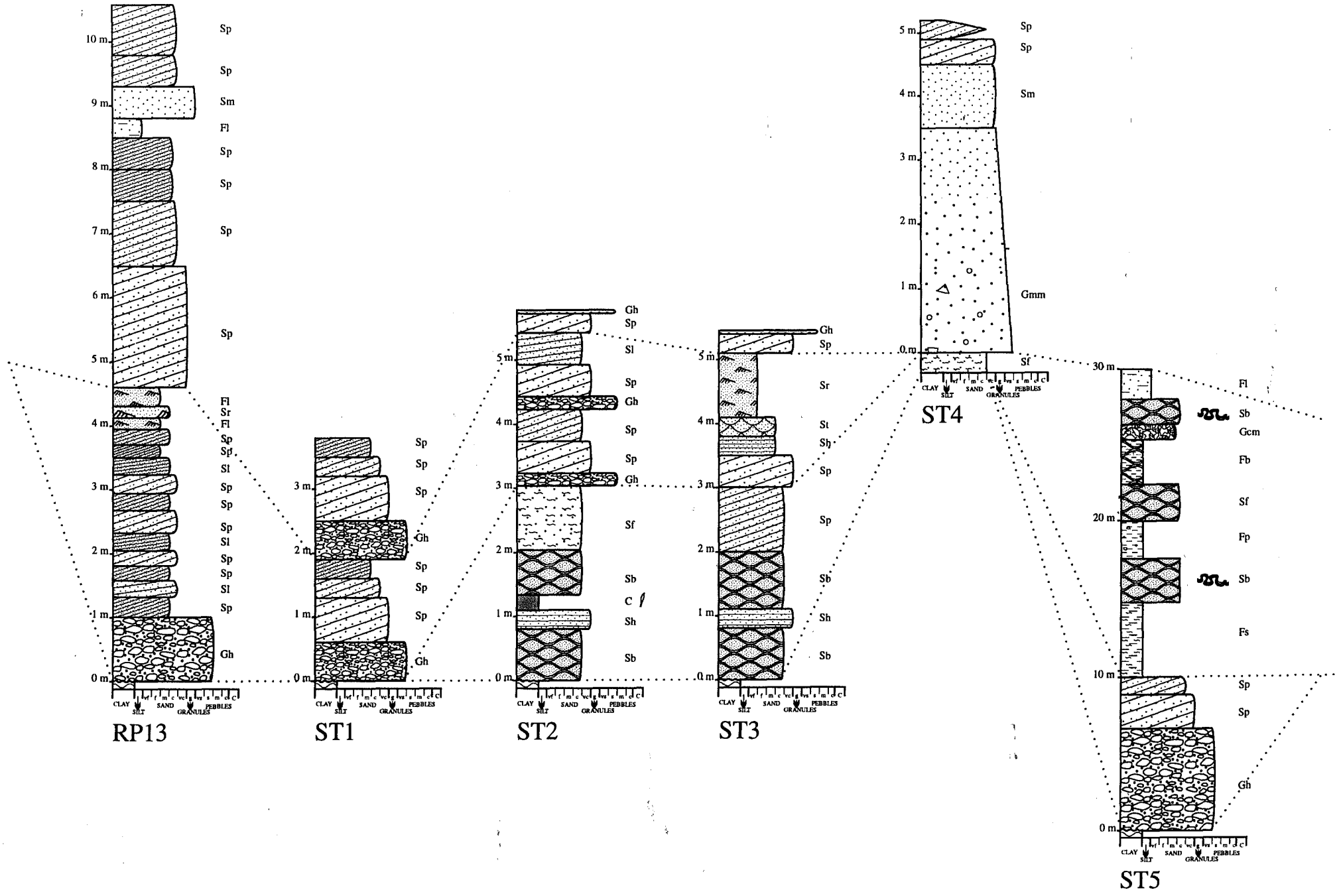

C.

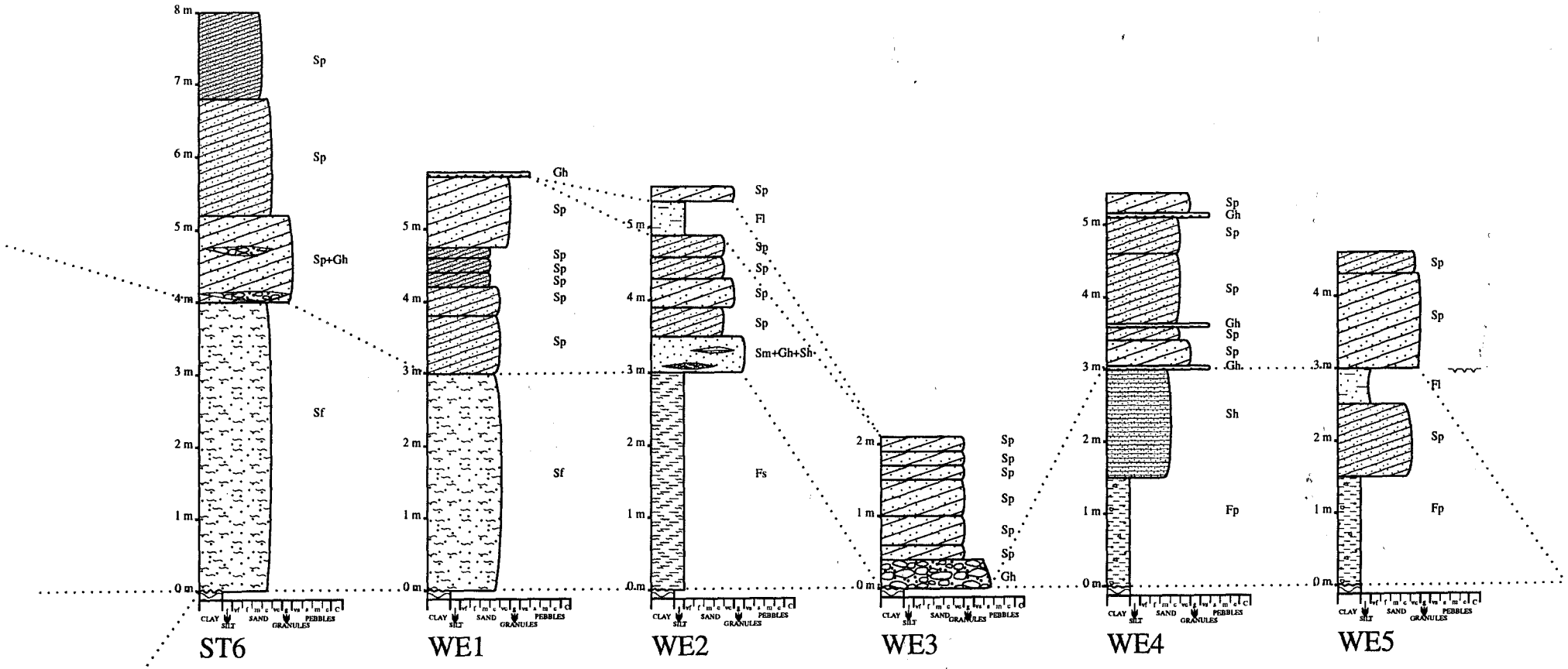
8 m
7 m
6 m
5 m
4 m
3 m
2 m
1 m
0 m
Sp
Sp
Sp+Gh
Sf
ST6
Gh
Sp
Sp
Sp
Sp
Sp
Sf
WE1
Sp
Fl
Sp
Sp
Sp
Sp
Sm+Gh+Sh
Fs
WE2
Sp
Sp
Sp
Sp
Sp
Sp
Gh
WE3
Sp
Gh
Sp
Sp
Gh
Sp
Sp
Gh
Sh
Fp
WE4
Sp
Sp
Fl
Sp
Fp
WE5
CLAY
SILT
SAND
GRANULES
PEBBLES

D.

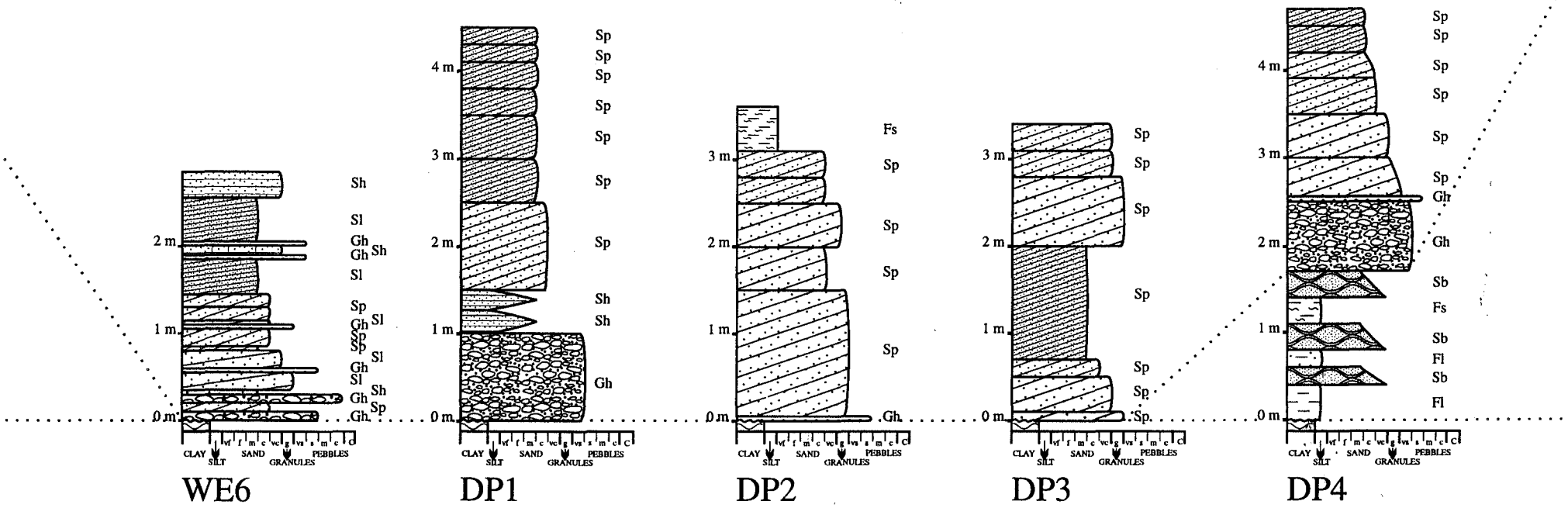
WE6
DP1
DP2
DP3
DP4
0 m
1 m
2 m
3 m
4 m
CLAY
SILT
SAND
GRANULES
PEBBLES

E.

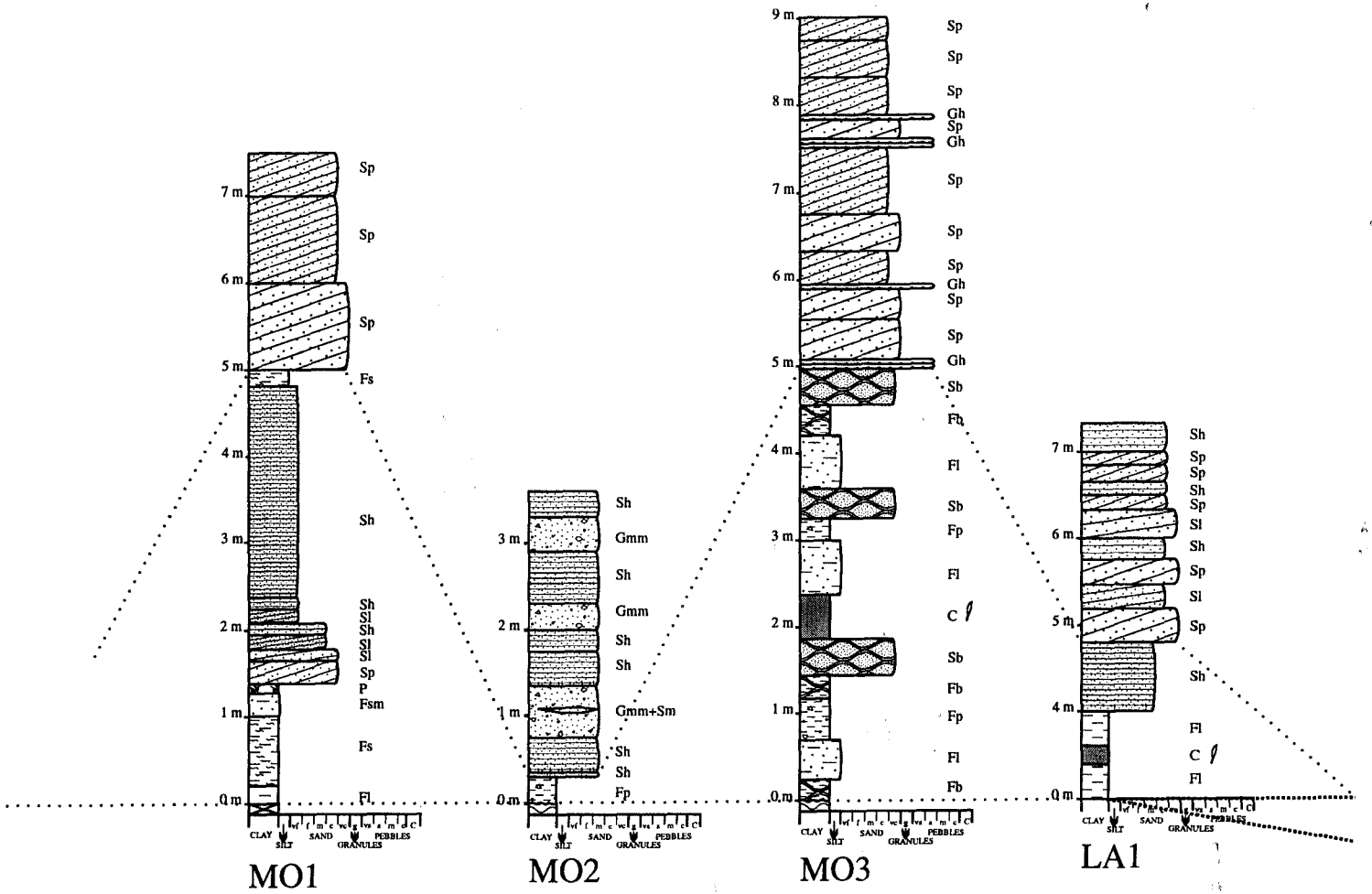

F.

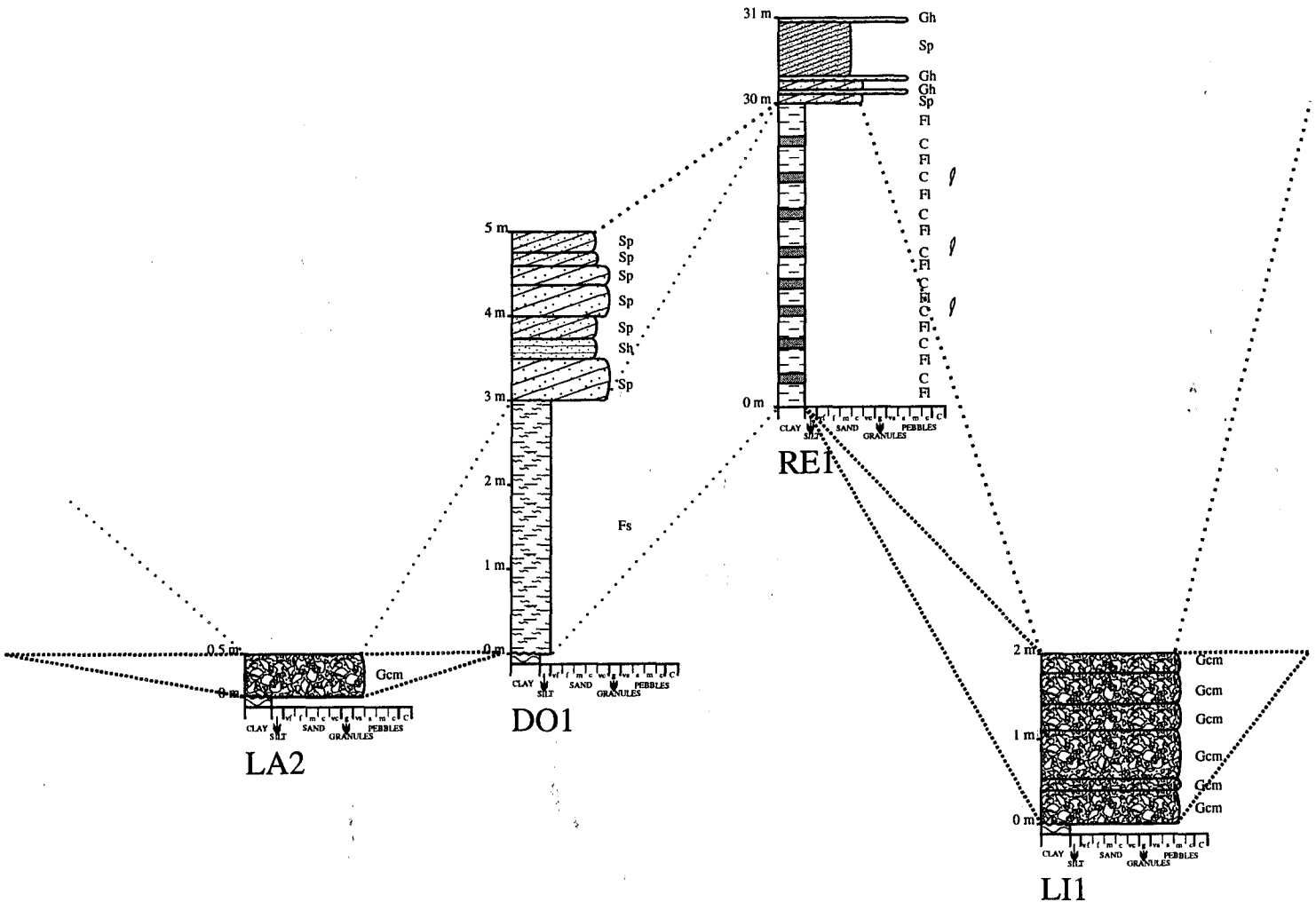
31 m
30 m
0 m
Gh
Sp
Gh
Gh
Sp
Fl
C
Fl
C
Fl
C
Fl
C
Fl
C
Fl
C
Fl
C
Fl
C
Fl
C
Fl
RE1
5 m
4 m
3 m
2 m
1 m
0 m
Sp
Sp
Sp
Sp
Sp
Sh
Sp
Fs
DO1
0.5 m
0 m
Gcm
LA2
2 m
1 m
0 m
Gcm
Gcm
Gcm
Gcm
Gcm
Gcm
LI1
CLAY
SILT
SAND
GRANULES
PEBBLES

G.

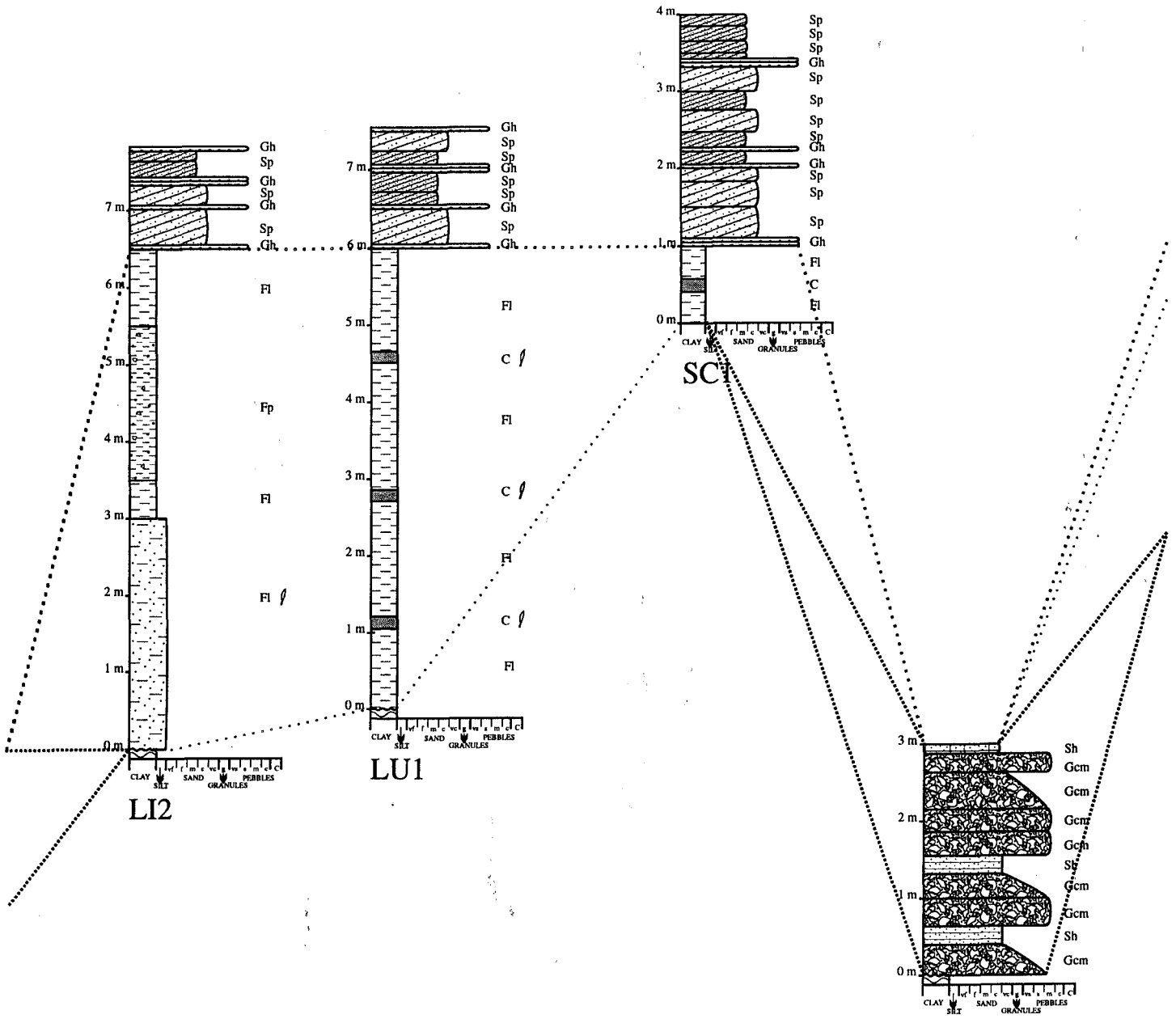
LI2
LU1
SC1
KI1
Gh
Sp
Fl
Fp
C
Sh
Gcm
7 m
6 m
5 m
4 m
3 m
2 m
1 m
0 m
CLAY
SILT
SAND
GRANULES
PEBBLES

H.

~NE

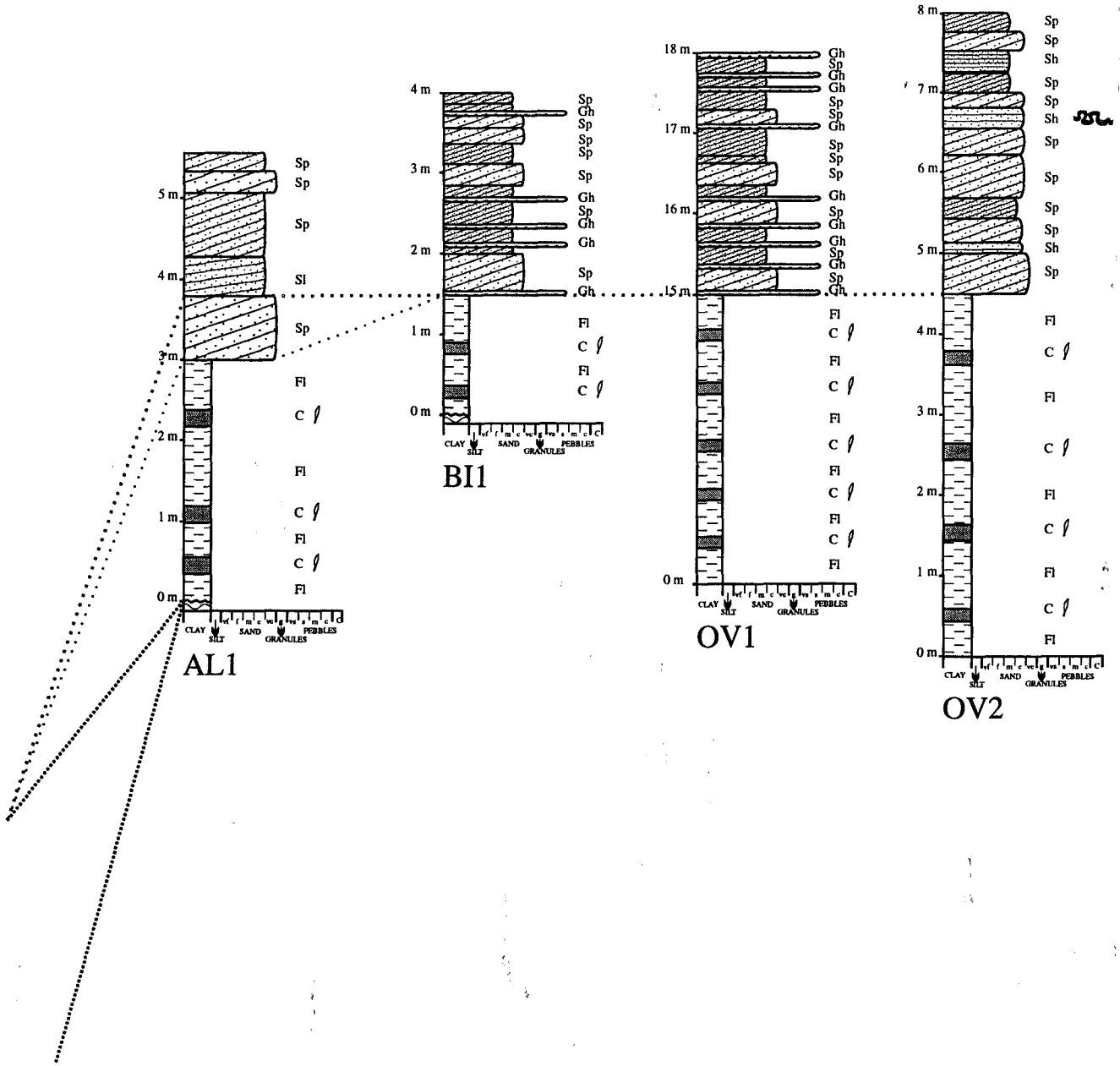

I.

3.

~NE

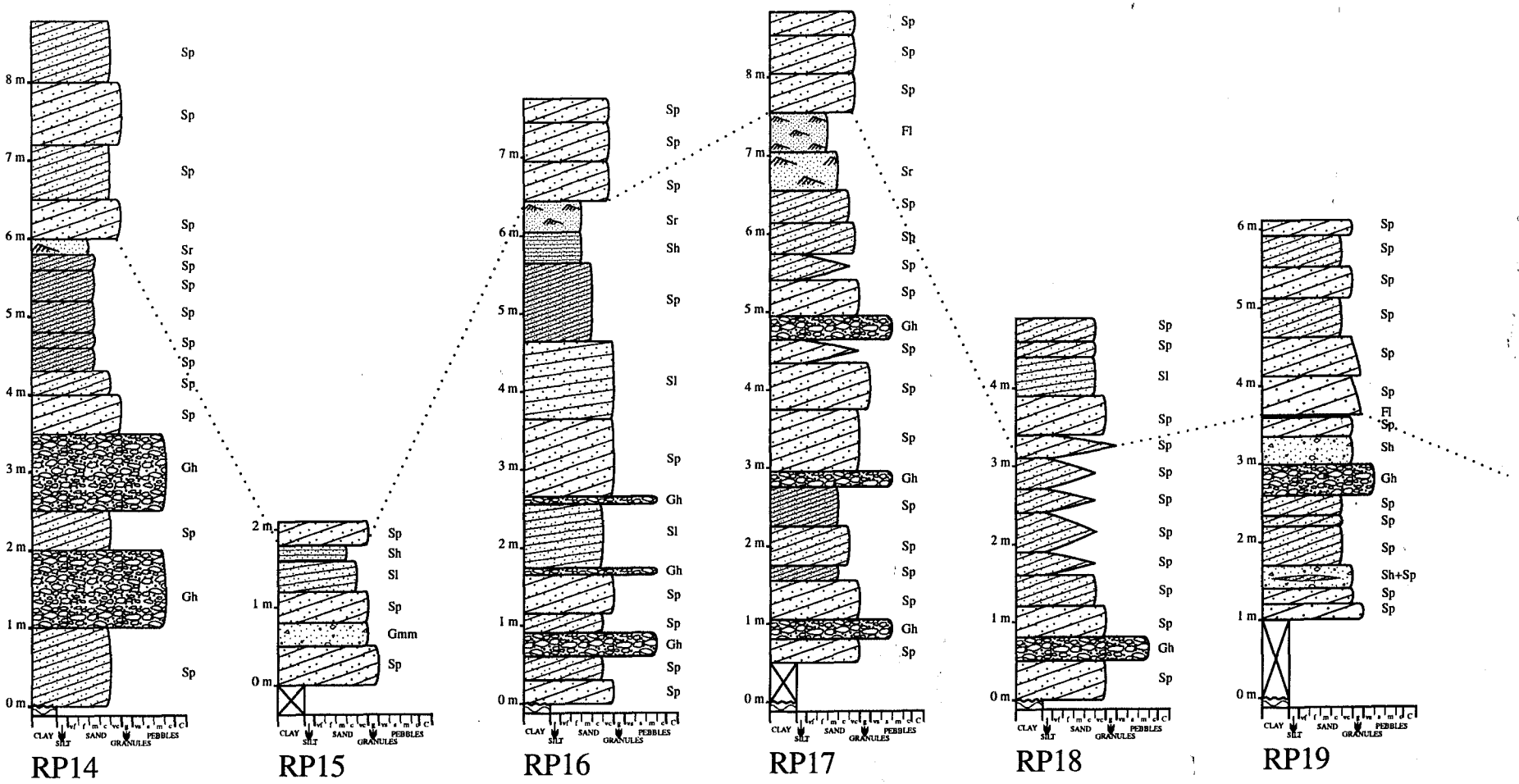
RP14
RP15
RP16
RP17
RP18
RP19
CLAY
SILT
SAND
GRANULES
PEBBLES

A.

~SW

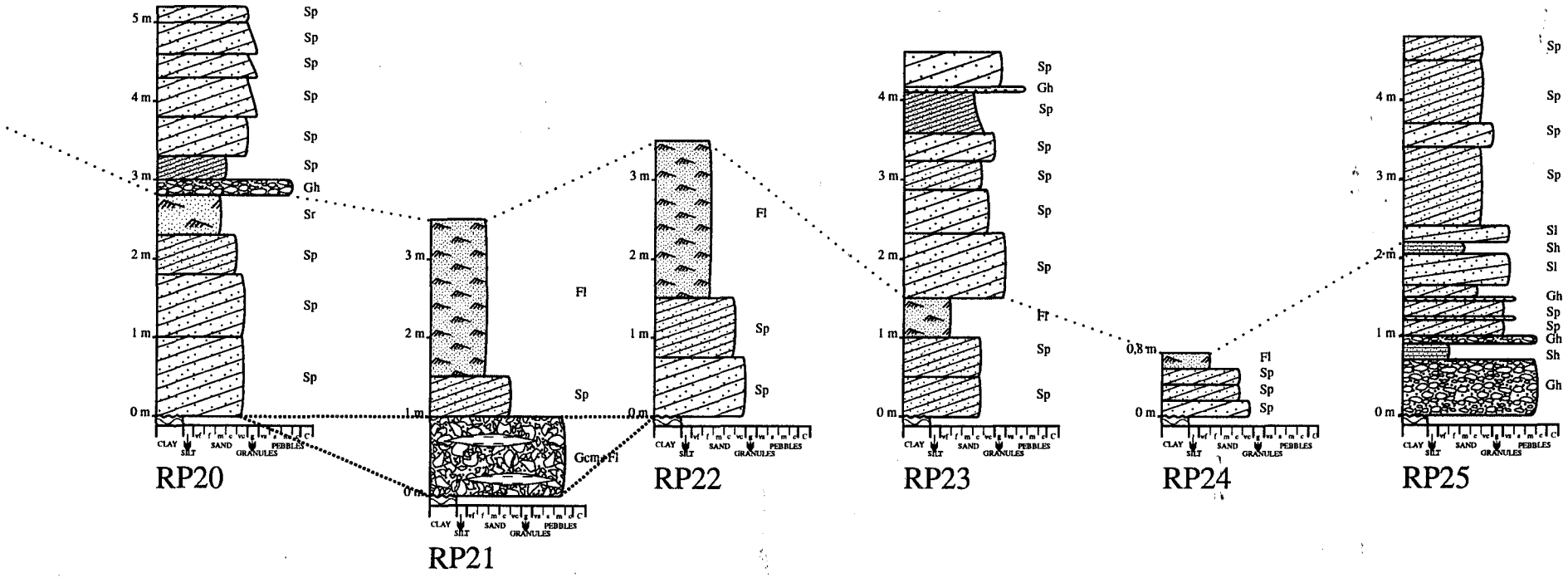
5 m
4 m
3 m
2 m
1 m
0 m
Sp
Sp
Sp
Sp
Sp
Sp
Gh
Sr
Sp
Sp
Sp
CLAY
SILT
SAND
GRANULES
PEBBLES
RP20
Fl
Sp
Gcm, Fl
RP21
Fl
Sp
Sp
RP22
Sp
Gh
Sp
Sp
Sp
Sp
Fl
Sp
Sp
RP23
0,8 m
Fl
Sp
Sp
Sp
RP24
Sp
Sp
Sp
Sl
Sh
Sl
Gh
Sp
Sp
Gh
Sh
Gh
RP25

B.

4.

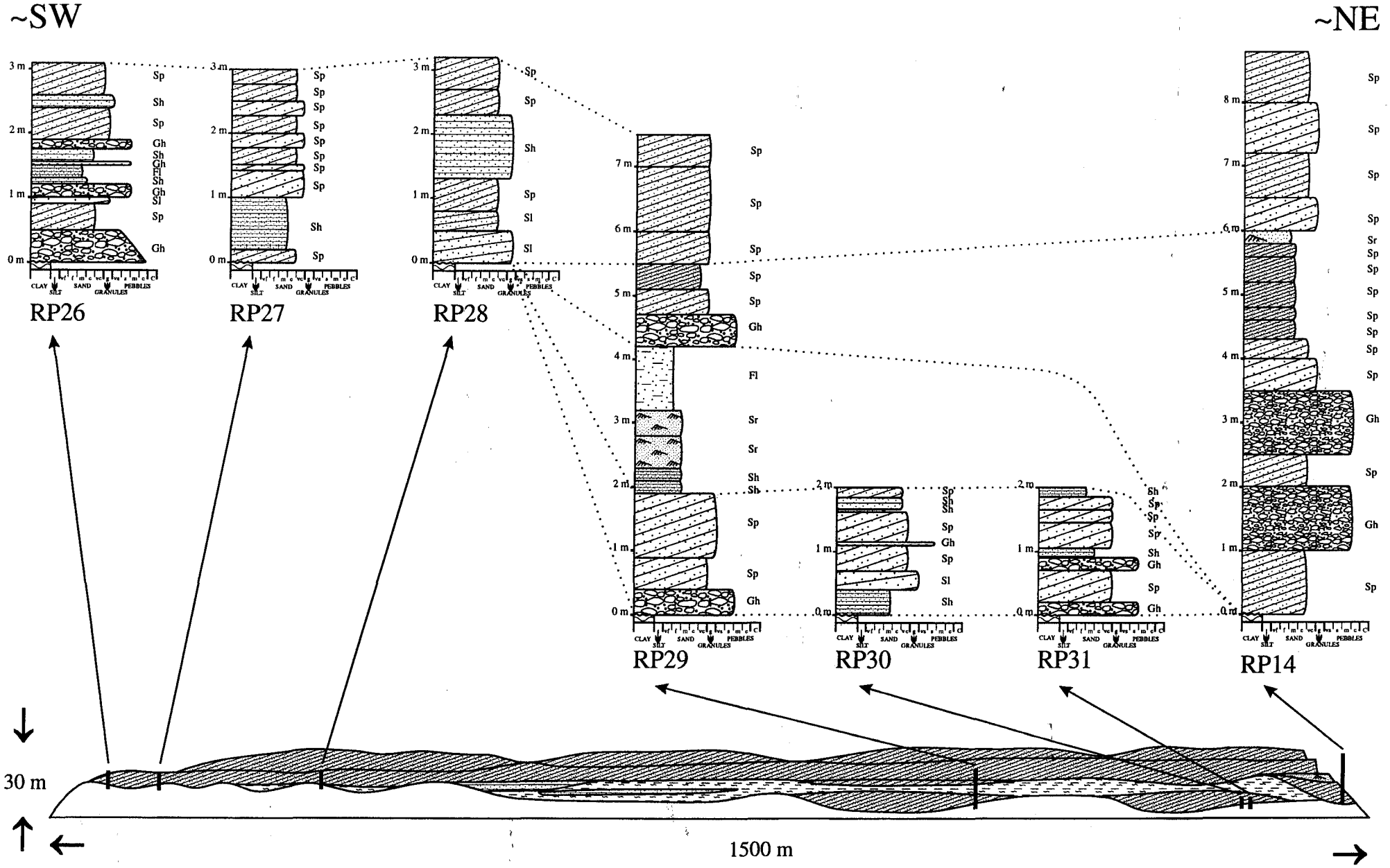
~SW
~NE
RP26
RP27
RP28
RP29
RP30
RP31
RP14
30 m
1500 m

~W ~E

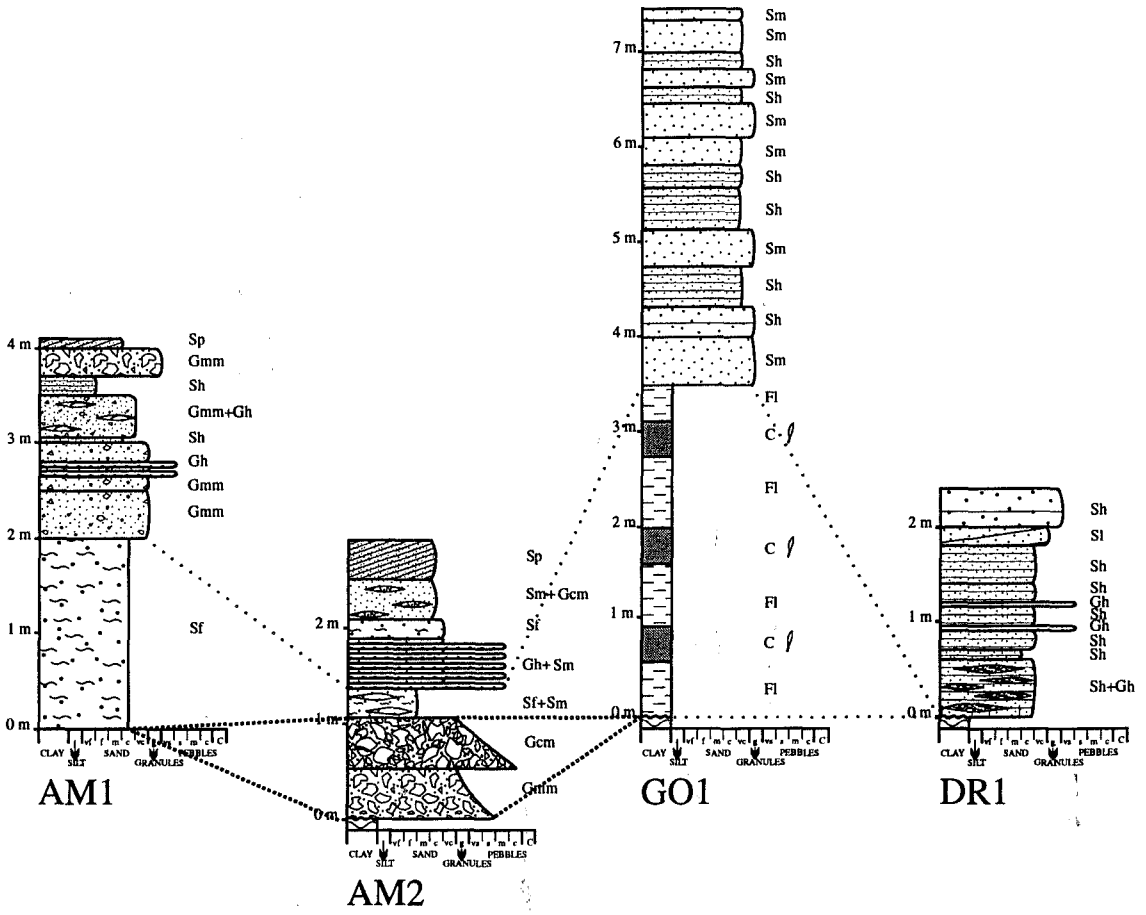
4 m
3 m
2 m
1 m
0 m
Sp
Gmm
Sh
Gmm+Gh
Sh
Gh
Gmm
Gmm
Sf
AM1
2 m
1 m
0 m
Sp
Sm+Gcm
Sf
Gh+Sm
Sf+Sm
Gcm
Gmm
AM2
7 m
6 m
5 m
4 m
3 m
2 m
1 m
0 m
Sm
Sm
Sh
Sm
Sh
Sm
Sm
Sh
Sh
Sm
Sh
Sh
Sm
Fl
C
Fl
C
Fl
C
Fl
GO1
2 m
1 m
0 m
Sh
Sl
Sh
Sh
Sh
Sh
Sh+Gh
DR1
CLAY
SILT
SAND
GRANULES
PEBBLES

6.

~NW

~SE

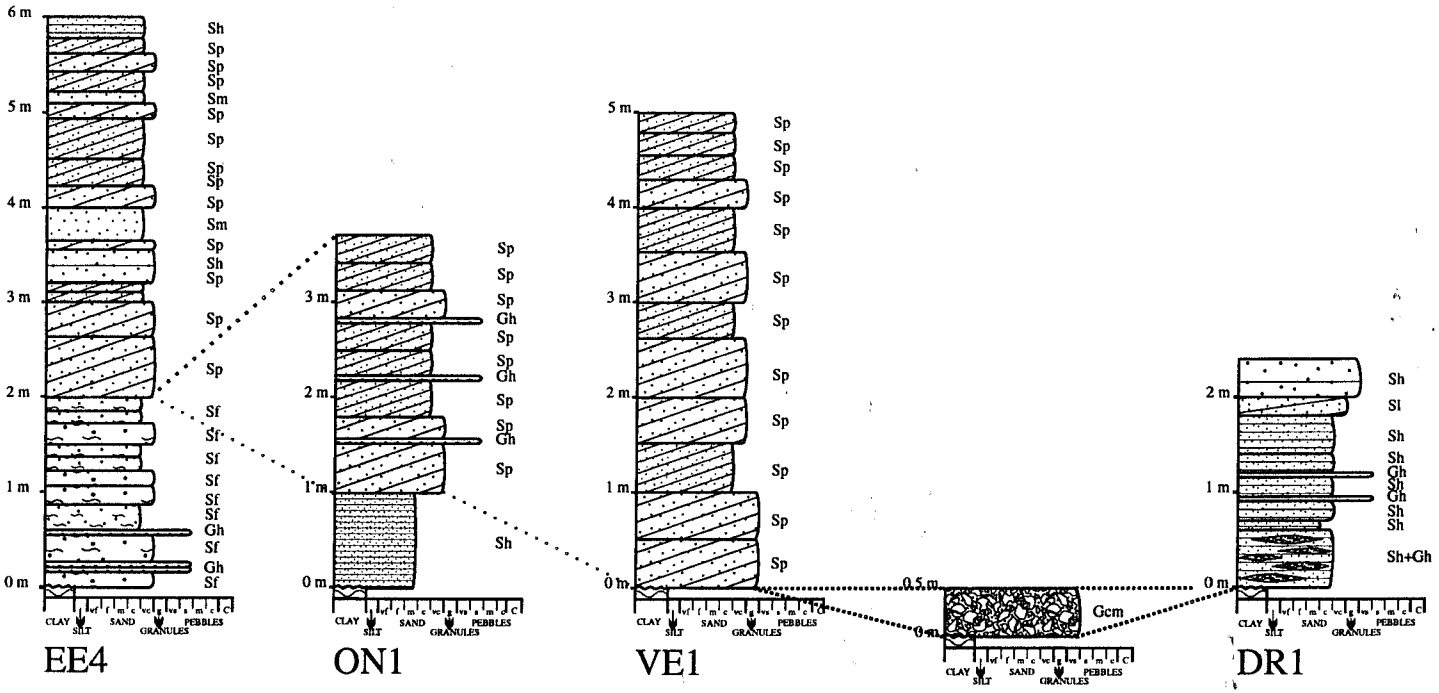
6 m
5 m
4 m
3 m
2 m
1 m
0 m
Sh
Sp
Sm
Sf
Gh
Gcm
Sl
Sh+Gh
CLAY
SILT
SAND
GRANULES
PEBBLES
EE4
ON1
VE1
LA2
DR1

APPENDIX 2

Clast statistical analyses

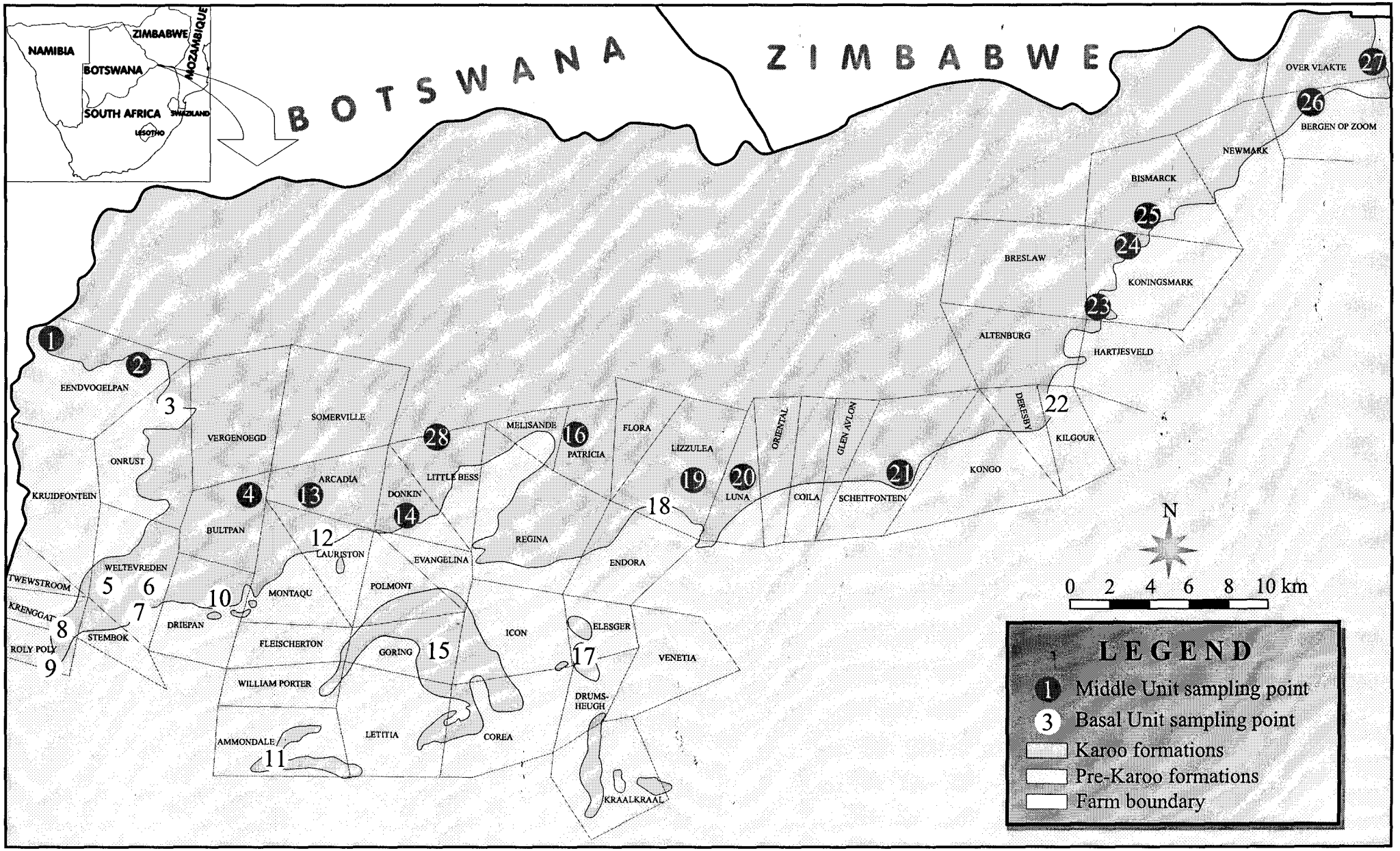

Fig. I. Map showing the sampling points for the clast statistical tests

EENDVOGELPAN1

C-axis	A-axis	Round.	Spher.	C-axis	A-axis	Round.	Spher.
-3,33	-3,91	3,5	1	-3,33	-3,33	3,5	1
-3,33	-3,91	3,5	2	-3,33	-3,33	4,5	1
-3,33	-3,91	4,5	2	-3,91	-4,32	3,5	2
-3,33	-3,91	4,5	2	-4,32	-4,32	3,5	1
-3,91	-3,91	3,5	1	-3,33	-3,33	3,5	1
-3,91	-4,32	4,5	2	-3,33	-3,33	4,5	1
-3,33	-3,91	3,5	2	-4,32	-4,32	3,5	1
-3,33	-3,33	3,5	1	-3,33	-3,33	3,5	2
-2,33	-2,33	3,5	1	-3,33	-3,33	3,5	1
-3,33	-3,33	3,5	1	-3,33	-3,91	3,5	2
-4,62	-5,31	3,5	2	-3,33	-4,9	3,5	2
-3,91	-4,9	3,5	2	-2,33	-3,91	3,5	2
-2,33	-2,33	3,5	1	-3,33	-3,33	3,5	1
-3,91	-3,91	3,5	1	-3,33	-3,91	3,5	2
-3,91	-4,32	3,5	2	-3,33	-3,33	3,5	1
-3,33	-3,33	3,5	1	-3,33	-3,33	4,5	1
-3,33	-3,33	3,5	1	-2,33	-3,33	4,5	2
-2,33	-2,33	3,5	1	-3,91	-4,32	3,5	2
-2,33	-2,33	3,5	1	-3,91	-4,32	3,5	2
-2,33	-2,33	3,5	1	-3,33	-3,33	3,5	1
-3,33	-3,91	3,5	2	-3,91	-3,91	3,5	1
-3,33	-3,91	3,5	2	-3,91	-4,32	3,5	1
-3,33	-3,33	3,5	1	-3,33	-4,32	3,5	2
-2,33	-3,33	3,5	2	-3,33	-4,32	3,5	2
-3,33	-3,33	3,5	1	-3,33	-3,33	3,5	1
-3,33	-3,33	3,5	1	-3,33	-3,33	3,5	1
-3,33	-3,33	3,5	1	-2,33	-3,33	3,5	2
-3,91	-3,91	3,5	1	-3,33	-3,91	3,5	2
-3,91	-4,62	3,5	2	-3,33	-3,91	3,5	2
-3,91	-4,32	3,5	2	-3,33	-3,33	3,5	1
-2,33	-2,33	3,5	1	-3,33	-3,33	3,5	1
-2,33	-2,33	3,5	1	-2,33	-3,33	3,5	2
-2,33	-3,33	3,5	2	-3,91	-3,91	3,5	1
-2,33	-2,33	3,5	1	-2,33	-3,33	3,5	1
-3,33	-5,12	3,5	2	-2,33	-2,33	3,5	1
-3,33	-4,32	3,5	2	-2,33	-2,33	3,5	1
-3,33	-3,91	3,5	2	-2,33	-2,33	3,5	1
-3,33	-3,33	3,5	1	-2,33	-2,33	3,5	1
-3,33	-3,33	3,5	1	-3,33	-3,33	3,5	1
-2,33	-2,33	3,5	1	-2,33	-2,33	3,5	1
-3,33	-3,33	3,5	1	-3,33	-3,91	3,5	2
-3,33	-4,9	3,5	2	-3,33	-3,91	3,5	2
-3,91	-4,62	3,5	2	-3,91	-4,32	3,5	2
-3,91	-4,32	3,5	2	-2,33	-2,33	4,5	2
-3,91	-3,91	3,5	1	-2,33	-3,33	4,5	2
-3,33	-4,32	3,5	2	-3,91	-4,32	3,5	2
-2,33	-2,33	3,5	1	-3,91	-4,62	3,5	2
-3,33	-3,33	3,5	1	-3,91	-3,91	3,5	1
-2,33	-2,33	3,5	1	-3,91	-3,91	3,5	1
-3,91	-3,91	3,5	1	-3,91	-3,91	3,5	1

EENDVOGELPAN1

Clast size distribution

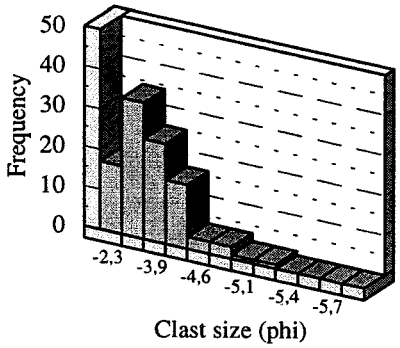

Clast roundness
(-3.91 phi)

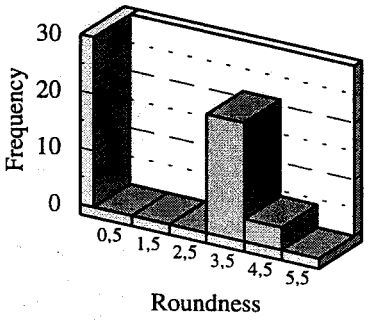

Clast roundness
(-3.33 phi)

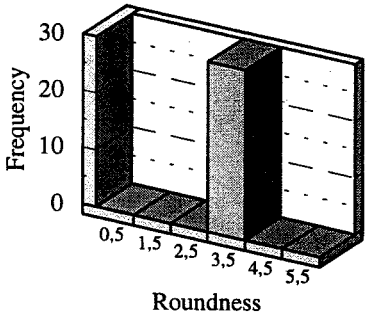

Clast Sphericity

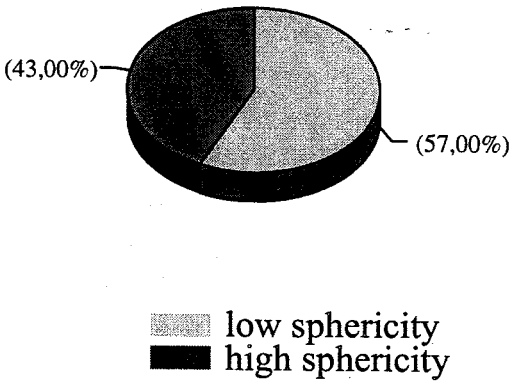

EENDVOGELPAN2

C-axis	A-axis	Round.	Spher.	C-axis	A-axis	Round.	Spher.
-3,91	-5,12	3,5	2	-2,33	-3,33	3,5	2
-4,32	-4,32	3,5	1	-3,91	-3,91	3,5	1
-3,33	-4,32	2,5	2	-3,91	-3,91	2,5	1
-3,33	-3,33	2,5	2	-3,33	-3,91	2,5	2
-3,33	-3,33	2,5	1	-3,33	-4,32	2,5	2
-3,33	-3,33	1,5	1	-2,33	-3,91	3,5	2
-3,33	-3,33	1,5	1	-3,33	-3,33	2,5	1
-4,32	-4,32	1,5	1	-4,62	-5,12	2,5	2
-2,33	-3,33	1,5	2	-3,33	-4,32	2,5	2
-2,33	-3,91	1,5	2	-3,33	-4,62	2,5	1
-3,33	-3,91	1,5	1	-2,33	-3,91	3,5	2
-3,91	-4,32	2,5	2	-2,33	-3,33	3,5	2
-4,32	-4,32	3,5	1	-2,33	-3,33	3,5	2
-4,32	-4,62	2,5	1	-2,33	-4,32	3,5	2
-3,33	-3,33	2,5	1	-3,33	-3,91	3,5	2
-3,33	-3,91	2,5	2	-3,33	-3,91	3,5	1
-3,91	-5,12	3,5	2	-2,33	-4,32	3,5	2
-3,33	-3,33	2,5	1	-3,33	-4,32	2,5	2
-3,33	-4,32	2,5	2	-2,33	-3,33	3,5	2
-4,32	-4,32	3,5	1	-3,33	-4,32	2,5	2
-3,33	-4,62	3,5	2	-3,33	-4,32	3,5	2
-3,33	-3,33	2,5	1	-3,91	-3,91	2,5	1
-3,33	-4,32	3,5	2	-3,33	-5,31	3,5	2
-3,33	-3,33	2,5	1	-3,91	-3,91	3,5	1
-3,33	-3,91	2,5	1	-3,33	-4,62	2,5	2
-3,91	-5,48	3,5	2	-3,33	-3,91	2,5	1
-4,32	-4,62	3,5	2	-3,91	-3,91	2,5	1
-3,56	-4,9	3,5	2	-3,33	-4,32	3,5	2
-2,33	-4,32	3,5	2	-3,33	-3,33	2,5	1
-3,91	-4,32	2,5	2	-3,91	-4,9	3,5	2
-3,91	-3,91	3,5	1	-2,33	-4,62	3,5	2
-2,33	-4,32	3,5	2	-4,32	-4,62	2,5	2
-4,32	-4,62	3,5	2	-3,33	-4,32	3,5	2
-4,32	-4,9	3,5	2	-3,33	-4,62	2,5	2
-3,91	-4,32	2,5	2	-4,62	-5,31	2,5	2
-3,33	-4,62	2,5	1	-4,62	-5,12	2,5	1
-3,91	-5,48	2,5	2	-4,32	-5,12	2,5	2
-3,91	-4,32	2,5	1	-3,33	-4,32	2,5	1
-3,33	-3,33	2,5	1	-2,33	-4,32	2,5	2
-3,33	-4,62	2,5	2	-4,32	-5,12	2,5	2
-3,91	-3,91	2,5	1	-3,33	-4,32	3,5	2
-2,33	-3,33	3,5	2	-4,32	-5,31	2,5	2
-3,33	-3,33	3,5	1	-4,62	-4,9	3,5	1
-3,91	-4,62	2,5	2	-3,33	-3,33	3,5	1
-3,91	-3,91	3,5	1	-3,91	-4,9	3,5	2
-3,91	-4,32	2,5	2	-3,91	-3,91	2,5	1
-3,33	-3,33	3,5	1	-4,32	-4,32	2,5	1
-2,33	-2,33	2,5	1	-3,91	-3,91	2,5	1
-3,33	-3,91	2,5	2	-4,9	-4,9	3,5	1
-2,33	-3,33	2,5	2	-3,91	-3,91	3,5	1

EENDVOGELPAN2

Clast size distribution

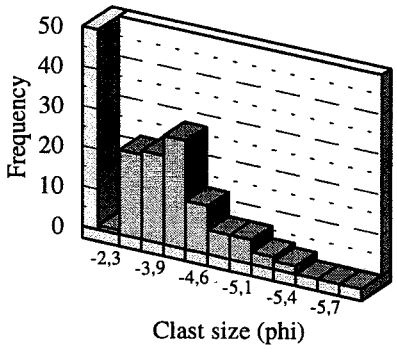

Clast roundness

(-3.91 phi)

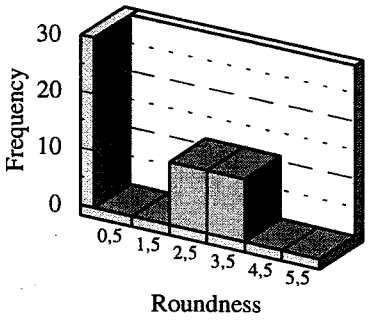

Clast roundness

(-3.33 phi)

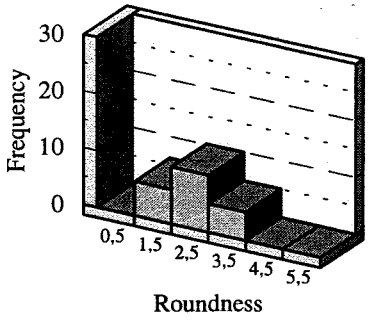

Clast Sphericity

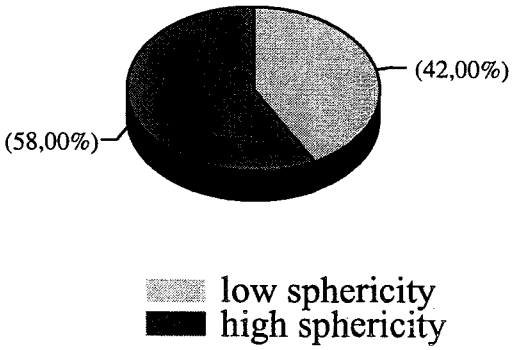

ONRUST

C-axis	A-axis	Round.	Spher.	C-axis	A-axis	Round.	Spher.
-3,33	-3,33	1,5	1	-3,33	-3,33	2,5	1
-3,33	-3,33	1,5	1	-2,33	-7,22	1,5	2
-2,33	-3,33	1,5	2	-2,33	-3,33	1,5	2
-2,33	-3,33	1,5	1	-3,33	-3,33	2,5	1
-2,33	-3,91	2,5	2	-3,91	-3,91	3,5	1
-3,33	-3,91	2,5	2	-2,33	-4,62	2,5	2
-3,33	-4,62	1,5	2	-3,33	-3,91	1,5	2
-2,33	-2,33	1,5	1	-2,33	-4,62	1,5	2
-2,33	-2,33	1,5	1	-2,33	-3,33	1,5	2
-2,33	-2,33	1,5	1	-3,33	-3,91	2,5	2
-2,33	-4,32	2,5	2	-3,33	-3,33	2,5	1
-3,33	-3,33	2,5	1	-3,33	-3,33	1,5	1
-3,33	-3,33	2,5	1	-3,33	-3,91	1,5	2
-3,33	-3,33	1,5	1	-3,33	-3,33	3,5	1
-3,33	-3,33	1,5	1	-2,33	-3,33	2,5	2
-3,33	-3,33	1,5	1	-2,33	-2,33	1,5	1
-3,33	-3,33	1,5	1	-3,33	-3,91	1,5	1
-3,33	-3,33	2,5	1	-2,33	-2,33	1,5	1
-3,33	-3,91	2,5	1	-2,33	-2,33	3,5	1
-2,33	-2,33	2,5	1	-2,33	-3,91	3,5	1
-3,33	-3,91	3,5	1	-3,91	-4,32	3,5	2
-2,33	-3,91	3,5	2	-2,33	-3,33	2,5	1
-3,33	-4,32	3,5	2	-2,33	-2,33	1,5	1
-2,33	-3,33	2,5	1	-2,33	-2,33	2,5	1
-2,33	-3,33	1,5	1	-3,33	-4,9	3,5	2
-3,33	-3,33	2,5	1	-3,33	-3,91	3,5	2
-3,33	-3,33	2,5	1	-2,33	-3,33	2,5	2
-3,33	-3,33	0,5	1	-3,33	-3,91	2,5	2
-3,33	-3,91	0,5	1	-3,33	-3,33	2,5	1
-2,33	-2,33	1,5	1	-3,33	-3,91	2,5	2
-3,33	-3,91	2,5	1	-2,33	-2,33	2,5	1
-3,33	-3,91	3,5	1	-2,33	-3,91	1,5	2
-3,33	-3,33	2,5	1	-3,33	-3,91	2,5	1
-2,33	-4,32	2,5	2	-2,33	-3,33	1,5	1
-3,91	-3,91	1,5	1	-3,33	-3,91	2,5	2
-3,33	-3,91	3,5	2	-3,33	-3,33	3,5	1
-2,33	-3,33	3,5	1	-3,33	-3,91	2,5	2
-2,33	-3,33	2,5	1	-3,33	-4,32	3,5	2
-2,33	-3,91	3,5	2	-3,33	-4,32	2,5	2
-3,33	-3,91	2,5	2	-3,33	-3,91	3,5	2
-3,91	-4,62	2,5	2	-3,33	-3,33	2,5	1
-3,33	-3,91	3,5	1	-2,33	-2,33	2,5	1
-3,33	-3,91	1,5	1	-2,33	-3,33	2,5	2
-3,33	-3,91	3,5	2	-2,33	-3,33	2,5	2
-3,33	-3,33	4,5	1	-3,33	-3,33	3,5	1
-3,33	-4,32	3,5	2	-3,33	-3,91	1,5	2
-3,33	-4,32	1,5	2	-2,33	-2,33	3,5	1
-3,33	-3,33	1,5	1	-3,33	-4,32	2,5	2
-2,33	-2,33	2,5	1	-3,33	-3,33	2,5	1
-3,33	-3,91	1,5	2	-2,33	-3,33	2,5	2

ONRUST

Clast size distribution

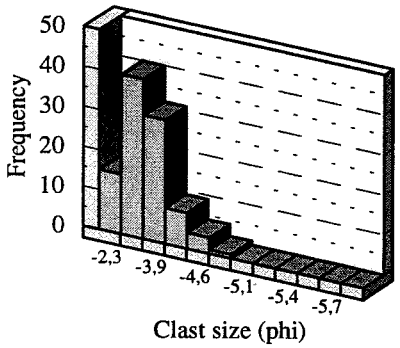

Clast roundness
(-3.91 phi)

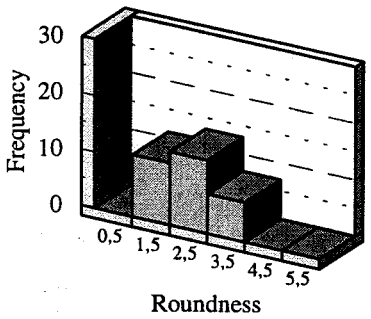

Clast roundness
(-3.33 phi)

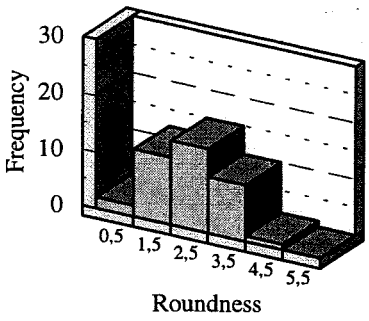

Clast Sphericity

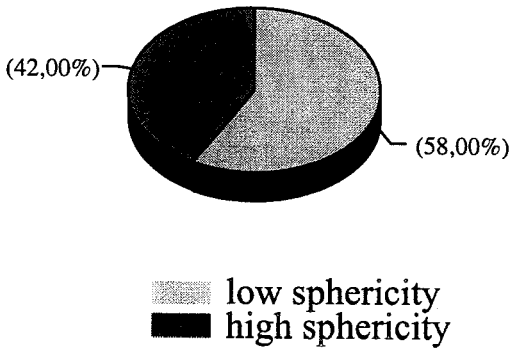

BULTPAN

C-axis	A-axis	Round.	Spher.	C-axis	A-axis	Round.	Spher.
-4,32	-4,9	3,5	2	-2,33	-2,33	2,5	1
-3,91	-5,31	3,5	2	-2,33	-2,33	2,5	1
-3,91	-4,32	3,5	1	-2,33	-2,33	2,5	1
-3,91	-4,32	2,5	2	-2,33	-2,33	3,5	1
-3,91	-4,32	2,5	2	-2,33	-2,33	2,5	1
-3,91	-4,32	2,5	1	-3,33	-3,33	2,5	1
-3,33	-3,91	3,5	1	-3,91	-4,62	3,5	2
-3,33	-3,33	2,5	1	-3,33	-3,33	3,5	1
-3,91	-4,32	3,5	2	-3,33	-4,32	3,5	2
-3,91	-4,32	3,5	2	-3,91	-3,91	3,5	1
-4,32	-4,32	3,5	1	-3,33	-3,33	3,5	1
-3,91	-4,32	3,5	1	-3,33	-4,32	2,5	2
-4,32	-5,12	2,5	2	-4,32	-4,32	3,5	1
-3,91	-4,9	2,5	2	-3,91	-3,91	3,5	1
-3,91	-3,91	3,5	1	-4,32	-5,31	3,5	2
-3,91	-4,32	2,5	2	-3,91	-3,91	3,5	1
-4,32	-4,62	2,5	1	-3,91	-3,91	2,5	1
-4,32	-4,32	2,5	1	-3,91	-3,91	2,5	1
-4,32	-4,32	3,5	1	-3,91	-4,32	2,5	2
-3,91	-3,91	3,5	1	-3,91	-3,91	3,5	1
-3,91	-4,32	3,5	1	-2,33	-3,33	2,5	2
-3,33	-3,33	2,5	1	-3,33	-3,33	2,5	1
-3,33	-4,32	2,5	2	-3,33	-3,91	3,5	1
-4,32	-4,32	2,5	1	-3,91	-4,32	2,5	2
-4,32	-4,32	3,5	1	-4,32	-4,32	3,5	1
-4,32	-4,32	2,5	1	-3,33	-4,32	2,5	1
-3,91	-4,62	3,5	2	-3,33	-3,91	2,5	1
-3,91	-3,91	3,5	1	-3,33	-4,32	3,5	2
-3,33	-3,91	3,5	1	-3,33	-3,91	3,5	1
-3,91	-3,91	3,5	1	-3,91	-4,32	2,5	1
-3,91	-3,91	3,5	1	-3,91	-3,91	3,5	1
-3,91	-4,32	2,5	1	-3,91	-4,32	3,5	2
-4,32	-4,62	2,5	2	-3,33	-3,33	2,5	1
-4,32	-4,9	3,5	2	-4,32	-4,9	3,5	2
-4,32	-4,32	3,5	1	-4,32	-4,9	3,5	2
-3,91	-4,32	3,5	2	-3,33	-3,33	2,5	1
-3,91	-3,91	2,5	1	-3,33	-3,33	3,5	1
-3,33	-3,91	2,5	2	-3,33	-3,33	3,5	1
-3,33	-3,33	3,5	1	-3,33	-3,33	2,5	1
-3,33	-3,33	2,5	1	-3,33	-3,33	3,5	1
-3,33	-3,91	2,5	2	-3,91	-4,32	2,5	1
-2,33	-2,33	3,5	1	-3,33	-4,32	2,5	2
-3,91	-3,91	3,5	1	-3,91	-3,91	3,5	1
-3,33	-4,32	2,5	2	-3,33	-4,32	3,5	2
-3,91	-3,91	3,5	1	-3,91	-3,91	3,5	1
-3,91	-4,32	3,5	2	-3,33	-3,33	3,5	1
-3,33	-4,32	2,5	2	-2,33	-2,33	3,5	1
-2,33	-3,33	2,5	1	-3,33	-3,33	3,5	1
-3,91	-4,32	3,5	2	-3,33	-3,33	2,5	1
-3,91	-4,62	3,5	2	-3,33	-3,91	2,5	2

BULTPAN

Clast size distribution

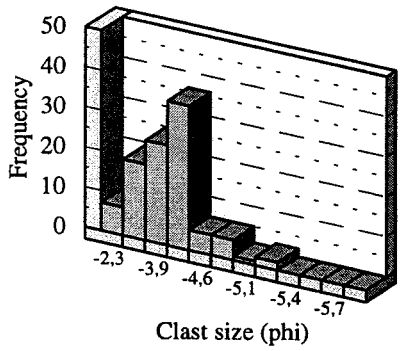

Clast roundness

(-3.91 phi)

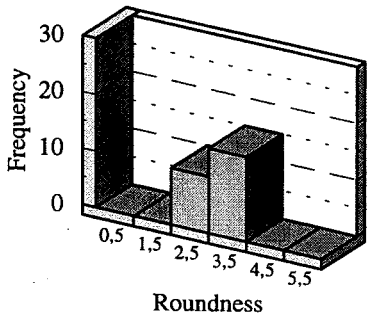

Clast roundness

(-3.33 phi)

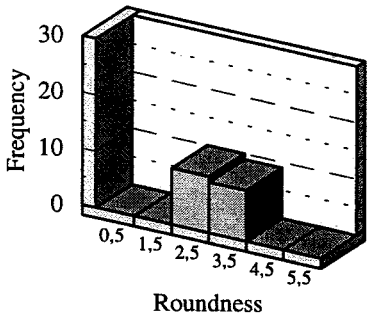

Clast Sphericity

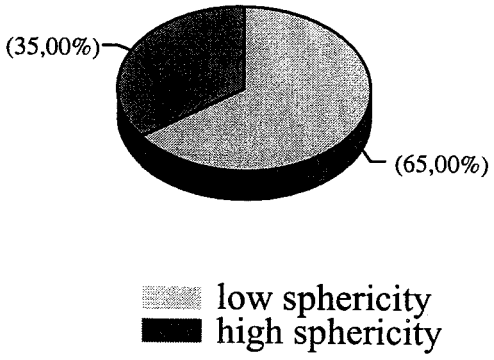

WELTEVREDEN1

C-axis	A-axis	Round.	Spher.	C-axis	A-axis	Round.	Spher.
-3,33	-3,33	3,5	1	-2,33	-3,33	2,5	2
-3,33	-4,32	3,5	2	-2,33	-3,33	3,5	2
-3,91	-3,91	3,5	1	-3,91	-3,91	3,5	1
-3,33	-3,33	3,5	1	-3,33	-4,32	4,5	2
-3,33	-4,32	3,5	2	-3,91	-3,91	2,5	1
-3,91	-3,91	2,5	1	-3,33	-3,33	2,5	1
-3,91	-3,91	2,5	1	-2,33	-4,62	4,5	2
-3,91	-3,91	3,5	1	-3,91	-4,62	2,5	2
-3,33	-3,91	3,5	2	-3,33	-4,32	3,5	2
-2,33	-3,33	2,5	2	-3,91	-3,91	5,5	1
-3,33	-3,33	4,5	1	-3,33	-4,32	5,5	2
-3,91	-3,91	4,5	1	-3,33	-3,91	2,5	2
-2,33	-3,33	3,5	2	-2,33	-2,33	2,5	1
-3,91	-4,32	3,5	2	-3,33	-3,33	5,5	1
-3,91	-4,32	2,5	2	-3,33	-3,33	5,5	1
-3,33	-3,91	4,5	2	-3,91	-3,91	5,5	1
-3,91	-4,32	3,5	2	-2,33	-3,33	4,5	2
-3,33	-3,33	3,5	1	-2,33	-3,33	4,5	2
-3,33	-3,91	4,5	2	-3,33	-3,91	5,5	2
-3,33	-3,91	5,5	2	-3,33	-3,33	5,5	1
-3,33	-3,33	4,5	1	-3,33	-3,33	4,5	1
-3,33	-3,33	3,5	1	-3,91	-3,91	2,5	1
-2,33	-4,62	5,5	2	-3,33	-3,91	2,5	2
-3,33	-3,33	2,5	1	-3,33	-3,91	2,5	2
-3,33	-3,91	1,5	2	-2,33	-2,33	2,5	1
-3,33	-3,33	5,5	1	-2,33	-2,33	4,5	1
-3,33	-3,33	5,5	1	-3,33	-3,91	1,5	2
-3,91	-3,91	1,5	1	-3,33	-3,33	2,5	1
-3,33	-3,33	3,5	1	-3,33	-3,33	2,5	1
-3,33	-3,91	3,5	2	-3,33	-3,33	3,5	1
-3,91	-4,62	2,5	2	-3,91	-3,91	2,5	1
-2,33	-3,91	4,5	2	-3,91	-3,91	1,5	1
-2,33	-3,91	2,5	2	-3,33	-4,32	3,5	2
-3,33	-3,91	1,5	2	-2,33	-3,33	4,5	2
-3,33	-3,33	1,5	2	-2,33	-3,91	4,5	2
-3,91	-3,91	2,5	1	-3,33	-3,33	4,5	1
-3,91	-4,32	3,5	2	-3,91	-3,91	2,5	1
-3,33	-3,91	3,5	2	-3,91	-3,91	1,5	1
-3,33	-3,91	3,5	2	-2,33	-3,33	4,5	2
-3,91	-4,62	3,5	2	-2,33	-2,33	3,5	1
-3,33	-3,33	5,5	1	-3,33	-3,33	4,5	1
-3,91	-3,91	2,5	1	-2,33	-3,33	4,5	2
-3,33	-3,91	5,5	2	-3,33	-3,91	2,5	2
-3,33	-3,33	2,5	1	-3,33	-3,91	3,5	2
-3,33	-3,91	3,5	2	-2,33	-3,91	2,5	2
-3,91	-3,91	2,5	1	-2,33	-4,32	2,5	2
-2,33	-3,91	2,5	2	-3,33	-3,91	2,5	2
-3,33	-3,33	2,5	1	-2,33	-3,33	2,5	2
-3,33	-3,33	3,5	1	-3,33	-3,33	5,5	1
-2,33	-2,33	2,5	1	-3,33	-4,32	3,5	2

WELTEVREDEN1

Clast size distribution

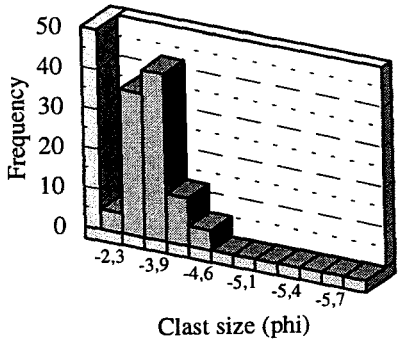

Clast roundness
(-3.91 phi)

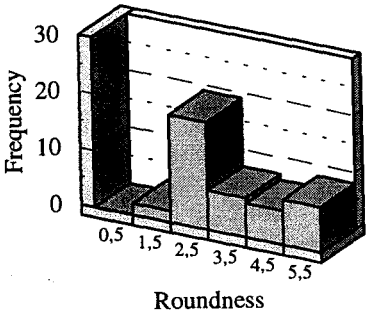

Clast roundness
(-3.33 phi)

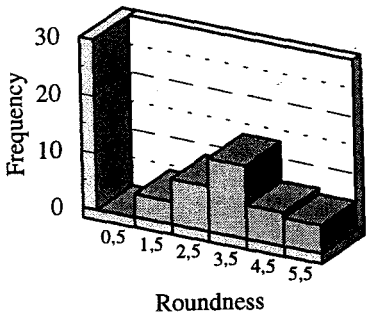

Clast Sphericity

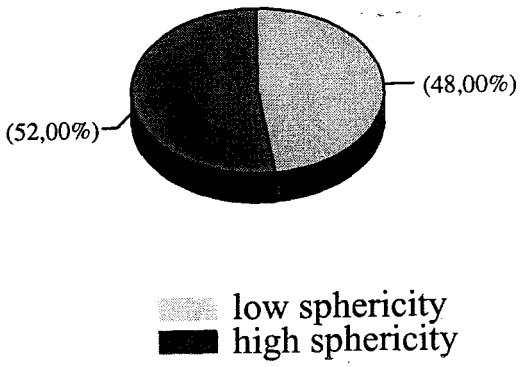

WELTEVREDEN2

C-axis	A-axis	Round.	Spher.	C-axis	A-axis	Round.	Spher.
-2,33	-2,33	1,5	1	-3,33	-3,33	3,5	1
-2,33	-2,33	1,5	1	-2,33	-3,33	2,5	2
-2,33	-2,33	1,5	1	-3,33	-3,33	2,5	1
-2,33	-2,33	1,5	1	-3,33	-3,33	3,5	1
-2,33	-3,33	0,5	2	-2,33	-3,33	3,5	2
-2,33	-3,33	0,5	2	-2,33	-3,33	2,5	2
-2,33	-2,33	2,5	1	-2,33	-3,91	1,5	2
-3,33	-3,91	1,5	2	-3,33	-3,91	3,5	2
-2,33	-2,33	1,5	1	-3,91	-3,91	1,5	1
-3,33	-3,33	1,5	1	-3,91	-3,91	1,5	1
-2,33	-2,33	0,5	1	-3,91	-3,91	2,5	2
-2,33	-3,33	1,5	1	-2,33	-2,33	1,5	1
-2,33	-3,33	1,5	2	-2,33	-2,33	2,5	1
-2,33	-3,33	0,5	1	-3,33	-3,33	2,5	1
-2,33	-2,33	0,5	1	-2,33	-2,33	2,5	1
-2,33	-3,33	0,5	2	-2,33	-2,33	3,5	1
-2,33	-3,33	0,5	2	-2,33	-3,33	3,5	2
-3,33	-3,33	0,5	2	-2,33	-3,33	2,5	1
-3,33	-3,33	0,5	1	-2,33	-2,33	1,5	1
-2,33	-2,33	1,5	1	-3,91	-3,91	1,5	1
-3,33	-3,33	2,5	1	-2,33	-2,33	0,5	1
-2,33	-2,33	2,5	1	-2,33	-3,91	4,5	2
-2,33	-2,33	2,5	1	-3,33	-3,33	1,5	1
-3,33	-4,32	2,5	2	-2,33	-2,33	0,5	1
-2,33	-2,33	2,5	2	-2,33	-3,33	2,5	2
-2,33	-3,33	2,5	2	-3,91	-4,32	1,5	2
-3,33	-3,33	2,5	1	-2,33	-3,33	3,5	2
-2,33	-3,33	2,5	2	-3,33	-3,33	2,5	2
-3,91	-3,91	2,5	1	-3,33	-3,91	2,5	2
-2,33	-2,33	2,5	1	-2,33	-3,33	3,5	2
-3,33	-3,33	2,5	1	-3,33	-3,33	4,5	1
-2,33	-3,91	2,5	2	-3,33	-3,33	3,5	1
-2,33	-3,33	2,5	2	-2,33	-3,33	3,5	2
-2,33	-2,33	2,5	1	-3,33	-3,33	2,5	1
-2,33	-3,33	3,5	2	-3,33	-3,33	1,5	1
-2,33	-2,33	1,5	1	-2,33	-2,33	1,5	1
-2,33	-2,33	2,5	1	-2,33	-3,33	2,5	2
-3,33	-3,91	2,5	2	-3,91	-3,91	1,5	1
-3,33	-3,91	3,5	2	-2,33	-2,33	1,5	1
-2,33	-3,33	0,5	2	-2,33	-3,33	2,5	2
-2,33	-2,33	0,5	1	-3,33	-3,33	2,5	1
-2,33	-3,33	2,5	2	-3,33	-3,33	2,5	1
-2,33	-3,33	1,5	2	-3,33	-3,33	2,5	1
-3,33	-3,91	1,5	2	-2,33	-3,91	1,5	2
-3,91	-4,32	1,5	2	-2,33	-3,33	1,5	2
-2,33	-3,91	1,5	2	-2,33	-2,33	1,5	1
-2,33	-3,33	2,5	2	-3,33	-3,33	1,5	1
-3,33	-4,32	3,5	2	-2,33	-3,33	2,5	2
-2,33	-3,33	2,5	2	-3,33	-3,33	2,5	1
-2,33	-3,33	3,5	2	-2,33	-2,33	1,5	1

WELTEVREDEN2

Clast size distribution

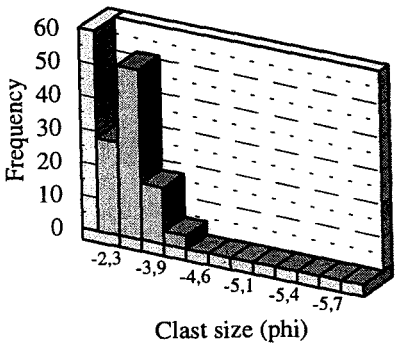

Clast roundness
(-3.91 phi)

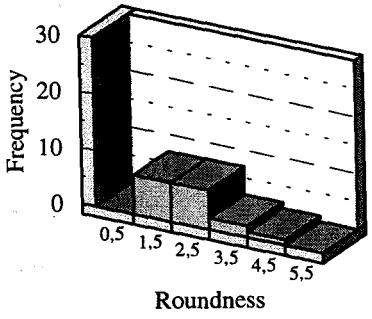

Clast roundness
(-3.33 phi)

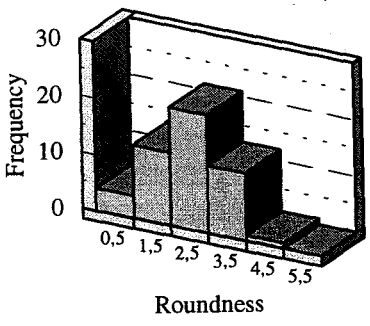

Clast Sphericity

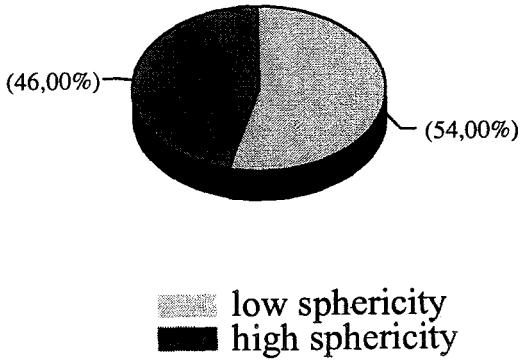

WELTEVREDEN3

C-axis	A-axis	Round.	Spher.	C-axis	A-axis	Round.	Spher.
-3,33	-4,32	0,5	2	-2,33	-3,91	4,5	2
-3,33	-3,91	2,5	2	-2,33	-3,33	4,5	2
-2,33	-3,33	2,5	1	-3,91	-3,91	3,5	1
-3,33	-3,91	2,5	2	-4,32	-4,9	1,5	2
-3,91	-4,32	2,5	2	-3,91	-4,32	2,5	2
-3,33	-3,33	2,5	1	-3,91	-4,32	2,5	2
-3,91	-3,91	2,5	1	-3,91	-3,91	1,5	1
-2,33	-3,33	3,5	2	-3,33	-3,91	3,5	2
-3,33	-3,91	2,5	2	-3,33	-4,62	4,5	2
-3,33	-3,91	3,5	2	-3,33	-4,32	2,5	2
-3,33	-3,91	2,5	2	-2,33	-3,33	2,5	2
-3,33	-3,91	3,5	2	-4,32	-4,9	2,5	2
-3,91	-4,32	4,5	2	-3,91	-4,9	1,5	2
-4,32	-4,9	1,5	2	-3,91	-4,62	2,5	2
-4,32	-4,32	3,5	1	-3,33	-4,32	1,5	2
-3,33	-3,91	2,5	1	-3,33	-3,91	3,5	2
-3,33	-3,33	4,5	1	-3,33	-4,32	2,5	2
-2,33	-3,33	4,5	2	-3,91	-4,9	1,5	2
-3,33	-3,91	4,5	1	-3,91	-4,32	1,5	2
-3,91	-4,32	2,5	2	-3,33	-4,32	3,5	2
-2,33	-4,62	3,5	2	-3,33	-3,91	4,5	2
-2,33	-3,91	3,5	2	-3,33	-3,33	3,5	1
-3,91	-3,91	4,5	1	-2,33	-3,91	2,5	2
-3,91	-3,91	4,5	1	-3,33	-3,91	3,5	2
-4,32	-4,62	2,5	2	-3,33	-3,91	2,5	2
-3,33	-3,33	2,5	1	-3,33	-4,32	2,5	2
-3,33	-4,32	2,5	2	-2,33	-3,33	3,5	2
-2,33	-3,91	2,5	2	-2,33	-3,33	3,5	2
-2,33	-2,33	1,5	1	-2,33	-3,33	5,5	2
-3,33	-3,33	3,5	1	-3,33	-3,91	5,5	2
-3,33	-3,91	2,5	2	-3,33	-3,91	3,5	2
-3,33	-3,33	4,5	1	-3,33	-3,33	3,5	2
-3,33	-3,33	3,5	1	-3,33	-3,33	2,5	1
-3,33	-3,33	4,5	1	-3,33	-3,33	4,5	1
-3,33	-3,33	2,5	1	-3,33	-3,33	1,5	1
-3,91	-4,32	3,5	2	-3,91	-3,91	2,5	2
-2,33	-3,33	3,5	1	-3,91	-4,32	3,5	2
-4,9	-5,31	0,5	2	-3,91	-3,91	2,5	1
-4,32	-4,32	1,5	1	-3,33	-4,32	2,5	2
-2,33	-4,32	3,5	2	-2,33	-2,33	3,5	1
-3,33	-3,91	2,5	1	-2,33	-2,33	4,5	1
-3,33	-3,91	2,5	2	-3,91	-4,62	2,5	2
-4,9	-5,12	0,5	2	-3,91	-4,32	4,5	2
-2,33	-4,9	1,5	2	-3,33	-4,32	4,5	2
-2,33	-3,91	2,5	2	-2,33	-2,33	4,5	1
-2,33	-3,91	2,5	2	-3,91	-4,32	2,5	2
-3,33	-3,33	1,5	1	-3,33	-3,91	3,5	2
-4,62	-4,9	0,5	2	-3,33	-3,91	5,5	1
-3,33	-3,91	3,5	2	-3,91	-3,91	5,5	1
-2,33	-3,33	4,5	2	-3,91	-3,91	3,5	1

WELTEVREDEN3

Clast size distribution

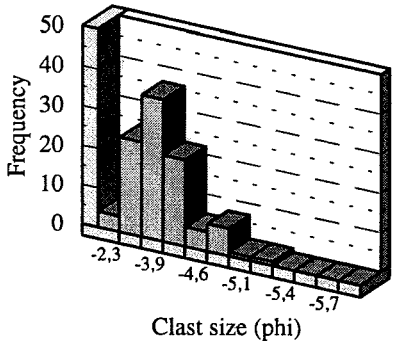

Clast roundness

(-3.91 phi)

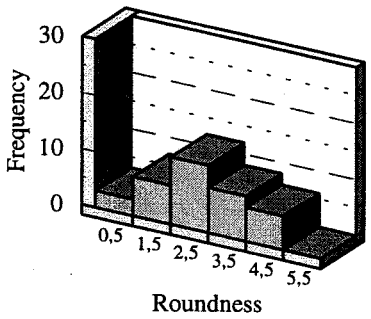

Clast roundness

(-3.33 phi)

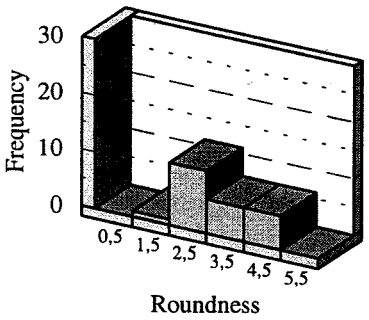

Clast Sphericity

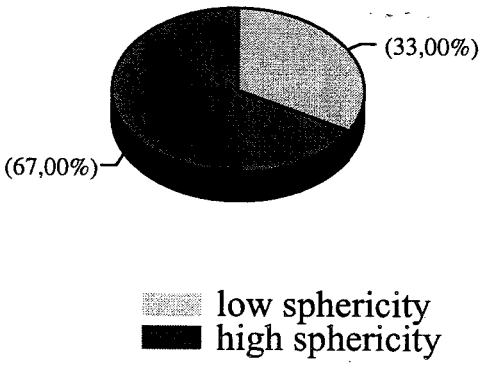

ROLY POLY1

C-axis	A-axis	Round.	Spher.	C-axis	A-axis	Round.	Spher.
-4,32	-4,9	1,5	2	-4,32	-6,32	0,5	2
-3,33	-4,62	1,5	2	-2,33	-2,33	0,5	1
-3,33	-3,91	3,5	2	-2,33	-2,33	2,5	1
-3,33	-3,91	2,5	2	-2,33	-2,33	3,5	1
-2,33	-2,33	2,5	1	-2,33	-2,33	0,5	1
-2,33	-3,33	2,5	2	-2,33	-2,33	4,5	1
-2,33	-3,91	2,5	2	-2,33	-2,33	2,5	1
-2,33	-2,33	4,5	1	-3,33	-3,33	3,5	1
-5,31	-7,22	5,5	2	-2,33	-3,33	2,5	1
-3,56	-4,32	3,5	2	-2,33	-3,33	4,5	2
-2,33	-4,62	1,5	2	-2,33	-2,33	3,5	2
-3,33	-3,33	3,5	1	-3,91	-4,32	0,5	2
-3,33	-3,33	3,5	1	-3,33	-3,33	3,5	1
-2,33	-3,33	2,5	2	-3,33	-3,91	2,5	2
-2,33	-3,33	2,5	2	-3,33	-3,91	0,5	2
-2,33	-4,32	2,5	2	-3,33	-3,91	1,5	2
-2,33	-2,33	2,5	1	-2,33	-3,91	4,5	2
-3,33	-3,33	3,5	1	-2,33	-3,33	2,5	2
-3,33	-4,32	2,5	2	-2,33	-3,33	4,5	2
-3,33	-3,91	3,5	2	-2,33	-3,33	0,5	2
-2,33	-2,33	2,5	1	-2,33	-3,33	3,5	2
-2,33	-3,91	4,5	2	-2,33	-3,91	4,5	2
-3,33	-3,33	2,5	1	-3,91	-3,91	2,5	2
-3,33	-3,33	2,5	1	-2,33	-3,33	3,5	2
-3,33	-3,91	4,5	2	-3,33	-3,91	4,5	2
-2,33	-3,33	3,5	2	-2,33	-3,91	4,5	2
-3,33	-4,32	2,5	2	-3,33	-3,33	2,5	2
-2,33	-3,91	3,5	2	-3,33	-3,33	0,5	1
-3,33	-3,33	4,5	1	-2,33	-3,33	2,5	2
-3,33	-3,33	4,5	1	-3,91	-3,91	0,5	1
-2,33	-3,33	2,5	2	-2,33	-2,33	3,5	1
-3,91	-3,91	4,5	1	-3,33	-3,33	2,5	1
-2,33	-2,33	2,5	1	-2,33	-4,32	3,5	2
-3,33	-3,33	2,5	1	-3,33	-4,32	0,5	2
-3,33	-3,91	2,5	2	-2,33	-2,33	1,5	1
-2,33	-2,33	2,5	1	-2,33	-2,33	3,5	1
-3,33	-3,91	1,5	2	-3,33	-3,91	2,5	2
-3,33	-4,32	0,5	2	-3,91	-4,32	0,5	2
-3,33	-3,33	3,5	1	-2,33	-2,33	3,5	1
-3,33	-3,33	4,5	1	-2,33	-2,33	4,5	1
-2,33	-3,33	1,5	2	-3,33	-3,33	2,5	1
-3,33	-3,91	3,5	2	-3,91	-3,91	0,5	1
-3,33	-4,32	2,5	2	-3,33	-3,91	2,5	2
-2,33	-3,33	0,5	2	-3,33	-3,91	2,5	2
-4,32	-4,9	0,5	1	-3,33	-3,33	3,5	2
-2,33	-3,33	2,5	2	-2,33	-2,33	2,5	1
-3,33	-4,32	3,5	2	-3,91	-3,91	3,5	2
-3,33	-4,32	2,5	2	-2,33	-3,33	4,5	2
-4,32	-5,31	0,5	2	-3,33	-3,33	0,5	1
-2,33	-3,33	3,5	2	-2,33	-3,33	2,5	1

ROLY POLY1

Clast size distribution

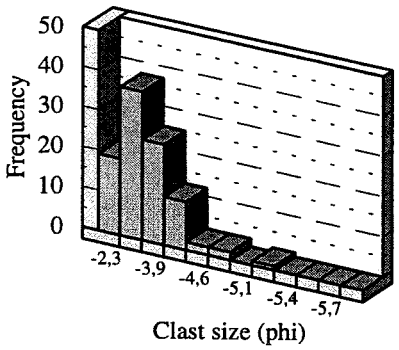

Clast roundness
(-3.91 phi)

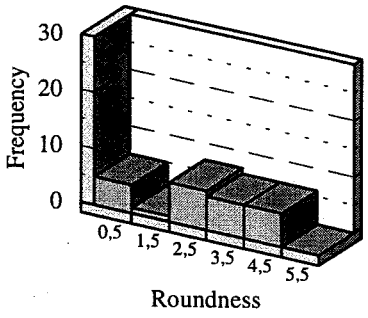

Clast roundness
(-3.33 phi)

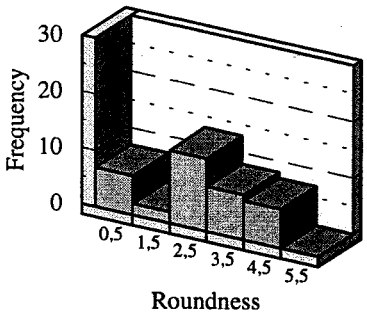

Clast Sphericity

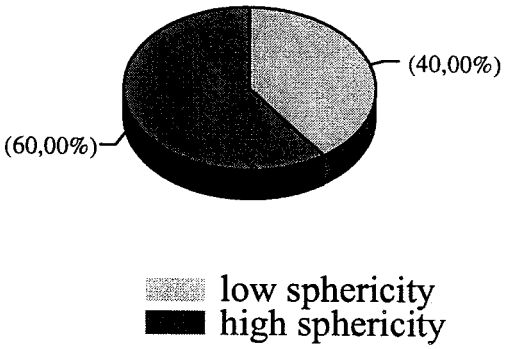

ROLY POLY2

C-axis	A-axis	Round.	Spher.	C-axis	A-axis	Round.	Spher.
-3,91	-4,32	5,5	2	-4,32	-4,32	3,5	1
-3,56	-3,91	0,5	1	-3,91	-3,91	3,5	1
-3,33	-4,32	1,5	2	-3,33	-3,33	3,5	1
-3,91	-4,32	5,5	2	-3,33	-3,91	2,5	2
-4,62	-5,12	4,5	2	-3,91	-4,32	5,5	1
-3,91	-3,91	3,5	1	-2,33	-3,33	2,5	1
-3,91	-3,91	3,5	2	-4,32	-4,62	2,5	2
-3,33	-3,33	5,5	1	-2,33	-2,33	2,5	1
-3,91	-4,32	3,5	2	-3,33	-3,33	2,5	1
-3,33	-3,33	2,5	1	-3,91	-4,62	3,5	2
-3,33	-3,91	2,5	1	-2,33	-3,33	4,5	2
-3,91	-3,91	4,5	1	-3,33	-4,62	1,5	2
-3,33	-3,33	3,5	1	-3,91	-4,9	3,5	2
-2,33	-3,33	2,5	2	-4,62	-4,9	4,5	2
-3,33	-4,32	3,5	2	-3,91	-3,91	5,5	1
-3,91	-4,32	2,5	2	-3,91	-3,91	4,5	1
-3,33	-3,33	3,5	1	-3,91	-4,32	2,5	2
-3,33	-3,91	3,5	2	-3,91	-4,32	4,5	2
-4,32	-4,32	3,5	1	-3,33	-3,33	3,5	1
-3,33	-3,91	2,5	2	-4,32	-5,31	2,5	2
-2,33	-2,33	3,5	2	-4,62	-5,31	2,5	2
-3,33	-3,91	4,5	2	-2,33	-2,33	4,5	1
-3,91	-3,91	4,5	2	-2,33	-2,33	4,5	1
-3,91	-3,91	3,5	1	-2,33	-2,33	2,5	1
-2,33	-3,33	2,5	2	-2,33	-3,33	1,5	2
-3,33	-3,91	4,5	2	-2,33	-2,33	3,5	1
-2,33	-5,31	5,5	2	-3,33	-3,91	4,5	1
-2,33	-2,33	2,5	1	-4,32	-5,12	3,5	2
-3,33	-3,33	2,5	1	-3,33	-3,33	3,5	1
-4,62	-4,62	3,5	1	-5,12	-5,31	3,5	1
-3,33	-3,33	3,5	1	-3,91	-4,32	3,5	2
-4,32	-5,63	5,5	2	-4,9	-5,9	2,5	2
-4,62	-5,63	0,5	2	-3,91	-3,91	4,5	2
-4,32	-5,63	1,5	2	-3,33	-3,33	3,5	1
-3,91	-4,32	1,5	2	-4,32	-4,9	1,5	2
-4,62	-5,31	3,5	2	-2,33	-2,33	4,5	1
-3,33	-3,33	2,5	1	-3,91	-3,91	4,5	1
-2,33	-2,33	2,5	1	-3,33	-4,32	2,5	2
-3,33	-3,33	1,5	1	-3,33	-3,91	3,5	2
-2,33	-3,91	2,5	1	-2,33	-2,33	3,5	1
-3,33	-4,32	2,5	2	-3,33	-3,91	2,5	2
-4,32	-4,62	2,5	2	-3,33	-4,32	2,5	2
-3,91	-4,9	3,5	2	-3,33	-3,33	1,5	1
-4,32	-4,9	2,5	2	-3,33	-3,33	4,5	1
-3,33	-3,91	3,5	2	-2,33	-3,33	3,5	2
-3,91	-4,32	3,5	2	-3,33	-4,32	3,5	2
-3,33	-4,32	2,5	2	-3,33	-3,33	3,5	1
-2,33	-3,91	3,5	2	-4,62	-4,9	2,5	1
-4,32	-4,9	4,5	1	-4,9	-5,9	2,5	2
-3,33	-4,62	1,5	2	-2,33	-2,33	1,5	1

ROLY POLY2

Clast size distributio

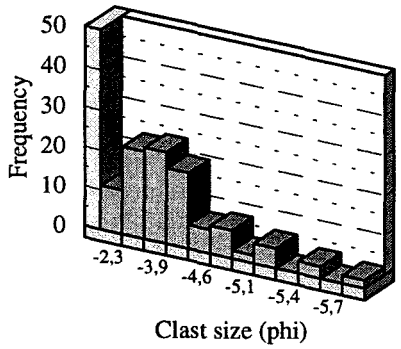

Clast roundness
(-3.91 phi)

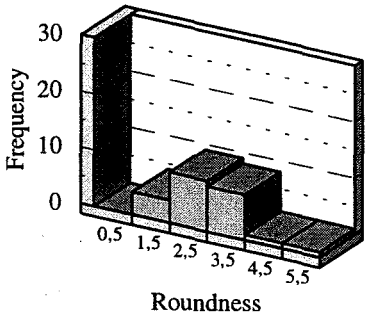

Clast roundness
(-3.33 phi)

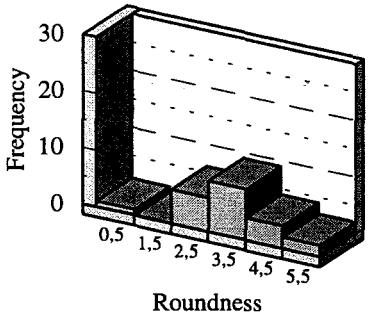

Clast Sphericity

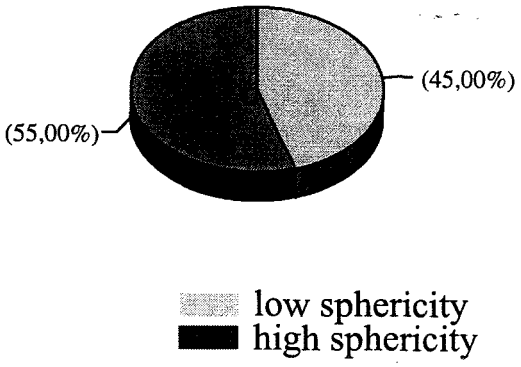

DRIEPAN

C-axis	A-axis	Round.	Spher.	C-axis	A-axis	Round.	Spher.
-2,33	-3,33	3,5	2	-3,33	-3,91	4,5	2
-2,33	-3,33	3,5	2	-3,91	-4,32	2,5	2
-2,33	-2,33	2,5	1	-2,33	-3,91	4,5	2
-3,91	-4,32	4,5	2	-2,33	-3,91	4,5	2
-3,33	-3,91	4,5	2	-3,33	-3,91	2,5	2
-2,33	-2,33	3,5	1	-2,33	-3,33	2,5	2
-3,33	-3,33	4,5	1	-2,33	-3,33	2,5	2
-3,33	-3,33	4,5	1	-3,33	-3,33	2,5	2
-3,33	-3,33	4,5	1	-2,33	-3,91	3,5	2
-2,33	-3,33	4,5	2	-2,33	-2,33	4,5	1
-3,33	-3,33	3,5	1	-3,91	-3,91	4,5	1
-3,33	-3,33	3,5	1	-3,91	-4,32	3,5	2
-3,33	-3,33	2,5	1	-3,33	-3,33	3,5	1
-2,33	-3,33	4,5	2	-3,33	-3,33	3,5	1
-2,33	-2,33	3,5	1	-3,33	-3,33	3,5	1
-2,33	-3,33	3,5	2	-3,33	-3,33	3,5	1
-3,33	-4,32	2,5	2	-2,33	-3,33	3,5	1
-3,33	-3,91	3,5	2	-2,33	-3,33	3,5	1
-3,33	-3,91	2,5	2	-2,33	-3,33	3,5	1
-3,33	-3,91	3,5	2	-4,32	-4,32	3,5	1
-3,33	-3,33	4,5	1	-3,33	-3,91	2,5	2
-3,91	-3,91	3,5	2	-3,33	-3,91	2,5	2
-3,33	-3,33	4,5	1	-3,33	-3,91	2,5	2
-3,33	-3,33	4,5	1	-3,33	-3,33	1,5	1
-3,33	-3,33	4,5	1	-3,33	-3,33	2,5	1
-2,33	-3,33	2,5	1	-3,33	-3,33	2,5	1
-3,33	-3,91	4,5	2	-3,91	-3,91	2,5	1
-3,33	-3,91	3,5	2	-3,33	-3,33	3,5	1
-3,33	-3,91	5,5	2	-3,33	-3,91	3,5	2
-3,33	-3,33	4,5	1	-2,33	-3,33	4,5	2
-3,91	-3,91	3,5	2	-2,33	-3,91	3,5	2
-3,33	-4,32	4,5	2	-2,33	-2,33	2,5	1
-3,33	-3,33	3,5	1	-2,33	-2,33	2,5	1
-3,33	-3,33	2,5	1	-2,33	-2,33	2,5	1
-2,33	-2,33	2,5	1	-2,33	-2,33	2,5	1
-3,33	-4,32	3,5	2	-2,33	-2,33	2,5	1
-3,33	-3,33	2,5	1	-2,33	-2,33	2,5	1
-2,33	-2,33	2,5	1	-2,33	-2,33	2,5	1
-2,33	-2,33	2,5	1	-2,33	-2,33	2,5	1
-3,91	-3,91	1,5	1	-2,33	-2,33	2,5	1
-3,33	-3,33	3,5	1	-3,33	-4,32	4,5	2
-2,33	-3,33	2,5	1	-3,33	-3,33	3,5	1
-2,33	-3,33	4,5	2	-2,33	-3,33	4,5	2
-3,91	-4,32	2,5	2	-2,33	-2,33	4,5	1
-3,33	-3,91	3,5	2	-2,33	-3,33	4,5	2
-2,33	-3,91	3,5	2	-2,33	-3,33	5,5	2
-3,33	-4,32	3,5	2	-2,33	-3,33	2,5	2
-3,33	-4,32	3,5	2	-2,33	-2,33	2,5	1
-2,33	-3,91	2,5	2	-3,33	-3,91	5,5	2
-3,33	-3,33	3,5	2	-2,33	-2,33	2,5	1

DRIEPAN

Clast size distribution

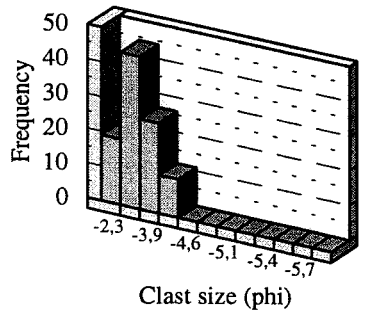

Clast roundness

(-3.91 phi)

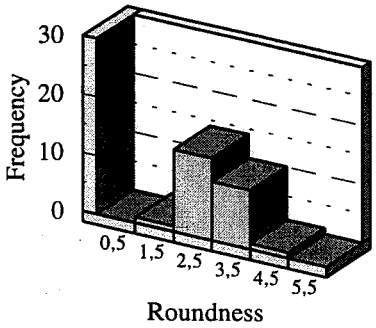

Clast roundness

(-3.33 phi)

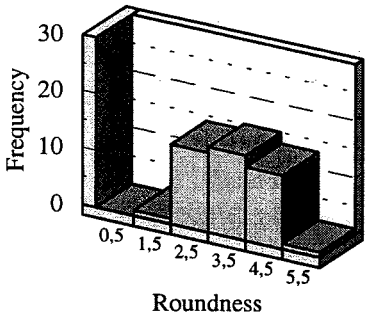

Clast Sphericity

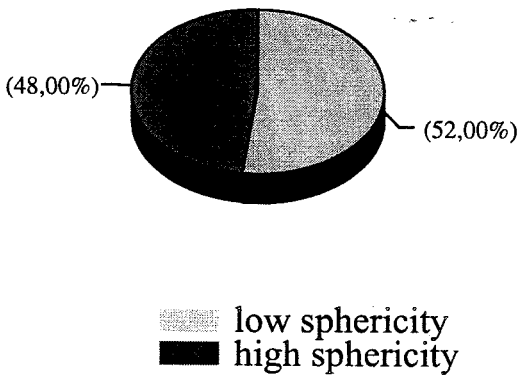

AMMONDALE

C-axis	A-axis	Round.	Spher.	C-axis	A-axis	Round.	Spher.
-2,33	-4,32	1,5	2	-3,33	-4,9	3,5	2
-3,33	-3,33	2,5	1	-2,33	-2,33	2,5	1
-3,33	-3,91	3,5	2	-2,33	-2,33	3,5	1
-4,32	-4,32	2,5	1	-4,62	-5,63	2,5	2
-3,33	-3,91	1,5	2	-4,9	-5,48	2,5	2
-3,91	-4,32	1,5	2	-3,33	-4,32	3,5	2
-3,33	-3,91	2,5	2	-3,91	-4,62	3,5	2
-3,33	-3,91	3,5	2	-3,33	-3,33	2,5	1
-3,91	-3,91	3,5	1	-3,33	-3,33	2,5	1
-3,33	-3,91	1,5	2	-3,33	-3,33	3,5	1
-3,33	-3,91	2,5	2	-3,33	-3,91	3,5	2
-3,33	-3,33	1,5	2	-4,32	-4,9	2,5	2
-3,33	-3,91	2,5	2	-3,33	-3,33	2,5	1
-3,91	-4,32	3,5	2	-2,33	-2,33	2,5	1
-3,33	-4,62	3,5	2	-2,33	-2,33	2,5	1
-3,33	-3,33	1,5	1	-2,33	-2,33	2,5	1
-3,33	-3,33	2,5	1	-2,33	-2,33	2,5	1
-3,33	-3,33	3,5	1	-2,33	-2,33	2,5	1
-3,33	-3,33	1,5	1	-2,33	-2,33	2,5	1
-3,91	-4,32	3,5	2	-2,33	-2,33	2,5	1
-3,33	-3,33	1,5	1	-2,33	-2,33	2,5	1
-3,91	-3,91	3,5	1	-2,33	-2,33	2,5	1
-3,33	-4,32	3,5	2	-3,91	-4,32	2,5	2
-3,33	-3,91	2,5	2	-4,32	-4,9	2,5	2
-3,33	-3,33	3,5	1	-3,91	-4,32	3,5	2
-3,91	-3,91	2,5	1	-3,33	-3,33	3,5	1
-3,33	-3,33	3,5	1	-3,91	-4,32	3,5	2
-3,91	-3,91	2,5	1	-3,33	-3,33	2,5	1
-3,91	-4,32	3,5	2	-3,33	-3,33	2,5	1
-3,91	-3,91	2,5	1	-2,33	-2,33	2,5	1
-3,33	-4,32	2,5	2	-2,33	-2,33	2,5	1
-3,33	-3,91	3,5	2	-2,33	-2,33	2,5	1
-2,33	-2,33	2,5	1	-2,33	-2,33	2,5	1
-3,91	-3,91	3,5	1	-2,33	-2,33	2,5	1
-2,33	-2,33	2,5	1	-3,33	-3,33	1,5	1
-2,33	-2,33	4,5	1	-3,33	-3,33	3,5	1
-3,91	-4,9	3,5	2	-3,33	-3,33	2,5	1
-2,33	-3,33	3,5	2	-3,33	-3,33	1,5	1
-2,33	-3,33	3,5	2	-3,33	-3,33	1,5	1
-2,33	-3,33	3,5	2	-3,91	-3,91	1,5	1
-2,33	-2,33	3,5	1	-3,33	-3,91	3,5	2
-3,33	-3,33	2,5	1	-2,33	-3,33	1,5	1
-3,33	-4,62	2,5	2	-2,33	-3,33	3,5	2
-2,33	-4,62	2,5	2	-3,33	-3,91	3,5	2
-3,33	-3,33	1,5	1	-3,91	-3,91	3,5	1
-4,9	-4,9	2,5	1	-3,91	-3,91	3,5	1
-3,33	-3,33	3,5	1	-3,33	-3,33	3,5	1
-3,33	-3,33	2,5	1	-3,33	-3,33	2,5	1
-2,33	-2,33	3,5	1	-3,33	-3,33	3,5	1
-4,32	-4,62	2,5	2	-5,12	-5,12	0,5	1

AMMONDALE

Clast size distribution

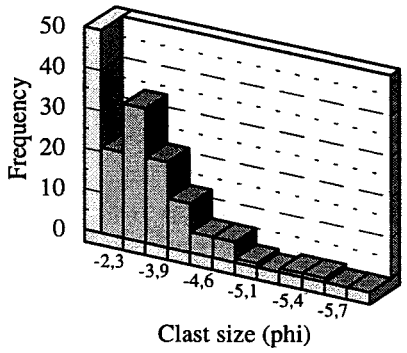

Clast roundness
(-3.91 phi)

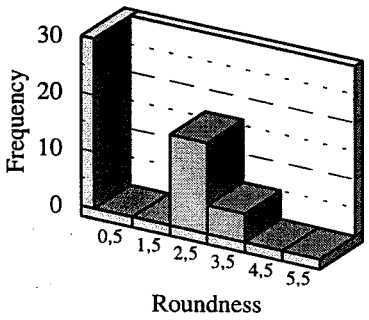

Clast roundness
(-3.33 phi)

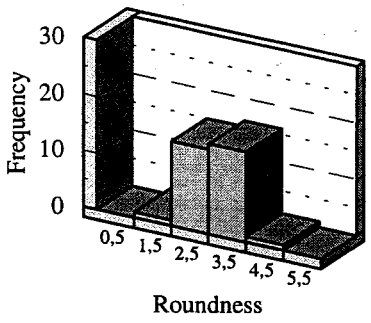

Clast Sphericity

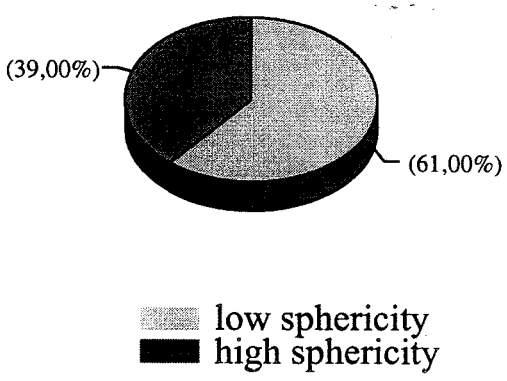

LAURISTON

C-axis	A-axis	Round.	Spher.	C-axis	A-axis	Round.	Spher.
-4,62	-4,9	1,5	1	-3,33	-4,62	3,5	2
-3,33	-3,33	1,5	1	-3,33	-3,33	2,5	1
-3,33	-3,91	1,5	2	-3,91	-4,9	2,5	2
-3,33	-3,33	1,5	1	-3,91	-4,9	2,5	2
-3,33	-3,33	1,5	1	-3,33	-3,91	3,5	2
-2,33	-3,33	2,5	2	-3,91	-4,62	3,5	2
-2,33	-3,33	2,5	2	-4,62	-5,63	2,5	2
-3,33	-3,33	2,5	1	-4,9	-4,9	3,5	1
-3,33	-3,91	1,5	2	-3,33	-3,33	2,5	1
-3,33	-3,33	1,5	1	-3,33	-3,91	3,5	1
-3,33	-3,91	1,5	2	-2,33	-2,33	2,5	1
-2,33	-2,33	1,5	1	-3,33	-3,91	2,5	2
-3,33	-3,33	1,5	1	-2,33	-2,33	2,5	1
-2,33	-3,33	1,5	1	-3,91	-3,91	2,5	1
-3,33	-3,91	2,5	2	-3,33	-3,91	0,5	2
-2,33	-3,33	1,5	2	-4,62	-4,62	2,5	1
-3,33	-3,33	1,5	1	-3,91	-4,32	2,5	2
-3,33	-3,33	1,5	1	-3,91	-4,32	2,5	2
-3,33	-3,33	1,5	1	-3,33	-3,91	2,5	2
-2,33	-3,91	3,5	2	-3,33	-3,33	2,5	1
-3,33	-3,33	1,5	1	-2,33	-2,33	3,5	1
-3,33	-3,33	1,5	1	-3,33	-3,33	3,5	1
-2,33	-2,33	2,5	1	-3,33	-3,33	1,5	1
-3,33	-4,32	2,5	2	-2,33	-3,33	2,5	2
-3,91	-3,91	1,5	1	-3,33	-3,33	2,5	1
-2,33	-2,33	1,5	1	-2,33	-3,33	1,5	1
-2,33	-2,33	1,5	1	-2,33	-2,33	1,5	1
-2,33	-2,33	1,5	1	-2,33	-3,91	1,5	2
-2,33	-2,33	1,5	1	-2,33	-4,32	0,5	2
-2,33	-2,33	1,5	1	-2,33	-3,33	0,5	2
-2,33	-2,33	1,5	1	-3,33	-4,32	1,5	2
-2,33	-2,33	1,5	1	-3,33	-3,33	1,5	1
-2,33	-2,33	1,5	1	-2,33	-3,33	1,5	1
-2,33	-2,33	1,5	1	-2,33	-4,32	2,5	2
-2,33	-2,33	1,5	1	-3,33	-4,32	2,5	2
-2,33	-2,33	1,5	1	-3,33	-3,91	1,5	2
-2,33	-2,33	1,5	1	-3,33	-3,91	1,5	2
-2,33	-2,33	1,5	1	-2,33	-2,33	1,5	1
-2,33	-2,33	1,5	1	-2,33	-3,33	2,5	2
-2,33	-2,33	1,5	1	-2,33	-2,33	2,5	1
-3,33	-3,91	2,5	2	-2,33	-2,33	2,5	1
-3,33	-3,33	1,5	1	-2,33	-2,33	2,5	1
-3,33	-3,33	1,5	1	-2,33	-2,33	2,5	1
-3,33	-3,33	1,5	1	-2,33	-2,33	2,5	1
-3,33	-3,33	2,5	1	-2,33	-2,33	2,5	1
-4,32	-4,62	3,5	2	-3,33	-3,33	1,5	1
-3,33	-3,33	2,5	1	-3,33	-3,33	3,5	1
-3,33	-3,33	2,5	1	-3,33	-3,33	1,5	1
-3,33	-3,91	2,5	2	-3,33	-3,33	2,5	1
-3,33	-5,32	2,5	2	-3,33	-3,91	2,5	2

LAURISTON

Clast size distribution

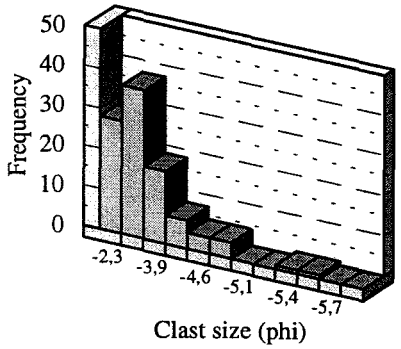

Clast roundness
(-3.91 phi)

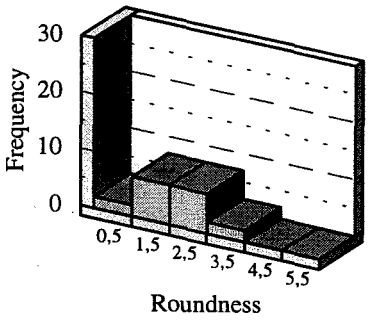

Clast roundness
(-3.33 phi)

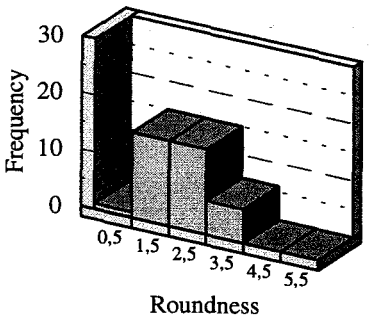

Clast Sphericity

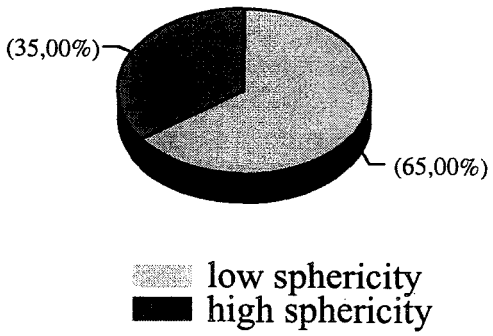

ARCADIA

C-axis	A-axis	Round.	Spher.	C-axis	A-axis	Round.	Spher.
-3,33	-3,91	3,5	2	-3,33	-3,91	2,5	2
-3,33	-3,91	3,5	2	-3,33	-3,91	2,5	2
-3,33	-4,32	2,5	2	-3,33	-3,91	3,5	2
-3,33	-4,32	3,5	2	-3,33	-3,33	3,5	1
-3,33	-4,32	3,5	2	-3,33	-3,33	3,5	1
-3,33	-4,32	3,5	2	-3,33	-4,32	3,5	2
-3,91	-3,91	2,5	1	-2,33	-3,33	3,5	2
-3,33	-3,91	3,5	2	-2,33	-3,33	3,5	2
-3,33	-3,91	3,5	2	-3,91	-4,62	2,5	2
-3,33	-3,91	3,5	1	-3,91	-3,91	3,5	1
-3,91	-4,9	2,5	2	-3,33	-3,91	4,5	2
-3,91	-4,32	2,5	2	-3,33	-4,32	3,5	2
-3,33	-4,32	2,5	2	-4,32	-5,12	2,5	2
-3,33	-3,33	3,5	1	-3,33	-4,32	3,5	2
-3,33	-3,33	3,5	1	-2,33	-3,91	3,5	2
-3,33	-4,32	3,5	2	-3,33	-3,91	2,5	2
-2,33	-2,33	1,5	1	-3,33	-3,33	3,5	1
-3,33	-3,33	3,5	1	-3,33	-3,33	2,5	1
-3,33	-3,91	3,5	2	-3,91	-4,32	2,5	2
-3,33	-4,32	3,5	2	-3,33	-3,91	3,5	2
-2,33	-3,91	4,5	2	-3,33	-4,32	2,5	2
-3,91	-3,91	3,5	1	-2,33	-3,91	2,5	2
-2,33	-3,91	3,5	2	-3,91	-3,91	2,5	1
-2,33	-4,32	3,5	2	-3,33	-3,33	4,5	1
-4,32	-4,32	3,5	1	-3,33	-3,91	4,5	2
-3,33	-3,33	3,5	1	-3,33	-3,91	3,5	2
-2,33	-2,33	4,5	1	-2,33	-2,33	4,5	1
-3,91	-4,32	3,5	2	-2,33	-2,33	4,5	1
-3,33	-3,33	3,5	1	-3,33	-3,33	1,5	1
-3,91	-4,32	2,5	2	-3,33	-3,91	3,5	1
-3,33	-3,91	3,5	2	-2,33	-3,91	3,5	2
-3,33	-3,33	3,5	1	-3,33	-3,91	3,5	2
-2,33	-2,33	3,5	1	-2,33	-3,91	2,5	2
-3,91	-3,91	3,5	1	-3,33	-3,91	3,5	2
-3,33	-3,91	3,5	2	-3,33	-3,91	4,5	2
-3,33	-3,91	3,5	2	-3,33	-3,91	3,5	2
-3,33	-3,33	4,5	1	-3,33	-3,91	3,5	2
-3,33	-3,33	3,5	1	-3,33	-3,33	4,5	1
-3,33	-3,91	3,5	2	-3,91	-4,32	3,5	2
-3,33	-3,91	3,5	2	-3,33	-3,91	3,5	2
-3,33	-3,91	3,5	2	-2,33	-2,33	3,5	1
-3,33	-3,91	4,5	2	-2,33	-2,33	3,5	1
-3,33	-3,91	3,5	2	-2,33	-3,33	3,5	2
-3,33	-3,91	3,5	2	-3,33	-4,32	3,5	2
-3,33	-3,91	3,5	2	-3,33	-3,33	3,5	1
-3,33	-3,33	3,5	1	-3,33	-3,91	3,5	2
-2,33	-3,91	3,5	2	-3,33	-3,91	3,5	2
-3,33	-3,91	3,5	2	-3,33	-3,33	3,5	1
-3,33	-3,33	3,5	1	-3,33	-4,32	3,5	2
-3,91	-4,32	3,5	2	-2,33	-3,33	3,5	2

ARCADIA

Clast size distribution

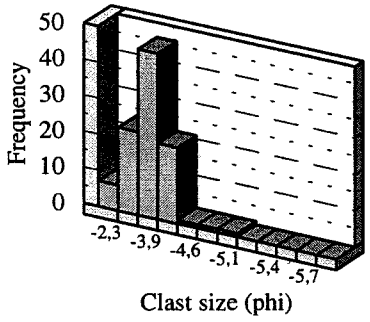

Clast roundness
(-3.91 phi)

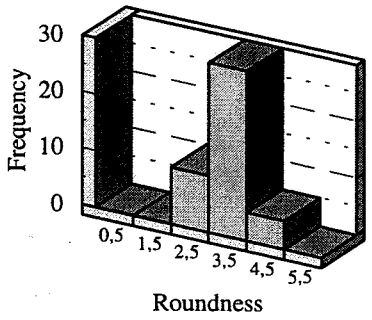

Clast roundness
(-3.33 phi)

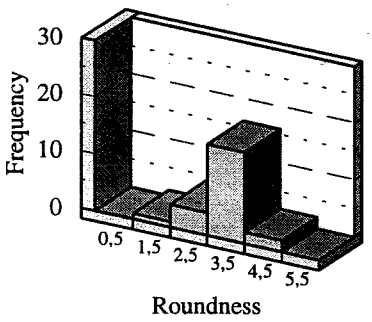

Clast Sphericity

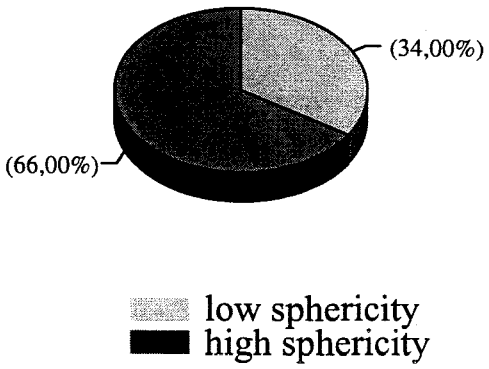

DONKIN

C-axis	A-axis	Round.	Spher.	C-axis	A-axis	Round.	Spher.
-3,33	-3,33	0,5	1	-3,91	-4,32	2,5	2
-4,32	-4,62	3,5	2	-3,91	-3,91	3,5	1
-4,32	-4,62	3,5	2	-3,91	-4,9	3,5	2
-4,32	-4,62	3,5	2	-3,33	-4,32	3,5	2
-3,91	-4,32	2,5	2	-3,33	-3,91	3,5	2
-4,32	-4,32	3,5	1	-3,33	-3,91	3,5	1
-3,33	-4,32	3,5	1	-3,33	-3,91	3,5	1
-2,33	-3,33	2,5	1	-3,33	-3,33	4,5	1
-3,33	-3,33	3,5	1	-3,33	-3,33	3,5	1
-3,33	-3,91	2,5	1	-2,33	-3,33	3,5	2
-2,33	-2,33	3,5	1	-3,33	-3,33	3,5	1
-2,33	-3,33	2,5	2	-4,9	-5,12	3,5	1
-3,91	-4,32	3,5	2	-3,33	-3,33	3,5	1
-3,91	-4,32	3,5	2	-4,32	-4,62	3,5	2
-3,33	-3,33	3,5	1	-3,91	-3,91	3,5	1
-3,33	-3,33	3,5	1	-3,33	-3,91	2,5	2
-3,33	-3,33	3,5	1	-2,33	-3,33	3,5	2
-3,33	-3,91	3,5	2	-3,33	-3,33	3,5	1
-2,33	-2,33	3,5	1	-3,33	-3,33	3,5	1
-2,33	-3,33	2,5	1	-3,33	-3,91	2,5	2
-3,33	-3,33	2,5	1	-3,33	-3,91	3,5	2
-2,33	-3,33	2,5	1	-2,33	-3,33	3,5	2
-2,33	-2,33	2,5	1	-4,32	-4,9	3,5	2
-3,33	-3,33	3,5	1	-4,9	-4,9	3,5	1
-2,33	-3,33	2,5	2	-2,33	-2,33	4,5	1
-3,91	-4,32	3,5	2	-3,33	-3,33	3,5	1
-3,91	-3,91	3,5	1	-3,33	-3,91	3,5	2
-3,33	-3,91	2,5	1	-3,33	-3,91	1,5	1
-2,33	-3,33	2,5	2	-2,33	-2,33	3,5	1
-2,33	-3,33	3,5	2	-3,33	-3,33	2,5	1
-2,33	-3,33	2,5	1	-3,33	-3,91	3,5	2
-2,33	-2,33	3,5	1	-3,33	-3,33	3,5	1
-3,91	-4,32	3,5	1	-3,33	-3,91	3,5	2
-3,91	-4,32	3,5	2	-3,33	-3,33	3,5	1
-3,33	-4,32	3,5	2	-3,91	-4,62	3,5	2
-3,33	-3,91	3,5	2	-4,62	-4,62	3,5	1
-2,33	-3,33	3,5	2	-3,33	-3,33	2,5	1
-3,33	-3,91	3,5	1	-3,33	-3,33	3,5	1
-4,32	-4,32	3,5	1	-2,33	-2,33	2,5	1
-4,32	-4,9	3,5	2	-3,33	-3,91	3,5	2
-3,33	-3,91	3,5	1	-4,32	-4,62	3,5	2
-2,33	-3,33	2,5	1	-2,33	-3,33	3,5	2
-2,33	-2,33	3,5	1	-3,91	-3,91	2,5	1
-4,32	-4,32	3,5	1	-3,33	-3,91	3,5	2
-3,33	-3,33	2,5	1	-3,33	-3,91	3,5	2
-3,33	-3,33	3,5	1	-3,33	-3,33	2,5	1
-3,91	-3,91	3,5	1	-2,33	-3,33	4,5	2
-3,33	-3,91	3,5	2	-2,33	-3,33	3,5	2
-3,91	-4,32	3,5	2	-3,33	-3,91	2,5	1
-3,33	-3,91	3,5	2	-3,33	-4,62	3,5	2

DONKIN

Clast size distribution

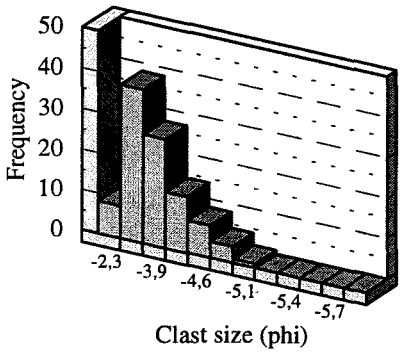

Clast roundness
(-3.91 phi)

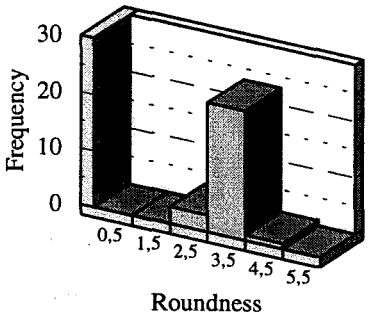

Clast roundness
(-3.33 phi)

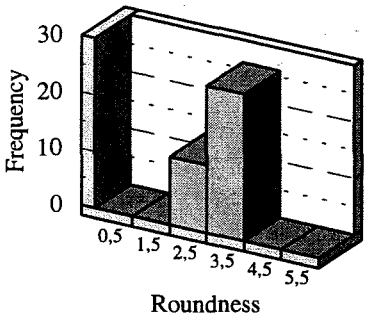

Clast Sphericity

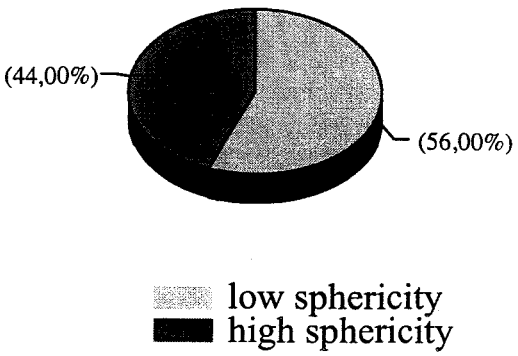

GORING

C-axis	A-axis	Round.	Spher.	C-axis	A-axis	Round.	Spher.
-3,33	-3,33	3,5	1	-3,33	-3,91	3,5	2
-2,33	-3,33	3,5	1	-3,91	-4,9	3,5	2
-3,91	-5,12	3,5	2	-3,91	-4,32	3,5	2
-2,33	-2,33	3,5	1	-3,33	-3,33	3,5	1
-3,33	-3,33	3,5	1	-3,33	-3,91	3,5	2
-3,33	-4,32	3,5	2	-2,33	-2,33	3,5	1
-4,32	-5,12	3,5	2	-2,33	-2,33	3,5	1
-3,33	-3,33	3,5	1	-2,33	-2,33	3,5	1
-4,32	-4,62	3,5	2	-3,33	-3,91	3,5	2
-4,32	-4,62	3,5	2	-4,32	-4,9	3,5	2
-3,91	-4,32	3,5	2	-3,91	-4,9	4,5	2
-3,33	-3,33	3,5	1	-4,32	-4,32	3,5	2
-3,33	-4,32	3,5	2	-3,33	-3,91	3,5	2
-3,91	-4,62	3,5	2	-2,33	-2,33	3,5	1
-2,33	-2,33	3,5	1	-3,33	-3,33	3,5	1
-2,33	-2,33	3,5	1	-3,33	-3,33	4,5	1
-2,33	-3,91	3,5	2	-2,33	-3,33	3,5	2
-3,33	-3,33	3,5	1	-3,33	-3,33	3,5	1
-2,33	-2,33	3,5	1	-2,33	-3,33	3,5	2
-3,91	-3,91	3,5	1	-3,33	-3,33	3,5	1
-2,33	-2,33	3,5	1	-2,33	-3,91	3,5	2
-3,33	-3,33	3,5	1	-2,33	-2,33	3,5	1
-3,91	-4,32	3,5	2	-2,33	-3,33	3,5	2
-3,91	-4,32	3,5	2	-3,33	-3,33	3,5	1
-3,91	-3,91	3,5	1	-3,33	-3,91	3,5	2
-3,91	-4,32	3,5	2	-3,33	-3,91	3,5	2
-2,33	-3,91	3,5	2	-3,33	-3,91	3,5	2
-3,91	-3,91	3,5	1	-2,33	-2,33	3,5	1
-3,33	-3,91	3,5	2	-2,33	-2,33	3,5	1
-3,91	-3,91	3,5	1	-3,33	-3,33	3,5	1
-4,32	-5,12	3,5	2	-2,33	-3,33	3,5	2
-3,91	-5,12	3,5	2	-3,33	-3,33	4,5	1
-2,33	-3,33	3,5	2	-2,33	-3,33	3,5	2
-2,33	-2,33	3,5	1	-2,33	-3,91	3,5	2
-2,33	-3,33	3,5	2	-2,33	-3,33	3,5	2
-2,33	-3,91	3,5	2	-2,33	-2,33	3,5	1
-2,33	-2,33	3,5	1	-3,33	-3,91	3,5	2
-3,33	-4,32	3,5	2	-2,33	-4,9	3,5	2
-3,91	-4,62	3,5	2	-3,33	-3,91	3,5	2
-3,91	-4,32	3,5	2	-4,32	-4,9	3,5	2
-3,33	-4,32	3,5	2	-2,33	-3,33	3,5	2
-3,33	-3,33	3,5	1	-3,33	-4,9	3,5	2
-3,91	-3,91	3,5	1	-3,33	-3,91	3,5	2
-3,91	-3,91	3,5	1	-3,91	-4,9	3,5	2
-3,91	-4,32	3,5	2	-2,33	-3,33	3,5	2
-3,33	-3,33	3,5	1	-2,33	-3,33	3,5	2
-3,33	-3,91	3,5	2	-3,33	-3,33	3,5	1
-3,91	-4,9	3,5	2	-2,33	-3,33	3,5	2
-3,91	-3,91	3,5	1	-3,33	-3,91	3,5	2
-3,33	-3,33	3,5	1	-3,91	-4,62	3,5	2

GORING

Clast size distribution

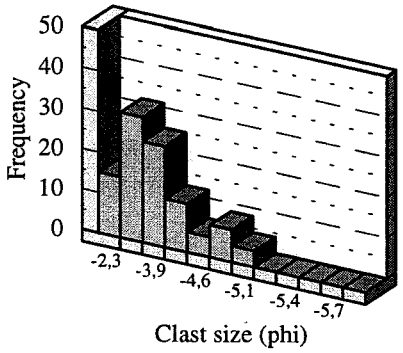

Clast roundness

(-3.91 phi)

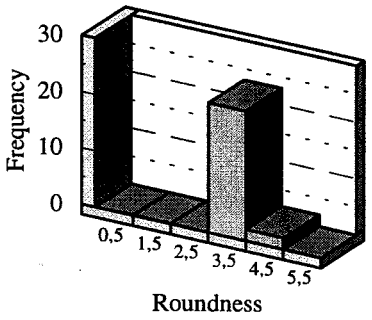

Clast roundness

(-3.33 phi)

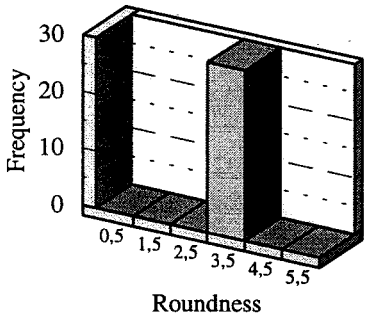

Clast Sphericity

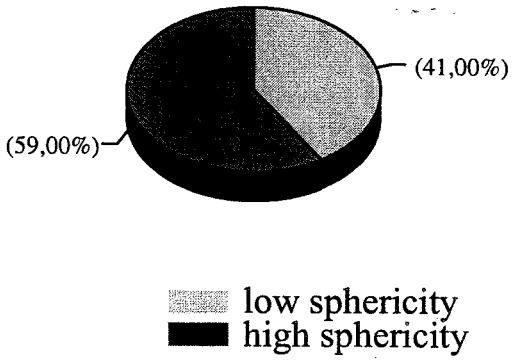

PATRICIA

C-axis	A-axis	Round.	Spher.	C-axis	A-axis	Round.	Spher.
-3,91	-4,32	3,5	2	-2,33	-2,33	2,5	1
-3,91	-3,91	4,5	1	-3,33	-4,32	3,5	2
-4,32	-4,32	2,5	1	-3,33	-4,32	3,5	1
-3,33	-3,91	3,5	2	-2,33	-3,33	3,5	2
-3,33	-4,32	2,5	2	-2,33	-2,33	3,5	1
-3,91	-3,91	3,5	1	-3,33	-3,33	3,5	1
-3,33	-3,91	3,5	2	-4,32	-4,62	3,5	1
-3,33	-3,91	3,5	2	-3,91	-4,32	3,5	2
-3,91	-4,32	3,5	1	-3,91	-4,32	3,5	2
-4,32	-4,32	3,5	1	-3,91	-4,32	3,5	2
-4,32	-4,32	3,5	1	-3,33	-3,33	2,5	1
-3,33	-3,91	3,5	2	-3,33	-3,91	3,5	2
-3,91	-3,91	3,5	1	-3,33	-3,91	2,5	2
-3,91	-3,91	3,5	1	-3,33	-4,32	3,5	2
-3,33	-3,91	3,5	2	-3,33	-3,91	3,5	2
-3,91	-4,62	3,5	2	-3,33	-3,91	2,5	2
-3,91	-4,62	3,5	2	-3,33	-3,91	3,5	1
-3,33	-4,32	3,5	2	-3,33	-3,33	3,5	1
-3,33	-3,91	3,5	2	-3,33	-3,33	3,5	1
-3,33	-3,91	2,5	2	-3,91	-4,32	2,5	2
-3,91	-4,32	3,5	2	-3,33	-3,33	3,5	1
-4,62	-4,62	3,5	1	-3,33	-3,33	3,5	1
-4,32	-4,32	4,5	1	-2,33	-3,33	3,5	2
-3,33	-4,32	3,5	2	-3,33	-3,33	3,5	1
-3,33	-3,91	3,5	2	-3,33	-3,33	2,5	1
-3,33	-3,33	3,5	1	-3,33	-3,91	3,5	1
-3,33	-3,91	3,5	2	-4,32	-4,32	3,5	1
-3,33	-3,91	2,5	2	-4,32	-4,62	3,5	1
-3,33	-3,91	2,5	2	-3,33	-3,91	3,5	2
-3,33	-3,33	3,5	1	-3,33	-3,33	3,5	1
-3,33	-3,91	3,5	2	-3,33	-3,91	3,5	2
-3,33	-3,33	2,5	1	-3,33	-3,91	3,5	1
-2,33	-2,33	3,5	1	-3,33	-3,33	3,5	1
-2,33	-3,33	3,5	1	-3,33	-3,91	3,5	2
-2,33	-3,33	2,5	2	-2,33	-3,33	3,5	2
-3,33	-3,33	3,5	1	-3,33	-3,33	3,5	1
-2,33	-3,33	3,5	2	-2,33	-2,33	3,5	1
-3,33	-3,91	3,5	2	-2,33	-2,33	2,5	1
-3,33	-3,91	2,5	2	-2,33	-3,33	3,5	2
-3,33	-3,91	3,5	2	-3,33	-3,33	3,5	1
-3,33	-3,33	3,5	1	-3,33	-3,33	2,5	1
-3,33	-3,91	3,5	2	-3,33	-3,33	3,5	1
-2,33	-3,33	2,5	1	-3,91	-3,91	3,5	1
-2,33	-3,91	3,5	2	-3,33	-4,32	3,5	2
-3,91	-3,91	3,5	1	-3,33	-4,32	3,5	2
-3,33	-3,91	3,5	2	-4,32	-4,32	3,5	1
-3,91	-4,62	3,5	2	-4,62	-4,9	3,5	1
-3,33	-4,32	3,5	2	-3,33	-4,62	3,5	2
-3,91	-3,91	3,5	1	-3,91	-4,32	3,5	2
-3,33	-4,32	3,5	2	-2,33	-2,33	3,5	1

PATRICIA

Clast size distribution

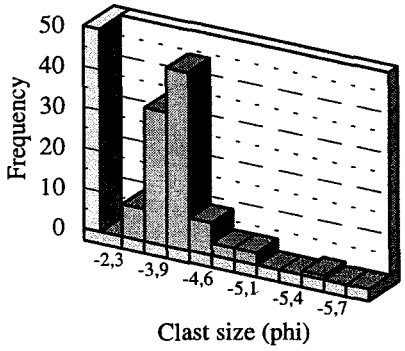

Clast roundness
(-3.91 phi)

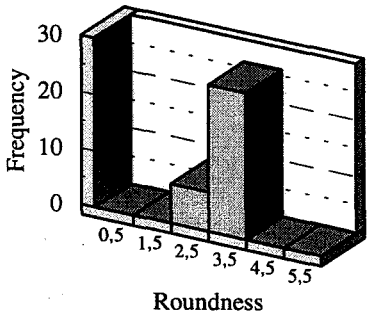

Clast roundness
(-3.33 phi)

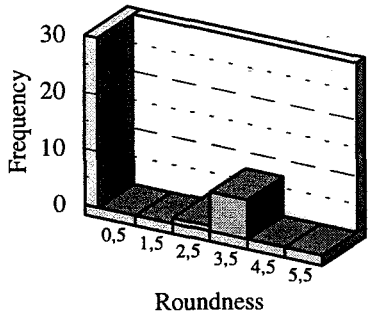

Clast Sphericity

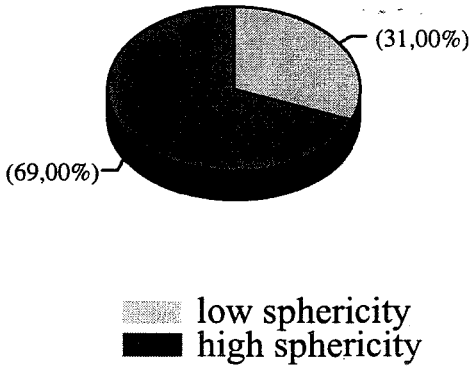

DRUMSHEUGH

C-axis	A-axis	Round.	Spher.	C-axis	A-axis	Round.	Spher.
-2,33	-2,33	3,5	1	-3,33	-3,91	3,5	2
-2,33	-2,33	2,5	1	-3,33	-3,91	3,5	2
-2,33	-2,33	2,5	1	-3,33	-3,91	2,5	2
-2,33	-2,33	3,5	1	-3,91	-3,91	3,5	1
-2,33	-2,33	3,5	1	-3,33	-3,91	3,5	2
-2,33	-2,33	3,5	1	-3,33	-3,91	2,5	2
-2,33	-2,33	3,5	1	-3,33	-3,91	3,5	2
-2,33	-2,33	3,5	1	-3,91	-3,91	3,5	1
-2,33	-2,33	3,5	1	-3,33	-4,32	2,5	2
-2,33	-2,33	3,5	1	-3,33	-4,32	3,5	2
-2,33	-2,33	3,5	1	-3,33	-4,32	3,5	2
-2,33	-2,33	3,5	1	-3,33	-4,32	3,5	2
-2,33	-2,33	4,5	1	-3,33	-4,32	3,5	2
-2,33	-2,33	3,5	1	-3,91	-4,32	3,5	2
-2,33	-2,33	3,5	1	-4,32	-4,32	4,5	1
-2,33	-2,33	3,5	1	-3,33	-4,32	3,5	2
-2,33	-2,33	3,5	1	-3,33	-4,32	3,5	2
-2,33	-2,33	3,5	1	-3,91	-4,32	3,5	2
-2,33	-2,33	3,5	1	-3,33	-4,32	3,5	2
-3,33	-3,33	3,5	1	-4,32	-4,32	3,5	1
-2,33	-3,33	3,5	2	-3,33	-4,32	3,5	2
-2,33	-3,33	3,5	2	-2,33	-4,32	3,5	2
-2,33	-3,33	3,5	2	-3,33	-4,32	3,5	2
-3,33	-3,33	2,5	1	-3,33	-4,32	3,5	2
-2,33	-3,33	3,5	2	-4,32	-4,32	3,5	1
-3,33	-3,33	3,5	1	-3,91	-4,32	3,5	2
-2,33	-3,33	2,5	2	-3,33	-4,32	3,5	2
-2,33	-3,33	3,5	2	-3,91	-4,32	3,5	2
-3,33	-3,33	3,5	1	-3,91	-4,32	3,5	2
-2,33	-3,33	4,5	2	-4,32	-4,32	3,5	1
-2,33	-3,33	3,5	2	-3,91	-4,32	3,5	1
-3,33	-3,33	4,5	1	-3,91	-4,32	3,5	2
-3,33	-3,33	2,5	1	-3,91	-4,62	3,5	2
-3,33	-3,33	3,5	1	-3,91	-4,62	3,5	2
-3,33	-3,33	3,5	1	-3,91	-4,62	2,5	2
-3,33	-3,33	3,5	1	-3,33	-4,62	3,5	2
-3,33	-3,33	3,5	1	-3,91	-4,62	3,5	2
-3,33	-3,33	3,5	1	-3,91	-4,9	3,5	2
-3,33	-3,33	4,5	1	-3,91	-4,9	3,5	2
-3,33	-3,33	3,5	1	-4,62	-4,9	3,5	2
-3,33	-3,91	3,5	2	-3,91	-4,9	3,5	2
-3,33	-3,91	3,5	2	-3,91	-4,9	3,5	2
-3,33	-3,91	3,5	2	-4,32	-4,9	3,5	2
-3,91	-3,91	3,5	1	-3,91	-5,12	3,5	2
-3,33	-3,91	2,5	2	-3,33	-5,12	3,5	2
-3,33	-3,91	3,5	2	-4,62	-5,12	3,5	2
-3,91	-3,91	3,5	1	-3,91	-5,12	3,5	2
-3,33	-3,91	3,5	2	-4,32	-5,31	3,5	2
-3,91	-3,91	4,5	1	-3,91	-5,63	3,5	2
-3,33	-3,91	3,5	2	-4,32	-5,63	3,5	2

DRUMSHEUGH

Clast size distribution

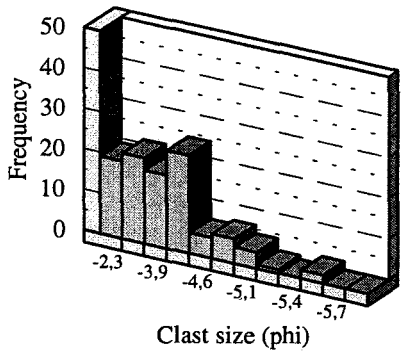

Clast roundness
(-3.91 phi)

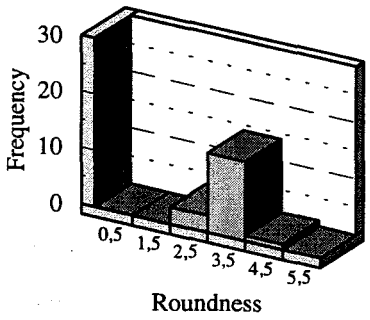

Clast roundness
(-3.33 phi)

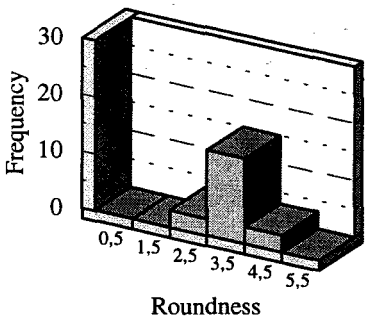

Clast Sphericity

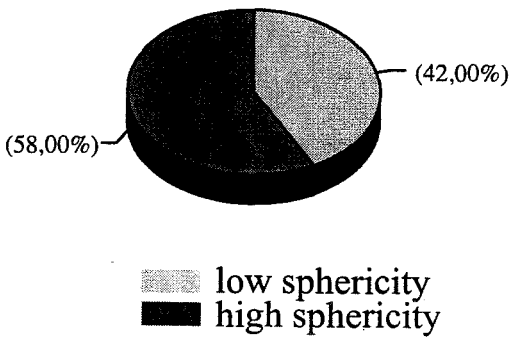

LIZZULEA1

C-axis	A-axis	Round.	Spher.	C-axis	A-axis	Round.	Spher.
-4,32	-5,31	1,5	2	-2,33	-2,33	1,5	1
-4,32	-4,32	1,5	2	-2,33	-2,33	1,5	1
-3,91	-4,32	1,5	2	-2,33	-2,33	1,5	1
-4,32	-5,12	1,5	2	-2,33	-3,33	1,5	2
-3,33	-3,91	1,5	2	-3,91	-4,9	1,5	2
-3,91	-3,91	1,5	1	-4,32	-4,9	1,5	2
-3,91	-4,32	1,5	2	-3,91	-5,12	1,5	2
-4,32	-4,62	1,5	1	-3,33	-4,32	1,5	2
-4,32	-4,9	1,5	2	-4,32	-4,9	1,5	2
-3,33	-3,33	1,5	1	-3,33	-4,32	1,5	2
-4,62	-4,62	1,5	1	-4,9	-5,63	1,5	2
-3,33	-4,32	1,5	2	-4,32	-4,9	1,5	2
-2,33	-3,33	1,5	1	-5,12	-6,12	2,5	2
-3,33	-3,33	1,5	1	-3,33	-4,32	1,5	2
-2,33	-3,33	1,5	1	-3,33	-3,33	2,5	1
-3,33	-3,33	1,5	1	-3,33	-4,9	1,5	2
-4,32	-5,31	2,5	2	-3,91	-5,12	1,5	2
-3,33	-3,33	1,5	1	-3,33	-3,33	1,5	1
-3,33	-4,32	1,5	2	-3,33	-3,33	1,5	1
-3,91	-4,32	1,5	2	-3,33	-3,33	1,5	1
-3,33	-4,32	1,5	2	-3,33	-3,33	1,5	1
-4,32	-4,9	1,5	2	-3,91	-3,91	1,5	1
-3,33	-4,32	1,5	2	-4,32	-4,62	1,5	2
-2,33	-3,33	1,5	2	-3,33	-4,32	1,5	2
-3,33	-3,33	1,5	1	-2,33	-2,33	1,5	1
-3,91	-3,91	1,5	1	-2,33	-2,33	1,5	1
-3,33	-3,91	1,5	1	-2,33	-3,91	1,5	2
-3,33	-4,32	1,5	2	-2,33	-3,91	1,5	2
-3,91	-4,9	1,5	2	-4,32	-4,62	1,5	2
-3,33	-3,33	1,5	1	-3,91	-4,32	1,5	2
-3,33	-3,33	1,5	1	-3,33	-4,32	1,5	2
-3,33	-4,32	2,5	2	-3,91	-4,32	1,5	2
-3,33	-5,12	1,5	2	-3,33	-3,91	2,5	2
-3,33	-3,33	2,5	1	-3,33	-3,33	1,5	1
-3,33	-4,32	2,5	2	-3,91	-3,91	1,5	1
-4,32	-4,32	1,5	1	-2,33	-3,33	1,5	1
-2,33	-3,33	1,5	2	-3,33	-4,9	1,5	2
-3,33	-3,91	1,5	2	-3,91	-3,91	2,5	1
-3,33	-3,91	1,5	2	-4,32	-4,9	2,5	2
-3,33	-3,33	1,5	1	-3,33	-3,33	2,5	1
-3,91	-4,32	1,5	2	-3,33	-4,32	2,5	2
-3,33	-3,33	1,5	1	-3,33	-3,91	1,5	2
-3,33	-3,33	0,5	1	-3,33	-3,91	1,5	2
-3,33	-3,91	1,5	2	-3,33	-3,33	1,5	1
-3,33	-3,33	1,5	1	-3,91	-5,63	1,5	2
-3,33	-3,91	1,5	2	-4,32	-5,31	2,5	2
-3,91	-4,32	1,5	2	-3,91	-4,9	2,5	2
-4,32	-4,9	1,5	2	-3,33	-5,63	1,5	2
-2,33	-3,91	1,5	2	-2,33	-3,91	1,5	2
-3,33	-3,91	1,5	2	-2,33	-3,91	1,5	2

LIZZULEA1

Clast size distribution

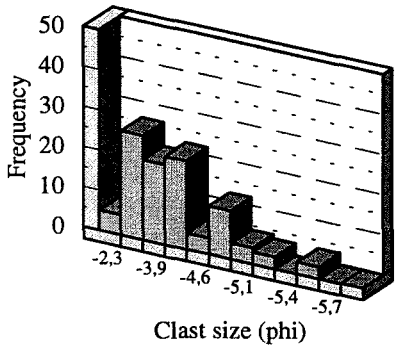

Clast roundness
(-3.91 phi)

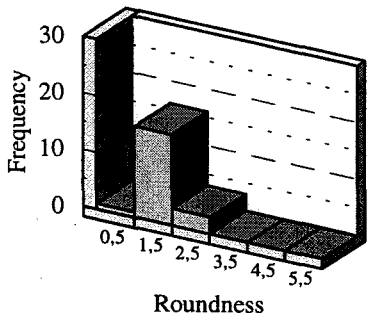

Clast roundness
(-3.33 phi)

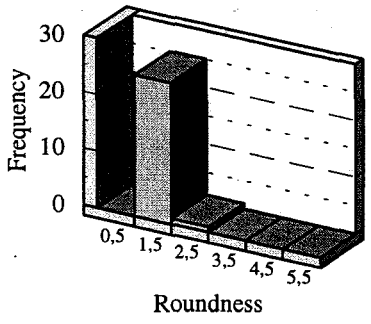

Clast Sphericity

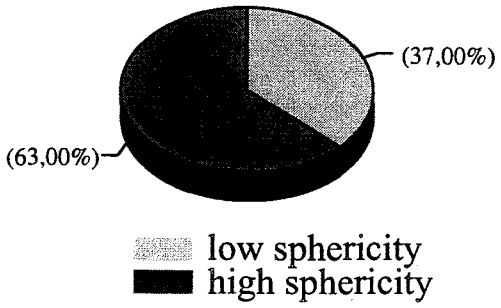

LIZZULEA2

C-axis	A-axis	Round.	Spher.	C-axis	A-axis	Round.	Spher.
-4,32	-4,32	3,5	1	-2,33	-2,33	3,5	1
-4,32	-4,62	3,5	2	-3,33	-3,91	3,5	2
-2,33	-2,33	3,5	1	-2,33	-2,33	3,5	1
-3,91	-4,32	3,5	2	-2,33	-2,33	3,5	1
-3,91	-4,9	3,5	2	-4,32	-4,32	3,5	1
-3,33	-3,91	3,5	2	-3,33	-3,91	3,5	2
-3,33	-3,91	3,5	2	-2,33	-2,33	3,5	1
-3,33	-4,32	3,5	2	-3,33	-3,33	2,5	1
-3,91	-4,62	3,5	2	-3,33	-3,33	3,5	1
-4,32	-4,32	3,5	1	-2,33	-4,32	3,5	2
-3,91	-3,91	3,5	1	-3,33	-3,91	4,5	2
-3,33	-3,91	3,5	2	-3,33	-4,9	4,5	2
-3,91	-4,62	3,5	2	-3,33	-3,33	4,5	1
-3,33	-3,33	3,5	1	-2,33	-3,33	3,5	2
-2,33	-2,33	3,5	1	-2,33	-2,33	3,5	2
-3,33	-4,32	3,5	2	-2,33	-2,33	3,5	1
-3,33	-3,33	3,5	1	-3,33	-3,91	3,5	2
-2,33	-2,33	3,5	1	-2,33	-2,33	4,5	1
-2,33	-2,33	3,5	1	-3,33	-3,33	3,5	1
-3,91	-4,32	3,5	2	-2,33	-2,33	3,5	1
-3,33	-3,91	3,5	2	-2,33	-2,33	3,5	1
-4,32	-4,9	3,5	2	-4,62	-4,62	2,5	1
-3,91	-4,32	3,5	2	-3,91	-4,9	3,5	2
-3,33	-3,33	3,5	1	-4,32	-5,12	3,5	2
-2,33	-3,33	2,5	2	-3,91	-4,62	3,5	2
-2,33	-2,33	3,5	1	-3,33	-4,32	3,5	2
-3,33	-3,91	3,5	2	-2,33	-2,33	3,5	1
-3,33	-3,33	3,5	1	-2,33	-3,33	3,5	2
-2,33	-2,33	3,5	1	-2,33	-3,33	3,5	2
-2,33	-3,33	3,5	2	-2,33	-2,33	3,5	1
-4,32	-5,12	3,5	2	-2,33	-3,33	3,5	1
-3,33	-3,91	3,5	2	-2,33	-2,33	3,5	1
-3,91	-5,12	3,5	2	-3,33	-3,33	3,5	1
-2,33	-2,33	3,5	1	-3,91	-4,62	4,5	2
-2,33	-2,33	3,5	1	-3,33	-3,91	3,5	2
-2,33	-2,33	3,5	1	-2,33	-2,33	3,5	1
-3,33	-3,33	3,5	1	-2,33	-3,33	3,5	2
-3,56	-4,32	3,5	2	-3,33	-3,33	3,5	1
-3,33	-3,33	3,5	1	-3,33	-3,33	3,5	1
-2,33	-2,33	3,5	1	-3,91	-4,9	3,5	2
-3,33	-3,91	3,5	2	-4,32	-4,32	3,5	1
-3,91	-4,62	3,5	2	-4,32	-4,32	3,5	1
-2,33	-3,33	3,5	2	-3,91	-4,32	3,5	2
-4,32	-5,31	3,5	2	-3,33	-4,62	3,5	2
-3,33	-4,32	3,5	2	-4,32	-4,32	3,5	1
-4,32	-4,9	3,5	2	-3,91	-4,32	3,5	1
-3,91	-4,32	3,5	2	-2,33	-3,33	3,5	2
-3,91	-4,32	3,5	2	-3,91	-4,62	3,5	2
-2,33	-2,33	3,5	1	-3,91	-4,62	3,5	2
-3,91	-4,32	3,5	2	-2,33	-2,33	3,5	1

LIZZULEA2

Clast size distribution

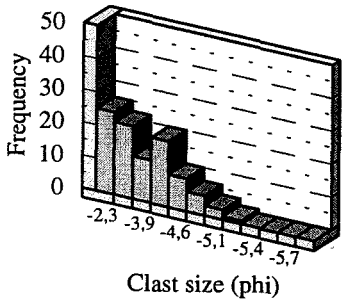

Clast roundness

(-3.91 phi)

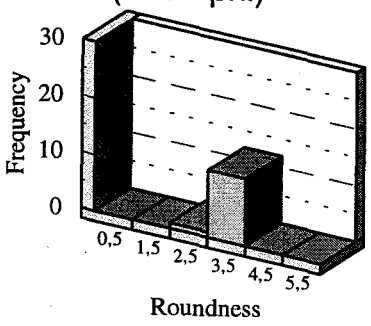

Clast roundness

(-3.33 phi)

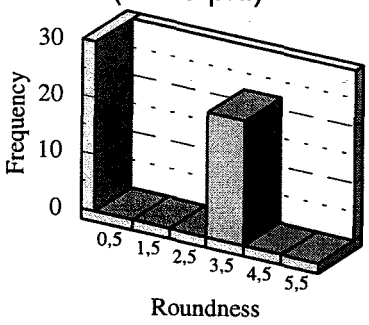

Clast Sphericity

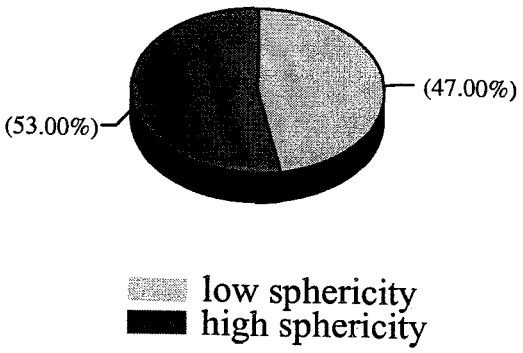

LUNA

C-axis	A-axis	Round.	Spher.	C-axis	A-axis	Round.	Spher.
-3,33	-4,62	2,5	2	-2,33	-3,33	3,5	1
-3,91	-3,91	2,5	2	-3,33	-4,32	3,5	2
-2,33	-3,33	3,5	1	-2,33	-2,33	3,5	1
-2,33	-3,91	3,5	2	-2,33	-2,33	3,5	1
-2,33	-3,91	3,5	2	-2,33	-2,33	3,5	1
-3,33	-3,91	3,5	2	-2,33	-2,33	3,5	1
-3,91	-4,62	3,5	2	-2,33	-2,33	3,5	1
-3,33	-3,33	3,5	1	-2,33	-2,33	3,5	1
-3,91	-4,32	3,5	2	-2,33	-2,33	3,5	1
-3,33	-3,91	3,5	2	-2,33	-2,33	3,5	1
-3,91	-4,32	3,5	2	-2,33	-2,33	3,5	1
-4,62	-5,12	3,5	2	-2,33	-2,33	3,5	1
-2,33	-2,33	3,5	1	-2,33	-2,33	3,5	1
-2,33	-2,33	3,5	1	-2,33	-2,33	3,5	1
-2,33	-2,33	3,5	1	-2,33	-2,33	3,5	1
-2,33	-2,33	3,5	1	-2,33	-2,33	3,5	1
-2,33	-2,33	3,5	1	-2,33	-2,33	3,5	1
-2,33	-2,33	3,5	1	-2,33	-2,33	3,5	1
-2,33	-2,33	3,5	1	-2,33	-2,33	3,5	1
-2,33	-2,33	3,5	1	-2,33	-2,33	3,5	1
-2,33	-2,33	3,5	1	-2,33	-2,33	3,5	1
-2,33	-2,33	3,5	1	-2,33	-2,33	3,5	1
-2,33	-2,33	3,5	1	-3,91	-4,32	3,5	2
-2,33	-2,33	3,5	1	-3,91	-4,32	3,5	2
-2,33	-2,33	3,5	1	-2,33	-3,33	3,5	2
-2,33	-2,33	3,5	1	-2,33	-3,91	3,5	2
-2,33	-2,33	3,5	1	-3,33	-3,33	3,5	1
-2,33	-2,33	3,5	1	-2,33	-3,33	3,5	2
-2,33	-2,33	3,5	1	-2,33	-3,33	3,5	2
-2,33	-2,33	3,5	1	-3,33	-3,33	3,5	1
-3,33	-3,91	3,5	2	-3,91	-3,91	3,5	1
-3,33	-3,91	3,5	2	-3,33	-3,91	3,5	2
-4,32	-4,32	3,5	1	-3,33	-3,91	3,5	2
-3,33	-3,91	3,5	2	-3,91	-4,32	4,5	2
-2,33	-3,33	3,5	2	-3,33	-4,32	3,5	2
-3,91	-4,32	3,5	2	-3,33	-4,32	3,5	2
-3,33	-3,33	3,5	1	-3,33	-4,32	3,5	2
-3,33	-3,91	3,5	2	-3,33	-3,91	3,5	2
-3,91	-3,91	3,5	1	-3,91	-3,91	2,5	1
-2,33	-3,33	3,5	2	-3,33	-3,91	2,5	2
-3,33	-3,33	3,5	1	-3,33	-3,91	3,5	2
-3,33	-3,33	3,5	1	-3,33	-3,33	3,5	1
-4,32	-4,32	3,5	1	-3,33	-3,91	3,5	1
-3,33	-3,91	3,5	2	-2,33	-4,32	3,5	2
-3,33	-4,32	3,5	2	-3,33	-3,91	3,5	2
-2,33	-3,91	3,5	2	-3,33	-4,62	3,5	2
-4,32	-4,9	3,5	2	-2,33	-3,33	3,5	2
-4,32	-4,32	2,5	1	-2,33	-2,33	3,5	1
-3,91	-3,91	2,5	1	-3,33	-3,91	3,5	2
-3,33	-3,33	2,5	1	-3,33	-4,32	3,5	2

LUNA

Clast size distribution

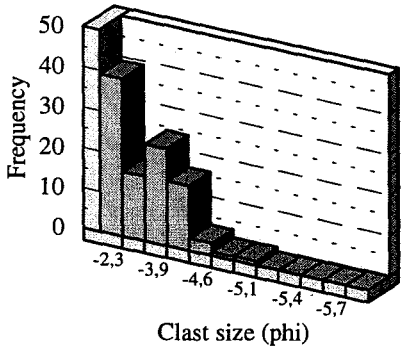

Clast roundness
(-3.91 phi)

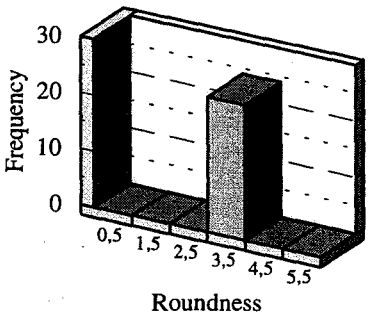

Clast roundness
(-3.33 phi)

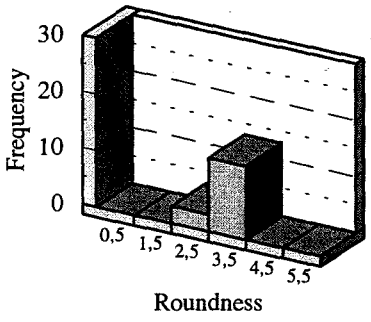

Clast Sphericity

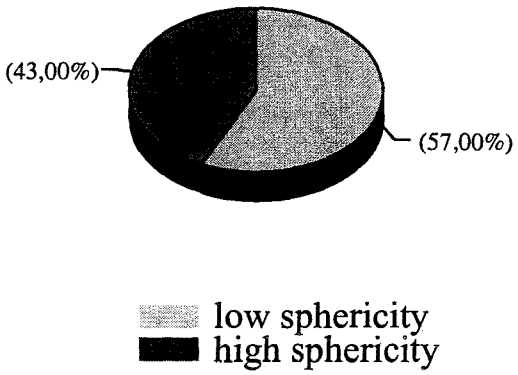

SCHIETFONTEIN

C-axis	A-axis	Round.	Spher.	C-axis	A-axis	Round.	Spher.
-3,33	-3,91	4,5	2	-3,91	-4,32	3,5	2
-2,33	-3,33	3,5	2	-3,33	-4,32	3,5	2
-2,33	-2,33	3,5	1	-2,33	-3,33	3,5	2
-2,33	-3,33	2,5	2	-2,33	-3,33	3,5	2
-3,33	-3,33	3,5	1	-2,33	-3,33	2,5	2
-3,33	-3,33	2,5	1	-3,33	-4,32	2,5	2
-3,91	-4,32	2,5	2	-3,91	-3,91	3,5	2
-3,33	-3,91	2,5	2	-3,33	-3,33	3,5	1
-3,33	-3,33	3,5	1	-3,33	-3,33	3,5	1
-3,33	-3,33	3,5	1	-3,33	-3,33	3,5	1
-3,91	-3,91	3,5	1	-3,33	-3,33	2,5	1
-3,33	-3,33	3,5	1	-2,33	-2,33	3,5	1
-2,33	-4,32	3,5	2	-3,33	-3,33	2,5	1
-2,33	-2,33	4,5	1	-3,33	-3,33	2,5	1
-2,33	-2,33	4,5	1	-3,33	-4,62	3,5	2
-3,91	-3,91	2,5	1	-3,33	-3,91	3,5	2
-3,33	-3,33	3,5	1	-3,33	-3,33	3,5	1
-2,33	-2,33	3,5	1	-3,33	-4,32	3,5	2
-2,33	-2,33	4,5	1	-3,33	-3,33	3,5	1
-2,33	-2,33	3,5	1	-3,33	-3,33	3,5	1
-3,33	-3,33	4,5	1	-3,91	-3,91	2,5	1
-3,33	-3,33	3,5	1	-2,33	-3,33	2,5	2
-3,33	-3,91	2,5	1	-3,33	-4,62	2,5	1
-3,33	-3,91	2,5	2	-3,33	-4,9	2,5	2
-3,33	-3,91	3,5	2	-3,33	-3,91	3,5	2
-3,91	-3,91	3,5	2	-2,33	-3,91	3,5	2
-3,33	-3,91	3,5	2	-3,33	-4,32	2,5	2
-3,33	-3,91	3,5	2	-3,91	-3,91	3,5	1
-2,33	-3,33	2,5	2	-3,33	-3,33	3,5	1
-3,33	-3,91	2,5	2	-3,33	-3,33	3,5	1
-3,33	-3,91	2,5	2	-3,91	-3,91	3,5	1
-2,33	-2,33	1,5	1	-3,91	-3,91	2,5	1
-2,33	-3,33	3,5	2	-3,91	-3,91	2,5	1
-3,33	-4,32	3,5	2	-3,33	-3,91	2,5	2
-2,33	-3,33	3,5	2	-3,33	-3,33	2,5	1
-3,33	-3,33	2,5	1	-3,33	-3,91	3,5	2
-3,91	-3,91	3,5	1	-3,33	-4,32	3,5	2
-3,33	-3,91	3,5	2	-3,33	-3,33	3,5	1
-3,33	-3,91	3,5	2	-3,33	-3,33	3,5	1
-3,33	-3,91	3,5	2	-3,33	-3,91	2,5	2
-3,91	-3,91	3,5	1	-2,33	-2,33	3,5	1
-3,33	-3,91	3,5	2	-2,33	-2,33	3,5	1
-3,33	-3,33	3,5	1	-2,33	-2,33	3,5	1
-3,91	-4,32	3,5	2	-2,33	-2,33	3,5	1
-3,91	-4,62	3,5	2	-2,33	-2,33	3,5	1
-3,91	-4,62	3,5	2	-2,33	-2,33	3,5	1
-3,91	-4,32	3,5	2	-2,33	-2,33	3,5	1
-3,33	-3,33	3,5	1	-2,33	-2,33	3,5	1
-3,33	-3,91	2,5	2	-2,33	-2,33	3,5	1
-3,91	-4,32	3,5	2	-2,33	-2,33	3,5	1

SCHIETFONTEIN

Clast size distribution

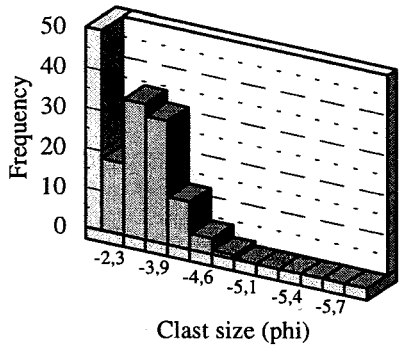

Clast roundness
(-3.91 phi)

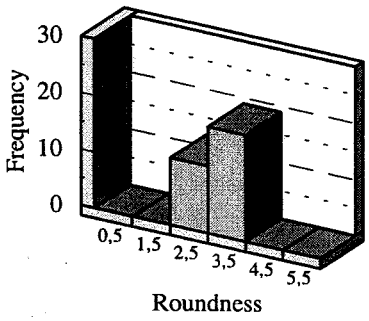

Clast roundness
(-3.33 phi)

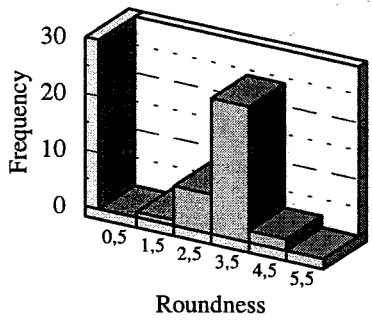

Clast Sphericity

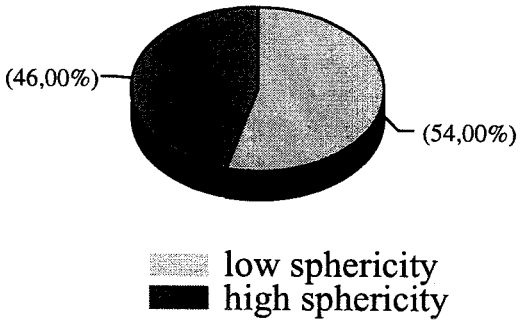

KILGOUR

C-axis	A-axis	Round.	Spher.	C-axis	A-axis	Round.	Spher.
-4,32	-5,12	0,5	2	-2,33	-3,91	0,5	2
-3,91	-4,32	0,5	2	-3,91	-3,91	1,5	1
-3,91	-5,31	0,5	2	-3,33	-3,91	1,5	2
-3,91	-4,9	0,5	2	-3,33	-3,91	1,5	2
-3,33	-3,33	0,5	1	-3,91	-3,91	1,5	1
-3,33	-3,33	0,5	1	-3,91	-4,32	1,5	2
-3,91	-5,12	1,5	2	-3,33	-3,33	0,5	1
-3,33	-3,91	0,5	1	-3,33	-3,91	1,5	1
-4,32	-4,62	1,5	2	-3,33	-3,91	1,5	1
-3,91	-4,62	2,5	1	-4,62	-5,12	1,5	1
-3,33	-3,91	1,5	2	-2,33	-2,33	1,5	1
-3,33	-4,32	0,5	2	-2,33	-2,33	1,5	1
-2,33	-3,91	0,5	2	-2,33	-2,33	0,5	1
-2,33	-2,33	1,5	1	-2,33	-2,33	0,5	1
-5,31	-6,12	0,5	2	-2,33	-2,33	0,5	1
-3,91	-3,91	1,5	1	-2,33	-2,33	0,5	1
-3,33	-4,32	1,5	2	-3,33	-3,91	1,5	2
-3,91	-4,32	0,5	1	-3,91	-4,9	1,5	2
-3,91	-3,91	1,5	1	-3,91	-4,32	1,5	2
-4,9	-5,31	0,5	1	-3,91	-4,32	1,5	1
-3,91	-4,32	0,5	2	-2,33	-3,33	0,5	2
-3,91	-5,12	1,5	2	-2,33	-3,33	0,5	2
-4,32	-4,32	1,5	1	-3,33	-3,91	0,5	1
-3,33	-3,91	1,5	1	-3,33	-4,32	1,5	2
-3,33	-3,91	1,5	2	-3,33	-4,32	1,5	2
-3,33	-4,32	1,5	2	-2,33	-2,33	1,5	1
-4,32	-5,48	0,5	2	-2,33	-2,33	1,5	1
-4,62	-5,63	1,5	2	-2,33	-3,33	1,5	2
-3,91	-4,32	0,5	2	-2,33	-3,91	1,5	2
-3,33	-3,91	0,5	2	-3,33	-4,62	0,5	1
-2,33	-3,33	0,5	2	-3,33	-3,33	0,5	1
-2,33	-2,33	0,5	1	-3,91	-4,32	1,5	1
-4,32	-4,9	0,5	2	-3,33	-3,33	1,5	1
-3,91	-4,32	1,5	2	-3,33	-3,33	1,5	1
-3,91	-4,32	2,5	2	-3,33	-3,33	1,5	1
-3,33	-3,33	2,5	1	-3,33	-3,91	1,5	2
-4,62	-4,9	1,5	1	-4,32	-4,32	1,5	1
-3,91	-5,12	0,5	1	-2,33	-4,32	1,5	2
-4,32	-5,12	0,5	2	-2,33	-3,33	0,5	2
-4,32	-4,9	1,5	2	-3,33	-3,91	0,5	1
-4,9	-5,48	0,5	2	-3,33	-3,33	0,5	1
-4,9	-5,48	0,5	2	-3,33	-3,33	0,5	1
-3,33	-4,62	1,5	2	-3,33	-4,32	0,5	2
-3,91	-4,32	0,5	2	-2,33	-3,91	1,5	2
-4,9	-5,31	1,5	2	-3,33	-3,33	0,5	1
-3,91	-4,62	1,5	2	-3,33	-3,33	0,5	1
-4,62	-5,48	3,5	1	-3,91	-4,32	1,5	2
-3,33	-4,32	3,5	2	-3,33	-3,33	1,5	1
-4,32	-4,62	1,5	2	-2,33	-2,33	0,5	1
-4,32	-4,62	3,5	2	-2,33	-3,33	0,5	1

KILGOUR

Clast size distribution

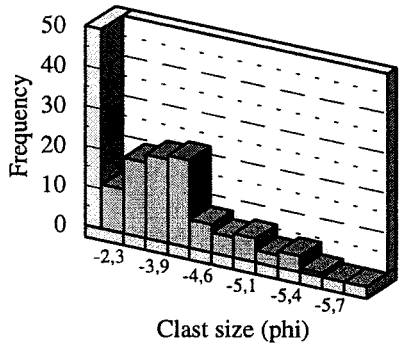

Clast roundness

(-3.91 phi)

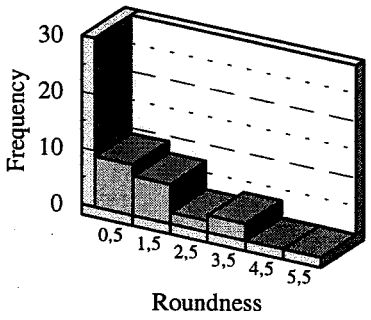

Clast roundness

(-3.33 phi)

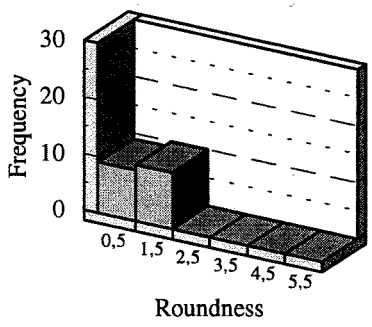

Clast Sphericity

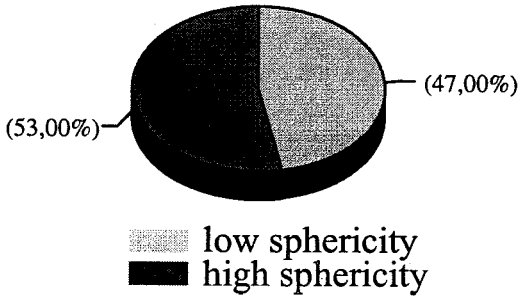

KONINGSMARK1

C-axis	A-axis	Round.	Spher.	C-axis	A-axis	Round.	Spher.
-3,33	-4,91	3,5	2	-3,33	-3,33	3,5	1
-3,33	-3,91	3,5	2	-3,33	-3,33	3,5	1
-3,33	-3,91	3,5	2	-3,33	-3,33	3,5	1
-3,33	-3,91	3,5	2	-3,33	-3,91	3,5	2
-2,33	-2,33	3,5	1	-3,33	-4,32	3,5	2
-2,33	-3,91	3,5	2	-3,91	-4,62	3,5	2
-2,33	-4,32	3,5	2	-3,91	-4,32	3,5	2
-2,33	-2,33	3,5	1	-3,33	-3,33	3,5	1
-4,32	-4,62	3,5	2	-2,33	-3,33	3,5	2
-3,33	-4,32	3,5	2	-3,33	-3,33	3,5	1
-3,33	-4,32	3,5	2	-2,33	-3,33	3,5	1
-4,32	-4,32	3,5	1	-2,33	-2,33	3,5	1
-3,33	-3,33	3,5	1	-2,33	-2,33	3,5	1
-3,91	-3,91	3,5	1	-3,33	-3,33	3,5	1
-3,33	-3,33	3,5	1	-2,33	-2,33	3,5	1
-3,33	-4,32	3,5	2	-2,33	-3,33	3,5	1
-3,33	-3,33	3,5	1	-2,33	-3,33	3,5	1
-3,33	-4,62	3,5	2	-2,33	-3,33	3,5	1
-3,33	-3,33	3,5	1	-3,91	-3,91	3,5	1
-2,33	-2,33	3,5	1	-4,32	-5,31	3,5	2
-3,33	-3,91	3,5	2	-4,62	-4,9	3,5	1
-2,33	-2,33	3,5	1	-3,91	-4,32	3,5	1
-3,91	-4,9	3,5	2	-2,33	-3,33	3,5	2
-3,91	-3,91	3,5	1	-3,33	-3,91	3,5	2
-3,33	-4,32	3,5	2	-3,33	-3,91	3,5	2
-3,33	-3,91	3,5	2	-3,33	-4,32	3,5	2
-3,91	-3,91	3,5	1	-3,33	-3,33	3,5	1
-3,33	-3,33	3,5	1	-3,33	-3,91	3,5	2
-3,33	-3,33	3,5	1	-2,33	-3,91	3,5	2
-3,33	-3,33	3,5	1	-2,33	-2,33	3,5	1
-3,91	-5,31	3,5	2	-2,33	-2,33	3,5	1
-3,33	-4,32	3,5	2	-2,33	-2,33	3,5	1
-3,33	-3,91	3,5	2	-3,33	-3,91	3,5	2
-3,33	-4,32	3,5	2	-3,91	-3,91	3,5	1
-2,33	-3,33	3,5	2	-2,33	-3,91	3,5	2
-3,33	-3,33	3,5	1	-2,33	-2,33	3,5	1
-3,91	-4,9	3,5	2	-3,33	-3,33	3,5	1
-3,91	-3,91	3,5	1	-3,33	-3,33	3,5	1
-3,33	-4,32	3,5	2	-3,91	-3,91	3,5	1
-3,91	-4,62	3,5	2	-3,33	-4,32	3,5	2
-3,91	-3,91	3,5	1	-2,33	-2,33	3,5	1
-3,33	-3,33	3,5	1	-3,33	-3,33	3,5	1
-3,33	-4,32	3,5	2	-3,91	-4,32	3,5	2
-3,33	-3,91	3,5	2	-3,91	-3,91	3,5	1
-3,33	-3,91	3,5	2	-3,91	-4,32	3,5	2
-3,33	-4,9	3,5	2	-3,33	-3,33	3,5	1
-3,91	-4,62	3,5	2	-3,91	-3,91	3,5	1
-4,32	-4,62	3,5	2	-3,91	-3,91	3,5	1
-3,33	-3,91	3,5	2	-2,33	-2,33	3,5	1
-3,91	-4,32	3,5	2	-3,91	-4,32	3,5	2

KONINGSMARK1

Clast size distribution

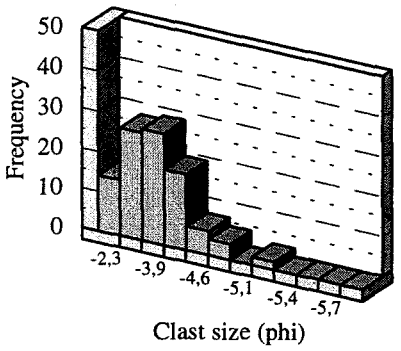

Clast roundness

(-3.91 phi)

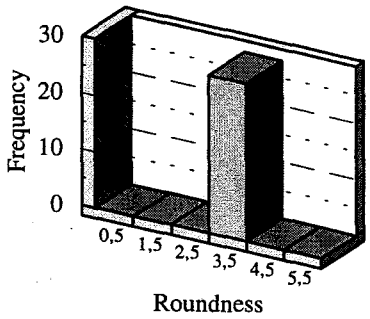

Clast roundness

(-3.33 phi)

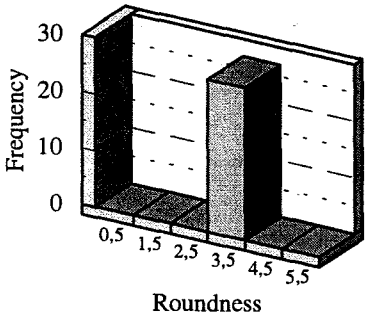

Clast Sphericity

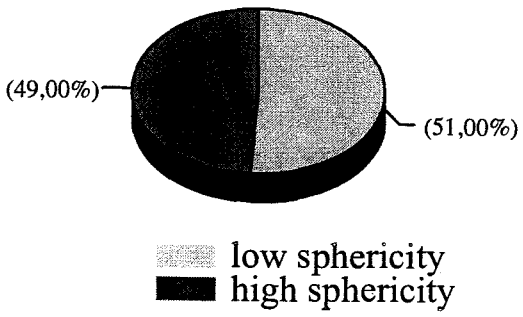

C-axis	A-axis	Round.	Spher.	C-axis	A-axis	Round.	Spher.
-3,33	-3,33	3,5	1	-2,33	-2,33	2,5	1
-3,33	-3,33	3,5	1	-2,33	-2,33	2,5	1
-3,33	-3,33	3,5	1	-2,33	-2,33	2,5	1
-3,33	-3,33	3,5	1	-2,33	-2,33	2,5	1
-3,33	-3,33	3,5	1	-2,33	-2,33	2,5	1
-3,33	-3,33	3,5	1	-2,33	-2,33	2,5	1
-3,33	-3,33	3,5	1	-2,33	-2,33	2,5	1
-3,33	-3,33	3,5	1	-2,33	-2,33	2,5	1
-3,33	-3,33	3,5	1	-2,33	-2,33	2,5	1
-3,33	-3,33	3,5	1	-2,33	-2,33	2,5	1
-3,33	-3,33	3,5	1	-2,33	-2,33	2,5	1
-3,33	-3,33	3,5	1	-2,33	-2,33	2,5	1
-3,33	-3,33	3,5	1	-2,33	-2,33	2,5	1
-3,33	-3,33	3,5	1	-2,33	-2,33	2,5	1
-3,33	-3,33	3,5	1	-2,33	-2,33	2,5	1
-3,33	-3,33	3,5	1	-2,33	-2,33	2,5	1
-3,33	-3,33	3,5	1	-2,33	-2,33	2,5	1
-3,33	-3,33	3,5	1	-2,33	-2,33	2,5	1
-3,33	-3,33	3,5	1	-2,33	-2,33	2,5	1
-3,33	-3,33	3,5	1	-2,33	-2,33	2,5	1
-2,33	-2,33	2,5	1	-2,33	-2,33	2,5	1
-2,33	-2,33	2,5	1	-2,33	-2,33	2,5	1
-2,33	-2,33	2,5	1	-2,33	-2,33	2,5	1
-2,33	-2,33	2,5	1	-2,33	-3,33	3,5	2
-2,33	-2,33	2,5	1	-2,33	-3,33	3,5	2
-2,33	-2,33	2,5	1	-2,33	-3,33	3,5	2
-2,33	-2,33	2,5	1	-2,33	-3,33	3,5	2
-2,33	-2,33	2,5	1	-2,33	-3,33	3,5	2
-2,33	-2,33	2,5	1	-2,33	-2,33	3,5	1
-2,33	-2,33	2,5	1	-2,33	-2,33	3,5	1
-2,33	-2,33	2,5	1	-2,33	-2,33	3,5	1
-2,33	-2,33	2,5	1	-2,33	-2,33	3,5	1
-2,33	-2,33	2,5	1	-2,33	-2,33	3,5	1
-2,33	-2,33	2,5	1	-2,33	-2,33	3,5	1
-2,33	-2,33	2,5	1	-2,33	-2,33	3,5	1
-2,33	-2,33	2,5	1	-2,33	-3,33	3,5	1
-2,33	-2,33	2,5	1	-2,33	-3,33	3,5	1
-2,33	-2,33	2,5	1	-2,33	-3,33	3,5	1
-2,33	-2,33	2,5	1	-2,33	-3,33	3,5	1
-2,33	-2,33	2,5	1	-2,33	-3,33	3,5	1
-2,33	-2,33	2,5	1	-2,33	-3,33	3,5	1
-2,33	-2,33	2,5	1	-2,33	-3,33	3,5	1
-2,33	-2,33	2,5	1	-2,33	-3,33	3,5	1
-2,33	-2,33	2,5	1	-2,33	-3,33	3,5	1
-2,33	-2,33	2,5	1	-2,33	-3,33	3,5	1
-2,33	-2,33	2,5	1	-2,33	-3,33	3,5	1
-2,33	-2,33	2,5	1	-2,33	-3,33	3,5	1
-2,33	-2,33	2,5	1	-2,33	-3,33	3,5	1
-2,33	-2,33	2,5	1	-2,33	-3,33	3,5	1
-2,33	-2,33	2,5	1	-2,33	-3,33	3,5	1

KONINGSMARK2

Clast size distribution

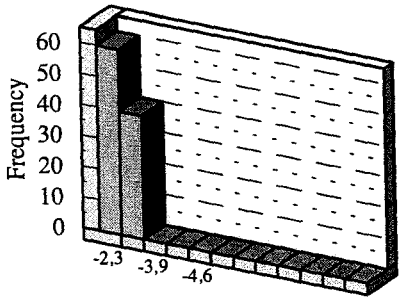

Clast size (phi)

Clast roundness

(-3.33 phi)

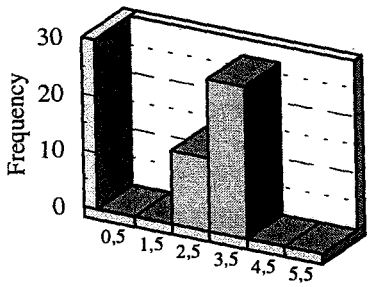

Roundness

Clast Sphericity

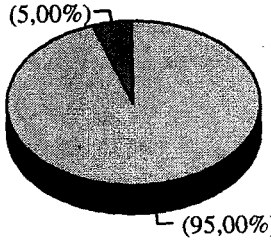

low sphericity
high sphericity

BISMARCK

C-axis	A-axis	Round.	Spher.	C-axis	A-axis	Round.	Spher.
-4,32	-4,62	2,5	2	-3,33	-3,91	3,5	2
-3,33	-3,33	2,5	1	-3,91	-4,9	2,5	2
-3,33	-3,33	3,5	1	-3,33	-4,62	3,5	2
-3,33	-3,33	3,5	1	-3,91	-4,32	3,5	2
-3,33	-3,91	3,5	2	-3,33	-3,91	2,5	2
-4,32	-4,32	2,5	1	-2,33	-3,33	2,5	1
-2,33	-3,33	2,5	1	-3,91	-4,62	2,5	2
-2,33	-3,33	3,5	2	-2,33	-4,32	3,5	2
-3,33	-3,33	3,5	1	-3,91	-3,91	3,5	1
-4,32	-4,9	2,5	2	-3,91	-5,12	3,5	2
-4,32	-4,32	2,5	1	-4,32	-4,62	3,5	1
-4,62	-4,62	2,5	1	-3,33	-4,32	3,5	2
-3,91	-4,62	2,5	2	-3,91	-4,62	3,5	2
-4,32	-4,32	2,5	1	-3,91	-3,91	3,5	1
-3,33	-3,91	3,5	2	-3,91	-3,91	3,5	1
-4,32	-4,32	3,5	1	-3,91	-4,62	3,5	2
-3,91	-3,91	2,5	1	-3,33	-4,32	3,5	2
-4,32	-4,32	2,5	1	-3,91	-3,91	3,5	1
-3,91	-4,62	2,5	2	-3,33	-3,91	3,5	1
-3,33	-3,91	2,5	1	-3,33	-3,91	3,5	1
-2,33	-3,33	3,5	1	-3,91	-4,9	3,5	2
-3,33	-3,91	2,5	2	-2,33	-2,33	1,5	1
-3,33	-3,33	1,5	1	-3,33	-3,33	3,5	1
-3,33	-4,62	1,5	2	-3,91	-4,62	3,5	2
-3,91	-4,32	3,5	2	-3,91	-4,32	2,5	2
-3,33	-3,91	4,5	1	-3,33	-4,32	2,5	2
-4,32	-4,32	2,5	1	-3,91	-4,32	2,5	2
-3,91	-4,32	2,5	2	-4,32	-4,32	2,5	2
-3,33	-4,32	3,5	2	-2,33	-3,91	1,5	2
-3,33	-3,91	1,5	2	-3,91	-4,32	2,5	2
-2,33	-3,33	1,5	2	-3,33	-4,32	2,5	2
-2,33	-4,32	3,5	2	-3,33	-4,32	3,5	2
-2,33	-3,33	2,5	2	-3,91	-3,91	2,5	1
-3,33	-3,91	3,5	1	-3,33	-3,91	3,5	2
-3,33	-4,32	3,5	2	-4,32	-4,9	3,5	2
-4,32	-5,12	3,5	2	-3,91	-4,32	3,5	2
-3,33	-3,33	2,5	1	-3,91	-3,91	2,5	1
-2,33	-3,91	-4,9	2	-4,62	-4,9	3,5	2
-3,91	-4,32	2,5	2	-4,32	-5,48	3,5	2
-3,91	-4,32	1,5	2	-4,32	-4,62	2,5	2
-2,33	-3,33	2,5	2	-3,91	-4,32	3,5	2
-3,33	-3,91	2,5	2	-3,33	-4,32	3,5	2
-3,33	-3,33	2,5	1	-3,33	-4,32	3,5	2
-3,33	-3,91	2,5	2	-3,91	-4,9	2,5	2
-3,33	-3,33	2,5	1	-3,91	-3,91	3,5	1
-3,33	-3,91	3,5	1	-3,33	-4,32	2,5	2
-3,33	-3,91	2,5	2	-3,91	-4,32	2,5	1
-2,33	-2,33	2,5	1	-3,91	-4,62	2,5	2
-3,33	-4,32	3,5	2	-3,91	-4,32	2,5	1
-2,33	-3,33	2,5	2	-4,32	-4,32	3,5	1

BISMARCK

Clast size distribution

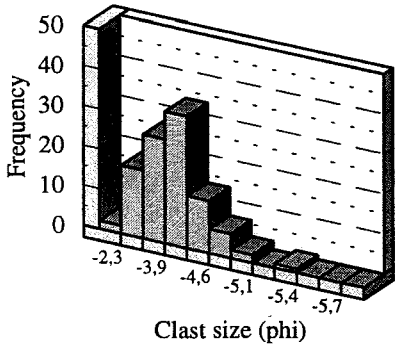

Clast roundness
(-3.91 phi)

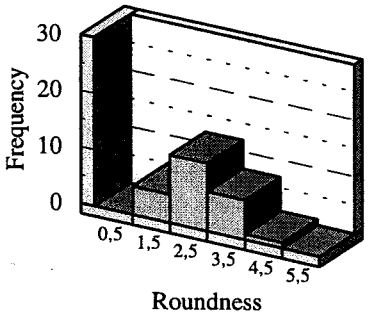

Clast roundness
(-3.33 phi)

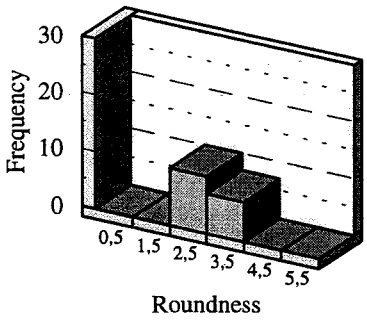

Clast Sphericity

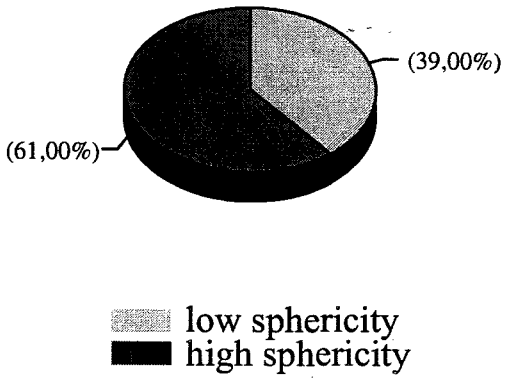

BERGEN OP ZOOM

C-axis	A-axis	Round.	Spher.	C-axis	A-axis	Round.	Spher.
-4,32	-4,9	4,5	2	-3,33	-4,32	3,5	2
-3,91	-4,32	3,5	2	-2,33	-2,33	3,5	1
-3,91	-3,91	3,5	1	-2,33	-2,33	3,5	1
-4,32	-5,63	3,5	2	-3,91	-4,32	3,5	2
-3,91	-4,9	3,5	2	-3,91	-4,9	3,5	2
-3,33	-3,91	3,5	2	-3,91	-4,62	3,5	2
-4,32	-5,31	3,5	2	-3,33	-4,32	3,5	2
-3,33	-3,33	3,5	1	-2,33	-2,33	3,5	1
-2,33	-2,33	3,5	1	-3,33	-3,91	3,5	2
-3,33	-3,33	3,5	1	-2,33	-2,33	3,5	1
-4,9	-4,9	3,5	1	-2,33	-3,33	3,5	2
-3,91	-5,63	3,5	2	-4,62	-5,31	3,5	2
-3,91	-3,91	3,5	1	-3,33	-4,32	3,5	2
-3,91	-3,91	3,5	1	-3,91	-3,91	3,5	1
-4,32	-4,62	3,5	2	-2,33	-2,33	3,5	1
-3,33	-3,33	3,5	1	-3,33	-4,9	3,5	2
-3,33	-3,91	3,5	2	-3,33	-3,91	3,5	2
-3,33	-3,33	3,5	1	-3,33	-5,12	3,5	2
-4,32	-4,62	3,5	2	-3,91	-4,9	3,5	2
-3,33	-3,91	4,5	2	-4,62	-5,31	3,5	2
-2,33	-3,33	3,5	2	-5,31	-5,31	3,5	1
-4,62	-4,62	3,5	1	-4,62	-5,48	3,5	2
-3,33	-3,91	3,5	2	-3,33	-3,33	3,5	1
-3,33	-4,62	3,5	2	-2,33	-2,33	3,5	1
-4,32	-4,32	3,5	1	-2,33	-2,33	3,5	1
-4,32	-5,31	3,5	2	-2,33	-2,33	3,5	1
-4,62	-5,31	3,5	2	-4,32	-5,12	3,5	2
-3,33	-3,91	4,5	2	-4,62	-4,62	3,5	1
-2,33	-3,33	3,5	2	-4,32	-5,12	3,5	2
-3,33	-4,32	3,5	2	-4,32	-5,31	3,5	2
-3,33	-3,91	3,5	2	-4,32	-4,9	3,5	2
-3,91	-4,32	3,5	2	-3,33	-4,32	4,5	2
-3,33	-3,91	3,5	2	-4,32	-4,32	3,5	1
-2,33	-3,33	3,5	2	-4,32	-4,9	3,5	2
-3,33	-3,91	3,5	2	-3,91	-4,9	3,5	2
-3,33	-3,33	3,5	1	-4,32	-5,31	3,5	2
-3,33	-3,91	3,5	2	-2,33	-2,33	3,5	1
-4,32	-4,9	3,5	2	-2,33	-2,33	3,5	1
-3,91	-5,12	3,5	2	-2,33	-2,33	3,5	1
-2,33	-2,33	3,5	1	-3,91	-3,91	3,5	1
-2,33	-2,33	3,5	1	-2,33	-3,33	3,5	2
-3,91	-4,62	3,5	2	-2,33	-3,33	3,5	2
-3,33	-4,62	3,5	2	-3,33	-3,33	4,5	1
-4,32	-4,32	3,5	1	-2,33	-2,33	3,5	1
-4,32	-4,32	3,5	1	-3,33	-3,91	3,5	1
-3,33	-3,91	3,5	2	-2,33	-2,33	4,5	1
-3,33	-4,32	3,5	2	-3,91	-4,32	3,5	2
-4,62	-4,9	2,5	2	-4,62	-5,31	3,5	2
-3,33	-4,32	3,5	2	-3,91	-4,62	3,5	2
-3,33	-4,32	3,5	2	-3,33	-3,91	3,5	2

BERGEN OP ZOOM

Clast size distribution

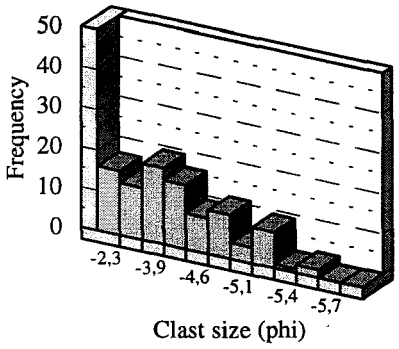

Clast roundness

(-3.91 phi)

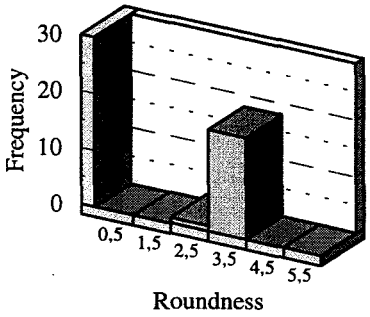

Clast roundness

(-3.33 phi)

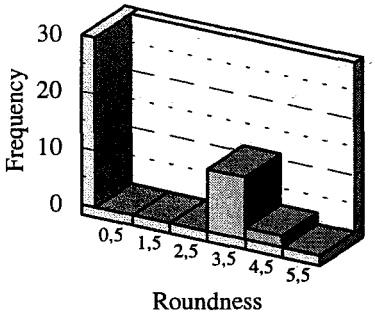

Clast Sphericity

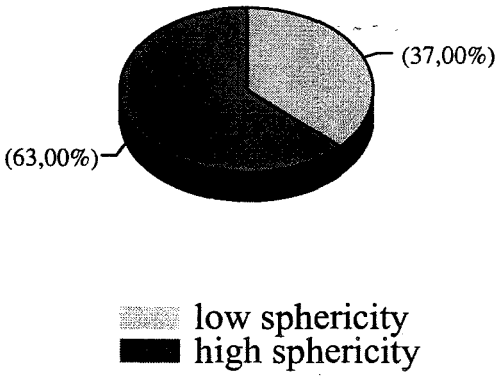

OVERVLAKTE

C-axis	A-axis	Round.	Spher.	C-axis	A-axis	Round.	Spher.
-3,91	-4,32	3,5	1	-3,33	-4,32	3,5	2
-3,91	-4,32	3,5	1	-4,32	-4,9	3,5	2
-3,91	-4,32	3,5	2	-3,91	-4,32	3,5	2
-4,32	-5,12	2,5	2	-3,33	-4,32	3,5	2
-3,91	-4,32	3,5	2	-3,33	-3,91	2,5	2
-3,33	-4,32	3,5	2	-3,91	-3,91	3,5	1
-4,62	-5,12	3,5	2	-3,33	-4,62	3,5	2
-3,91	-4,62	3,5	2	-3,33	-3,91	3,5	2
-3,33	-4,32	3,5	2	-3,33	-4,32	3,5	2
-4,32	-5,12	3,5	2	-3,33	-3,91	3,5	2
-3,91	-3,91	2,5	1	-3,33	-4,62	3,5	2
-4,32	-4,32	3,5	1	-3,33	-3,91	2,5	2
-3,33	-3,91	2,5	1	-5,12	-5,63	3,5	2
-3,91	-3,91	2,5	1	-4,32	-4,62	3,5	2
-3,91	-3,91	3,5	1	-3,33	-3,91	3,5	1
-3,91	-4,32	2,5	2	-3,33	-3,91	3,5	2
-3,33	-3,91	3,5	1	-3,33	-3,91	3,5	1
-3,33	-3,33	3,5	1	-3,33	-3,91	3,5	1
-3,33	-4,32	3,5	2	-3,91	-3,91	2,5	1
-3,91	-4,32	3,5	2	-4,32	-4,9	2,5	2
-3,33	-4,32	3,5	2	-3,33	-3,91	3,5	2
-3,91	-4,32	3,5	2	-2,33	-3,91	3,5	2
-3,33	-3,91	3,5	2	-4,32	-4,32	3,5	1
-3,91	-4,62	3,5	2	-3,91	-3,91	2,5	1
-3,91	-4,32	3,5	2	-3,91	-3,91	2,5	1
-3,91	-4,32	3,5	1	-3,91	-4,32	3,5	1
-3,33	-3,91	3,5	2	-3,91	-4,32	2,5	2
-3,33	-4,62	3,5	2	-3,91	-4,32	3,5	2
-3,91	-4,32	3,5	2	-3,33	-3,33	3,5	1
-3,91	-3,91	3,5	1	-3,33	-3,91	3,5	1
-3,91	-4,32	3,5	2	-3,33	-4,32	3,5	2
-3,91	-3,91	3,5	1	-3,91	-4,32	3,5	2
-3,91	-4,32	3,5	2	-3,33	-4,32	3,5	2
-3,33	-4,32	2,5	2	-3,91	-4,32	3,5	2
-4,32	-4,62	3,5	2	-3,33	-3,91	3,5	1
-3,33	-4,32	2,5	2	-2,33	-3,33	3,5	2
-3,33	-3,91	3,5	2	-2,33	-3,33	3,5	1
-3,91	-3,91	3,5	1	-3,33	-3,91	3,5	2
-3,33	-3,91	3,5	2	-4,32	-4,32	3,5	2
-3,33	-4,32	2,5	2	-3,91	-4,32	3,5	2
-3,91	-4,32	3,5	2	-4,32	-4,32	3,5	1
-3,91	-4,32	3,5	2	-4,32	-4,9	3,5	2
-3,91	-4,62	3,5	2	-3,33	-4,32	3,5	2
-3,33	-3,91	3,5	1	-2,33	-4,32	3,5	2
-3,33	-3,33	3,5	2	-3,33	-3,91	3,5	2
-3,33	-3,33	3,5	1	-3,91	-4,32	3,5	2
-3,33	-3,33	3,5	1	-3,91	-4,32	3,5	2
-3,91	-4,32	3,5	2	-3,33	-3,91	3,5	2
-3,33	-4,32	3,5	2	-3,91	-4,32	3,5	2
-3,33	-3,91	3,5	2	-3,33	-3,33	3,5	1

OVERVLAKTE

Clast size distribution

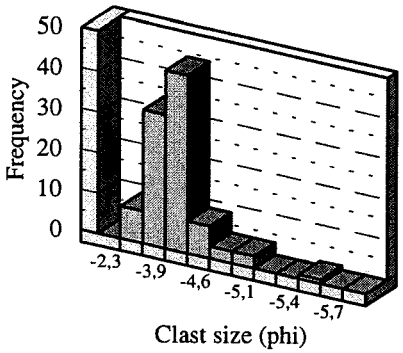

Clast roundness
(-3.91 phi)

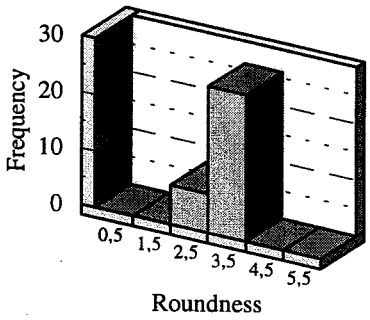

Clast roundness
(-3.33 phi)

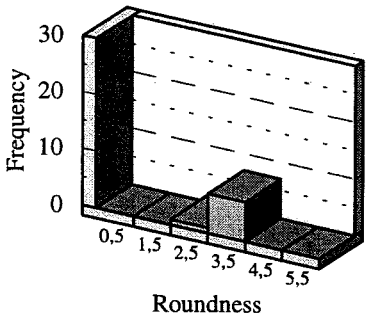

Clast Sphericity

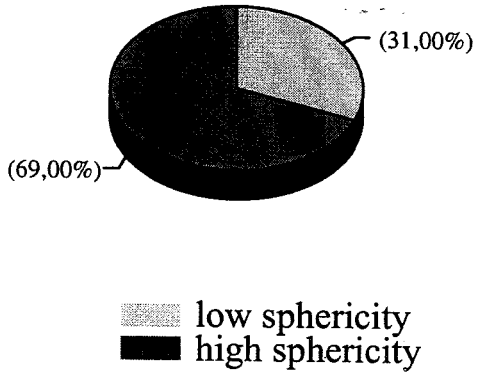

LITTLE BESS

C-axis	A-axis	Round.	Spher.	C-axis	A-axis	Round.	Spher.
-4.62	-5.48	2.5	1	-3.91	-4.32	2.5	1
-4.32	-5.48	3.5	2	-3.91	-4.32	2.5	1
-3.33	-5.31	2.5	2	-3.91	-4.32	3.5	2
-3.33	-5.12	3.5	1	-3.33	-4.32	2.5	2
-4.62	-5.12	2.5	1	-3.33	-3.91	3.5	1
-4.32	-4.9	3.5	2	-3.91	-3.91	3.5	2
-4.62	-4.9	2.5	1	-3.91	-3.91	3.5	1
-4.32	-4.9	3.5	2	-3.91	-3.91	3.5	2
-3.33	-4.9	2.5	2	-3.33	-3.91	3.5	2
-3.91	-4.9	3.5	2	-2.33	-3.91	3.5	1
-4.32	-4.9	3.5	2	-3.91	-3.91	3.5	2
-4.9	-4.9	4.5	2	-4.32	-3.91	3.5	1
-4.32	-4.62	3.5	2	-3.91	-3.91	3.5	2
-4.62	-4.62	3.5	2	-3.33	-3.91	3.5	1
-3.91	-4.62	3.5	2	-3.91	-3.91	3.5	1
-3.33	-4.62	3.5	2	-3.91	-3.91	2.5	1
-4.32	-4.62	2.5	1	-3.33	-3.91	3.5	2
-3.91	-4.62	2.5	2	-3.91	-3.91	2.5	1
-3.91	-4.62	2.5	1	-3.33	-3.91	2.5	1
-3.91	-4.62	3.5	2	-3.33	-3.91	2.5	2
-3.91	-4.62	3.5	1	-3.33	-3.91	2.5	1
-3.91	-4.62	3.5	2	-3.33	-3.91	3.5	1
-3.91	-4.62	3.5	2	-3.33	-3.91	3.5	1
-3.91	-4.62	2.5	1	-3.33	-3.91	3.5	1
-3.91	-4.62	3.5	1	-2.33	-3.91	3.5	1
-3.91	-4.32	3.5	1	-3.33	-3.91	3.5	1
-3.91	-4.32	3.5	2	-3.33	-3.91	3.5	2
-4.32	-4.32	2.5	2	-3.33	-3.91	2.5	2
-4.32	-4.32	2.5	2	-3.33	-3.91	2.5	2
-4.32	-4.32	3.5	2	-3.91	-3.91	3.5	2
-4.32	-4.32	2.5	2	-3.33	-3.91	3.5	2
-4.32	-4.32	3.5	1	-3.91	-3.91	3.5	2
-4.32	-4.32	2.5	2	-3.33	-3.91	3.5	2
-3.33	-4.32	3.5	2	-3.33	-3.91	3.5	2
-3.33	-4.32	2.5	2	-3.33	-3.91	3.5	2
-4.32	-4.32	2.5	2	-3.33	-3.91	3.5	2
-3.33	-4.32	3.5	2	-3.33	-3.33	3.5	2
-3.33	-4.32	2.5	2	-2.33	-3.33	3.5	2
-3.91	-4.32	3.5	2	-3.33	-3.33	2.5	2
-3.91	-4.32	2.5	1	-3.33	-3.33	2.5	2
-3.91	-4.32	3.5	2	-3.33	-3.33	2.5	1
-3.33	-4.32	3.5	2	-3.33	-3.33	2.5	1
-3.33	-4.32	2.5	2	-3.33	-3.33	3.5	1
-3.91	-4.32	3.5	1	-3.91	-3.33	3.5	1
-4.32	-4.32	3.5	2	-2.33	-3.33	3.5	2
-3.91	-4.32	3.5	1	-3.33	-3.33	3.5	1
-4.32	-4.32	3.5	1	-3.33	-3.33	3.5	1
-4.32	-4.32	3.5	2	-3.33	-3.33	3.5	2
-3.33	-4.32	3.5	1	-2.33	-2.33	4.5	1
-3.91	-4.32	3.5	1	-3.91	-2.33	3.5	1

LITTLE BESS

Clast size distribution

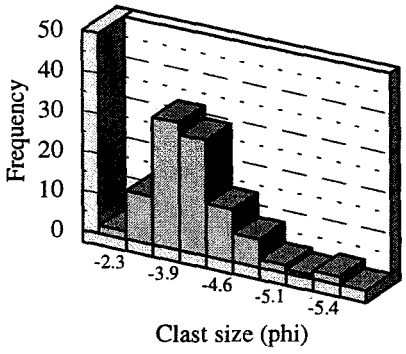

Clast roundness
(-3.91 phi)

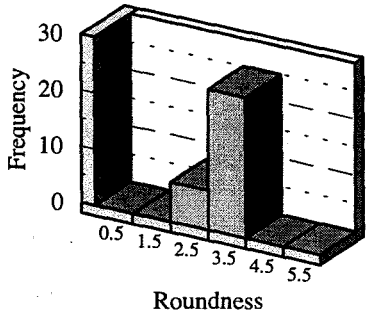

Clast roundness
(-3.33 phi)

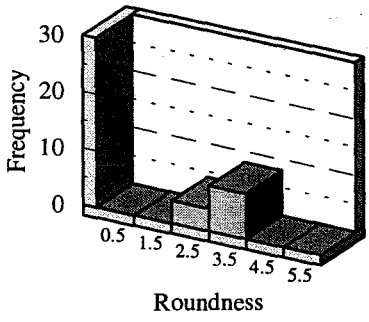

Clast Sphericity

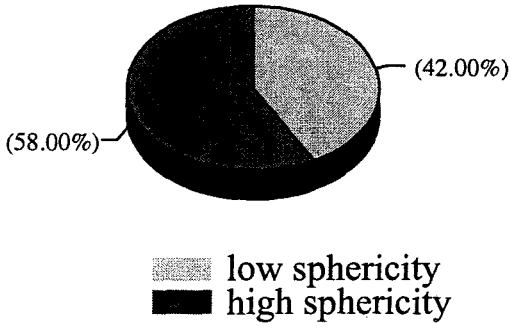

EENDVOGELPAN1	C-axis	A-axis	Roundness	Sphericity
Mean	-3,2519	-3,5869	3,59	1,43
Standard Error	0,06037	0,07385	0,02876	0,04975
Median	-3,33	-3,33	3,5	1
Mode	-3,33	-3,33	3,5	1
Standard Deviation	0,60375	0,73857	0,28762	0,49756
Variance	0,36452	0,54548	0,08272	0,24757
Kurtosis	-0,77766	-0,41883	6,59456	-1,9571
Skewness	0,36187	0,21402	2,90913	0,28710
Range	2,29	2,98	1	1
Count	100	100	100	100
Smallest(1)	-4,62	-5,31	4,5	1
Largest(1)	-2,33	-2,33	0,05637	2
Confidence Level(0.95)	0,118334	0,14475	0,05637	0,09752

EENDVOGELPAN2	C-axis	A-axis	Roundness	Sphericity
Mean	-3,4917	-4,1737	2,87	1,58
Standard Error	0,06669	0,06249	0,05972	0,04960
Median	-3,33	-4,32	2,5	2
Mode	-3,33	-4,32	2,5	2
Standard Deviation	0,66695	0,62498	0,59721	0,49604
Variance	0,44482	0,39060	0,35666	0,24606
Kurtosis	-0,4772	-0,27265	-0,65780	-1,93069
Skewness	0,32015	0,07973	-0,35127	-0,32913
Range	2,57	3,15	2	1
Count	100	100	100	100
Smallest(1)	-4,9	-5,48	1,5	1
Largest(1)	-2,33	-2,33	3,5	2
Confidence Level(0,95)	0,13072	0,12249	0,11705	0,09722

ONRUST	C-axis	A-axis	Roundness	Sphericity
Mean	-2,9632	-3,5651	2,37	1,42
Standard Error	0,05211	0,07245	0,08122	0,04960
Median	-3,33	-3,33	2,5	1
Mode	-3,33	-3,33	2,5	1
Standard Deviation	0,52118	0,72457	0,81221	0,49604
Variance	0,27163	0,52500	0,65969	0,24606
Kurtosis	-1,5635	5,57563	-0,6313	-1,9306
Skewness	0,26889	-0,92513	0,12870	0,32913
Range	1,58	4,89	4	1
Count	100	100	100	100
Smallest(1)	-3,91	-7,22	0,5	1
Largest(1)	-2,33	-2,33	4,5	2
Confidence Level(0,95)	0,10214	0,14201	0,15919	0,09722

BULTPAN	C-axis	A-axis	Roundness	Sphericity
Mean	-3,6403	-3,9619	3,06	1,35
Standard Error	0,05457	0,06548	0,04988	0,04793
Median	-3,91	-3,91	3,5	1
Mode	-3,91	-4,32	3,5	1
Standard Deviation	0,54577	0,65484	0,49888	0,47937
Variance	0,29786	0,42882	0,24888	0,22979
Kurtosis	0,61845	0,78682	-1,97976	-1,6251
Skewness	0,95987	0,79133	-0,24544	0,63858
Range	1,99	2,98	1	1
Count	100	100	100	100
Smallest(1)	-4,32	-5,31	2,5	1
Largest(1)	-2,33	-2,33	3,5	2
Confidence Level(0,95)	0,10696	0,12834	0,09778	0,09395

WELTEVREDEN1	C-axis	A-axis	Roundness	Sphericity
Mean	-3,245	-3,7069	3,49	1,52
Standard Error	0,05567	0,05025	0,11677	0,05021
Median	-3,33	-3,91	3,5	2
Mode	-3,33	-3,91	2,5	2
Standard Deviation	0,55675	0,50257	1,16770	0,50211
Variance	0,30997	0,25257	1,36353	0,25212
Kurtosis	-0,74598	0,93437	-0,84925	-2,03449
Skewness	0,61130	0,65409	0,29162	-0,08128
Range	1,58	2,29	4	1
Count	100	100	100	100
Smallest(1)	-3,91	-4,62	1,5	1
Largest(1)	-2,33	-2,33	5,5	2
Confidence Level(0,95)	0,10912	0,09850	0,22886	0,09841

WELTEVREDEN2	C-axis	A-axis	Roundness	Sphericity
Mean	-2,7464	-3,1882	2,11	1,46
Standard Error	0,05652	0,05999	0,09628	0,05009
Median	-2,33	-3,33	2,5	1
Mode	-2,33	-3,33	2,5	1
Standard Deviation	0,56525	0,59990	0,96289	0,50090
Variance	0,31951	0,35988	0,92717	0,25090
Kurtosis	-0,99865	-0,90657	-0,42258	-2,0141
Skewness	-0,78865	0,25591	0,09612	0,16296
Range	1,58	1,99	4	1
Count	100	100	100	100
Smallest(1)	-3,91	-4,32	0,5	1
Largest(1)	-2,33	-2,33	4,5	2
Confidence Level(0,95)	0,11078	0,11757	0,18872	0,09817

WELTEVREDEN3	C-axis	A-axis	Roundness	Sphericity
Mean	-3,3371	-3,9287	3,04	1,67
Standard Error	0,06606	0,05905	0,11583	0,04725
Median	-3,33	-3,91	2,5	2
Mode	-3,33	-3,91	2,5	2
Standard Deviation	0,66062	0,59056	1,15836	0,47258
Variance	0,43643	0,34876	1,34181	0,22333
Kurtosis	-0,47981	0,67926	-0,31249	-1,49128
Skewness	0,13314	0,38953	0,02024	-0,73413
Range	2,57	2,98	5	1
Count	100	100	100	100
Smallest(1)	-4,9	-5,31	0,5	1
Largest(1)	-2,33	-2,33	5,5	2
Confidence Level(0.95)	0,12948	0,11574	0,22703	0,09262

ROLY POLY1	C-axis	A-axis	Roundness	Sphericity
Mean	-2,9623	-3,5496	2,7	1,6
Standard Error	0,06646	0,08444	0,12870	0,04923
Median	-3,33	-3,33	2,5	2
Mode	-2,33	-3,33	2,5	2
Standard Deviation	0,66460	0,84446	1,28707	0,49236
Variance	0,44169	0,71312	1,65656	0,24242
Kurtosis	0,09680	3,36564	-0,63458	-1,86592
Skewness	-0,67517	-0,94720	-0,26684	-0,41449
Range	2,98	4,89	5	1
Count	100	100	100	100
Smallest(1)	-5,31	-7,22	0,5	1
Largest(1)	-2,33	-2,33	5,5	2
Confidence Level(0.95)	0,13026	0,16551	0,25226	0,09650

ROLY POLY2	C-axis	A-axis	Roundness	Sphericity
Mean	-3,5142	-3,984	3,25	1,55
Standard Error	0,07450	0,08814	0,11315	0,05
Median	-3,33	-3,91	3,5	2
Mode	-3,33	-3,91	3,5	2
Standard Deviation	0,74509	0,88143	1,13150	0,5
Variance	0,55515	0,77693	1,28030	0,25
Kurtosis	-0,68812	-0,24364	-0,22077	-1,99873
Skewness	0,18243	0,09417	0,04002	-0,2040
Range	2,79	3,57	5	1
Count	100	100	100	100
Smallest(1)	-5,12	-5,9	0,5	1
Largest(1)	-2,33	-2,33	5,5	2
Confidence Level(0,95)	0,14603	0,17275	0,22177	0,09799

DRIEPAN	C-axis	A-axis	Roundness	Sphericity
Mean	-2,9621	-3,3997	3,41	1,48
Standard Error	0,05814	0,06198	0,09	0,05021
Median	-3,33	-3,33	3,5	1
Mode	-3,33	-3,33	2,5	1
Standard Deviation	0,58147	0,61988	0,9	0,50211
Variance	0,33810	0,38425	0,81000	0,25212
Kurtosis	-1,36648	-0,58317	-0,74027	-2,03449
Skewness	-0,08648	0,48646	0,26473	0,08128
Range	1,99	1,99	4	1
Count	100	100	100	100
Smallest(1)	-4,32	-4,32	1,5	1
Largest(1)	-2,33	-2,33	5,5	2
Confidence Level(0.95)	0,11396	0,12149	0,17639	0,09841

AMMONDALE	C-axis	A-axis	Roundness	Sphericity
Mean	-3,2562	-3,566	2,74	1,39
Standard Error	0,06906	0,08288	0,07401	0,04902
Median	-3,33	-3,33	2,5	1
Mode	-3,33	-3,33	2,5	1
Standard Deviation	0,69069	0,82888	0,74018	0,49020
Variance	0,47706	0,68704	0,54787	0,24030
Kurtosis	-0,30392	-0,53093	-0,20776	-1,82723
Skewness	-0,17241	-0,05780	-0,41772	0,45794
Range	2,79	3,3	4	1
Count	100	100	100	100
Smallest(1)	-5,12	-5,63	0,5	1
Largest(1)	-2,33	-2,33	4,5	2
Confidence Level(0,95)	0,13537	0,16245	0,14507	0,09607

LAURISTON	C-axis	A-axis	Roundness	Sphericity
Mean	-3,0249	-3,381	2,06	1,35
Standard Error	0,06550	0,08191	0,07152	0,04793
Median	-3,33	-3,33	1,5	1
Mode	-3,33	-3,33	1,5	1
Standard Deviation	0,65507	0,81910	0,71520	0,47937
Variance	0,42912	0,67092	0,51151	0,22979
Kurtosis	-0,24553	-0,43578	-0,34705	-1,62511
Skewness	-0,49026	-0,30462	0,37649	0,63858
Range	2,57	3,3	3	1
Count	100	100	100	100
Smallest(1)	-4,9	-5,63	0,5	1
Largest(1)	-2,33	-2,33	3,5	2
Confidence Level(0,95)	0,12839	0,16054	0,14017	0,09395

ARCADIA	C-axis	A-axis	Roundness	Sphericity
Mean	-3,2352	-3,7812	3,4	1,66
Standard Error	0,04968	0,05507	0,05945	0,04760
Median	-3,33	-3,91	3,5	2
Mode	-3,33	-3,91	3,5	2
Standard Deviation	0,49680	0,55077	0,59458	0,47609
Variance	0,24681	0,30334	0,35353	0,22666
Kurtosis	0,11805	1,46199	1,48614	-1,56124
Skewness	0,62947	0,97058	-0,55897	-0,68585
Range	1,99	2,79	3	1
Count	100	100	100	100
Smallest(1)	-4,32	-5,12	1,5	1
Largest(1)	-2,33	-2,33	4,5	2
Confidence Level(0,95)	0,09737	0,10794	0,11653	0,09331

DONKIN	C-axis	A-axis	Roundness	Sphericity
Mean	-3,3203	-3,7291	3,25	1,44
Standard Error	0,06774	0,06452	0,05751	0,04988
Median	-3,33	-3,91	3,5	1
Mode	-3,33	-3,33	3,5	1
Standard Deviation	0,67742	0,64551	0,57515	0,49888
Variance	0,45890	0,41669	0,33080	0,24888
Kurtosis	-0,53521	-0,02396	4,89500	-1,97976
Skewness	0,00536	0,24938	-1,56421	0,24544
Range	2,57	2,79	4	1
Count	100	100	100	100
Smallest(1)	-4,9	-5,12	0,5	1
Largest(1)	-2,33	-2,33	4,5	2
Confidence Level(0,95)	0,13277	0,12651	0,11272	0,09778

GORING	C-axis	A-axis	Roundness	Sphericity
Mean	-3,1927	-3,7055	3,53	1,59
Standard Error	0,06869	0,07909	0,01714	0,04943
Median	-3,33	-3,91	3,5	2
Mode	-3,33	-3,33	3,5	2
Standard Deviation	0,68691	0,79090	0,17144	0,49431
Variance	0,47184	0,62552	0,02939	0,24434
Kurtosis	-1,34620	-0,57348	29,8977	-1,90035
Skewness	0,10241	0,18542	5,59464	-0,37157
Range	1,99	2,79	1	1
Count	100	100	100	100
Smallest(1)	-4,32	-5,12	3,5	1
Largest(1)	-2,33	-2,33	4,5	2
Confidence Level(0,95)	0,13463	0,15501	0,03360	0,09688

PATRICIA	C-axis	A-axis	Roundness	Sphericity
Mean	-3,3894	-3,8166	3,35	1,51
Standard Error	0,05673	0,05661	0,04113	0,05024
Median	-3,33	-3,91	3,5	2
Mode	-3,33	-3,91	3,5	2
Standard Deviation	0,56739	0,56614	0,41132	0,50241
Variance	0,32193	0,32052	0,16919	0,25242
Kurtosis	0,09668	0,73606	1,56072	-2,03955
Skewness	0,28962	0,84241	-1,05524	-0,04061
Range	2,29	2,57	2	1
Count	100	100	100	100
Smallest(1)	-4,62	-4,9	2,5	1
Largest(1)	-2,33	-2,33	4,5	2
Confidence Level(0.95)	0,11120	0,11096	0,08061	0,09847

DRUMSHEUGH	C-axis	A-axis	Roundness	Sphericity
Mean	-3,2785	-3,7781	3,46	1,58
Standard Error	0,06791	0,08928	0,03999	0,04960
Median	-3,33	-3,91	3,5	2
Mode	-3,33	-4,32	3,5	2
Standard Deviation	0,67913	0,89287	0,39999	0,49604
Variance	0,46122	0,79722	0,15999	0,24606
Kurtosis	-1,02287	-0,72076	3,41028	-1,93069
Skewness	0,17633	0,26508	-0,33704	-0,32913
Range	2,29	3,3	2	1
Count	100	100	100	100
Smallest(1)	-4,62	-5,63	2,5	1
Largest(1)	-2,33	-2,33	4,5	2
Confidence Level(0,95)	0,13310	0,17499	0,07839	0,09722

LIZZULEA1	C-axis	A-axis	Roundness	Sphericity
Mean	-3,4793	-4,0817	1,62	1,63
Standard Error	0,06578	0,07865	0,03561	0,04852
Median	-3,33	-3,91	1,5	2
Mode	-3,33	-3,33	1,5	2
Standard Deviation	0,65782	0,78657	0,35618	0,48523
Variance	0,43273	0,61870	0,12686	0,23545
Kurtosis	-0,2524	-0,08866	3,16618	-1,73619
Skewness	0,17135	0,01869	1,66633	-0,54675
Range	2,79	3,79	2	1
Count	100	100	100	100
Smallest(1)	-5,12	-6,12	0,5	1
Largest(1)	-2,33	-2,33	2,5	2
Confidence Level(0,95)	0,12893	0,15416	0,06981	0,09510

LIZZULEA2	C-axis	A-axis	Roundness	Sphericity
Mean	-3,23	-3,6501	3,52	1,53
Standard Error	0,07399	0,09194	0,02835	0,05016
Median	-3,33	-3,91	3,5	2
Mode	-2,33	-2,33	3,5	2
Standard Deviation	0,73995	0,91944	0,28355	0,50161
Variance	0,54753	0,84537	0,08040	0,25161
Kurtosis	-1,37741	-1,21099	9,95383	-2,02603
Skewness	0,02374	0,22612	0,68789	-0,12205
Range	2,29	2,98	2	1
Count	100	100	100	100
Smallest(1)	-4,62	-5,31	2,5	1
Largest(1)	-2,33	-2,33	4,5	2
Confidence Level(0.95)	0,14502	0,18020	0,05557	0,09831

LUNA	C-axis	A-axis	Roundness	Sphericity
Mean	-2,9321	-3,3099	3,44	1,43
Standard Error	0,06800	0,08609	0,02777	0,04975
Median	-2,33	-3,33	3,5	1
Mode	-2,33	-2,33	3,5	1
Standard Deviation	0,68008	0,86091	0,27779	0,49756
Variance	0,46251	0,74117	0,07717	0,24757
Kurtosis	-1,00887	-1,49710	9,03288	-1,95712
Skewness	-0,56777	-0,02710	-2,21315	0,28710
Range	2,29	2,79	2	1
Count	100	100	100	100
Smallest(1)	-4,62	-5,12	2,5	1
Largest(1)	-2,33	-2,33	4,5	2
Confidence Level(0,95)	0,13329	0,16873	0,05444	0,09752

SCHIETFONTEIN	C-axis	A-axis	Roundness	Sphericity
Mean	-3,1444	-3,5159	3,26	1,46
Standard Error	0,05650	0,06805	0,05526	0,05009
Median	-3,33	-3,33	3,5	1
Mode	-3,33	-3,33	3,5	1
Standard Deviation	0,56506	0,68057	0,55267	0,50090
Variance	0,31929	0,46318	0,30545	0,25090
Kurtosis	-1,09257	-0,54080	0,43201	-2,01413
Skewness	0,4140	0,45995	-0,41790	0,16296
Range	1,58	2,57	3	1
Count	100	100	100	100
Smallest(1)	-3,91	-4,9	1,5	1
Largest(1)	-2,33	-2,33	4,5	2
Confidence Level(0,95)	0,11075	0,13339	0,10832	0,09817

KILGOUR	C-axis	A-axis	Roundness	Sphericity
Mean	-3,4824	-4,0321	1,15	1,53
Standard Error	0,07653	0,08810	0,06871	0,05016
Median	-3,33	-3,91	1,5	2
Mode	-3,33	-4,32	1,5	2
Standard Deviation	0,76533	0,88108	0,68718	0,50161
Variance	0,58574	0,77631	0,47222	0,25161
Kurtosis	-0,63590	-0,23883	2,20399	-2,02603
Skewness	0,06097	0,24610	1,15537	-0,12205
Range	2,98	3,79	3	1
Count	100	100	100	100
Smallest(1)	-5,31	-6,12	0,5	1
Largest(1)	-2,33	-2,33	3,5	2
Confidence Level(0,95)	0,15000	0,17269	0,13468	0,09831

KONINGSMARK1	C-axis	A-axis	Roundness	Sphericity
Mean	-3,2759	-3,7461	3,5	1,49
Standard Error	0,06115	0,07379	0	0,05024
Median	-3,33	-3,91	3,5	1
Mode	-3,33	-3,91	3,5	1
Standard Deviation	0,61158	0,73792	0	0,50241
Variance	0,37403	0,54453	0	0,25242
Kurtosis	-0,71886	-0,21352	-	-2,03955
Skewness	0,33608	0,40453	-	0,04061
Range	2,29	2,98	0	1
Count	100	100	100	100
Smallest(1)	-4,62	-5,31	3,5	1
Largest(1)	-2,33	-2,33	0	2
Confidence Level(0.95)	0,11986	0,14463	0	0,09847

KONINGSMARK2	C-axis	A-axis	Roundness	Sphericity
Mean	-2,53408	-2,72795	2,96938	1,05102
Standard Error	0,04051	0,04919	0,05016	0,02211
Median	-2,33	-2,33	2,5	1
Mode	-2,33	-2,33	2,5	1
Standard Deviation	0,40510	0,49199	0,50162	0,22117
Variance	0,16410	0,24205	0,25163	0,04891
Kurtosis	0,22850	-1,85906	-2,0262	15,4936
Skewness	-1,49139	-0,42344	0,12459	4,14461
Range	1	1	1	1
Count	100	100	100	100
Smallest(1)	-3,33	-3,33	2,5	1
Largest(1)	-2,33	-2,33	3,5	2
Confidence Level(0,95)	0,08020	0,09740	0,09931	0,04378

BISMARCK	C-axis	A-axis	Roundness	Sphericity
Mean	-3,5441	-4,1067	2,836	1,61
Standard Error	0,06185	0,05524	0,10073	0,04902
Median	-3,33	-4,32	2,5	2
Mode	-3,33	-4,32	3,5	2
Standard Deviation	0,61852	0,55246	1,00739	0,49020
Variance	0,38256	0,30522	1,01485	0,24030
Kurtosis	-0,22076	0,95823	34,63890	-1,82723
Skewness	0,62775	0,58896	-4,67077	-0,45794
Range	2,29	3,15	9,4	1
Count	100	100	100	100
Smallest(1)	-4,62	-5,48	-4,9	1
Largest(1)	-2,33	-2,33	4,5	2
Confidence Level(0,95)	0,12122	0,10828	0,19744	0,09607

BERGEN OP ZOOM	C-axis	A-axis	Roundness	Sphericity
Mean	-3,5214	-4,0447	3,55	1,63
Standard Error	0,07833	0,09660	0,02611	0,04852
Median	-3,33	-4,32	3,5	2
Mode	-3,33	-3,91	3,5	2
Standard Deviation	0,78335	0,96602	0,26111	0,48523
Variance	0,61365	0,93320	0,06818	0,23545
Kurtosis	-0,89306	-0,70267	10,9966	-1,73619
Skewness	0,18808	0,48474	2,30129	-0,54675
Range	2,98	3,3	2	1
Count	100	100	100	100
Smallest(1)	-5,31	-5,63	2,5	1
Largest(1)	-2,33	-2,33	4,5	2
Confidence Level(0.95)	0,15353	0,18933	0,05117	0,09510

OVERVLAKTE	C-axis	A-axis	Roundness	Sphericity
Mean	-3,6501	-4,184	3,35	1,69
Standard Error	0,04733	0,04132	0,03588	0,04648
Median	-3,91	-4,32	3,5	2
Mode	-3,33	-4,32	3,5	2
Standard Deviation	0,47339	0,41321	0,35887	0,46482
Variance	0,22410	0,17074	0,12878	0,21606
Kurtosis	1,30087	1,40105	2,00121	-1,33114
Skewness	0,25412	-0,24790	-1,99037	-0,83419
Range	2,79	2,3	1	1
Count	100	100	100	100
Smallest(1)	-5,12	-5,63	2,5	1
Largest(1)	-2,33	-3,33	3,5	2
Confidence Level(0,95)	0,09278	0,08098	0,07033	0,09110

LITTLE BESS	C-axis	A-axis	Roundness	Sphericity
Mean	-3.707	-4.1589	3.2	1.58
Standard Error	0.05286	0.05590	0.05025	0.04966
Median	-3.91	-4.32	3.5	2
Mode	-3.33	-3.91	3.5	2
Standard Deviation	0.52868	0.55905	0.50251	0.49603
Variance	0.27950	0.31253	0.25252	0.24606
Kurtosis	0.48490	1.34973	-0.74870	-1.9306
Skewness	0.43692	0.43684	-0.38987	-0.3291
Range	2.57	3.15	2	1
Count	100	100	100	100
Smallest(1)	-4.9	-5.48	2.5	1
Largest(1)	-2.33	-2.33	4.5	2
Confidence Level(0.95)	0.10362	0.10957	0.098491	0.09722

APPENDIX 3

Borehole records

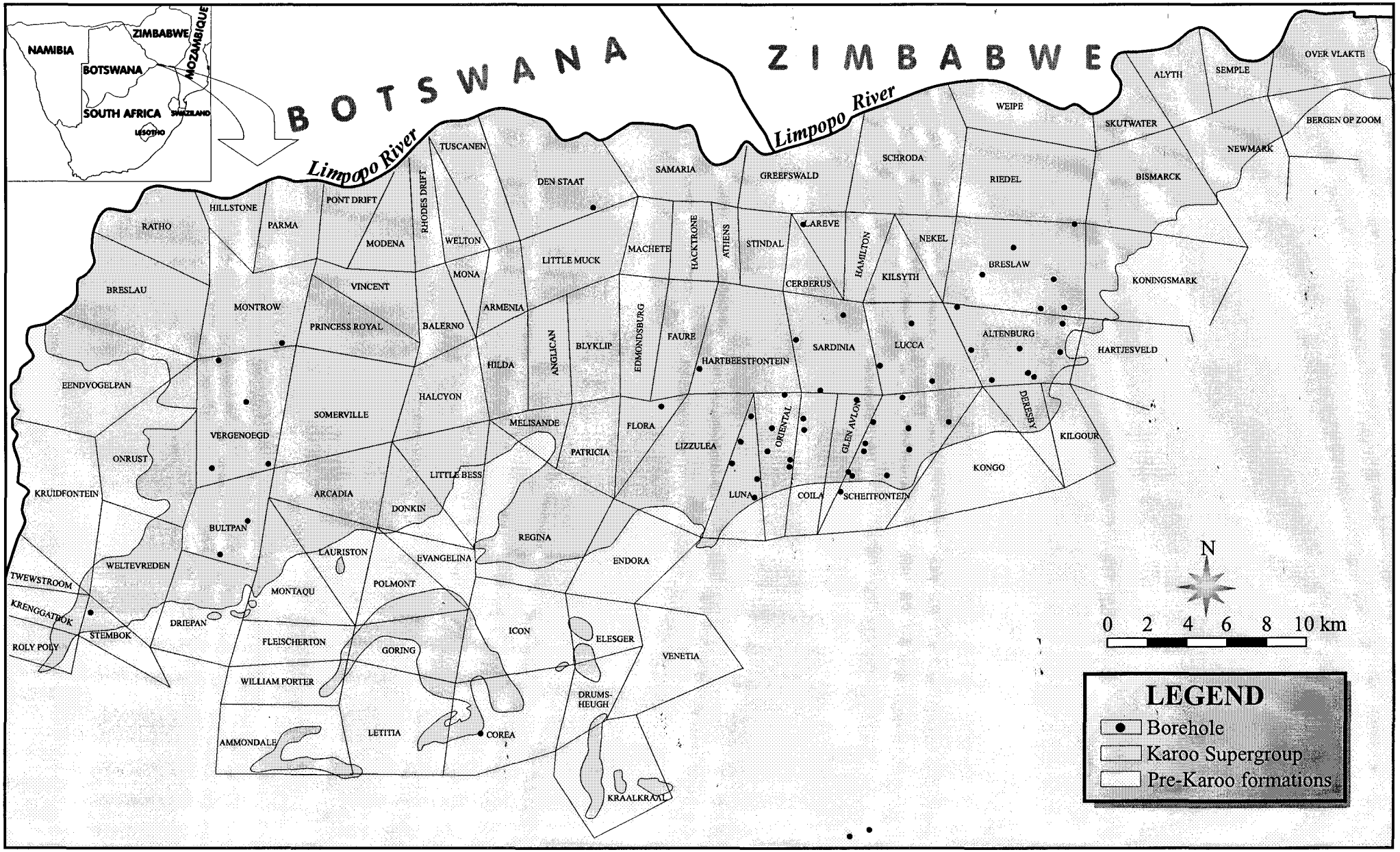

Fig. I. Map showing the position of the boreholes.

Bore-hole	Total thickness of Basal Unit	Thickness of the coarse unit	Thickness of the fine unit	Thickness of the coal zone	Thickness of the oxidative / reductive coarse units		Thickness of the oxidative / reductive fine units		Depositional environment
Har-1	68.37		49.69	18.68			1.00	48.69	Swamp & floodplain lake - distal
Lun-1	85.65	3.13	67.96	14.56		3.13	9.78	58.18	Swamp & floodplain lake - distal & proximal
Lun-2	66.15	3.10	50.74	12.31		3.10	10.54	40.20	Swamp & floodplain lake - distal & proximal
Lun-3	50.68		37.55	13.13			8.15	29.4	Swamp & floodplain lake - distal
Lun-4	79.98	15.93	51.25	12.80		15.93	45.14	6.11	Swamp & floodplain lake (distal & proximal)
Lun-6	53.25	1.22	40.27	11.76		1.22	4.96	35.31	Swamp & floodplain lake - distal & proximal
Coi-2	61.39	0.30	47.46	13.63		0.30	10.82	36.64	Swamp & floodplain lake - distal
Coi-3	46.36	11.68	24.32	10.36		11.68	7.13	17.19	Swamp & floodplain lake - distal & proximal
Gle-1	51.72		39.45	12.27			10.97	28.48	Swamp & floodplain lake - distal
Ori-1	57.96		41.65	16.31			8.62	33.03	Swamp & floodplain lake - distal
Ori-2	64.92		50.95	13.97			9.45	41.5	Swamp & floodplain lake - distal
Ori-3	61.90		48.06	13.84			12.21	35.85	Swamp & floodplain lake - distal
Ori-4	33.25	4.00	21.64	7.61		4.00	6.85	14.79	Swamp & floodplain lake - distal & proximal

Bore-hole	Total thickness of Basal Unit	Thickness of the coarse unit	Thickness of the fine unit	Thickness of the coal zone	Thickness of the oxidative / reductive coarse units		Thickness of the oxidative / reductive fine units		Depositional environment
Ori-5	39.02		29.70	9.32			5.22	24.48	Swamp & floodplain lake - distal
Bul-2	104.55	38.41	51.54	14.6		38.41		51.54	Channel, swamp & floodplain lake -proximal
Bul-3	56.08	13.19	29.05	13.84		13.19		29.05	Channel, swamp & floodplain lake - distal
Ver-1	27.01	7.83	11.17	8.01		7.83	0.38	10.79	Channel, swamp & floodplain lake - distal
Ver-2	77.72	7.00	62.12	8.60		7.00	6.21	55.91	Channel, swamp & floodplain lake-distal
Ver-3	68.58	18.04	38.37	12.17		18.64		38.37	Channel, swamp & floodplain lake - distal
Ver-4	21.03	8.53	11.00	1.50		8.53		11.00	Channel, swamp & floodplain lake -proximal
Den-1	100.40	27.35	60.43	12.62		27.35	5.16	55.27	Channel, swamp & floodplain lake - proximal & distal
Sch-1	58.52		49.83	8.69			9.78	40.05	Swamp & floodplain lake - distal
Sch-2	49.62	4.88	35.69	9.05		4.88	9.46	26.23	Swamp & floodplain lake - distal & proximal
Sch-3	55.81	3.62	40.00	12.19		3.62	4.82	35.18	Swamp & floodplain lake - distal & proximal
Sch-4	44.81	7.08	29.89	7.84		7.08	0.73	29.16	Swamp & floodplain lake - distal & proximal
Sch-5	45.05	5.62	30.19	9.24		5.62	5.63	24.56	Swamp & floodplain lake - distal & proximal

Bore-hole	Total thickness of Basal Unit	Thickness of the coarse unit	Thickness of the fine unit	Thickness of the coal zone	Thickness of the oxidative / reductive coarse units		Thickness of the oxidative / reductive fine units		Depositional environment
Sch-6	38.10		30.17	7.93			7.18	22.99	Swamp & floodplain lake - distal
Sch-7	76.02	9.51	53.83	12.68		9.51	7.25	46.58	Channel, swamp & floodplain lake - distal
Sch-8	42.98	3.42	29.53	10.03	0.34	3.08	10.00	19.53	Swamp & floodplain lake - distal & proximal
Sch-9	40.06		29.33	10.73			6.50	22.83	Swamp & floodplain lake - distal
Sch-10	46.91	4.45	33.98	8.48		4.45	4.41	29.57	Swamp & floodplain lake - distal & proximal
Sch-11	14.55	7.62	6.93			7.62	0.82	6.11	Swamp & floodplain lake - distal (with dropstone?)
Alt-1	34.53	3.11	22.46	8.96		3.11	0.46	22.00	Channel, swamp & floodplain lake - distal
Alt-2	55.50	1.52	43.83	10.15		1.52	7.25	36.58	Swamp & floodplain lake - distal & proximal
Alt-3	40.57	0.30	33.72	6.55		0.30	3.53	30.19	Swamp & floodplain lake - distal
Alt-4	36.46	9.97	19.15	7.34		9.97	7.40	11.75	Swamp & floodplain lake - distal (with dropstone?)
Alt-5	48.24	7.80	33.86	6.58		7.80	6.24	27.62	Swamp & floodplain lake - distal (with dropstone?)
Alt-6	38.61	6.33	28.17	4.11	0.60	5.73	0.45	27.72	Swamp & floodplain lake - distal & proximal
Alt-7	39.14		30.05	9.09			0.21	29.84	Swamp & floodplain lake - distal

Bore-hole	Total thickness of Basal Unit	Thickness of the coarse unit	Thickness of the fine unit	Thickness of the coal zone	Thickness of the oxidative / reductive coarse units		Thickness of the oxidative / reductive fine units		Depositional environment
Luc-1	42.06	9.88	24.35	7.83		9.88	3.03	21.32	Swamp & floodplain lake - distal (with dropstone?)
Luc-2	48.72	0.30	35.77	12.65		0.30	7.71	28.06	Swamp & floodplain lake - distal
Luc-3	82.17	7.25	64.98	9.94		7.25		64.98	Swamp & floodplain lake - distal & proximal
Sar-1	58.53	1.63	45.56	11.34		1.63	7.00	38.56	Swamp & floodplain lake - distal
Sar-2	47.85	4.66	34.75	8.44		4.66	2.35	32.40	Swamp & floodplain lake - distal (with dropstone?)
Sar-3	71.06	4.91	52.86	13.29		4.91	8.29	44.57	Channel, swamp & floodplain lake - distal
Rev-1	56.69	2.74	41.55	12.40		2.74	0.32	41.23	Channel, swamp & floodplain lake - distal
Bre-1	41.67		32.43	9.24			2.43	30.00	Swamp & floodplain lake - distal
Bre-2	47.88	7.22	33.99	6.67		7.22	0.54	33.45	Channel, swamp & floodplain lake - distal (with dropstone?)
Bre-3	33.01		27.92	5.09			0.45	27.47	Swamp & floodplain lake - distal
Bre-4	35.97		30.95	5.02			5.95	25.00	Swamp & floodplain lake - distal
Bre-5	51.00	22.00	24.50	4.50		22.00		24.50	Channel, swamp & floodplain lake - distal
Bre-6	45.00	6.00	19.00	20.00		6.00		19.00	Channel, swamp & floodplain lake - distal

Bore-hole	Total thickness of Basal Unit	Thickness of the coarse unit	Thickness of the fine unit	Thickness of the coal zone	Thickness of the oxidative / reductive coarse units		Thickness of the oxidative / reductive fine units		Depositional environment
Flo-1	41.00	14.00	18.00	10.00		14.00	3.5	14.50	Channel, swamp & floodplain lake - distal
Ste-1	54.00	25.00	25.00	4.00		25.00		25.00	Swamp & floodplain lake - proximal
Bro-1	111.00	48.00	44.00	19.00		48.00		44.00	Channel, swamp & floodplain lake - distal
Del-1	82.00	6.00	32.00	44.00		6.00		32.00	Channel, swamp & floodplain lake - distal
Mon-1	86.00	33.00	43.00	10.00		33.00		43.00	Channel, swamp & floodplain lake - proximal & distal
Cor-1	92.00	53.00	6.00	33.00		53.00		6.00	Channel, swamp & floodplain lake - distal
Alt-8	65.00	11.00	16.00	38.00		11.00	5.00	11.00	Channel, swamp & floodplain lake -proximal

Bore-hole	Total thickness of Middle Unit	Thickness of the coarse unit	Thickness of the fine unit	Thickness of the oxidative / reductive coarse units		Thickness of the oxidative / reductive fine units		Depositional environment
Har-1	16.95	4.45	12.50		4.45	0.50	12.00	Channel & overbank
Lun-1	18.71	6.15	12.56	6.00	0.15	2.79	9.77	Channel & overbank
Lun-2	6.09	3.96	2.13		3.96	2.13		Channel & overbank
Lun-3	4.67	4.67			4.67			Channel
Lun-4	13.11	5.58	7.53		5.58	0.75	6.78	Channel & overbank
Lun-6	6.49	3.46	3.03		3.46		3.03	Channel & overbank
Coi-2	7.19	5.06	2.13		5.06		2.13	Channel & overbank
Coi-3	13.38	0.40	12.98		0.40		12.98	Channel & overbank
Gle-1	25.09	6.80	18.29		6.80		18.29	Channel & overbank
Ori-1	35.61	19.58	16.03	9.75	9.83	4.65	11.38	Channel & overbank
Ori-2	23.78	6.70	17.08		6.70	3.68	13.40	Channel & overbank
Ori-3	31.37	4.85	26.52		4.85	7.40	19.12	Channel & overbank
Ori-4	12.47	5.46	7.01		5.46	0.70	6.31	Channel & overbank
Ori-5	12.98	3.90	9.08		3.90	0.90	8.18	Channel & overbank
Ver-1	8.84	5.31	3.53		5.31	3.53		Channel & overbank
Ver-2	46.22	34.64	11.58		34.64	10.00	1.58	Channel & overbank
Ver-3	8.23	8.23			8.23			Channel
Den-1	26.21	21.52	4.69		21.52	0.50	4.19	Channel & overbank
Sch-1	16.77	3.66	13.11		3.66		13.11	Channel & overbank
Sch-2	22.70	9.20	13.50	0.23	8.97	3.93	9.57	Channel & overbank

Bore-hole	Total thickness of Middle Unit	Thickness of the coarse unit	Thickness of the fine unit	Thickness of the oxidative / reductive coarse units		Thickness of the oxidative / reductive fine units		Depositional environment
Sch-3	5.76	2.22	3.54		2.22	0.35	3.19	Channel & overbank
Sch-4	5.79	3.11	2.68	0.31	2.80		2.68	Channel & overbank
Sch-5	33.87	6.34	27.53		6.34	7.16	20.37	Channel & overbank
Sch-7	14.81	10.24	4.57		10.24	0.45	4.12	Channel & overbank
Sch-8	6.40	3.96	2.44		3.96		2.44	Channel & overbank
Sch-9	2.01	2.01		2.01				Channel
Alt-1	6.31	6.31		6.31				Channel
Alt-2	6.98	6.98		0.40	6.58			Channel
Alt-3	12.16	4.24	7.92		4.24	4.66	3.26	Channel & overbank
Alt-6	37.37	15.75	21.62	2.40	13.35	12.03	9.59	Channel & overbank
Luc-1	18.72	6.71	12.01		6.71	0.15	11.86	Channel & overbank
Luc-2	11.98	5.88	6.10		5.88	0.60	5.50	Channel & overbank
Luc-3	13.22	4.08	9.14		4.08	8.22	0.92	Channel & overbank
Sar-1	40.20	7.28	32.92	2.68	4.60	13.83	19.09	Channel & overbank
Sar-2	6.80	3.75	3.05		3.75		3.05	Channel & overbank
Sar-3	7.10	6.27	0.83		6.27		0.83	Channel & overbank
Rev-1	37.19	19.60	17.59		19.60	8.10	9.49	Channel & overbank
Bre-1	17.28	7.53	9.75		7.53	1.00	8.75	Channel & overbank
Bre-2	29.54	8.41	21.13	0.30	8.11	8.13	13.00	Channel & overbank
Bre-3	7.71	6.00	1.71	0.30	5.70	0.71	1.00	Channel & overbank

Bore-hole	Total thickness of Middle Unit	Thickness of the coarse unit	Thickness of the fine unit	Thickness of the oxidative / reductive coarse units		Thickness of the oxidative / reductive fine units		Depositional environment
Bre-4	6.10	3.35	2.75		3.35	0.27	2.48	Channel & overbank
Bre-5	14.00	7.00	7.00		7.00		7.00	Channel & overbank
Bre-6	36.00	3.00	33.00		3.00		27.00	Channel & overbank
Flo-1	27.00	2.00	25.00		2.00	18.00	7.00	Channel & overbank
Del-1	10.00	10.00		10.00				Channel
Mon-1	26.00	14.00	12.00	10.00	4.00	12.00		Channel & overbank
Cor-1	15.00	4.50	10.50	3.50	1.00	6.50	4.00	Channel & overbank
Alt-8	30.00	11.00	19.00		11.00	11.00	8.00	Channel & overbank

Bore-hole	Total thick-ness of the Upper Unit	Num-ber of FUC	Thick-ness of FUC	Thick-ness of the coarse unit	Thick-ness of the fine unit	Thick-ness of the oxidative reductive coarse units		Thick-ness of the oxidative reductive fine units		Thickness of coarse units with carbonate glaebules	Thickness of fine units with carbonate glaebules	Thickness of conglomerate beds within the coarse unit	Depositional environment
Har-1	63.71			4.88	34.75	4.88		34.75		0	0		Overbank with sandbody
		1	?	24.08	?	12.04	12.04			0			Channel
Lun-1	69.69	2+ 0.5	?	6.10	?	6.10				0			Channel
			19.81	4.88	14.94	4.88		14.94		0	14.94		Channel
			26.52	10.67	15.85	10.67		15.85		0	0	0.6	Channel
					17.25			17.25			0		Overbank
Lun-2	113.38	3+ 0.5	?	24.57	?	24.57				0		0.91	Channel
			13.80	8.50	5.30	8.5		5.3		0	5.30		Channel
			20.42	9.24	11.19	9.24		11.19		0	11.19		Channel
			17.70	15.05	2.65	15.05		2.65		0	0	0.12	Channel
					36.88			24.58	12.30		0		Overbank
Lun-3	31.7			6.40	25.30	6.4		12.65	12.65	0	0		Overbank with sandbody
Lun-4	46.82				46.82			46.82			24.69		Overbank

Bore-hole	Total thick-ness of the Upper Unit	Num-ber of FUC	Thick-ness of FUC	Thick-ness of the coarse unit	Thick-ness of the fine unit	Thick-ness of the oxidative reductive coarse units	Thick-ness of the oxidative reductive fine units	Thickness of coarse units with carbonate glaebules	Thickness of fine units with carbonate glaebules	Thickness of conglomerate beds within the coarse unit	Depositional environment
Coi-2	110.58	1+0.5	?	20.72	?	20.72		0			Channel
			10.97	10.97	0	10.97		0			Channel
					14.81		14.81		0		Overbank
		3	17.18	14.02	3.16	14.02	3.16	0	0		Channel
			14.59	12.15	2.44	12.15	2.44	0	0		Channel
			19.20	19.20	0	19.20		0			Channel
					13.11		6.55 6.55		0		Overbank
Coi-3	71.93			4.45 7.93 7.31 8.53	43.71	28.22	43.71	0	0		Overbank with sandbody
Gle-1	110.95	1+0.5	?	20.30	?	20.3		0			Channel
			21.03	9.94	11.09	9.94	11.09	0	0	2.93	Channel
				5.82	30.57	5.82	30.57	0	0		Overbank with sandbody
		1	21.34	14.02	7.32	14.02	7.32	0	0		Channel
				2.7 2.13 0.6	3.23 1.4 1.83	5.43	6.46	0	0		Levee

Bore-hole	Total thick-ness of the Upper Unit	Num-ber of FUC	Thick-ness of FUC	Thick-ness of the coarse unit	Thick-ness of the fine unit	Thick-ness of the oxidative reductive coarse units	Thick-ness of the oxidative reductive fine units	Thickness of coarse units with carbonate glaebules	Thickness of fine units with carbonate glaebules	Thickness of conglomerate beds within the coarse unit	Depositional environment
Ori-1	81.08	0.5	?	20.42	?	20.42		0			Channel
					28.96		28.96		28.96		Overbank
		2	?	5.79	?	5.79		0			Channel
			25.91	14.02	11.89	14.02	11.89	0	11.89	0.15	Channel
Ori-2	83.5	1	19.81	13.22	6.58	13.22	6.58	0	0		Channel
					37.18		37.18		0		Overbank
		1	?	14.33	?	14.33		0			Channel
					12.19		12.19		0		Overbank
Ori-3	55.78	1	14.94	12.81	2.13	12.81	2.13	0	2.13	0.91	Channel
				2.72	5.18	5.86	6.73	0	5.18		Levee
				3.14	1.55						
					28.25		28.25		3.96		Overbank
Ori-4	37.8				37.8		37.8		0		Overbank
Ori-5	21.95				21.95		21.95		0		Overbank

Bore-hole	Total thick-ness of the Upper Unit	Num-ber of FUC	Thick-ness of FUC	Thick-ness of the coarse unit	Thick-ness of the fine unit	Thick-ness of the oxidative reductive coarse units		Thick-ness of the oxidative reductive fine units		Thickness of coarse units with carbonate glaebules	Thickness of fine units with carbonate glaebules	Thickness of conglomerate beds within the coarse unit	Depositional environment
Den-1	202.68	0.5	?	6.07	?	6.07				6.07			Channel
		9	11.31	11.31	0	11.31				6.49			Channel
			6.89	6.89	0	6.89				6.88			Channel
			7.13	7.13	0	7.13				0			Channel
			12.98	12.98	0	12.98				0			Channel
			29.08	29.08	0	20.85	8.23			0			Channel
			10.97	10.97	0	8.54	2.43			0			Channel
			25.60	25.60	0	25.6				0			Channel
			12.77	12.77	0	12.77				0			Channel
			14.66	14.66	0	14.66				0		0.88	Channel
					17.37			17.37			17.37		Overbank
		1	?	10.24	?	10.24				3.96			Channel
					37.61			35.61	2		1.53		Overbank
Sch-1	94.19	0.5	?	11.77	?	11.77				0			Channel
					48.28			48.28			0		Overbank
		1	22.56	18.6	3.96	12.8	5.8	3.96		0	0		Channel
					11.58			9.14	2.44		0		Overbank

Bore-hole	Total thick-ness of the Upper Unit	Num-ber of FUC	Thick-ness of FUC	Thick-ness of the coarse unit	Thick-ness of the fine unit	Thick-ness of the oxidative reductive coarse units		Thick-ness of the oxidative reductive fine units		Thickness of coarse units with carbonate glaebules	Thickness of fine units with carbonate glaebules	Thickness of conglomerate beds within the coarse unit	Depositional environment
Sch-2	56.29			9.76 3.64	42.89	13.4		42.89		0	15.54		Overbank with sandbody
Sch-3	26.81			4.87	21.94	4.87		21.94		0	0		Overbank with sandbody
Sch-4	25.77	0.5	?	10.66	?	6.7	3.96			0			Channel
					15.11			1	14.11		0		Overbank
Sch-5	24.4				24.4			24.4			0		Overbank
Sch-6	32.04	0.5	?	9.14	?	9.14				0			Channel
					22.9			11.45	11.45		0		Overbank
Alt-1	29.75	0.5	?	10.67	?	1.67	9			0			Channel
					19.08			17.08	2		0		Overbank
Alt-2	12.79			3.65	9.14	0.36	3.29	1	8.14	0	0		Overbank with sandbody
Luc-1	14.68			2.01	12.67		2.01		12.67	0	0		Overbank with sandbody
Luc-2	35.66	1+0.5	?	8.53	?	0.53	8			0			Channel
			8.93	6.31	2.62	6	0.31	2	0.62	0	2.62		Channel
					18.20			12.5	5.7		0		Overbank

Bore-hole	Total thick-ness of the Upper Unit	Num-ber of FUC	Thick-ness of FUC	Thick-ness of the coarse unit	Thick-ness of the fine unit	Thick-ness of the oxidative reductive coarse units		Thick-ness of the oxidative reductive fine units		Thickness of coarse units with carbonate glaebules	Thickness of fine units with carbonate glaebules	Thickness of conglomerate beds within the coarse unit	Depositional environment
Luc-3	89.19				25.30			25.30			25.30		Overbank
		1+0.5	?	6.40	?	3.1	3.3			0			Channel
			29.54	20.70	8.84	15	5.7	8.84		0	8.84		Channel
					27.95			7.18	20.77		0		Overbank
Sar-1	89.92			3.62	3.62	14.48		14.48		14.48	14.48		Levee
				3.62	3.62								
				3.62	3.62								
				3.62	3.62								
					60.96			60.96			0		Overbank
Sar-2	107.9	0.5	?	24.69	?	24.69				0			Channel
				3.23	55.29	3.23		55.29		0	36.88		Overbank with sandbody
		1	?	24.69	?	2.69	22			0			Channel
Sar-3	46.41			6.70	39.71	6.70		39.71		0	26		Overbank with sandbody
Rev-1	206.93	??	??	153.9	0	153.9				69.92			Channel
				4.93	48.1	4.93		48.1		4.93	48.1		Overbank with sandbody

Bore-hole	Total thick-ness of the Upper Unit	Num-ber of FUC	Thick-ness of FUC	Thick-ness of the coarse unit	Thick-ness of the fine unit	Thick-ness of the oxidative reductive coarse units		Thick-ness of the oxidative reductive fine units		Thickness of coarse units with carbonate glaebules	Thickness of fine units, with carbonate glaebules	Thickness of conglomerate beds within the coarse unit	Depositional environment
Bre-1	13.58	0.5	?	4.57	?	4.57				0			Channel
				2.83	6.18	0.3	2.53	6.18		0	0		Overbank with sandbody
Bre-2	18.58	0.5	?	2.74	?	2.74				0			Channel
					15.84			15.84			15.84		Overbank
Bre-5	18.00			4.00	14.00	4.00		14.00					Overbank with sandbody
Bre-6	27.00				27.00			19.00	8.00				Overbank
Flo-1	31.00				31.00			31.00					Overbank
Del-1	45.00				45.00			16.00	29.00				Overbank
Mon-1	40.00			6.00	14.00	6.00		14.00					Overbank with sandbody
				2.00	18.00	2.00		18.00					Overbank with sandbody
Cor-1	20.00				20.00			18.00	2.00				Overbank

APPENDIX 4

Thin section descriptions

I. Formation name & geographic location

Basal Unit - Karoo Supergroup; Altenburg Farm@old diamond digging place - ALT1

II. Texture

A. Grain size and sorting

- ➢*1-2 mm very coarse sand (80%) & 2-4 mm granules (20%)*
- ➢*well sorted*

B. Grain shape

- ➢*xenomorph*
- ➢*angular, subangular > subrounded*
- ➢*low (70%) & high (30%) sphericity grains*

C. Stage of textural maturity

- ➢*submature*

D. Fabric

- ➢*massive*
- ➢*matrix:grain 0:100 => grain supported*
- ➢*grains show point contacts*
- ➢*25% porosity (i.e. pore-filling cement plus present porosity)*

III. Mineral composition

Percentage of quartz: 100%

- ➢*80% monocrystalline & 20% polycrystalline*
- ➢*80% undulatory & 20% nonundulatory*
- ➢*polycrystalline grain size/ crystal size in the polycrystalline grains/ crystal number/ crystal shape & boundaries*
  1 mm (coarse sand) / 0.2 mm (fine sand) / plenty / elongated crystals with sutured contacts
  1 mm (coarse sand) / 0.2 mm (fine sand) / plenty / equal crystals with non-sutured contacts

IV. Diagenetic features

- ➢*sparite cement*
- ➢*Fe-oxides present as extremely rare blebs*

V. Classification

- ✧*sparite cemented quartz arenite*

I. Formation name & geographic location

Middle Unit (lower part) - Karoo Supergroup; Altenburg Farm - ALT2

II. Texture

A. Grain size and sorting

- ➢*0.125-0.25 mm fine sand (10%), 0.25-0.5 mm medium sand (50%), 0.5-1 mm coarse sand (25%) & 1-2 mm very coarse sand (15%)*
- ➢*the upward fining cycles are well sorted*

B. Grain shape

- ➢*xenomorph, but there are a few euhedral quartz grains with angular authigenic overgrowth rims*
- ➢*rounded >> subrounded*
- ➢*low (50%) & high (50%) sphericity grains*

C. Stage of textural maturity

- ➢*supermature*

D. Fabric

- ➢*slight lamination due to the upward fining cycles determined by*
- ➢*matrix:grain 0:100 => grain supported*
- ➢*grains closely packed: concavo-convex contacts due to the slight authigenic overgrowth of the quartz crystals*
- ➢*5% porosity (i.e. pore-filling cement plus present porosity)*

III. Mineral composition

Percentage of quartz: 100%

- ➢*98% monocrystalline & 2%. polycrystalline*
- ➢*60% undulatory & 40% nonundulatory*
- ➢*polycrystalline grain size/ crystal size in the polycrystalline grains/ crystal number/ crystal shape & boundaries 1 -2 mm (very coarse sand) / 0.2 mm (fine sand size) / plenty / irregular, subequal with sutured contacts*

IV. Diagenetic features

- ➢*authigenic overgrowth of the quartz crystals*
- ➢*goethite & quartz cement*
- ➢*Fe-oxides present as grain coatings (there are only a few grain contacts without limonite rim) & numerous crystals*

V. Classification

- ✧*quartz arenite*

I. Formation name & geographic location

Basal Unit - Karoo Supergroup; Ammondale Farm - AMM1

II. Texture

A. Grain size and sorting

➢*0.06-0.125 mm very fine sand (10%), 0.125-0.25 mm fine sand (10%), 0.5-1 mm very coarse sand (67%) & 2-4 mm granules (10%) & 4-8 mm small pebble (3%)*

➢*very poorly sorted*

B. Grain shape

➢*xenomorph*

➢*angular, subangular > subrounded*

➢*low (85%) & high (15%) sphericity*

C. Stage of textural maturity

➢*submature*

D. Fabric

➢*massive*

➢*matrix:grain 30:70 => matrix supported*

➢*0-5% porosity (i.e. pore-filling cement plus present porosity)*

III. Mineral composition

A. Grains:

1. Percentage of quartz: >95%

➢*90% monocrystalline & 10% polycrystalline*

➢*90% undulatory & 10% nonundulatory*

➢*polycrystalline grain size/ crystal size in the polycrystalline grains/ crystal number/ crystal shape & boundaries*
2.4-4 mm (granule) / 1 mm (coarse sand) / 3-8 / irregular, subequant with sutured contacts
1 mm (coarse sand) 1 mm (coarse sand) / 8 / elongated with sutured contacts

➢*grain size 0.06-0.125 mm very fine sand (10%), 0.125-0.25 mm fine sand (10%), 0.5-1 mm coarse sand (67%) & 2-4 mm granules (10%) & 4-8 mm small pebble (3%)*

2. Percentage of feldspar: 1%

➢*multiple (tartan) twins*

➢*advanced alteration (to mass of sericite and muscovite forming ghost crystals); many grains (~40%) show clouding of elongated, randomly oriented micas*

➢*grain size 0.5-1mm (coarse sand)*

3. Percentage of lithic fragments: 1-2%

➢*feldspar-quartz rich fragments of an unidentified metamorphic rock(s)*

➢*grain size 0.5-1 mm coarse sand (60%) & 2-4 mm granules (40%)*

4. Percentage of mica: 2%

➢*muscovite*

➢*grain size 0.125-0.25 mm fine sand (60%) & 0.5-1 mm coarse sand (40%)*

B. Matrix: 30%

➢*clay 40%*

➢*mica 40%*

➢*quartz & miscellaneous 20%*

IV. Diagenetic features

➢*limonite rich silica cement*

➢*Fe-oxides present as diffuse microcrystalline stain of the matrix & very rare blebs*

V. Classification

✧*quartzwacke*

I. Formation name & geographic location

Basal Unit - Karoo Supergroup; Ammondale Farm - AMM3

II. Texture

A. Grain size and sorting

- ➢*0.06-0.125 mm very fine sand (10%), 0.25-0.5 mm medium sand (37%), 0.5-1 mm coarse sand (40%), 1-1.2 mm very coarse sand (10%) & 4-8 mm small pebble (3%)*
- ➢*very poorly sorted*

B. Grain shape

- ➢*xenomorph*
- ➢*subangular-angular (the fine polycrystalline grains tend to be more rounded, while the feldspars are angular)*
- ➢*low (80%) & high (20%) sphericity grains*

C. Stage of textural maturity

- ➢*immature*

D. Fabric

- ➢*slight lamination determined by the blade or lath-shaped clay minerals of the matrix (diagenetic Fe-oxides along the bedding plane also indicate the lamination), other grains randomly orientated*
- ➢*matrix:grain 60:40 => matrix supported*
- ➢*0-5% porosity (i.e. pore-filling cement plus present porosity)*

III. Mineral composition

A. Grains:

1. Percentage of quartz: 87%
   - ➢*85% monocrystalline & 15% polycrystalline*
   - ➢*80% undulatory & 20% nonundulatory*
   - ➢*polycrystalline grain size/ crystal size in the polycrystalline grains/ crystal number/ crystal shape & boundaries 1-1.2 m (very coarse sand) / 0.4-1 mm (medium-coarse sand) / 3-8 / irregular, subequant and a few lenticular crystals with sutured contacts and only one grain: 1.2 mm (very coarse sand) / 0.1 mm (fine silt) / plenty / subequant, lenticular crystals with sutured contacts*
   - ➢*grain size 0.06-0.125 mm very fine sand (11%), 0.25-0.5 mm medium sand (36%), 0.5-1 mm coarse sand (40%), 1-1.2 mm very coarse sand (10%) & 4-8 mm small pebble (3%)*
2. Percentage of feldspar: 4%
   - ➢*90% multiple (tartan, albite) & 10% simple twins*
   - ➢*altered (broken down to micas and clay minerals)*
   - ➢*grain size 0.25-0.5 mm (medium sand)*
3. Percentage of lithic fragments: 1%
   - ➢*feldspar-quartz rich fragments of an unidentified metamorphic rock(s)*
   - ➢*all fragments are angular, subangular*
   - ➢*grain size ~0.5 mm (coarse sand)*
4. Percentage of micas: 8%
   - ➢*muscovite*
   - ➢*grain size 0.25-0.5 mm (medium sand)*
5. Percentage of other terrigenous minerals: <<0.01%
   - ➢*opaque minerals, zircon*
   - ➢*grain size 0.06-0.125 mm (very fine sand) + one zircon of 0.4 mm (medium sand)*

B. Matrix: 60%

- ➢*clay 70%*
- ➢*biotite 20%*
- ➢*quartz & miscellaneous 10%*

IV. Diagenetic features

- ➢*limonite rich silica cement*
- ➢*Fe-oxides present as diffuse microcrystalline stain of the matrix & very rare blebs*

V. Classification

- ✧*lithic greywacke*

I. Formation name & geographic location

Upper Unit - Karoo Supergroup; Balerno Farm - BAL1A

II. Texture

A. Grain size and sorting

➢*0.032-0.062 mm coarse silt (50%) & 0.062-0.125 mm very fine sand (50%)*

➢*moderately sorted*

B. Grain shape

➢*xenomorph*

➢*subrounded >> subangular, rounded*

➢*low (40%) & high (60%) sphericity*

C. Stage of textural maturity

➢*mature*

D. Fabric

➢*massive*

➢*matrix:grain 80:20 => matrix supported & abundant grain supported clusters (F- (floating) fabrics with GS- (grain supported) clusters)*

➢*quartz grains show strong embayment dissolution features*

➢*~20% porosity (i.e. pore-filling cement plus present porosity)*

III. Mineral composition

A. Grains:

1. Percentage of quartz: 99.9%

➢*100% monocrystalline & 0% polycrystalline*

➢*80% undulatory & 20% non-undulatory*

➢*grain size 0.032-0.062 mm coarse silt (50%) & 0.062-0.125 mm very fine sand (50%)*

2. Percentage of feldspar: <0.1% but more than BAL1B

➢*multiple (tartan, albite) twins*

➢*mostly slightly altered (cloudy, brownish in PPL), but there are some ghost grains too (only the nuclei is twinned feldspar, the rest of the grain is replaced by calcite)*

➢*grain size 0.062-0.125 mm (very fine sand)*

3. Percentage of other terrigenous minerals: <0.01%

➢*opaque minerals, zircon, tourmaline, green hornblende*

➢*grain size ~0.1 mm (very fine sand)*

B. Matrix: 80%

➢*cryptocrystalline silica << microquartz >75%*

➢*length-fast chalcedony 20%*

➢*traces of microsparite cement <5%*

IV. Other features

A. Voids *(diameter: 0.5-0.8 mm) filled by:*

➢*fibrous, radial, length-fast chalcedony => microquartz*

➢*Fe-oxide banded crytocrystalline silica => microquartz => equant megaquartz (in the void center)*

➢*fibrous, radial, multi-generation lutecite ("zebraic chalcedony") - in a few voids only*

➢*crystal/bundle size increases toward the center of the void*

B. Tubules *(width: ~0.2 mm; length: 1-2 mm) filled by:*

➢*double layer of 0.1 mm thick fibrous, radial, length-fast chalcedony*

C. Veins *(width: 1.2 mm) filled by:*

➢*Fe-oxide banded crytocrystalline silica (0.14 mm) => length-fast chalcedony(0.14 mm) => finely laminated, Fe-oxide banded crytocrystalline silica (0.14 mm) => equant megaquartz (in the vein center)(0.14 mm)*

➢*Fe-oxide banded crytocrystalline silica (0.04 mm) => fibrous, radial, length-fast chalcedony (0.15mm)*

D. Cavities *(diameter: 0.5-0.8 mm) enveloped by:*

➢*0.1 mm thick finely laminated, Fe-oxide banded crytocrystalline silica => 0.05 mm thick megaquartz wall*

V. Diagenetic features

➢*Fe-oxides present as rare grain coatings (there are some grain contacts without limonite rim) & very rare blebs.*

VI. Classification

✧*gradational silcrete (sample taken from the transition of the silcrete and calcrete)*

I. Formation name & geographic location

Upper Unit - Karoo Supergroup; Balerno Farm - BAL1B

II. Texture

A. Grain size and sorting

➢*0.032-0.062 mm coarse silt (50%) & 0.062-0.125 mm very fine sand (50%)*

➢*moderately sorted*

B. Grain shape

➢*xenomorph*

➢*subrounded >> subangular, rounded*

➢*low (40%) & high (60%) sphericity*

C. Stage of textural maturity

➢*mature*

D. Fabric

➢*massive*

➢*matrix:grain 70:30 => matrix supported*

➢*predominantly F- (floating) fabrics, but very few GS- (grain supported) clusters*

➢*quartz grains show strong embayment dissolution features*

➢*~45% porosity (i.e. cavernous rock)*

III. Mineral composition

A. Grains:

1. Percentage of quartz: 99%

➢*100% monocrystalline & 0% polycrystalline*

➢*80% undulatory & 20% non-undulatory*

➢*grain size 0.032-0.062 mm coarse silt (50%) & 0.062-0.125 mm very fine sand (50%)*

2. Percentage of feldspar: <0.1% but less than BAL1A

➢*multiple (tartan, albite) twins*

➢*slightly altered (cloudy, brownish in PPL)*

➢*grain size 0.062-0.125 mm (very fine sand)*

3. Percentage of other terrigenous minerals: <0.01%

➢*opaque minerals, zircon, tourmaline*

➢*grain size ~0.1 mm (very fine sand)*

B. Matrix: 70%

➢*cryptocrystalline silica >> microquartz 80%*

➢*length-fast chalcedony 20%*

IV. Other features

A. Spherical voids *(diameter: 0.5-0.8 mm) filled by:*

➢*fibrous, radial, multi-generation, length-fast chalcedony*

➢*fibrous, radial, length-fast chalcedony => equant megaquartz (in the void center)*

➢*Fe-oxide banded crytocrystalline silica => microquartz => length-fast chalcedony*

➢*fibrous, radial, multi-generation lutecite ("zebraic chalcedony") - in a few voids only*

➢*crystal/bundle size increases toward the center of the void*

B. Tubules *(width: 0.2 mm; length: 1-2 mm) filled by:*

➢*double layer of 0.1 mm thick fibrous, radial, length-fast chalcedony*

C. Veins *(width: 2 mm) filled by:*

➢*finely laminated, Fe-oxide banded crytocrystalline silica alternating with length-fast chalcedony (0.2 mm) => Fe-oxide laminae => length-fast chalcedony(0.2mm) => Fe-oxide laminae => Fe-oxide banded crytocrystalline silica alternating with length-fast chalcedony (0.2 mm) (in the vein center)*

➢*single layer of 0.04-0.2mm thick fibrous, radial, length-fast chalcedony*

V. Diagenetic features

➢*Fe-oxides present as rare grain coatings (there are some grain contacts without limonite rim) & very rare blebs*

VI. Classification

✧*gradational silcrete*

I. Formation name & geographic location

Upper Unit - Karoo Supergroup; Balerno Farm - BAL2

II. Texture

A. Gain size and sorting

- ➢*0.031-0.06 mm coarse silt (40%), 0.062-0.125 mm very fine sand (40%), 0.125-0.25 mm fine sand (15%) & 0.25-0.5 mm medium sand (5%)*
- ➢*poorly sorted*

B. Grain shape

- ➢*xenomorph*
- ➢*subrounded, subangular > rounded*
- ➢*low (35%) & high (65%) sphericity*

C. Stage of textural maturity

- ➢*mature*

D. Fabric

- ➢*massive*
- ➢*matrix:grain 80:20 => matrix supported*
- ➢*grains float in sparry calcite matrix, grain concentration decrease from inside (0%) toward the margin (20%)of the separia*
- ➢*quartz grains show strong embayment dissolution features*
- ➢*0-5% porosity (i.e. pore-filling cement plus present porosity)*

III. Mineral composition

A. Grains:

1. Percentage of quartz: 100%
   - ➢*100% monocrystalline & 0% polycrystalline*
   - ➢*60% undulatory & 40% nonundulatory*
   - ➢*grain size 0.062-0.125 mm very fine sand*
2. Percentage of other terrigenous minerals: <0.01%
   - ➢*opaque minerals, zircon*
   - ➢*grain size ~0.1 mm (very fine sand)*

B. Matrix: 80%

- ➢*sparry calcite: coarsely crystalline (0.25-1 mm), whereas the wedge-shaped cracks are filled by very coarsely crystalline (1-4 mm) calcite only*

IV. Classification

- ✧*septaria*

I. Formation name & geographic location

Upper Unit - Karoo Supergroup; Balerno Farm - BAL5

II. Texture

A. Grain size and sorting

➢*0.031-0.062 mm coarse silt (30%); 0.062-0.125 mm very fine sand (40%); 0.125-0.25 mm fine sand (15%) & 0.25-0.5 mm medium sand (15%)*

➢*poorly sorted*

B. Grain shape

➢*xenomorph*

➢*subrounded, rounded >> subangular (coarse sand grains well rounded or rounded)*

➢*low (35%) & high (65%) sphericity*

C. Stage of textural maturity

➢*mature*

D. Fabric

➢*massive*

➢*matrix:grain 20:80 => grain supported (host rock), microquartz cemented, poorly sorted quartzwacke. Adjacent to the bone fragment, this quartz arenite shows progressive grain displacement, therefore the fabric is matrix supported: the detrital quartz grains float in a hematite matrix. Further away from the bone fragment, the matrix supported fabric shows advanced grain displacement, the matrix is sparite.and/or cryptocrystalline silica/microquartz.*

➢*0-5% porosity (i.e. pore-filling cement plus present porosity)*

III. Mineral composition

A. Grains:

1. Percentage of quartz: 99%

➢*100% monocrystalline & 0% polycrystalline*

➢*60% undulatory & 40% nonundulatory*

➢*except for the original host rock, all grains show embayment dissolution features*

➢*grain size 0.062-0.125 mm (very fine sand)*

2. Percentage of feldspar: <1%

➢*multiple (tartan, albite) twins*

➢*slightly altered (sericitisation)*

➢*grain size 0.062-0.125 mm (very fine sand)*

3. Percentage of other terrigenous minerals: <0.01%

➢*opaque minerals, zircon*

➢*grain size 0.062-0.125 mm (very fine sand)*

B. Matrix: 20%

➢*microquartz, sparite, hematite, clay*

IV. Other features

Voids *(diameter: 0.5-1 mm) developed only in the parts with sparite/cryptocrystalline silica/microquartz matrix & filled by:*

➢*fibrous, radial, length-fast chalcedony*

➢*fibrous, radial, length-fast chalcedony => microquartz*

➢*fibrous, radial, length-fast chalcedony => equant megaquartz*

➢*fibrous, radial lutecite ("zebraic chalcedony")*

V. Diagenetic features

➢*Fe-oxides present as very rare blebs*

VI. Classification

✧*calcretized and silcretized quartzwacke and a bone fragment surrounded by a hematite corona*

I. Formation name & geographic location

Middle Unit (lower part) - Karoo Supergroup; Bismarck Farm - BIS1

II. Texture

A. Grain size and sorting

➢*0.25-0.5 mm medium sand (20%), 0.5-1 mm coarse sand (60%) & 1-2 mm very coarse sand (20%)*

➢*poorly sorted*

B. Grain shape

➢*xenomorph, but there are a few euhedral quartz grains with angular authigenic overgrowth rims*

➢*subrounded >> rounded*

➢*low (50%) & high (50%) sphericity grains*

C. Stage of textural maturity

➢*mature*

D. Fabric

➢*massive*

➢*matrix:grain 0:100 => grain supported*

➢*closely packed: concavo-convex contacts due to the slight authigenic overgrowth of the quartz crystals*

➢*10% porosity (i.e. pore-filling cement plus present porosity)*

III. Mineral composition

Percentage of quartz: 100%

➢*70% monocrystalline & 30% polycrystalline*

➢*70% undulatory & 30% nonundulatory*

➢*a few quartz grains have zircon and other needle-shaped microliths*

➢*polycrystalline grain size/ crystal size in the polycrystalline grains/ crystal number/ crystal shape & boundaries*

1 -2 mm (very coarse sand) / 0.2 mm or more (fine sand) / plenty / irregular, subequal crystals with sutured contacts

2 mm (very coarse sand) / 0.5-1 mm (coarse sand) / 4 / irregular, subequal crystals with sutured contacts

1 mm (coarse sand) / 0.2 mm or less (fine sand) / plenty / irregular, subequal crystals with sutured contacts

IV. Diagenetic features

➢*the authigenic overgrowth of the quartz grains pre-dates the limonite cementation and coating of the grains as most the overgrowths also have a thin rim of limonite*

➢*silica, limonite cement*

➢*Fe-oxides present as grain coatings (there are some grain contacts without limonite rim) & very rare blebs*

V. Classification

✧*quartz arenite*

I. Formation name & geographic location

Upper Unit - Karoo Supergroup; Blyklip Farm - BLY3

II. Texture

A. Grain size and sorting

- ➢*0.125-0.25 mm fine sand (10%); 0.5-1 mm coarse sand (70%); 1-2 mm very coarse sand (10%); 2-4 mm granule (5%) & 4-8 mm small pebble (5%)*
- ➢*moderately sorted*

B. Grain shape

- ➢*xenomorph*
- ➢*subrounded, rounded, well rounded quartz grains, rounded feldspar & well rounded calcrete glaebule particles*
- ➢*low (35%) & high (65%) sphericity*

C. Stage of textural maturity

- ➢*mature*

D. Fabric

- ➢*massive*
- ➢*matrix:grain 5:95 => grain supported*
- ➢*grains show point contacts*
- ➢*25% porosity (i.e. pore-filling cement plus present porosity)*

III. Mineral composition

A. Grains:

1. Percentage of quartz: 30%
   - ➢*75% monocrystalline & 25% polycrystalline*
   - ➢*80% undulatory & 20% nonundulatory*
   - ➢*polycrystalline grain size/ crystal size in the polycrystalline grains/ crystal number/ crystal shape & boundaries*
     0.5-1 mm (coarse sand) / ~0.25 mm (medium) / 3 / irregular with non-sutured contacts
     0.5-1 mm (coarse sand) / <0.1 mm (fine) / plenty / irregular with non-sutured contacts
   - ➢*grain size 0.25-0.5 mm medium sand (10%), 0.5-1 mm coarse sand (85%) & 1-2 mm very coarse sand (5%)*
2. Percentage of feldspar: 10%
   - ➢*multiple (albite, tartan) twins*
   - ➢*slightly altered (sericitisation; cloudy, brownish in PPL))*
   - ➢*grain size 0.25-0.5 mm medium sand (30%) & 0.5-1 mm coarse sand (70%)*
3. Percentage of lithic fragments: 60%
   - ➢*consisting of carbonate glaebules (99%) & bone fragments (<1%)*
   - ➢*carbonate glaebules consists of:*
     - ○*5% <u>septaria</u>: radial wedge-shaped cracks filled by sparite; <1% very fine silt size quartz grains floating in micrite matrix*
     - ○*95% <u>nodule</u>:*
       - ●*5%: elongated or spherical inhomogenities filled by microsparite or sparite; <1% very fine silt size quartz grains floating in otherwise micrite matrix.*
       - ●*75%: <10% very fine silt size quartz grains floating in otherwise micrite matrix*
       - ●*15%: >10% very fine silt size quartz grains floating in otherwise micrite matrix*
       - ●*5%: <10% very fine silt size quartz grains floating in microsparite matrix; one glaebule has a bone fragment nucleus*
   - ➢*grain size 1-2 mm very coarse sand (33%), 2-4 mm granule (33%) & 4-8 mm small pebble (33%)*
4. Percentage of other terrigenous minerals: <0.01%
   - ➢*opaque minerals, zircon*
   - ➢*grain size 0.062-0.125 mm (very fine sand)*

B. Matrix: 15%

- ➢*consists of subrounded-subangular quartz (99%) & feldspar(<1%) grains*
- ➢*mean grain size 0.062-0.125 mm very fine sand*

IV. Diagenetic features

- ➢*sparite, limonite cement*
- ➢*Fe-oxides present as grain coatings & very rare blebs*

V. Classification

- ✧*litharenite* (clast supported, pebbly-granular calcrete glaebular coarse sandstone)

I. Formation name & geographic location

Upper Unit - Karoo Supergroup; Breslau Farm - BRE1

II. Texture

A. Grain size and sorting

- ➢*0.062-0.125 mm very fine sand (90%) & 0.25-0.5 mm medium sand (10%)*
- ➢*moderately sorted*

B. Grain shape

- ➢*xenomorph*
- ➢*subrounded >> rounded > subangular*
- ➢*low (40%) & high (60%) sphericity*

C. Stage of textural maturity

- ➢*mature*

D. Fabric

- ➢*slight lamination determined by the blade or lath-shaped grains*
- ➢*matrix:grain 0:100 => grain supported*
- ➢*grains show point contacts*
- ➢*20% porosity (i.e. pore-filling cement plus present porosity)*

III. Mineral composition

Grains:

1. Percentage of quartz: ~94%
   - ➢*95% monocrystalline & 5% polycrystalline (90% of the large grains are polycrystalline)*
   - ➢*60% undulatory & 40% nonundulatory*
   - ➢*polycrystalline grain size/ crystal size in the polycrystalline grains/ crystal number/ crystal shape & boundaries*
     0.25-0.5 mm (medium sand) / 0.02 mm (medium silt) / plenty / elongated with non-sutured contacts
     0.25-0.5 mm (medium sand) / 0.02 mm (medium silt) / plenty / irregular, subequant with sutured contacts
   - ➢*grain size 0.062-0.125 mm very fine sand (90%) & 0.25-0.5 mm medium sand (10%)*
2. Percentage of feldspar: ~5%
   - ➢*multiple (tartan, albite) twins*
   - ➢*slightly altered (sericitisation)*
   - ➢*grain size 0.062-0.125 mm very fine sand (95%) & 0.25-0.5 mm medium sand (5%)*
3. Percentage of chert: <1%
   - ➢*grain size 0.25-0.5 mm (medium sand)*
4. Percentage of other terrigenous minerals: <0.01%
   - ➢*opaque minerals, zircon, tourmaline*
   - ➢*grain size ~0.1 mm (very fine sand)*

IV. Diagenetic features

- ➢*silica, limonite cement*
- ➢*Fe-oxides present as grain coatings (there are some grain contacts without limonite rim) & very rare blebs*

V. Classification

- ✧*quartz arenite - subarkose*

I. Formation name & geographic location

Upper Unit - Karoo Supergroup; Breslau Farm - BRE2

II. Texture

A. Grain size and sorting

- ➢*0.031-0.06 mm coarse silt (30%), 0.062-0.125 mm very fine sand (50%), 0.125-0.25 mm fine sand (15%) & 0.25-0.5 mm medium sand (5%)*
- ➢*poorly sorted*

B. Grain shape

- ➢*xenomorph*
- ➢*subrounded, subangular > rounded*
- ➢*low (35%) & high (65%) sphericity*

C. Stage of textural maturity

- ➢*mature*

D. Fabric

- ➢*massive*
- ➢*matrix:grain 70:30 => matrix supported*
- ➢*grains float in sparry calcite matrix*
- ➢*quartz grains show strong embayment dissolution features*
- ➢*0-5% porosity (i.e. pore-filling cement plus present porosity)*

III. Mineral composition

A. Grains:

1. Percentage of quartz: 100%
   - ➢*100% monocrystalline & 0% polycrystalline*
   - ➢*70% undulatory & 30% nonundulatory*
   - ➢*grain size 0.062-0.125 mm very fine sand*
2. Percentage of other terrigenous minerals: <0.01%
   - ➢*opaque minerals, zircon*
   - ➢*grain size ~0.1 mm (very fine sand)*

B. Matrix: 70%

- ➢*sparry calcite: very coarsely crystalline (1-4 mm)*

IV. Classification

- ✧*part of a giant concretion*

I. Formation name & geographic location

Basal Unit - Karoo Supergroup; Cirencester Farm - CIR1

II. Texture

A. Mean grain size and sorting

- ➢*0.06-0.125 mm very fine sand (10%), 0.25-0.5 mm medium sand (20%), 0.5-1 mm coarse sand (55%) & 1-1.2 mm very coarse sand (15%)*
- ➢*very poorly sorted*

B. Grain shape

- ➢*xenomorph*
- ➢*very angular > angular*
- ➢*low (80%) & high (20%) sphericity grains*

C. Stage of textural maturity

- ➢*immature*

D. Fabric

- ➢*slight lamination determined by the blade or lath-shaped mica minerals of the matrix. The laminated matrix wraps around the coarser detrital grains.*
- ➢*matrix:grain 50:50 => matrix supported*
- ➢*0-5% porosity (i.e. pore-filling cement plus present porosity)*

III. Mineral composition

A. Grains:

1. Percentage of quartz: 100%
   - ➢*monocrystalline 85% vs. polycrystalline 15%*
   - ➢*undulatory 90% vs. nonundulatory 10%*
   - ➢*polycrystalline grain size/ crystal size in the polycrystalline grains/ crystal number/ crystal shape & boundaries*
     1.4-2 mm(very coarse sand) / 0.2 and 1.2 mm (fine to very coarse sand) / 5 or less / irregular, subequant and a few elongated crystals with sutured contacts
     0.4-0.8 mm(coarse sand) / 0.2 mm or less (medium or finer sand) / 5 or more / irregular, subequant and a few elongated crystals with sutured contacts
   - ➢*grain size 0.06-0.125 mm very fine sand (10%), 0.25-0.5 mm medium sand (20%), 0.5-1 mm coarse sand (55%) & 1-1.2 mm very coarse sand (15%)*
2. Percentage of other terrigenous minerals (including mica): <<0.01%
   - ➢*opaque minerals, zircon, mica*
   - ➢*grain size 0.06-0.125 mm (very fine sand)*

B. Matrix: 50%

- ➢*clay 80%*
- ➢*mica 10%*
- ➢*quartz & miscellaneous 10%*

IV. Diagenetic features

- ➢*limonite rich silica cement*
- ➢*Fe-oxides present as diffuse microcrystalline stain in the matrix & very rare blebs*

V. Classification

- ✧*quartzwacke*

I. Formation name & geographic location

Basal Unit - Karoo Supergroup; Donkin Farm - DON1

II. Texture

A. Grain size and sorting

- ➢*0.125-0.25 mm fine sand (10%), 0.5-1 mm coarse sand (40%) & 1-2 mm very coarse sand (50%)*
- ➢*moderately sorted*

B. Grain shape

- ➢*xenomorph*
- ➢*subangular, angular >> subrounded*
- ➢*low (50%) & high (50%) sphericity grains*

C. Stage of textural maturity

- ➢*submature*

D. Fabric

- ➢*massive*
- ➢*matrix:grain 0:100 => grain supported*
- ➢*grains show point contacts*
- ➢*35% porosity (i.e. pore-filling cement plus present porosity)*

III. Mineral composition

Grains:

Percentage of quartz: 100%

- ➢*85% monocrystalline vs.15% polycrystalline*
- ➢*85% undulatory vs.15% nonundulatory*
- ➢*polycrystalline grain size/ crystal size in the polycrystalline grains/ crystal number/ crystal shape & boundaries*
  0.5-1 mm (coarse sand) / 0.25 mm (medium sand) / plenty / irregular, subequant crystals with sutured contacts

IV. Diagenetic features

- ➢*silica cement*
- ➢*Fe-oxides present as blebs & euhedral hematite crystals*

V. Classification

- ✧*quartz arenite*

I. Formation name & geographic location

Basal Unit - Karoo Supergroup; Donkin Farm - DON2A

II. Texture

A. Mean grain size and sorting

- ➢*0.25-0.5 mm medium sand (50%) & 1-2 mm very coarse (50%)*
- ➢*moderately sorted*

B. Grain shape

- ➢*xenomorph*
- ➢*subangular > subrounded*
- ➢*low (40%) & high (60%) sphericity grains*

C. Stage of textural maturity

- ➢*submature*

D. Fabric

- ➢*massive*
- ➢*matrix:grain 0:100 => grain supported*
- ➢*grains show point contacts*
- ➢*35% porosity (i.e. pore-filling cement plus present porosity)*

III. Mineral composition

Grains:

1. Percentage of quartz: 99%
   - ➢*85% monocrystalline & 15% polycrystalline*
   - ➢*60% undulatory & 40% nonundulatory*
   - ➢*polycrystalline grain size/crystal size in the polycrystalline grains/crystal number/crystal shape & boundaries*
     0.5-1 mm (coarse sand)/0.25 mm (medium sand)/plenty/irregular, subequant crystals with sutured contacts
     0.5-1 mm (coarse sand)/0.25 mm (medium sand)/plenty/elongated, subequant crystals - sutured contacts
   - ➢*grain size 0.25-0.5 mm medium sand (49%) & 1-2 mm very coarse (51%)*
2. Percentage of feldspar: <1%
   - ➢*multiple twins (albite)*
   - ➢*altered (sericitisation)*
   - ➢*grain size 0.25-0.5 mm (medium sand)*
3. Percentage of lithic fragments: <0.01%
   - ➢*quartz-muscovite rich metamorphic rock fragment*
   - ➢*grain size: undulatory quartz - ~1 mm (coarse sand); muscovite - 0.2 mm (fine sand)*
4. Percentage of micas: <0.01%
   - ➢*muscovite*
   - ➢*grain size 0.25 mm (fine medium sand)*

IV. Diagenetic features

- ➢*limonite & silica (chalcedony) cement*
- ➢*Fe-oxides present as blebs & euhedral hematite crystals*

V. Classification

- ✧*quartz arenite*

I. Formation name & geographic location

Middle Unit (lower part)- Karoo Supergroup; Donkin Farm - DON2B

II. Texture

A. Grain size and sorting

- ➢1-2 *mm very coarse sand (10%) & 0.5-1 mm coarse sand (90%)*
- ➢*moderately sorted*

B. Grain shape

- ➢*xenomorph*
- ➢*subrounded > rounded*
- ➢*low (50%) & high (50%) sphericity grains*

C. Stage of textural maturity

- ➢*supermature*

D. Fabric

- ➢*massive*
- ➢*matrix:grain 0:100 => grain supported*
- ➢*grains closely packed: point contacts*
- ➢*30% porosity (i.e. pore-filling cement plus present porosity)*

III. Mineral composition

Percentage of quartz: 100%

- ➢*90% monocrystalline & 10% polycrystalline*
- ➢*70% undulatory & 30% nonundulatory*
- ➢*50% of the monocrystalline grains contain subparallel lines of very small bubles/vacuoles. Usually these grains show intensive cracking and undulatory extinction.*
- ➢*some monocrystalline grains have lath shaped, 0.2 mm long mineral inclusions*
- ➢*polycrystalline grain size/ crystal size in the polycrystalline grains/ crystal number/ crystal shape & boundaries 1-2 m(very coarse sand) / 0.25 mm or more (medium or coarser sand) / plenty / irregular, subequant crystals with sutured contacts*

IV. Diagenetic features

- ➢*silica & limonite cement*
- ➢*Fe-oxides present as grain coatings & numerous blebs*

V. Classification

- ✧*(vein) quartz arenite*

I. Formation name & geographic location

Basal Unit - Karoo Supergroup; Drumsheugh Farm - DRU2

The slide consists of two different rock types:

A. II. Texture

A. Grain size and sorting

- ➢*0.25-0.5 mm medium (10%), 0.5-1 mm coarse sand (70%) & 1-2 mm very coarse sand (20%)*
- ➢*poorly sorted*

B. Grain shape

- ➢*xenomorph*
- ➢*subangular >> subrounded*
- ➢*low (50%) & high (50%) sphericity grains*

C. Stage of textural maturity

- ➢*immature*

D. Fabric

- ➢*massive*
- ➢*matrix:grain 5:95 => grain supported*
- ➢*grains show point (40%) & concavo-convex (60%) contacts*
- ➢*0-5% porosity (i.e. pore-filling cement plus present porosity)*

III. Mineral composition

A. Grains:

Percentage of quartz: ~100%

- ➢*98% monocrystalline & 2% polycrystalline*
- ➢*80% undulatory & 20% nonundulatory*
- ➢*polycrystalline grain size/ crystal size in the polycrystalline grains/ crystal number/ crystal shape & boundaries*
  1-2 mm (very coarse sand) / 0.5-1 mm (coarse sand) / 5 / irregular, subequant crystals with sutured contacts, and there is one
  4.5 mm (fine pebble)/ 2-4 mm (granules) / 3 / irregular, subequant crystals with non-sutured contacts.

B. Matrix: 5%

- ➢*clay 90%*
- ➢*quartz & miscellaneous 10%*

IV. Diagenetic features

- ➢*limonite rich silica cement*
- ➢*Fe-oxides present as diffuse microcrystalline stain of the matrix & very rare blebs*

V. Classification

- ✧*quartz arenite*

B. II. Texture

A. Grain size and sorting

➢*0.06-0.125 mm very fine sand (40%) & 0.25-0.5 mm medium (60%)*

➢*moderately sorted*

B. Grain shape

➢*xenomorph*

➢*subrounded (70%) & subangular (30%)*

➢*low (30%) & high (70%) sphericity grains*

C. Stage of textural maturity

➢*immature*

D. Fabric

➢*vague lamination due to the lath shaped minerals of the matrix*

➢*matrix:grain 75:25 => matrix supported*

➢*0% porosity (i.e. pore-filling cement plus present porosity)*

III. Mineral composition

A. Grains:

Percentage of quartz: 100%

➢*100% monocrystalline & 0% polycrystalline*

➢ *80% undulatory & 20% nonundulatory*

B. Matrix: 75%

➢*clay 80%*

➢*quartz & miscellaneous 20%*

IV. Diagenetic features

➢*limonite rich silica cement*

➢*Fe-oxides present as diffuse microcrystalline stain of the matrix & very rare blebs*

V. Classification

✧*quartz grain rich mudstone*

I. Formation name & geographic location

Middle Unit (lower part) - Karoo Supergroup; Eendvogelpan - EEN1

II. Texture

A. Grain size and sorting

➢*0.25-0.5 mm medium sand (20%), 0.5-1 mm coarse (60%), 2-4 mm granule (15%) & 4-8 mm small pebble (5%)*

➢*poorly sorted*

B. Grain shape

➢*xenomorph, but there are a very few euhedral quartz grains with angular, very thin authigenic overgrowth rims*

➢*subrounded >> subangular > rounded*

➢*low (40%) & high (60%) sphericity grains*

C. Stage of textural maturity

➢*submature*

D. Fabric

➢*massive*

➢*matrix:grain 0:100 => grain supported*

➢*grains show point contacts*

➢*40% porosity (i.e. pore-filling cement plus present porosity)*

III. Mineral composition

Grains:

1. Percentage of quartz: 99%

➢*70% monocrystalline & 30% polycrystalline*

➢*65% undulatory & 35% nonundulatory*

➢*about 5% of the quartz grains contain subparallel lines of very small bubles/vacuoles. Usually these grains show intensive cracking and undulatory extinction.*

➢*about 5% of the quartz grains have needle-shaped microliths*

➢*polycrystalline grain size/ crystal size in the polycrystalline grains/ crystal number/ crystal shape & boundaries*
2-4 mm (granules) / 0.5-1 mm (coarse sand) / plenty / irregular, subequant crystals with sutured contacts
2-4 mm (granules) / 0.5-1 mm (coarse sand) / plenty / irregular, elongated crystals with sutured contacts

➢*grain size 0.25-0.5 mm medium sand (20%), 0.5-1 mm coarse (60%) & 2-4 mm granule (& larger) (20%)*

2. Percentage of mica: <1 %

➢*muscovite*

➢*grain size 0.25-0.5 mm (medium sand)*

3. Percentage of other terrigenous minerals: <0.01%

➢*opaque minerals, zircon, tourmaline*

➢*grain size medium sand (medium sand)*

IV. Diagenetic features

➢*authigenic overgrowth of the quartz crystals*

➢*limonite & silica cement*

➢*Fe-oxides present as grain coatings & numerous blebs*

V. Classification

✧*pebbly quartz arenite*

I. Formation name & geographic location

Middle Unit (medial part) - Karoo Supergroup; Eendvogelpan Farm - EEN3

II. Texture

A. Grain size and sorting

- ➢*0.25-0.5 mm medium sand (10%), 0.5-1 mm coarse sand (80%) & 1-2 mm very coarse sand (10%)*
- ➢*moderately sorted*

B. Grain shape

- ➢*xenomorph, but there are a very few euhedral quartz grains with angular, very thin authigenic overgrowth rims*
- ➢*rounded > subrounded*
- ➢*low (60%) & high (40%) sphericity grains*

C. Stage of textural maturity

- ➢*supermature*

D. Fabric

- ➢*massive*
- ➢*matrix:grain 0:100 => grain supported*
- ➢*grains show point contacts*
- ➢*40% porosity (i.e. pore-filling cement plus present porosity)*

III. Mineral composition

Percentage of quartz: 100%

- ➢*90% monocrystalline & 10% polycrystalline*
- ➢*70% undulatory & 30% nonundulatory*
- ➢*about 5% of the quartz grains contain subparallel lines of very small bubles/vacuoles. Usually these grains show intensive cracking and undulatory extinction.*
- ➢*polycrystalline grain size/ crystal size in the polycrystalline grains/ crystal number/ crystal shape & boundaries*

  0.5-1 m (coarse sand) / 0.2 mm (fine sand) / plenty / irregular, subequant crystals with sutured contacts and a few grains with elongated crystals with sutured contacts

IV. Diagenetic features

- ➢*authigenic overgrowth of the quartz crystals*
- ➢*silica & limonite cement*
- ➢*Fe-oxides present as grain coatings & numerous blebs*

V. Classification

- ✧*quartz arenite*

I. Formation name & geographic location

Basal Unit - Karoo Supergroup; Eendvogelpan - EEN5A

II. Texture

A. Grain size and sorting

- ➢*0.125-0.25 mm fine sand (10%), 0.5-1 mm coarse (35%) & 1-2 mm very coarse (55%)*
- ➢*moderately sorted*

B. Grain shape

- ➢*xenomorph*
- ➢*subangular, angular > subrounded*
- ➢*low (70%) & high (30%) sphericity grains*

C. Stage of textural maturity

- ➢*submature*

D. Fabric

- ➢*massive*
- ➢*matrix:grain 10:90 => grain supported*
- ➢*grain show point contacts*
- ➢*35% porosity (i.e. pore-filling cement plus present porosity)*

III. Mineral composition

A. Grains:

1. Percentage of quartz: 100%
   - ➢*80% monocrystalline & 20% polycrystalline*
   - ➢*60% undulatory & 40% nonundulatory*
   - ➢*a few quartz grains have zircon and other needle-shaped microliths*
   - ➢*polycrystalline grain size/ crystal size in the polycrystalline grains/ crystal number/ crystal shape & boundaries*
     1-2 mm (very coarse sand) / 0.5 mm (coarse sand)/ plenty / irregular, subequant crystals with sutured contacts
2. Percentage of other terrigenous minerals: <<0.01%
   - ➢*opaque minerals, zircon, tourmaline*
   - ➢*grain size 0.125-0.25 mm (fine sand)*

B. Matrix: 10%

- ➢*clay 60%*
- ➢*quartz & miscellaneous 40%*

IV. Diagenetic features

- ➢*limonite rich silica cement*
- ➢*Fe-oxides present as diffuse microcrystalline stain of the matrix & blebs*

V. Classification

- ✧*quartz arenite*

I. Formation name & geographic location

Middle Unit (lower part) - Karoo Supergroup; Eendvogelpan - EEN8

II. Texture

A. Grain size and sorting

➢*0.25-0.5 mm medium sand (20%), 0.5-1 mm coarse sand (70%) & 1-2 mm very coarse sand (10%)*

➢*moderately sorted*

B. Grain shape

➢*xenomorph,*

➢*subrounded >> rounded*

➢*low (60%) & high (40%) sphericity grains*

C. Stage of textural maturity

➢*supermature*

D. Fabric

➢*massive*

➢*matrix:grain 0:100 => grain supported*

➢*grains show point contacts*

➢*35% porosity (i.e. pore-filling cement plus present porosity)*

III. Mineral composition

Grains:

1. Percentage of quartz: 100%

➢*95% monocrystalline & 5% polycrystalline*

➢*65% undulatory & 35% nonundulatory*

➢*a few quartz grains have zircon and other needle-shaped microliths*

➢*polycrystalline grain size/ crystal size in the polycrystalline grains/ crystal number/ crystal shape & boundaries*
0.5-1 m (coarse sand) / 0.2 mm (fine sand size) / plenty / irregular, subequant crystals with sutured contacts

2. Percentage of other terrigenous minerals: <<0.01%

➢*Fe-oxides, zircon, tourmaline*

➢*grain size medium sand (medium sand)*

IV. Diagenetic features

➢*limonite & silica cement*

➢*Fe-oxides present as grain coatings & numerous blebs*

V. Classification

✧*quartz arenite*

I. Formation name & geographic location

Upper Unit - Karoo Supergroup; Faure Farm - FAU1

II. Texture

A. Grain size and sorting

- ➢*0.062-0.125 mm very fine sand (90%) & 0.5-1 mm coarse sand (10%)*
- ➢*moderately sorted*

B. Grain shape

- ➢*xenomorph*
- ➢*subrounded >> rounded > subangular (coarse sand fraction predominantly rounded)*
- ➢*low (65%) & high (35%) sphericity (coarse sand fraction predominantly spheric)*

C. Stage of textural maturity

- ➢*mature*

D. Fabric

- ➢*slight lamination determined by the coarse sand grains*
- ➢*matrix:grain 0:100 => grain supported*
- ➢*grains show point contacts*
- ➢*15% porosity (i.e. pore-filling cement plus present porosity)*

III. Mineral composition

Grains:

1. Percentage of quartz: ~95%
   - ➢*95% monocrystalline & 5% polycrystalline*
   - ➢*80% undulatory & 20% non-undulatory*
   - ➢*polycrystalline grain size/ crystal size in the polycrystalline grains/ crystal number/ crystal shape & boundaries 0.5-1 mm (coarse sand) / 0.25 mm (medium sand) / 5-6 / irregular, subquant with non-sutured contacts*
   - ➢*grain size 0.062-0.125 mm very fine sand (90%) & 0.5-1 mm coarse sand (10%)*
2. Percentage of feldspar: ~5%
   - ➢*multiple (tartan, albite) twins*
   - ➢*slightly altered (sericitisation)*
   - ➢*grain size 0.062-0.125 mm very fine sand (90%) & 0.5-1 mm coarse sand (10%)*
3. Percentage of other terrigenous minerals: <0.01%
   - ➢*opaque minerals, zircon (well rounded), green hornblende*
   - ➢*grain size ~0.1 mm (very fine sand)*

IV. Diagenetic features

- ➢*silica, limonite cement*
- ➢*Fe-oxides present as rare grain coatings (there are some grain contacts without limonite rim) & very rare blebs*

V. Classification

- ✧*quartz arenite - subarkose*

I. Formation name & geographic location

Clarens Formation - Karoo Supergroup; Greefswald Farm - GRE1

This sample was taken from the columnar sandstone pillars identified as fossil termite nests.

II. Texture

A. Grain size and sorting

➢*0.125-0.25 mm fine sand (20%) & 0.25-0.5 mm medium sand (80%)*

➢*moderately sorted*

B. Grain shape -

➢*xenomorph, but there are a few euhedral quartz grains with angular authigenic overgrowth rims*

➢*subrounded - rounded (coarser sand fraction predominantly rounded)*

➢*low (45%) & high (55%) sphericity (coarser sand fraction predominantly spheric)*

C. Stage of textural maturity

➢*mature*

D. Fabric

➢*massive*

➢*matrix:grain 0:100 => grain supported*

➢*point contacts*

➢*20% porosity (i.e. pore-filling cement plus present porosity)*

III. Mineral composition

Grains:

A. Percentage of quartz: ~99%

➢*100% monocrystalline & 0% polycrystalline*

➢*60% undulatory & 40% non-undulatory*

➢*grain size 0.125-0.25 mm fine sand (20%) & 0.25-0.5 mm medium sand (80%)*

B. Percentage of chert: <1%

➢*grain size 0.125-0.25 mm (fine sand)*

C. Percentage of other terrigenous minerals: <<0.01%

➢*opaque minerals, zircon*

➢*grain size ~0.1 mm (very fine sand)*

IV. Diagenetic features

➢*silica cement*

➢*Fe-oxides are sporadic, only present as very rare blebs*

V. Classification

✧*quartz arenite*

I. Formation name & geographic location

Clarens Formation - Karoo Supergroup; Greefswald Farm - GRE2

II. Texture

A. Grain size and sorting

- ➢*0.062-0.125 mm very fine sand (97%) & 0.5-1 mm coarse sand (3%)*
- ➢*the modal sizes well sorted, the overall sorting is moderate*

B. Grain shape

- ➢*xenomorph*
- ➢*subrounded >> rounded > subangular (coarse sand fraction predominantly very well rounded)*
- ➢*low (45%) & high (55%) sphericity (coarse sand fraction predominantly spheric)*

C. Stage of textural maturity

- ➢*mature*

D. Fabric

- ➢*massive*
- ➢*perhaps bioturbated - there are two 3 mm long, 2 mm wide elongated voids. One void is filled by 0.03-0.06 mm (coarse silt) grains floating in limonite cement, the other one is empty, but wrapped by a 0.5 mm thick layer of coarse silt floating in limonite cement.*
- ➢*matrix:grain 0:100 => grain supported*
- ➢*point contacts*
- ➢*20% porosity (i.e. pore-filling cement plus present porosity)*

III. Mineral composition

Grains:

A. Percentage of quartz: ~98%

- ➢*100% monocrystalline & 0% polycrystalline*
- ➢*60% undulatory & 40% non-undulatory*
- ➢*grain size 0.062-0.125 mm very fine sand (97%) & 0.5-1 mm coarse sand (3%)*

B. Percentage of feldspar: ~1%

- ➢*multiple (tartan, albite) twins*
- ➢*slightly altered (cloudy, brownish in PPL)*
- ➢*grain size 0.062-0.125 mm (very fine sand)*

C. Percentage of chert: ~1%

- ➢*grain size 0.062-0.125 mm (very fine sand)*

D. Percentage of other terrigenous minerals: <0.01%

- ➢*opaque minerals, zircon, green hornblende*
- ➢*grain size ~0.1 mm (very fine sand)*

IV. Diagenetic features

- ➢*silica cement*
- ➢*except for the bioturbated zones, the Fe-oxides are sporadic, only present as rare grain coatings (there are some grain contacts without limonite rim) & blebs*

V. Classification

- ✧*quartz arenite*

I. Formation name & geographic location

Middle Unit (medial part) - Karoo Supergroup; Halcyon Farm - HAL1

II. Texture

A. Grain size and sorting

➢*0.03-0.06 mm coarse silt (84%), 1-2 mm very coarse sand (15%) & 2-4 mm granules (1%)*

➢*overall sample moderately sorted, very coarse sand well sorted*

B. Grain shape

➢*xenomorph*

➢*subrounded, rounded >> subangular (very coarse sand grains well rounded or rounded)*

➢*low (35%) & high (65%) sphericity*

C. Stage of textural maturity

➢*submature*

D. Fabric

➢*cross-lamination determined by the blade or lath-shaped silt grains and grain size changes. Coarser grains lined up at the bottom of the cosets.*

➢*matrix:grain 15:85 => grain supported*

➢*grains show point contacts*

➢*0-5% porosity (i.e. pore-filling cement plus present porosity)*

III. Mineral composition

A. Grains (only >silt size):

1. Percentage of quartz: 98%

➢*85% monocrystalline & 15% polycrystalline*

➢*80% undulatory & 20% nonundulatory*

➢*polycrystalline grain size/crystal size in the polycrystalline grains/crystal number/crystal shape & boundaries 1-2 mm (very coarse sand) / 0.25-0.5 mm (medium silt) / plenty / irregular with non-sutured contacts*

➢*grain size 1-2 mm (very coarse sand)*

2. Percentage of feldspar: <1%

➢*multiple (albite) twins*

➢*slightly altered (sericitisation)*

➢*grain size 0.062-0.125 mm (very fine sand)*

3. Percentage of lithic fragments: <1%

➢*subrounded red mudstone*, metamorphic rock fragment (feldspar & polycrystalline quartz)

➢*grain size 2-4 mm (very fine sand)*

4. Percentage of other terrigenous minerals: <0.01%

➢*opaque minerals, zircon, green hornblende*

➢*grain size 0.062-0.125 mm (very fine sand)*

B. Matrix (whole rock): 15%

➢*limonite-rich clay 60%*

➢*quartz & miscellaneous 40%*

IV. Diagenetic features

➢*silica cement*

➢*Fe-oxides present as grain coatings around the very coarse sand grains only (most of the grain contacts are separated by thin limonite rims) & very rare blebs*

V. Classification

✧*quartz arenite (cross-laminated, muddy coarse siltstone with some cosets containing well rounded, 1-4 mm quartz grains at their base.)*

I. Formation name & geographic location

Middle Unit (medial part) - Karoo Supergroup; Halcyon Farm - HAL2

II. Texture

This sample consists of two rock types: red, fine (0.008-0.015 mm) silty mudstone (20%) & green, muddy coarse (0.031-0.06 mm) siltstone (80%). These two rock types form micro-scale flaser bedding.

A. Grain size and sorting

- ➢*mud (15%); 0.008-0.015 mm fine silt (15%); 0.031-0.06 mm coarse silt (69%) & 0.25-0.5 mm medium sand (<1%)(scattered through)*
- ➢*moderately sorted*

B. Grain shape

- ➢*xenomorph*
- ➢*subangular, subrounded (medium sand grains rounded or subrounded)*
- ➢*low (65%) & high (35%) sphericity*

C. Stage of textural maturity

- ➢*immature silty mudstone & mature muddy siltstone*

D. Fabric

- ➢*micro-scale flaser bedding with cross-lamination in the muddy siltstone*
- ➢*matrix:grain 90:10 => matrix supported silty mudstone & matrix:grain 10:90 => grain supported muddy siltstone*
- ➢*grains show point contacts in the muddy siltstone*
- ➢*0-5% porosity (i.e. pore-filling cement plus present porosity)*

III. Mineral composition

A. Grains:

1. Percentage of quartz: 99%
   - ➢*99% monocrystalline & 1% polycrystalline*
   - ➢*80% undulatory & 20% nonundulatory*
   - ➢*polycrystalline grain size/ crystal size in the polycrystalline grains/ crystal number/ crystal shape & boundaries 0.25-0.5 mm (medium sand) / 0.1 mm (very fine sand) / < 5 / irregular with non-sutured contacts*
   - ➢*grain size 0.031-0.06 mm (coarse silt)*
2. Percentage of feldspar: 1%
   - ➢*multiple (albite) twins*
   - ➢*slightly altered (sericitisation)*
   - ➢*grain size 0.031-0.06 mm (coarse silt)*
3. Percentage of other terrigenous minerals: <0.01%
   - ➢*opaque minerals, zircon, green hornblende*
   - ➢*grain size 0.031-0.06 mm (coarse silt)*

B. Matrix: 10-90%

- ➢*clay 60%*
- ➢*quartz & miscellaneous 40%*

IV. Diagenetic features

- ➢*silica cement*
- ➢*Fe-oxides present as blebs & diffuse stain in the interstitial material*

V. Classification

- ✧*flaser bedded quartz arenite (muddy siltstone) & silty mudstone*

I. Formation name & geographic location

Middle Unit (medial part) - Karoo Supergroup; Halcyon Farm - HAL3

II. Texture

A. Grain size and sorting

- ➢*0.015-0.031 mm medium silt (70%) & 0.031-0.06 mm coarse silt (30%)*
- ➢*moderately sorted*

B. Grain shape

- ➢*xenomorph*
- ➢*subangular, subrounded*
- ➢*low (65%) & high (35%) sphericity*

C. Stage of textural maturity

- ➢*submature*

D. Fabric

- ➢*cross-lamination determined by lineation of the blade or lath-shaped silt grains; mineralogical and grain size changes*
- ➢*matrix:grain 20:80 => grain supported*
- ➢*grains show point contacts*
- ➢*0-5% porosity (i.e. pore-filling cement plus present porosity)*

III. Mineral composition

A. Grains:

1. Percentage of quartz: 99%
   - ➢*100% monocrystalline & 0% polycrystalline*
   - ➢60% *undulatory & 40% nonundulatory*
   - ➢*grain size 0.015-0.031 mm medium silt (70%) & 0.031-0.06 mm coarse silt (30%)*
2. Percentage of feldspar: 1%
   - ➢*multiple (albite) twins*
   - ➢*slightly altered (sericitisation)*
   - ➢*grain size 0.031-0.06 mm (coarse silt)*
3. Percentage of other terrigenous minerals: <1%
   - ➢*opaque minerals, zircon, tourmaline, green hornblende*
   - ➢*80% of the grains are found in just two cross-laminae*
   - ➢*grain size 0.015-0.031 mm (medium silt)*

B. Matrix: 20%

- ➢*clay 60%*
- ➢*quartz 40%*

IV. Diagenetic features

- ➢*silica cement*
- ➢*Fe-oxides present as very rare blebs*

V. Classification

- ✧*quartz arenite (cross-laminated muddy siltstone)*

I. Formation name & geographic location

transition between the lower and medial parts of the Middle Unit - Karoo Supergroup; Halcyon Farm - HAL6

II. Texture

A. Grain size and sorting

- ➢*0.5-1 mm coarse sand (88%), 1-2 mm very coarse (10%) & 2-4 mm granule sized muddy coarse (0.031-0.06 mm) siltstone clasts (2%)*
- ➢*moderately*

B. Grain shape

- ➢*xenomorph*
- ➢*rounded, subrounded >> subangular (the silt grains in the siltstone clasts are subangular)*
- ➢*low (15%) & high (85%) sphericity (the silt grains in the siltstone clasts low (65%) & high (35%) sphericity)*

C. Stage of textural maturity

- ➢*originally mature, but due to the infiltrated muddy siltstone and mudstone, the whole rock seems to be immature*

D. Fabric

- ➢*massive*
- ➢*matrix:grain 40:60 => predominantly grain supported, but there are matrix supported patches*
- ➢*grains show point contacts where grain supported, but there are loosely packed patches where matrix supported*
- ➢*0-5% porosity (i.e. pore-filling cement plus present porosity)*

III. Mineral composition

A. Grains:

1. Percentage of quartz: 98%
   - ➢98% *monocrystalline & 2% polycrystalline*
   - ➢*70% undulatory & 30% nonundulatory*
   - ➢*polycrystalline grain size/crystal size in the polycrystalline grains/crystal number/crystal shape & boundaries 0.5-1 mm (coarse sand) / 0.2 mm (fine sand) / < 5 / irregular with non-sutured contacts*
   - ➢*mean grain size 0.5-1 mm (coarse sand)*
2. Percentage of lithic fragments: 2%
   - ➢*muddy coarse (0.031-0.06 mm) siltstone clasts and one bone fragment (0.4 X 0.7 mm)*
   - ➢*the clasts show soft sedimentary deformations*
   - ➢*mean grain size 2-4 mm (granule)*

B. Matrix: 40%

- ➢*clay 60%*
- ➢*quartz: 0.031-0.06 mm coarse silt 38% & 0.06-0.125 mm very fine sand 2%*
- ➢*the matrix is inhomogeneous consisting of clean clay (60%); coarse silty mud (20%) as well as muddy coarse silt(20%) patches. There are no differences between the later matrix type and the muddy coarse siltstone clasts.*

IV. Diagenetic features

- ➢*silica, limonite cement*
- ➢*Fe-oxides present as grain coatings (there are some grain contacts without limonite rim) & blebs*

V. Classification

- ✧*quartzwacke with pene-contemporaneous silty-muddy matrix*

I. Formation name & geographic location

Middle Unit (lower part) - Karoo Supergroup; Halcyon Farm - HAL7

II. Texture

A. Grain size and sorting

➢*0.25-0.5 mm medium sand (50%); 1-2 mm very coarse sand (15%); 2-4 mm granule (15%); 4-8 mm small pebble (15%) & 8-16 mm medium pebble (5%)*

➢poorly *sorted*

B. Grain shape

➢*xenomorph*

➢*subrounded, subangular >> rounded*

➢*low (65%) & high (35%) sphericity*

C. Stage of textural maturity

➢*mature (but poorly sorted)*

D. Fabric

➢*massive*

➢*matrix:grain 0:100 => grain supported*

➢*grains show point contacts*

➢*20% porosity (i.e. pore-filling cement plus present porosity)*

III. Mineral composition

Grains:

1. Percentage of quartz: 100%

➢*80% monocrystalline & 20% polycrystalline*

➢*80% undulatory & 20% nonundulatory*

➢*polycrystalline grain size/crystal size in the polycrystalline grains/crystal number/crystal shape & boundaries*

4-16 mm (pebbles) / >0.25 mm (>medium sand) / <5 / irregular with non-sutured contacts

2-4 mm (granules) / <0.25 mm (fine&very fine sand) / >5 / irregular with non-sutured contacts

2. Percentage of other terrigenous minerals: <0.01%

➢*opaque minerals, zircon, tourmaline, green hornblende*

➢*grain size 0.25-0.5 mm (medium sand)*

IV. Diagenetic features

➢*limonite cement*

➢*Fe-oxides present as grain coatings (most of the grain contacts are separated by thin limonite rims) & very rare blebs*

V. Classification

✧*pebbly quartz arenite*

I. Formation name & geographic location

Upper Unit - Karoo Supergroup; Halcyon Farm - HAL8

II. Texture

A. Grain size and sorting

- ➢*0.062-0.125 mm very fine sand (90%) & 0.125-0.25 mm fine sand (10%)*
- ➢*moderately sorted*

B. Grain shape

- ➢*xenomorph*
- ➢*subrounded > rounded, subangular (fine sand fraction predominantly rounded)*
- ➢*low (50%) & high (50%) sphericity*

C. Stage of textural maturity

- ➢*mature*

D. Fabric

- ➢*slight lamination determined by the blade or lath-shaped grains*
- ➢*matrix:grain 0:100 => grain supported*
- ➢*grains show point contacts, loosely packed*
- ➢*20% porosity (i.e. pore-filling cement plus present porosity)*

III. Mineral composition

Grains:

1. Percentage of quartz: ~95%
   - ➢*100% monocrystalline & 0% polycrystalline*
   - ➢*80% undulatory & 20% nonundulatory*
   - ➢*grain size 0.062-0.125 mm very fine sand (90%) & 0.125-0.25 mm fine sand (10%)*
2. Percentage of feldspar: ~4%
   - ➢*multiple (tartan, albite) twins*
   - ➢*grain size 0.062-0.125 mm very fine sand (95%) & 0.125-0.25 mm fine sand (5%)*
3. Percentage of mica: <1%
   - ➢*muscovite*
   - ➢*grain size ~0.1 mm (very fine sand)*
4. Percentage of other terrigenous minerals: <0.01%
   - ➢*opaque minerals, zircon, tourmaline, green hornblende*
   - ➢*grain size ~0.1 mm (very fine sand)*

IV. Diagenetic features

- ➢*silica, limonite cement*
- ➢*Fe-oxides present as rare grain coatings (there are some grain contacts without limonite rim) & very rare blebs*

V. Classification

- ✧*quartz arenite*

I. Formation name & geographic location

Upper Unit - Karoo Supergroup; Hilda Farm - HIL2

II. Texture

A. Grain size and sorting

- ➢*0.125-0.25 mm fine sand (1%); 0.5-1 mm coarse sand (26%); 1-2 mm very coarse sand (24%); 2-4 mm granule (24%) & 4-8 mm small pebble (25%)*
- ➢*moderately sorted*

B. Grain shape

- ➢*xenomorph*
- ➢*rounded > subrounded > subangular*
- ➢*low (35%) & high (65%) sphericity*

C. Stage of textural maturity

- ➢*mature*

D. Fabric

- ➢*slight normal grading indicated by the decrease of the carbonate glaebules from small pebble to coarse grain sand size*
- ➢*matrix:grain 15:85 => grain supported*
- ➢*grains show point contacts*
- ➢*20% porosity (i.e. pore-filling cement plus present porosity)*

III. Mineral composition

A. Grains:

1. Percentage of quartz: 2%
   - ➢98% *monocrystalline & 2% polycrystalline*
   - ➢*50% undulatory & 50% nonundulatory*
   - ➢*polycrystalline grain size/crystal size in the polycrystalline grains/crystal number/crystal shape & boundaries 0.4 mm (medium sand) / ~0.125 mm (fine) / 3 / irregular with sutured contacts*
   - ➢*grain size 0.5-1 mm (coarse sand)*
2. Percentage of feldspar: 1%
   - ➢*multiple (albite, tartan) twins*
   - ➢*grain size 0.25-0.5 mm (medium sand)*
3. Percentage of lithic fragments: 97%
   - ➢*consisting of carbonate glaebules (99%), 1 laminated fine silty mudstone & bone fragments (<1%)*
   - ➢*carbonate glaebules consists of:*
     - ○*10% <u>septaria</u>: radial wedge-shaped cracks filled by sparite; <1% very fine silt size quartz grains floating in micrite matrix*
     - ○*5% <u>concretion</u>: curvilinear circumgranular cracks filled with sparite & microspaite; one concretion has a feldspar fragment nucleus*
     - ○*85% <u>nodule</u>:*
       - ●*20%: elongated or spherical inhomogenities filled by microsparite or sparite; <10% very fine silt size quartz grains floating in otherwise micrite matrix*
       - ●*30%: <1% very fine silt size quartz grains floating in microsparite matrix*
       - ●*50%: >10% very fine silt size quartz grains floating in microsparite matrix*
   - ➢*grain size 0.5-1 mm coarse sand (24.5%); 1-2 mm very coarse sand (24.5%), 2-4 mm granule (25%) & 4-8 mm small pebble (26%)*
4. Percentage of other terrigenous minerals: <0.01%
   - ➢*opaque minerals, zircon*
   - ➢*grain size 0.062-0.125 mm (very fine sand)*

B. Matrix: 15%

- ➢*consists of subrounded-subangular quartz (99%) & feldspar(1%) grains*
- ➢*grain size 0.062-0.125 mm very fine sand*

IV. Diagenetic features

- ➢ *limonite (80%) & micrite (20%) cement*
- ➢*Fe-oxides present as very rare blebs*

V. Classification

- ✧*litharenite*

I. Formation name & geographic location

Upper Unit - Karoo Supergroup; Hillstone Farm - HILL1

II. Texture

A. Grain size and sorting

➢*0.062-0.125 mm very fine sand (10%), 0.125-0.25 mm fine sand (60%) & 0.25-0.50 mm medium sand (30%)*

➢*poorly-moderately sorted*

B. Grain shape

➢*xenomorph*

➢*subrounded, subangular>> rounded*

➢*low (40%) & high (60%) sphericity*

C. Stage of textural maturity

➢*mature*

D. Fabric

➢*massive*

➢*matrix:grain 40:60 => matrix supported & grain supported clusters*

➢*F- (floating) & GS- (grain supported) fabric patches*

➢*only matrix supported quartz grains show embayment dissolution features*

➢*<10% porosity (i.e. pore-filling cement plus present porosity)*

III. Mineral composition

A. Grains:

1. Percentage of quartz: 99%

➢*97% monocrystalline & 3% polycrystalline*

➢*70% undulatory & 30% non-undulatory*

➢*polycrystalline grain size/ crystal size in the polycrystalline grains/ crystal number/ crystal shape & boundaries 0.6 mm (coarse sand) / 0.2 mm (medium silt) / 3 / irregular with non-sutured contacts*

➢*grain size 0.062-0.125 mm very fine sand (10%), 0.125-0.25 mm fine sand (60%) & 0.25-0.50 mm medium sand (30%)*

2. Percentage of feldspar: <1%

➢*multiple (tartan, albite) twins*

➢*slightly altered (cloudy, brownish in PPL)*

➢*grain size 0.062-0.125 mm (very fine sand)*

3. Percentage of other terrigenous minerals: <0.01%

➢*Fe-oxides, zircon, tourmaline*

➢*grain size ~0.1 mm (very fine sand)*

B. Matrix: 40%

➢*microquartz*

IV. Other features

A. Voids *(diameter: 0.5-0.8 mm) filled by:*

➢*fibrous, radial, length-fast chalcedony*

➢*fibrous, radial, length-fast chalcedony => microquartz*

➢*Fe-oxide banded crytocrystalline silica => fibrous, radial, length-fast chalcedony => equant megaquartz*

➢*fibrous, radial, multi-generation lutecite ("zebraic chalcedony")*

➢*microquartz => equant megaquartz*

➢*crystal/bundle size increases toward the center of the void*

➢*sparry calcite (only in 5 voids)*

B. Tubules *(width: ~0.2 mm; length: 1-2 mm) filled by:*

➢*Fe-oxide banded crytocrystalline silica => fibrous, radial, length-fast chalcedony => equant megaquartz*

C. Detrital grains *(<1%) enveloped by:*

➢*0.02 mm single microquartz wall*

D. Cavities *(diameter: 0.5-1 mm) enveloped by:*

➢*0.02 mm single microquartz wall*

V. Diagenetic features

➢*Fe-oxides present as crystals & blebs*

VI. Classification

✧*massive silcrete*

I. Formation name & geographic location

Clarens Formation - Karoo Supergroup; Hillstone Farm - HILL2

II. Texture

A. Grain size and sorting

- ➢*0.062-0.125 mm very fine sand (30%), 0.125-0.25 mm fine sand (40%) & 0.25-0.50 mm medium sand (30%)*
- ➢*moderately sorted*

B. Grain shape

- ➢*xenomorph (40%) & euhedral(60%) - due to authigenic overgrowth of a few quartz crystals (original grain margin outlined by a very thin limonite rim)*
- ➢*subrounded > rounded (the xenomorph grains only)*
- ➢*low (40%) & high (60%) sphericity*

C. Stage of textural maturity

- ➢*mature*

D. Fabric

- ➢*massive*
- ➢*except for the completely homogenous fabric, there is no other microscopic evidence of the bioturbation, although the section was taken form a vertical, tube shaped (diameter 6 cm) weathered-out animal(?) burrow*
- ➢*matrix:grain 0:100 => grain supported*
- ➢*closely packed grains due to authigenic overgrowth of a few quartz crystals*
- ➢*5% porosity (i.e. pore-filling cement plus present porosity)*

III. Mineral composition

Grains:

1. Percentage of quartz: ~96%
   - ➢*100% monocrystalline & 0% polycrystalline*
   - ➢*60% undulatory & 40% non-undulatory*
   - ➢*grain size 0.06-0.125 mm very fine sand (30%), 0.125-0.25 mm fine sand (40%) & 0.25-0.5 mm medium sand (30%)*
2. Percentage of feldspar: ~4%
   - ➢*multiple (albite) twins*
   - ➢*10% slightly altered (cloudy, brownish in PPL)*
   - ➢*grain size 0.06-0.125 mm very fine sand (30%), 0.125-0.25 mm fine sand (40%) & 0.25-0.5 mm medium sand (30%)*
3. Percentage of other terrigenous minerals: <0.01%
   - ➢*opaque minerals, zircon, tourmaline, green hornblende*
   - ➢*grain size ~0.1 mm (very fine sand)*

IV. Diagenetic features

- ➢*authigenic overgrowth of a few quartz crystals*
- ➢*silica, limonite cement*
- ➢*Fe-oxides present as very rare grain coatings (there are some grain contacts without limonite rim) & blebs*

V. Classification

- ✧*quartz arenite*

I. Formation name & geographic location

Basal Unit- Karoo Supergroup; Kilgour - KIL1

II. Texture

A. Grain size and sorting

- ➢*0.25-0.5 mm medium sand (5%), 0.5-1 mm coarse sand (65%) & 1-2 mm very coarse sand (30%)*
- ➢*poorly sorted*

B. Grain shape

- ➢*xenomorph*
- ➢*subangular >> subrounded*
- ➢*low (60%) & high (40%) sphericity grains*

C. Stage of textural maturity

- ➢*submature*

D. Fabric

- ➢*massive*
- ➢*matrix:grain 0:100 => grain supported*
- ➢*grains show concavo-convex contacts*
- ➢*20% porosity (i.e. pore-filling cement plus present porosity)*

III. Mineral composition

Grains:

1. Percentage of quartz: 99 %
   - ➢*82% monocrystalline & 18% polycrystalline*
   - ➢*80% undulatory & 20% nonundulatory*
   - ➢*polycrystalline grain size/crystal size in the polycrystalline grains/crystal number/crystal shape & boundaries 0.5-1 mm (coarse sand)/0.25 mm (medium sand)/plenty/irregular, subequant crystals with sutured contacts*
   - ➢*grain size 0.25-0.5 mm medium sand (<4%), 0.5-1 mm coarse sand (65%) & 1-2 mm very coarse sand (30%)*
2. Percentage of mica: <1 %
   - ➢*muscovite*
   - ➢*grain size 0.25 mm (fine medium sand)*

IV. Diagenetic features

- ➢*limonite rich silica (chalcedony) cement*
- ➢*Fe-oxides present as blebs & euhedral hematite crystals*

V. Classification

- ✧*quartz arenite*

I. Formation name & geographic location

Basal Unit - Karoo Supergroup; Lauriston Farm - LAU3

II. Texture

A. Grain size and sorting

- ➢*0.06-0.125 mm very fine sand (5%), 0.25-0.5 mm medium (15%), 0.5-1 mm coarse sand (20%) & 1-2 mm very coarse sand (60%)*
- ➢*poorly sorted*

B. Grain shape

- ➢*xenomorph*
- ➢*subangular > subrounded*
- ➢*low (50%) & high (50%) sphericity grains*

C. Stage of textural maturity

- ➢*submature*

D. Fabric

- ➢*massive*
- ➢*matrix:grain 0:100 => grain supported*
- ➢*grains show concavo-convex contacts*
- ➢*10% porosity (i.e. pore-filling cement plus present porosity)*

III. Mineral composition

Grains:

1. Percentage of quartz: 99%
   - ➢*70% monocrystalline & 30% polycrystalline*
   - ➢*60% undulatory & 40% nonundulatory*
   - ➢*polycrystalline grain size/ crystal size in the polycrystalline grains/ crystal number/ crystal shape & boundaries 0.5-1 mm (coarse sand) / 0.25 mm (medium sand) / plenty / irregular, subequant crystals with sutured contacts*
   - ➢*grain size 0.06-0.125 mm very fine sand (>4%), 0.25-0.5 mm medium (18%), 0.5-1 mm coarse sand (18%) & 1-2 mm very coarse sand (60%)*
2. Percentage of feldspar: <0.5%
   - ➢*multiple twins (albite)*
   - ➢*altered (sericitisation)*
   - ➢*mean grain size 0.1 mm (very fine sand)*
3. Percentage of mica: <0.5%
   - ➢*muscovite*
   - ➢*mean grain size 0.1 mm (very fine sand)*
   - ➢*hydromuscovite*
   - ➢*mean grain size 0.25-0.50 mm (medium sand)*

IV. Diagenetic features

- ➢*limonite & silica cement*
- ➢*Fe-oxides present as blebs & crystals*

V. Classification

- ✧*quartz arenite*

I. Formation name & geographic location

Basal Unit - Karoo Supergroup; Lauriston Farm - LAU4

II. Texture

A. Grain size and sorting

- ➢*0.125-0.25 mm fine sand (40%) & 0.25-0.5 mm medium sand (60%)*
- ➢*moderately sorted*

B. Grain shape

- ➢*xenomorph*
- ➢*angular, subangular > subrounded*
- ➢*low (85%) & high (15%) sphericity*

C. Stage of textural maturity

- ➢*mature*

D. Fabric

- ➢*slight lamination could be traced due to the laminae of diagenetic Fe-oxides*
- ➢*matrix:grain 70:30 => matrix supported (about 50% of the matrix consists of ghost crystals perhaps formed through the advanced alteration of feldspars)*
- ➢*0% porosity (i.e. pore-filling cement plus present porosity)*

III. Mineral composition

A. Grains:

1. Percentage of quartz: 93%
   - ➢*90% monocrystalline &10% polycrystalline*
   - ➢*90% undulatory & 10% nonundulatory*
   - ➢*polycrystalline grain size/crystal size in the polycrystalline grains/crystal number/crystal shape & boundaries*
     0.8 mm (coarse sand) / 0.05 mm (silt) / plenty / irregular, subequant >> elongated with sutured contacts
     0.4 mm (medium sand) / 0.1 mm (very fine sand) / 5-10 or plenty / irregular, subequant >> elongated with sutured contacts
   - ➢*grain size 0.125-0.25 mm fine sand (40%) & 0.25-0.5 mm medium sand (60%)*
2. Percentage of feldspar: ~4%
   - ➢*multiple (albite - thin laminae) twins*
   - ➢*advanced alteration (to sericite and muscovite, with plenty ghost crystals); many grains show clouding of elongated, randomly orientated microlithes (sericite and muscovite)*
   - ➢*grain size 0.125-0.25 mm fine sand (40%) & 0.25-0.5 mm medium sand (60%)*
3. Percentage of lithic fragments: ~1%
   - ➢*metamorphic rock (biotite schist) (The biotite wraps around the quartz grains.)*
   - ➢*all fragments are angular, subangular*
   - ➢*grain size 0.3-0.5 mm (medium sand)*
4. Percentage of mica: ~2%
   - ➢*biotite, muscovite*
   - ➢*grain size 0.3-0.5 mm (medium sand)*

B. Matrix: 70%

- ➢*quartz 90%*
- ➢*mica, clay & miscellaneous 10%*

IV. Diagenetic features

- ➢*limonite rich silica cement*
- ➢*Fe-oxides present as diffuse microcrystalline stain of the matrix & very rare blebs*

V. Classification

- ✧*quartzwacke*

I. Formation name & geographic location

Upper Unit - Karoo Supergroup; Little Muck Farm - LIT1

II. Texture

A. Grain size and sorting

➢*0.031-0.062 mm coarse silt (30%); 0.062-0.125 mm very fine sand (40%); 0.125-0.25 mm fine sand (15%) & 0.25-0.5 mm medium sand (15%)*

➢*poorly sorted*

B. Grain shape

➢*xenomorph*

➢*subrounded, rounded >> subangular (coarse sand grains well rounded or rounded)*

➢*low (35%) & high (65%) sphericity*

C. Stage of textural maturity

➢*mature*

D. Fabric

➢*massive*

➢*matrix:grain 20:80 => grain supported with matrix supported clusters (only where the matrix is sparry calcite)*

➢*grains show point contacts, in the matrix supported clusters the grains are displaced*

➢*10% porosity (i.e. pore-filling cement plus present porosity)*

III. Mineral composition

A. Grains:

1. Percentage of quartz: 99%

➢*100% monocrystalline & 0% polycrystalline*

➢*60% undulatory & 40% nonundulatory*

➢*grain size 0.062-0.125 mm (very fine sand)*

2. Percentage of feldspar: <1%

➢*multiple (tartan, albite) twins*

➢*slightly altered (sericitisation)*

➢*grain size 0.062-0.125 mm (very fine sand)*

3. Percentage of other terrigenous minerals: <0.01%

➢*opaque minerals, zircon*

➢*grain size 0.062-0.125 mm (very fine sand)*

B. Matrix: 20%

➢*clay 20%*

➢*microquartz 70%*

➢*sparry calcite 10%*

IV. Diagenetic features

➢*Fe-oxides present as grain coatings (there are some grain contacts without limonite rim) & very rare blebs*

V. Classification

✧*quartz wacke*

I. Formation name & geographic location

Clarens Formation - Karoo Supergroup; Little Muck Farm - LIT2

II. Texture

A. Grain size and sorting

- ➢*0.062-0.125 mm very fine sand (69%), 0.25-0.50 mm medium sand (20%), 0.5-1 mm coarse sand (10%) & 2-4 mm granule 1%*
- ➢*moderately sorted*

B. Grain shape

- ➢*xenomorph but there are a few euhedral quartz grains as well due to the authigenic overgrowth*
- ➢*subrounded >> subangular > rounded*
- ➢*low (35%) & high (65%) sphericity*

C. Stage of textural maturity

- ➢*mature*

D. Fabric

- ➢*massive*
- ➢*matrix:grain 0:100 => grain supported*
- ➢*grains show point contacts*
- ➢*20% porosity (i.e. pore-filling cement plus present porosity)*

III. Mineral composition

Grains:

1. Percentage of quartz: 94%
   - ➢*100% monocrystalline & 0% polycrystalline*
   - ➢*70% undulatory & 30% nonundulatory*
   - ➢*grain size 0.06-0.125 mm very fine sand (70%), 0.25-0.50 mm medium sand (20%), 0.5-1 mm coarse sand (10%*
2. Percentage of feldspar: ~5%
   - ➢*multiple (tartan, albite) twins*
   - ➢*slightly altered (sericitisation, brownish clouding)*
   - ➢*grain size 0.062-0.125 mm (very fine sand)*
3. Percentage of lithic fragments: >1%
   - ➢*angular, subangular silcrete granules*
   - ➢*grain size 2-4 mm (granules)*
4. Percentage of other terrigenous minerals: <0.01%
   - ➢*opaque minerals, zircon, tourmaline*
   - ➢*grain size 0.062-0.125 mm (very fine sand)*

IV. Diagenetic features

- ➢*authigenic overgrowth of the quartz crystals*
- ➢*microquartz (<20 μm) and chalcedony cement*
- ➢*Fe-oxides present as grain coatings (there are some grain contacts without limonite rim) & very rare blebs*

V. Classification

- ✧*quartz arenite - subarkose*

I. Formation name & geographic location

Clarens Formation - Karoo Supergroup; Little Muck Farm - LIT3

II. Texture

A. Grain size and sorting

➢*0.062-0.125 mm very fine sand (90%) & 0.5-1 mm coarse sand (10%)*

➢*moderately sorted*

B. Grain shape

➢*xenomorph*

➢*subrounded, rounded >> subangular (coarse sand grains well rounded or rounded)*

➢*low (35%) & high (65%) sphericity*

C. Stage of textural maturity

➢*mature*

D. Fabric

➢*massive*

➢*matrix:grain 0:100 => grain supported*

➢*grains show point contacts*

➢*10% porosity (i.e. pore-filling cement plus present porosity)*

III. Mineral composition

Grains:

1. Percentage of quartz: 99%
   - ➢*100% monocrystalline & 0% polycrystalline*
   - ➢*80% undulatory & 20% nonundulatory*
   - ➢*grain size 0.062-0.125 mm (very fine sand)*
2. Percentage of feldspar: 1%
   - ➢*multiple (tartan, albite) twins*
   - ➢*slightly altered (sericitisation)*
   - ➢*grain size 0.062-0.125 mm (very fine sand)*
3. Percentage of other terrigenous minerals: <0.01%
   - ➢*opaque minerals, zircon, tourmaline, green hornblende*
   - ➢*grain size 0.062-0.125 mm (very fine sand)*

IV. Diagenetic features

➢*silica cement*

➢*Fe-oxides present as very rare blebs*

V. Classification

✧*quartz arenite*

I. Formation name & geographic location

Upper Unit - Karoo Supergroup; Little Muck Farm - LIT4

II. Texture

A. Grain size and sorting

➢*0.062-0.125 mm very fine sand (90%) & 0.5-1 mm coarse sand (10%)*

➢*well sorted*

B. Grain shape

➢*xenomorph*

➢*subrounded, rounded > subangular*

➢*low (30%) & high (70%) sphericity*

C. Stage of textural maturity

➢*mature*

D. Fabric

➢*massive*

➢*matrix:grain 95:5 => matrix supported F- (floating) & abundant GS- grain supported (matrix:grain 10:80) fabric clusters*

➢*quartz grains show strong embayment dissolution features*

➢*~20% porosity (i.e. pore-filling cement plus present porosity)*

III. Mineral composition

A. Grains:

1. Percentage of quartz: 99%

➢*100% monocrystalline & 0% polycrystalline*

➢*60% undulatory & 40% nonundulatory*

➢*grain size 0.062-0.125 mm very fine sand (90%) & 0.5-1 mm coarse sand (10%)*

2. Percentage of feldspar: <1%

➢*multiple (tartan, albite) twins*

➢*slightly altered (sericitisation)*

➢*grain size 0.062-0.125 mm (very fine sand)*

3. Percentage of other terrigenous minerals: <0.01%

➢*opaque minerals, zircon, tourmaline, green hornblende*

➢*grain size 0.062-0.125 mm (very fine sand)*

B. Matrix: (5-)90%

➢*cryptocrystalline silica*

IV. Other features

A. Voids *(diameter: 0.5-0.8 mm) filled by:*

➢*Fe-oxide banded crytocrystalline silica => fibrous, radial, length-fast chalcedony*

➢*Fe-oxide banded crytocrystalline silica => microquartz => equant megaquartz (in the void center)*

➢*Fe-oxide banded crytocrystalline silica => fibrous, radial, length-fast chalcedony => microquartz => equant megaquartz*

➢*laminated Fe-oxides => Fe-oxide banded crytocrystalline silica => microquartz => equant megaquartz*

➢*laminated Fe-oxides => laminated crytocrystalline silica => equant megaquartz*

➢*crystal/bundle size increases toward the center of the void*

B. Tubules *(width: ~0.2 mm; length: 1-2 mm) filled by:*

➢*Fe-oxide banded crytocrystalline silica => microquartz => fibrous, radial, length-fast chalcedony*

➢*Fe-oxide banded crytocrystalline silica => fibrous, radial, length-fast chalcedony => microquartz => equant megaquartz*

C. Veins *(width: 0.1-1 mm) filled by:*

➢*Fe-oxide banded crytocrystalline silica => length-fast chalcedony => finely laminated, Fe-oxide banded crytocrystalline silica => equant megaquartz (in the vein center)*

➢*Fe-oxide banded crytocrystalline silica => fibrous, radial, length-fast chalcedony*

D. Cavities *(diameter: 0.8-1.6 mm) enveloped by walls consisting of:*

➢*laminated, Fe-oxide banded crytocrystalline silica => length-fast chalcedony => megaquartz*

➢*microquartz*

➢*0.062-0.125 mm (very fine) detrital quartz grains floating in Fe-oxide matrix (similar fabric visible in WEI6 - bioturbation burrow)*

V. Diagenetic features

➢*Fe-oxides present as very rare blebs*

VI. Classification

✧*massive silcrete*

I. Formation name & geographic location

Middle Unit (lower part) - Karoo Supergroup; Lizzulea Farm - LIZ1

II. Texture

A. Grain size and sorting

- ➢*0.25-0.5 mm medium sand (10%), 0.5-1 mm coarse sand (80%) & 1-2 mm very coarse sand(10%)*
- ➢*moderately sorted*

B. Grain shape

- ➢*xenomorph, but there are a few euhedral quartz grains with angular authigenic overgrowth rims*
- ➢*well rounded, rounded >> subrounded, subanuglar*
- ➢*low (50%) and high (50%) sphericity grains*

C. Stage of textural maturity

- ➢*supermature*

D. Fabric

- ➢*massive*
- ➢*matrix:grain 0:100 => grain supported*
- ➢*grains very closely packed, but only a few grains have sutured contacts*
- ➢*10% porosity (i.e. pore-filling cement plus present porosity)*

III. Mineral composition

Percentage of quartz: 100%

- ➢*98% monocrystalline & 2% polycrystalline*
- ➢*70% undulatory & 30% nonundulatory*
- ➢*polycrystalline grain size/ crystal size in the polycrystalline grains/ crystal number/ crystal shape & boundaries*
  0.4 mm (medium sand) / 0.2 mm or less (medium or finer sand) / plenty / irregular, subequant with sutured contacts

IV. Diagenetic features

- ➢*authigenic overgrowth of the quartz crystals*
- ➢*silica & limonite cement*
- ➢*Fe-oxides present as blebs clusters and rare grain coatings (there are grain contacts without limonite rim)*

V. Classification

- ✧*quartz arenite*

I. Formation name & geographic location

Middle Unit (lower part) - Karoo Supergroup; Lizzulea Farm - LIZ3

II. Texture

A. Grain size and sorting

- ➢*0.5-1 mm coarse sand (40%) & 1-2 mm very coarse sand (60%) (there is a 1 cm pebble of vein quartz)*
- ➢*moderately sorted*

B. Grain shape

- ➢*xenomorph,*
- ➢*subrounded > rounded*
- ➢*low (50%) & high (50%) sphericity grains*

C. Stage of textural maturity

- ➢*supermature*

D. Fabric

- ➢*massive*
- ➢*matrix:grain 0:100 => grain supported*
- ➢*grains very loosely packed, rarely show point contacts*
- ➢*40% porosity (i.e. pore-filling cement plus present porosity)*

III. Mineral composition

Percentage of quartz: 100%

- ➢*monocrystalline 95% vs. polycrystalline 5%*
- ➢*undulatory 70% vs. nonundulatory 30%*
- ➢*<5% of the quartz grains have zircon and other needle-shaped microliths*
- ➢*polycrystalline grain size/ crystal size in the polycrystalline grains/ crystal number/ crystal shape & boundaries 0.5-1 mm (coarse sand) / 0.2 mm (fine sand) / plenty / irregular, subequant crystals with sutured contacts*

IV. Diagenetic features

- ➢*limonite cement*
- ➢*Fe-oxides present as thick grain coatings resulting in the "cement-supported" fabric*

V. Classification

- ✧*pebbly quartz arenite*

I. Formation name & geographic location

Upper Unit - Karoo Supergroup; Lizzulea Farm - LIZIIA

II. Texture

A. Grain size and sorting

- ➢*0.02 medium silt (60%) & 0.05 mm coarse silt (40%)*
- ➢*moderately sorted individual laminae*

B. Grain shape

- ➢*xenomorph*
- ➢*subrounded >> subangular > rounded*
- ➢*low (35%) & high (65%) sphericity*

C. Stage of textural maturity

- ➢*mature*

D. Fabric

- ➢*slight lamination due to grain size changes & gradual development of matrix supported fabric form grains supported*
- ➢*matrix:grain 40:60 => grain & matrix supported laminae*
- ➢*grains show point contacts*
- ➢*15% porosity (i.e. pore-filling cement plus present porosity)*

III. Mineral composition

A. Grains:

1. Percentage of quartz: 100%
   - ➢*100% monocrystalline & 0% polycrystalline*
   - ➢55% *undulatory & 45% nonundulatory*
   - ➢*grain size 0.02 medium silt (60%) & 0.05 mm coarse silt (40%)*
2. Percentage of other terrigenous minerals: <0.01%
   - ➢*opaque minerals, tourmaline, zircon*
   - ➢*grain size 0.05 mm coarse silt*

B. Matrix: 40%

- ➢*clay & micirte*

IV. Diagenetic features

- ➢*limonite rich sparite cement*
- ➢*Fe-oxides present as rare grain coatings (there are some grain contacts without limonite rim) & very rare blebs*

V. Classification

- ✧*quartzwacke (laminated quartz silstone)*

I. Formation name & geographic location

Upper Unit - Karoo Supergroup; Lizzulea Farm - LIZIIB

II. Texture

A. Mean grain size and sorting

- ➢*0.125-0.25 mm fine sand (10%); 1-2 mm very coarse sand (30%) & 2-4 mm granule (60%)*
- ➢*moderately sorted individual laminae*

B. Grain shape

- ➢*xenomorph*
- ➢*well rounded*
- ➢*low (35%) & high (65%) sphericity*

C. Stage of textural maturity

- ➢*mature*

D. Fabric

- ➢*slight lamination due to grain size changes; there are two, normal graded granule & one very coarse sand laminae*
- ➢*matrix:grain 5:95 => grain supported*
- ➢*grains show point contacts*
- ➢*20% porosity (i.e. pore-filling cement plus present porosity)*

III. Mineral composition

A. Grains:

1. Percentage of quartz: 1.5%
   - ➢*100% monocrystalline & 0% polycrystalline*
   - ➢*70% undulatory & 30% nonundulatory*
   - ➢*grain size 0.125-0.25 mm medium sand*
2. Percentage of feldspar: <1%
   - ➢*multiple (albite, tartan) twins*
   - ➢*grain size 0.25-0.5 mm medium sand*
3. Percentage of lithic fragments: 97.5%
   - ➢*consisting of carbonate glaebules (99%) & bone fragments (<1%)*
   - ➢*carbonate glaebules consists of:*
     - ○*2% septaria: radial wedge-shaped cracks filled by sparite; <1% very fine silt size quartz grains floating in micrite matrix*
     - ○*98% nodule:* ●*7%: elongated or spherical inhomogenities filled by microsparite or sparite; <10% very fine silt size quartz grains floating in otherwise micrite matrix.*
       - ●*70%: <10% very fine silt size quartz grains floating in micrite matrix*
       - ●*20%: >10% very fine silt size quartz grains floating in micrite matrix*
       - ●*3%: <10% very fine silt size quartz grains floating in microsparite matrix*
   - ➢*grain size 0.125-0.25 mm medium sand (8%), 0.5-1 mm coarse sand (24.5%); 1-2 mm very coarse sand (24.5%), 2-4 mm granule (25%) & 4-8 mm small pebble (26%)*

B. Matrix: 5%

- ➢*consists of subangular quartz grains*
- ➢*grain size 0.062-0.125 mm very fine sand*

IV. Diagenetic features

- ➢ *limonite rich micrite, sparite cement*
- ➢*Fe-oxides present as very rare blebs*

V. Classification

- ✧*litharenite*

I. Formation name & geographic location

Upper Unit - Karoo Supergroup; Machete Farm - MAC1

II. Texture

A. Grain size and sorting

- ➢*0.062-0.125 mm very fine sand (40%); 0.125-0.25 mm fine sand (40%); 2-4 mm granule (20%) & 4-8 mm small pebble (10%)*
- ➢*poorly sorted*

B. Grain shape

- ➢*xenomorph*
- ➢*subrounded, rounded, subangular*
- ➢*low (35%) & high (65%) sphericity*

C. Stage of textural maturity

- ➢*mature*

D. Fabric

- ➢*massive*
- ➢*matrix:grain 0:100 => grain supported*
- ➢*grains show point contacts*
- ➢*0-5% porosity (i.e. pore-filling cement plus present porosity)*

III. Mineral composition

Grains:

1. Percentage of quartz: 85%
   - ➢*100% monocrystalline & 0% polycrystalline*
   - ➢*70% undulatory & 30% nonundulatory*
   - ➢*grain size 0.062-0.125 mm very fine sand (45%); 0.125-0.25 mm fine sand (45%) & 2-4 mm granule (5%)*
2. Percentage of lithic fragments: 15%
   - ➢*80%: subrounded, Fe-oxide free, slightly silcretized very fine sandstone fragments (the quartz grains are moderately displaced by the cryptocrystalline and/or chalcedony matrix => GS- fabric)*
   - ➢*20%: subangular, Fe-oxide free, silcrete fragments (the very rare quartz grains float in the cryptocrystalline and/or chalcedony matrix => M- fabric)*
   - ➢*grain size 2-4 mm granule (25%) & 4-8 mm fine pebble (75%)*
3. Percentage of other terrigenous minerals: <0.01%
   - ➢*opaque minerals, zircon, tourmaline, green hornblende*
   - ➢*grain size 0.062-0.125 mm (very fine sand)*

IV. Diagenetic features

- ➢*limonite, microquartz cement*
- ➢*Fe-oxides present as grain coatings (there are some grain contacts without limonite rim) & blebs*

V. Classification

- ✧*sublitharenite*

I. Formation name & geographic location

Basal Unit - Karoo Supergroup; Montagu Farm - MOG8

II. Texture

A. Grain size and sorting

- ➢*0.125-0.25 mm fine sand (40%), 0.25-0.5 mm medium sand (35%), 0.51 mm coarse sand (10%), 1-2 mm very coarse sand (10%) & 2-4 mm granules (5%)*
- ➢*very poorly sorted*

B. Grain shape

- ➢*xenomorph*
- ➢*very angular > angular*
- ➢*low (80%) & high (20%) sphericity grains*

C. Stage of textural maturity

- ➢*immature*

D. Fabric

- ➢*slight lamination due to the blade or lath-shaped minerals of the matrix. The laminated matrix asymmetrically wraps around the coarser detrital grains.*
- ➢*matrix:grain 80:20 => matrix supported*
- ➢*0-5% porosity (i.e. pore-filling cement plus present porosity)*

III. Mineral composition

A. Grains:

1. Percentage of quartz: 99%
   - ➢*90% monocrystalline & 10% polycrystalline*
   - ➢*70% undulatory (~50% slightly undulatory only) & 30% nonundulatory*
   - ➢*the larger quartz grain show a web of randomly orientated, elongated, needle-shaped cracks*
   - ➢*polycrystalline grain size/ crystal size in the polycrystalline grains/ crystal number/ crystal shape & boundaries*

     1.6–2 mm (very coarse sand) / 0.05-0.2 mm (silt and fine sand) / plenty /irregular, subequant with non-sutured, straight contacts, slightly disintegrated

     1-1.6 mm (very coarse sand) /0.4 -0.8 mm (medium-coarse sand) / ~5 / irregular, subequant with non-sutured, straight contacts, slightly disintegrated
2. Percentage of feldspar: ~1%
   - ➢*multiple (albite - thin laminae) twins*
   - ➢*advanced alteration (to mass of sericite and muscovite, with plenty ghost crystals); many grain show clouding*
   - ➢*grain size 0.2 mm (fine sand)*

B. Matrix: 80%

- ➢*clay 90%*
- ➢*quartz, mica & miscellaneous 10%*

IV. Diagenetic features

- ➢*limonite rich silica cement*
- ➢*Fe-oxides present as diffuse microcrystalline stain of the matrix & very rare blebs*

V. Classification

- ✧*(vein) quartz grain rich mudstone*

I. Formation name & geographic location

Basal Unit - Karoo Supergroup; Montagu Farm - MOG10A

II. Texture

A. Grain size and sorting

- ➢*0.1250.25 mm fine sand (5%), 0.5 mm medium (coarse) sand (20%), 1-2 mm very coarse sand (35%) & 2-4 mm granules (40%)*
- ➢*poorly sorted*

B. Grain shape

- ➢*xenomorph*
- ➢*subrounded > subangular*
- ➢*low (60%) & high (40%) sphericity grains*

C. Stage of textural maturity

- ➢*submature*

D. Fabric

- ➢*massive*
- ➢*grains randomly orientated*
- ➢*matrix:grain 0:100 => grain supported*
- ➢*grains show point contacts*
- ➢*35% porosity (i.e. pore-filling cement plus present porosity)*

III. Mineral composition

Grains:

1. Percentage of quartz: 99%
   - ➢*40% monocrystalline & 60% polycrystalline*
   - ➢*80% undulatory & 20% nonundulatory*
   - ➢*about 5% of the monocrystalline quartz grains show characteristics of vein quartz*
   - ➢*polycrystalline grain size/crystal size in the polycrystalline grains/crystal number/crystal shape & boundaries*
     2-4 mm (granules) / 0.25 mm (medium sand) / plenty / irregular, subequant crystals with sutured contacts
     2-4 mm (granules) / 0.25 mm (medium sand) / plenty / irregular, subequant crystals with non-sutured contacts (granite?)
     1-2 mm (very coarse sand) / 0.2 mm (fine sand) / plenty / irregular, subequant crystals with sutured contacts
   - ➢*grain size 0.125-0.25 mm fine sand (<4%), 0.5 mm medium (coarse) sand (20%), 1-2 mm very coarse sand (35%) & 2-4 mm granules (40%)*
2. Percentage of mica: <1%
   - ➢*muscovite*
   - ➢*grain size 0.2 mm (fine sand)*

IV. Diagenetic features

- ➢*microsparite cement*
- ➢*Fe-oxides present as quite rare blebs*

V. Classification

- ✧*quartz arenite*

I. Formation name & geographic location

Basal Unit - Karoo Supergroup; Montagu Farm - MOG10B

II. Texture

A. Grain size and sorting

- ➢*0.125-0.25 mm fine sand (1%), 0.25-0.5 mm medium sand (50%), 0.5-1 mm coarse sand (40%) & 1-2 mm very coarse (9%)*
- ➢*poorly sorted*

B. Grain shape

- ➢*xenomorph*
- ➢*subrounded > subangular*
- ➢*low (60%) & high (40%) sphericity grains*

C. Stage of textural maturity

- ➢*submature*

D. Fabric

- ➢*massive*
- ➢*matrix:grain 0:100 => grain supported*
- ➢*grains show point contacts*
- ➢*30% porosity (i.e. pore-filling cement plus present porosity)*

III. Mineral composition

Grains:

1. Percentage of quartz: 99%
   - ➢*80% monocrystalline & 20% polycrystalline*
   - ➢*70% undulatory & 30% nonundulatory*
   - ➢*polycrystalline grain size/crystal size in the polycrystalline grains/crystal number/crystal shape & boundaries*
   - ➢*0.5-1mm (coarse sand)/0.25 mm (medium sand)/plenty/irregular, subequant crystals with sutured contacts*
   - ➢*grain size 0.25-0.5 mm medium sand (50%), 0.5-1 mm coarse sand (40%) & 1-2 mm very coarse (10%)*
2. Percentage of mica: 1%
   - ➢*muscovite*
   - ➢*grain size 0.125-0.25 mm (fine sand)*

IV. Diagenetic features

- ➢*microsparite cement*
- ➢*Fe-oxides present as quite rare blebs*

V. Classification

- ✧*quartz arenite*

I. Formation name & geographic location

Upper Unit - Karoo Supergroup; Montrow Farm - MON2

II. Texture

A. Grain size and sorting

- ➢*0.125-0.25 mm fine sand (2%); 0.5-1 mm coarse sand (6%); 1-2 mm very coarse sand (18%); 2-4 mm granule (47%) & 4-8 mm small pebble (27%)*
- ➢*moderately sorted*

B. Grain shape

- ➢*xenomorph*
- ➢*subrounded, rounded quartz grains, well rounded calcrete glaebule particles*
- ➢*low (35%) & high (65%) sphericity*

C. Stage of textural maturity

- ➢*mature*

D. Fabric

- ➢*massive*
- ➢*matrix:grain 15:85 => grain supported*
- ➢*grains show point contacts*
- ➢*20% porosity (i.e. pore-filling cement plus present porosity)*

III. Mineral composition

A. Grains:

1. Percentage of quartz: 10%
   - ➢*50% monocrystalline & 50% polycrystalline*
   - ➢*70% undulatory & 30% nonundulatory*
   - ➢*polycrystalline grain size/ crystal size in the polycrystalline grains/ crystal number/ crystal shape & boundaries 0.5-1 mm (coarse sand) / ~0.25 mm (medium) / 2-4 / elongated&irregular with non-sutured contacts*
   - ➢*grain size 0.25-0.5 mm medium sand (20%), 0.5-1 mm coarse sand (60%) & 2-4 mm granule (20%)*
2. Percentage of feldspar: <1%
   - ➢*multiple (albite) twins*
   - ➢*grain size 0.25-0.5 mm medium sand*
3. Percentage of lithic fragments: ~90%
   - ➢*consisting of carbonate glaebules (99%) & bone fragments (<1%)*
   - ➢*carbonate glaebules consists of:*
     - ○*5% <u>septaria</u>: radial wedge-shaped cracks filled by sparite; <1% very fine silt size quartz grains floating in micrite matrix*
     - ○*10% <u>concretion</u>: curvilinear circumgranular cracks filled by sparite & microspaite*
     - ○*85% <u>nodule</u>:*
       - ●*5%: elongated, tabular or spherical inhomogenities filled by microsparite or sparite; <1% very fine silt size quartz grains floating in otherwise micrite matrix.*
       - ●*65%: <10% very fine silt size quartz grains floating in micrite matrix*
       - ●*30%: <10% very fine silt size quartz grains floating in microsparite matrix*
   - ➢*grain size 1-2 mm very coarse sand (20%), 2-4 mm granule (50%) & 4-8 mm small pebble (30%)*
4. Percentage of other terrigenous minerals: <0.01%
   - ➢*opaque minerals, zircon*
   - ➢*grain size 0.062-0.125 mm (very fine sand)*

B. Matrix: 15%

- ➢*consists of subrounded-subangular quartz grains*
- ➢*grain size 0.062-0.125 mm very fine sand*

IV. Diagenetic features

- ➢*sparite cement*

V. Classification

- ✧*litharenite*

I. Formation name & geographic location

Upper Unit - Karoo Supergroup; Nekel Farm - NEK1

II. Texture

A. Grain size and sorting

- ➢*0.5-1 mm coarse sand (40%);1-2 mm very coarse sand (35%); 2-4 mm granule (20%) & 4-8 mm small pebble (5%)*
- ➢*moderately sorted*

B. Grain shape

- ➢*xenomorph*
- ➢*subrounded, rounded quartz grains, well rounded calcrete glaebules, siltstone & very fine sandstone particles*
- ➢*low (35%) & high (65%) sphericity*

C. Stage of textural maturity

- ➢*mature*

D. Fabric

- ➢*massive*
- ➢*matrix:grain 15:85 => grain supported*
- ➢*grains show point contacts*
- ➢*20% porosity (i.e. pore-filling cement plus present porosity)*

III. Mineral composition

A. Grains:

1. Percentage of quartz: 2%
   - ➢*100% monocrystalline & 0% polycrystalline*
   - ➢*50% undulatory & 50% nonundulatory*
   - ➢*grain size 0.5-1 mm coarse sand (55%) &1-2 mm very coarse sand (45%)*
2. Percentage of lithic fragments: 98%
   - ➢*consists of carbonate glaebules (99%) & silstone-very fine sandstones (1%)*
   - ➢*carbonate glaebules consists of:*
     - ○*5% <u>septaria</u>: radial wedge-shaped cracks filled by sparite; <1% very fine silt size quartz grains floating in micrite matrix*
     - ○*95% <u>nodule</u>:* ●*15%: elongated or spherical inhomogenities filled by microsparite or sparite; <1% very fine silt size quartz grains floating in otherwise micrite matrix.*
       ●*85%: >1% to 85% very fine silt size quartz grains floating in microsparite matrix*
   - ➢*grain size 2-4 mm granule (80%) & 4-8 mm small pebble (20%)*
3. Percentage of other terrigenous minerals: <0.01%
   - ➢*opaque minerals, tourmaline*
   - ➢*grain size 0.062-0.125 mm (very fine sand)*

B. Matrix: 15%

- ➢*consists of subrounded-subangular quartz (98%) & feldspar(2%) grains*
- ➢*grain size 0.062-0.125 mm very fine sand (50%), 0.125-0.25 mm fine sand (40%) & 0.25-0.5 mm medium sand (10%)*

IV. Diagenetic features

- ➢*sparite cement*
- ➢*Fe-oxides present as very rare blebs*

V. Classification

- ✧*litharenite* (clast supported, pebbly-granular calcrete glaebular corase-very coarse sandstone)

I. Formation name & geographic location

Upper Unit - Karoo Supergroup; Nekel Farm - NEK2

II. Texture

A. Grain size and sorting

- ➢*0.031-0.06 mm coarse silt (70%) & 0.062-0.125 mm very fine sand (30%)*
- ➢*well sorted*

B. Grain shape

- ➢*xenomorph*
- ➢*subrounded, subangular > rounded*
- ➢*low (35%) & high (65%) sphericity*

C. Stage of textural maturity

- ➢*mature*

D. Fabric

- ➢*massive*
- ➢*matrix:grain 90:10 => matrix supported*
- ➢*grains float in sparry calcite matrix*
- ➢*quartz grains show strong embayment dissolution features*
- ➢*0-5% porosity (i.e. pore-filling cement plus present porosity)*

III. Mineral composition

A. Grains:

1. Percentage of quartz: 100%
   - ➢*100% monocrystalline & 0% polycrystalline*
   - ➢*70% undulatory & 30% nonundulatory*
   - ➢*grain size 0.062-0.125 mm very fine sand*
2. Percentage of other terrigenous minerals: <0.01%
   - ➢*opaque minerals, zircon*
   - ➢*grain size ~0.1 mm (very fine sand)*

B. Matrix: 90%

- ➢*sparry calcite: medium crystalline (0.062-0.25 mm), whereas the wedge-shaped cracks are filled by extremely coarsely crystalline (>4 mm) calcite only*

IV. Classification

- ➢*septaria*

I. Formation name & geographic location

Middle Unit (lower part) - Karoo Supergroup; Overvlakte Farm - OVE2

II. Texture

A. Grain size and sorting

➢*0.25-0.5 mm medium sand grain (80%) & 0.5-1 mm coarse sand (20%)*

➢*well sorted*

B. Grain shape

➢*xenomorph, but there are a few euhedral quartz grains with angular authigenic overgrowth rims*

➢*subrounded > rounded*

➢*low (60%) & high sphericity grains (40%)*

C. Stage of textural maturity

➢*supermature*

D. Fabric

➢*massive*

➢*matrix:grain 0:100 => grain supported*

➢*grains very closely packed: concavo-convex contacts (20% of the grains have sutured contacts)*

➢*5% porosity (i.e. pore-filling cement plus present porosity)*

III. Mineral composition

Grains:

1. Percentage of quartz: 100%

➢*monocrystalline 98% vs. polycrystalline 2%*

➢*undulatory 70% vs. nonundulatory 30%*

➢*one monocrystaline quartz has a zircon inclusion*

➢*70% of the quartz grains have a ~0.01 mm thick coating which shows higher order interference colour*

➢*polycrystalline grain size/crystal size in the polycrystalline grains/crystal number/crystal shape & boundaries*
0.5-1 m (coarse sand) / 0.25 mm (medium sand) / plenty / irregular, subequant with sutured contacts
0.25-0.5 mm (medium sand) / 0.1 mm (very fine sand) / plenty / irregular, subequant with sutured contacts

2. Percentage of other terrigenous minerals: <<0.01%

➢*opaque minerals, zircon, tourmaline*

➢*grain size medium sand (medium sand)*

IV. Diagenetic features

➢*the authigenic overgrowth of the quartz grains post-dates the limonite coating of the grains as the limonite rim is outlining the original subrounded, rounded grains*

➢*silica & limonite cement*

➢*Fe-oxides present as very thin grain coatings and rare blebs clusters*

V. Classification

✧*quartz arenite*

I. Formation name & geographic location

Upper Unit - Karoo Supergroup; Parma Farm - PAR1A

II. Texture

A. Grain size and sorting

- ➢*0.062-0.125 mm very fine sand*
- ➢*well sorted*

B. Grain shape

- ➢*xenomorph*
- ➢*subrounded >> rounded, subangular*
- ➢*low (35%) & high (65%) sphericity*

C. Stage of textural maturity

- ➢*mature*

D. Fabric

- ➢*massive*
- ➢*matrix:grain 0:100 => grain supported*
- ➢*grains show point contacts*
- ➢*15% porosity (i.e. pore-filling cement plus present porosity)*

III. Mineral composition

Grains:

1. Percentage of quartz: 98%
   - ➢*100% monocrystalline & 0% polycrystalline*
   - ➢*70% undulatory & 30% nonundulatory*
   - ➢*grain size 0.062-0.125 mm very fine sand*
2. Percentage of feldspar: ~2%
   - ➢*multiple (tartan, albite) twins*
   - ➢*slightly altered (sericitisation)*
   - ➢*grain size 0.062-0.125 mm very fine sand (*
3. Percentage of other terrigenous minerals: <0.01%
   - ➢*opaque minerals, zircon*
   - ➢*grain size ~0.1 mm (very fine sand)*

IV. Diagenetic features

- ➢*silica, limonite & very little microsparite cement*
- ➢*Fe-oxides present as diffuse interstitial material & very rare blebs*

V. Classification

- ✧*quartz arenite*

I. Formation name & geographic location

Upper Unit - Karoo Supergroup; Pondrif Farm - PON1A

II. Texture

A. Grain size and sorting

- ➢*0.062-0.125 mm very fine sand*
- ➢*moderately sorted*

B. Grain shape

- ➢*xenomorph*
- ➢*subrounded >> rounded, subangular*
- ➢*low (30%) & high (70%) sphericity*

C. Stage of textural maturity

- ➢*mature*

D. Fabric

- ➢*massive*
- ➢*matrix:grain 0:100 => grain supported*
- ➢*grains show point contacts*
- ➢*15% porosity (i.e. pore-filling cement plus present porosity)*

III. Mineral composition

Grains:

1. Percentage of quartz: 98%
   - ➢*100% monocrystalline & 0% polycrystalline*
   - ➢*70% undulatory & 30% nonundulatory*
   - ➢*grain size 0.062-0.125 mm (very fine sand)*
2. Percentage of feldspar: ~2%
   - ➢*multiple (tartan, albite) twins*
   - ➢*slightly altered (sericitisation)*
   - ➢*grain size 0.062-0.125 mm (very fine sand)*
3. Percentage of other terrigenous minerals: <0.01%
   - ➢*opaque minerals, zircon*
   - ➢*grain size ~0.1 mm (very fine sand)*

IV. Diagenetic features

- ➢*microsparite & silica cement*
- ➢*Fe-oxides present as diffuse interstitial material & very rare blebs*

V. Classification

- ✧*quartz arenite*

I. Formation name & geographic location

Clarens Formation - Karoo Supergroup; Pontdrift - PON2

II. Texture

A. Grain size and sorting

- ➢*0.062-0.125 mm very fine sand (33%), 0.125-0.25 mm fine sand (33%) & 0.25-0.50 mm medium sand (33%)*
- ➢*the individual laminae moderately sorted*

B. Grain shape

- ➢*xenomorph & a few euhedral grains due to authigenic quartz overgrowth*
- ➢*subrounded >> rounded > subangular (coarse sand fraction predominantly rounded)*
- ➢*low (25%) & high (75%) sphericity*

C. Stage of textural maturity

- ➢*mature*

D. Fabric

- ➢*laminated: the very fine-fine and medium grains form weakly defined, graded laminae*
- ➢*matrix:grain 0:100 => grain supported*
- ➢*closely packed grains with a few point contacts*
- ➢*10% porosity (i.e. pore-filling cement plus present porosity)*

III. Mineral composition

Grains:

1. Percentage of quartz: ~99.9%
   - ➢*100% monocrystalline & 0% polycrystalline*
   - ➢*70% undulatory & 30% non-undulatory*
   - ➢*grain size 0.062-0.125 mm very fine sand (33%), 0.125-0.25 mm fine sand (33%) & 0.25-0.50 mm medium sand (33%)*
2. Percentage of feldspar: ~0.1%
   - ➢*multiple (albite) twins*
   - ➢*grain size 0.062-0.125 mm (very fine sand)*
3. Percentage of other terrigenous minerals: <0.01%
   - ➢*opaque minerals, zircon, green hornblende*
   - ➢*grain size ~0.1 mm (very fine sand)*

IV. Diagenetic features

- ➢*authigenic quartz overgrowth*
- ➢*silica, limonite cement*
- ➢*Fe-oxides present as rare grain coatings (there are some grain contacts without limonite rim) & blebs*

V. Classification

- ✧*quartz arenite*

I. Formation name & geographic location

Clarens Formation - Karoo Supergroup; Princes Royal Farm - PRI1

II. Texture

A. Grain size and sorting

- ➢*0.062-0.125 mm very fine sand (90%) & 0.25-0.5 mm medium sand (10%)*
- ➢*moderately well sorted*

B. Grain shape

- ➢*xenomorph, but there are a few euhedral quartz grains with angular authigenic overgrowth rims*
- ➢*subrounded >> subangular > rounded (the xenomorf grains only)*
- ➢*low (40%) & high (60%) sphericity*

C. Stage of textural maturity

- ➢*mature*

D. Fabric

- ➢*massive*
- ➢*perhaps bioturbated - there is a 0.5 cm wide, 3 cm long, "J" shaped tubule containing 98% of the medium sand grains. This zone is only moderately sorted and has diffuse margins.*
- ➢*matrix:grain 0:100 => grain supported*
- ➢*closely packed grains due to the slight authigenic overgrowth of the quartz crystals*
- ➢*<10% porosity (i.e. pore-filling cement plus present porosity)*

III. Mineral composition

Grains:

1. Percentage of quartz: ~99%
   - ➢*100% monocrystalline & 0% polycrystalline*
   - ➢*70% undulatory & 30% non-undulatory*
   - ➢*grain size 0.062-0.125 mm very fine sand (90%) & 0.25-0.5 mm medium sand (10%)*
2. Percentage of feldspar: ~1%
   - ➢*multiple (tartan, albite) twins*
   - ➢*slightly altered (cloudy, brownish in PPL)*
   - ➢*grain size 0.062-0.125 mm (very fine sand)*
3. Percentage of other terrigenous minerals: <0.01%
   - ➢*opaque minerals, zircon, tourmaline*
   - ➢*grain size ~0.1 mm (very fine sand)*

IV. Diagenetic features

- ➢*authigenic overgrowth of the quartz crystals*
- ➢*microquartz (<20 μm), limonite cement*
- ➢*Fe-oxides present as rare blebs*

V. Classification

- ✧*quartz arenite*

I. Formation name & geographic location

Clarens Formation - Karoo Supergroup; Princes Royal Farm - PRI2

II. Texture

A. Grain size and sorting

- ➢*0.5-1 mm coarse sand*
- ➢*well sorted*

B. Grain shape

- ➢*xenomorph (40%) & euhedral(60%) - due to recrystallization perhaps generated by the inplacement of the adjacent dolerite dyke. The hexagonal bipyramid crystals commonly grew toward the center of a few large pores.*
- ➢*rounded*
- ➢*low (40%) & high (60%) sphericity*

C. Stage of textural maturity

- ➢*mature*

D. Fabric

- ➢*massive*
- ➢*matrix:grain 5:95 => grain supported*
- ➢*very closely packed grain clusters due to the authigenic overgrowth of the quartz crystals resulting in a few sutured grain contacts as well*
- ➢*20% porosity (i.e. pore-filling cement plus present porosity)*

III. Mineral composition

A. Grains:

Percentage of quartz: 100%

- ➢*100% monocrystalline & 0% polycrystalline*
- ➢*60% slightly undulatory & 40% non-undulatory*
- ➢*grain size 0.5-1 mm (coarse sand)*

B. Matrix: 5%

- ➢*mixture of microquartz, limonite, mica and clay*

IV. Diagenetic features

- ➢*authigenic overgrowth of the quartz crystals*
- ➢*microquartz (<20 μm), limonite cement*
- ➢*Fe-oxides present as rare & very thin grain coatings (there are some grain contacts without limonite rim)*

V. Classification

- ✧*slightly recrystallized quartz arenite*

I. Formation name & geographic location

Upper Unit - Karoo Supergroup; Ratho Farm - RAT2

II. Texture

A. Grain size and sorting

- ➢*0.031-0.06 mm coarse silt (30%), 0.062-0.125 mm very fine sand (50%), 0.125-0.25 mm fine sand (15%) & 0.25-0.5 mm medium sand (5%)*
- ➢*poorly sorted*

B. Grain shape

- ➢*xenomorph*
- ➢*subrounded, subangular > rounded*
- ➢*low (35%) & high (65%) sphericity*

C. Stage of textural maturity

- ➢*mature*

D. Fabric

- ➢*massive*
- ➢*matrix:grain 80:20 => matrix supported*
- ➢*grains float in sparry calcite matrix*
- ➢*quartz grains show strong embayment dissolution features*
- ➢*0-5% porosity (i.e. pore-filling cement plus present porosity)*

III. Mineral composition

A. Grains:

1. Percentage of quartz: 100%
   - ➢*100% monocrystalline & 0% polycrystalline*
   - ➢*70% undulatory & 30% nonundulatory*
   - ➢*grain size 0.062-0.125 mm very fine sand*
2. Percentage of other terrigenous minerals: <0.01%
   - ➢*opaque minerals, zircon*
   - ➢*grain size ~0.1 mm (very fine sand)*

B. Matrix: 80%

- ➢*sparry calcite: coarsely- very coarsely crystalline (0.25-4 mm)*

IV. Classification

- ✧*Carbonate glaebule (part of a giant carbonate concretion)*

I. Formation name & geographic location

Upper Unit - Karoo Supergroup; Ratho Farm - RAT4

II. Texture

A. Grain size and sorting

- ➢*0.062-0.125 mm very fine sand (40%),0.125-0.25 mm fine sand (40%) & 0.25-0.5 mm medium sand (20%)*
- ➢*individual laminae well sorted*

B. Grain shape

- ➢*xenomorph*
- ➢*subrounded , subangular > rounded*
- ➢*low (35%) & high (65%) sphericity grains*

C. Stage of textural maturity

- ➢*submature*

D. Fabric

- ➢*lamination caused by grain size changes*
- ➢*matrix:grain 0:100 => grain supported*
- ➢*grains very loosely packed: point contacts*
- ➢*30% porosity (i.e. pore-filling cement plus present porosity)*

III. Mineral composition

Grains:

1. Percentage of quartz: 98%
   - ➢*100% monocrystalline & 0% polycrystalline*
   - ➢*80% undulatory & 20% nonundulatory*
   - ➢*grain size 0.062-0.125 mm very fine sand (40%),0.125-0.25 mm fine sand (40%) & 0.25-0.5 mm medium sand (20%)*
2. Percentage of feldspar: 2%
   - ➢*multiple (albite, tartan) twins*
   - ➢*strongly altered to calcite, ghost grains*
   - ➢*grain size 0.062-0.125 mm very fine sand (40%),0.125-0.25 mm fine sand (40%) & 0.25-0.5 mm medium sand (20%)*
3. Percentage of other terrigenous minerals: <0.01%
   - ➢*opaque minerals, zircon, tourmaline, green hornblende*
   - ➢*80% of the grains are found in cross-laminae*
   - ➢*grain size 0.015-0.031 mm (medium silt)*

IV. Other features

Voids *(diameter: 0.2-0.8 mm) filled by:*

- ➢*microsparite-micite - resembling hair-rootlet molds*

V. Diagenetic features

- ➢*silica (10%), sparry calcite (90%) cement*
- ➢*Fe-oxides present as grain coatings & very rare blebs*

VI. Classification

- ✧*quartz arenite (cross-laminated siltstone)*

I. Formation name & geographic location

Basal Unit - Karoo Supergroup; Regina Farm - REG2

II. Texture

A. Grain size and sorting

- ➢*0.125-0.25 mm fine sand (35%), 0.25-0.5 mm medium sand (30%), 1-2 mm very coarse sand (30%) & 2-4 mm granules (5%)*
- ➢*poorly sorted*

B. Grain shape

- ➢*xenomorph, but there are a few euhedral quartz grains with angular authigenic overgrowth rims*
- ➢*angular > subangular*
- ➢*low (85%) & high (15%) sphericity grains*

C. Stage of textural maturity

- ➢*immature*

D. Fabric

- ➢*lamination due to the blade or lath-shaped minerals of the matrix. The laminated matrix wraps around the coarser detrital grains.*
- ➢*matrix:grain 35:65 => matrix supported*
- ➢*0-5% porosity (i.e. pore-filling cement plus present porosity)*

III. Mineral composition

A. Grains:

1. Percentage of quartz: 100%
   - ➢*70% monocrystalline & 30% polycrystalline*
   - ➢*90% undulatory & 10% nonundulatory*
   - ➢*polycrystalline grain size/crystal size in the polycrystalline grains/crystal number/crystal shape & boundaries 1-1.4 mm(very coarse sand) / 0.2-0.8 mm (fine-medium sand) / 5 or less / irregular, subequant with sutured contacts*
   - ➢*grain size 0.125-0.25 mm fine sand (35%), 0.25-0.5 mm medium sand (30%), 1-2 mm very coarse sand (30%) & 2-4 mm granules (5%)*
2. Percentage of other terrigenous minerals: <<0.01%
   - ➢*opaque minerals, zircon*
   - ➢*grain size 0.125-0.25 mm (fine sand)*

B. Matrix: 35%

- ➢*clay 70%*
- ➢*quartz & miscellaneous 30%*

IV. Diagenetic features

- ➢*authigenic overgrowth of the quartz crystals*
- ➢*silica cement*
- ➢*Fe-oxides present as diffuse microcrystalline stain in the matrix & rare blebs*

V. Classification

- ✧*quartzwacke*

I. Formation name & geographic location

Basal Unit - Karoo Supergroup; Regina Farm - REG5

II. Texture

A. Grain size and sorting

- ➢*0.125-0.25 mm fine sand (50%), 0.25-0.5 mm medium sand (25%), 1-2 mm very coarse sand (20%) & 2-4 mm granule (5%)*
- ➢*very poorly sorted*

B. Grain shape

- ➢*xenomorph*
- ➢*angular > subangular (most of the larger grains are subangular)*
- ➢*low (85%) & high (15%) sphericity grains*

C. Stage of textural maturity

- ➢*immature*

D. Fabric

- ➢*lamination due to the blade or lath-shaped micas & quartz of the matrix as well as diagenetic Fe-oxides precipitated along the bedding plane. The laminated matrix wraps around the coarser detrital grains*
- ➢*matrix:grain 60:40 => matrix supported*
- ➢*0-5% porosity (i.e. pore-filling cement plus present porosity)*

III. Mineral composition

A. Grains:

1. Percentage of quartz: 93%
   - ➢*85% monocrystalline & 15% polycrystalline*
   - ➢*90% undulatory & 10% nonundulatory*
   - ➢*polycrystalline grain size/crystal size in the polycrystalline grains/crystal number/crystal shape & boundaries*
     1.4-2 mm (very coarse sand) / 0.2-0.4 mm (medium sand) and 0.8-1 mm (coarse sand) / 5 or more /irregular, subequant with sutured contacts
     1 mm (coarse sand) / 0.2-0.4 mm (fine-medium sand) / 5 or more / irregular, subequant with sutured contacts
   - ➢*grain size 0.125-0.25 mm fine sand (49%), 0.25-0.5 mm medium sand (26%), 1-2 mm very coarse sand (21%) & 2-4 mm granule (4%)*
2. Percentage of feldspar: 1%
   - ➢*multiple (tartan 85% & albite 15%) twins*
   - ➢*sericitization*
   - ➢*grain size 0.25-0.5 mm (medium sand)*
3. Percentage of lithic fragments: 2%
   - ➢*feldspar-quartz rich fragments*
   - ➢*metamorphic rock (biotite schist) (The biotite wrap around the quartz grains.)*
   - ➢*all fragments are angular, subangular*
   - ➢*grain size 1.4-2 mm very coarse sand (50%) & 2-4 mm granule (50%)*
4. Percentage of micas: 5%
   - ➢*biotite >> muscovite*
   - ➢*grain size 0.125-0.25 mm fine sand (95%) & 0.5-1 mm medium sand (5%)*
5. Percentage of other terrigenous minerals: <<0.01%
   - ➢*opaque minerals, zircon*
   - ➢*grain size 0.125-0.25 mm (fine sand)*

B. Matrix: 60%

- ➢*clay 70%*
- ➢*biotite 20%*
- ➢*quartz & miscellaneous 10%*

IV. Diagenetic features

- ➢*limonite rich silica cement*
- ➢*Fe-oxides present as diffuse microcrystalline stain in the matrix & extremely rare blebs*

V. Classification

- ✧*biotite rich lithic greywacke*

I. Formation name & geographic location

Middle Unit (lower part) - Karoo Supergroup; Regina Farm - REG7

II. Texture

A. Grain size and sorting

- ➢*0.25-0.5 mm medium sand (50%) & 0.5-1 mm coarse sand (50%)*
- ➢*moderately sorted*

B. Grain shape

- ➢*xenomorph, but there are a few euhedral quartz grains with angular authigenic overgrowth rims*
- ➢*subrounded > subangular*
- ➢*low (60%) & high (40%) sphericity grains*

C. Stage of textural maturity

- ➢*mature*

D. Fabric

- ➢*massive*
- ➢*matrix:grain 8:92 => grain supported*
- ➢*grains show point contacts*
- ➢*15% porosity (i.e. pore-filling cement plus present porosity)*

III. Mineral composition

A. Grains:

Percentage of quartz: 100%

- ➢*85% monocrystalline & 15% polycrystalline*
- ➢*75% undulatory & 25% nonundulatory*
- ➢*polycrystalline grain size/crystal size in the polycrystalline grains/crystal number/crystal shape & boundaries 0.8-1.2 mm (coarse & very coarse sand) / 0.2 mm (fine sand) / plenty / irregular, subequant and a few elongated crystals with sutured contacts*

B. Matrix: 8%

- ➢*clay 60%*
- ➢*quartz & miscellaneous 40%*

IV. Diagenetic features

- ➢*limonite rich silica cement*
- ➢*Fe-oxides present as diffuse microcrystalline stain of the matrix & clusters of blebs*

V. Classification

- ✧*quartz arenite*

I. Formation name & geographic location

Basal Unit - Karoo Supergroup; Roly-Poly-Farm - ROL3

II. Texture

A. Grain size and sorting

➢*0.02 mm medium silt (80%), 0.06-0.125 mm very fine sand (10%) & 0.125-0.25 mm fine sand (10%)*

➢*moderately sorted*

B. Grain shape

➢*xenomorph*

➢*subrounded = subangular*

➢*low (60%) & high (40%) sphericity grains*

C. Stage of textural maturity

➢*submature*

D. Fabric

➢*lamination caused by flat lying mica flakes*

➢*matrix:grain 0:100 => grain supported*

➢*grains very closely packed: concavo-convex contacts (100%)*

➢*5% porosity (i.e. pore-filling cement plus present porosity)*

III. Mineral composition

Grains:

1. Percentage of quartz: 97%
   - ➢*100% monocrystalline & 0% polycrystalline*
   - ➢*50% undulatory & 50% nonundulatory*
   - ➢*grain size 0.02 mm medium silt (81%), 0.06-0.125 mm very fine sand (9%) & 0.125-0.25 mm fine sand (9%)*
2. Percentage of feldspar: 1%
   - ➢*multiple twins (tartan)*
   - ➢*altered (sericitisation)*
   - ➢*grain size 0.06-0.125 mm very fine sand (50%) & 0.125-0.25 mm fine sand (50%)*
3. Percentage of micas: 2%
   - ➢*biotie*
   - ➢*grain size 0.06-0.125 mm (very fine sand)*
   - ➢*muscovite (hydromuscovite)*
   - ➢*grain size 0.02 mm (medium silt) & 0.125-0.25 mm (fine sand)*
4. Percentage of other terrigenous minerals: <0.01%
   - ➢*opaque minerals, zircon*
   - ➢*grain size 0.062-0.125 mm (very fine sand)*

IV. Diagenetic features

➢*silica cement*

➢*Fe-oxides present as rare blebs & crystals*

V. Classification

✧*quartz arenite (siltstone)*

I. Formation name & geographic location

Basal Unit - Karoo Supergroup; Stembok Farm, near the long bore hole of DeBeers - STE2

II. Texture

A. Grain size and sorting

➢*0.125-0.25 mm fine sand (25%), 0.25-0.5 mm medium sand (40%), 1-2 mm very coarse sand (30%) & 2-4 mm granules (5%)*

➢*very poorly sorted*

B. Grain shape

➢*xenomorph*

➢*very angular > angular*

➢*low (80%) & high (20%) sphericity grains*

C. Stage of textural maturity

➢*immature*

D. Fabric

➢*massive*

➢*matrix:grain 40:60 => matrix supported*

➢*0-5% porosity (i.e. pore-filling cement plus present porosity)*

III. Mineral composition

A. Grains:

1. Percentage of quartz: ~100%

➢*90% monocrystalline & 10% polycrystalline*

➢*90% undulatory & 10% nonundulatory*

➢*polycrystalline grain size/crystal size in the polycrystalline grains/crystal number/crystal shape & boundaries*
2 mm (granule) / 0.2 to 0 .6 mm (medium to coarse sand) / 5-6 / irregular, subequant with sutured contacts
1.6 mm (very coarse sand) / 0.4 to 0 .8 mm (medium to coarse sand) / <5 / subequant with sutured contacts
0.8 mm (coarse sand) / <0.1 (less than very fine sand) / plenty / irregular, subequant with sutured contacts

2. Percentage of other terrigenous minerals: <0.01%

➢*opaque minerals, zircon*

➢*grain size 0.125-0.25 mm (fine sand)*

B. Matrix: 40%

➢*clay 95%*

➢*quartz & miscellaneous 5%*

IV. Diagenetic features

➢*silica cement*

➢*Fe-oxides present as diffuse microcrystalline stain in the matrix & rare blebs*

V. Classification

✧*quartzwacke*

I. Formation name & geographic location

Basal Unit - Karoo Supergroup; Stembok Farm - STE3

II. Texture

A. Grain size and sorting

- ➢*0.125-0.25 mm fine sand (70%), 0.25-0.5 mm medium sand (5%), 0.51 mm coarse sand (10%), 1-2 mm very coarse sand (10%) & 2-4 mm granules (5%)*
- ➢*very poorly sorted*

B. Grain shape

- ➢*xenomorph*
- ➢*very angular > angular*
- ➢*low (80%) & high (20%) sphericity grains*

C. Stage of textural maturity

- ➢*immature*

D. Fabric

- ➢*slight lamination due to the blade or lath-shaped minerals of the matrix. The laminated matrix asymmetrically wraps around the coarser detrital grains.*
- ➢*matrix:grain 75:25 => matrix supported*
- ➢*0-5% porosity (i.e. pore-filling cement plus present porosity)*

III. Mineral composition

A. Grains:

1. Percentage of quartz: 99%
   - ➢*98% monocrystalline & 2% polycrystalline*
   - ➢*90% undulatory & 10% nonundulatory*
   - ➢*polycrystalline grain size/ crystal size in the polycrystalline grains/ crystal number/ crystal shape & boundaries 1.4-2 mm(very coarse sand) / 0.4 and 1.2 mm (medium-very coarse sand) / 5 or less / irregular, subequant and a few elongated crystals with sutured contacts*
   - ➢*grain size 0.125-0.25 mm fine sand (70%), 0.25-0.5 mm medium sand (5%), 0.51 mm coarse sand (10%), 1-2 mm very coarse sand (10%) & 2-4 mm granules (5%)*
2. Percentage of mica: <1%
   - ➢*biotite altered, slight pleochroism*
   - ➢*grain size 0.25-0.5 mm (medium sand)*
3. Percentage of other terrigenous minerals: <<0.01%
   - ➢*opaque minerals, zircon*
   - ➢*grain size 0.125-0.25 mm (fine sand)*

B. Matrix: 75%

- ➢*clay 80%*
- ➢*quartz & miscellaneous 20%*

IV. Diagenetic features

- ➢*silica cement*
- ➢*Fe-oxides present as diffuse microcrystalline stain in the matrix & rare blebs*

V. Classification

- ✧*quartz grain rich mudstone*

I. Formation name & geographic location

Upper Unit - Karoo Supergroup; Princes Royal Farm @ Tsolwe - TSO1

II. Texture

A. Grain size and sorting

- ➢*0.062-0.125 mm very fine sand (50%) & 0.125-0.25 mm fine sand (50%)*
- ➢*well sorted*

B. Grain shape

- ➢*xenomorph*
- ➢*subrounded, rounded >> subangular*
- ➢*low (35%) & high (65%) sphericity*

C. Stage of textural maturity

- ➢*mature*

D. Fabric

- ➢*massive*
- ➢*matrix:grain 20:80 => grain supported*
- ➢*grains are loosely packed & show point contacts*
- ➢*0-5% porosity (i.e. pore-filling cement plus present porosity)*

III. Mineral composition

A. Grains:

1. Percentage of quartz: 99%
   - ➢*100% monocrystalline & 0% polycrystalline*
   - ➢60% *undulatory & 40% nonundulatory*
   - ➢*grain size 0.062-0.125 mm (very fine sand)*
2. Percentage of feldspar: <1%
   - ➢*multiple (tartan, albite) twins*
   - ➢*slightly altered (sericitisation)*
   - ➢*grain size 0.062-0.125 mm very fine sand (50%) & 0.125-0.25 mm fine sand (50%)*
3. Percentage of other terrigenous minerals: <0.01%
   - ➢*opaque minerals, zircon*
   - ➢*grain size 0.062-0.125 mm (very fine sand)*

B. Matrix: 20%

- ➢*microquartz*

IV. Other features

40% of the rock consists of 1.4-10 mm thick microquartz veins

- ➢*the veins are parallel to the original bedding*
- ➢*10% of the veins show M- (matrix) fabric, the rest is clean microquartz*
- ➢*within the veins there vertically and subhorizontally oriented tubules (length 1-2 mm) and voids (diameters 0.04/0.1/0.2/0.5 mm) filled by fibrous, radial length-slow chalcedony bundles; fibrous, radial lutecite ("zebraic chalcedony"); length-fast chalcedony and macroquartz.*

V. Diagenetic features

- ➢*silica, limonite & <1% sparry calcite cement*
- ➢*Fe-oxides present as grain coatings (there are some grain contacts without limonite rim) & very rare blebs*

VI. Classification

- ✧*partially silcretized quartz arenite*

I. Formation name & geographic location

Upper Unit - Karoo Supergroup; Balerno Farm @ Tsolwe -TSO2

II. Texture

A. Grain/clast size and sorting

- ➢*0.25-0.5 mm medium sand (10%), 0.5-1 mm coarse sand (60%), 1-2 mm very coarse sand (10%), 2-4 mm granule (10%) & 4-8 mm small pebble (10%)*
- ➢*poorly sorted*

B. Grain/clast shape

- ➢*xenomorph*
- ➢*subrounded, subangular*
- ➢*low (40%) & high (60%) sphericity*

C. Stage of textural maturity

- ➢*submature*

D. Fabric

- ➢*massive*
- ➢*matrix:clast 60:40 => matrix supported*
- ➢*grains/clasts are loosely packed*
- ➢*0-5% porosity (i.e. pore-filling cement plus present porosity)*

III. Mineral composition

A. Grains/clasts:

1. Percentage of rock fragments: 100%
   - ➢*grains of the very fine sandstone (80%) and medium siltstone (20%) clasts consist of 100% monocrystalline quartz with 80% undulatory & 20% non-undulatory extinction*
   - ➢*all clasts show grain supported internal fabric*
   - ➢*80% of the clasts have Fe-oxide rich matrix*
   - ➢*80% of the clasts are coated by 0.02 mm film of microquartz*
   - ➢*grain size 0.5-1 mm coarse sand (60%), 0.25-0.5 mm medium sand (10%), 1-2 mm very coarse sand (10%), 2-4 mm granule (10%) & 4-8 mm fine pebble (10%)*
2. Percentage of other terrigenous minerals: <0.01%
   - ➢*opaque minerals, zircon, tourmaline, green hornblende*
   - ➢*grain size ~0.1 mm (very fine sand)*

B. Matrix: 60%

- ➢*microquartz >75%*
- ➢*coarse silty clay <25%*

IV. Other features

A. Voids *(diameter: 0.2-0.4 mm) filled by:*

- ➢*Fe-oxide rimmed microquartz band => equant megaquartz (in the void center)*

B. Veins *(width: 0.5 m) filled by:*

- ➢*microquartz*
- ➢*apart from the straight, cross cutting veins there are web-like vein structures with crenulated walls as well*

C. Cavities *(diameter: 0.5-0.8 mm) enveloped by:*

- ➢*0.02 mm thick microquartz wall*

V. Diagenetic features

- ➢*Fe-oxides present as grain/clast coatings and rare blebs*

VI. Classification

- ✧*lithic greywacke - matrix supported massive breccia (Gmm) interwoven by microquartz veins*

I. Formation name & geographic location

Clarens Formation - Karoo Supergroup; Weipe Farm - WEI6

II. Texture

A. Grain size and sorting

- ➢*0.125-0.25 mm fine sand*
- ➢*well sorted*

B. Grain shape

- ➢*xenomorph, but there are a few euhedral quartz grains with angular authigenic overgrowth rims*
- ➢*rounded, subrounded > subangular (the xenomorf grains only)*
- ➢*low (50%) & high (50%) sphericity*

C. Stage of textural maturity

- ➢*supermature*

D. Fabric

- ➢*massive*
- ➢*bioturbation burrow (0.5 cm in diameter) with a 2 mm thick wall consisting of 0.03-0.06 mm (coarse silt) detrital grains floating in limonite cement*
- ➢*matrix:grain 0:100 => grain supported*
- ➢*very closely packed grain due to the authigenic overgrowth of the quartz crystals*
- ➢*<5% porosity (i.e. pore-filling cement plus present porosity)*

III. Mineral composition

Grains:

1. Percentage of quartz: ~95.5%
   - ➢*100% monocrystalline & 0% polycrystalline*
   - ➢*60% undulatory & 40% non-undulatory*
   - ➢*grain size 0.125-0.25 mm (fine sand)*
2. Percentage of feldspar: ~3.5%
   - ➢*multiple (tartan, albite) twins*
   - ➢*slightly altered (cloudy, brownish in PPL)*
   - ➢*grain size 0.125-0.25 mm (fine sand)*
3. Percentage of chert: <1%
   - ➢*grain size 0.125-0.25 mm (fine sand)*
4. Percentage of other terrigenous minerals: <0.01%
   - ➢*opaque minerals, zircon, green hornblende*
   - ➢*grain size ~0.1 mm (very fine sand)*

IV. Diagenetic features

- ➢*the authigenic overgrowth of the quartz grains post-dates the limonite coating of the grains as the limonite rim is outlining the original rounded, subrounded grains*
- ➢*silica, limonite cement*
- ➢*Fe-oxides present as rare grain coatings (there are some grain contacts without limonite rim)*

V. Classification

- ✧*quartz arenite*

I. Formation name & geographic location

Basal Unit - Karoo Supergroup; Weltevreden Farm - WEL2

II. Texture

A. Mean grain size and sorting

➢*0.125-0.25 mm fine sand (20%), 0.2-0.4 mm medium sand (60%) &1-1.2 mm very coarse sand (20%)*

➢*very poorly sorted*

B. Grain shape

➢*xenomorph*

➢*angular, subangular >> subrounded*

➢*low (80%) & high (20%) sphericity grains*

C. Stage of textural maturity

➢*immature*

D. Fabric

➢*slight lamination determined by the blade or lath-shaped clay minerals of the matrix. Lower, right corner of the slide displays a soft sedimentary deformation in form of a "plastic fold". The laminated matrix wraps around the coarser detrital grains.*

➢*matrix:grain 70:30 => matrix supported*

➢*0-5% porosity (i.e. pore-filling cement plus present porosity)*

III. Mineral composition

A. Grains:

1. Percentage of quartz: 99%

➢*90% monocrystalline & 10% polycrystalline*

➢*90% undulatory & 10% nonundulatory*

➢*polycrystalline grain size/ crystal size in the polycrystalline grains/ crystal number/ crystal shape & boundaries 1-1.4 mm(very coarse sand) / 0.2-0.4 mm (fine-medium sand) / 5 or less / irregular, subequant and a few lenticular crystals with sutured contacts*

➢*grain size 0.25-0.5 mm fine sand (20%), 0.2-0.4 mm medium sand (60%) &1-1.2 mm very coarse sand (20%)*

2. Percentage of mica: <1%

➢*biotite altered, slight pleochroism*

➢*grain size 0.25-0.5 mm (medium sand)*

3. Percentage of other terrigenous minerals: <0.01%

➢*opaque minerals, zircon*

➢*grain size 0.25-0.5 mm (fine sand)*

B. Matrix: 70%

➢*clay 90%*

➢*quartz & miscellaneous 10%*

IV. Diagenetic features

➢*silica cement*

➢*Fe-oxides present as diffuse microcrystalline stain in the matrix & rare blebs*

V. Classification

✧*clay rich quartzwacke*

I. Formation name & geographic location

Basal Unit - Karoo Supergroup; Weltevreden Farm - WEL6

II. Texture

A. Grain size and sorting

➢*0.125-0.25 mm fine sand (50%), 0.25-0.5 mm medium sand (20%) & 1-2 mm very coarse sand (30%)*

➢*very poorly sorted*

B. Grain shape

➢*xenomorph*

➢*angular, subangular >> subrounded*

➢*low (80%) & high (20%) sphericity grains*

C. Stage of textural maturity

➢*immature*

D. Fabric

➢*slight lamination determined by the blade or lath-shaped mica and clay minerals of the matrix*

➢*matrix:grain 60:40 => matrix supported*

➢*0-5% porosity (i.e. pore-filling cement plus present porosity)*

III. Mineral composition

A. Grains:

1. Percentage of quartz: ~100%

➢*monocrystalline 95% vs. polycrystalline 5%*

➢*undulatory 90% vs. nonundulatory 10%*

➢*polycrystalline grain size/ crystal size in the polycrystalline grains/ crystal number/ crystal shape & boundaries*
2.5-4 mm (granules) / 0.2 to 0 .6 mm (medium to coarse sand) / 20 or mores / irregular, subequant and a few elongated crystals with sutured contacts
2 mm (granules) / 1 to 1 .6 mm (very coarse sand) / 3 / subequant and elongated crystals with sutured contacts
1.2 mm (very coarse sand) / 0.4 to 0 .8 mm (medium to coarse sand size) / 5 or less / irregular, subequant and a few elongated crystals with sutured contacts

2. Percentage of other terrigenous minerals: <<0.01%

➢*opaque minerals, zircon*

➢*grain size 0.25-0.5 mm (fine sand)*

B. Matrix: 60%

➢*clay 97%*

➢*quartz & miscellaneous 3%*

IV. Diagenetic features

➢*silica cement*

➢*Fe-oxides present as diffuse microcrystalline stain in the matrix & rare blebs*

V. Classification

✧*clay rich quartzwacke*

I. Formation name & geographic location

Basal Unit - Karoo Supergroup; Weltevreden Farm - WEL14

II. Texture

A. Grain size and sorting

- ➢*0.02 mm medium silt (50%) & 0.06-0.125 mm very fine sand (50%)*
- ➢*moderately sorted, but the individual laminae well sorted*

B. Grain shape

- ➢*xenomorph*
- ➢*subrounded > subangular*
- ➢*low (30%) & high sphericity grains (70%)*

C. Stage of textural maturity

- ➢*mature*

D. Fabric

- ➢*lamination caused by grain size changes, flat lying mica flakes & elongated quartz grains*
- ➢*matrix:grain 0:100 => grain supported*
- ➢*grains very closely packed: point contacts (40%) & concavo-convex contacts (60%)*
- ➢*30% porosity (i.e. pore-filling cement plus present porosity)*

III. Mineral composition

Grains:

1. Percentage of quartz: 98%
   - ➢*monocrystalline 100% vs. polycrystalline 0%*
   - ➢*undulatory 80% vs. nonundulatory 20%*
   - ➢*grain size 0.02 mm medium silt (50%) & 0.06-0.125 mm very fine sand (50%)*
2. Percentage of mica: 2%
   - ➢*muscovite*
   - ➢*grain size 0.062-0.125 mm (very fine sand)*
3. Percentage of other terrigenous minerals: <0.01%
   - ➢*opaque minerals, zircon*
   - ➢*grain size 0.062-0.125 mm (very fine sand)*

IV. Diagenetic features

- ➢*silica cement*
- ➢*Fe-oxides present as blebs & crystals*

V. Classification

- ✧*quartz arenite (siltstone)*

I. Formation name & geographic location

Basal Unit - Karoo Supergroup; Weltevreden Farm - WEL18

II. Texture

A. Mean grain size and sorting

➢*0.125-0.25 mm fine sand (10%), 0.25-0.5 mm medium (40%) & 0.5-1 mm coarse sand (50%)*

➢*poorly sorted*

B. Grain shape

➢*xenomorph*

➢*subangular >> subrounded , angular*

➢*low (40%) & high (60%) sphericity grains*

C. Stage of textural maturity

➢*submature*

D. Fabric

➢*slight lamination determined by the blade or lath-shaped mica and clay minerals of the matrix*

➢*matrix:grain 20:80 => grain & matrix supported*

➢*where grain supported, the grains show point contacts*

➢*0-5% porosity (i.e. pore-filling cement plus present porosity)*

III. Mineral composition

A. Grains:

1. Percentage of quartz: 99%

➢*40% monocrystalline & 60% polycrystalline*

➢*95% undulatory & 5% nonundulatory*

➢*polycrystalline grain size/ crystal size in the polycrystalline grains/ crystal number/ crystal shape & boundaries 0.5-1 mm (coarse sand) / 0.25 mm (medium sand) / plenty / irregular, subequant crystals with sutured contacts*

➢*grain size 0.125-0.25 mm fine sand (10%), 0.25-0.5 mm medium (40%) & 0.5-1 mm coarse sand (50%)*

2. Percentage of feldspar: 1%

➢*multiple twins (tartan)*

➢*altered (sericitisation)*

➢*grain size 0.25-0.5 mm (medium sand)*

3. Percentage of other minerals: <<0.01%

➢*opaque minerals, zircon*

➢*grain size 0.25-0.5 mm (fine sand)*

B. Matrix: 20%

➢*clay 80%*

➢*quartz & miscellaneous 3%*

IV. Diagenetic features

➢*silica cement*

➢*Fe-oxides present as diffuse microcrystalline stain in the matrix & rare blebs*

V. Classification

✧*quartzwacke*